

University of Mississippi

eGrove

Electronic Theses and Dissertations

Graduate School

2011

Part A: Studies Towards Total Synthesis of an Anticancer and Antifungal Natural Product, Pseudolaric Acid B; Part B: Synthesis and Biological Evaluation of Berkeleyamide a and Its Derivatives

Swapnil Jayant Kulkarni

Follow this and additional works at: <https://egrove.olemiss.edu/etd>

 Part of the [Pharmacy and Pharmaceutical Sciences Commons](#)

Recommended Citation

Kulkarni, Swapnil Jayant, "Part A: Studies Towards Total Synthesis of an Anticancer and Antifungal Natural Product, Pseudolaric Acid B; Part B: Synthesis and Biological Evaluation of Berkeleyamide a and Its Derivatives" (2011). *Electronic Theses and Dissertations*. 175.

<https://egrove.olemiss.edu/etd/175>

This Dissertation is brought to you for free and open access by the Graduate School at eGrove. It has been accepted for inclusion in Electronic Theses and Dissertations by an authorized administrator of eGrove. For more information, please contact egrove@olemiss.edu.

PART A: STUDIES TOWARDS TOTAL SYNTHESIS OF AN ANTICANCER AND
ANTIFUNGAL NATURAL PRODUCT, PSEUDOLARIC ACID B;
PART B: SYNTHESIS AND BIOLOGICAL EVALUATION OF BERKELEYAMIDE A AND
ITS DERIVATIVES.

A Dissertation

Presented in partial fulfillment of requirements for the degree of

Doctor of Philosophy

in the Department of Medicinal Chemistry

The University of Mississippi

by

SWAPNIL J KULKARNI

MAY 2011

Copyright Swapnil J. Kulkarni 2011

ALL RIGHTS RESERVED

ABSTRACT

Part A: Studies towards total synthesis of an antifungal and anticancer agent, Pseudolaric acid B

Marked by the uncontrolled cell proliferation, cancer is one of the deadliest diseases, accounting for about 7.0 million deaths in 2007. Cancer is second leading cause of death worldwide, according to the American Cancer Society. Cancer chemotherapy has evolved through many years of painstaking research, and as a result, today we are able to cure at least some of cancers. One of the major impediments in the development of new drugs for treating cancer is that most of the approved drugs are themselves toxic and produce drug resistance during the initial exposure of these drugs. Thus there is a continued need to search for new/better drugs. Over the years, numerous natural products have been identified as leads for the drug discovery and development process. Some of the most well-known examples are Taxol, vincristine, vinblastine, Camptothecin and Etoposide

Pseudolaric acid B is a diterpenoidal natural product isolated from the extract of the root bark of *Pseudolarix kaempferi*, is a Chinese herbal medicine called *Tu Jin Pi*, which has been used for many years against fungal infections of the skin and nails. Studies of the bark of this plant have led to the isolation of several novel diterpene acids, namely pseudolaric acids A (PLAA, **1**), B (PLAB, **2**), C (PLAC, **3**) and B-Glycoside (PLAB-Gly, **4**)⁴⁻⁶.

We hereby report our studies towards the synthesis of PLAB using a model substrate. We have accomplished the synthesis of the model system, which can now be applied to the total

synthesis of PLAB. Key steps of our approach include Lewis acid mediated Diels Alder (DA) cycloaddition to give a bicyclo [2.2.2] acid, and a cationic 1,2- rearrangement. Series of functional group transformation reactions of the DA adduct, epoxidation, a tandem ring-opening-ring closing event, decarboxylation, and an enhanced Wagner-Meerwein rearrangement afforded a bicyclo [3.2.1] core **3.22**. Unfortunately, X-ray analyses of the bicyclo derivative revealed an inverted relative configuration. All the approaches to solving this end stage problem will be presented in the dissertation. Finally, we were able to obtain the crucial intermediate **3.22**, with the desired relative stereochemistry. With this intermediate in hand we have started efforts to complete the total synthesis of PLAB.

Part B: Synthesis and biological evaluation of Berkeleyamide A and its derivatives

Interleukin-1 β converting enzyme (ICE), also known as caspase-1, responsible for the cleavage and activation of interleukin-1 β (IL-1 β) to its active form (17K), is involved in the pathogenesis of several auto immune inflammatory disorders. Subsequent research over the years suggests that ICE plays a pivotal role in regulation of proinflammatory cytokines and its inhibition can be a potential therapeutic target for the treatment of immune-mediated inflammatory diseases.

Recently several interesting secondary metabolites have been isolated from the rare microbes evolved in extreme ecosystems such as a Berkeley Pit Lake in search of potential anticancer and antimicrobial agents. One such natural product, Berkeleyamide A, isolated from the fungi *Penicillium rubrum*, inhibited caspase-1 (ICE) and the signal transducing enzyme

matrix metalloproteinase-3 (MMP-3) in a low micromolar range. Herein we report an efficient total synthesis of (-)-berkeleyamide A. The total synthesis was accomplished in overall 18% yield, starting from *N*-Boc-*L*-leucinal, employing Evans' *syn*-aldol reaction of *N*-acyl-4*R*-benzyl oxazolidin-2-one as the key step. Excellent enantioselectivity (more than 95% ee) was obtained with a good yield (75%) for the crucial C-C bond formation key reaction step. In summary, our synthetic endeavor of (-)-berkeleyamide A is very efficient, scalable and highly diastereoselective with the flexibility to develop various analogues of the natural product. Using this modular approach, we accomplished syntheses of four other diastereomers. We have also carried out molecular docking studies to predict the binding mode of berkeleyamide A in the ICE active site. Furthermore, we designed a library of compounds as potential caspase-1 inhibitors based on berkeleyamide A scaffold.

Finally we carried out biological evaluation of Berkeleyamide A and its derivatives. We tested these compounds for caspase-1 inhibition, antifungal, antimalarial, antileishmanial and cytotoxic activities. However, berkeleyamide A and its derivatives failed to show promise in any of these assays.

DEDICATION

Dedicated To My Parents

Mrs. Shilpa J Kulkarni & Mr. Jayant K Kulkarni

To Whose Vision And Tireless Encouragement,

I Owe All My Success And Good Life Here

ACKNOWLEDGMENTS

I would like to thank all those individuals, institutions and grants which have helped to make this project successful. In particular, I would like to express my sincere gratitude and appreciation to:

Dr. Mitchell A. Avery, my major advisor, for his patience, guidance and support throughout this project. I highly appreciate his vision and open-mindedness in encouraging my creativity and independent research potential. I acknowledge his fortitude during the most difficult times in my graduate studies as well as research endeavours.

Dr. Stephen J. Cutler and Dr. John S. Williamson for their unwavering support and valuable guidance during my graduate studies and job search phase and also for serving on my dissertation committee.

Dr. Takashi Tomioka, for his insightful comments and also for serving on my dissertation committee.

Dr. Christopher McCurdy for his constant support and encouragement and for serving as a references from time-to-time.

Dr. Amar Chittiboyina, Dr. Blake Watkins and Dr. Ekambaram Pedduri for providing invaluable guidance and help in the research studies of my dissertation project. My fellow graduate students, from Dr. Avery's group and all the other friends from the department for making this long journey a memorable one.

JD Williams Library, The Science Library and the inter-library loan facility for providing with literature and books required for successful completion of this project.

My close friends, Dr. Nidhi Singh, Dr.Yatin Shukla and Dr.Parag Budukh for their unending support and friendship and for making the time in graduate school an unforgettable experience.

My best friend Dr. Pankaj Daga whose unrelenting support and assistance saw me through the difficult times and for facilitating the formatting of my dissertation document report.

My sister, Smita Kulkarni-Dixit and Sister-in-law, Charuta Upadhye-Modak for their eternal love and support.

My wife, Dr. Sampada Upadhye-Kulkarni whose unwavering love, encouragement and assistance proved extremely therapeutic in completion of my dissertation.

My parents –in-law, Mrs. Sulabha B Upadhye and Mr. Bhaskar Upadhye for supporting my every endeavour and encouraging me to complete my PhD.

My parents, Mrs. Shilpa J Kulkarni and Mr. Jayant Kulkarni for their unending love, sacrifice and vision which brought me to this day.

I will reap the benefits of their tireless work in making me the person that I am today and for that, I am eternally grateful to them.

Last but not the least, I thank God for making this dissertation see the light of the day.

TABLE OF CONTENTS

PARTA: STUDIES TOWARDS TOTAL SYNTHESIS OF PSEUDOLARIC ACID B

1.	PSEUDOLARIC ACID B -INTRODUCTION	1
1.1	Isolation of various pseudolaric acids.....	2
1.2	Structure elucidation	5
1.3	Biological activities	
1.3.1.	Antifungal	5
1.3.2	Antifertility	6
1.3.3.	Anti angiogenesis.....	7
1.4	PLAB binding site.....	10
1.5	Other activities	11
1.6	PLAB as a potential Anticancer agent	12
1.7	Structure Activity Relationship of Pseudolaric acid B	13
1.7.1	Antifungal SAR	14
1.7.1	Antiangiogenesis SAR.....	15
1.8	Synthetic approaches towards Pseudolaric acid A and B	
1.8.1.	Pan's Approach.....	18
1.8.2.	Chiu' intial Approach	19
1.8.3.	Bai's Approac	20
1.8.4	Chiu's total synthesis of pseudolaric acid A.....	22
1.8.5	Trost's total synthesis of pseudolaric acid B	27
2.	PRIOR WORK IN OUR RESEARCH GROUP	32
3.	STUDIES TOWARDS TOTAL SYNTHESIS OF PSEUDOLARIC ACID B	
3.1.	Synthetic Approach 1.....	43
3.2.	Synthesis of Model system	45
3.3.	Strategies to obtain the desired rearranged compound 3.22	51
3.3.1.	Strategy I.....	51
3.3.2.	Startegy II.....	55
3.3.3.	Startegy III	56
3.3.4.	Startegy IV	57
3.3.5.	Startegy V	58

3.4	Alternative route for total synthesis of PLAB	64
3.5	Progress for alternative route	65
3.6.	Future direction.....	68
4.	EXPERIMENTAL- PSEUDOLARIC ACID B	69

**PART B: SYNTHESIS AND BIOLOGICAL EVALUATION OF BERKELEYAMIDE A
AND ITS DERIVATIVES**

5. INTRODUCTION- CASPASE-1

5.1.	Caspases classification.....	181
5.2.	Zymogen Activation	182
5.3.	Caspase-1 also know as interleukin 1 β -converting enzyme (ICE).....	183
5.4.	Role of Caspase-1	183
5.5	Activation of Caspase-1	184
5.6	Structure of Caspase-1	185
5.7	Active site of caspase-1	186
5.8.	Allosteric site in caspase-1.....	188
5.9.	Catalytic mechanism of caspase-1 mediated hydrolysis of peptide bond.....	189
5.10.	Caspase-1 and Diseases	
5.10.1	Epilepsy and ICE	192
5.10.2	ICE and multiple sclerosis	193
5.10.3	ICE and Rheumatoid Arthritis	194
5.10.2	ICE and other diseases	194
5.11	Development of ICE inhibitors.....	195
5.11.1	Substrate Specificity for caspase-1	196
5.12	Caspase-1 Inhibitors in literature	200

**6. SYNTHESIS AND BIOLOGICAL EVALUATION OF
BERKELEYAMIDE A AND ITS DERIVATIVES**

6.1.	Introduction.....	207
6.2.	Structure of Berkeleyamide A	208
6.3.	Route-1 proposed synthesis for berkeleyamide A	209
6.4.	Need for asymmetric route	213
6.5.	Prior work	214

6.6.	Route-2 Total synthesis of Berkeleyamide A	217
6.6.1	Synthesis of Aldehyde 6.24	218
6.6.2	Synthesis of Chiral imide.....	219
6.6.3	Asymmetric aldol reaction.....	222
6.7	Moshers's method.....	224
6.8	Crystal structure of berkeleyamide A derivative	227
6.9	Synthesis of diastereomers of berkeleyamide-A.....	229
6.10	Anti-Aldol reaction	232
6.11	Design of Caspase-1 inhibitors based on berkeleyamide A scaffold	
6.11.1	Background.....	236
6.11.2	ICE active site –Quick Summary.....	237
6.11.3	Rational design of Caspase-1 inhibitor	239
6.11.4	Molecular docking protocol.....	239
6.11.5	Pose Validation	240
6.12	Design of ICE inhibitors	245
6.13	Biological Evaluation.....	252
6.14	Conclusion	257
7.	EXPERIMENTAL- BEREKELEYAMIDE A	259
8.	BIBLIOGRAPHY	365
9.	VITA	386

List of Tables

Table 1.1: Structures of various pseudolaric acids till date	1
Table 1.2 Cytotoxic activity of PLAB on different human cancer cells (IC ₅₀).....	9
Table 1.3: Biological evaluation of derivatives of PLAB against cancer cell lines	17
Table 5.1: Caspase-1 Inhibitors from literature	202
Table 6.1: Different catalyst and reaction conditions for Knoevenagel reaction	211
Table 6.2: Reaction conditions for cyclization (All reactions carried out in Microwave at normal absorption).....	212
Table 6.3: Structures of proposed novel ICE inhibitors based on 1 scaffold	246
Table 6.4: Biological evaluation of berkeleyamide A and their derivatives against Caspase-1	253
Table:6.5 Biological evaluation of berkeleyamide A and its derivatives : Anti-leishmanial Assay	254
Table 6.6: Biological evaluation of berkeleyamide A and its derivatives: Anti-Malarial Assay.....	254
Table 6.7a : Biological evaluation of berkeleyamide A and its derivatives : Anti-fungal Assay	255
Table 6.7b : Biological evaluation of berkeleyamide A and its derivatives : Anti-fungal Assay.....	255
Table 6.8: Standards used for Antifungal assay.....	256
Table 6.9: Biological evaluation of berkeleyamide A and its derivatives for Cytotoxicity Assay	256

List of figures

Figure 1.1. Common scaffold of pseudolaric acid	1
Figure 1.2: Pseudolaric acids with modified seven membered ring	2
Figure 1.3: Structure activity relationship of pseudolaric acids.	13
Figure 3.1: ORTEP plot of the X-ray crystal structure of the ketone 3.23 depicting the relative stereochemistry	48
Figure 3.2: Molecular energy calculation for the ketone 3.22.....	50
Figure 3.3: Molecular energy calculation for the ketone 3.23.....	50
Figure 3.4: Ball and stick representation of 3.44.....	61
Figure 3.5: Ortep diagram for Diol	63
Figure 3.6: ORTEP representation of ketone 3.22.....	63
Figure 5.1: Maturation of Caspase-1	182
Figure 5.2. Cartoon representation of caspase-1.....	186
Figure 5.3. Cartoon depiction of caspase-1 active site with cysteine 285 covalently attached to the inhibitor.....	187
Figure 5.4: Allosteric site of Caspase-1	189
Figure 5.5.: Detailed Mechanism of hydrolysis of peptide bond catalyzed by Caspase-1	191
Figure 5.6.: Typical caspase-1 inhibitor	196
Figure 5.7.: Types of caspase-1 inhibitors.....	197
Figure 5.8.: Different warhead groups used in caspase-1 inhibitors.....	198
Figure 5.9.: Crucial hydrogen bonding interaction in P2-P3 region of caspase-1 inhibitor	199
Figure 5.10. Depiction of active site of Caspase-1 with bound inhibitor Ac-YVAD-CHO, as reported in the co-crystal structure	200
Figure 6.1. Possible diastereomers of Berkeleyamide	208
Figure 6.2. Configurational correlation model for (<i>R</i>)-MTPA and (<i>S</i>)-MTPA Derivatives	225
Figure 6.3: Mosher ester analysis confirming the <i>S</i> -configuration of the aldol adduct.....	226
Figure 6.4: ORTEP representation of crystal structure of derivative of berkeleyamide A	228
Figure 6.5: Rationale for anti-aldol product.	235
Figure 6.6: Depiction of active site residues of Caspase-1 with bound inhibitor Ac-YVAD-CHO	238
Figure 6.7: Ligplot depiction of Z-VAD-FMK in the Caspase-1 active site in the co-crystal structure 2HBQ.	241

Figure 6.8: Pose validation studies. Ligand in green is the native ligand which was extracted and docked in the active site.	242
Figure 6.9: Overlay of 6.1 (docked in ICE active site) shown in magenta with Z-VAD-FMK shown in green in the ICE active site	243
Figure 6.10: The overlay of 6.1 (magenta) and Z-VAD-FMK (green) in the active site of ICE. The active site is shown as van der Waals surface.	244
Figure 6.11: Overlay of all eight diastereomers docked in to the ICE active site. 6.1 is shown in green and SSS diastereomer is shown in magenta	244
Figure 6.12: General protocol for docking	247
Figure 6.13: Overlay of SJK-2 (Magenta) and native ligand in Green in ICE active site shown as van der waals surface.....	248
Figure 6.14: Ligand Interaction Diagram for native ligand Z-VAD-FMK in ICE active site.....	249
Figure 6.15: Ligand Interaction Diagram for SJK-1 in ICE active site.....	250

List of Scheme's

Scheme 1.1: Pans retrosynthetic plan.	18
Scheme 1.2: Synthesis of lactone 1.3.....	19
Scheme 1.3: Chiu's synthesis of 1.35 using reductive aldol.....	20
Scheme 1.4: Bai's retrosynthesis of PLAA	21
Scheme 1.5: Bai's synthesis of hemiacetal intermediate 1.48 for synthesis of PLAA.....	22
Scheme 1.6: Chiu's retrosynthetic analysis for synthesis of PLAA... ..	23
Scheme 1.7: Synthesis of compound 1.59.. ..	24
Scheme 1.8: Completion of Total synthesis of PLAA.....	26
Scheme 1.9 : Trost's retrosynthetic approach	27
Scheme 1.10: Trost's synthesis of crucial intermediate 1.66.....	28
Scheme 1.11 Trost's completion of total synthesis of PLAB	29
Scheme 2.1: Retrosynthetic Scheme for PLAB	32
Scheme 2.2 : Degradation of PLAC	33
Scheme 2.3: Reconstruction of pseudolaric acid B from crucial intermediate 2.1	34
Scheme 2.4. More detailed Retrosynthetic Analysis for Pseudolaric Acid B... ..	35
Scheme 2.5: Synthesis of the model system... ..	37
Scheme 2.6: Synthesis of diene derivative 2.5... ..	37
Scheme 2.7 Intramolecular Diels-Alder approach.....	38
Scheme 2.8: DA using maelic anhydride.....	39
Scheme 2.9: Decarboxylation and lactonization using NaOH and Pb(OAc) ₄	39

Scheme 2.10 lead tetraacetate decarboxylation, mechanistic insights.....	40
Scheme 2.11 Synthesis of lactone 2.41.....	41
Scheme 3.1: Retrosynthetic Analysis for Pseudolaric Acid B.....	43
Scheme 3.2 : Retrosynthetic scheme for model system.....	44
Scheme 3.3 : Synthesis of diene 20... ..	45
Scheme 3.4: Synthesis of rearranged ketone 3.23... ..	47
Scheme 3.5: Mechanistic insights in to Wagner-Meerwien type rearrangement... ..	49
Scheme 3.6 : Barton decarboxylation... ..	52
Scheme 3.7: Barton decarboxylation mechanism... ..	53
Scheme 3.8: Mechanistic insights for formation of [2.2.2] intermediate... ..	53
Scheme 3.9: Attempted synthesis of the trihydroxy derivative 3.37... ..	54
Scheme 3.10: Attempts to rearrange the epoxide 3.19 to give desired ketoester 3.39.	55
Scheme 3.11: Acid mediated Rearrangement of lactone 3.41... ..	56
Scheme 3.12: Attempted synthesis of Benzyloxy Ketone 3.45... ..	58
Scheme 3.13. Proposed synthetic route for strategy V.. ..	59
Scheme 3.14: Synthesis of ene-ketone 3.44... ..	60
Scheme 3.15: Mechanism of dehydration of tertiary alcohol using burgess reagent.. ..	60
Scheme 3.16 : Completion of synthesis of crucial intermediate 3.10... ..	62
Scheme 3.17: Route 2 retrosynthetic analysis... ..	65
Scheme 3.18: Route 2; attempted synthesis of intermediate 3.66	66
Scheme 3.19: Future directions... ..	68
Scheme 6.1: Proposed synthesis of berkeleyamide A	209
Scheme 6.2: Synthesis of disubstituted Pyrrolidone scaffold.....	210
Scheme 6.3. Retrosynthetic analysis for Berkeleyamide A by Brimble <i>et al</i>	214
Scheme 6.4: synthesis of chiral alkene 6.14	215
Schemes 6.5: Completion of synthesis of Berkeleyamide A by Brimble.....	216
Scheme 6.6 : Route-2 retrosynthetic analysis of 6.1.....	217
Scheme 6.7: Synthesis of aldehyde fragment 6.24	218
Scheme 6.8: Synthesis of γ -N-Boc-oxazolidinone fragment 6.30	220
Scheme 6.9 : Synthesis of aldol adduct 6.31	221
Scheme 6.10: Synthesis of Azido chiral imide derivative 6.33	222
Scheme 6.11: Crimmin's Aldol protocol	223
Scheme 6.12: Mosher ester synthesis	225
Scheme 6.13: Synthesis of 6.1	226
Scheme 6.14: Dinitrobenzoyl derivative of Ketal.....	228
Scheme 6.15: Synthesis of Berkeleyamide A and its epimer; 6.42	230

Scheme 6.16: Synthesis of Diastereomers of Berkeleyamide A.....	231
Scheme 6.17: Oppolzer's protocol.....	232
Scheme 6.18: Evans anti-aldol protocol	233
Scheme 6.19: Synthesis of diastereomer of Berkeleyamide using Ghosh's Methodology ..	234

CHAPTER 1
PSEUDOLARIC ACID B-INTRODUCTION

Cancer is one of the deadliest diseases, accounting for about 7.0 million deaths in 2007. Cancer is, in fact, the second leading cause of death worldwide, according to the American Cancer Society.¹ Cancer chemotherapy has evolved through many years of painstaking research, and as a result, today we are able to cure at least some types of cancers. One of the major impediments in the development of new drugs for treating cancer is that most of the approved drugs are themselves toxic, and over a period of time, cancers develop resistance to existing drugs. Thus there is a continued need to search for new and better anti-cancer drugs. By far, chemotherapy is one of the most important and effective methods to treat or control cancer.

Over the years, numerous natural products have been identified as leads in various drug discovery programs.^{2, 3} The past two decades have seen a considerable number of new chemical entities either derived from natural products or that are natural product themselves. Newman and Cragg published a critical review on the impact of natural products on developing novel anti-cancer agents. In this review, they analyzed sources of new chemical entities (NCE) reported in the literature from 1981-2008. Their analysis suggests that between 1981-2008, more than 50% of the sources of NCE's had natural product origins (natural product, natural product derivatives or natural product inspired). Moreover, almost 80% of anti-cancer agents and 68% of antiinfective agents are from natural product sources. Some of the well-known examples are: Taxol, rapamycin, statins and several β -lactam antibiotics.²⁻⁴

Our research group is involved in the total synthesis of biologically important natural products. Our aim is to explore natural product leads, build natural product derived library and study their structure activity relationship in quest of potent inhibitors of several important biological targets.

Pseudolaric acids are novel diterpenoidal acids isolated from the root and trunk bark of *Pseudolarix kaempferi* Gordon (*Pinaceae*). The crude alcoholic extract of the plant (called “*Tu-jin-pi*”) has been used for decades in China for the treatment of the fungal infections of skin and nail.⁵ The antifungal activity of *Pseudolarix kaempferi* was reported in the literature in late 1950’s, and later detailed investigation of the extract led to the isolation and identification of the major antifungal component, pseudolaric acids. To date, more than 20 diterpenoids have been isolated with unique tricyclic scaffold. Up until March 2011, over 170 publications have been reported in the literature covering different aspect of studies on the pseudolaric acids. The pseudolaric acids and its derivatives have exhibited an array biological properties such as antifungal, anti-fertility, cytotoxic and anti-angiogenic.^{5,6}

Pseudolaric acids, with their diverse biological properties and unusual tricyclic structures, have attracted the attention of a number of research groups, resulting in several studies directed towards the total synthesis of the natural product.

1.1 Isolation of various pseudolaric acids:

The Cortex pseudolaricis was extracted with either benzene or percolated with 95% ethanol.⁷ Over 20 Pseudolaric acids have been reported in the literature with Pseudolaric acid A and B being the first ones to be isolated and characterized. Most of the pseudolaric acids have a common scaffold, with variations only at either of R1, R2 and R3 positions. Few of them were derivatives of pseudolaric acid A with modifications mainly on the seven membered ring and a couple of them were pseudolaric acid B derivative with truncated side chain (Figure 1.1).⁶ A comparative study analyzing the composition of the extracts of “*tu jin pi*” from different regions in the Republic of China showed some variation in the ratio of components. However, the major

components in crude extract were in the following order; pseudolaric acid B (PLAB) (1.2) and its glycoside derivative, pseudolaric acid A PLAA (1.1) and its glycoside derivative 1.5, pseudolaric acid C.⁸ One of the common protocols for isolation of pseudolaric acids was extraction of the benzene extract with sodium bicarbonate solution followed by acidification of the aqueous extract with hydrochloric acid leading to precipitation of the mixtures of pseudolaric acids. Pure pseudolaric acids can then be obtained via silica gel column chromatography.^{7,9}

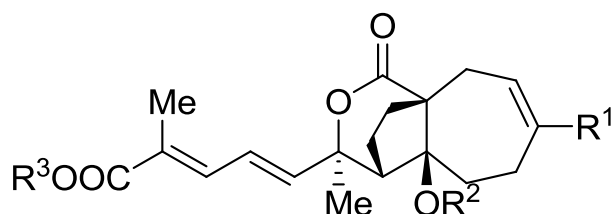


Figure 1.1. Common scaffold of pseudolaric acid

Table 1.1: Structures of various Pseudolaric acids till date ^{6,9-17}

	Name	R1	R2	R3
1.1	Pseudolaric acid A	Me	Ac	H
1.2	Pseudolaric acid B	CO ₂ Me	Ac	H
1.3	Pseudolaric acid C1	CO ₂ Me	H	H
1.4	Pseudolaric acid C2	CO ₂ H	Ac	H
1.5	Pseudolaric acid A <i>O</i> -β-D-glucopyranoside	Me	Ac	β-D-glucose
1.6	Pseudolaric acid B <i>O</i> -β-D-glucopyranoside	CO ₂ Me	Ac	β-D-glucose
1.7	Demethoxydeacetoxypseudolaric acid B	CO ₂ H	H	H
1.8	Pseudolaric acid B 2,3-dihydroxypropyl ester	CO ₂ Me	Ac	CH ₂ CH(OH)CH ₂ OH
1.9	Pseudolaric acid B 6- <i>O'</i> -acetyl- <i>O</i> -β-D-glucopyranoside	CO ₂ Me	Ac	6'- <i>O</i> -acetyl-β-D-glucose

1.10	Deacetylpseudolaric acid A	Me	H	H
1.11	Pseudolaric acid A methyl ester	Me	Ac	Me
1.12	Pseudolaric acid B methyl ester	CO ₂ Me	Ac	Me
1.13	Deacetylpseudolaric acid A <i>O</i> -β-D-glucopyranoside	Me	H	β-D-glucose
1.14	Deacetylpseudolaric acid A 2,3-dihydroxypropyl ester	Me	H	CH ₂ CH(OH)CH ₂ OH
1.15	Deacetylpseudolaric acid B 2,3-dihydroxypropyl ester	CO ₂ Me	H	CH ₂ CH(OH)CH ₂ OH

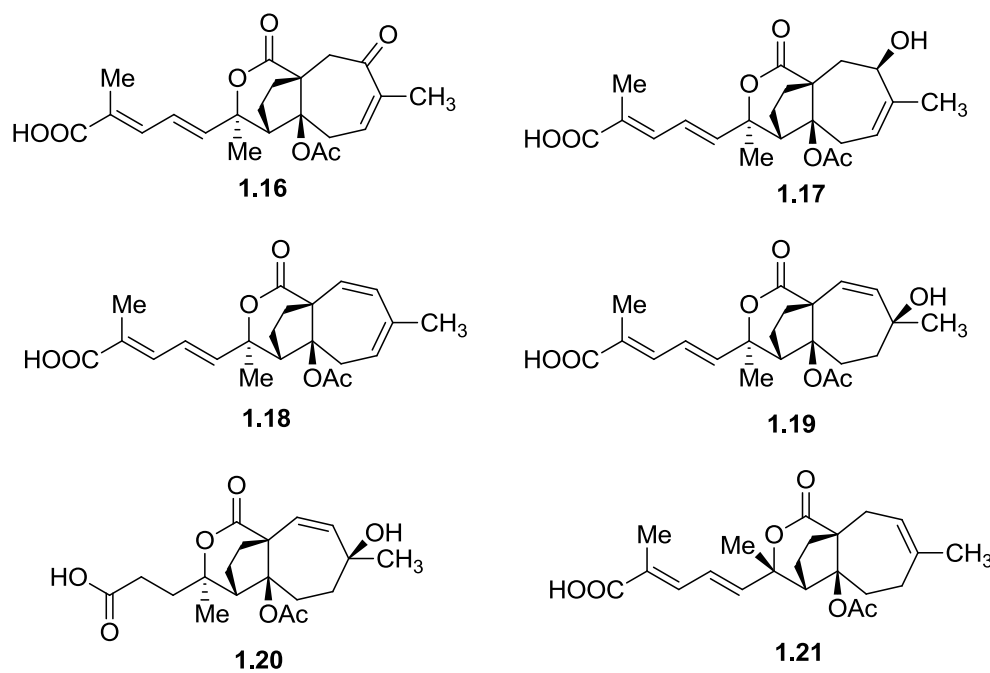


Figure 1.2: Pseudolaric acids with modified seven membered ring

1.2 Structure Elucidation:

Zhou's research group¹⁸ performed thorough structural elucidation studies, including degradation analysis, functional group transformations, NMR, mass spectroscopy and IR on pseudolaric acids.^{19, 20} Lin *et al*²¹, using X-ray crystallographic analysis, unambiguously assigned relative stereochemistry and structure of 1.1 (Figure 1.1) while absolute configuration of 1.2 was confirmed to be 3S, 4S,10R,11R by use of the circular dichroism method. Hamburger *et al*²² carried out NMR(1D&2D) and molecular modeling studies to investigate the conformation of 1.2. Their NOEs studies revealed close spatial relationship of H3, H12 and H13. Furthermore, their molecular modeling studies were in corroboration with NOE studies suggesting that the lactone ring adopting a half-planar conformation.²² Recently the absolute chemistry and structures of both 1.1 and 1.2 were also confirmed by total synthesis.^{23, 24}

1.3 Biological properties and Mechanism of Action of Pseudolaric acid B

1.3.1 Antifungal Activity

The extract of *Pseudolarix kaempferi* has long been used in China traditionally to treat fungal infections of skin.⁵ Hufford *et al* led a systematic investigation into the bioactivity-guided fractionation of *P. kaempferi* to identify the active constituents responsible for its antifungal activity.²⁵ The authors recognized Pseudolaric acid B as the major constituent responsible for antifungal activity of *P. kaempferi*. In their study, PLAB was found to be particularly active against *Trichophyton mentagrophytes*, *Twrtlopsispetrophium*, *Mirrospwum gypseum*, and *Candida* species and the in vitro efficacy of PLAB was found to be comparable to amphoterecin B, a well known antifungal compound. In order to identify the structural features required for antifungal activity, the authors further synthesized various methylated and hydrolyzed

derivatives of PLAB. The SAR studies demonstrated that neither the methylated nor the hydrolyzed compounds showed any antifungal activity. This led to the conclusion that acetoxy group and the C-18 free acid in PLAB moiety are necessary for antifungal activity. Compound 3, as well as its monopotassium and monosodium salts of PLAB exhibited marginal micromolar level antifungal activity against *C. albicans*. PLAB was evaluated for its ability to reduce the *C. albicans* infection in murine kidney candidiasis model. PLAB was found to exhibit significant antifungal activity against *C. albicans* in murine kidney candidiasis model.²⁵

Avery *et al* demonstrated the concentration-dependent activation effect of PLAB for the nuclear peroxisome proliferator-activator (PPAR) α , γ and δ isoforms in CV-1 and H4IIEC3 cell lines. Since the peroxisome proliferator- activated receptors (PPARs) are important for the membrane integrity and lipid metabolism of *Candida* species, it was speculated by the authors that the activation of PPAR isoforms may be the plausible mechanism of anti-fungal activity of PLAB.²⁶

1.3.2 Antifertility Activity

In a study by Zhang et al, Pseudolaric acid B has demonstrated anti-fertility activity by decreasing the fertilization rate of hamster ova. But no effect of PLAB on spermatozoa activity or fertilizing ability of hamster was observed in this study.²⁷ Anti-fertility activity of PLAB was evaluated in several animal models, including rats, dogs, and hamsters. Although there was a transient reduction in the progesterone levels of the animals treated with PLAB, termination of pregnancies were not observed in these cases.²⁷

1.3.3 Anti-cancer activity

Apart from antifungal and anti-fertility activities of PLAB, it was shown to exhibit cytotoxicity towards several cancer cell lines including those of the lung, colon, breast, brain and kidney by Pan *et al.*²⁸ It was discovered that minor structural modifications of the functional groups led to significant reduction in cytotoxic activity of PLAB. The target for anticancer activity of PLAB and PLAA was also not known and elucidated.

1.3.4 Angiogenesis

Angiogenesis is a pivotal factor in tumor progression, and it is known that inhibition of angiogenesis is a potential anti-cancer target. Recently, studies have shown that PLAB exerted potent anti-angiogenic effects *in vitro*, which was evaluated by vascular endothelial cell proliferation, migration and tube formation assays. Moreover, PLAB also showed repression of *in vivo* angiogenesis in the Matrigel plug and chicken chorioallantoic membrane assay.²⁹⁻³² Anti-angiogenic activity of PLAB was the result of a dual mechanism. First, PLAB blocked vascular endothelial growth factor (VEGF) mediated anti-apoptotic effect and induced cell death in endothelial cells. The increased apoptosis of endothelial cell was due to the inhibition of VEGF stimulated tyrosine kinase phosphorylation of the kinase insert domain-containing receptor/fetal liver kinase-1 (KDR/flk-1), resulting in the inhibition of Akt and ERK phosphorylation.³¹ Second, PLAB inhibited the secretion of the angiogenic factor VEGF from breast tumor cells via reduction of hypoxia-inducible factor-1 α (HIF-1 α) protein by inducing its ubiquitin-proteasome mediated degradation. Hypoxia inducible factor-1 is a heterodimer composed of HIF-1 α and HIF-1 β . HIF-1 α is a key transcription factor responsible for angiogenesis in hypoxic conditions.

Overexpression of HIF-1 α protein is demonstrated in several types of cancers and its degradation can be considered as a promising target in anti-angiogenesis.^{30, 31}

Molecular target of PLAB has been recently identified as microtubules which have been proved to be one of the most validated targets for anticancer drug development.³³ Microtubules are polymers of α -tubulin and β -tubulin heterodimers playing an essential role in the organization, development and preservation of cell shape, transport of important components of cells, cell signaling, in cell division and mitosis. Microtubules are long filamentous tubeshaped protein polymers present in all eukaryotic cells which undergo dynamic polymerization (two non-equilibrium dynamic states; dynamic instability and treadmilling) to facilitate cell mitosis and division.^{34, 35} Wong *et al* demonstrated that PLAB is a novel microtubule destabilizing agent *in vitro* as well as *in vivo*, and more importantly, it circumvents the P-glycoprotein overexpression induced drug resistance.^{36, 37} Consistent with previous reports³⁸, they also found PLAB displayed significant cytotoxicity (Table 1) (mean IC₅₀ 0.9 μ g/ml) against various human cell lines. Furthermore, with the use of NIH-3T3 cells transfected with V1 isoform, the authors demonstrated that PLAB selectively halts the progression of actively proliferating cancer cells. PLAB induced G₂-M cell cycle arrest for cell types from different tissues liver (HepG2), breast (MCF-7), colon (SW620), and cervical (HeLa) in a time dependant manner. To completely understand the mechanism of PLAB induced cell cycle arrest, HepG2 cells were treated with PLAB along with other G₂-M cell cycle arrest agents etoposide (topoisomerase II inhibitors) and nocodazole (microtubule-targeting agent). PLAB and nocodazole, unlike etoposide, did not have any effect on G2 checkpoint proteins and upregulated cyclin B1, a marker for mitotic arrest. This suggests that PLAB may arrest mitotic phase of the cell cycle which was further confirmed by examining the effect of PLAB on microtubules organization by use of immunofluorescence

staining of α -tubulin. Wong and associates treated HeLa cells and umbilical vascular endothelial cells with PLAB (2 $\mu\text{mol/L}$) which resulted in the disruption of microtubule fibres, abnormal formation of multipolar spindles and subsequent cell cycle arrest at prometaphase in a time dependent manner. This study suggests that PLAB is a microtubule destabilizing agent and exerts its cytotoxicity in a manner similar to that of colchicine and vinblastine. PLAA also shows similar microtubule destabilization leading to apoptosis but is far less potent than PLAB.^{36, 37}

Table 1.2 Cytotoxic activity of PLAB on different human cancer cells (IC_{50})³⁸

Cancer Cells	IC_{50} ($\mu\text{mol/L}$)	Cancer Cells	IC_{50} ($\mu\text{mol/L}$)
BGC-823	1.13 ± 0.24	Ketr3	3.58 ± 2.42
HeLa	0.50 ± 0.19	A-2780	0.87 ± 0.08
A549	5.20 ± 0.26	Skov3	0.74 ± 0.28
HCT-8	1.20 ± 0.02	Mcf-7	4.25 ± 1.37
HT-29	0.68 ± 0.03	EJ	1.04 ± 0.50
KB	0.17 ± 0.035	HKC	5.77 ± 0.65

(Table 1.2 adapted from reference no. 38)

1.4 PLAB binding site

Wong *et al* examined the microtubule polymerization *in vitro* in the presence of PLAB, paclitaxel and colchicine.^{36,37} As expected, paclitaxel increased tubulin polymerization due to its stabilizing effects on the microtubules. On the other hand, PLAB and colchicine treatment reduced the microtubule assembly in dose dependent manner suggesting that PLAB directly interacts with tubulin. Furthermore, most of the known microtubule-disrupting agents interact with either the vinca domain or the colchicine site of tubulin. Hence they carried out further studies to probe the binding site of PLAB with the aid of [³H]colchicine and [³H]vinblastine competition-binding assays. PLAB was able to displace [³H]colchicine from the binding site when its concentration was increased gradually while [³H]vinblastine remained bounded to the binding site. This study implies that PLAB may interact with the colchicines binding domain in a competitive fashion and does not interact with the vinblastine binding domain. The fact that PLAB only displaced colchicine at a higher concentration and given their structural disparity, suggest that PLAB binds to a distinct novel binding site on tubulin that induces conformational changes to the colchicine site and weakens colchicine binding. The observations that PLAB may bind to a distinct tubulin binding site corroborated with research findings from Tong's research group³². They carried out the studies to probe the effects on the dynamics and conformation of tubulin induced by binding of PLAB. To confirm that PLAB interacts directly with tubulin, investigations were carried out to see the effects of PLAB on intrinsic tryptophan fluorescence of tubulin. The tubulin has eight tryptophan residues in its primary structure and intrinsic tryptophan fluorescence is a measure of conformational state of tubulin. PLAB enhanced the intrinsic fluorescence, while vinblastine and colchicine decreased the intrinsic tryptophan fluorescence of tubulin. Also, the far-UV CD showed some change in the secondary helical

structure of the protein suggesting that PLAB binds to tubulin which brings a unique change in its conformation. Furthermore, unlike vinblastine and colchicine, PLAB increased the fluorescence intensity of the tubulin bis-ANS (bis-ANS binds stoichiometrically with tubulin and the complex is used to probe the conformational status of tubulin) complex. Additionally, PLAB did not have any effects on the tubulin cysteine residues, which was measured by 2, 4 Dinitrothiocyanobenzene (DNTB) titration assay. Tubulin has reactive sulphhydryl groups (of Cysteine residues) located in the area, which is especially crucial for polymerization, and any changes in reactivity of these functional group is a measure of conformational change of the protein. DNTB is used to titrate the number of sulphhydryl groups in a protein. While colchicine and vinblastine caused a decrease in the number of reactive thiol groups, PLAB did not have any effect on the accessibility of sulphhydryl groups on tubulin. Both these studies (bis-ANS-Tubulin complex and DNTB titration of thiol groups) together indicate that PLAB indeed binds to a novel, distinct binding site different than that of colchicine and vinblastine, However, the exact binding site is yet to be determined. It is safe to conclude that neither vinblastine nor colchicine competitively inhibits PLAB binding to tubulin.³²

1.5 Explanation of other biological properties of PLAB

The identification of tubulin as the molecular target of the pseudolaric acids has helped to solve the puzzle regarding mechanisms for their other biological activities. Though there is no direct evidence, a plausible mechanism of antimicrobial activity of pseudolaric acids can be microtubule destabilization in the microbes. There is a high structural similarity between tubulins of lower and higher organisms, which makes the above assumption more logical. Along the same lines, the anti-fertility activities of 1.1 and 1.2 can be explained and is most probably due to the suppression of angiogenesis and inhibition of cell division during formation and development of

the embryo. Lastly, the reduction of HIF-1 α protein and subsequently inhibition of angiogenesis can be attributed to their effect on the depolymerization of microtubules as other microtubule-targeting molecules, such as 2-methoxyestradiol or phenyl-3-(2-chloroethyl) urea have shown similar outcomes.³⁷

1.6 PLAB as a potential Anticancer agent:

Acquired drug resistance is one of the major hurdles in anti-infective and anti-cancer drug development. Multi drug resistant tumour cells are characterized by the overexpression of the P-glycoprotein (P-gp) efflux pump. These P-gp efflux pumps are responsible for the development of resistance in tumor cells to many drugs including tubulin-binding agents. Wong *et al* demonstrated that PLAB's cytotoxicity was only slightly reduced (2 fold) compared to cytotoxicity of doxorubicin (17 fold decrease) in cells that ectopically overexpressed P-gp proteins. Furthermore, PLAB also showed a better cytotoxicity profile than taxol in a paclitaxel-selective P-gp overexpressing cell line and multidrug-resistant liver cancer cell line from the parental cell line. These results suggest that PLAB is not a P-gp substrate and able to circumvent P-gp mediated drug resistance in tumor cells. Furthermore, Wong and coworkers also demonstrated *in vivo* efficacy of PLAB by using a xenograft mouse model. In this study, PLAB treatment resulted in tumor suppression in a dose-dependent manner. Moreover, PLAB treatment not only reduced the tumor growth of a taxol-resistant liver cancer but also did not show any signs of toxicity or weight loss in the animals, indicating that PLAB is selective against tumors *in vivo*.^{36,37}

In summary, it is quite clear that PLAB, with its multiple modes of action, inhibition of angiogenesis, as well as microtubule destabilization, and by virtue of its ability to circumvent P-gp mediated drug resistance, is a good lead in anti-cancer drug development.

1.7 Structure Activity Relationship of Pseudolaric acid B

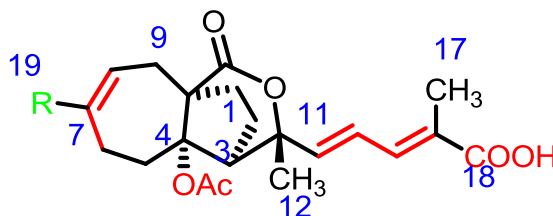


Figure 1.3: Structure activity relationship of pseudolaric acids. The portion of molecule shown in red indicates forbidden modifications and the one displayed in green indicates allowed modification

Several research groups have synthesized numerous derivatives of PLAB and PLAA in an effort to identify their SAR which ultimately will aid in the design of more potent analogs of pseudolaric acid. They have tested PLAB, PLAA, other naturally occurring pseudolaric acids as well as synthetic derivatives for antifungal and antiangiogenic activities. Interestingly, the SAR profile of PLAB and PLAA for all the above mentioned activities is nearly the same. Core structure of pseudolaric acid (PLAB and PLAA), along with its functional group, is absolutely necessary for the activity. Most of the chemical modifications resulted in reduced or completely abolished activity with exception of derivatives, which were either equipotent or more potent than parent natural products (PLAB and PLAA)

1.7.1 Antifungal SAR^{25, 39, 40}

1) The compounds exhibiting antifungal activity have amphipathic properties. All of them have a hydrophobic polycyclic rigid carboskeleton and a hydrophilic region of an unsaturated carboxylic acid chain.

2) R1 tolerates some lipophilic substituents, but overall, carboxylic methyl ester and methyl functional groups as found in PLAB and PLAA respectively were the most active compounds. Substitution at R1 with CO₂Et, -CO₂(n-Pr) and -CO₂(n-Bu) decreased the antifungal activity.

3) The double bond at C-7 position is important for antifungal activity and any modification of the double bond, even migration renders the resulting compound inactive.

4) The side chain is absolutely essential for the activity. Saturation of the two double bonds or modification of the double bonds resulted in diminished activity. Shortening or lengthening of the side chain had a similar fate.

5) The free carboxylic acid group in the side chain was found to be necessary for antifungal activity. Ester, amide and even naturally occurring glycoside had little to no activity, however, the sodium and potassium salts of PLAB retain the activity. Surprisingly, the NH-(thiazol-2-yl) amide derivative exhibited better antifungal profile than the parent natural product against *Epidermophyton floccosum*⁴⁰

6) Finally, C-4 acetyl group is optimal for antifungal activity

1.7.2 Antiangiogenic SAR⁴¹

Same research group carried out SAR studies for antiangiogenic activity, and the SAR is as follows:

1) All the compounds that showed antiangiogenic activity were amphipathic in nature same as is the case for antifungal activity. All derivatives shared this common feature: presence of a hydrophobic domain comprising of constrained tricyclic ring on the western hemisphere and a relatively hydrophilic (*E*)-methylpentadienoic acid side chain on the eastern hemisphere of the molecule.

(2) Major difference in the antiangiogenic and antifungal SAR for PLAB was seen at R1 substitution. A bulky hydrophobic R group at C-7 increased the antiangiogenic and/or anticancer activity by almost 3-4 folds. Table 1.3 shows the amide and ester derivatives of PLAB tested against human microvascular endothelial cells (HMEC-1), human premyelocytic leukemia (HL-60), human lung cancer cell (A-549), human breast cancer cells (MB-MDA-468), human liver cells (BEL-7402), human colon cell HCT116 and human cervical cancer cell (HeLa) *in vitro*.

4) Presence of Δ^7 is crucial for antiangiogenic activity and saturation or modification of the double bond leads to loss of activity. This probably suggests that the double between C-7 and C-8 might lock the molecule in a favorable bioactive conformation (Not supported by any data).

5) The side chain is absolutely essential for the activity and either saturation of the two double bonds or shortening or lengthening of the side chain resulted in analogs to greatly decrease or no activity.

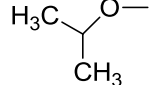
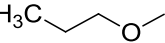
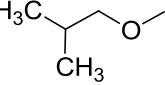
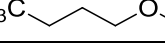
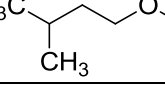
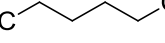
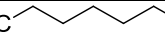
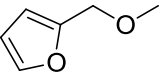
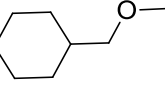
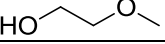
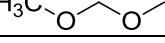
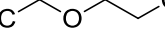
6) Several research groups have made numerous ester and amide analogs with different degrees of structural complexities; however, no substitution is tolerated and the free carboxylic acid functional group is critical for antiangiogenic activity

7) Any other structural changes in the seven-membered ring, like saturation or migration of the Δ^7 double bond and/or oxygenation at C-7 or C-8 will render the analogs inactive.

8) Finally, as in the case of antifungal SAR, the acetoxy group at C-4 is crucial for the activity. The replacement, hydrolysis or the elimination of the acetoxy group, significantly attenuated the antiangiogenic and anticancer activity.

The SAR studies PLAB showed that most of the structural feature must be retained in order to preserve the antifungal, antiangiogenic and cytotoxic activity. To obtain significantly more potent analogs from PLAB, studies are warranted to identify the exact target site on tubulin. Once the active site is known, molecular modeling studies (docking) can be used to study the binding interactions of PLAB and PLAA with tubulin active site. After understanding the key protein-ligand interactions, better analogs can be designed with improved biological as well as pharmacokinetic profile.

Table 1.3: Biological evaluation of ester derivatives of PLAB against several cancer cell lines⁴¹

	R ¹	IC ₅₀ (μM)					
		HMEC-1	HL-60	A-549	MB-MDA-468	HCT116	Hela
1.1	(Plab) H ₃ CO—	0.803±0.00	0.235±0.07	1.162±0.36	0.596±0.22	0.136±0.03	0.497±0.15
1.1a	H ₃ CHN—	>5.00	>5.00	>5.00	-	-	-
1.1b	H ₃ C—O—	1.047±0.01	0.5±0.266	1.992±0.02	0.587±0.11	0.670±0.02	0.756±0.11
1.1c		0.199±0.00	0.242±0.01	0.608±0.01	0.332±0.04	0.367±0.04	0.427±0.23
1.1d		0.238±0.04	0.190±0.03	0.677±0.11	0.243±0.02	0.234±0.03	0.262±0.01
1.1e		0.278±0.09	0.171±0.00	0.649±0.00	0.239±0.02	0.243±0.03	0.262±0.01
1.1f		0.195±0.00	0.198±0.05	0.567±0.02	0.245±0.07	0.257±0.04	0.163±0.08
1.1g		0.757±0.03	0.316±0.01	0.726±0.01	0.27±0.098	0.394±0.06	0.426±0.25
1.1h		0.216±0.01	0.264±0.00	0.676±0.11	0.298±0.08	0.304±0.03	0.212±0.05
1.1i		0.569±0.14	0.658±0.02	0.756±0.00	0.657±0.08	0.641±0.00	0.565±0.15
1.1j		0.562±0.04	0.459±0.31	0.74±0.03	0.377±0.07	0.419±0.09	0.550±0.12
1.1k		0.335±0.02	0.421±0.24	0.666±0.06	1.973±0.12	1.563±0.59	2.291±0.38
1.1l		>5.00	>5.00	>5.00	-	-	-
1.1m		>5.00	>5.00	>5.00	-	-	-
1.1n		>5.00	>5.00	>5.00	-	-	-

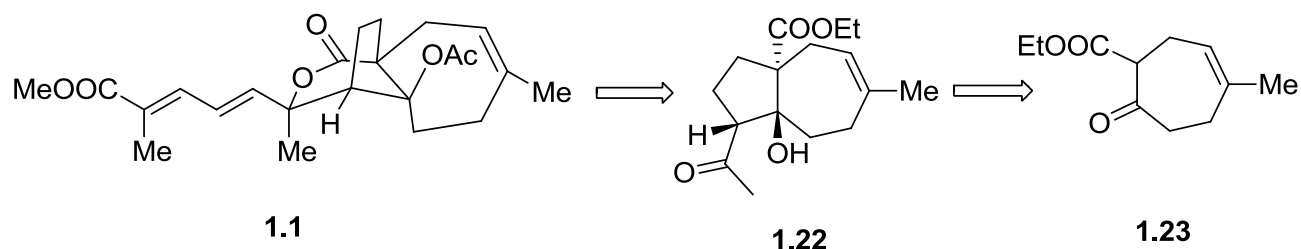
(This table is adapted from Yang et.al. *J Med Chem* **2008**, 51, 77-85)

1.8 Synthetic studies on Pseudolaric acid (A and B):

To date, several efforts towards the total synthesis of pseudolaric acids have been published in the literature by few research groups. However, only Chiu's group and Trost's group have succeeded in completing the total synthesis of 1.1 and 1.2 respectively.

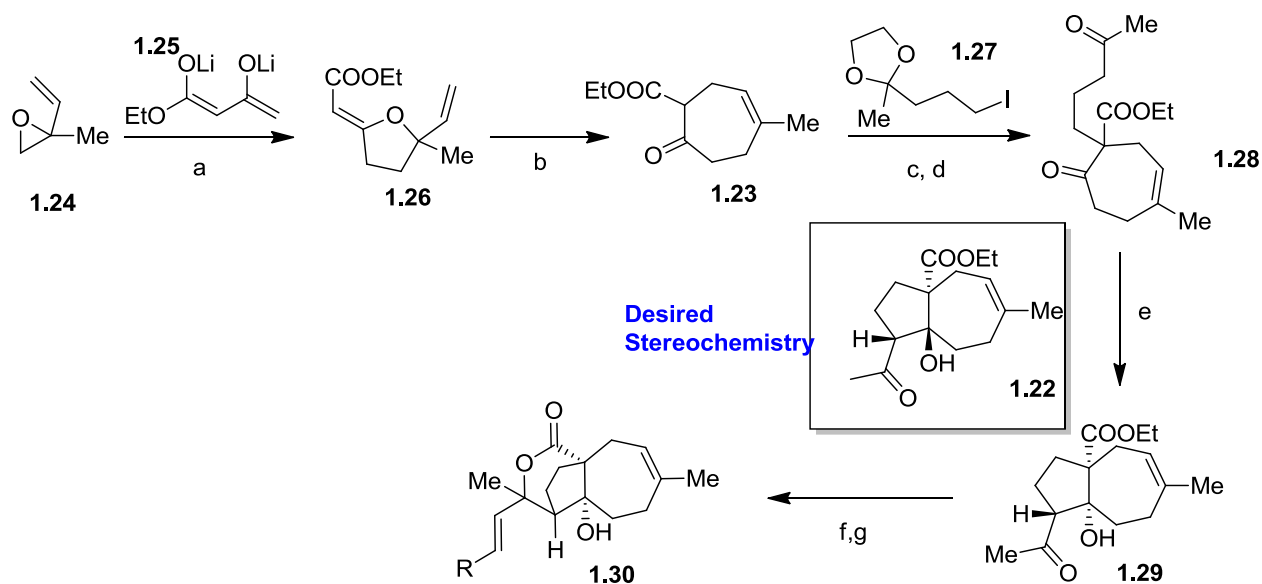
1.8.1 Pan's PLAA synthetic studies ^{6, 42}:

First synthetic study towards pseudolaric acid A was reported by Pan and associates in 1989. In their retrosynthetic analysis given below they envisioned intermediate **1.22** to be crucial for the completion of total synthesis of PLAA. Their approach was to construct all the rings in the tricyclic core sequentially starting from the β -keto ester derivative **1.23**



Scheme 1.1: Pan's retrosynthetic plan

The synthesis of seven membered ring beta ketoester began with nucleophilic ring opening of the vinyl epoxide by the dianion of ethyl acetoacetate to give a hemiketal. The hemiketal was subsequently dehydrated using tosic acid to give tetrahydrofuran derivative **1.26**, which under thermal conditions underwent claisen rearrangement to give **1.23**. β -ketoester **1.23** was alkylated to give compound **1.28**, which was then subjected to base-mediated aldol reaction to give **1.29**. Aldol adduct was treated with organolithium reagent to give diol, which was treated with sodium hydride to give lactone **1.30**. The eventual completion of synthesis of PLAA and determination of relative stereochemistry was reported by this group. Later on, Chiu *et al* proved that the aldol adduct formed was actually **1.29** instead of the **1.22** and had undesired cis-fused ring junction.

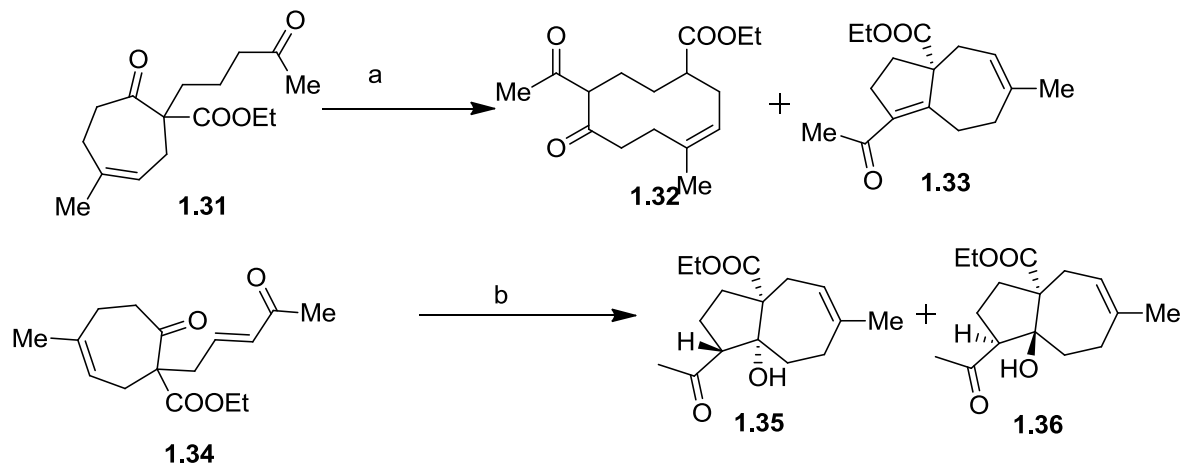


Scheme 1.2: Synthesis of lactone 1.30

Reagents and conditions: (a) Tosic acid (b) heat (c) K_2CO_3 , toluene, 18-crown ether (d) dil. Acetic acid (e) 0.5 equiv. KOtBu, 1 : 1 THF-tBuOH, 70%; (f) **1.27**, nBuLi, THF, $-78^\circ C$, (g) NaH, RT, 1 h, 83%.

1.8.2 Chiu's initial studies⁴³

Chiu and associates decided to revisit the strategy employed by Pan, i.e. sequential construction of the three rings of PLAA. However, Pan's earlier aldol reaction could not be reproduced instead a carbocycle was obtained. Further analysis suggested that aldol adduct formed which degraded under basic condition in a retro aldol fashion.



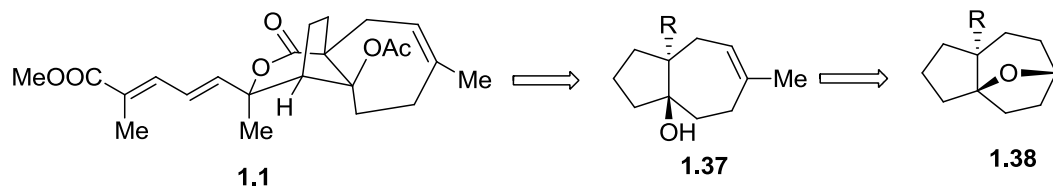
Scheme 1.3: Chiu's synthesis of **1.35** using reductive aldol.

Reagents and condition Reagents and conditions: (a) 0.5 equiv. KOtBu, 1 : 1 THF (b) [Ph₃PCuH]₆, PhMe, -23 °C, 0.5 h, 66% : 16% (**1.34**:**1.35**).

After this failure, Chiu's research group investigated a reductive aldol cyclization of α,β -unsaturated ketone **1.34** catalyzed by copper reagent [Ph₃PCuH]₆ (Scheme 1.3). Primarily two aldol products were formed; **1.35** and **1.36** (66:16 %) in good yields and the relative stereochemistry of both the products were determined by X-ray crystallographic analysis. Unfortunately, none of them had the desired relative stereochemistry required to complete the total synthesis of PLAA

1.8.3 Bai's studies^{44, 45}

Bai was the first one to explore an asymmetric route for the construction of tricyclic core of PLAA using chiral pool synthesis starting with D (-)-mannitol. Their retro synthetic approach is delineated in the scheme given below

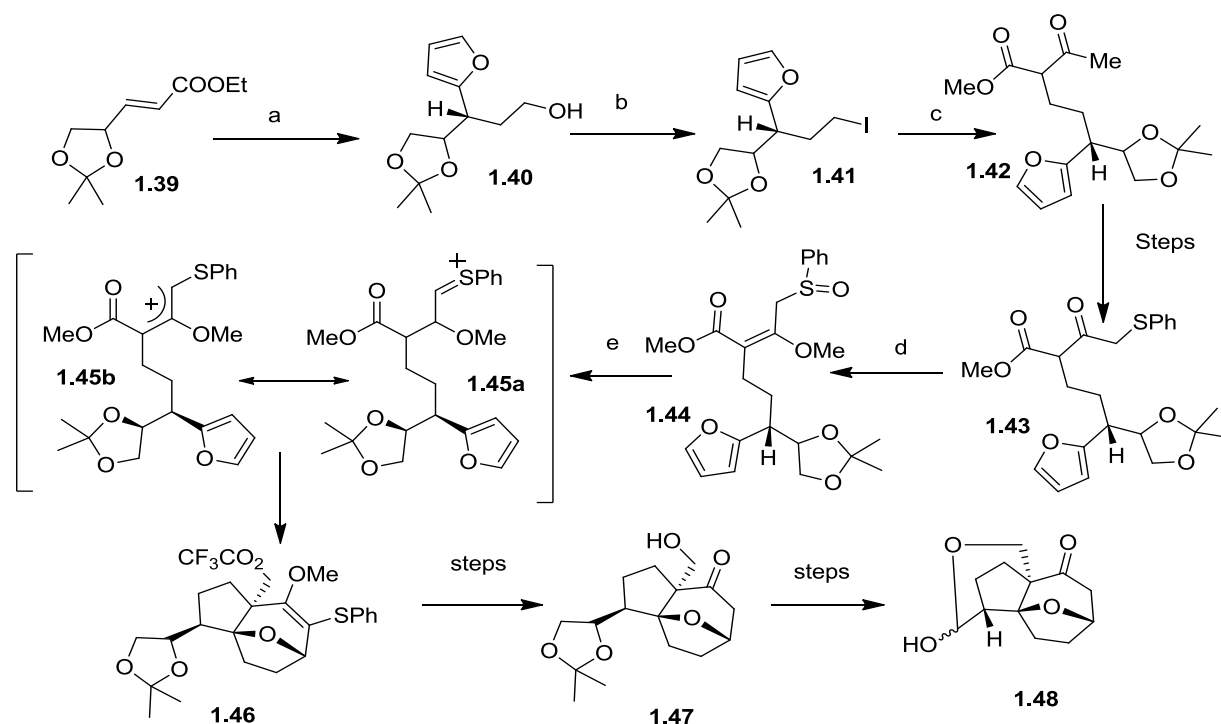


Scheme 1.4: Bai's retrosynthesis of PLAA

The key step employed by Bai was Harmata's generation of allylic cation for tandem Pummerer rearrangement and intramolecular [4+3] cycloaddition to build the 5,7 fused ring system. α,β unsaturated ester **1.39** derived from D-(-)-mannitol was subjected to furyllithium conjugate addition in highly diastereoselective fashion, and the resultant ester was reduced using LAH to give alcohol **1.40** in moderate yields over two steps. The alcohol was converted to iodide **1.41** and was alkylated with methyl acetoacetate furnishing **1.42**. Compound **1.42** was deprotonated and quenched with diphenyl disulfide to give sulfide **1.43**, which was then oxidized and alkylated in situ to give E-enol ether **1.44**. The enol ether was reduced using dibal, and the obtained alcohol was subjected to tandem Pummerer rearrangement and intramolecular [4+3] cycloaddition. The thionium ion formed in situ in the Pummerer rearrangement undergoes intramolecular [4 + 3] cycloaddition with furan moiety of **1.45b** affording a trans fused 5,7 fused ring compound **1.46**. The absolute stereochemistry at C-1 and C-2 was established by NOESY experiments to be *trans*; similar to that of PLAA. However, stereochemistry at center 3 required inversion to advance the synthesis of PLAA and was done in the following manner. Reduction of double bond, desulfurization, hydrolysis of enol ether and detrifluoroacetylation of **1.46** were carried out in one pot using H₂ - Raney Ni affording acetone **1.47** which cleaved in oxidative fashion to furnish aldehyde. Aldehyde (**1.47a**) was epimerized to enol, which underwent intramolecular

hemiacetalization in acidic environment to give hemiacetal **1.48** in very moderate yield.

Completion of the total synthesis is yet to be reported.^{44, 45}



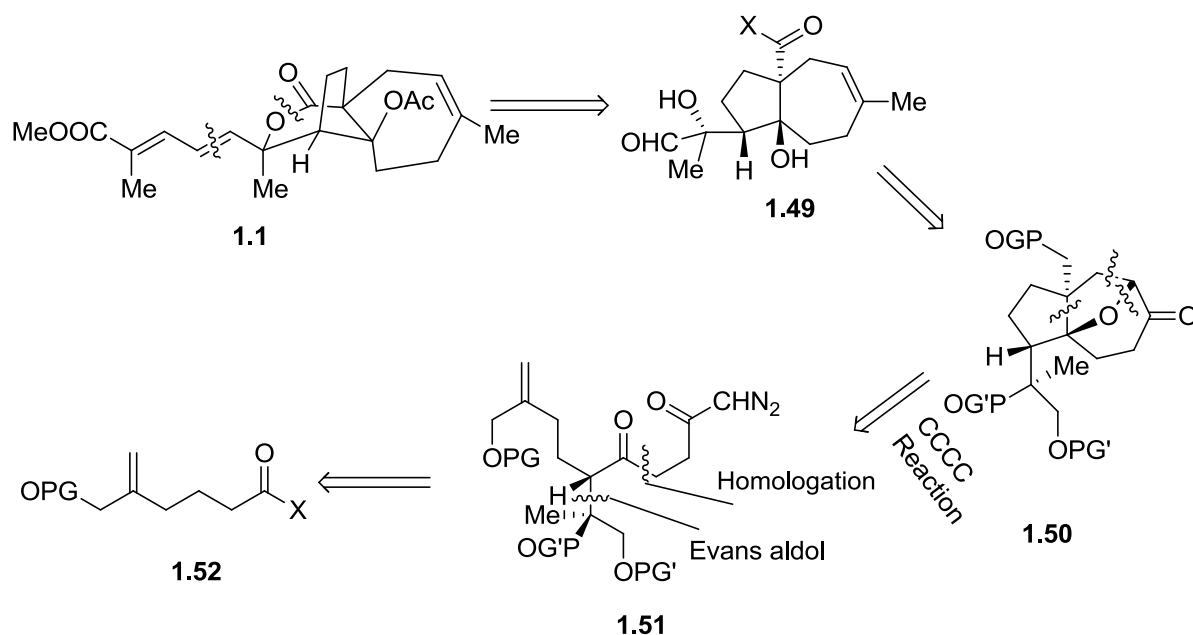
Scheme 1.5: Bai's synthesis of hemiacetal intermediate **1.48** for synthesis of PLAA

Reagents and conditions: (a) i) 2-furyllithium, dr > 20:1; ii) LAH (b) I₂, PPh₃ (c) methyl acetoacetate, NaH; (d) Oxidation (e) (CF₃CO)₂O, 2, 6-lutidine, CH₂Cl₂, RT, overnight, 50% (dr > 95%); (f) CF₃COOH, CHCl₃, reflux, 12 h, 33% (60% of 85 recovered).

1.8.4 Chiu's total synthesis

Chiu's group reported the first total synthesis of PLAA in 2006. Given below is their retrosynthetic scheme 1.6, which relies on cleavage of lactone and HWE disconnection of PLAA to give a crucial aldehyde intermediate **1.49**. They envisioned the aldehyde from a octahydro epoxyazulene intermediate **1.50**, which, in turn, can be visualized from a intramolecular carbene cyclization cycloaddition (CCCC) cascade reaction starting from the diazo ketone **1.51**. They

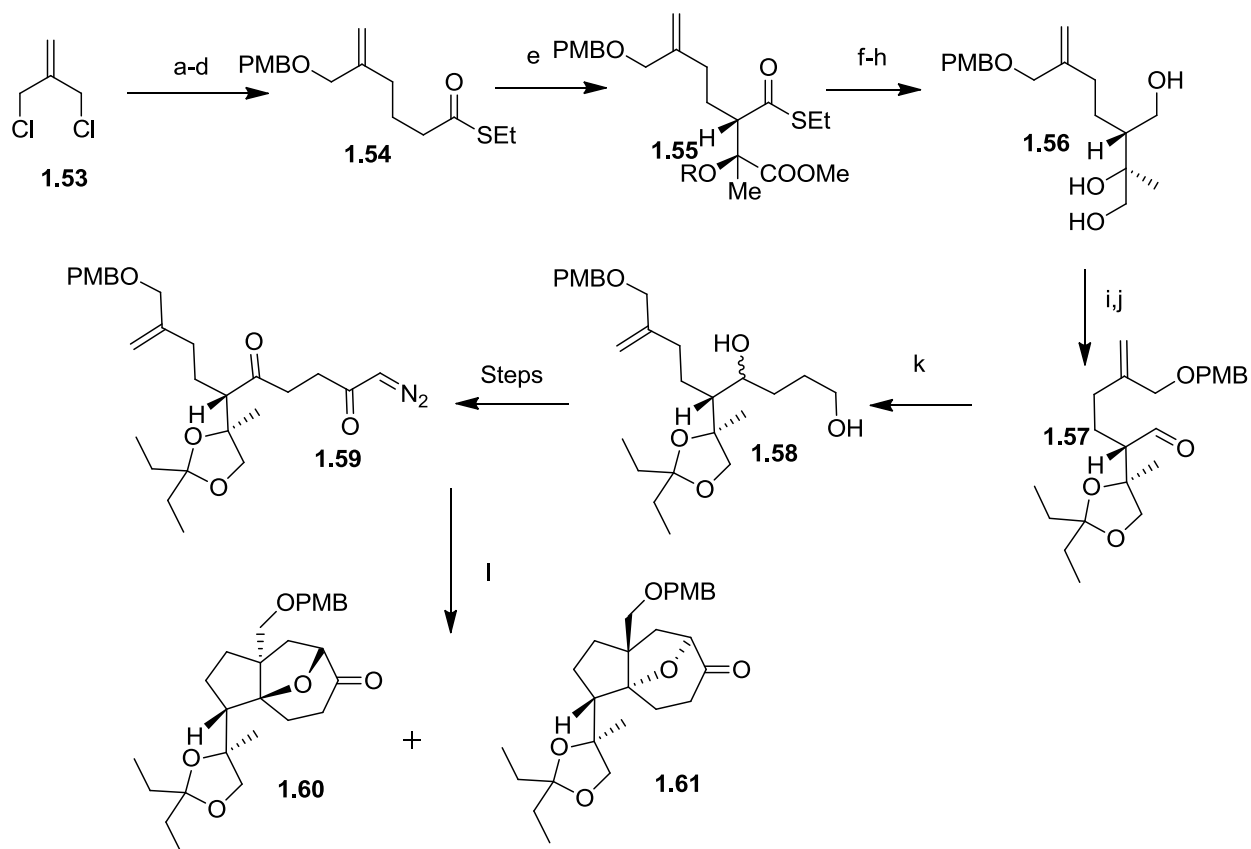
proposed the synthesis of diazo ketone from compound **1.52** via asymmetric Evans aldol reaction and homologation.



Scheme 1.6: Chiu's retrosynthetic analysis for synthesis of PLAA

Retrosynthetic Analysis

Synthesis began by *p*-methoxy benzyloxy monosubstitution of commercially available allyl dichloride to give allyl chloride **1.53**, which was then alkylated with zinc homoenolate of methyl 3-iodopropionate affording ester **1.54**. The ester was converted to thioester and further transformed into silyl enol ether. The enol ether was then subjected to a [Cu][OTf]₂ catalyzed asymmetric aldol reaction with methyl pyruvate giving aldol adduct in 76% yield and more importantly with 88% ee. Tertiary hydroxy group generated having required absolute configuration was protected by TBS and the thioester group is reduced to aldehyde **1.55**. The aldehyde was then submitted to reduction with LAH giving a triol **1.56**. The 1,3 diol of **1.56** was protected as dioxalane and the remaining primary alcohol was oxidized using DMP to give aldehyde **1.57**.



Scheme 1.7: Synthesis of compound **1.59**

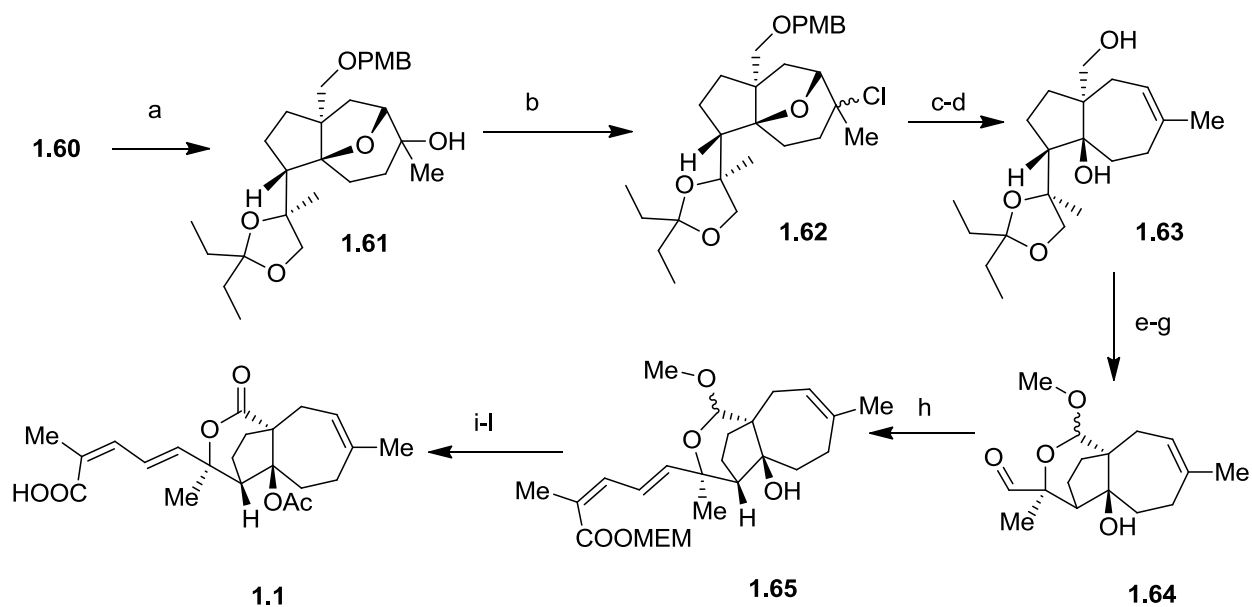
Reagents and conditions: a) NaH, PMBOH, THF, reflux, 61%; b) $\text{ICH}_2\text{CH}_2\text{CO}_2\text{Me}$, Zn(Cu), CuCN, 91%; c) NaOH, MeOH d) EtSH, DCC, DMAP, CH_2Cl_2 e) i) LDA, TESCl, THF, -78°C ; ii). $[\text{Cu}\{(\text{S,S})\text{-tBu-box}\}][\text{OTf}]_2$, methyl pyruvate, 88% ee; f) TBSOTf, 2,6-lutidine, DCM, RT, g) Et_3SiH , Pd/C, CH_2Cl_2 , h) LAH followed by TBAF, THF, i) 3,3-dimethoxypentane, PTSA, ; j) Dess–Martin periodinane, k) $\text{CIMgO}(\text{CH}_2)_3\text{MgCl}$, THF l) 3% $[\text{Rh}_2\{(\text{S})\text{-bptv}\}_4]$, PhCF_3 , 408°C , 82% yield (50% **21a**, 32% **21b**).

PMB = p-methoxybenzyl, DMA = *N,N*-dimethylacetamide, DCC = *N,N*-dicyclohexylcarbodiimide, DMAP = 4-dimethylaminopyridine, LDA = lithium diisopropylamide, TES = triethylsilyl, tBu-box = 2,20-methylenebis(4-tert-butyl-2-oxazoline), Tf = trifluoromethanesulfonyl, TBS = tert-butyldimethylsilyl, TBAF = tetrabutylammonium

fluoride, PTSA = p-toluenesulfonic acid, DMP = Dess–Martin periodinane, bptv = α -(tert-butyl)-1,3-dihydro-1,3-dioxo-2H-benz[f]isoindole-2-acetato, DMPU = 1,3-dimethylhexahydro-2-pyrimidinone, DDQ = 2,3-dichloro-5,6-dicyano-1,4-benzoquinone, CSA = camphorsulfonic acid.

The aldehyde **1.57** was homologated with Grignard reagent CIMgO (CH₂)₃MgCl developed by Normant *et al*; to give a diol, which was subjected to series of steps to give the crucial chiral diazoketone intermediate. The diazoketone **1.58**, was converted into the required cycloadduct **1.59** utilizing Hashimoto's chiral rhodium catalyst; [Rh₂{(S)-bptv}₄] catalyzed CCCC cascade reaction. Mechanistically, an electrophilic carbene generated from diazoketone **1.58** cyclized with the tethered carbonyl group to form a carbonyl ylide, which instantaneously undergoes intramolecular [5 + 2] cycloaddition.

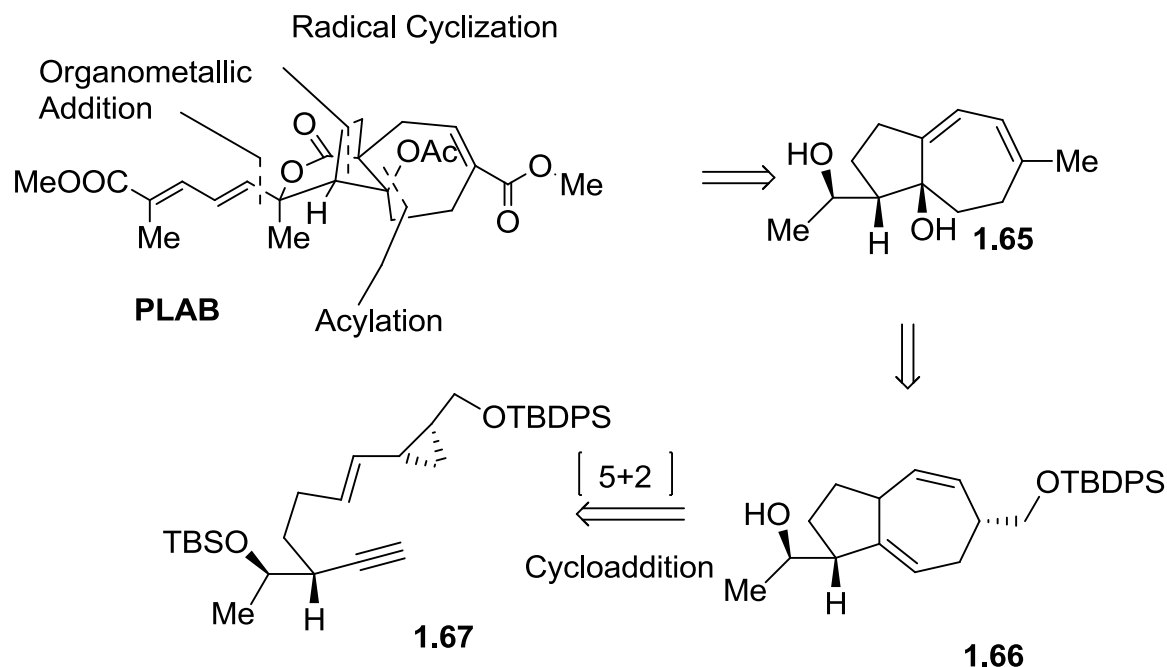
In this key reaction, cycloadduct obtained had all the requisites of stereochemistry; however, this reaction suffered from moderate diastereoselectivity (1.6:1). Ketone in the cycloadduct **1.60** was subjected to nucleophilic methyl magnesium bromide addition giving single diastereomer **1.61**. Tertiary alcohol containing compound **1.61** was treated with thionyl chloride giving mixture of chlorides **1.62**. This mixture was subjected to a reductive protocol that resulted in cleavage of oxygen bridge and installation of the double bond to give compound **1.63** with perhydroazulene core. Simple functional group transformation and deprotection furnished mixed acetal **1.64**. The primary alcohol in **1.64** was oxidized and homologated by a HWE reaction developed by Avery research group. Four routine functional group transformations yielded pseudolaric acid A in 26 linear step in 1.4% overall yield.^{23, 46, 47}



Scheme 1.8: Completion of Total synthesis of PLAA

Reagents and conditions: a) MeMgCl, THF, b) SOCl₂, DMPU, 0°C–RT; c) Na, Et₂O, reflux, 78% d) DDQ e) Dess–Martin periodinane, f) MeOH, CSA, RT, 95%; g) Dess–Martin periodinane; h) (E)-(EtO)₂POCH₂CH=C(CH₃)CO₂MEM, nBuLi, THF, 83%; i) 60% AcOH, j) Dess–Martin periodinane; k) 3N HCl/THF, RT, 66%; l) AcCl, DMAP, 80%. DMPU=1,3-dimethylhexahydro-2-pyrimidinone, DDQ=2,3-dichloro-5,6-dicyano-1,4-benzoquinone, CSA=camphorsulfonic acid, MEM=2-(methoxyethoxy)methyl.

1.8.5 Trost's synthesis of PLAB:

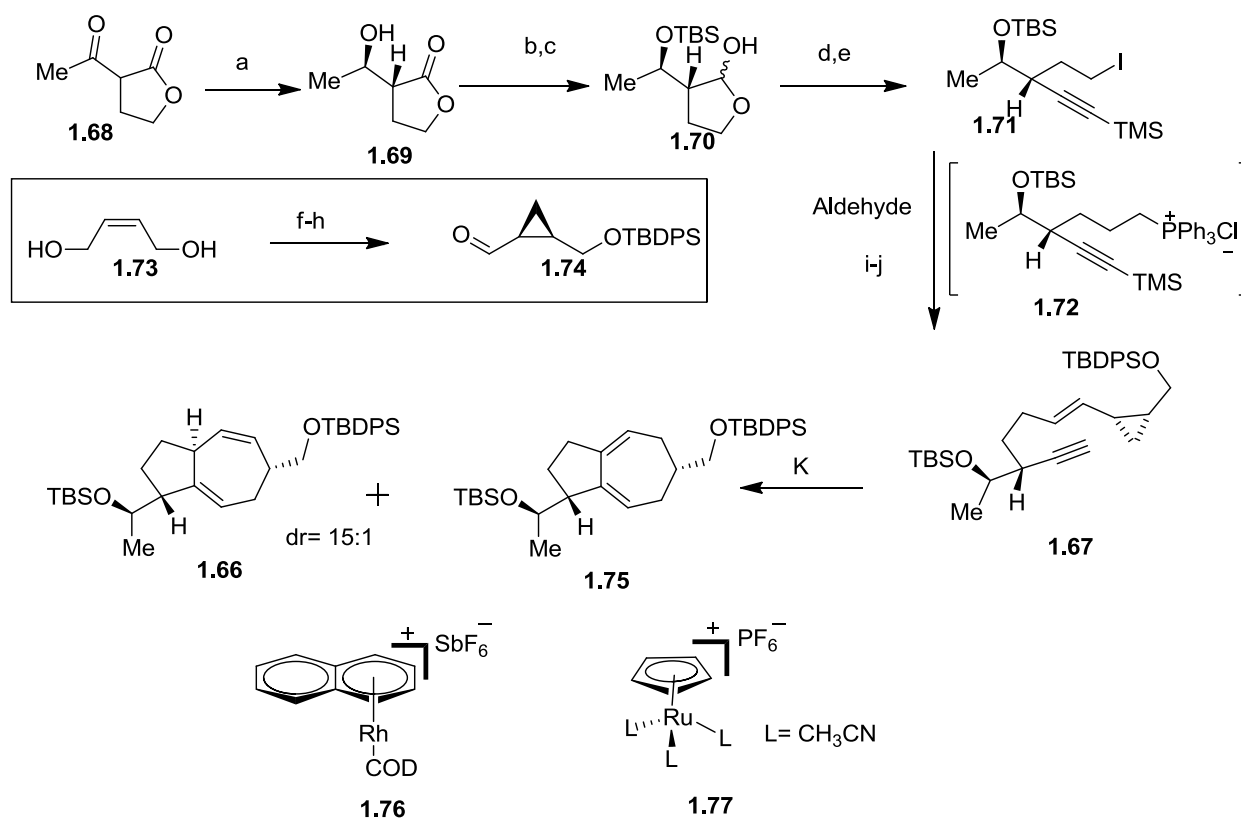


Scheme 1.9 : Trost's retrosynthetic approach

Trost's retrosynthetic approach

Trost's group reported the first asymmetric total synthesis of Pseudolaric acid B. Their synthetic approach (scheme 1.10) relies on building the polyhydroazulene scaffold via the Ru catalyzed intramolecular cycloaddition reaction of an alkyne and a vinylcyclopropane. The scaffold **1.66** can be further transformed into important precursor **1.65**, which, then can be subjected to a free radical mediated cyclization yielding the tricyclic core. The synthesis of vinylcyclopropane **1.67** was carried out in 10 steps in a modular fashion. Optically pure iodide **1.71** was obtained in 5 steps from 2-acetylbutyrolactone wherein the stereogenic center were set by use of Noyori reduction. To this end, the cyclopropyl aldehyde derivative was synthesized in three steps from cis-butenediol using Charette cyclopropanation. The iodide was homologated using triphenylphosphoniummethylide, and the resulting in phosphonium salt (not isolated) was immediately subjected to Schlosser-Wittig olefination with the aldehyde to give TMS protected

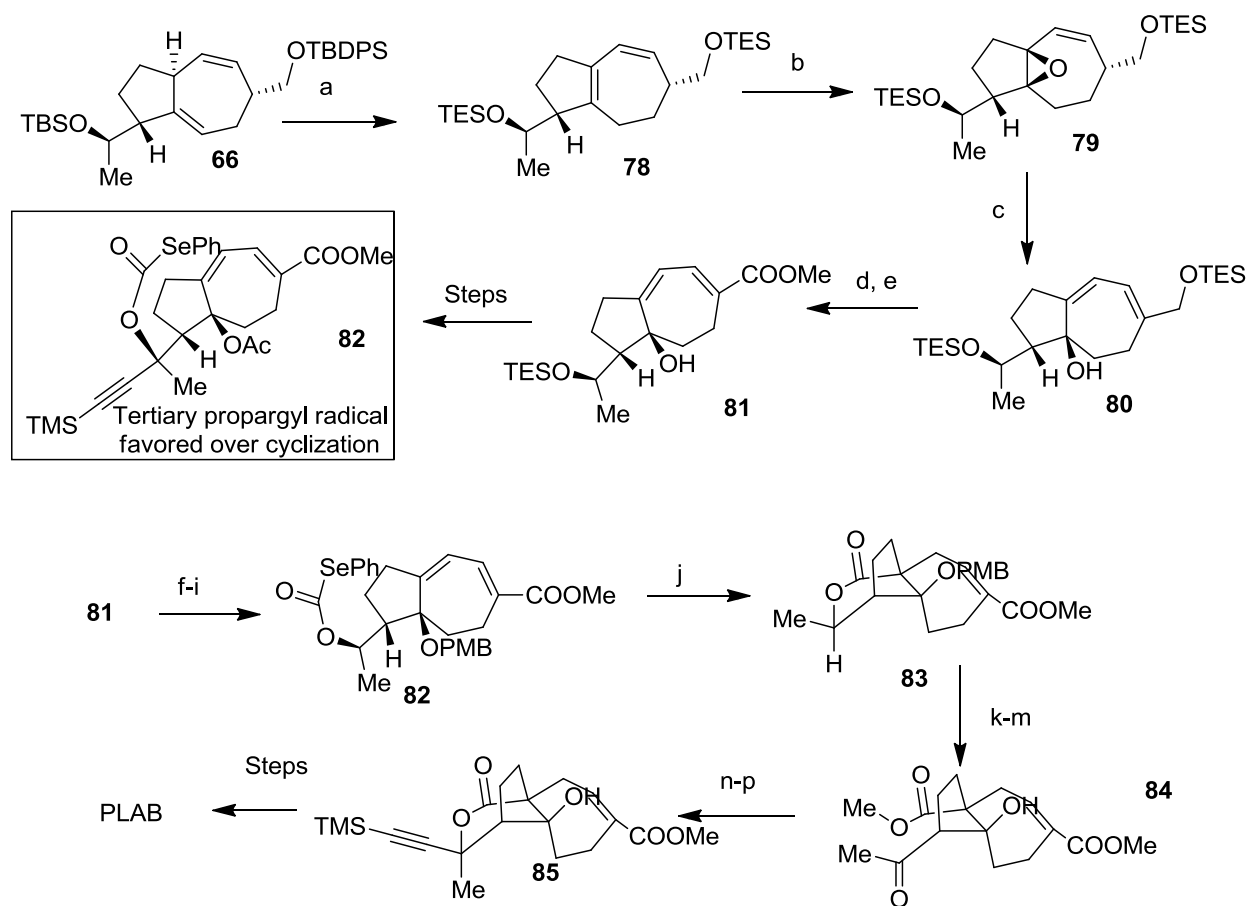
alkyne. Alkyne was subjected to deprotection to give the crucial intermediate required for [5+2] the cycloaddition reaction. The key cycloaddition reaction was carried out successfully using both by ruthenium based catalyst as well as rhodium based catalyst. However, with ruthenium (23 mol%) based catalyst only 48% yield was obtained, while in the case of rhodium catalyst (11 mol%) 88% yield was obtained for the required regioisomer. Lower yields obtained in the case of ruthenium based catalyst may be a result insertion of ruthenium in to labile bisallyl C-H bond leading to formation of Ru-cyclopentadienyl complex, finally, deactivating the catalyst.



Scheme 1.10: Trost's synthesis of crucial intermediate **1.66**

Reagents and Conditions: Conditions: (a) Noyori asymmetric reduction (b) TBSCl, imidazole, DMAP, DMF; (c) DIBAL-H, -78 °C; (d) TMSCHN₂, LDA, THF, -78 °C, then TMSCl, (e) PPh₃, I₂, imidazole, (f) TBDPSCl, imidazole, THF, 92%; (g) S Charette's auxiliary, CH₂Cl₂ (h)

Swern (i) (1) $\text{MePh}_3\text{P}+\text{Br}^-$, PhLi (2) **71**, PhLi/LiBr ; (3) **74**, $-78\text{ }^\circ\text{C}$, then PhLi/LiBr , (4) HCl , $-78\text{ }^\circ\text{C}$, then KO^tBu , $23\text{ }^\circ\text{C}$; (j) K_2CO_3 , MeOH , 58% (k) 11 mol % **1.76**



Scheme 1.11 Trost's completion of total synthesis of PLAB

Reagents and Conditions: (a) i) TBAF, 3 Å MS, ii) TESCl, imidazole, DMAP, DMF, 85%; (b) *m*-CPBA, (c) LDA, THF, (d) DDQ, pH 7 buffer, DCM; (e) MnO_2 , KCN, (f) TBAF (g) CDI, THF, quant; (h) Ph_2Se_2 , NaBH_4 , DMF, 92%; (i) $\text{PMBOC}(\text{NH})\text{CCl}_3$, 2 mol % $\text{Sc}(\text{OTf})_3$, (j) Bu_3SnH , 1,1'-azo(biscyclohexanecarbonitrile), (k) KOTMS, toluene, $120\text{ }^\circ\text{C}$, Me_2SO_4 , (l) Dess-Martin periodinane, NaHCO_3 , (m) DDQ (n) $\text{TMSCl} \cdot \text{CCl}_2 \cdot 2\text{LiCl}$, THF, $-78\text{ }^\circ\text{C}$ (o) Otera's catalyst, 12 toluene, $130\text{ }^\circ\text{C}$, 94%; (p) TBAF,

The diene was isomerized as well as deprotected by molecular sieve activated TBAF, and the diol obtained was protected with TES group. The use of TES protecting group allowed for diastereoselective epoxidation of the tetrasubstituted double bond using mCPBA. The eliminative epoxide opening by LDA afforded the *tert*-alcohol with required stereochemistry at C-4. Series of functional group transformation and deprotection gave the diol **1.81** in good yields. Next, alkoxy carbonyl radical mediated cyclization was used for formation of the lactone ring. Initial attempts of use of intermediate **1.82** with side chain precursor attached to it did not furnish any cyclized product due to predominant tertiary propargyl radical formation. Alternatively, use of the secondary alkoxy carbonyl selenium compound in radical cyclization protocol resulted in mixtures of double-bond isomers, which were treated then with DBU to give only the desired ester.^{24, 48}

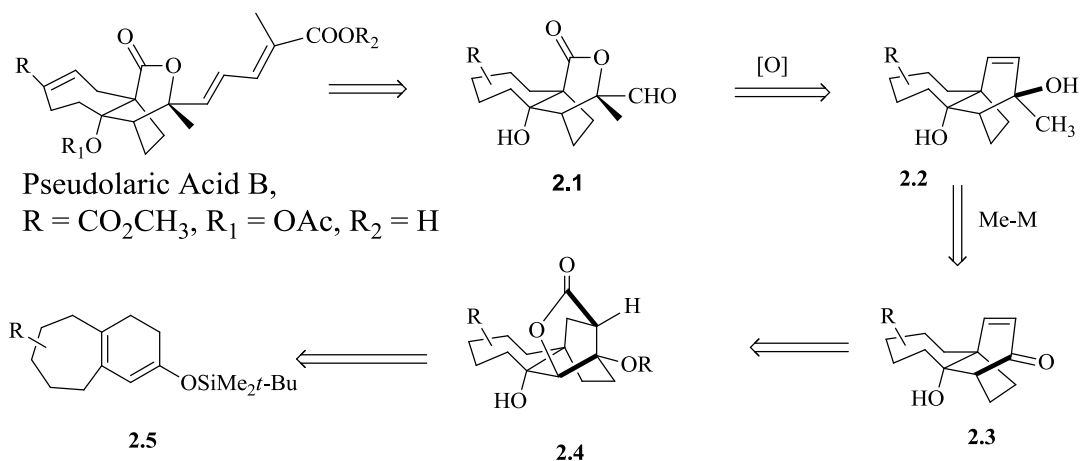
Finally, to install the side chain, it was imperative that the lactone be hydrolyzed and that the total synthesis of the natural product be completed. Lactone was hydrolyzed by using KOTMS, the acid was immediately esterified and the secondary alcohol was oxidized to give compound **1.84**. The PMB group was removed before mounting the side chain to prevent β -elimination. TMS-acetylene was added on to the ketone in the form of $\text{TMS}(\text{C})_2\text{CeCl}_2 \cdot 2\text{LiCl}$ to afford a Felkin-anh model favored alcohol at C-11 with required stereochemistry. The *tert* alcohol was then subjected to lactonization to form tricyclic core using Otera's catalyst. Finally PLAB was assembled by deprotection, scandium triflate catalyzed acetylation, hydrostannylation, and Stille coupling with the iodide.

In summary, Trost's group completed the total synthesis of plab using rhodium catalyzed [5+2] cycloaddition in 28 steps with overall 1.4% yield.

Chiu's and Trost's research group completed the total synthesis of PLAA and PLAB respectively. However, both the routes are very laborious and lengthy. A novel short route for synthesis of pseudolaric acids is warranted in order to carry out detailed structure activity relationship studies. The route should be amenable to scale-up in order to make several analogs of pseudolaric acid B in search of potent anticancer and antifungal agent.

CHAPTER 2
PRIOR WORK IN OUR LAB

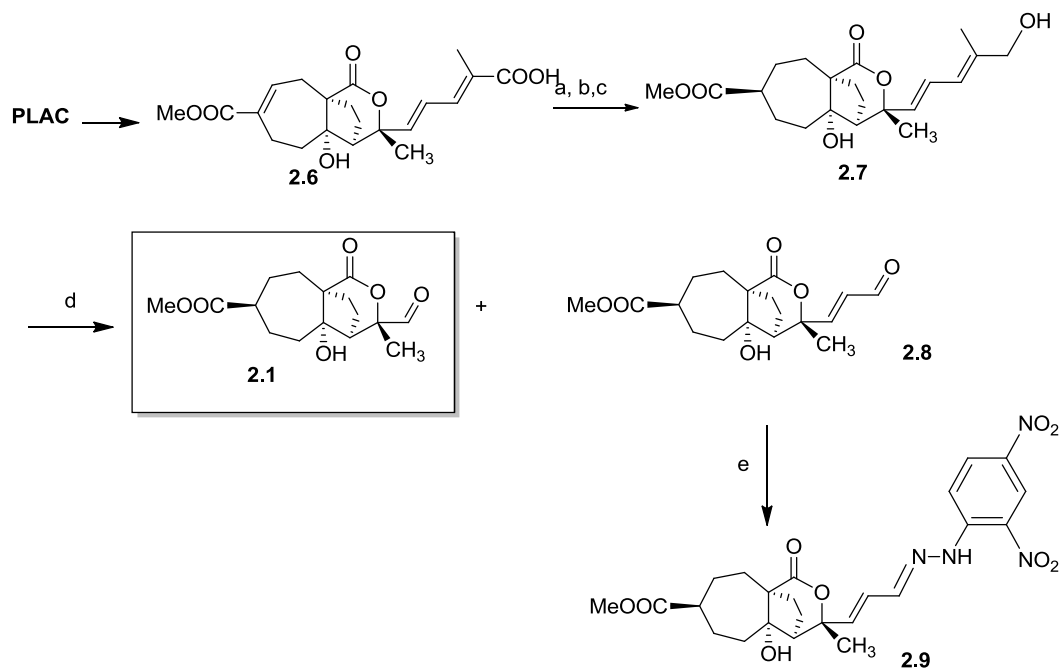
PLAB is one of the exciting natural products with intriguing biological properties and is a challenging synthetic target. We have been engaged in the semi-synthesis and total synthesis of PLAB, with the goal of performing structure-activity relationships in the pursuit of potent antifungal and anticancer agent. Our total synthetic plan was based on the fact that the tricyclic core of PLAB could be accessed through a Wagner-Meerwein-type (WM) rearrangement from intermediate **2.4**, followed by an oxidative ring opening and subsequent rearrangement of **2.2** to give an aldehyde **2.1** (Scheme **2.1**). In order to test the validity of intermediate **2.1** in completion of the total synthesis of PLAB, we decided to carry out degradation analysis of the natural product. In degradation analysis a natural product is broken down in a systematic manner until a crucial intermediate (in this case intermediate **2.1**) is identified and then from the crucial intermediate, the natural product is reconstructed.⁴⁹



Scheme 2.1: Retrosynthetic Scheme for PLAB

Intermediate **2.6** could be obtained by degradation of PLAC as shown in Scheme 2.2. (We chose PLAC for degradation to **2.6** over PLAB because it was found in higher yields during isolation of *Pseudolarix kaempferi* bark). Acid functional group in **2.6** was converted to acid chloride, which was reduced selective to alcohol in the presence of an ester using

LiAlH(OCMe₃)₃ (72%, 2 steps) and the endo double bond was reduced by using magnesium to give intermediate **2.7**.

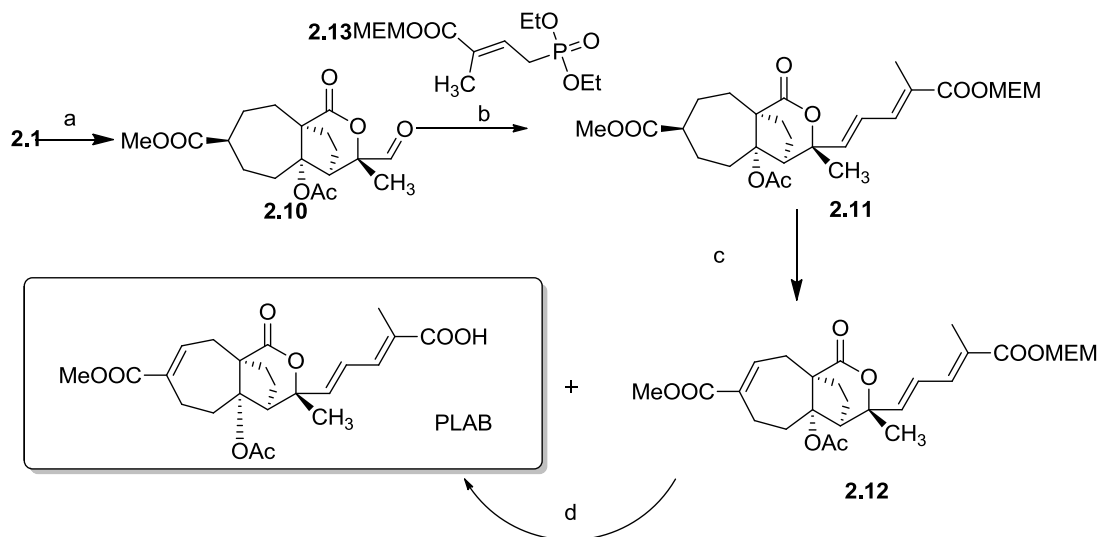


Scheme 2.2 : Degradation of PLAC

Reagents and conditions: (a) (i) SOCl₂, 70°C (ii) THF, -78°C, LiAlH(OCMe₃)₃; (b) Mg, MeOH, rt, (c) Ozonolysis (d) 2,4-(NO₂)₂C₆H₃NHNH₂, cat. HCl; (e) THF, -78°C, 1.1 equiv. LiAlH(OCMe₃)₃.

Ozonolysis, followed by reductive workup of diene **2.7**, provided two aldehydes; aldehyde **2.8** (major) and aldehyde **2.1** (minor). To confirm the absolute stereochemistry of the intermediate **2.8**, the aldehyde intermediate was transformed into a 2,4-dinitrophenyl hydrazone **2.9**. Single crystal obtained was resolved using X-ray crystal analysis. (scheme 2.2). Aldehyde intermediate **2.8** was converted to the required aldehyde **2.1** in two steps; reduction of aldehyde to allylic alcohol and ozonolysis of the allylic alcohol.

With intermediate **2.1** in hand, the next important task was to rebuild PLAB from the crucial intermediate **2.1**. The first step involving acetylation of the sterically hindered tertiary hydroxyl group proved to be difficult as anticipated. After few initial attempts, treatment of **2.1** with scandium triflate and Ac₂O in acetonitrile afforded acetate **2.13**, albeit with poor yield. The Aldehyde was subjected to a Wittig reaction to install the side chain, furnishing diene **2.11**

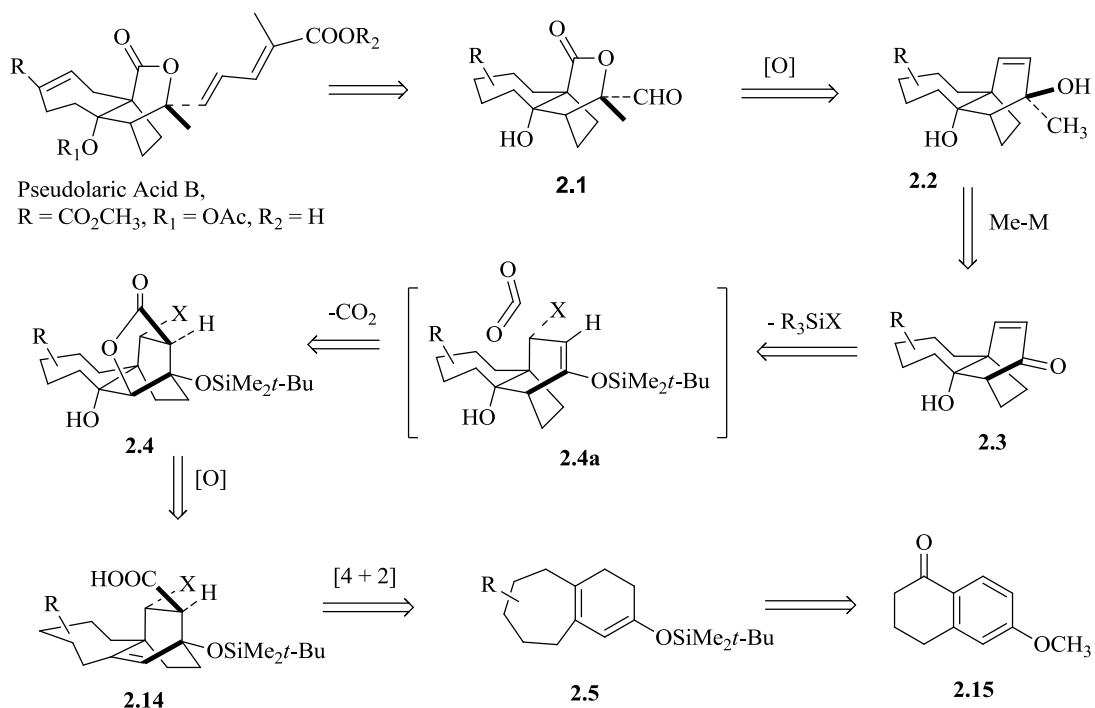


Scheme 2.3: Reconstruction of pseudolaric acid B from crucial intermediate **2.1**.

Reagents and conditions: (a) Ac₂O, MeCN, Sc(OTf)₃, -20 to 0°C; (b) (EtO)₂P(O)CH₂CHC(Me)-COOMEM, *n*-BuLi, THF, -20 to 0°C; (c) KHMDS, THF, -78°C, then PhSeCl, -23°C, then AcOH, H₂O₂; (d) AcOH, THF, H₂O, rt.

Final steps in total synthesis of PLAB were the regeneration of the *endo* double bond and the deprotection of the acid functional group. The *endo* double bond was reinstated by trapping potassium hexamethyldisilazane (KHMDS) mediated anion of ester with PhSeCl and the subsequent oxidative elimination of the selenium compound to give pseudolaric acid B as the major product.⁴⁹(scheme 2.3)

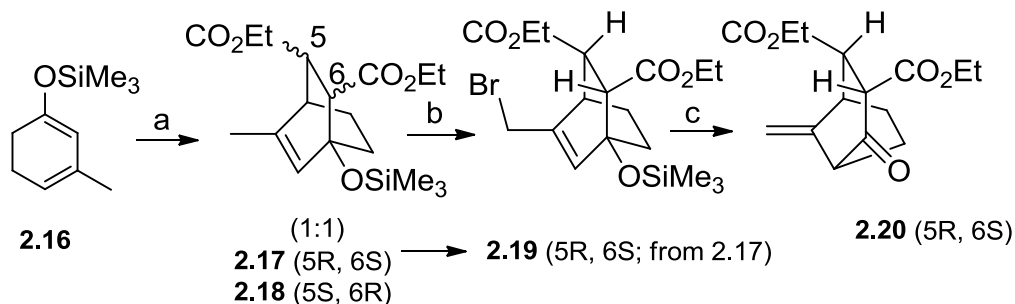
In summary, crucial intermediate **2.1** was identified for the completion total synthesis of PLAB. Furthermore, it was demonstrated that PLAB could be constructed from these intermediate aldehyde **2.1** in four steps. The key steps in the completion of the total synthesis were installation of acetyl group onto the hindered tertiary hydroxyl group, the building of side chain *via* a Horner-Wadsworth-Emmons reaction and reinstatement of the desired *endo* double bond by Selenylation and oxidative elimination sequence. The synthetic approach developed in our group is not only important for completion of total synthesis of PLAB but also for the synthesis of PLAB analogs (generation of diverse libraries). This route can also be used for radiolabeling of PLAB to probe its mechanism of action, especially useful in identifying the tubulin binding site.



Scheme 2.4. More detailed Retrosynthetic Analysis for Pseudolaric Acid B

With encouraging results from degradation analysis, the next task was to devise a strategy for synthesis of the crucial intermediate **2.1**, via Wagner-Meerwein arrangement of highly oxygenated species **2.4** (retrosynthetic 2.4 scheme detailed version).

An unreported aspect of the proposed [2.2.2]→[3.2.1] WM rearrangement, of having the bridgehead sp^3 -C of the bicyclo[2.2.2]octanyl core surrounded by α,β and γ -O atoms, a β -COOR moiety and possibly a fourth electron withdrawing γ -X group, was to be quickly ascertained. While it is accepted that the bridgehead β -O atom in WM rearrangements provides a rate accelerating effect (due to the contribution of lone pair electrons towards stabilization of the WM intermediates), a β -carboxyl group would be less likely to exert π -electron stabilization as this would require the prior enolization of the carboxyl moiety. In the model system chosen, the second γ -carboxyl group would roughly mimic the electron withdrawing capacity of an X group, thus suggesting that **2.14** should provide useful information regarding the likelihood of a successful rearrangement for **2.4** (or congener). In order to test these hypotheses, synthesis of **2.14** was smoothly accomplished as follows in Scheme 2.5. Diels Alder (DA) addition of diethylfumarate to 1-trimethylsilyoxy-3-methylcyclohexadiene **2.16** afforded a 1:1 mixture of [4+2] cycloadducts **2.17** and **2.18**. After chromatographic separation, **2.17** was arbitrarily chosen for allylic bromination to provide the allylic bromide **2.19** in 90% yield. Treatment of **2.19** with $AgClO_4$ in benzene resulted in the immediate precipitation of $AgBr$ and concomitant formation of the desired exocyclic product **2.20**, thus confirming our presumption that the bicyclic diester would undergo a Wagner-Meerwein shift.⁵⁰

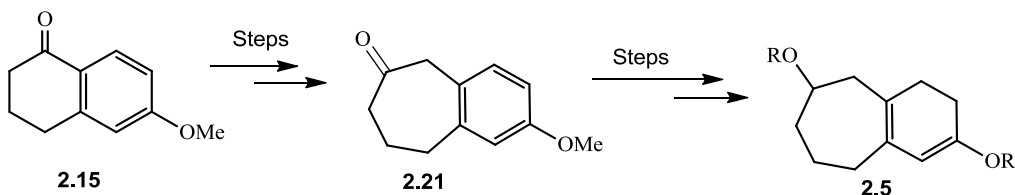


Scheme 2.5: Synthesis of the model system

Reactions and conditions: a) diethyl fumarate, heat; b) NBS, hv, and c) AgClO₄·H₂O, benzene.

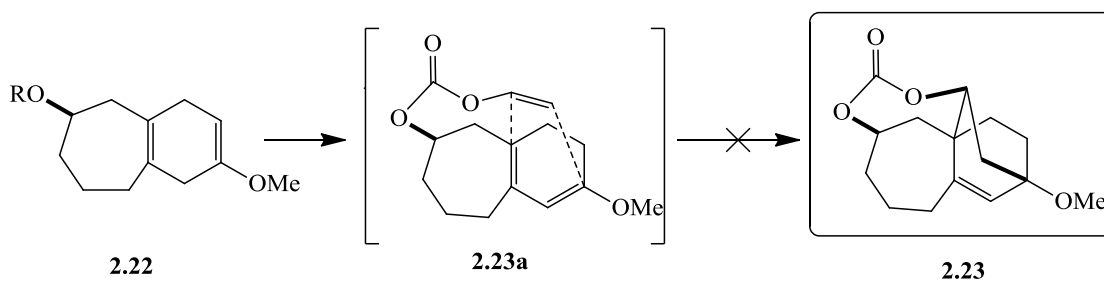
These results were suggestive that the key rearrangement step in the retrosynthetic analysis (Scheme 2.4) would be successful despite the electron withdrawing ester group(s). With this important finding in hand, we embarked upon the more complex ring-fused system intended to lead us to the natural product PLAB.

With success of Wagner-Meerwien rearrangement in the model system, next step was to test our hypotheses in actual substrate. After few initial attempts, the synthesis of diene **2.5** was successfully carried out with good yields starting from naphthalone derivative **2.15**. Key steps in this conversion were; dimethyl anion mediated one carbon Wittig reaction, Thallic (III) nitrate mediated oxidative ring expansion and birch reduction.



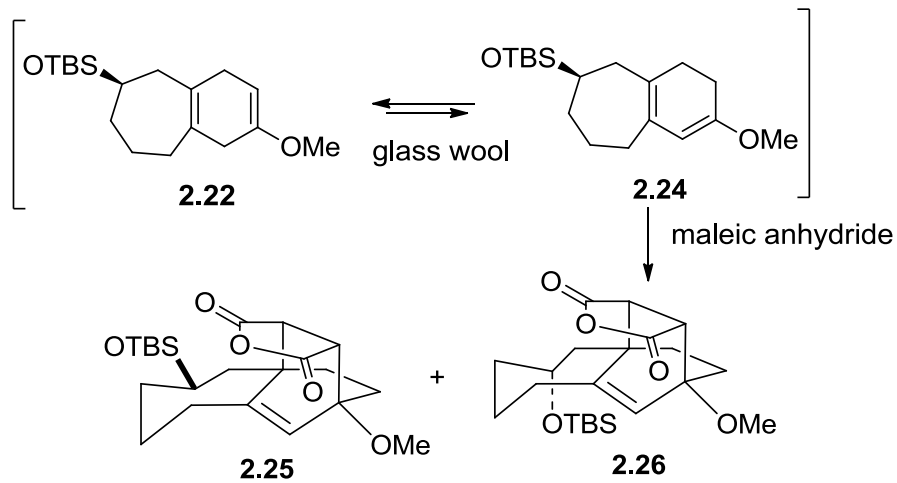
Scheme 2.6: Synthesis of diene derivative 2.5.

A more appealing approach to the DA adduct **2.14** involved the possibility of achieving an intramolecular Diels-Alder (IMDA) via the 7-membered ring R group tethered to the X position. To accomplish this 1,3 diene was acylated with appropriate acid chloride or silyl chloride (e.g. when R = $-\text{SiMe}_2\text{CH}=\text{CH}_2$; $-\text{SiMe}_2\text{CH}_2\text{CH}=\text{CH}_2$; $E\text{-COCH}=\text{CHCOOEt}$; $E\text{-COCH}=\text{CHCl}$). Unfortunately, of the several precursors synthesized and different reaction conditions attempted, all failed to successfully undergo IMDA reaction under a variety of cycloaddition conditions. It was felt that the IMDA precursors were not stable due to impurities catalyzing rapid thermal decomposition.

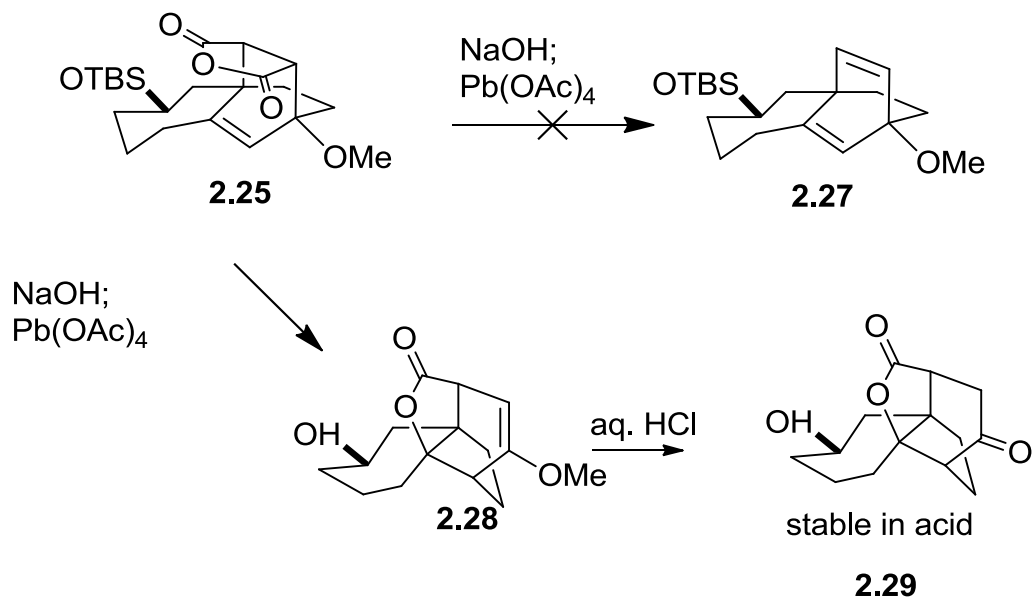


Scheme 2.7 Intramolecular Diels-Alder approach

After the difficulties encountered in the intramolecular approach, it was assumed that intermolecular reaction with maleic anhydride, a highly reactive dienophile, could at least serve to provide access to the ring system. Gratifyingly, the silyl-protected 1,4-diene **2.22** underwent cycloaddition with maleic anhydride in presence of glass wool to give the diastereomers **2.25** and **2.26**, in a ratio of 4:1, respectively. It was postulated that the dicarboxylic acids from hydrolysis of anhydride diastereomers **2.25** or **2.26** would undergo literature preceded decarboxylative olefin formation upon treatment with $\text{Pb}(\text{OAc})_4$, leading to a bicyclo[2.2.2]octadienyl functional arrangement as in **2.27**, Scheme 2.9.



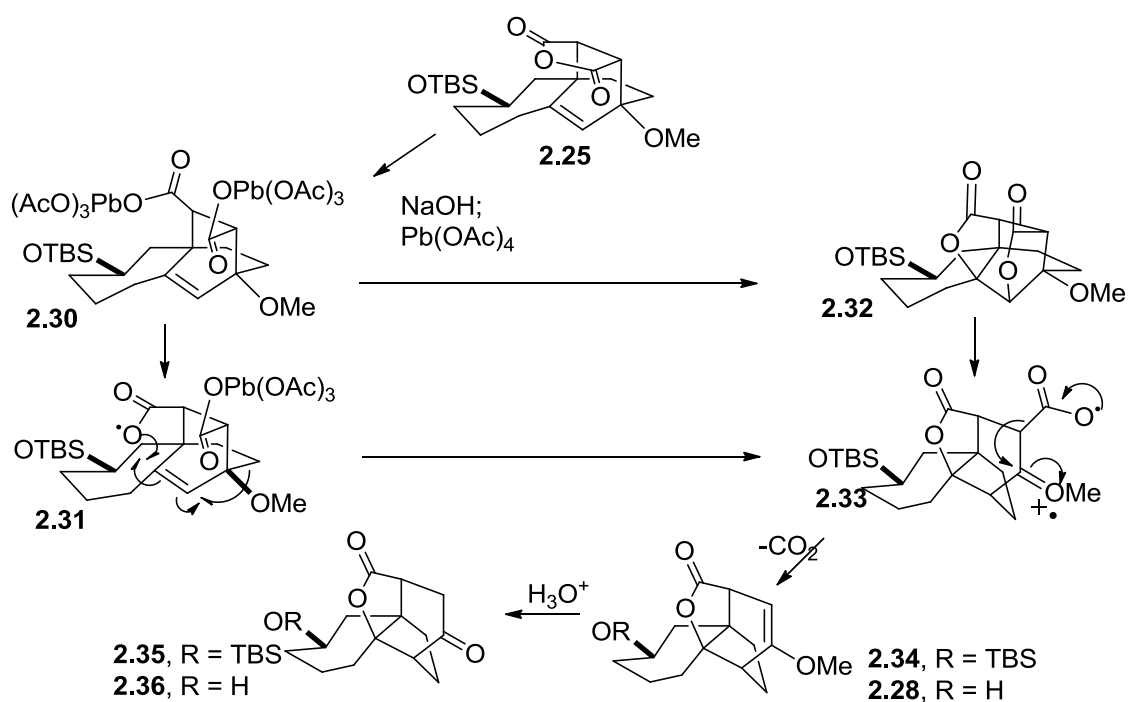
Scheme 2.8: DA using maleic anhydride



Scheme 2.9: Decarboxylation and lactonization using NaOH and Pb(OAc)₄

However, surprisingly, a single decarboxylation and lactone ring formation occurred in a good yield to provide the highly stable tetracyclic lactone **2.28**. In review of the mechanism of the

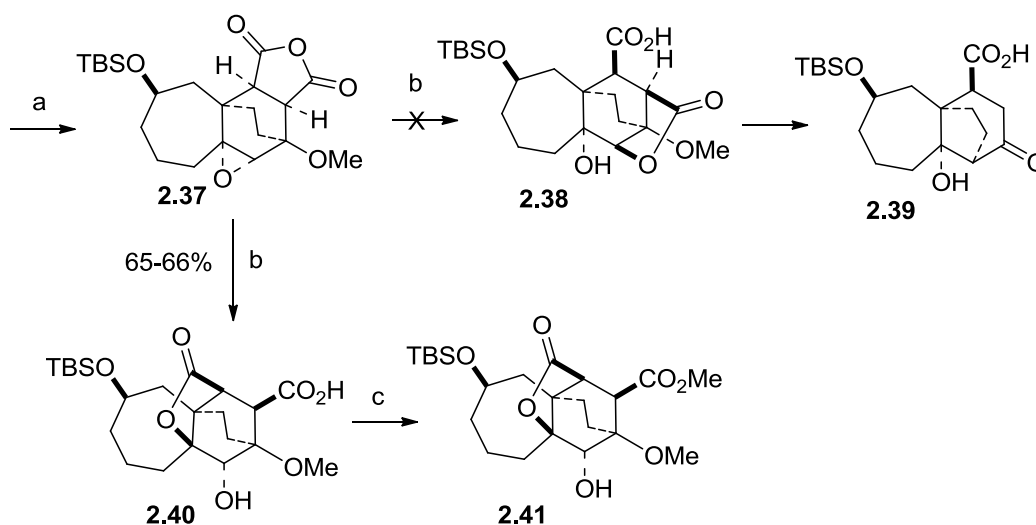
reaction, it was noted that the anhydride was hydrolyzed first with hydroxide ion to a dicarboxylate salt, which was treated directly *in vitro* with lead tetraacetate. The reaction was rapid and clean, and when stopped early, did not demonstrate the presence of mechanistically suggestive intermediates like the dilactone **2.32**. Instead, the product structure implies a mechanism, possibly radical, in which the bridging carboxyl radical **2.31** can undergo cyclization by a 5-*endo-tet* closure, with either simultaneous or stepwise bridge migration (WMR) leading to the enol ether intermediate **2.33**. Ensuing decarboxylation of **2.33** then finally gives the product di-ether **2.34**, or after *in situ* desilylation, the enol-ether alcohol **2.28**.



Scheme 2.10 lead tetraacetate decarboxylation, mechanistic insights

In an effort to make use of this remarkable reaction, elimination of water from **2.28** (acid treatment) was attempted but was not successful, the sole product being the stable keto-lactone

2.36, formed again in high yield. Attempts to reduce the lactone of **2.34** or **2.35** were also unsuccessful. The reticent behavior of the lactones **2.28** and **2.34-2.36** led to their eventual abandonment in order to explore similar Pb(IV) chemistry on the corresponding epoxide, which had the virtue of not having an available double bond to undergo lactone formation. Thus, epoxidation of the anhydride **2.25** gave the expected epoxide **2.37**. Upon exposure to NaOH, it was hoped that the other lactone would form by S_N2 ring opening from the less hindered secondary epoxide carbon to give lactone **2.38**.



Scheme 2.11 Synthesis of lactone **2.41**

Reactions and conditions a) *m*-CPBA, CH₂Cl₂; b) NaOH; H⁺; c) Me₂SO₄, Na₂CO₃, acetone.

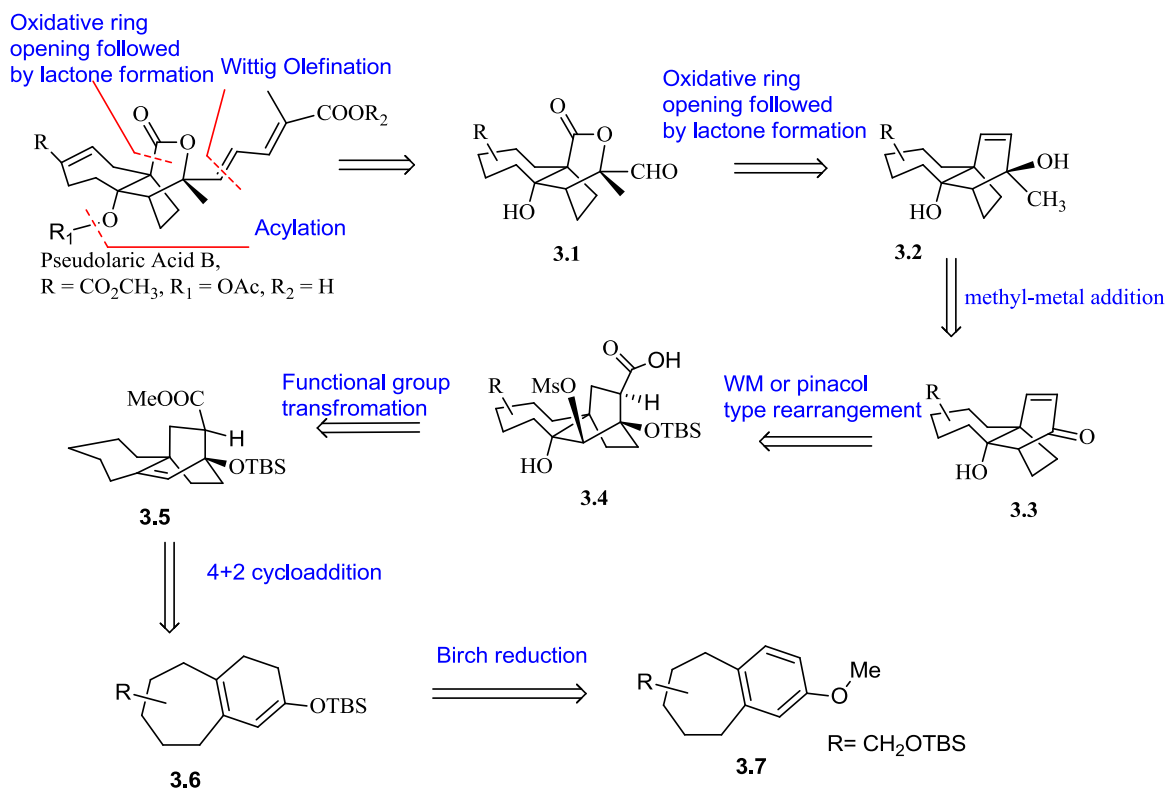
While **2.37** did lead to a 5-membered ring lactone-acid as hoped, once again bridgehead lactonization was the sole ring-opening product, lactone **2.40**. Unfortunately, all the approaches to make use of the remarkable lead tetracetate catalyzed reaction were futile.⁵⁰

Finally, we decided to examine was the use of an intermolecular DA reaction with methyl acrylate. This route would remove the second carboxyl moiety at the outset, thus eliminating the need for complicated interconversions. As before, the 1,4-diene was elected as a starting material using glass wool to effect *in situ* Lewis-Acid catalyzed isomerization of the 1,4-diene to the 1,3-diene. While this approach had been successfully employed with maleic anhydride, acrylates were polymerized before DA reaction could occur. While the possibility existed of returning to the earlier protocol of hydrolysis of the 1,4-dieneol ether to a β,γ -unsaturated enone which could then be enolized and trapped as the silyl 1,3-dieneol ether, we decided to set this system aside for the time being and work with a slightly simpler decalin system. Once details of the rearrangement could be solved, we felt we could more confidently return to the suberone like scaffold.

CHAPTER 3
STUDIES TOWARDS TOTAL SYNTHESIS OF
PSEUDOLARIC ACID B

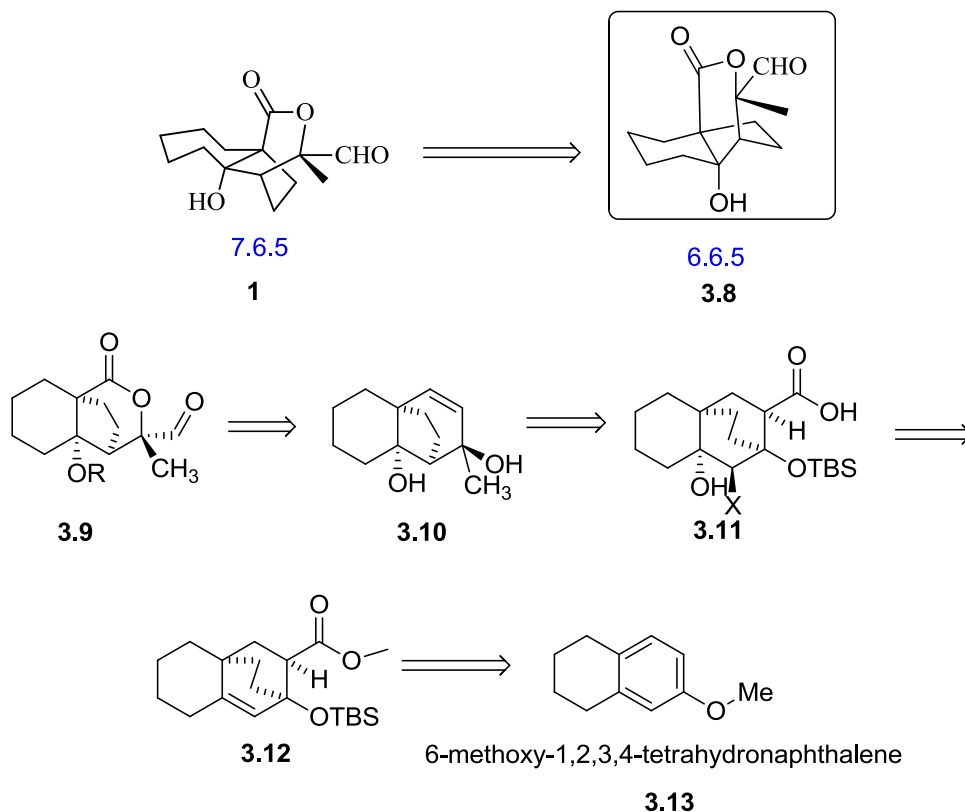
3.1 Synthetic Approach 1:

With the failure of IMDA and succinic anhydride intermolecular DA, we focused our attention on the methyl acrylate DA reaction. Given below is our revised retrosynthetic, scheme 3.1. Our synthetic plan is based on the fact that the tricyclic core of PLAB could be accessed through an oxidative ring opening and ensuing rearrangement of **3.2**. Intermediate **3.2** can be visualized via Wagner-Meerwein (WM) or a pinacol type rearrangement of highly oxygenated species⁵¹ **3.4**., which in turn can be envisioned as a Diels-Alder adduct **3.5**. The adduct **3.5** can be obtained via a Diels-Alder reaction between the electron rich diene **3.6** and appropriate dienophile.



Scheme 3.1: Retrosynthetic Analysis for Pseudolaric Acid B

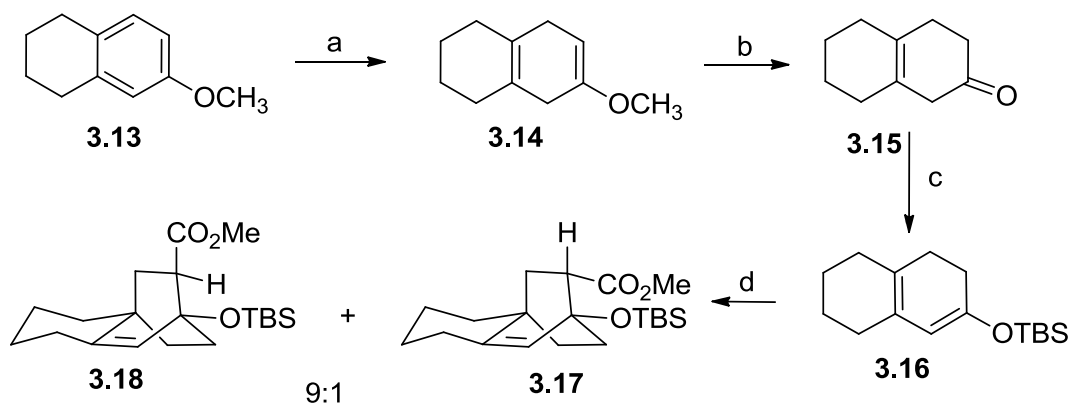
Diene **3.6** can be prepared from 2-methoxy-6,7,8,9-tetrahydro-5H-benzo[7]annulene. With our relay system established and crucial intermediates indentified, we wanted to quickly test our hypothesis. To facilitate this study, we chose to begin with a model system (Scheme 3.2), which can be accessed via readily available and inexpensive starting materials and which would provide quick access to the necessary Wagner-Meerwein precursor. With this precursor in hand, we could then determine the necessary conditions to bring about the molecular rearrangement.



Scheme 3.2 : Retrosynthetic scheme for model system

3.2 Synthesis of Model system:

Synthesis of the model system commenced with Birch reduction of commercially available 6-methoxy-1,2,3,4-tetrahydronaphthalene **3.13** to give the cross-conjugated diene **3.14** in 91% yield. Compound **3.14** readily underwent hydrolysis in the presence of catalytic amounts of oxalic acid in methanol/water mixture furnishing the unconjugated enone **3.15** in 78% yield (Scheme 6). The kinetically formed lithium enolate of **3.15** mediated by lithium diisopropyl amide, was trapped with *tert*-butyldimethylsilyl chloride in THF affording the TBS-protected, conjugated dienol ether **3.16**, in 82% yield. After screening through several protocols, Diels-Alder cycloaddition of methyl acrylate with **3.16** in the presence of trimethyl aluminum and diethyl aluminum chloride⁵² in THF at -20°C proceeded smoothly. It resulted in an 81% yield of a 9:1 mixture of *endo:exo* regioisomers **3.18** and **3.19**, respectively, which were readily separated by silica gel flash column chromatography.⁵³

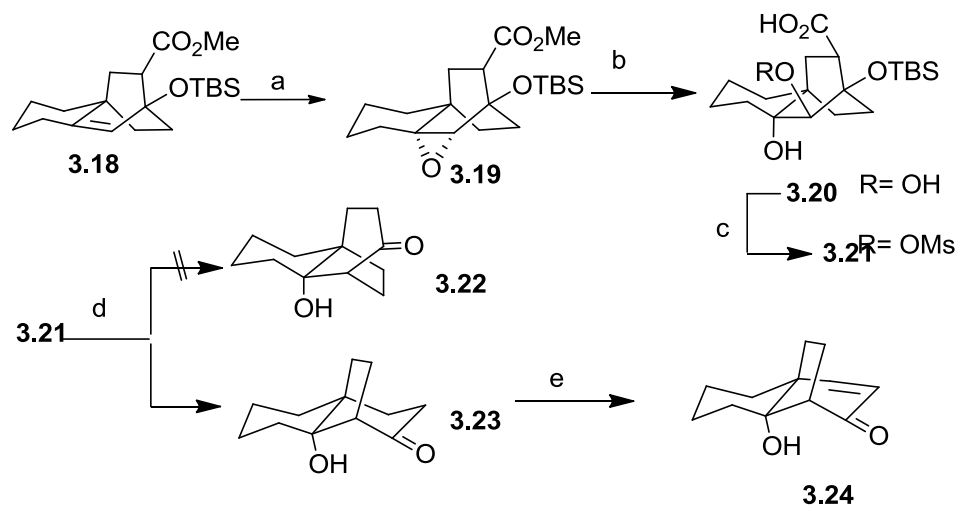


Scheme 3.3 : Synthesis of diene **20**

Reagents and conditions a) Li/NH₃, EtOH, Et₂O, -78°C, 91%; b) oxalic acid (cat.), MeOH/H₂O, RT, 78%; c) LDA, TBSCl, THF, -78°C-RT, 82%; d) methyl acrylate, Me₃Al, Et₂AlCl, THF, -20°C, 81%, 9:1.

Once the tricyclic architecture had been established, the next mission was to carry out the molecular rearrangement to obtain the crucial enone, which can then be oxidatively opened and rearranged to obtain the crucial aldehyde intermediate **3.9**. The classic Wagner-Meerwein rearrangement involves the use of free hydroxyls under acidic conditions. We subjected the tricyclic alkene **3.18** to mCPBA epoxidation (obtained exclusively only one isomer) followed by treatment with aqueous sodium hydroxide resulting in the opening of the epoxide and hydrolysis of the ester to give dihydroxy acid **3.20**. We believed that compound **3.20** had the right architecture required for Wagner-Meerwein type or a pinacol type rearrangement. Our initial attempts to rearrange **3.20** under Lewis acid or protic acid conditions proved to be unsuccessful. The dihydroxy acid was relatively unstable and instantaneously cyclized to the lactone under acidic conditions. To block this pathway and to accelerate or initiate the rearrangement, we decided to activate the hydroxyl group using a methane sulfonyl group. Treatment of the carboxylic acid **3.20** with methane sulfonyl chloride and triethylamine in dichloromethane at 0°C yielded compound **3.21**. After a quick filtration column, mesylate was dissolved in toluene and heated to 180°C for 4 hours in a sealed tube providing the rearranged tricyclic β -hydroxy ketone (either **3.22** or **3.23**), while yielding only a small amount of the lactone. The structure of the ketone was confirmed by NMR (1D and 2D) and spectroscopic techniques. There was a possibility of two isomers from this rearrangement; either it can be desired ketone **3.22** or undesired ketone **3.23**. At this time, it was crucial to investigate the relative stereochemistry of the product of rearrangement. Extensive 2D NMR studies conducted were inconclusive and could ascertain the relative stereochemistry of the product. Fortunately, we were able to crystallize the ketone from ethyl acetate and the single crystal obtained was submitted for X-ray

analysis. X-ray of ketone revealed that the tricyclic β -hydroxy ketone had undesired relative stereochemistry and indeed we had obtained ketone **3.24** instead of **3.23** (figure 3.1).



Scheme 3.4: Synthesis of rearranged ketone **3.23**

Reagents and conditions a) *m*-CPBA, NaHCO_3 , CH_2Cl_2 , 99%; b) NaOH (aq), 5:1 MeOH/ H_2O , RT, 70% c) MsCl, Et_3N , CH_2Cl_2 , 0 °C; d) toluene, 180 °C, 56% (2 steps) e) IBX, DMSO/Toluene, 75°C, 59%

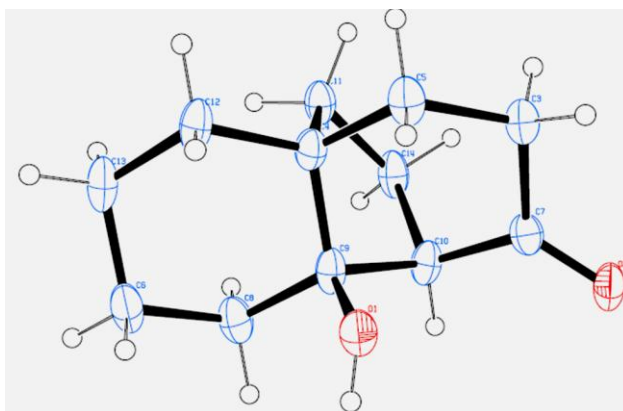
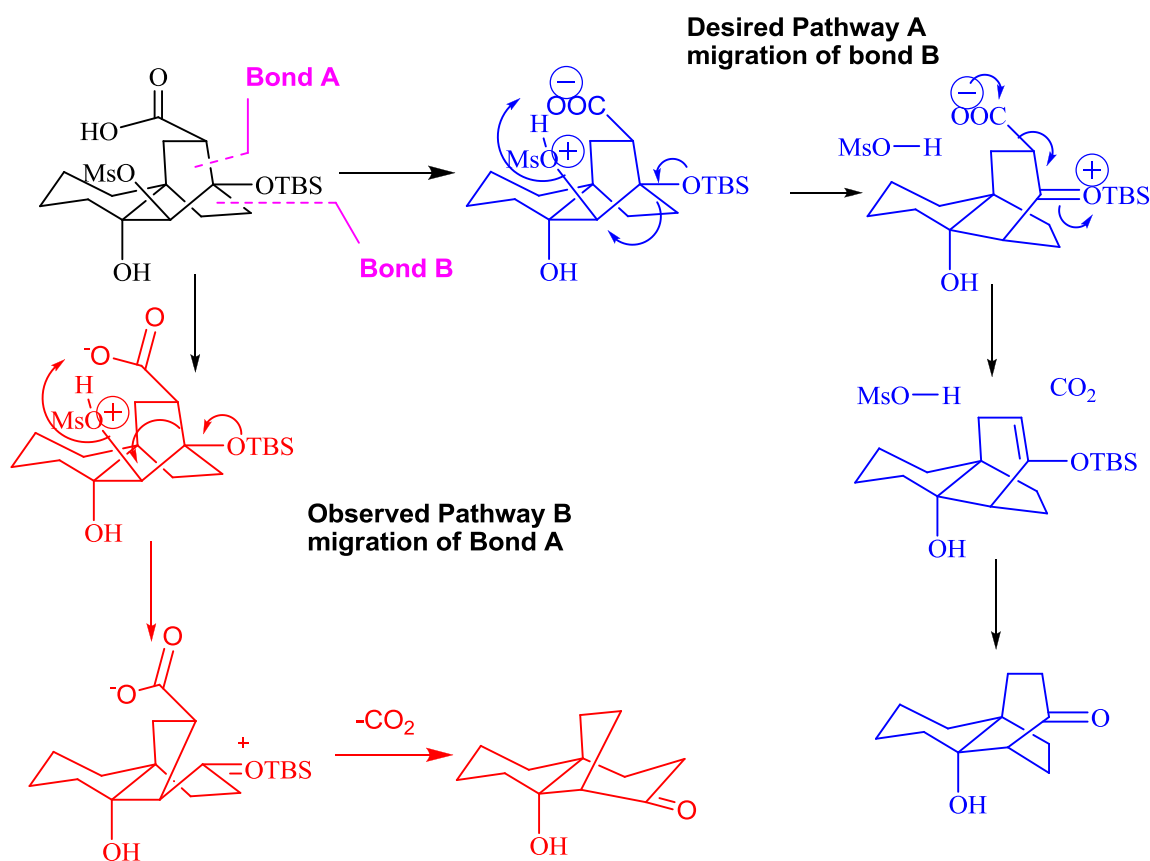


Figure 3.1: ORTEP plot of the X-ray crystal structure of the ketone **3.23** depicting the relative stereochemistry

To explain this unanticipated result, we postulated a step-wise mechanism pathway, as demonstrated in scheme 6. The reaction can proceed via two distinct pathways: Pathway A, where migration of bond B is favored or pathway B, where migration of bond A is preferred. In order to obtain our desired compound the course of the reaction should have been pathway A. In pathway A, migrating bond B is antiperiplanar to the leaving group suggesting a S_N2 type one step mechanism. Unfortunately, it seems that the rearrangement of the trihydroxy acid occurred via pathway B. In Pathway B, the leaving group is in the same plane as the migrating group, suggesting two step S_N1 type mechanism (formation of carbocation followed by migration of bond A, with sp^3 hybridized carbon almost getting sp^2 character). In our case, pathway B was favored, either due to a predominant S_N1 type mechanism, or due to higher migratory aptitude of carboxy substituted bond. Later we also calculated the total energies of both the ketones. The molecules were sketched using Maestro graphical user interface from Schrodinger. The two molecules were then subjected to energy minimization using OPLS2005 force-field. The minimized conformation were then used as a starting conformation for the geometry optimization using Jaguar module available in Schrodinger Suite. Jaguar is well-known and well-

established module for quantum chemical calculations. We used Hybrid Density Functional Theory (B3LYP) method with split basis set function (6-31G**) for geometry optimization. The energies of the two molecules were calculated and the energy difference is reported. These calculations also (slightly) supported the formation of more stable ketone **3.23**. The relative energy of isomer **3.22** was higher by ($\Delta E = E[3.23] - E[3.22] = -3.0 \text{ kcal/mol}$) 3.0 kcal/mol (figure 3.2 and 3.3)



Scheme 3.5: Mechanistic insights into Wagner-Meerwein type rearrangement

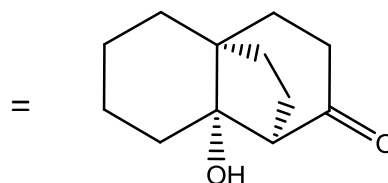
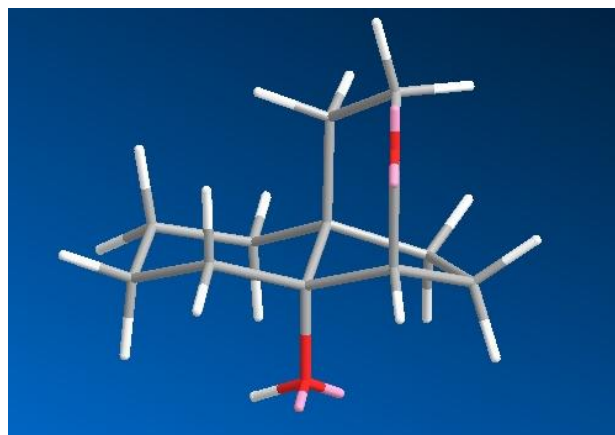


Figure 3.2: Molecular energy calculation for the ketone **3.22** T.E = 33.5599 kcal/mol (Chem3D)

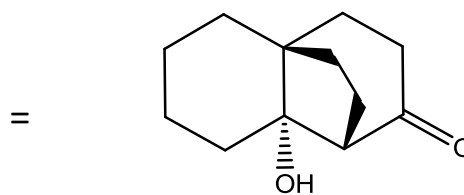
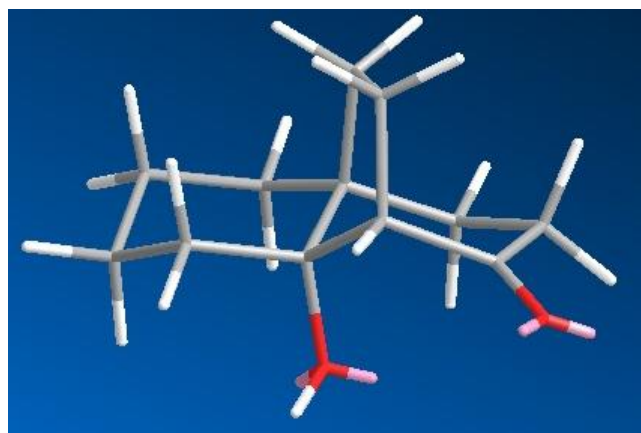


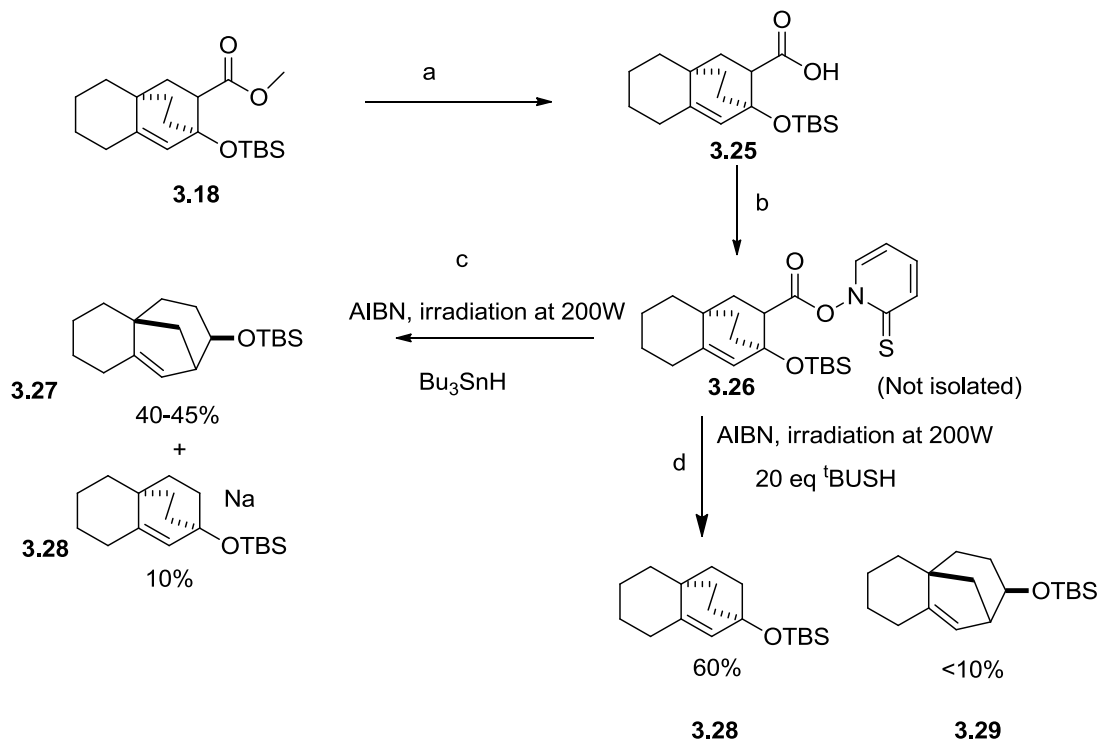
Figure 3.3: Molecular energy calculation for the ketone **3.23** T.E = 30.1534 kcal/mol (Chem 3D)

Though we were able to successfully accomplish a novel Wagner-Meerwien [2.2.2]→[3.2.1] type rearrangement, its application to the completion of total synthesis needed some fine tuning. Our strategy was to change the migratory aptitude in the rearrangement reaction to obtain ketone with required relative stereochemistry. In the next section, several approaches en route to obtaining the correct ketone will be described in details.

3.3 Strategies to obtain the desired rearranged compound

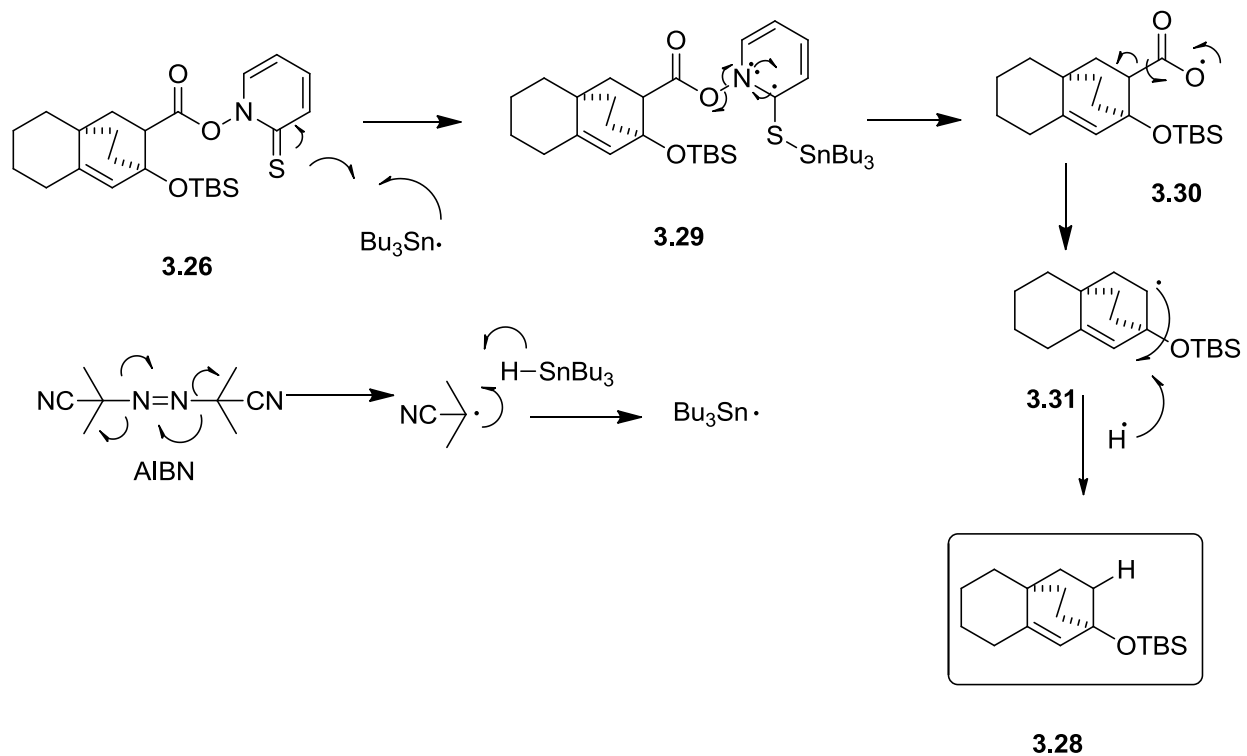
3.3.1 Strategy I

With the aim obtain ketone **3.22**, we decided to carry out the rearrangement without the carboxylic acid functional group attached to the tricyclic core **3.18**. After scrutinizing several protocols for decarboxylation, we planned to employ Barton decarboxylation on the tricyclic core (Scheme 3.6). However, Barton's decarboxylation did not proceed as smoothly as anticipated. When the reaction was carried out with only 1.0 equivalent of the radical quenching agent, *tert*-butyl thiol, compound **3.27** with a [3.2.1] rearranged core was obtained in about 50% yield, with the required [2.2.2] decarboxylated system **3.28** present in only around 10%. We rationalized the formation of **3.27** based on formation of cyclopropyl radical type intermediate **3.33**. The cyclopropyl intermediate then formed disintegrates to give more stable tertiary radical **3.34**. Reaction mechanism for decarboxylation as well as for unanticipated product **3.27** is given below (scheme **3.7 and 3.8**)

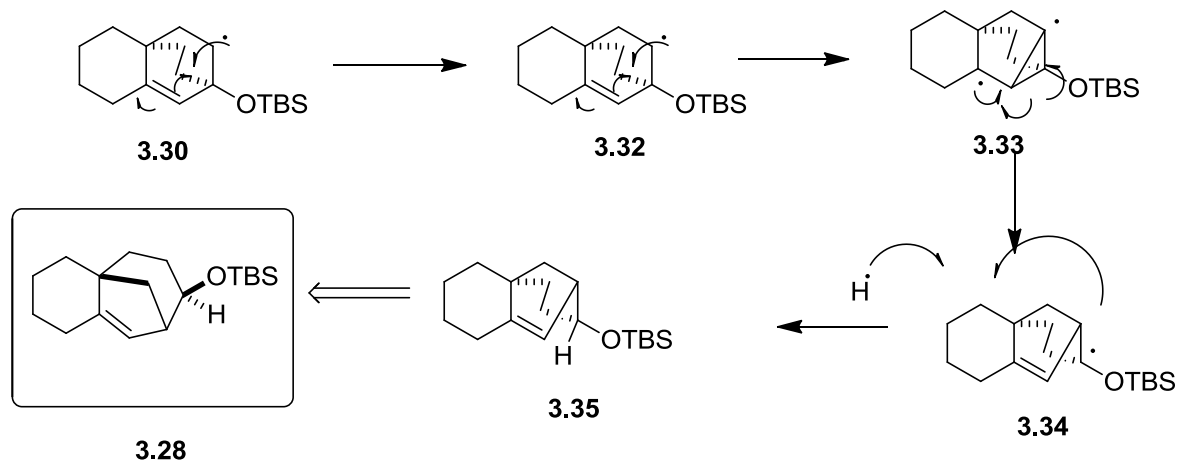


Scheme 3.6 : Barton decarboxylation

Reagents and conditions a) NaOH, 5:1 MeOH:H₂O, 69% b) isobutryl chlorformate, TEA, 2-Mercaptopyridine *N*-oxide c) AIBN, *t*-Bu₃SnH, hν 200 watt benzene d) AIBN, ^tBuSH, hν 200W, benzene.

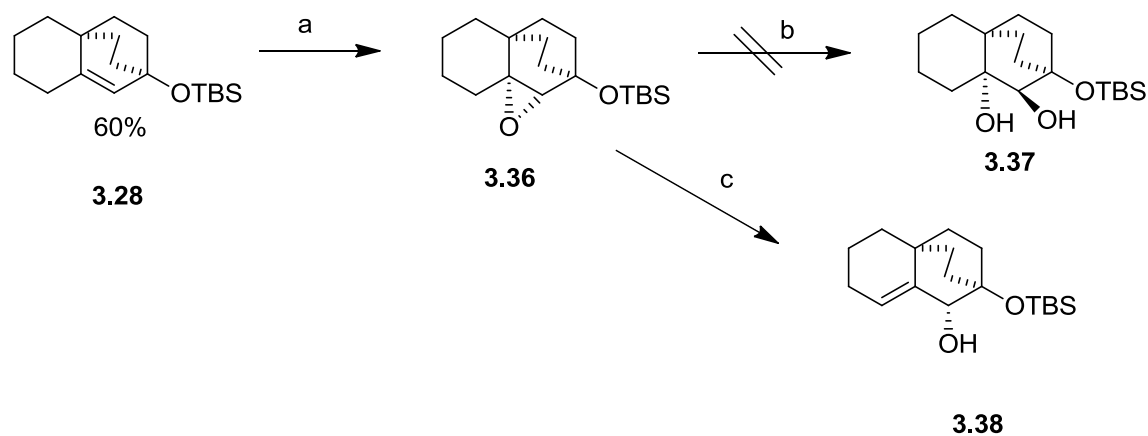


Scheme 3.7: Barton decarboxylation mechanism



Scheme 3.8: Mechanistic insights for formation of [2.2.2] intermediate

After ascertaining the mechanism of the rearrangement, we carried out the decarboxylation reaction with 20 equivalents of *tert*-butyl thiol (radical scavenger).^{54, 55} As anticipated, we were able to obtain the required [2.2.2] decarboxylated tricyclic system. With compound **3.28** in hand, treatment with mCPBA in DCM gave the epoxide **3.36**. The next step was the opening of this epoxide by a hydroxide nucleophile to give the tri hydroxy compound **3.37**. However, the epoxide was stable to alkaline hydrolysis conditions and highly unstable to acidic epoxide opening conditions. We are in the process of synthesizing more of alkene **3.28** and investigating conditions necessary to obtain the trihydroxy compound **3.37**, which will be further subjected to a Wagner-Meerwein/ pinacol type rearrangement.

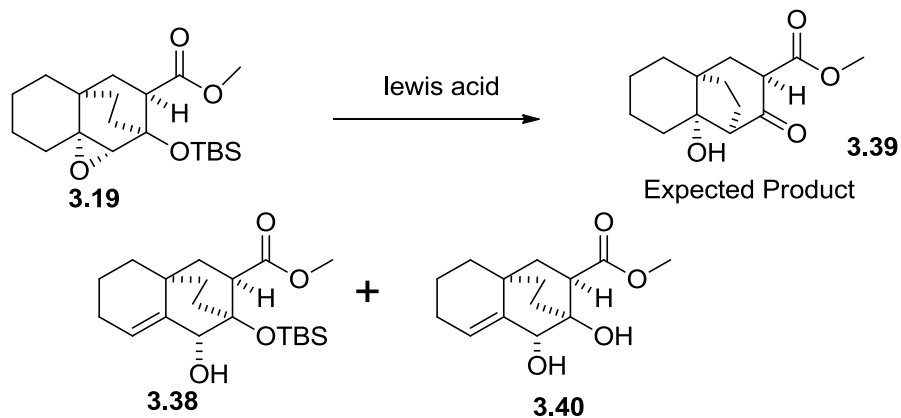


Scheme 3.9: Attempted synthesis of the trihydroxy derivative **3.37**

Reagents and Conditions: a) mCPBA, NaHCO₃, DCM b) NaOH, MeOH:water, 5:1 c) HClO₄, Acetone, water.

3.3.2 Strategy II

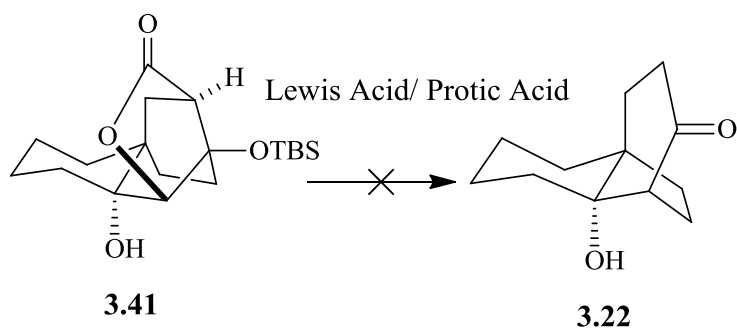
We then investigated the epoxide **3.19**, which was set up for a classic semi-pinacol type rearrangement. In a classical semi-pinacol type rearrangement, an epoxy alcohol in presence of a Lewis acid rearranges to give a pinacol type product.⁵⁶ The stereochemistry of the products generally depends on the Lewis acid catalysts used (however is hard to predict). When we subjected our epoxide to various lewis acid conditions, a mixture of products were obtained with majority of allylic alcohol **3.38**, TBS deprotected allylic alcohol **3.40** and some other unrecognizable compounds. However, none of the required compound was obtained



Scheme 3.10: Attempts to rearrange the epoxide **3.19** to give desired ketoester **3.39**

3.3.3. Strategy III

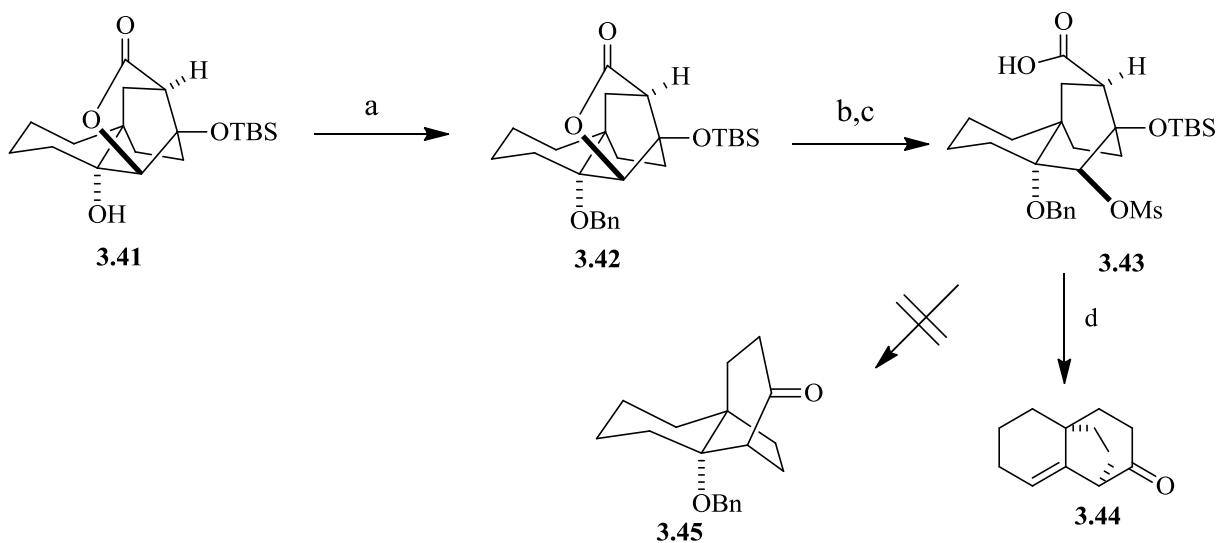
Next, we thought that the lactone would provide an efficient route to the Wagner-Meerwein rearrangement. Our initial thoughts were that the lactone would provide an efficient route to the Wagner-Meerwein rearrangement when treated with various Lewis or protic acids as the lactone oxygen atom (leaving group) was properly oriented (β -orientation) such that the backside sp^2 LUMO orbital would be facing the forming sp^2 HOMO orbital of the migrating ring methylene. While the reaction was certainly set-up stereoelectronically for a successful rearrangement, some unforeseen aspect of using an intramolecularly tethered leaving group interfered with the prospective rearrangement reaction. Thus, treatment of **52** with externally supplied reagent Lewis or protic acids resulted in some cases in dehydration by tertiary hydroxy group elimination, or alternatively, TBS deprotection from the angular hydroxyl moiety. However, no evidence of WM rearrangement reaction products (i.e. [2.2.2] \rightarrow [3.2.1]) were seen.



Scheme 3.11: Acid mediated Rearrangement of lactone **3.41**

3.3.4. Strategy IV

Further, it was deliberated that the desired ketone **3.22** may actually have formed, but because of the harsh conditions, there is a possibility of opening of the cyclic ketone **3.22** in a retro-aldol fashion and recyclization, in aldol fashion to yield the rearranged ketone **3.23**. Generally, such aldol reactions gives rise *syn* product. To test our hypothesis, the tertiary alcohol of the lactone **3.41** was protected with benzyl protecting group in a hope that the benzyl group would survive the harsh rearrangement condition. Benzylation of tertiary alcohol xx was a challenging task and was achieved using sodium hydride and benzyl bromide (surprisingly a very clean reaction). Then the benzyl lactone obtained was hydrolyzed with aqueous sodium hydroxide to hydroxy acid. The hydroxyl acid was then mesylated using mesyl chloride and triethyl amine to give mesylate **3.43**. Compound **3.43** was then subjected to the rearrangement conditions developed earlier, heating in a sealed tube in toluene at 180 °C. Surprisingly, an unanticipated β,γ unsaturated ketone **3.44** (desired product was β -benzyloxy ketone 41) and considerable amount of benzyl lactone **3.42** was isolated in the reaction (scheme 3.12)

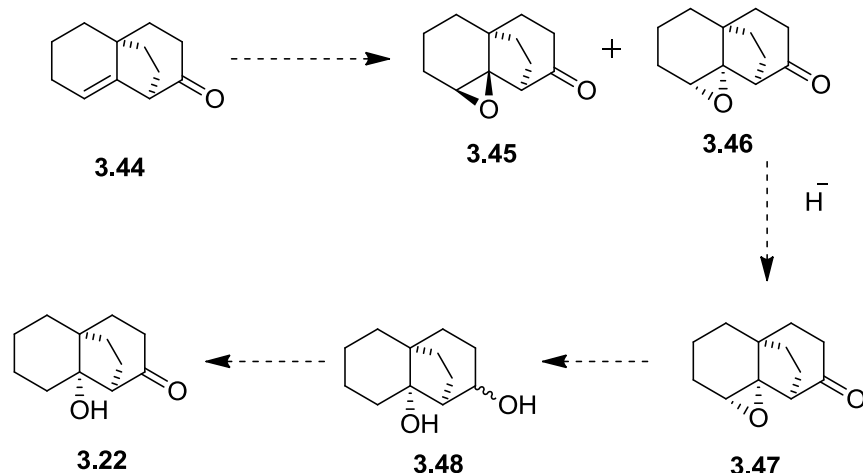


Scheme 3.12: Attempted synthesis of Benzyloxy Ketone 3.45

Reagents and Conditions: a) BnBr, NaH, DMF b) NaOH, MeOH:H₂O 68% c) MsCl, TEA, DCM d) Toluene, 180°C 48%.

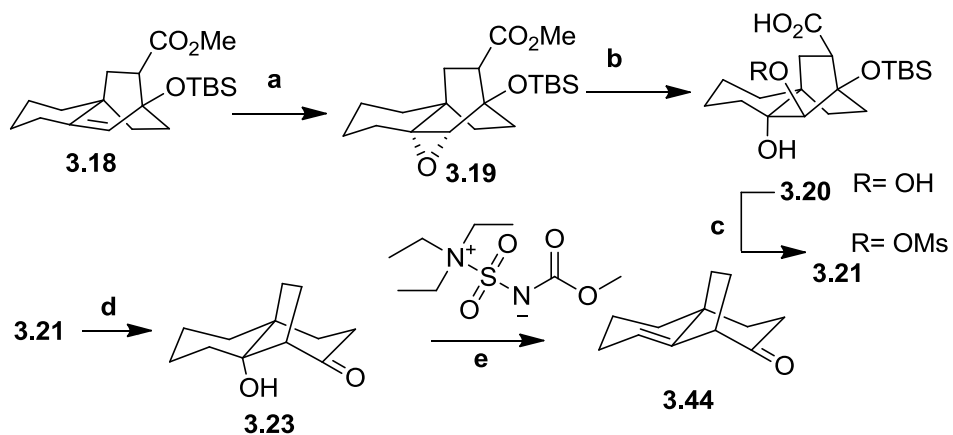
3.3.5. Strategy V

So far all the strategies adopted by us for fixing the relative stereochemistry of the obtained rearranged product 25 were futile. Hence, we decided to take an alternate route to complete our model. In strategy IV we had obtained β,γ unsaturated ketone 3.44. This ketone can be epoxidized to give (probably) a mixture of epoxides 3.45 and 3.46. After isolation and identification of the required epoxide 3.46, it can be subjected hydride mediated ring opening to yield a diol 3.48. Later the diol xx can be subjected to oxidation using Dess-Martin-Periodinane to yield required ketone 3.22.



Scheme 3.13. Proposed synthetic route for strategy V

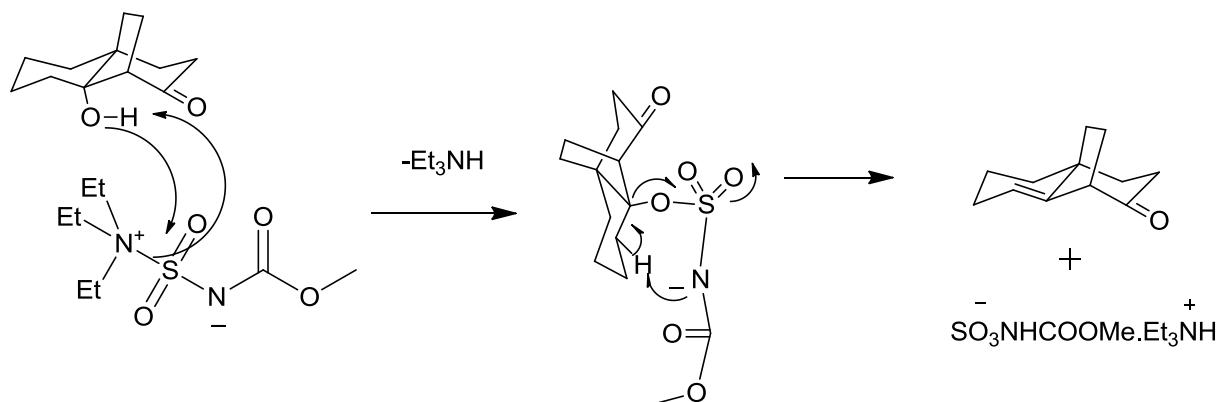
With the proposed route (scheme 3.13) in mind, we began the synthetic scheme with birch reduction the naphthalene derivative. As described earlier, the naphthalene derivative was converted in to *endo* DA adduct 3.18 in four steps. It is important to note that starting from the naphthalene derivative up until DA adduct no chromatographic purification were required. The DA adduct was converted to an α -epoxide **3.19**, which was subsequently hydrolyzed to give trihydroxy acid derivative. The compound **3.20** was converted into mesylate and converted to β -hydroxy ketone derivative xx using our novel Wagner-Meerwien type rearrangement. Once the *tert*-hydroxy ketone was obtained, several alcohol dehydration protocols were examined to obtain the ketone **3.44**. Exposing the ketone to amberlyst or tosic acid gave the desired product, albeit with poor yields. Hence we decided to explore relatively mild dehydration agents like Martin sulfurane reagent or Burgess reagent. Martin sulfurane afforded the required compound, however, the reaction did not go to completion. Finally, refluxing the *tert*-alcohol in anhydrous benzene in presence of burgess reagent furnished the trisubstituted alkene **3.44** in over 80% yield.



Scheme 3.14: Synthesis of ene-ketone 3.44

Reagents and conditions a) *m*-CPBA, NaHCO₃, CH₂Cl₂, 99%; b) NaOH (aq), 5:1 MeOH/H₂O, RT, 70% c) MsCl, Et₃N, CH₂Cl₂, 0 °C; d) toluene, 180 °C, 66% e) Burgess reagent, Benzene reflux 87%

Mechanism of dehydration using burgess reagent is given in scheme given below

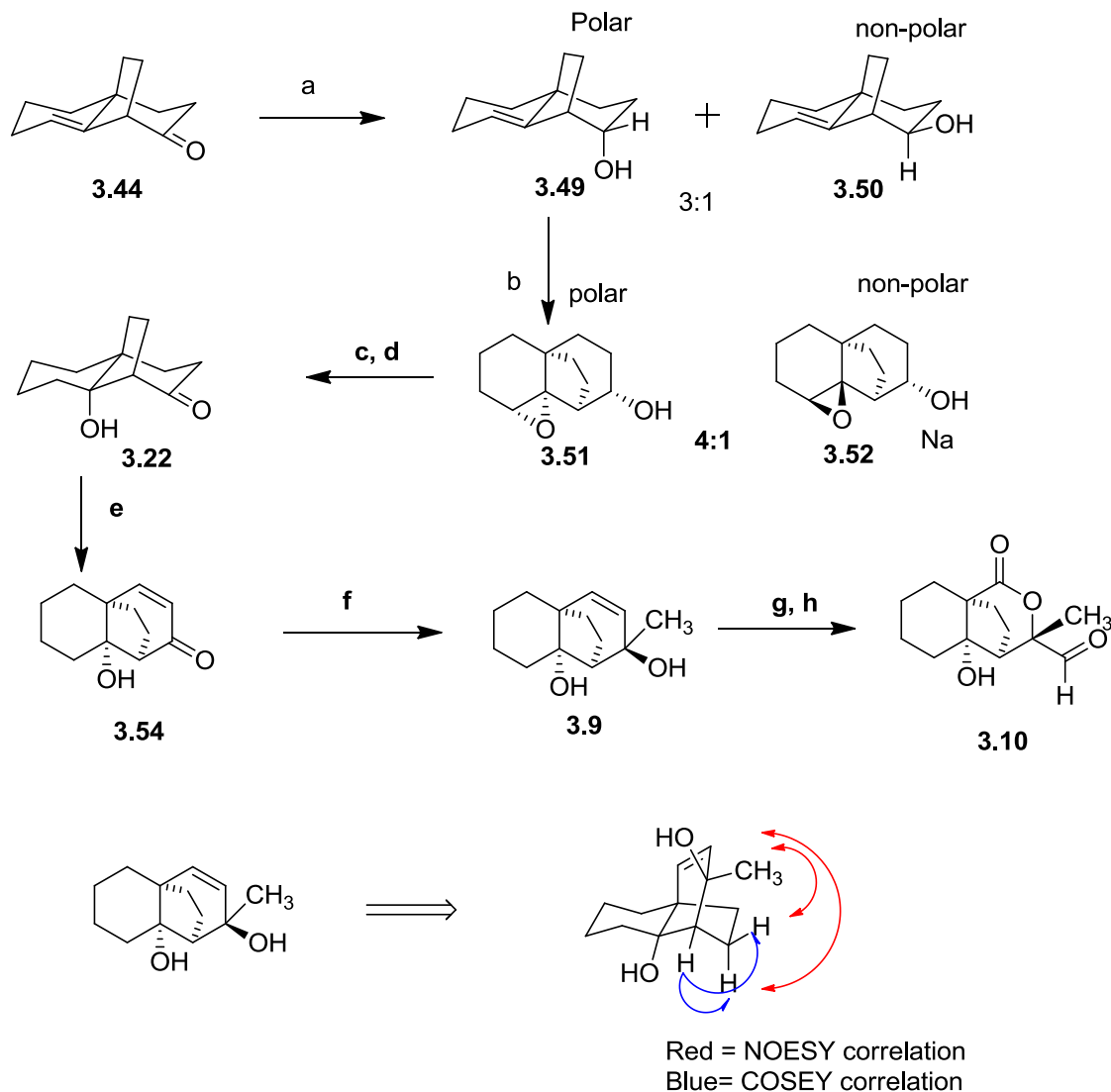


Scheme 3.15: Mechanism of dehydration of tertiary alcohol using burgess reagent

Once the alkene was obtained, it was submitted to the mCPBA mediated epoxidation. Unfortunately, the epoxidation of ketone did not proceed in a clean fashion. This may be due to the possibility of a Baeyer-Villiger Oxidation of ketone functionality giving rise to multiple products. In the lieu of this failure, we decided to convert the ketone functionality in **3.44** into a secondary alcohol. This was achieved by treating the ketone with sodium borohydride at 0 °C to give mixtures of alcohols 3.48 and 3.49 in 3:1 ratio. Each isomer was separated by flash column chromatography and fully characterized by 1D and 2D NMR. Alcohol 3.49 was carried forward in the epoxidation reaction producing a mixture of epoxide with moderate diastereoselectivity of 4:1. The moderate diastereoselectivity can be explained by the figure given below. The molecule **3.44** was sketched in Chem 3D and minimized using MM2 minimization. It can be seen from the figure 3.4 that the β -face of the alkene is only slightly more sterically hindered (presence of bridge methylene group) than the α -face of the molecule.



Figure 3.4: Ball and stick representation of 3.44



Scheme 3.16 : Completion of synthesis of crucial intermediate **3.10**

Reagents and conditions a) NaBH_4 THF, 89%; b) *m*-CPBA, NaHCO_3 , CH_2Cl_2 , 89%; c) LAH, THF 90% d) DMP, DCM 89 % e) IBX, DMSO:Toluene 1:2 80 °C 80% f) MeLi 1.6M in Ether, THF 91% g) O_3 DCM, DMS h) DMP, DCM 70% (2 steps)

The epoxide mixture obtained was purified using column chromatography and the alpha epoxide was forwarded in the scheme. Although pure diastereoselectivities were obtained at the ketone reduction and epoxide formation step, the unrequired isomers can be easily recycled and overall

of the α -epoxide can be increased. The epoxide **3.51** was ring opened using lithium aluminium hydride to give a diol and the diol was subsequently oxidized using Dess Marton periodinane oxidation to give the desired ketone **3.22**. The relative stereochemistry of the ketone was confirmed by X-ray crystal analysis of the ketone as well as of the precursor diol (Figure 3.5 and 3.6)

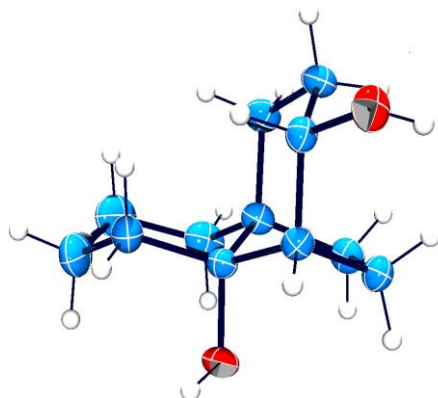


Figure 3.5: Ortep diagram for Diol

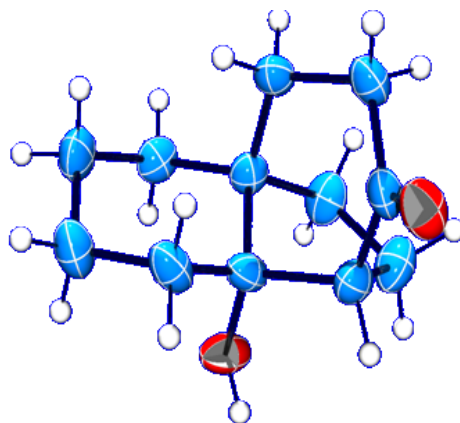


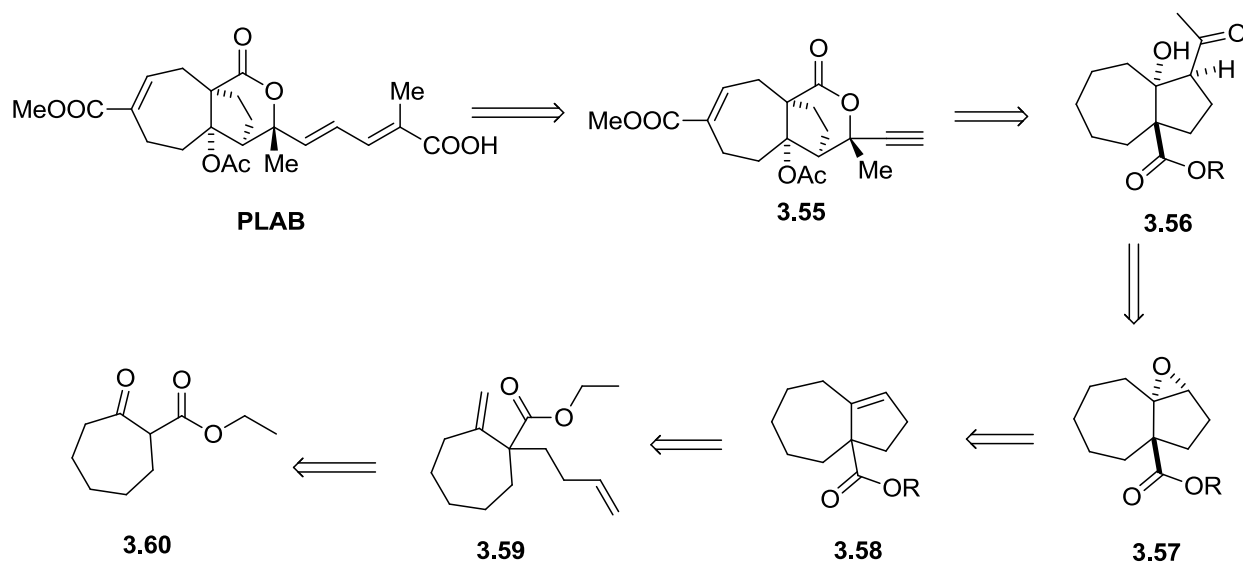
Figure 3.6: ORTEP representation of ketone **3.22**

Gratifyingly, the relative stereochemistry of the ketone is as desired. With ketone successfully synthesized, according to our synthetic plan, next task was introduction of unsaturation followed by methyl metal to give *tert*-Diol 3.9. Introduction of α,β unsaturation proved to be more difficult than anticipated, with routine sequence of phenylselenation followed by *in situ* oxidation/elimination resulted in very low yields. After few attempts, α,β unsaturation was obtained in acceptable yields using IBX in a solvent mixture of DMSO/toluene at 75°C for 2 hours (65-70% yield). Nucleophilic 1,2 Methyl lithium addition on the carbonyl group proceeded very smoothly at room temperature, giving rise to a single isomer. The relative stereochemistry was established by COSY and NOSEY ¹H-NMR (scheme 3.16) experiments and was found to be in accordance to our scheme. With the relative stereochemistry and structure of diol confirmed, final task was ozonolysis of the diene and subsequent lactol formation. Ozonolysis using standard conditions and reductive workup afforded lactol (not shown). The lactol without purification was immediately oxidized to give lactone **3.10**, the crucial intermediate. The structure and relative stereochemistry was confirmed using 2DNMR and other spectroscopic technique. Though the relative stereochemistry of intermediate **3.10** was confirmed by 2D NMR technique we still want to carry out X-ray crystal structure analysis to eliminate any doubts about the correctness of the structure.

3.4 Alternative route retrosynthesis

Simultaneously, we have designed an alternative route for synthesis of PLAB. It is known from several earlier approaches and Trost's completion of total synthesis of PLAB that the intermediate **3.56** is crucial for completion of the total synthesis of PLAB. We decide to use a model system to quickly investigate our hypothesis of constructing the intermediate **3.56** in

following manner. Delineated below, scheme 3.17, is our alternative retrosynthetic approach towards synthesis of the crucial intermediate. The crucial intermediate can be visualized from the trans fused 7+5 polyhydroazulene ring **3.57**. The epoxide can be prepared from the β - keto ester **3.60** in about 3 steps.

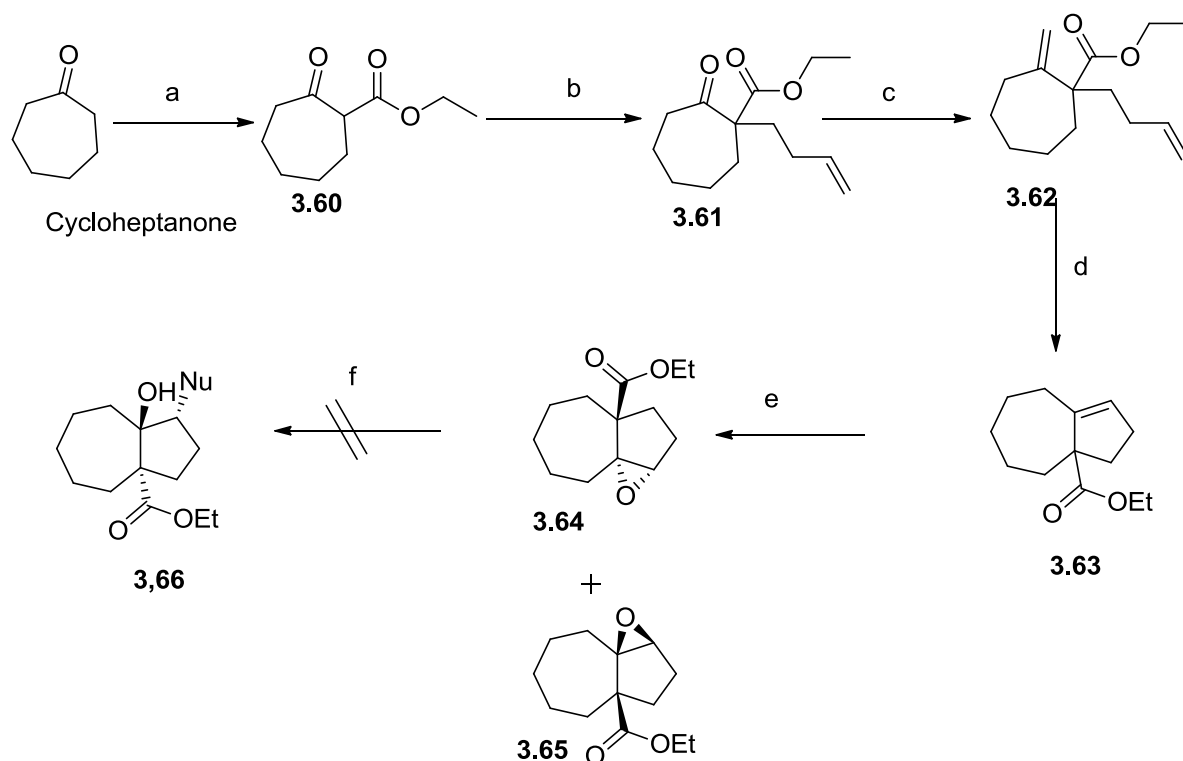


Scheme 3.17: Route 2 retrosynthetic analysis

3.5 Progress for alternative route

As per our retrosynthetic scheme, we began with synthesis of ethyl 2-oxocycloheptanecarboxylate **3.60** from cycloheptone in 75% yield. Then compound **3.61** was alkylated⁵⁷ using homoallyl bromide and potassium *tert*-butoxide to give compound **3.59** in 70% yield.^{58, 59} The next step was one carbon witting to obtain the diene **3.62**. Initial attempts to convert **3.61** to **3.62**, utilizing *n*-BuLi in THF to generate the triphenylphosphonium methyllide, resulted in relatively low yield. Recovery of starting material in this reaction suggested that enolization of the substrate was competing with the addition process. Changing solvents in the Wittig reaction from THF to DMSO and using dimsyl anion as the deprotonating species

(NaCH₂SOCH₃) allowed for a more selective addition to occur relative to unwanted deprotonation of the carbonyl, and improved the yield to about 70%. With diene **3.62** in hand, we subjected it to intramolecular ring closing metathesis using 10 mol% of Grubbs II generation catalyst. Gratifyingly, the reaction proceeded smoothly, giving alkene **3.63** in almost quantitative yield.⁶⁰ Epoxidation of alkene with mCPBA in DCM gave separable mixture of two epoxides; 6:4 (trans:syn) in 85% yield (**3.64:3.65**). Using examples from literature and 1D and 2D NMR spectroscopy, the non-polar epoxide **3.64** was identified as the required epoxide with trans relationship with the ester. With the required epoxide in hand, we decided to carry out opening of the epoxide with various nucleophiles. After using several different nucleophiles and different epoxide opening protocols⁶¹⁻⁶⁹ we were unable to obtain any desired product. The epoxide was either stable to most of the conditions or opened to give allylic alcohol or in some cases ester was attacked by the nucleophile with epoxide still intact. This suggests the epoxide is hindered and not susceptible to opening with nucleophiles.



Scheme 3.18: Route 2; attempted synthesis of intermediate **3.66**

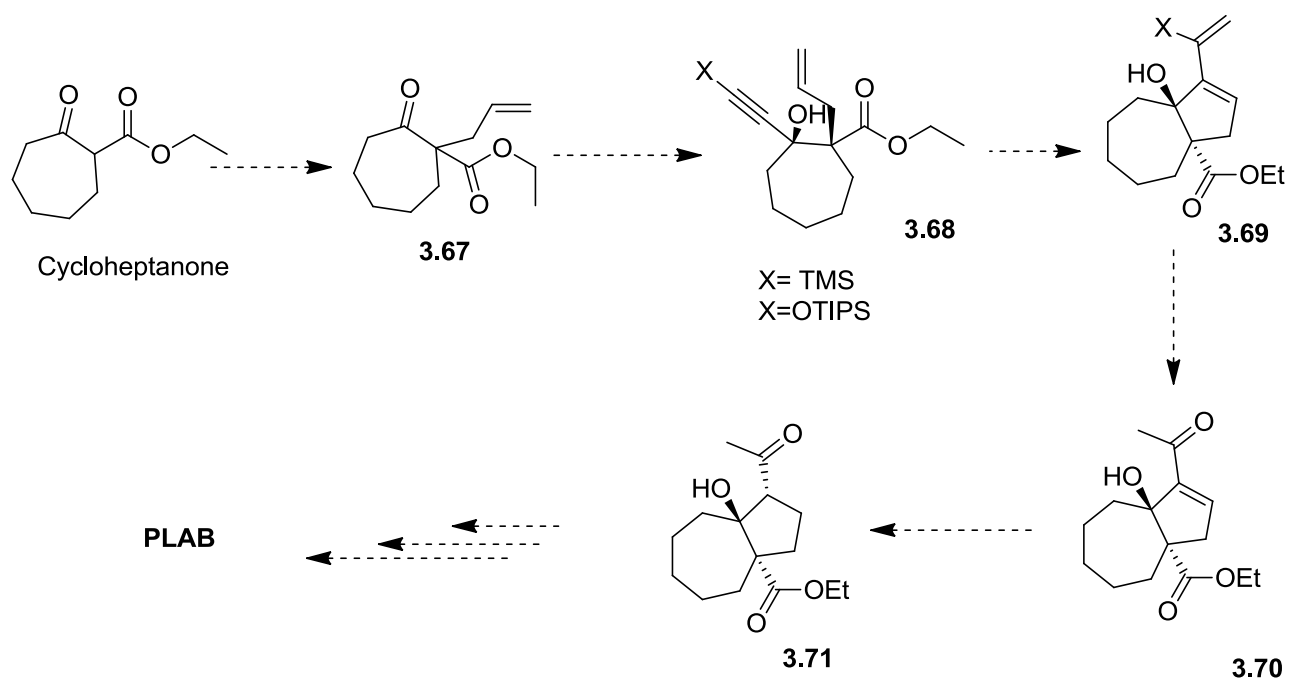
Reagents and conditions a) Diethyl carboxylate, NaH, DMF 75% b) 4-bromobut-1-ene, K^t OBu, DMSO 70% c) methyltriphenylphosphonium bromide, NaH, DMSO, 70% d) Grubbs II generation catalyst, DCM reflux 95% e) mCPBA, DCM, RT 85% f) alkyl, alkenyl, alkynyl grignards, or alkenyl, alkynyl lithium etc.

In summary, we have successfully accomplished the model studies directed toward the total synthesis of pseudolaric acid B starting from a commercially available naphthalene derivative. We demonstrated that our novel Wagner-Meerwein rearrangement can indeed be applied to completion of total synthesis of PLAB. However, a setback in our synthetic scheme was that the undesired ketone formation was favored over the desired ketone. Gratifyingly, we were able to invert the stereochemistry of the ketone in relatively acceptable yields in five steps. Currently we are in a process of streamlining our synthetic route, and then it will be applied towards the

synthesis of the natural product, PLAB. Furthermore, we also demonstrated a quick assembly of 5+7 membered ring using ring closing metathesis. The success of this route depends upon the ring opening of the epoxide with appropriate nucleophile. As this route is relatively short and elegant, more studies directed towards opening of sterically hindered epoxide are warranted.

3.6 Future Direction

With the route 2 failing to give desired product, we wish to investigate an alternative route to obtain the crucial intermediate **3.71**. The proposed route is delineated in scheme 3.19. The ethyl carboxylate cycloheptanone derivative can easily be alkylated with allyl bromide to give intermediate **3.67**, which in turn can be subjected to alkynyl metal addition to give corresponding tertiary alcohol **3.68**. This step is going to determine the stereochemistry of polyhydroazulene framework which will be formed in next step.



Scheme 3.19: Future directions

We intend to use an intramolecular delivery of the alkynyl species which will be tethered to the carboxylic acid, ensuring the attack of alkyne from the same side as that of carboxylic acid resulting in correct stereoisomer required for completion of total synthesis of PLAB. Once the correct stereochemistry is obtained, next crucial step is enyne-metathesis, which can be carried out using Grubbs II catalyst. With appropriate X group (TMS or OTIPS) it is possible to envision crucial intermediate **3.70** in few steps from **3.68**. Currently, to test our hypothesis synthesis of intermediate is being carried out in our laboratory and will be reported in due course.

CHAPTER 4
EXPERIMENTAL- PSEUDOLARIC ACID B

General Experimental

^1H and ^{13}C NMR spectra were measured in CDCl_3 or C_6D_6 on Bruker 400 MHz (100 MHz) or 500 MHz (125 MHz) machines. Chemical shifts were reported in ppm downfield from tetramethylsilane (δ) as the internal standard and coupling constants are in hertz (Hz). Assignment of proton resonances were confirmed by correlated spectroscopy. IR spectra were recorded using a universal attenuated total reflection sampling accessory with a Zinc Selenide crystal on a Perkin-Elmer Spectrum 100 FT-IR spectrometer. The high-resolution mass spectra (HRMS) were recorded on a Micromass Q-ToF Micro mass spectrometer with lock spray source. Optical rotations were measured on an Autopol V automatic polarimeter, from Rudolph Research Analytical in a 1 dm or a 5 dm cell. Melting points were measured on an OptiMelt[®] V.1.061 (Stanford Research systems) instrument and were uncorrected. The reaction progress was monitored on precoated silica gel G or GP Analtech TLC plates. Spots were visualized under 254 nm UV light and/or by dipping the TLC plate into a solution of 2 ml anisaldehyde and 10 ml glacial acetic acid and 5 ml H_2SO_4 in 340 ml MeOH followed by heating with a hot gun. Column chromatography was performed with Dynamic Adsorbents Inc. silica gel 60 (230-400 mesh). All the solvents (hexane, ethyl acetate, CH_2Cl_2 , Et_2O) were distilled prior to use. All reactions were performed under an atmosphere of argon using oven-dried glassware and standard syringe/septa techniques. The solvents THF and Et_2O were distilled from sodium-benzophenone, toluene, cyclohexane, benzene from sodium. CH_2Cl_2 was dried over P_2O_5 . DMF, NEt_3 , $^i\text{Pr}_2\text{NH}$ and $^i\text{Pr}_2\text{NEt}$ and were distilled from CaH_2 .

6-Methoxy-1,2,3,4,5,8-hexahydronaphthalene (3.14)

Ammonia (350 mL) was condensed into a 3-neck round-bottom flask at -78°C . Dry ether (50 mL) and dry ethanol (125 mL) were added via syringe followed by a solution of 6-methoxy-1,2,3,4-tetrahydronaphthalene (10g, 61.7 mmol, in 10 mL dry ether). Lithium metal (2.78g, 6.5 eq) was added piecewise. After the blue color faded (~ 1 hour), the cooling bath was removed, and the ammonia was allowed to evaporate overnight. Ether (200 mL) was added, and the mixture was washed with water (2 x 200 mL) and brine (100 mL). The ether layer was dried (MgSO_4) and concentrated to give 9.21g (91%) of a clear oil, which was mostly pure by TLC (20% EtOAc:hexanes). The product 3.14 was used in the next step without further purification. An aliquot was purified rapidly by column chromatography (silica gel, hexanes). IR (neat) 2924, 2827, 1703, 1671, 1218 cm^{-1} ; ^1H NMR (400 MHz, CDCl_3) δ 4.65 (d, $J = 3.1$ Hz, 1H), 3.78 (s, 1H), 3.56 (s, 3H), 2.79 – 2.53 (m, 5H), 1.91 (s, 4H), 1.74 – 1.56 (m, 5H). ^{13}C NMR (CDCl_3) δ 153.04, 125.86, 124.74, 90.54, 77.35, 77.03, 76.72, 53.74, 33.85, 31.96, 29.64, 29.25, 23.17, 22.92. HRMS (ESI) calcd. for $\text{C}_{11}\text{H}_{17}\text{O}$: 165.1279 $[\text{M}+\text{H}]^+$, found 165.1273.

3,4,5,6,7,8-Hexahydro-1H-naphthalene-2-one (3.15)

The dienol ether (8.83g, 54 mmol) was added to a solution of MeOH (47 mL) and H_2O (15 mL) followed by oxalic acid (486 mg, 0.1 eq). The mixture was stirred for 3 hours until no starting material remained by TLC (20% EtOAc/hexanes). The MeOH was removed by vacuum. EtOAc (60 mL) was added. The organic layer was washed with aqueous NaHCO_3 (saturated). The organic layer was dried (MgSO_4) and evaporated. The residue was purified by column chromatography (5% EtOAc:hexanes) to give 6.3g (78%) of the pure enone as a clear oil. IR

(neat) 3413, 2922, 1715, 1440, 815, 740 cm^{-1} ; ^1H NMR (400 MHz, CDCl_3) δ 2.74 (s, 2H), 2.49 (t, $J = 6.9$ Hz, 2H), 2.33 (s, 2H), 1.98 (s, 2H), 1.90 (s, 2H), 1.63 (dd, $J = 6.2, 3.2$ Hz, 4H) ^{13}C NMR (101 MHz, CDCl_3) δ 210.99, 128.60, 125.77, 77.43, 77.11, 76.79, 44.42, 38.96, 30.69, 29.73, 29.62, 22.85, 22.38. HRMS (ESI) calcd. for $\text{C}_{10}\text{H}_{14}\text{OK}$: 189.0677 $[\text{M}+\text{K}]^+$, found 189.0669.

***tert*-Butyl-(3,4,5,6,7,8-hexahydronaphthalene-2-yloxy)-dimethylsilane. (3.16)**

Freshly distilled diisopropylamine (0.98 mL) was added to dry THF (10 mL) in a round-bottom flask under argon. The solution was cooled to -18°C with a MeOH/ice bath. *n*-BuLi (2.79 mL, 2.5M) was added dropwise over 10 minutes. After an additional 15 minutes at -18°C , the solution was cooled to -78°C . The enone (3.15) (952 mg, 6.35 mmol) was dissolved in dry THF (2 mL) and added dropwise over 10 minutes to the LDA solution. After 30 minutes at -78°C , TBDMSCl (1.14g, 1.5 eq) in THF (1.5 mL) was added over 5 minutes via syringe. After 1 hour at -78°C , the solution was allowed to warm to RT overnight. After 24 hours the solvent was evaporated. Pentane was added, and the mixture was filtered through Celite to remove LiCl. Evaporation of the pentane gave a clear, yellow oil. The product was used without further purification. An aliquot was purified by column chromatography (silica, hexanes). The column was washed with 1% Et_3N :hexanes prior to purification. The product was isolated as a clear oil (1.37g, 82%). IR (neat) 2928, 2858, 1668, 1622, 1247, 838 cm^{-1} ; ^1H NMR (CDCl_3) δ 4.90 (s, 1H), 2.18 (m, 4H), 1.95 (m, 4H), 1.61 (m, 4H), 0.93 (s, 9H), 0.17 (m, 6H); ^{13}C NMR (CDCl_3) δ 151.5, 126.6, 122.3, 106.6, 32.0, 30.2, 29.8, 29.5, 29.3, 26.1, 23.6, 23.5, 18.5; HRMS (ESI) calcd. for $\text{C}_{16}\text{H}_{29}\text{OSi}$: 265.1981 $[\text{M}+\text{H}]^+$, found, 265.1975.

***endo*-8-(*tert*-Butyl dimethylsilyloxy) tricyclo[6.2.2.0^{1,6}] dodec-6-ene-9-carboxylic acid methyl ester (3.18) and *exo*-8-(*tert*-Butyl dimethylsilyloxy) tricyclo[6.2.2.0^{1,6}] dodec-6-ene-9-carboxylic acid methyl ester.(3.17)**

Methyl acrylate (858 μL , 820 mg, 2.5 eq) was dissolved in dry toluene (1.5 mL) and cooled to 0°C. $\text{Al}(\text{Me}_3)_3$ (170 μL) was added dropwise. After 15 minutes the temperature was lowered to -20°C, and Et_2AlCl (3.42 mL, 1.0 eq, 1M in hexanes) was added dropwise via syringe and syringe pump. After 15 minutes the diene (1g, 3.8 mmol) in dry toluene (9 mL) was added dropwise. The reaction was completed in 3 hours at -20°C. Water (5 mL) was added to quench the reaction, followed by HCl (10 mL, 2N). The aqueous layer was extracted with EtOAc. The organic layer was washed with brine and dried over MgSO_4 . The crude mixture was purified by column chromatography (silica, 3% EtOAc:hexanes) to give two products (1.07g, 81% total yield) in a 9:1 ratio as clear oils. Major isomer (*endo*): IR (neat) 2928, 2857, 1737, 1433, 1359, 1250, 1197, 837 cm^{-1} ; ^1H NMR (CDCl_3) δ 5.73 (s, 1H), 3.60 (s, 3H), 2.80 (dd, 1H, $J = 6.0$ Hz, $J = 9.5$ Hz), 2.31-2.21 (m, 2H), 1.70-1.29 (m, 12H), 0.86 (s, 9H), 0.11 (s, 3H), 0.10 (s, 3H); ^{13}C NMR (CDCl_3) δ 176.2, 143.8, 127.0, 51.7, 51.3, 39.5, 36.8, 36.5, 32.3, 32.3, 26.9, 25.9, 21.7, 19.8, 18.4, -1.8, -2.0; HRMS (ESI) calcd. for $\text{C}_{20}\text{H}_{35}\text{O}_3\text{Si}$: 351.2349 $[\text{M}+\text{H}]^+$, found, 351.2348; Anal. calcd. for $\text{C}_{20}\text{H}_{34}\text{O}_3\text{Si}$: C, 68.52, H, 9.78; found: C, Minor isomer (*exo*): IR (neat) 2930, 2859, 1732, 1460, 1354, 1261, 1203, 1163, 1105, 867, 834, 791 cm^{-1} ; ^1H NMR (CDCl_3) δ 5.83 (s, 1H), 3.67 (s, 3H), 2.55 (ddd, 1H, $J = 10.9$ Hz, $J = 5.9$ Hz, $J = 1.3$ Hz), 2.21 (m, 2H), 1.60-1.47 (m, 10H), 1.34-1.25 (m, 2H), 0.87 (s, 9H), 0.12 (s, 3H), 0.05 (s, 3H); ^{13}C NMR (CDCl_3) δ 176.1, 144.9, 130.3, 51.7, 50.7, 37.4, 36.6, 33.3, 32.3, 30.3, 27.0, 26.0, 21.8, 19.7, 18.4, -1.9, -2.1; HRMS (ESI) calcd. for $\text{C}_{20}\text{H}_{35}\text{O}_3\text{Si}$: 351.2349 $[\text{M}+\text{H}]^+$, found, 351.2352.

(1aR,8aR)-methyl 2-((tert-butyldimethylsilyl)oxy)octahydro-2,4a-ethanonaphtho[1,8a-b]oxirene-3-carboxylate (3.19)

The ester (5g, 1.4 mmol) was dissolved in CH₂Cl₂ (100 mL) and treated with NaHCO₃ (2.06g) with stirring. The suspension was cooled to 0°C and treated with *m*-CPBA (4.24g, 1.5 eq, 70%). The cooling bath was removed. The reaction was completed within 2 hours (TLC; 20% EtOAc:hexanes). The mixture was filtered, and the white solid was washed with CH₂Cl₂ (10 mL). The filtrate was washed with NaHCO₃ (sat, 2 x 20 mL) and dried over MgSO₄. Evaporation of the solvent gave a pale, yellow oil (5.21g, 99%). NMR showed none of the β-isomer. IR (neat) 2932, 2864, 1734, 1433, 1361, 1263, 1186, 1143, 871, 824, 781 cm⁻¹; ¹H NMR (CDCl₃) δ 3.67 (s, 3H), 3.11 (d, 1H, *J* = 0.8 Hz), 2.83 (dd, 1H, *J* = 10.5 Hz, *J* = 5.3 Hz), 2.33 (m, 1H), 2.22-2.14 (m, 1H), 1.89 (dt, 1H, *J* = 11.4 Hz, *J* = 4.3 Hz), 1.67 (m, 2H), 1.58-1.27 (m, 8H), 1.16 (dt, 1H, *J* = 12.1 Hz, *J* = 4.4 Hz), 0.86 (s, 9H), 0.17 (s, 3H), 0.10 (s, 3H); ¹³C NMR (CDCl₃) δ 176.6, 75.9, 61.9, 61.6, 51.9, 51.4, 36.6, 35.2, 34.1, 33.4, 32.6, 29.6, 25.9, 23.7, 22.5, 18.2, -2.1, -2.8; HRMS (ESI) calcd. for C₂₀H₃₅O₄Si: 367.2298 [M+H]⁺, found, 367.2302. Anal. for C₂₀H₃₄O₄Si: calcd: C, 65.53, H, 9.35; found: C, 65.91, H, 9.39.

8-(tert-Butyl dimethylsilyloxy)-6,7-dihydroxy tricyclo[6.2.2.0^{1,6}]dodecane-9-carboxylic acid (3.20)

Method A. The lactone (200 mg, 0.57 mmol) was dissolved in dry EtOH (16 mL) and treated with KOH (640 mg). The mixture was stirred overnight until no starting material remained (TLC, 20% EtOAc:hexanes). The solution was neutralized with HCl (1N). The product was extracted with EtOAc (4 x 15 mL). After drying with MgSO₄, the solvent was evaporated by vacuum to give the product as a white amorphous solid (196 mg, 93%).

Method B. The epoxide (5.2g, 1.4 mmol) was dissolved in MeOH (52 mL) and treated with a solution of NaOH (2.86g, 5eq. in 10 mL H₂O) with stirring. The solution was heated to reflux for 5 hours or until no starting material remained by TLC (20% EtOAc:hexanes). The MeOH was removed by vacuum. The residue was dissolved in CH₂Cl₂ (100 mL). HCl (3N) was added slowly with vigorous stirring until the reaction mixture was neutralized. Fast addition of the HCl leads to formation of a sticky mass. The aqueous layer was separated, and the organic layer was filtered. The white solid was washed with CH₂Cl₂ and ether (2.94g, 56%). mp °C; IR (KBr) 3509, 3288, 3269, 2942, 2919, 2858, 2641, 2621, 1681, 1470, 1260, 1143, 1004, 835, 773 cm⁻¹; ¹H NMR (DMSO-d₆) δ 4.35 (s, 1H), 4.04 (bs, 1H), 2.77 (t, 1H, *J* = 10.0 Hz), 1.97 (t, 1H, *J* = 11.4 Hz), 1.84 (m, 1H), 1.71 (m, 1H), 1.58-1.33 (m, 8H), 1.28-1.10 (m, 2H), 1.06 (d, 1H, *J* = 12.7 Hz), 0.81 (s, 9H), 0.09 (s, 3H), 0.06 (s, 3H); ¹³C NMR (DMSO-d₆) δ 178.6, 90.0, 84.5, 76.5, 75.7, 75.6, 49.6, 34.9, 34.1, 33.6, 30.7, 30.2, 26.5, 22.0, 21.4, 18.7, -1.2, -1.7; HRMS (ESI) calcd. for C₁₉H₃₃O₅Si: 369.2103 [M-H]⁻, found, 369.2095. Anal. calcd. for C₁₉H₃₄O₅Si: C, 61.58, H, 9.25; found: C, 61.57, H, 9.40.

(1S,4aS,8aS)-8a-hydroxyhexahydro-1H-1,4a-ethanonaphthalen-2(5H)-one (3.23)

The hydroxy acid (1.0 g, 2.7 mmol) was suspended in dry CH₂Cl₂ (30mL) and cooled to 0 °C. Et₃N (800 μL, 2.1 eq) was added dropwise. After 5 minutes, freshly distilled MsCl (440 μL, 2.1 eq) was added dropwise. After stirring at 0 °C for 30 minutes, the solution was allowed to warm to RT. The solvent was removed under vacuum, and the residue was dissolved in EtOAc (35 mL) and washed with 1M HCl (25 mL). The organic layer was washed with water (2 x 20 mL). The organic layer was washed with brine (20 mL) and dried with MgSO₄. Removal of the

solvent and filtration through a short pad of silica (3% MeOH/Chloroform) gave the mesylate, which was used without further purification.

The mesylate was dissolved in 800 mL of dry toluene and heated in an oil bath to 180 °C in a glass, high-pressure reaction vessel (Ace Glass, Inc., PN 8648-157) for 8 hours. The solvent was removed under vacuum, and the product was purified by column chromatography (silica, 15% EtOAc/Hexanes) to give 352 mg (67%, 2 steps) of a light tan solid.

IR (KBr) 3401, 2925, 2852, 1694, 1444, 1177, 1033, 1006, 800 cm^{-1} ; ^1H NMR (CDCl_3) δ 2.53-2.45 (m, 1H), 2.36 (m, 2H), 2.25 (dd, 1H, $J = 16.2$ Hz, $J = 7.0$ Hz), 2.12 (m, 1H), 1.98 (m, 1H), 1.86 (m, 1H), 1.68-1.35 (m, 10H); ^{13}C NMR (CDCl_3) δ 211.19, 80.85, 77.28, 77.02, 76.77, 61.58, 42.76, 35.37, 34.88, 34.06, 29.85, 29.08, 23.47, 21.28, 20.46.; HRMS (ESI) calcd. for $\text{C}_{12}\text{H}_{19}\text{O}_2$: 195.1379 $[\text{M}+\text{H}]^+$, found, 195.1393. anal. for $\text{C}_{12}\text{H}_{18}\text{O}_2$: calcd. C, 74.19, H, 9.34; found: C, 74.20, H, 9.52.

***endo*-8-(*tert*-Butyl dimethylsilyloxy) tricyclo[6.2.2.0^{1,6}]dodec-6-ene-9-carboxylic acid (3.25)**

The *endo* ester (3.83g, 1.1 mmol) was dissolved in MeOH (100 mL) at RT. An aqueous solution of NaOH (3.57g in 7 mL H_2O) was added slowly. The solution was heated to reflux for 12 hours or until no starting material remained by TLC (20% EtOAc:hexanes). (Prolonged heating resulted in substantial loss of product due to desilylation). The product mixture was acidified to pH 3 with HCl (2N), and the MeOH was removed by vacuum. The product was extracted with EtOAc (3 x 50 mL). The organic layer was dried (MgSO_4), and the solvent was removed by vacuum. The residue was purified by column chromatography (silica, 10% EtOAc:hexanes) to give 1.97g (67%) of the pure acid as a white solid. mp 61-63 °C (dec.); IR (KBr) 3473, 2934,

2859, 1761, 1703, 1256, 1197, 1109, 836, 775 cm^{-1} ; ^1H NMR (CDCl_3) δ 11.10 (bs, 1H), 5.66 (s, 1H), 2.67 (dd, 1H, $J = 9.9$ Hz, $J = 4.0$ Hz), 2.18 (m, 2H), 1.93 (td, $J = 9.2$ Hz, $J = 3.7$ Hz), 1.80-1.73 (m, 1H), 1.64-1.31 (m, 10H), 0.93 (s, 9H), 0.21 (s, 3H), 0.20 (s, 3H); ^{13}C NMR (CDCl_3) δ 175.5, 147.5, 124.8, 78.5, 50.6, 36.6, 35.8, 35.3, 33.9, 31.9, 26.9, 26.0, 21.5, 19.4, 18.3; HRMS (ESI) calcd. for $\text{C}_{19}\text{H}_{32}\text{ClO}_3\text{Si}$: 371.1815 $[\text{M}+\text{Cl}]^-$, found, 371.1849;

Synthesis of (3.28) tert-butyl(((2s,4ar)-3,4,5,6,7,8-hexahydro-2H-2,4a-ethanonaphthalen-2-yl)oxy)dimethylsilane

To stirred suspension of (2S,4aR)-2-((tert-butyl dimethylsilyl)oxy)-3,4,5,6,7,8-hexahydro-2H-2,4a-ethanonaphthalene-3-carboxylic acid **3.25** (50mg, 0.149 mmol) in Benzene (5.0 ml) was charged N-Methylmorpholine (0.033 ml, 0.297 mmol) at -30°C resulting in a pale yellow solution. To this after 15 mins was charged DCC (30.7 mg, 0.149 mmol) followed by 2-Mercapto pyridineoxide (37.8 mg, 0.297 mmol). The reaction mixture was brought to 0°C and stirred for 2-3 hrs. After 2 hrs t-Butylthiol (0.329 ml, 2.53 mmol) was charged to reaction mixture (suspension) slowly. The reaction mixture was then exposed to 300 hv light for 2 hrs. (Note The temperature was maintained $0-10^\circ\text{C}$ by ice water bath). Reaction was monitored by TLC. Reaction mixture was diluted with water and extracted with ether. The aqueous extract was carefully quenched with bleach in the hood. The organic layer was quickly washed with bleach followed by brine. The organic layer was dried over magnesium sulfate and evaporated under vacuum to give crude oil. The crude was purified by column chromatography using pentane to afford **3.28** tert-butyl(((2s,4ar)-3,4,5,6,7,8-hexahydro-2H-2,4a-ethanonaphthalen-2-yl)oxy)dimethylsilane (25.0mg, 0.085 mmol, 57.5 % yield) 2927.36 2866.22, 1477.98, 1448.69, 1253.83, 1069.83, 1008.05, 860.72, 772.99, 673.18 cm^{-1} ^1H NMR (400 MHz, CDCl_3) δ 5.77 (s, 1H), 2.21 (dt, $J = 6.7, 3.5$ Hz, 2H), 1.67 (td, $J = 10.1, 4.1$ Hz, 2H), 1.57 (dd, $J = 6.6, 3.2$ Hz, 4H),

1.45 (t, $J = 5.7$ Hz, 2H), 1.41 – 1.24 (m, 5H), 1.01 – 0.78 (m, 9H), 0.20 – 0.02 (m, 5H). ^{13}C NMR (101 MHz, CDCl_3) δ 143.29, 129.80, 77.30, 76.99, 76.67, 75.38, 36.02, 35.63, 33.26, 32.24, 26.66, 25.82, 21.63, 19.50, 17.96, -2.10. APCI (M+1) 293.21; (M+Na) 315.21

Synthesis of (3.27) tert-butyldimethyl(((4aR,7R)-1,2,3,4,5,6,7,8-octahydro-4a,8-methanobenzo[7]annulen-7-yl)oxy)silane

Same procedure was followed. Instead of using 17.0eq of t-Butyl thiol only 1.0 equivalent was used. Colorless oil. IR 2856, 1471, 1461.78, 1253.84, 1051.73, 772.99, 673.18 cm^{-1} . ^1H NMR (500 MHz, CDCl_3) δ 5.49 (s, 1H), 3.65 (ddd, $J = 9.3, 6.0, 2.9$ Hz, 1H), 2.46 – 2.36 (m, 2H), 2.02 – 1.95 (m, 1H), 1.78 – 1.54 (m, 7H), 1.38 – 1.21 (m, 6H), 1.00 (td, $J = 12.8, 5.5$ Hz, 1H), 0.90 (s, 9H), 0.09 – 0.02 (m, 6H). ^{13}C NMR (126 MHz, CDCl_3) δ 146.62, 121.27, 77.27, 77.02, 76.77, 70.02, 49.69, 46.55, 44.55, 36.77, 29.66, 26.88, 26.38, 26.36, 25.95, 22.86, 18.22, -4.60. APCI (M+1) 293.24

(3R,5aR,9aR,9bS)-3a-((tert-butyldimethylsilyl)oxy)-9a-hydroxydecahydro-2H-3,5a-methanonaphtho[1,2-b]furan-2-one (3.41)

The acid (226 mg, 0.67 mmol) was dissolved in CH_2Cl_2 (2 mL) and treated with *m*-CPBA (249 mg, 1.5 eq, 70%) at RT. The solution was stirred at RT for 3 hours, until no starting material remained by TLC (5% MeOH: CHCl_3). CH_2Cl_2 (10 mL) was added, and the mixture was washed with NaOH (1N, 4 x 20 mL) until no *meta*-chlorobenzoic acid remained. After drying (MgSO_4), the solvent was removed by vacuum to give the product as an amorphous white solid (110 mg, 46%). mp 204-205°C; IR (KBr) 3474, 2934, 2860, 1764, 1473, 1343, 1104, 994, 836,

774 cm^{-1} ; ^1H NMR (CDCl_3) δ 3.97 (s, 1H), 2.45 (d, 1H, $J = 10.9$ Hz), 2.07-1.96 (m, 2H), 1.92-1.79 (m, 2H), 1.60-1.48 (m, 5H), 1.47-1.39 (m, 2H), 1.29-1.18 (m, 3H), 0.83 (s, 9H), 0.13 (s, 3H), 0.11 (s, 3H); ^{13}C NMR (CDCl_3) δ ; HRMS (ESI) calcd. for $\text{C}_{19}\text{H}_{33}\text{O}_4\text{Si}$: 353.2142 $[\text{M}+\text{H}]^+$, found, 353.2147; Anal. calcd. for $\text{C}_{19}\text{H}_{32}\text{O}_4\text{Si}$: C, 64.73, H, 9.15; found C, 64.92, H, 9.29.

Synthesis of (1R,4aR)-3,4,6,7-tetrahydro-1H-1,4a-ethanonaphthalen-2(5H)-one (3.44)

To a solution of (1R,4aR,8aS)-8a-hydroxyhexahydro-1H-1,4a-ethanonaphthalen-2(5H)-one (470.0mg, 2.419 mmol) in anhydrous benzene was added at once Burgess Reagent (865 mg, 3.63 mmol). The resulting solution was refluxed under argon for 4 hrs or until completion of the reaction as indicated by TLC. After reaction was complete RM was diluted with ethyl acetate and washed with water followed by brine. The organic layer was dried over magnesium sulfate and evaporated under vacuum. The product was purified by Flash column chromatography (Hex:EtOAc 9:1) to give (1R,4aR)-3,4,6,7-tetrahydro-1H-1,4a-ethanonaphthalen-2(5H)-one (365.0mg, 2.071 mmol, 86 % yield) ^1H NMR (400 MHz, CDCl_3) δ 5.52 (t, $J = 3.6$ Hz, 1H), 3.10 (d, $J = 6.5$ Hz, 1H), 2.68 – 2.47 (m, 1H), 2.29 (tdd, $J = 27.5, 18.8, 8.7$ Hz, 2H), 1.95 (ddd, $J = 16.4, 7.7, 3.9$ Hz, 6H), 1.80 (ddd, $J = 18.1, 13.5, 6.7$ Hz, 4H), 1.66 – 1.58 (m, 3H), 1.58 – 1.44 (m, 3H). ^{13}C NMR (101 MHz, CDCl_3) δ 211.16, 136.39, 118.07, 77.36, 77.04, 76.73, 58.48, 40.58, 36.46, 34.93, 33.53, 27.55, 26.92, 25.03, 19.97. HRMS (ESI) calcd. for $\text{C}_{12}\text{H}_{16}\text{NaO}$: 199.1099 $[\text{M}+\text{Na}]^+$, found, 199.1143

(1R,2S,4aR)-2,3,4,5,6,7-hexahydro-1H-1,4a-ethanonaphthalen-2-ol (3.50) To a stirred solution of (1R,4aR)-3,4,6,7-tetrahydro-1H-1,4a-ethanonaphthalen-2(5H)-one (330.0mg, 1.872 mmol) at 0°C was carefully added sodium borohydride (70.8 mg, 1.872 mmol) keeping the

temperature below zero. Reaction was slowly brought to and stirring for 2hrs or until the completion of the reaction (monitored by TLC). Reaction was again cooled to 0°C and quenched with dropwise addition of water. Methanol was evaporated and crude obtained was dissolve in ethyl acetate. Oragnic layer was wahed with saturated ammonium chloride solution, brine and then was dried over magensium sulfate. After concentrartion of organic solvent colorless oily liquid was obtained. Crude was purified using flash colum chromatography (Hexane:EtoAc 7:3) to furnish

Polar-(1R,2R,4aR)-2,3,4,5,6,7-hexahydro-1H-1,4a-ethanonaphthalen-2-ol (3.49) and

NonPolar-(1R,2S,4aR)-2,3,4,5,6,7-hexahydro-1H-1,4a-ethanonaphthalen-2-ol (3.50)

(72.0mg, 0.404 mmol, 21.57 % yield) ¹H NMR (500 MHz, CDCl₃) δ 5.39 (t, *J* = 3.5 Hz, 1H), 3.85 – 3.66 (m, 1H), 2.61 – 2.50 (m, 1H), 1.95 (dd, *J* = 10.9, 6.2 Hz, 2H), 1.90 – 1.82 (m, 1H), 1.82 – 1.73 (m, 1H), 1.71 – 1.61 (m, 3H), 1.61 – 1.52 (m, 3H), 1.52 – 1.43 (m, 2H), 1.43 – 1.32 (m, 2H), 1.28 (dd, *J* = 12.3, 6.2 Hz, 1H). ¹³C NMR (126 MHz, CDCl₃) δ 147.48, 114.09, 77.25, 77.00, 76.75, 73.87, 49.44, 39.69, 36.51, 36.19, 34.08, 28.75, 24.98, 22.06, 20.24. ESI+ (M+1) 179.2

Polar-(1R,2R,4aR)-2,3,4,5,6,7-hexahydro-1H-1,4a-ethanonaphthalen-2-ol (3.49) (198.0mg,

1.111 mmol, 59.3 % yield) ¹H NMR (500 MHz, CDCl₃) δ 5.64 – 5.30 (m, 1H), 3.71 (s, 1H), 2.63 – 2.37 (m, 1H), 2.05 – 1.94 (m, 2H), 1.91 (s, 1H), 1.88 – 1.77 (m, 3H), 1.77 – 1.68 (m, 2H), 1.67 – 1.49 (m, 5H), 1.49 – 1.39 (m, 2H), 1.39 – 1.32 (m, 2H), 1.20 (dd, *J* = 11.9, 5.3 Hz, 1H). ¹³C NMR (126 MHz, CDCl₃) δ 145.79, 117.14, 77.25, 77.00, 76.75, 72.05, 48.64, 40.53, 35.84, 34.63, 34.59, 27.10, 25.66, 24.96, 20.08. ESI (M+Na) 201.13

Polar(3.51) (1aR,4aR,7R,8S,8aR)-octahydro-4a,8-ethanonaphtho[1,8a-b]oxiren-7-ol and Nonpolar (1aR,4aR,7R,8S,8aS)-octahydro-4a,8-ethanonaphtho[1,8a-b]oxiren-7-ol (3.52)

To stirred solution of (1R,2R,4aR)-2,3,4,5,6,7-hexahydro-1H-1,4a-ethanonaphthalen-2-ol (250.0 mg, 1.402 mmol) in DCM at was added sodium carbonate (130 mg, 1.543 mmol) and mCPBA (346 mg, 1.543 mmol) at once. After stirring for 1 hr the starting material disappeared, monoitotring by TLC. The reaction mixture was filtered through celite and celite was washed with 10ml additional DCM. Combined DCM was washed with 2.0M sodium bicarbonate and 0.1 NaOH to remove m-Chlorobenzoic acid. The organic layer was then washed with brine and dried over magnesium sulfate. DCM was evaporated under vacuum to give crude epoxide whihc was purified by column chromatogarchy to give colorless oil Nonpolar **3.52** (1aR,4aR,7R,8S,8aS)-octahydro-4a,8-ethanonaphtho[1,8a-b]oxiren-7-ol (170.0 mg, 0.875 mmol, 62.4 % yield) ¹H NMR (400 MHz, CDCl₃) δ 4.20 – 4.03 (m, 1H), 3.16 (d, *J* = 5.3 Hz, 1H), 2.14 – 1.84 (m, 6H), 1.76 – 1.57 (m, 5H), 1.57 – 1.44 (m, 3H), 1.44 – 1.32 (m, 3H), 1.28 (dd, *J* = 24.6, 8.6 Hz, 2H), 1.13 – 0.99 (m, 1H). ¹³C NMR (101 MHz, CDCl₃) δ 77.36, 77.04, 76.72, 70.06, 69.07, 58.62, 46.58, 36.50, 34.40, 29.82, 28.59, 28.26, 24.57, 19.22, 16.91. . ESI+ (M+Na) 217.10

and Polar **3.51**(1aR,4aR,7R,8S,8aR)-octahydro-4a,8-ethanonaphtho[1,8a-b]oxiren-7-ol (50.0mg, 0.257 mmol, 18.35 % yield) ¹H NMR (400 MHz, CDCl₃) δ 3.90 (d, *J* = 8.8 Hz, 1H), 3.45 (d, *J* = 3.2 Hz, 1H), 1.99 – 1.79 (m, 7H), 1.70 – 1.63 (m, 1H), 1.63 – 1.50 (m, 7H), 1.52 – 1.44 (m, 3H), 1.29 (dd, *J* = 16.7, 8.9 Hz, 2H). ¹³C NMR (101 MHz, CDCl₃) δ 77.33, 77.01, 76.69, 71.44, 70.72, 57.34, 47.63, 38.97, 33.37, 30.88, 29.14, 27.86, 22.15, 20.93, 16.41. ESI+ (M+Na) 217.13

(1S,2R,4aR,8aS)-octahydro-1H-1,4a-ethanonaphthalene-2,8a-diol (3.53)

To a stirred solution of (1aR,4aR,7R,8S,8aS)-octahydro-4a,8-ethanonaphtho[1,8a-b]oxiren-7-ol (54.0 mg, 0.278 mmol) at -20°C in THF (Volume: 1.0 ml) was added dropwise 3.5M LAH (0.199 ml, 0.695 mmol). The reaction was slowly brought to RT and was stirred until completion of reaction (Monitored by TLC). After completion of reaction mixture was again cooled to -20°C and quenched with 500 µl of MeOH followed by 500 µl rochelle salt solution. The reaction was stirred vigorously till solid precipitate was seen. The precipitate was filtered through celite. The celite was washed with 5.0ml ethyl acetate. The combined organic extract was washed with saturated ammonium chloride solution and brine. The organic layer was dried over magnesium sulfate and evaporated under vacuum. Crude was purified by column chromatography to give (1S,2R,4aR,8aS)-octahydro-1H-1,4a-ethanonaphthalene-2,8a-diol (38.5 mg, 0.196 mmol, 70.6 % yield) ¹H NMR (400 MHz, CDCl₃) δ 4.05 – 3.85 (m, 1H), 2.40 (s, 3H), 1.98 (d, *J* = 6.0 Hz, 1H), 1.89 (dd, *J* = 12.2, 5.5 Hz, 1H), 1.84 (d, *J* = 4.9 Hz, 1H), 1.79 (dd, *J* = 12.8, 5.6 Hz, 2H), 1.74 – 1.63 (m, 3H), 1.64 – 1.57 (m, 2H), 1.55 (d, *J* = 8.3 Hz, 1H), 1.48 (d, *J* = 9.0 Hz, 2H), 1.38 (tt, *J* = 12.4, 6.1 Hz, 3H), 1.04 (dd, *J* = 13.6, 6.9 Hz, 1H), 0.97 – 0.81 (m, 1H). ¹³C NMR (101 MHz, CDCl₃) δ 80.37, 77.36, 77.04, 76.72, 69.10, 52.24, 42.98, 33.99, 30.95, 30.65, 28.07, 27.47, 20.77, 20.58, 20.54. ESI+ (M+1) 197.14

(1S,4aS,8aS)-8a-hydroxyhexahydro-1H-1,4a-ethanonaphthalen-2(5H)-one (3.22)

To a stirred solution of (1S,2S,4aR,8aS)-octahydro-1H-1,4a-ethanonaphthalene-2,8a-diol (38.0mg, 0.194 mmol) in DCM (Volume: 1.0 ml) was added DMP (82 mg, 0.194 mmol) at RT. The reaction was complete within 30mins. DCM was recovered and diethyl ether was added to the residue. The suspension was filtered through celite and the organic layer was washed with saturated sodium bicarbonate solution, brine and dried over magnesium sulfate. Concentration of ether under vacuum afforded crude ketone which was purified by column chromatography to

give (1S,4aS,8aS)-8a-hydroxyhexahydro-1H-1,4a-ethanonaphthalen-2(5H)-one **3.22** (35.0mg, 0.178 mmol, 92 % yield) $\text{CHCl}_3/\nu_{\text{max}} \text{ cm}^{-1}$ 3389, 2915, 2850, 1690, 1159 ^1H NMR (500 MHz, CDCl_3) δ 2.52 (q, $J = 14.8$ Hz, 2H), 2.24 – 2.03 (m, 3H), 1.94 – 1.87 (m, 1H), 1.82 (dd, $J = 13.8$, 6.1 Hz, 1H), 1.68 (dt, $J = 13.2$, 8.4 Hz, 3H), 1.62 – 1.46 (m, 8H), 1.40 (dd, $J = 13.1$, 9.9 Hz, 1H). ^{13}C NMR (126 MHz, CDCl_3) δ 213.42, 81.79, 77.25, 77.00, 76.75, 61.51, 44.38, 33.98, 33.81, 30.75, 29.92, 29.52, 26.11, 20.32, 20.23. HRMS (ESI) calcd. for $\text{C}_{12}\text{H}_{19}\text{O}_2\text{Na}$: 212.1204 $[\text{M}+\text{Na}]^+$, found, 212.1213.

(1S,2R,4aR,8aS)-2-methyl-2,5,6,7,8,8a-hexahydro-1H-1,4a-ethanonaphthalene-2,8a-diol

(3.19)

To a stirred solution of the (1R,4aR,8aS)-8a-hydroxy-6,7,8,8a-tetrahydro-1H-1,4a-ethanonaphthalen-2(5H)-one (20.0 mg, 0.104 mmol) in THF (Volume: 1.0 ml) at RT was added methyl lithium (0.195 ml, 0.312 mmol) at once. (Note: adding methyl lithium at 0°C results in two products) After stirring for 15 min or till the starting material disappeared the reaction was quenched by addition of saturated ammonium chloride solution. The reaction mixture was diluted by ethyl acetate and organic layer was washed with brine. The organic extract was then dried over magnesium sulfate and evaporated under vacuum to give crude diol. Crude was purified using column chromatography ethyl acetate and hexanes (7:3) to afford (1S,2R,4aR,8aS)-2-methyl-2,5,6,7,8,8a-hexahydro-1H-1,4a-ethanonaphthalene-2,8a-diol (16.2 mg, 0.078 mmol, 74.8 % yield) ^1H NMR (400 MHz, CDCl_3) δ 5.62 (d, $J = 9.5$ Hz, 1H), 5.40 (d, $J = 9.3$ Hz, 1H), 2.32 (dd, $J = 20.5$, 10.4 Hz, 2H), 2.13 – 1.97 (m, 3H), 1.76 – 1.46 (m, 15H), 1.42 (t, $J = 9.1$ Hz,

4H), 1.32 (s, 3H). ¹³C NMR (126 MHz, MeOD) δ 139.54, 129.55, 80.19, 74.29, 55.66, 48.11, 47.94, 47.88, 47.77, 47.60, 47.43, 47.26, 47.09, 46.63, 34.16, 31.54, 30.44, 27.92, 22.90, 22.42, 20.87.

(1R,4aR,8aS)-8a-hydroxy-6,7,8,8a-tetrahydro-1H-1,4a-ethanonaphthalen-2(5H)-one (3.54)

To a stirred solution of (1R,4aR,8aS)-8a-hydroxyhexahydro-1H-1,4a-ethanonaphthalen-2(5H)-one (20.0 mg, 0.103 mmol) of mixture of Toluene (Ratio: 2.0, Volume: 2.0 ml) and DMSO (Ratio: 1.000, Volume: 1.000 ml) was added IBX (115 mg, 0.412 mmol). The reaction mixture was stirred at 90°C for 3-4hrs (Reaction monitored by TLC). After completion of reaction it was quenched with 2.0 ml water and extracted with ether. The organic layer washed with brine, dried over magnesium sulfate and evaporated under vacuum to give crude enone. The crude was carefully purified by column chromatography using ethyl acetate and hexanes. (8:2) to give (1R,4aR,8aS)-8a-hydroxy-6,7,8,8a-tetrahydro-1H-1,4a-ethanonaphthalen-2(5H)-one (15.3mg, 0.080 mmol, 77 % yield) White solid; mp 83-85 °C; IR cm⁻¹; ¹H NMR (400 MHz, CDCl₃) δ 6.91 (d, *J* = 9.7 Hz, 1H), 5.98 (dd, *J* = 9.7, 1.3 Hz, 1H), 2.73 (d, *J* = 7.3 Hz, 1H), 2.48 – 2.29 (m, 1H), 1.96 (ddd, *J* = 11.9, 9.6, 5.1 Hz, 2H), 1.91 – 1.73 (m, 5H), 1.72 – 1.64 (m, 2H), 1.63 – 1.47 (m, 5H), 1.47 – 1.39 (m, 1H), 1.26 (qd, *J* = 11.4, 5.9 Hz, 1H). ¹³C NMR (101 MHz, CDCl₃) δ 203.59, 160.76, 127.99, 82.33, 77.35, 77.03, 76.71, 60.81, 51.10, 32.76, 29.55, 28.94, 23.45, 22.54, 20.35. ¹³C NMR (CDCl₃) δ 202.5, 157.8, 127.9, 82.3, 60.3, 47.6, 31.9, 29.3, 26.8, 21.2, 20.9, 19.8; HRMS (ESI) calcd. for C₁₂H₁₇O₂: 193.1229 [M+H]⁺, found, 193.1221;

(3S,4R,4aS,8aS)-4a-hydroxy-3-methyl-1-oxooctahydro-4,8a-ethanoisochromene-3-carbaldehyde (3.10)

A stream of ozone was carefully bubbled through a solution of (1S,2R,4aR,8aS)-2-methyl-2,5,6,7,8,8a-hexahydro-1H-1,4a-ethanonaphthalene-2,8a-diol (16.0 mg, 0.077 mmol) in DCM (Volume: 1.0 ml) at -78 °C until distinctive blue color of ozone was clearly observed. The reaction was stirred at that temperature for 30mins. After 30 mins a stream of argon was passed through the solution to displace the ozone. To this solution at -78 °C was added DMS (0.011 ml, 0.154 mmol) and the reaction was allowed to warm up to RT and stirred for 6-8 hrs. Reaction was monitored by TLC and no starting material was observed after 7 hrs. Organic solvent was evaporated and crude lactol obtained was immediately dissolved in DCM. To a stirred solution of lactol; (1R,3S,4R,4aS,8aS)-1,4a-dihydroxy-3-methyloctahydro-4,8a-ethanoisochromene-3-carbaldehyde (13.0 mg, 0.054 mmol, 70.4 % yield) in DCM (Volume: 1.0 ml) was added DMP (32.6 mg, 0.077 mmol) at RT. The reaction was stirred no starting material was seen on TLC. DCM was recovered and diethyl ether was added to the residue. The suspension was filtered through celite and the organic layer was washed with saturated sodium bicarbonate solution, brine and dried over magnesium sulfate. Concentration of ether under vacuum afforded crude ketone which was purified by column chromatography to give colorless oily compound (3S,4R,4aS,8aS)-4a-hydroxy-3-methyl-1-oxooctahydro-4,8a-ethanoisochromene-3-carbaldehyde (9.3 mg, 0.039 mmol, 50.8 % yield)

¹H NMR (600 MHz, cdcl₃) δ 9.57 (s, 1H), 2.39 (d, *J* = 6.8 Hz, 1H), 2.31 (d, *J* = 13.3 Hz, 2H), 2.23 – 2.15 (m, 2H), 1.98 (d, *J* = 14.1 Hz, 2H), 1.87 – 1.78 (m, 5H), 1.77 – 1.73 (m, 2H), 1.67 – 1.59 (m, 5H), 1.57 – 1.47 (m, 8H), 1.42 – 1.32 (m, 2H), 1.30 (s, 1H), 1.22 (s, 1H). ¹³C NMR (126 MHz, CDCl₃) δ 201.62, 174.47, 86.70, 77.63, 77.30, 77.04, 76.79, 55.00, 48.85, 33.99, 32.49, 26.86, 23.95, 22.63, 22.01, 20.53.

ethyl 2-oxocycloheptanecarboxylate (3.60) and ethyl 2-hydroxycyclohept-1-enecarboxylate (3.60a)

ethyl 2-oxocycloheptanecarboxylate (3.60) (org.syn.coll. vol V p.198)

In a 100 mL 2 necked round-bottomed flask equipped with condenser and dropping funnel was added sodium Hydride mineral oil dispersion (4.99 g, 125 mmol). NaH mineral oil dispersion was then washed with benzene to remove mineral oil (2x50ml wash). Once the mineral oil was removed, fresh Benzene (50.0 ml) was charged and then Diethyl Carbonate (10.80 ml, 89 mmol) was added slowly and this mixture was heated to reflux. Cycloheptanone (5.26 ml, 44.6 mmol) was added dropwise through a dropping funnel over 3-4 hrs. After the addition was complete reflux was continued for another 30 mins and then reaction was cooled to RT. To the RM was then added acetic acid dropwise to give a pasty white solid. (pH acidic). To the pasty solid was added icecold water (exothermic reaction). The aqueous layer was extracted with ether and the combined organic extracts were washed with 1M Sodium Bicarbonate and brine. The organic layer was evaporated and crude oil obtained was purified by flash chromatography (1:10 EtOAc: Hexanes) to afford ethyl 2-oxocycloheptanecarboxylate (5.89 g, 32.0 mmol, 71.7 % yield) Note: Product obtained was mixture of Ketone 3.60 and its enol 3.60a. This mixture was carried forward as such in the next reaction. 2927, 2256.20, 1739.85, 1704, 1637.54, 1239.51, 1309.11, 1048 cm^{-1} ; ^1H NMR (400 MHz, cdcl_3) δ 12.69 (s), 4.25 – 3.99 (m), 3.47 (dd, $J = 10.3, 4.0$ Hz), 2.63 – 2.45 (m), 2.45 – 2.24 (m), 2.08 – 1.94 (m), 1.94 – 1.74 (m), 1.71 – 1.63 (m), 1.61 – 1.50 (m), 1.49 – 1.35 (m), 1.22 (dt, $J = 17.0, 7.1$ Hz). ^{13}C NMR (101 MHz,) δ 208.79, 179.34, 172.87, 170.36, 101.43, 77.32, 77.00, 76.68, 60.83, 60.11, 58.75, 58.72, 42.89, 35.17, 31.82, 29.47, 27.78, 27.39, 27.21, 24.45, 24.19, 14.07, 13.87. ESI+ ($\text{M}+\text{Na}$) 207.11

ethyl 1-(but-3-en-1-yl)-2-oxocycloheptanecarboxylate (3.61)

The ethyl 2-oxocycloheptanecarboxylate (2.0g, 10.86 mmol) was added dropwise to a stirred solution of Potassium t-butoxide (1.267 g, 11.29 mmol) in dry DMSO (5.0 ml). After 14-Bromo-1-butene (1.146 ml, 11.29 mmol) was added dropwise. After 5hrs at RT the solution was diluted with water. The layers were separated, the aqueous layer was extracted with Ether (3 x 25 mL) and the combined organic layers were washed with brine and dried over Magnesium Sulfate. Organic layer was evaporated under vacuum and crude oil obtained was purified by column chromatography (Hexanes: Ethyl acetate 95:5) to afford ethyl 1-(but-3-enyl)-2-oxocycloheptanecarboxylate (1.95 g, 8.18 mmol, 75 % yield) ^1H NMR (500 MHz, CDCl_3) δ 5.74 (ddt, $J = 16.5, 10.4, 6.3$ Hz, 1H), 4.94 (dd, $J = 36.3, 13.6$ Hz, 2H), 4.27 – 4.01 (m, 2H), 2.60 (ddd, $J = 12.3, 8.7, 3.5$ Hz, 1H), 2.42 (ddd, $J = 22.8, 12.1, 7.5$ Hz, 1H), 2.18 – 2.07 (m, 1H), 2.06 – 1.87 (m, 3H), 1.81 – 1.52 (m, 7H), 1.49 – 1.35 (m, 1H), 1.32 – 1.10 (m, 3H). ^{13}C NMR (126 MHz, CDCl_3) δ 209.27, 172.31, 137.96, 114.68, 77.35, 77.10, 76.84, 62.48, 60.97, 42.00, 34.56, 32.84, 29.83, 28.88, 25.51, 24.82, 14.06. ESI+ (M+1) 239.17

ethyl 1-(but-3-en-1-yl)-2-methylenecycloheptanecarboxylate (3.62)

In a 100 mL round-bottomed flask, Sodium hydride 60% (0.554 g, 13.85 mmol) was added along with 10ml DMSO and heated at 70°C for 1 hr. An additional 10ml DMSO was added followed by Methyl triphenylphosphonium bromide (4.95 g, 13.85 mmol). After 20 mins Alkneylated ketone (1.1g, 4.62 mmol) in (10 mL) DMSO was added slowly. RM stirred at this temperature till completion of reaction. Reaction monitored by TLC. After completion of the reaction it was diluted with water. The Aqueous layer was extarcted with ether and the combined organic layer was washed with sat. ammonium chloride solution followed by brine. The organic layer was dried over magnesium sulfate and evaporated under vacuum to give thick oil. The crude was

purified by flash chromatography (Hexanes:Et₂O 96:4) to afford ethyl 1-(but-3-enyl)-2-methylenecycloheptanecarboxylate (755 mg, 3.19 mmol, 69.2 % yield) ¹H NMR (500 MHz, CDCl₃) δ 7.35 (s, 1H), 5.83 (ddd, *J* = 16.7, 11.5, 6.5 Hz, 1H), 5.20 – 4.76 (m, 4H), 4.26 – 4.05 (m, 2H), 2.33 – 2.11 (m, 4H), 2.03 (ddd, *J* = 25.2, 16.9, 7.7 Hz, 4H), 1.58 (dddd, *J* = 33.0, 25.5, 16.9, 10.7 Hz, 11H), 1.27 (t, *J* = 7.1 Hz, 3H). ¹³C NMR (126 MHz, CDCl₃) δ 175.64, 152.63, 138.74, 114.29, 113.16, 77.27, 77.02, 76.76, 60.37, 54.84, 37.58, 34.94, 34.69, 30.95, 30.28, 29.52, 24.54, 14.14. ESI+ (M+1) 236.17

ethyl 2,3,3a,4,5,6,7,8-octahydroazulene-3a-carboxylate (3.63)

To a solution of ethyl 1-(but-3-enyl)-2-methylenecycloheptanecarboxylate (500 mg, 2.098 mmol) in degassed Toluene (2.0 ml) was added Grubbs Catalyst 2nd Generation (89 mg, 0.105 mmol) to give a yellow solution. Reaction mixture was refluxed for 5hrs. Toluene was evaporated under vacuum and residue obtained was dissolved in DCM and loaded on to column for purification using Hex:Et₂O 95:5. to afford ethyl 2,3,3a,4,5,6,7,8-octahydroazulene-3a-carboxylate (307 mg, 1.474 mmol, 70.3 % yield); ¹H NMR (500 MHz, CDCl₃) δ 5.53 (s, 1H), 4.16 (ddd, *J* = 14.1, 7.1, 2.4 Hz, 2H), 2.48 (dd, *J* = 12.1, 7.9 Hz, 1H), 2.41 – 2.29 (m, 2H), 2.29 – 2.13 (m, 3H), 2.03 (dd, *J* = 13.9, 7.2 Hz, 1H), 1.86 – 1.77 (m, 1H), 1.72 (dd, *J* = 13.9, 8.9 Hz, 3H), 1.68 – 1.61 (m, 3H), 1.50 – 1.33 (m, 4H), 1.27 (t, *J* = 7.1 Hz, 3H). ¹³C NMR (126 MHz, CDCl₃) δ 176.92, 147.62, 128.24, 77.27, 77.01, 76.76, 60.35, 60.27, 37.55, 36.40, 30.35, 30.32, 29.96, 29.20, 24.95, 14.22. ESI+ (M+1) 208.12

(1aS,3aS,8aR)-ethyl octahydro-1aH-azuleno[1,8a-b]oxirene-3a-carboxylate (3.64) and (1aS,3aR,8aR)-ethyl octahydro-1aH-azuleno[1,8a-b]oxirene-3a-carboxylate (3.65)

To a stirred solution of ethyl 2,3,3a,4,5,6,7,8-octahydroazulene-3a-carboxylate (200 mg, 0.960 mmol) in aDCM (2.0 ml) was charged MCPBA (m-Chloroperoxybenzoic acid) (258 mg, 1.152

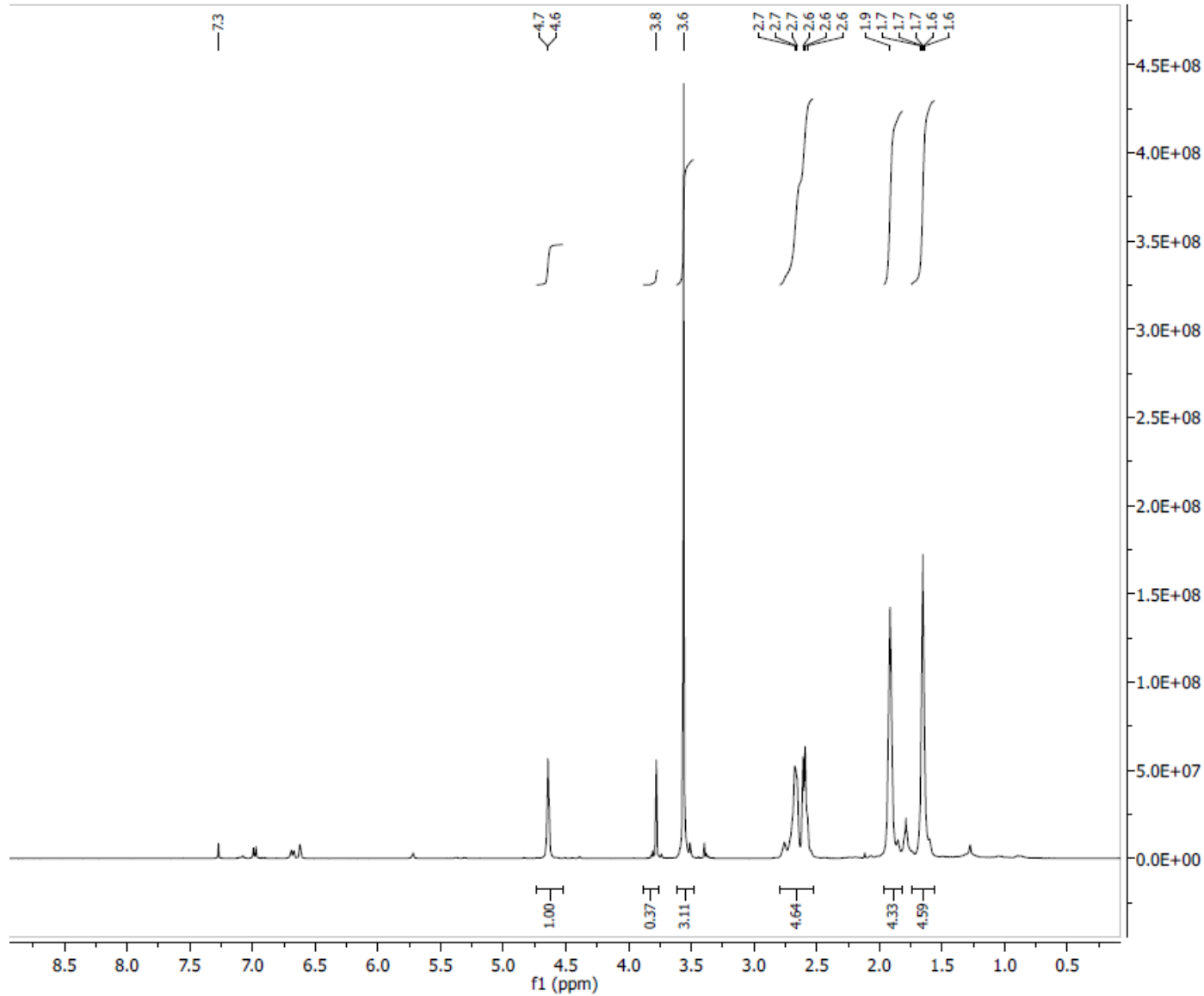
mmol) to give a white suspension. Reaction mixture was stirred for 2 hrs at RT. TLC showed completion of reaction with formation of two new spots. Reaction mixture was diluted with water and organic layer was separated. The DCM layer was washed with sat. NaHCO₃ and brine and then dried over magnesium sulfate. The organic layer was dried under vacuum and crude oil obtained was purified using column chromatography. Hex: Et₂O (9:1) to afford (Non polar on TLC) **3.64** (1aS,3aS,8aR)-ethyl octahydro-1aH-azuleno[1,8a-b]oxirene-3a-carboxylate (106mg, 0.473 mmol, 49.2 % yield) and (Slightly more Polar) **3.65** (1aS,3aR,8aR)-ethyl octahydro-1aH-azuleno[1,8a-b]oxirene-3a-carboxylate (95.0 mg, 0.424 mmol, 44.1 % yield)

(1aS,3aS,8aR)-ethyl octahydro-1aH-azuleno[1,8a-b]oxirene-3a-carboxylate (3.64)

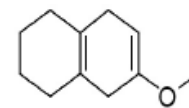
¹H NMR (400 MHz, CDCl₃) δ 4.27 – 4.11 (m, 2H), 3.35 (s, 1H), 2.44 – 2.32 (m, 1H), 2.12 (dd, *J* = 9.5, 3.6 Hz, 1H), 1.93 (dd, *J* = 13.6, 7.9 Hz, 1H), 1.84 (ddd, *J* = 5.8, 4.3, 1.6 Hz, 1H), 1.77 – 1.65 (m, 4H), 1.65 – 1.52 (m, 5H), 1.39 (ddt, *J* = 11.4, 9.0, 6.9 Hz, 2H), 1.27 (t, *J* = 7.1 Hz, 3H). ¹³C NMR (101 MHz, CDCl₃) δ 175.19, 77.34, 77.02, 76.70, 69.47, 64.72, 60.29, 54.78, 35.97, 32.80, 30.59, 27.07, 26.69, 26.30, 25.02, 14.20. ESI+ (M+Na) 207.11

(1aS,3aR,8aR)-ethyl octahydro-1aH-azuleno[1,8a-b]oxirene-3a-carboxylate (3.65)

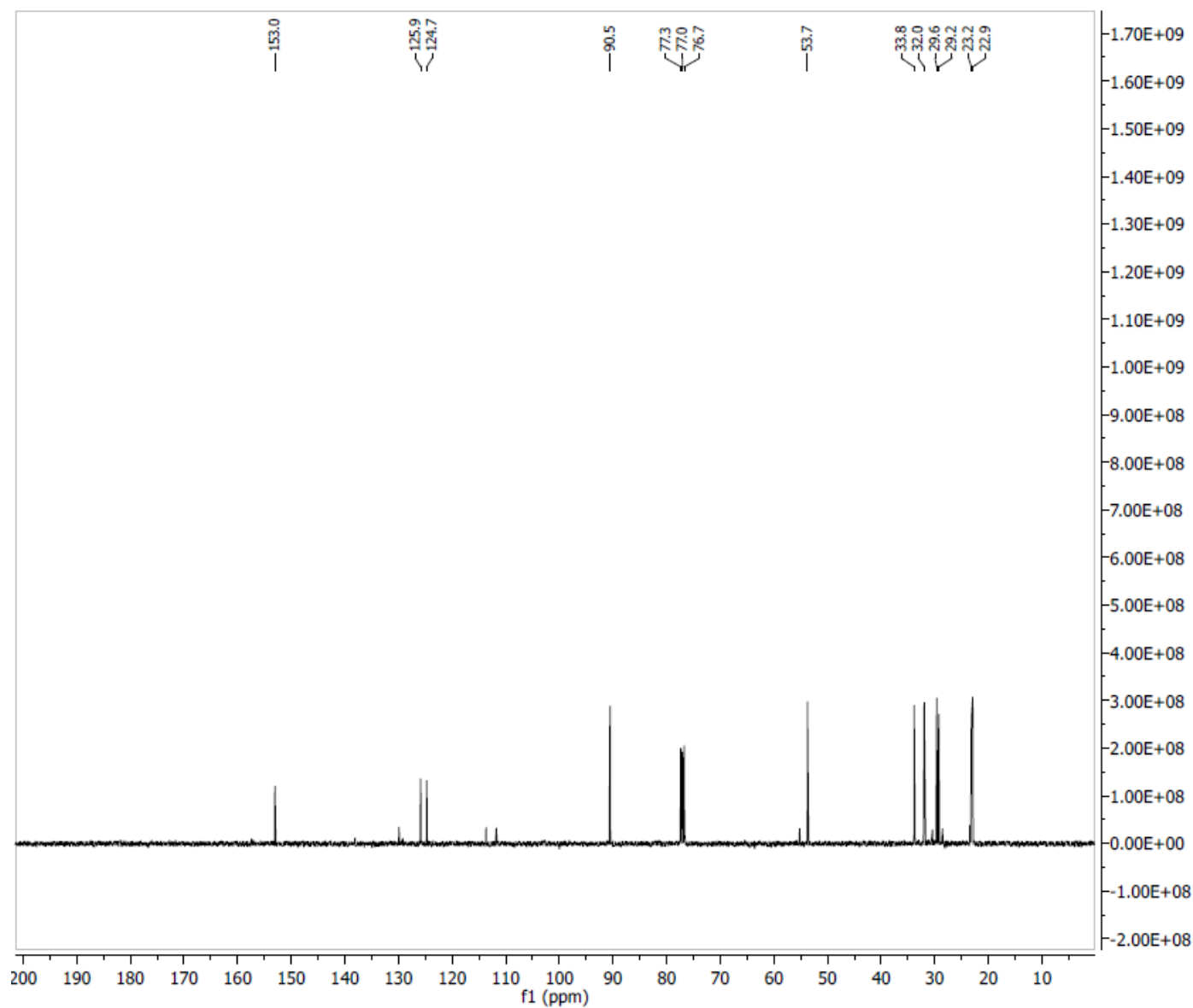
¹H NMR (400 MHz, CDCl₃) δ 4.34 – 4.08 (m, 2H), 3.28 (s, 1H), 2.41 (dd, *J* = 14.1, 11.7 Hz, 1H), 2.18 – 1.85 (m, 3H), 1.83 – 1.57 (m, 8H), 1.56 – 1.41 (m, 4H), 1.28 (dd, *J* = 13.6, 6.5 Hz, 4H). ¹³C NMR (126 MHz, CDCl₃) δ ¹³C NMR (101 MHz, CDCl₃) δ 175.56, 77.35, 77.03, 76.72, 70.41, 63.77, 60.39, 55.56, 35.19, 34.07, 30.87, 28.12, 25.81, 25.00, 23.55, 14.22. ESI+ (M+Na) 207.11



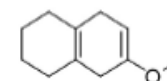
Parameter	Value
1 Spectrometer	spect
2 Solvent	CDCl3
3 Temperature	298.2
4 Pulse Sequence	zg30
5 Experiment	1D
6 Number of Scans	16
7 Receiver Gain	72
8 Relaxation Delay	1.0000
9 Pulse Width	10.2500
10 Acquisition Time	3.9846
11 Spectrometer Frequency	400.15
12 Spectral Width	8223.7
13 Lowest Frequency	-1640.8
14 Nucleus	1H
15 Acquired Size	32768
16 Spectral Size	32768



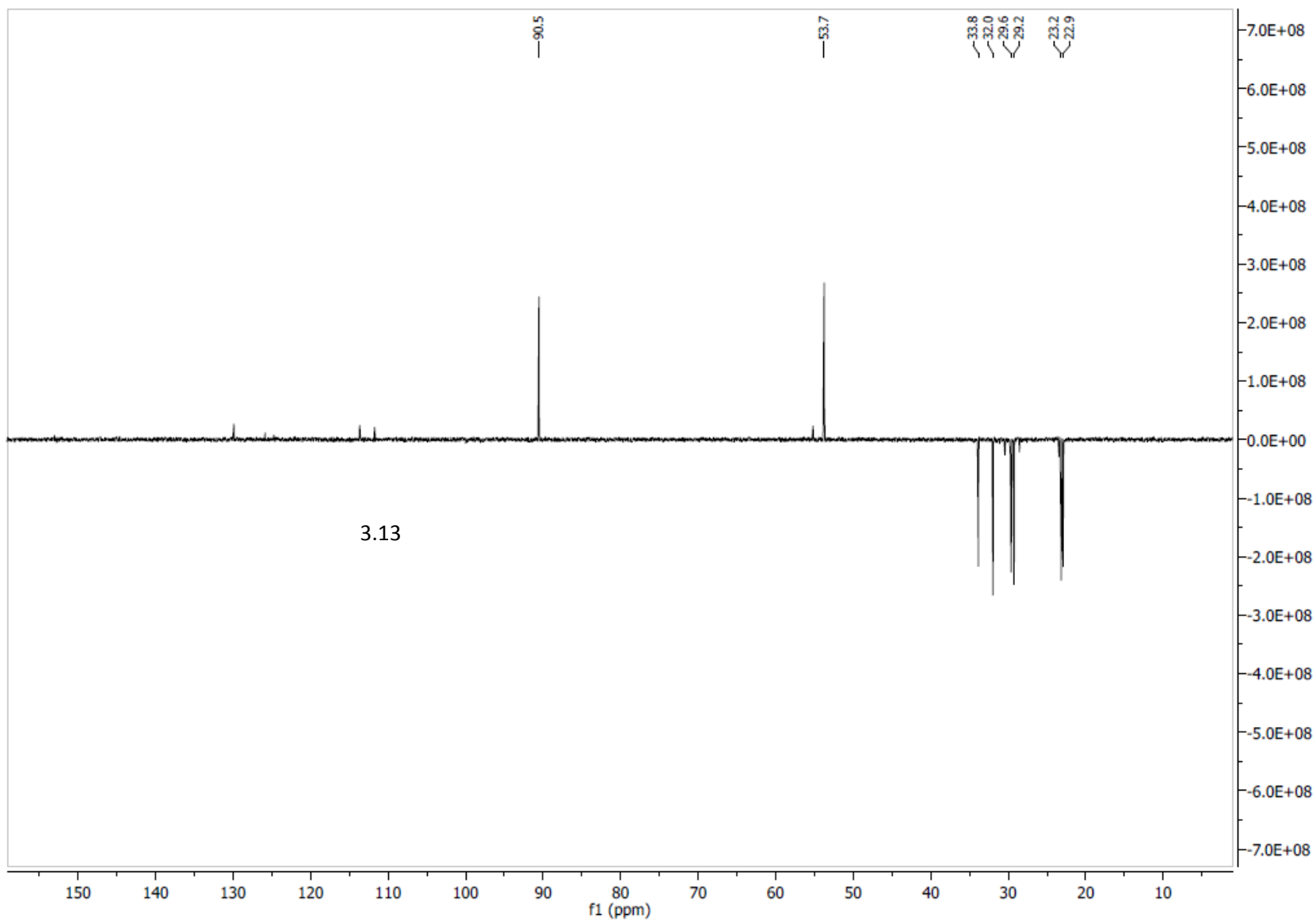
3.13

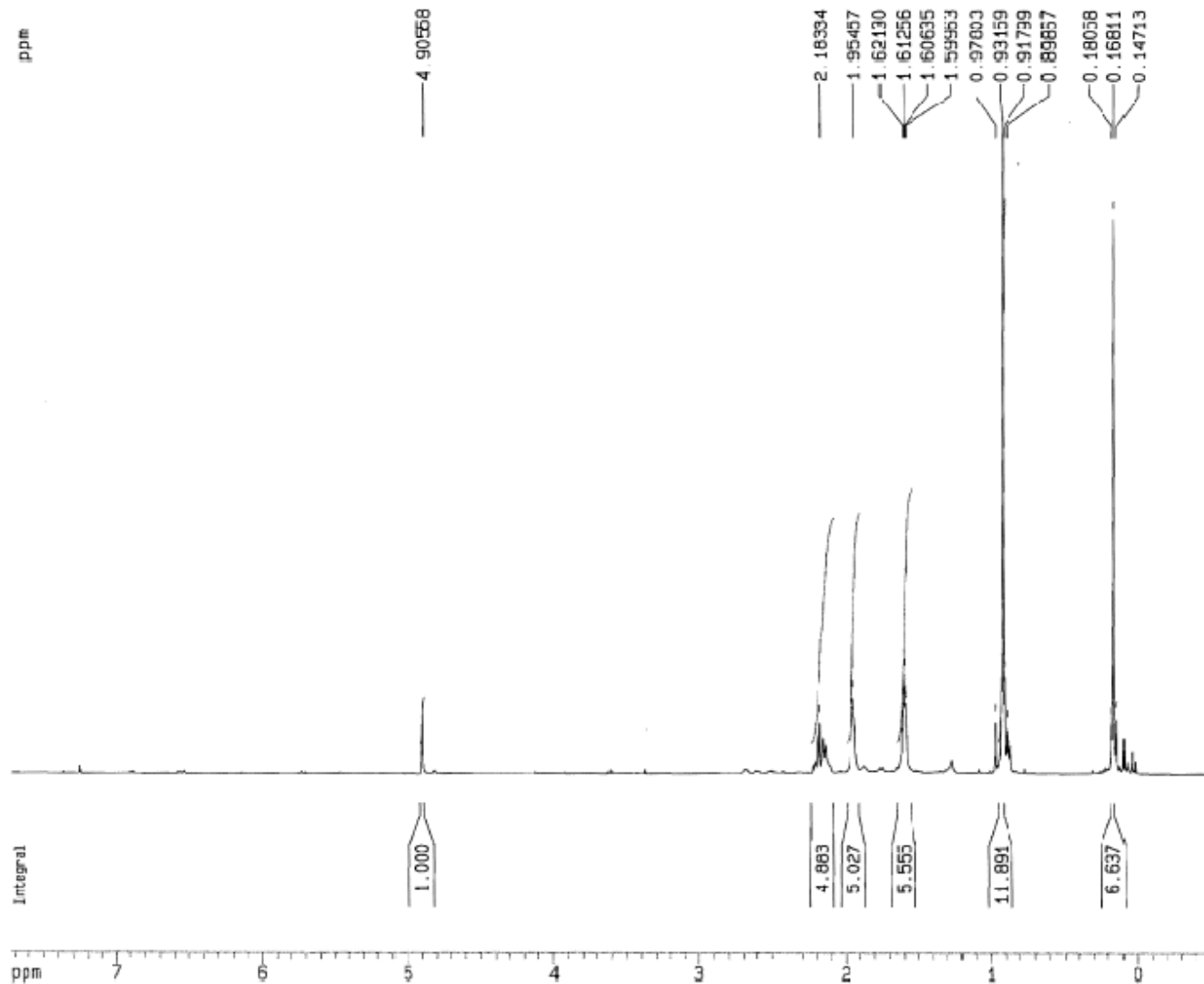


Parameter	Value
1 Spectrometer	spect
2 Solvent	CDCl3
3 Temperature	298.2
4 Pulse Sequence	zgpg30
5 Experiment	1D
6 Number of Scans	512
7 Receiver Gain	32800
8 Relaxation Delay	2.0000
9 Pulse Width	10.0000
10 Acquisition Time	1.3631
11 Spectrometer Frequency	100.62
12 Spectral Width	24038.5
13 Lowest Frequency	-1957.9
14 Nucleus	13C
15 Acquired Size	32768
16 Spectral Size	32768



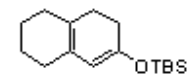
3.13



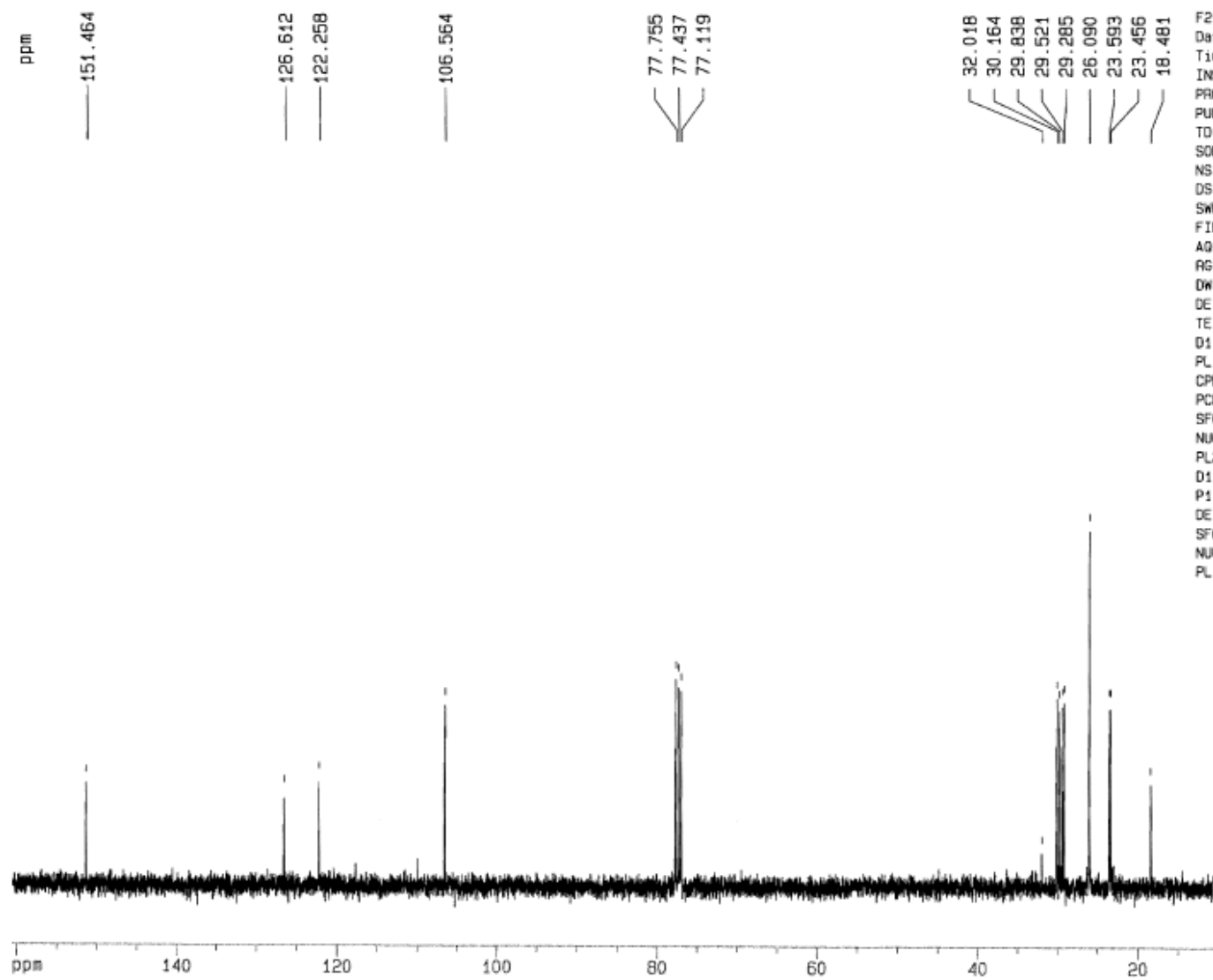


F2 - Acquisition Parameters
 Date_ 500000
 Time 9.34
 INSTRUM drx400
 PROBHD 5 mm Nalorac
 PULPROG zg30
 TD 32768
 SOLVENT1 CDCl3
 NS 8
 DS 0
 SWH 8250.825 Hz
 FIDRES 0.251795 Hz
 AQ 1.9857908 sec
 RG 40.3
 DW 60.600 usec
 DC 4.50 usec
 TE 300.0 K
 D1 1.00000000 sec
 P1 10.00 usec
 DE 4.50 usec
 SFO1 400.1324710 MHz
 NUC1 1H
 PL1 0.00 dB

F2 - Processing parameters
 SI 16384
 SF 400.1300092 MHz
 WDW EM
 SSB 0
 LB 0.30 HZ
 GB 0
 PC 1.00



3.14



F2 - Acquisition Parameters

Date_ 500000

Time 9.43

INSTRUM drx400

PROBHD 3 mm Nalorac

PULPROG zgdc30

TD 65536

SOLVENT CDCl3

NS 114

DS 2

SWH 22123.895 Hz

FIDRES 0.337584 Hz

AQ 1.4811636 sec

RG 8192

DW 22.500 usec

DE 4.50 usec

TE 300.0 K

D11 0.03000000 sec

PL12 18.00 dB

CPOPRG2 waltz15

PCPD2 100.00 usec

SFO2 400.1316005 MHz

NUC2 1H

PL2 0.00 dB

D1 2.00000000 sec

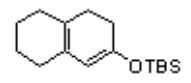
P1 9.00 usec

DE 4.50 usec

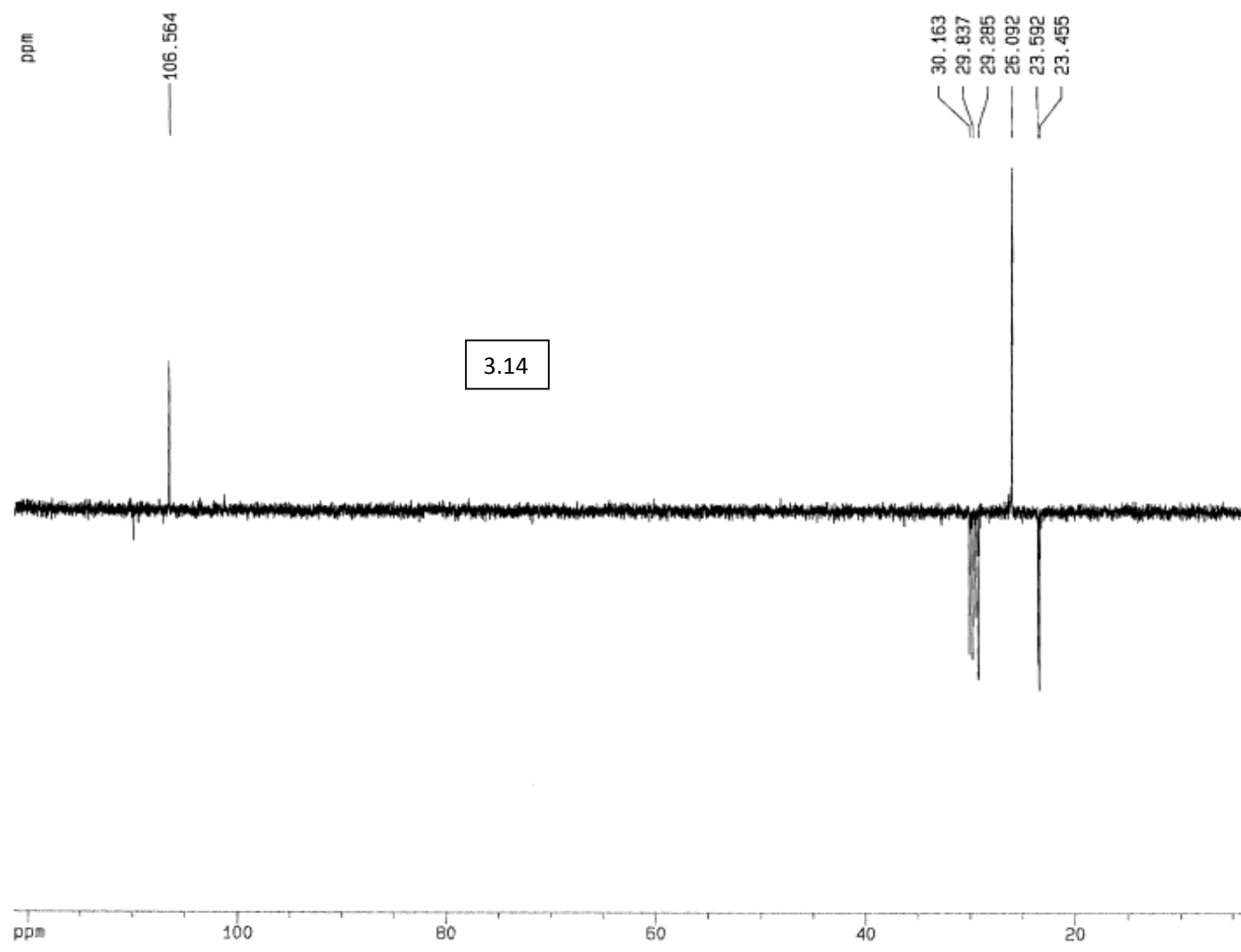
SFO1 100.6237964 MHz

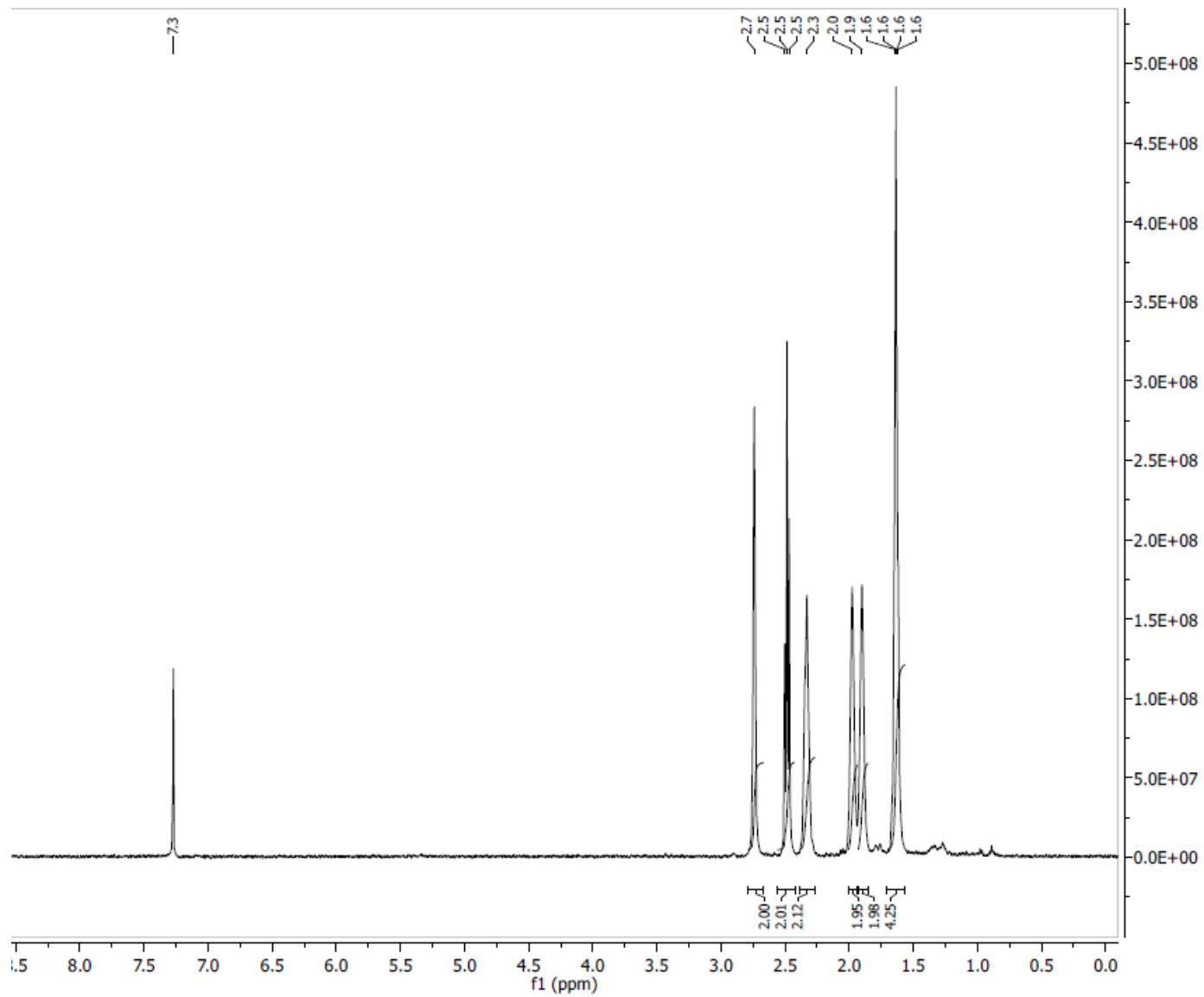
NUC1 13C

PL1 0.00 dB

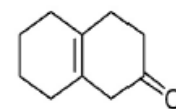


3.14

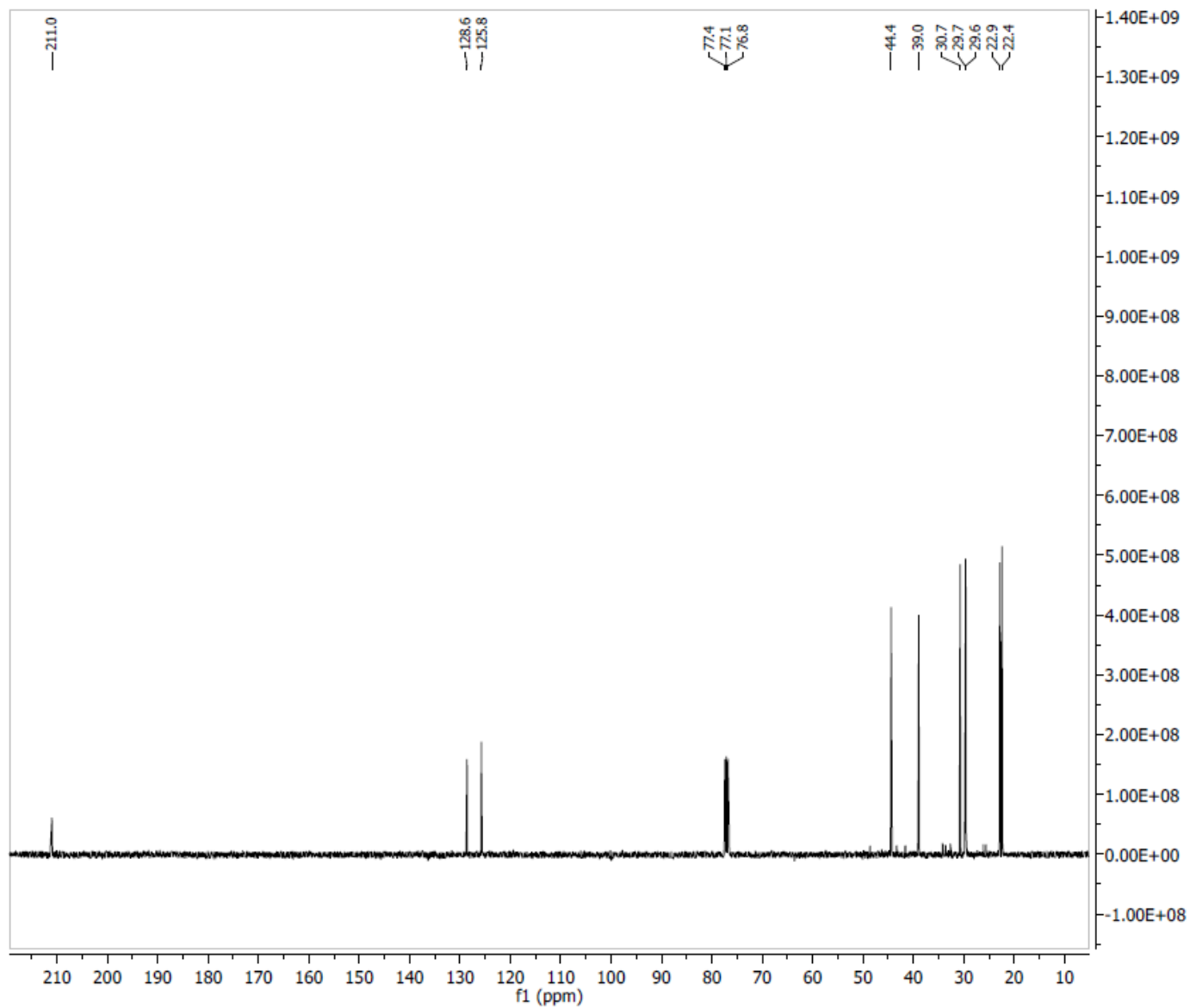




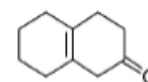
Parameter	Value
1 Spectrometer	spect
2 Solvent	CDC13
3 Temperature	298.2
4 Pulse Sequence	zg30
5 Experiment	1D
6 Number of Scans	2
7 Receiver Gain	456
8 Relaxation Delay	1.0000
9 Pulse Width	10.2500
10 Acquisition Time	3.9846
11 Spectrometer Frequency	400.15
12 Spectral Width	8223.7
13 Lowest Frequency	-1640.8
14 Nucleus	1H
15 Acquired Size	32768
16 Spectral Size	32768



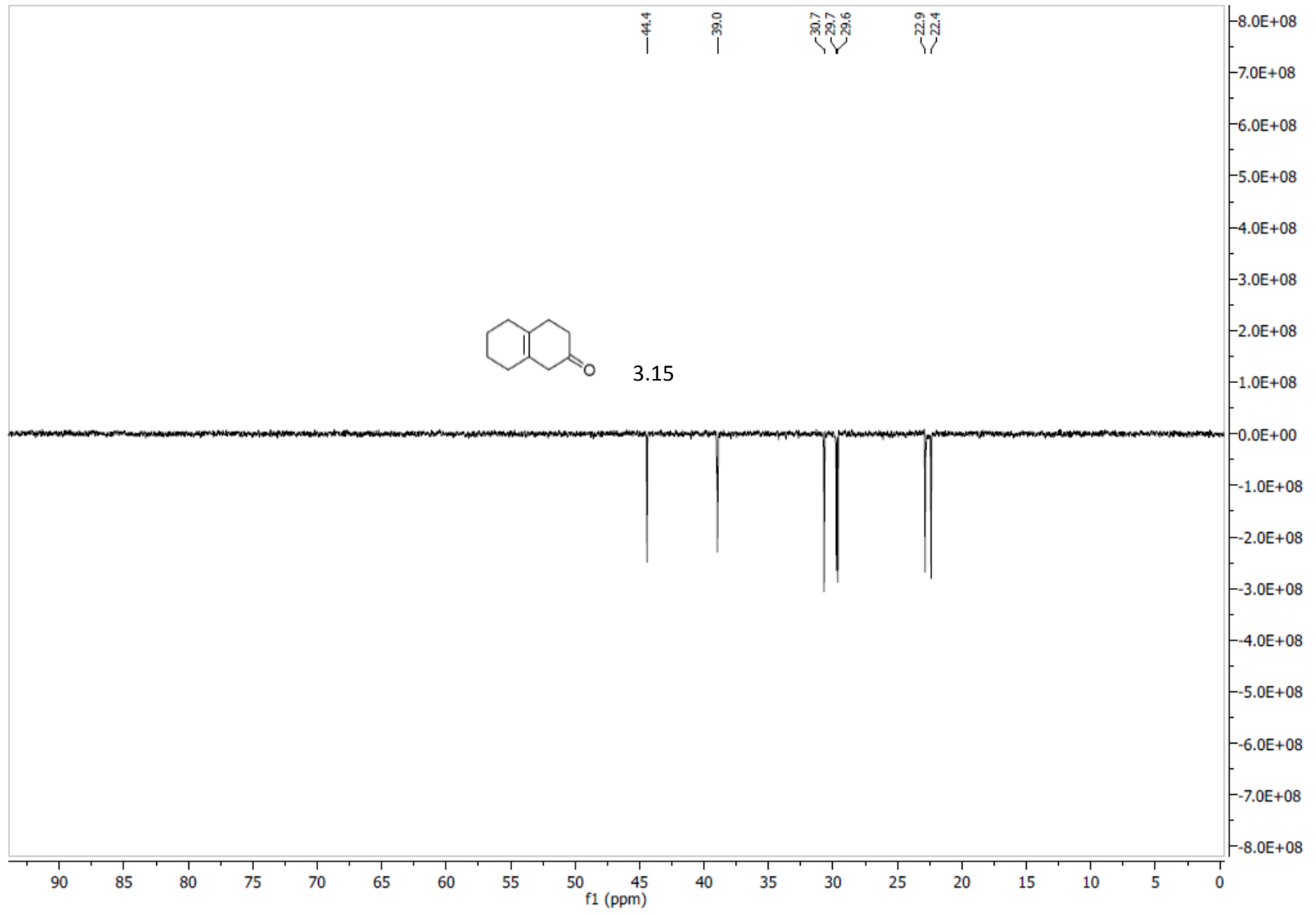
3.15

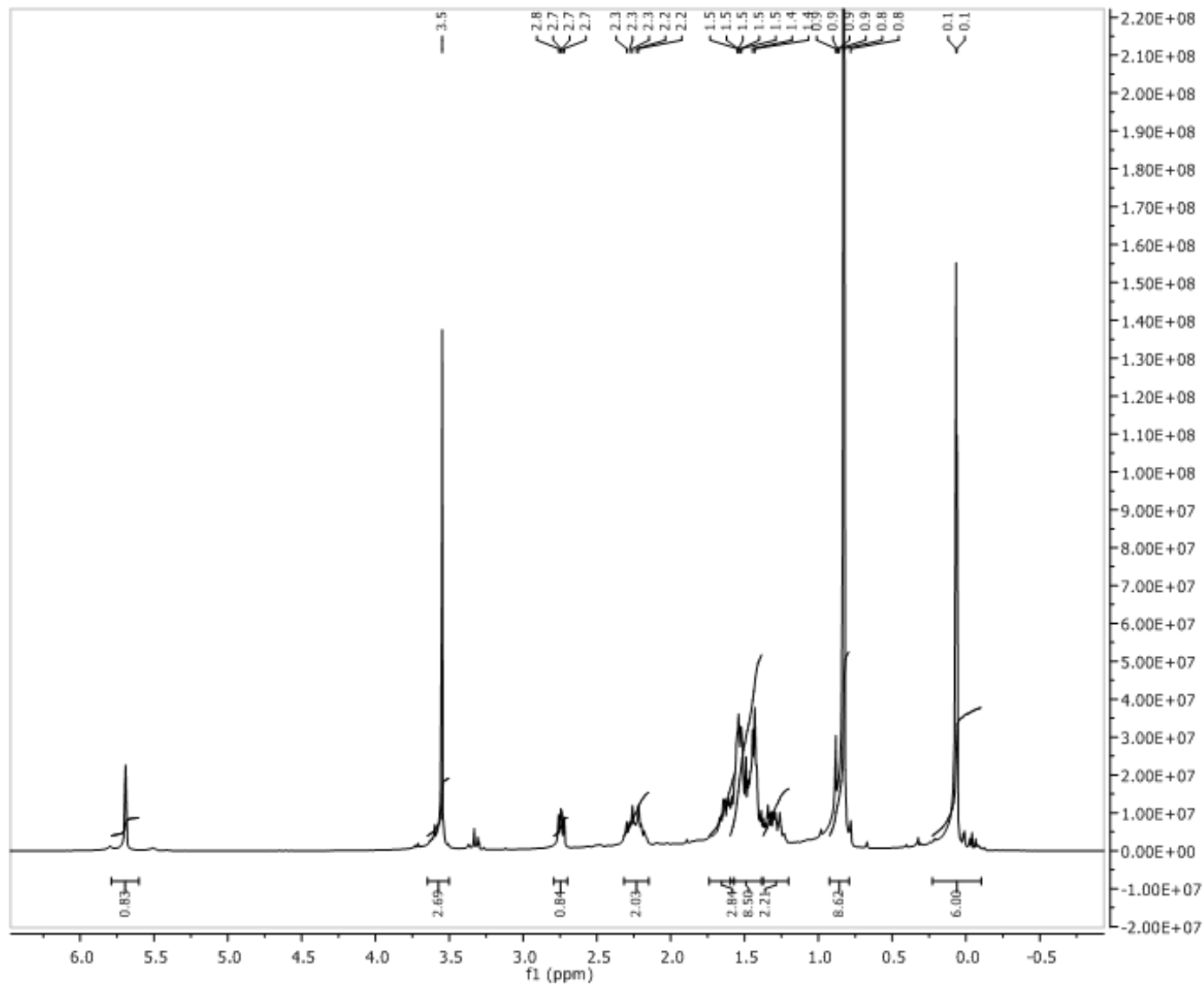


Parameter	Value
1 Spectrometer	spect
2 Solvent	CDCB
3 Temperature	298.2
4 Pulse Sequence	zgpg30
5 Experiment	1D
6 Number of Scans	512
7 Receiver Gain	32800
8 Relaxation Delay	2.0000
9 Pulse Width	10.0000
10 Acquisition Time	1.3631
11 Spectrometer Frequency	100.62
12 Spectral Width	24038.5
13 Lowest Frequency	-1957.9
14 Nucleus	13C
15 Acquired Size	32768
16 Spectral Size	32768

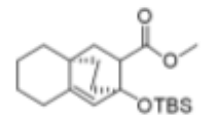


3.15

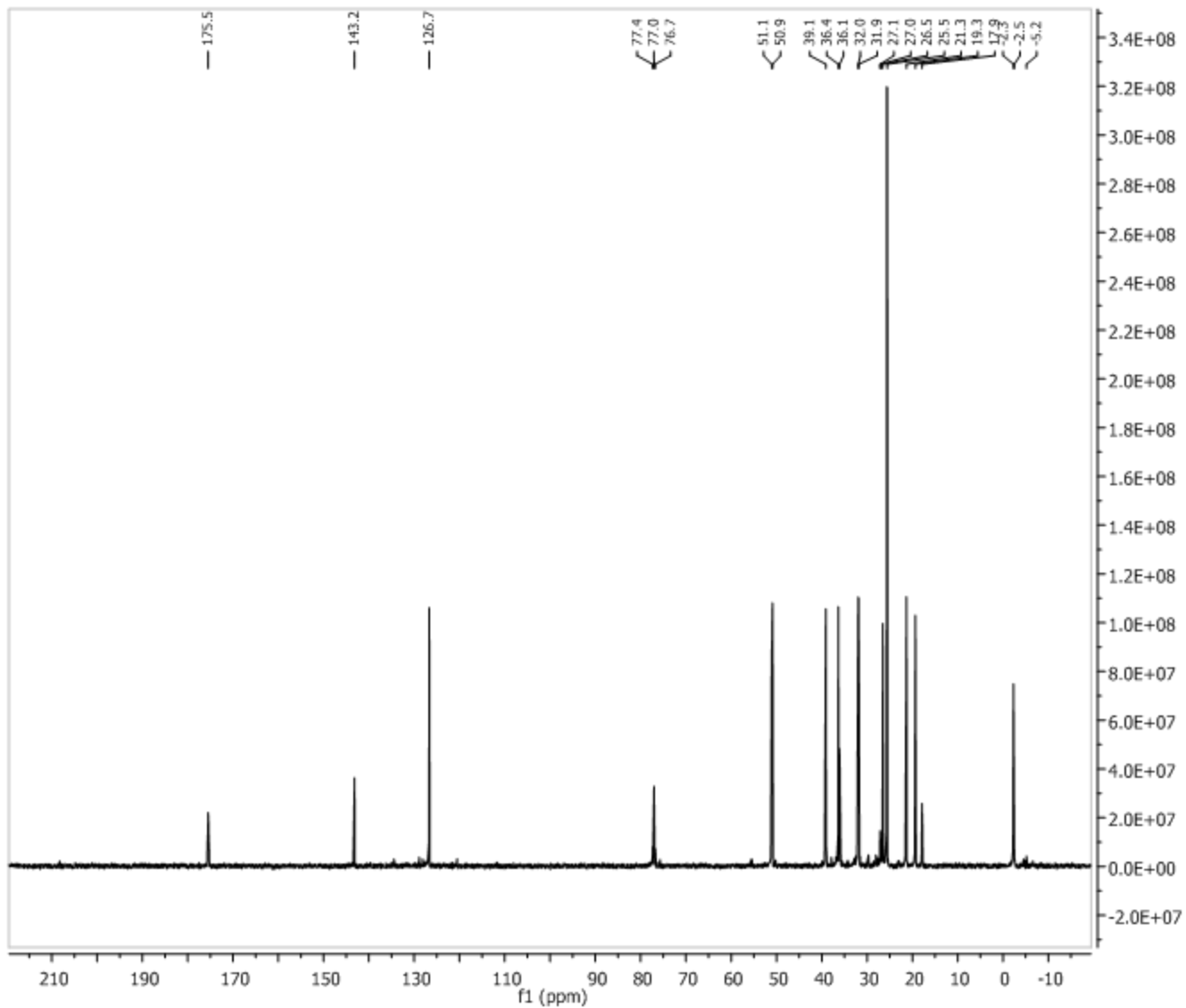




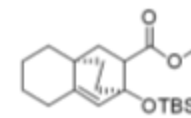
Parameter	Value
1 Spectrometer	spect
2 Solvent	CDCl3
3 Temperature	300.2
4 Pulse Sequence	zg30
5 Experiment	1D
6 Number of Scans	16
7 Receiver Gain	72
8 Relaxation Delay	1.0000
9 Pulse Width	10.0000
10 Acquisition Time	3.9846
11 Spectrometer Frequency	400.15
12 Spectral Width	8223.7
13 Lowest Frequency	-1640.8
14 Nucleus	1H
15 Acquired Size	32768
16 Spectral Size	32768



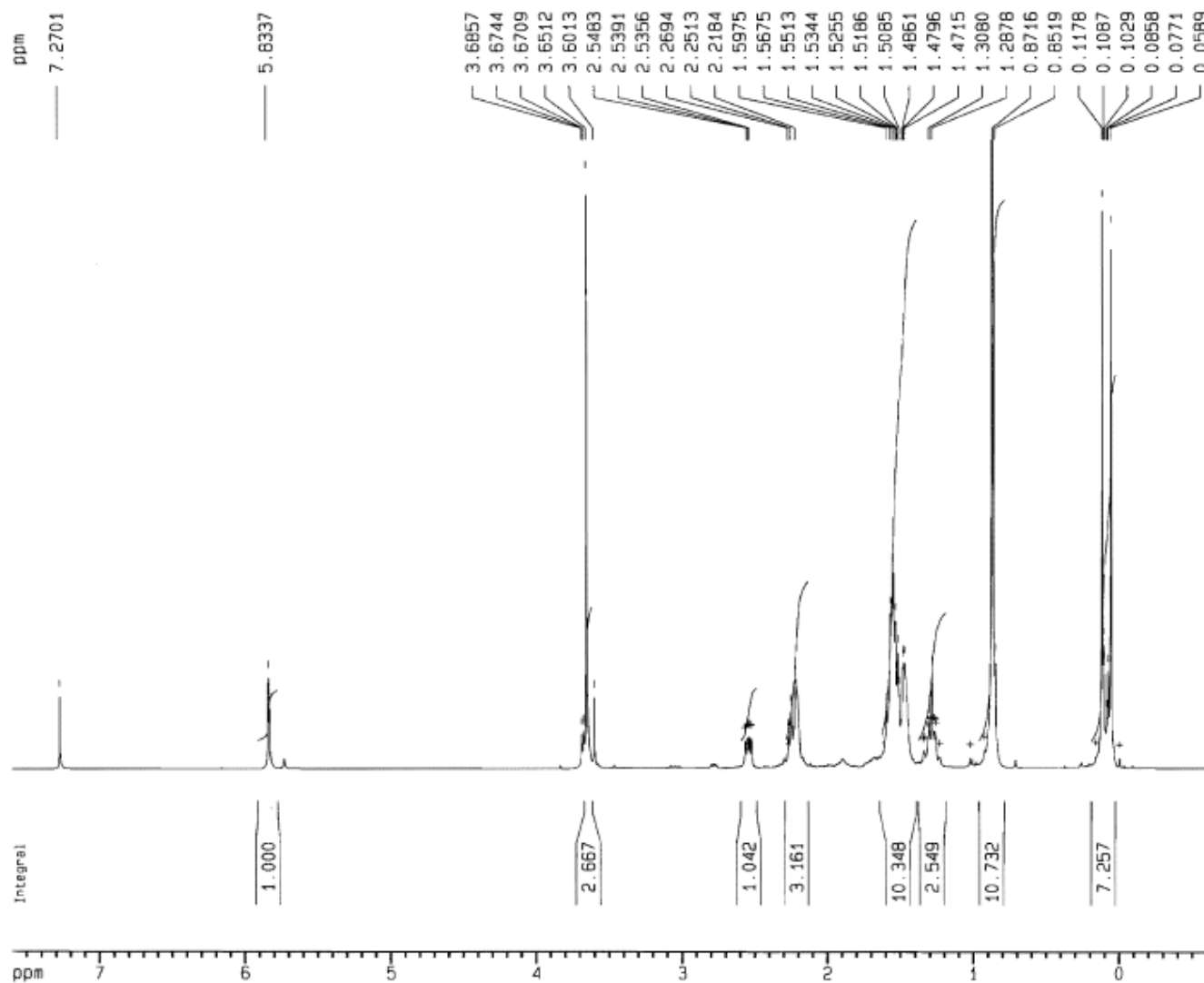
3.18



Parameter	Value
1 Spectrometer	spect
2 Solvent	CDCl3
3 Temperature	300.2
4 Pulse Sequence	zgpg30
5 Experiment	1D
6 Number of Scans	256
7 Receiver Gain	32800
8 Relaxation Delay	2.0000
9 Pulse Width	10.0000
10 Acquisition Time	1.3631
11 Spectrometer Frequency	100.62
12 Spectral Width	24038.5
13 Lowest Frequency	-1957.9
14 Nucleus	13C
15 Acquired Size	32768
16 Spectral Size	32768



3.18

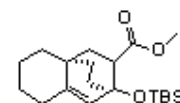


F2 - Acquisition Parameters

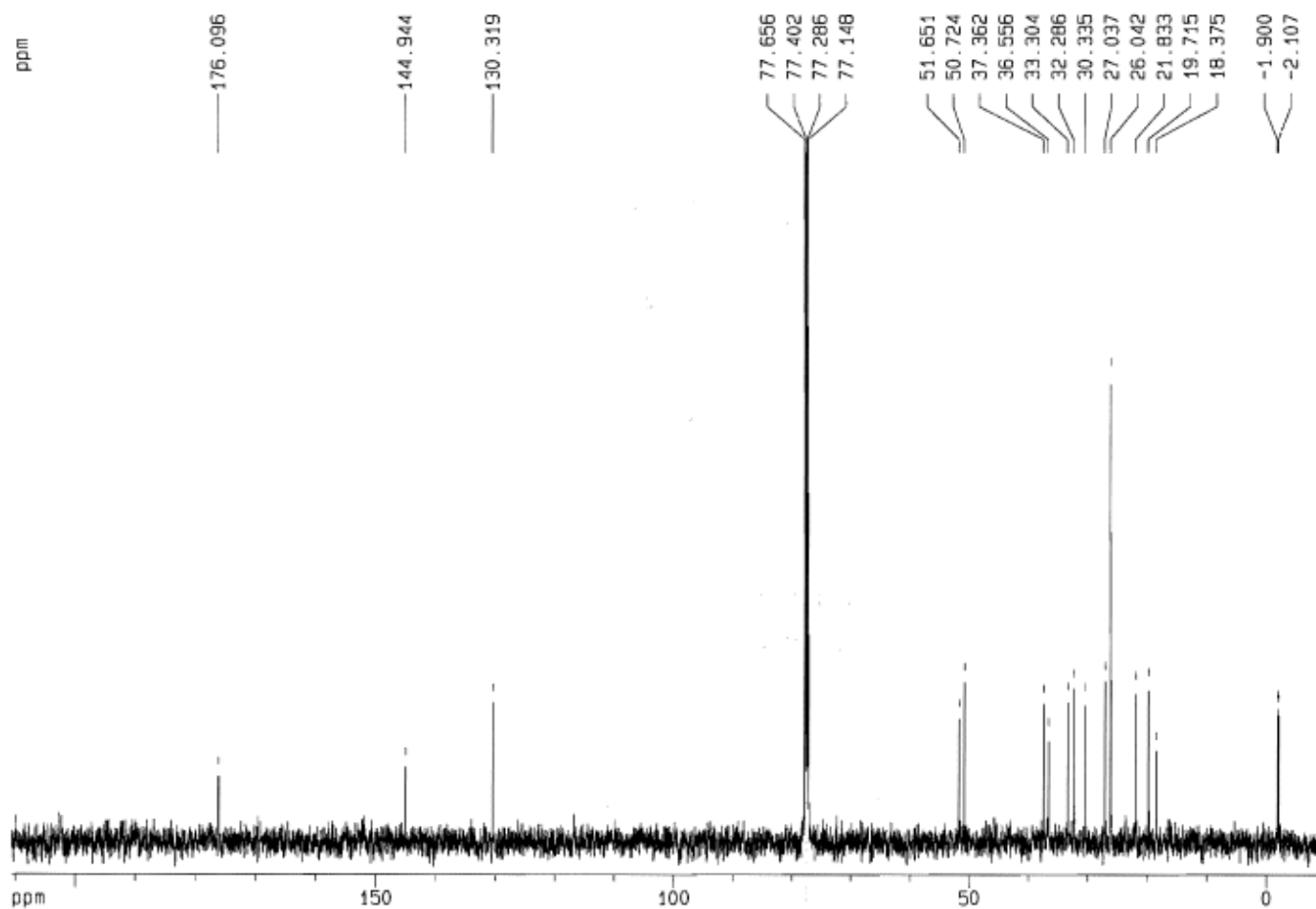
Date_	500000
Time	14.46
INSTRUM	drx400
PROBHD	3 mm Nalorac
PULPROG	zg30
TD	32768
SOLVENT	CDCl3
NS	8
DS	2
SWH	8250.825 Hz
FIDRES	0.251795 Hz
AQ	1.9857908 sec
RG	90.5
DM	60.600 usec
DE	4.50 usec
TE	300.0 K
D1	1.00000000 sec
P1	7.50 usec
DE	4.50 usec
SFO1	400.1324710 MHz
NUC1	1H
PL1	-3.00 dB

F2 - Processing parameters

SI	16384
SF	400.1300052 MHz
WDM	EM
SSB	0
LB	0.30 Hz
GB	0
PC	1.00



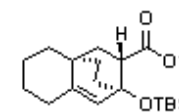
3.17



F2 - Acquisition Parameters
 Date_ 20001204
 Time 13.40
 INSTRUM spect
 PROBHD 3mm Nalorac Du
 PULPROG zgdc30
 TD 32768
 SOLVENT CDCl3
 NS 1024
 OS 0
 SMH 30303.031 Hz
 FIDRES 0.924775 Hz
 AQ 0.5407220 sec
 RG 8192
 DM 16.500 usec
 DE 5.93 usec
 TE 300.0 K
 D1 3.0000000 sec
 d11 0.0300000 sec

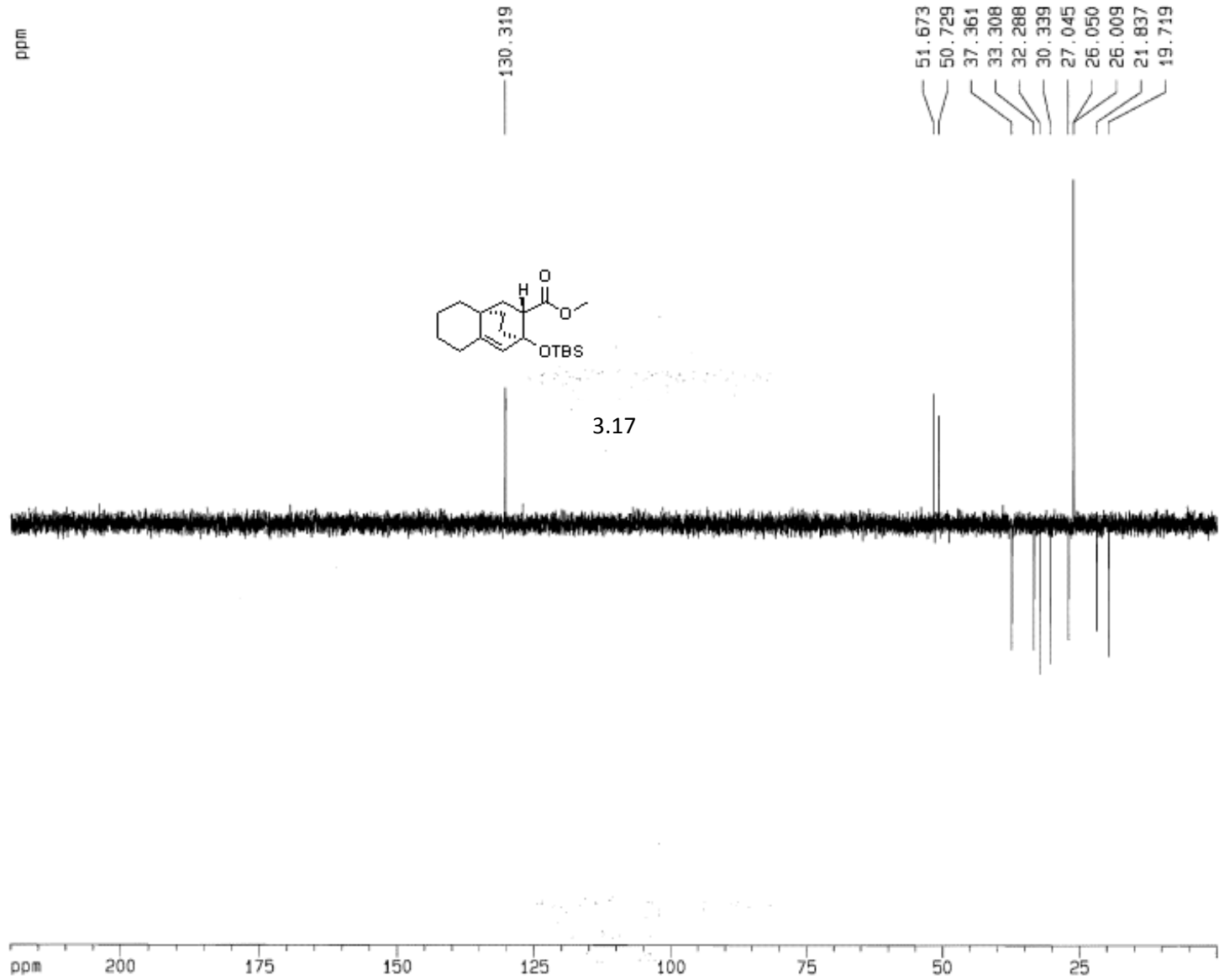
----- CHANNEL f1 -----
 NUC1 13C
 P1 8.00 usec
 PL1 3.00 dB
 SF01 125.7715724 MHz

----- CHANNEL f2 -----
 CPDPRG2 waltz16
 NUC2 1H
 PCPD2 100.00 usec
 PL2 3.00 dB
 PL12 22.00 dB
 SF02 500.1320005 MHz

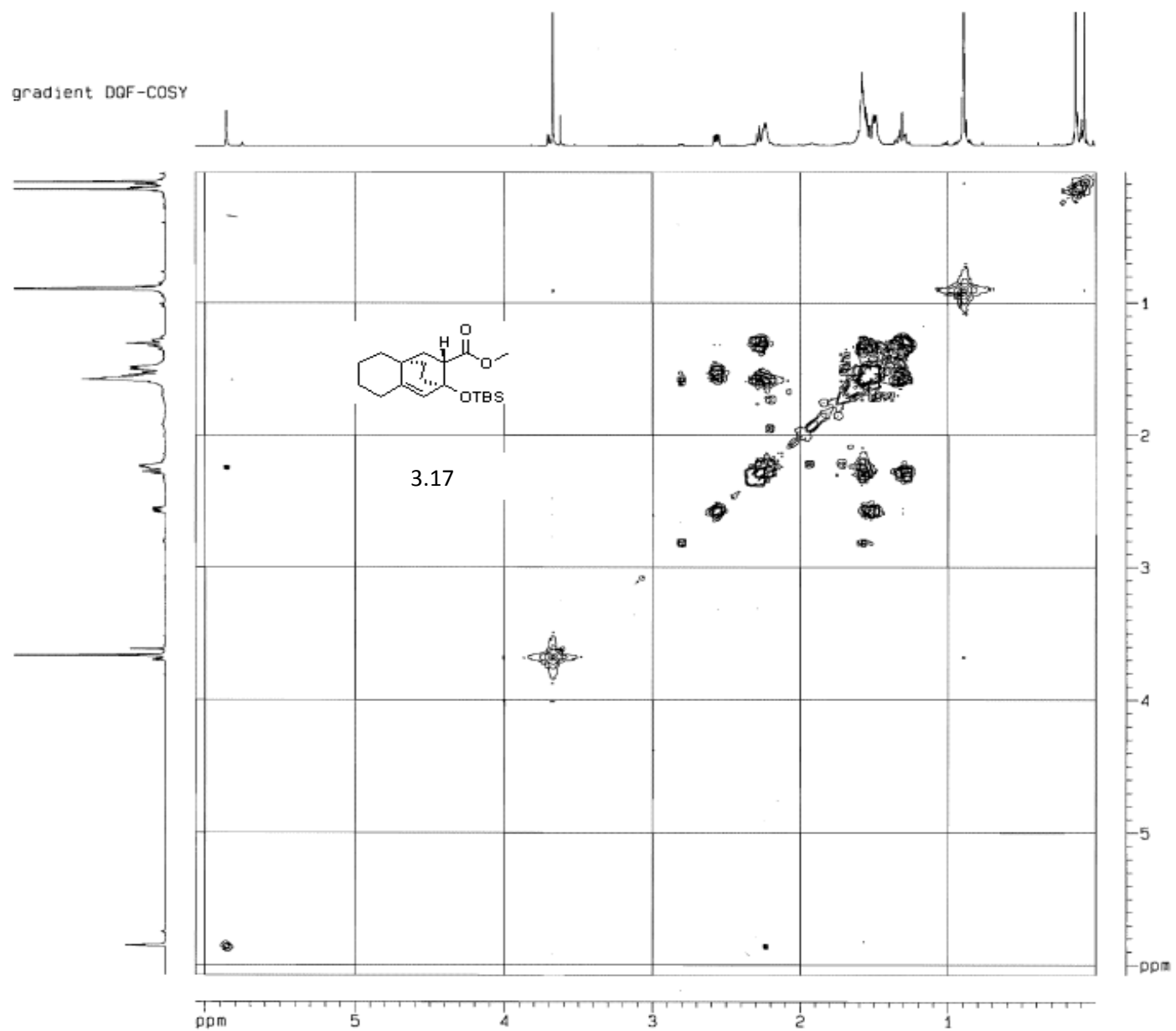


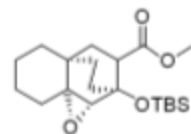
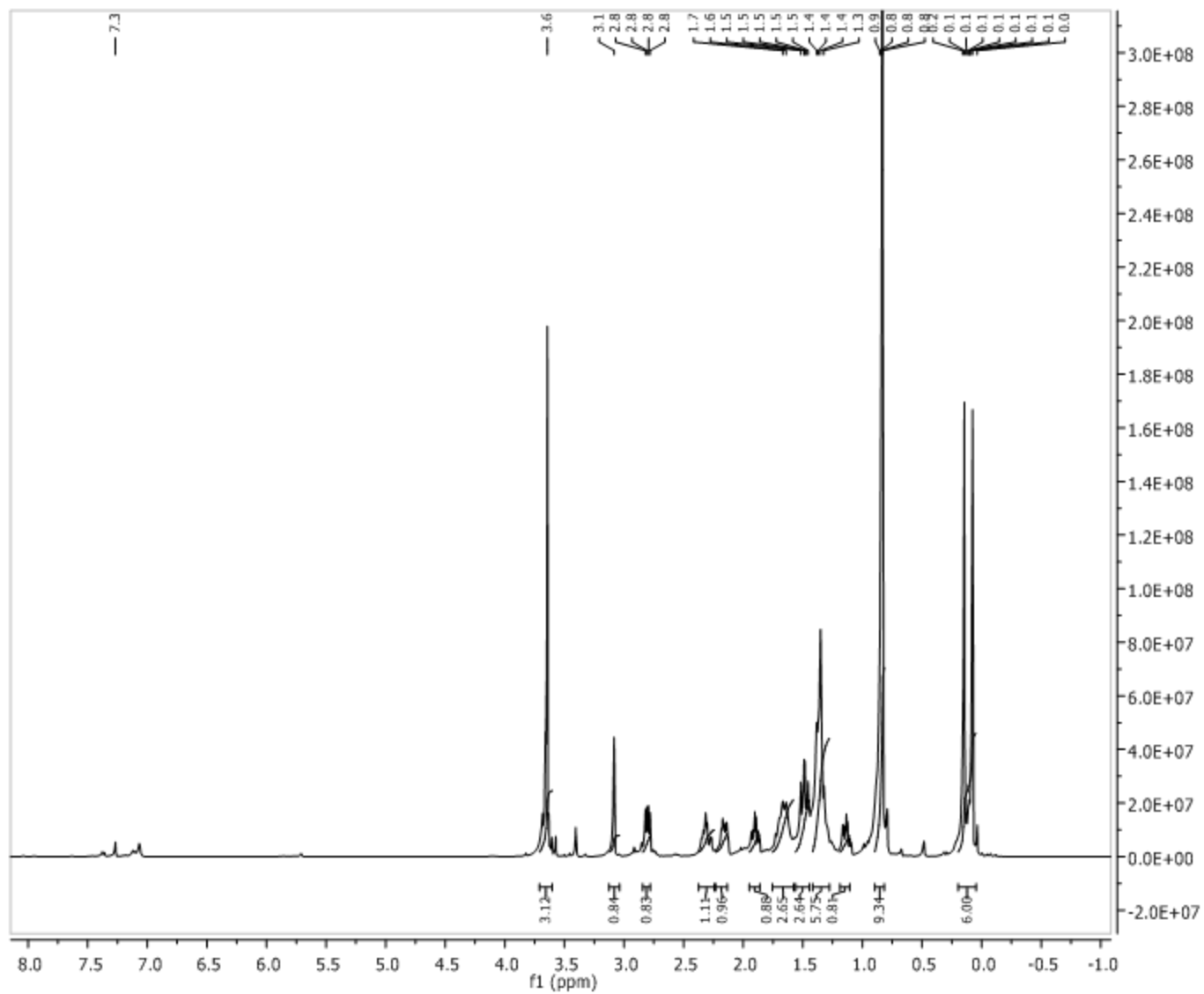
3.17

ppm

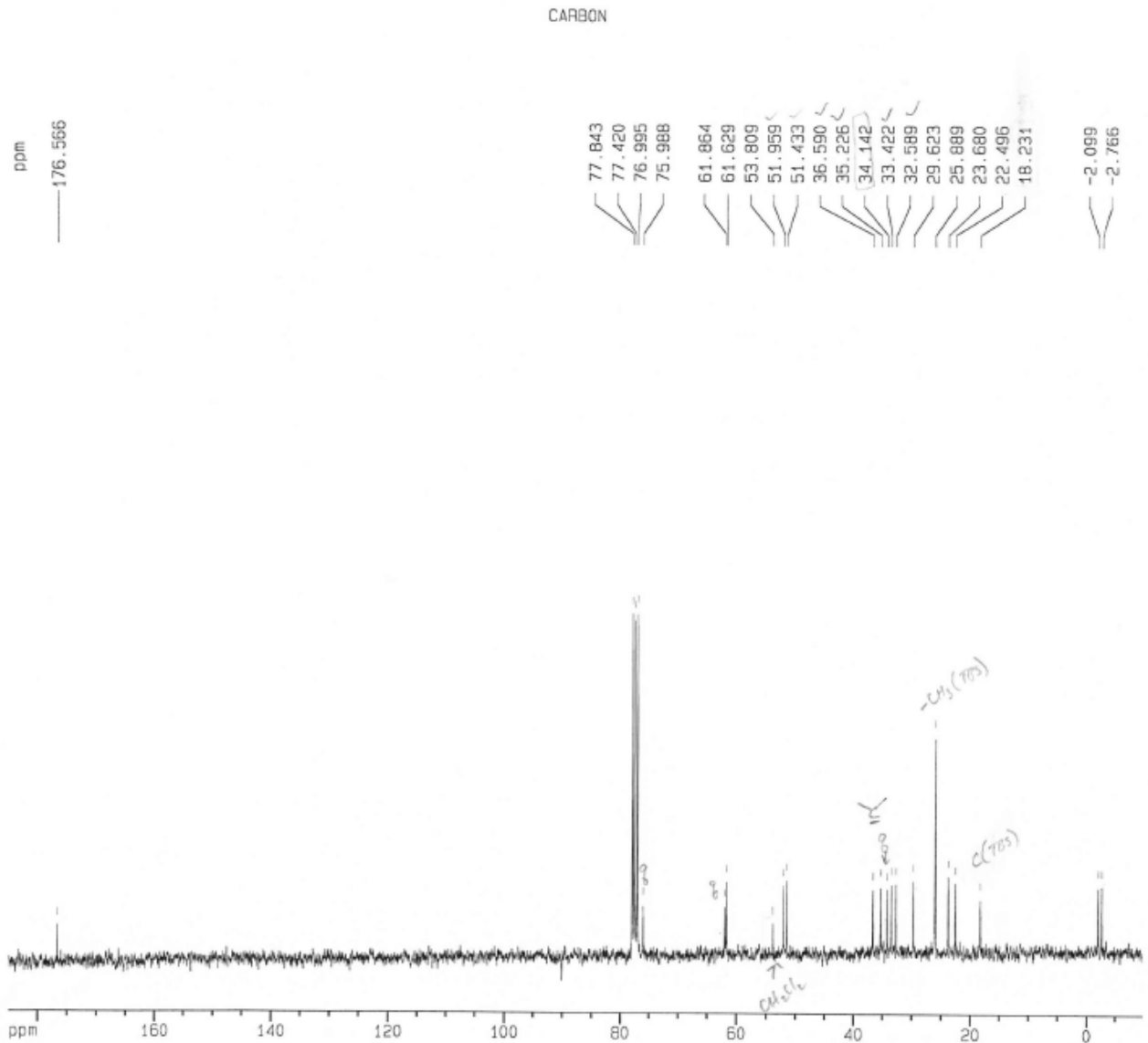


gradient DQF-COSY





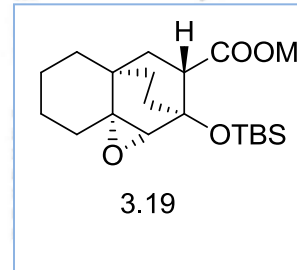
3.19

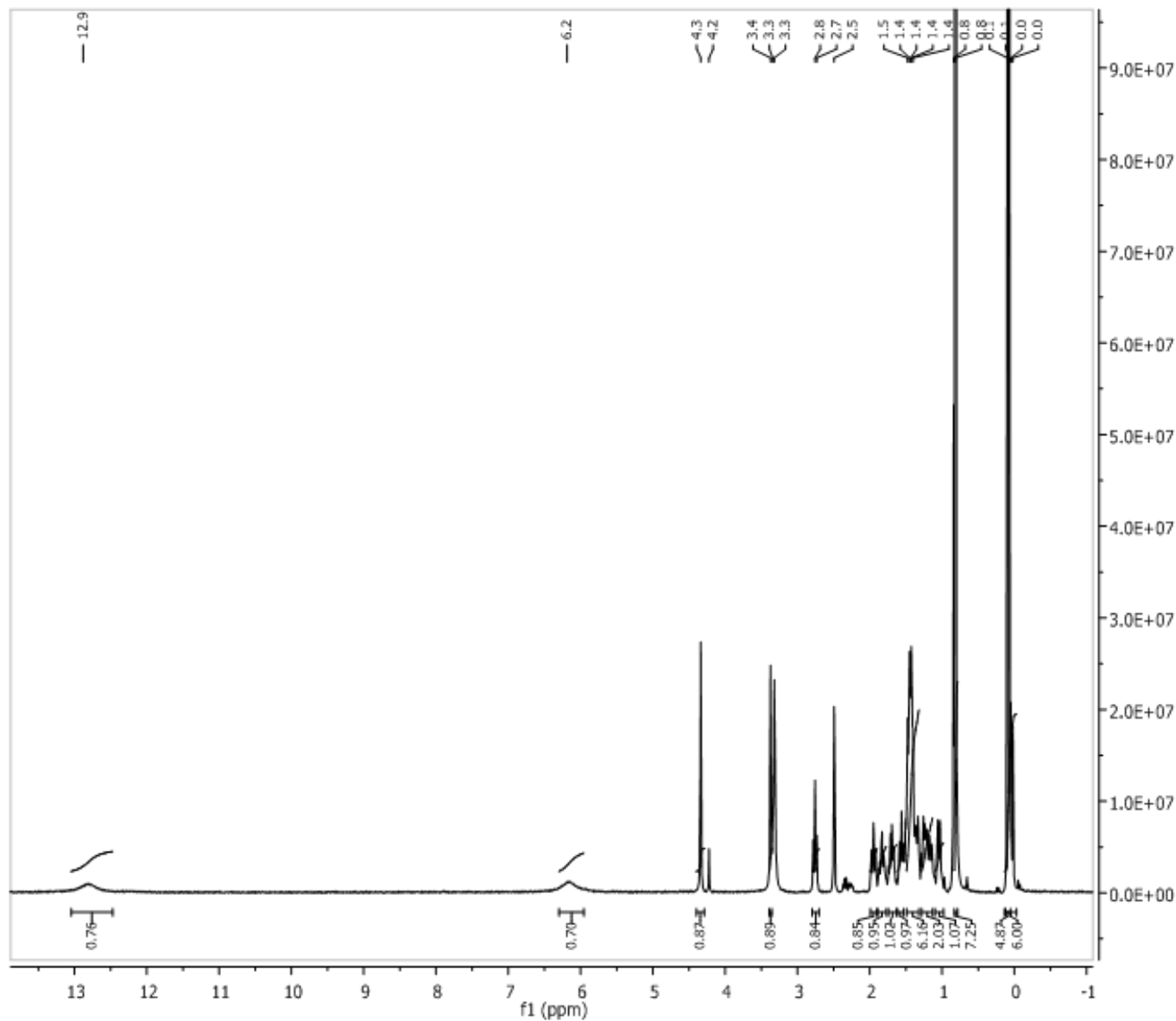


Current Data Parameters
 NAME epoxyDAester
 EXPNO 2
 PROCNO 1

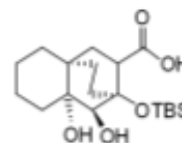
F2 - Acquisition Parameters
 Date_ 500000
 Time 15.32
 INSTRUM spect
 PROBHD 5 mm Nalorac
 PULPRDG zgpg30
 TD 32768
 SOLVENT CDCl3
 NS 1257
 DS 2
 SMH 16666.666 Hz
 FIDRES 0.508626 Hz
 AQ 0.9830900 sec
 RG 2298.8
 DM 30.000 usec
 DE 4.50 usec
 TE 300.0 K
 D11 0.0300000 sec
 PL12 18.00 dB
 CPDPRG2 waltz16
 PCPD2 90.00 usec
 SF02 300.1312005 MHz
 NUC2 1H
 PL2 -3.00 dB
 D1 3.0000000 sec
 P1 6.50 usec
 DE 4.50 usec
 SF01 75.4745111 MHz
 NUC1 13C
 PL1 -3.00 dB

F2 - Processing parameters
 SI 16384
 SF 75.4677190 MHz
 MDW EM
 SSB 0

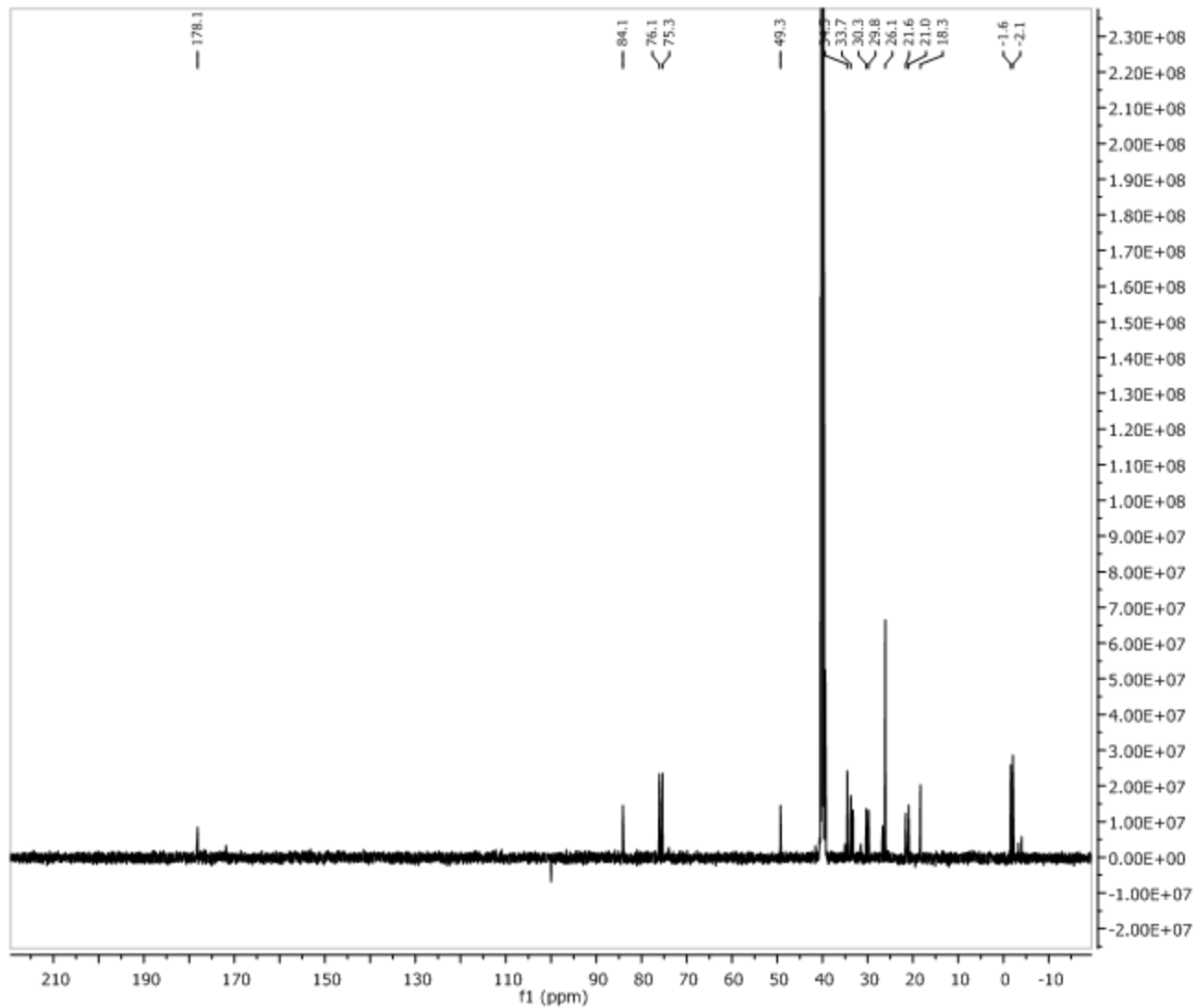




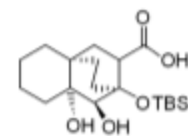
Parameter	Value
1 Spectrometer	spect
2 Solvent	DMSO
3 Temperature	298.2
4 Pulse Sequence	zg30
5 Experiment	1D
6 Number of Scans	4
7 Receiver Gain	256
8 Relaxation Delay	1.0000
9 Pulse Width	10.2500
10 Acquisition Time	3.9846
11 Spectrometer Frequency	400.15
12 Spectral Width	8223.7
13 Lowest Frequency	-1640.8
14 Nucleus	1H
15 Acquired Size	32768
16 Spectral Size	32768



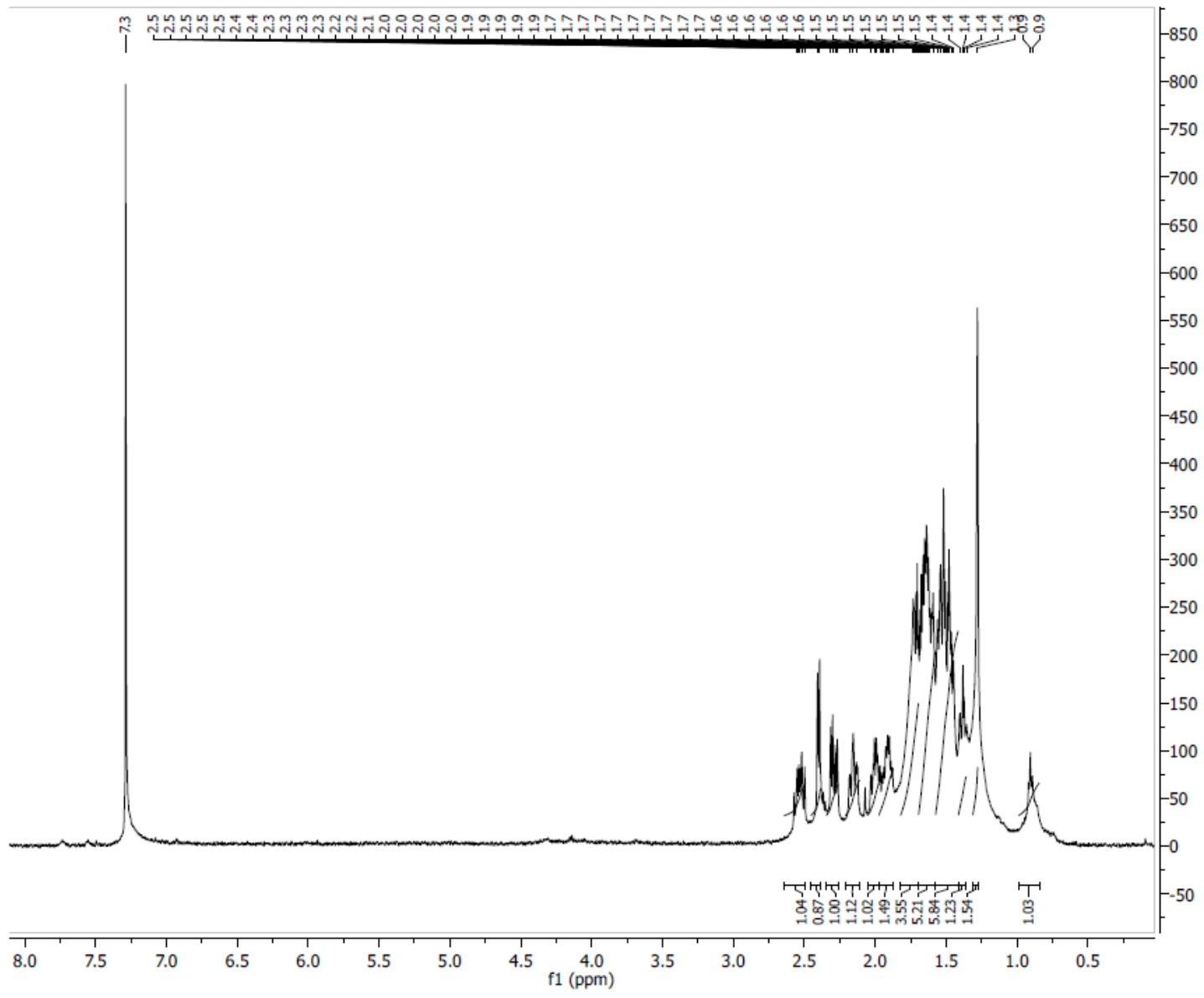
3.20



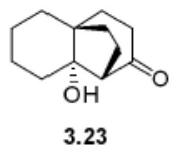
Parameter	Value
1 Spectrometer	spect
2 Solvent	DMSO
3 Temperature	298.2
4 Pulse Sequence	zgpg30
5 Experiment	1D
6 Number of Scans	2801
7 Receiver Gain	32800
8 Relaxation Delay	2.0000
9 Pulse Width	10.0000
10 Acquisition Time	1.3631
11 Spectrometer Frequency	100.62
12 Spectral Width	24038.5
13 Lowest Frequency	-1957.9
14 Nucleus	13C
15 Acquired Size	32768
16 Spectral Size	32768

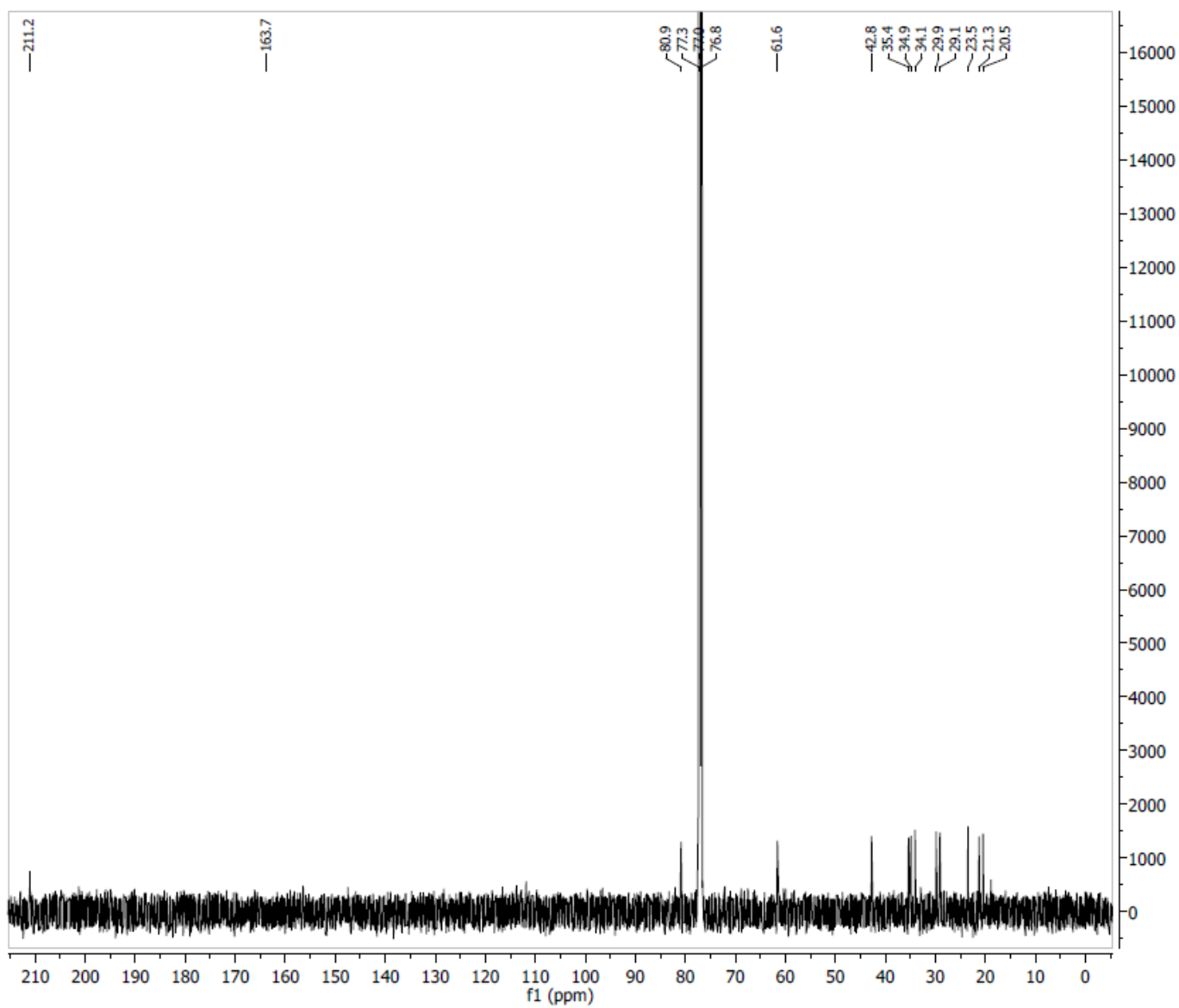


3.20

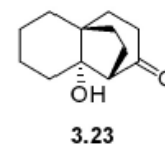


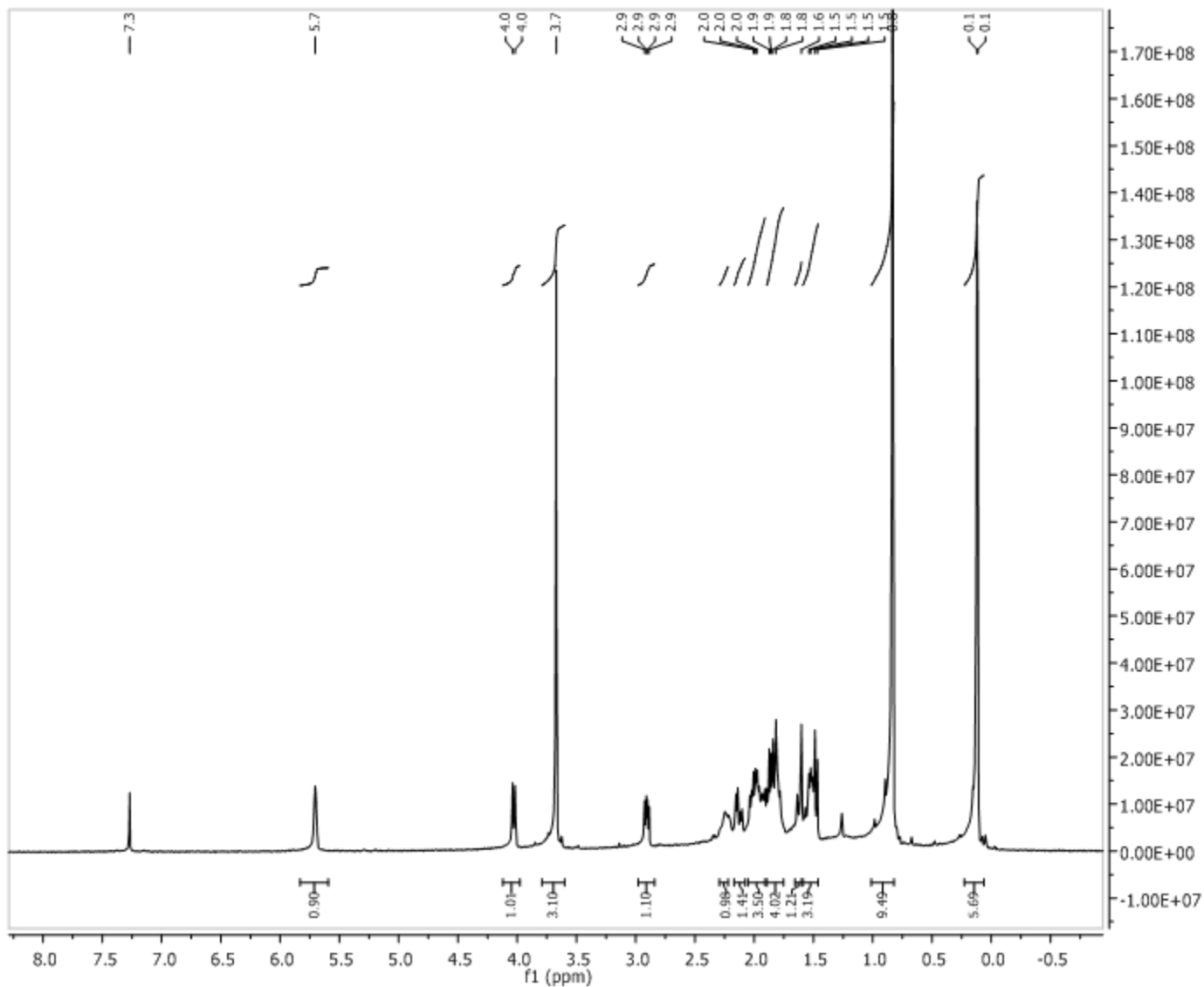
Parameter	Value
1 Spectrometer	spect
2 Solvent	CDCl3
3 Temperature	297.2
4 Pulse Sequence	zg30
5 Experiment	1D
6 Number of Scans	16
7 Receiver Gain	813
8 Relaxation Delay	1.0000
9 Pulse Width	11.0000
10 Acquisition Time	1.1698
11 Spectrometer Frequency	500.13
12 Spectral Width	7002.8
13 Lowest Frequency	-250.6
14 Nucleus	1H
15 Acquired Size	8192
16 Spectral Size	16384



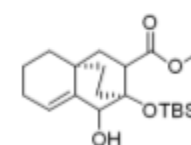


Parameter	Value
1 Spectrometer	spect
2 Solvent	CDCl3
3 Temperature	297.2
4 Pulse Sequence	zgpg30
5 Experiment	1D
6 Number of Scans	5120
7 Receiver Gain	9195
8 Relaxation Delay	3.0000
9 Pulse Width	11.0000
10 Acquisition Time	1.1797
11 Spectrometer Frequency	125.76
12 Spectral Width	27777.8
13 Lowest Frequency	-683.9

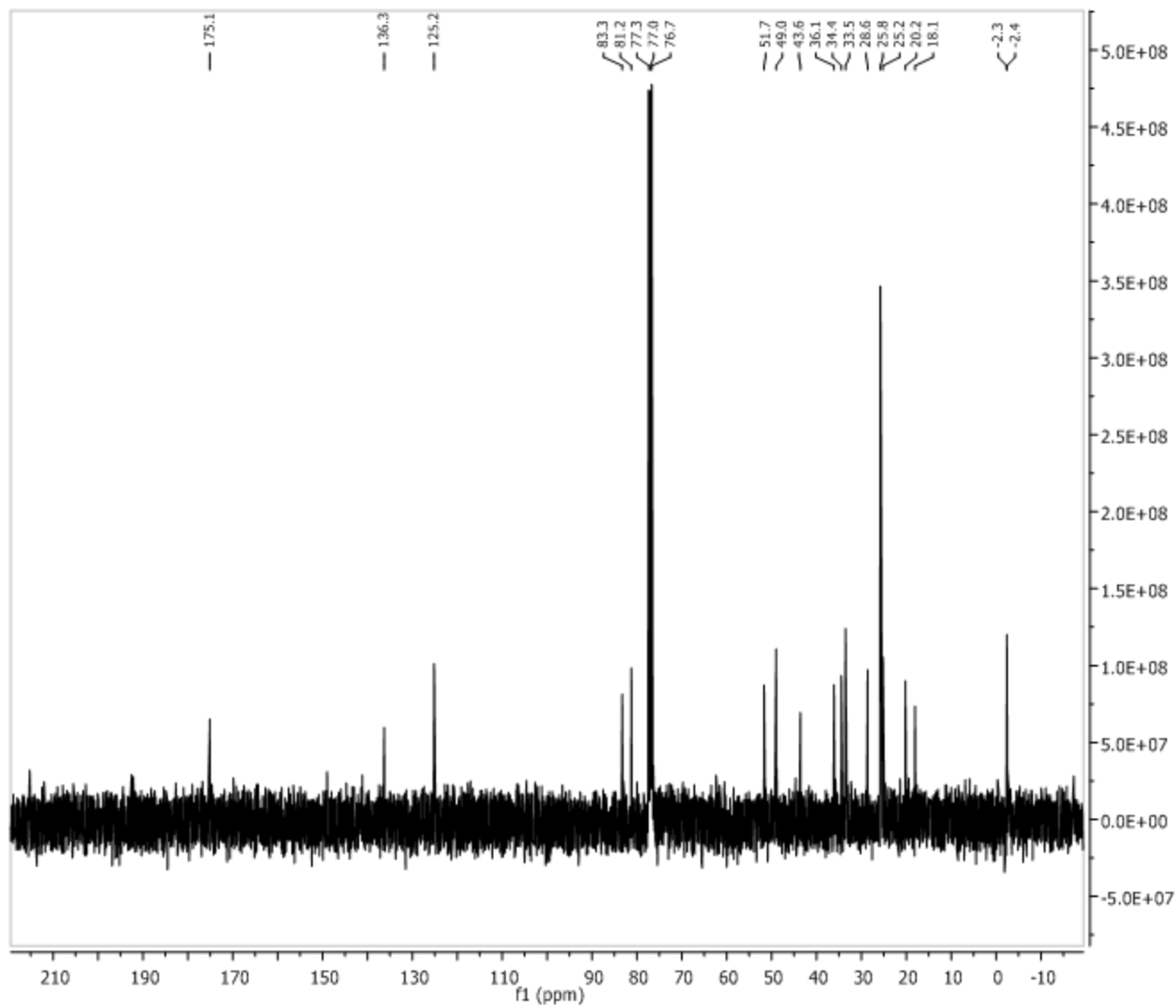




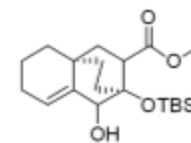
Parameter	Value
1 Spectrometer	spect
2 Solvent	CDCl3
3 Temperature	300.2
4 Pulse Sequence	zg30
5 Experiment	1D
6 Number of Scans	8
7 Receiver Gain	512
8 Relaxation Delay	1.0000
9 Pulse Width	10.0000
10 Acquisition Time	3.9846
11 Spectrometer Frequency	400.15
12 Spectral Width	8223.7
13 Lowest Frequency	-1640.8
14 Nucleus	1H
15 Acquired Size	32768
16 Spectral Size	32768



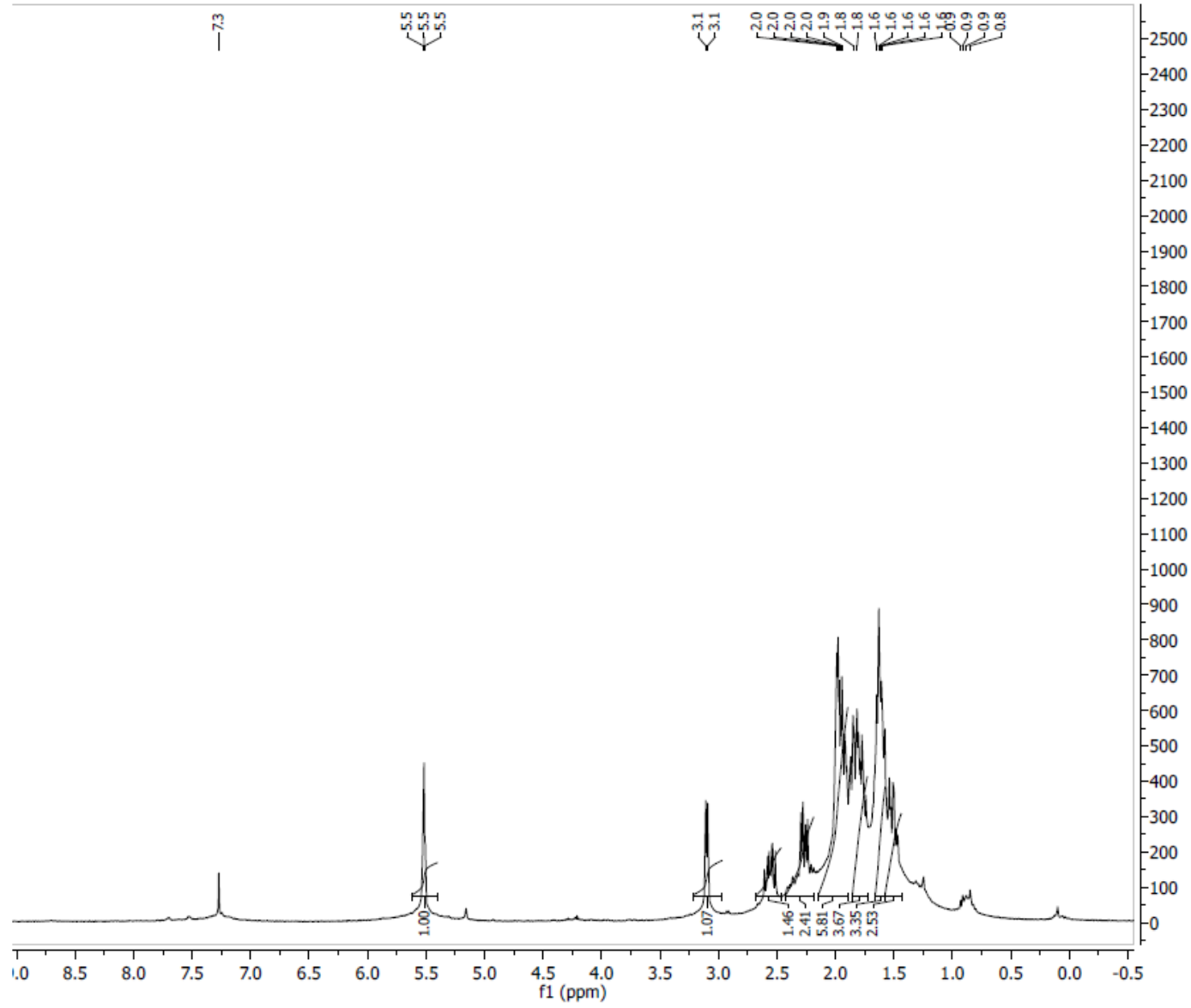
3.38



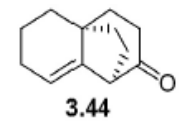
Parameter	Value
1 Spectrometer	spect
2 Solvent	CDCl3
3 Temperature	300.2
4 Pulse Sequence	zgpg30
5 Experiment	1D
6 Number of Scans	500
7 Receiver Gain	32800
8 Relaxation Delay	2.0000
9 Pulse Width	9.0000
10 Acquisition Time	1.3631
11 Spectrometer Frequency	100.62
12 Spectral Width	24038.5
13 Lowest Frequency	-1957.9
14 Nucleus	13C
15 Acquired Size	32768
16 Spectral Size	32768

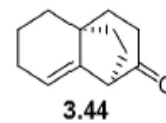
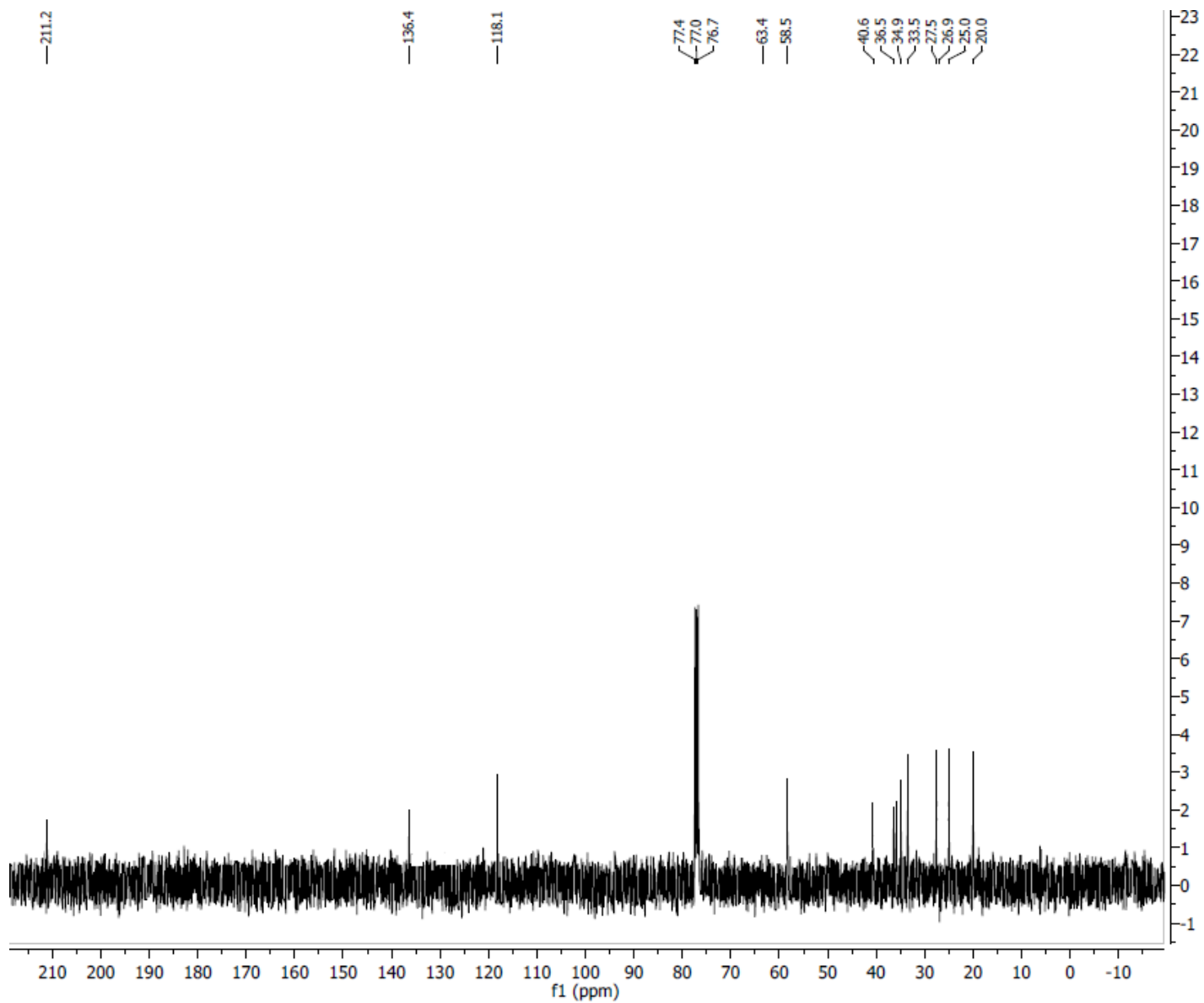


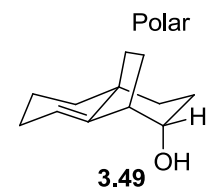
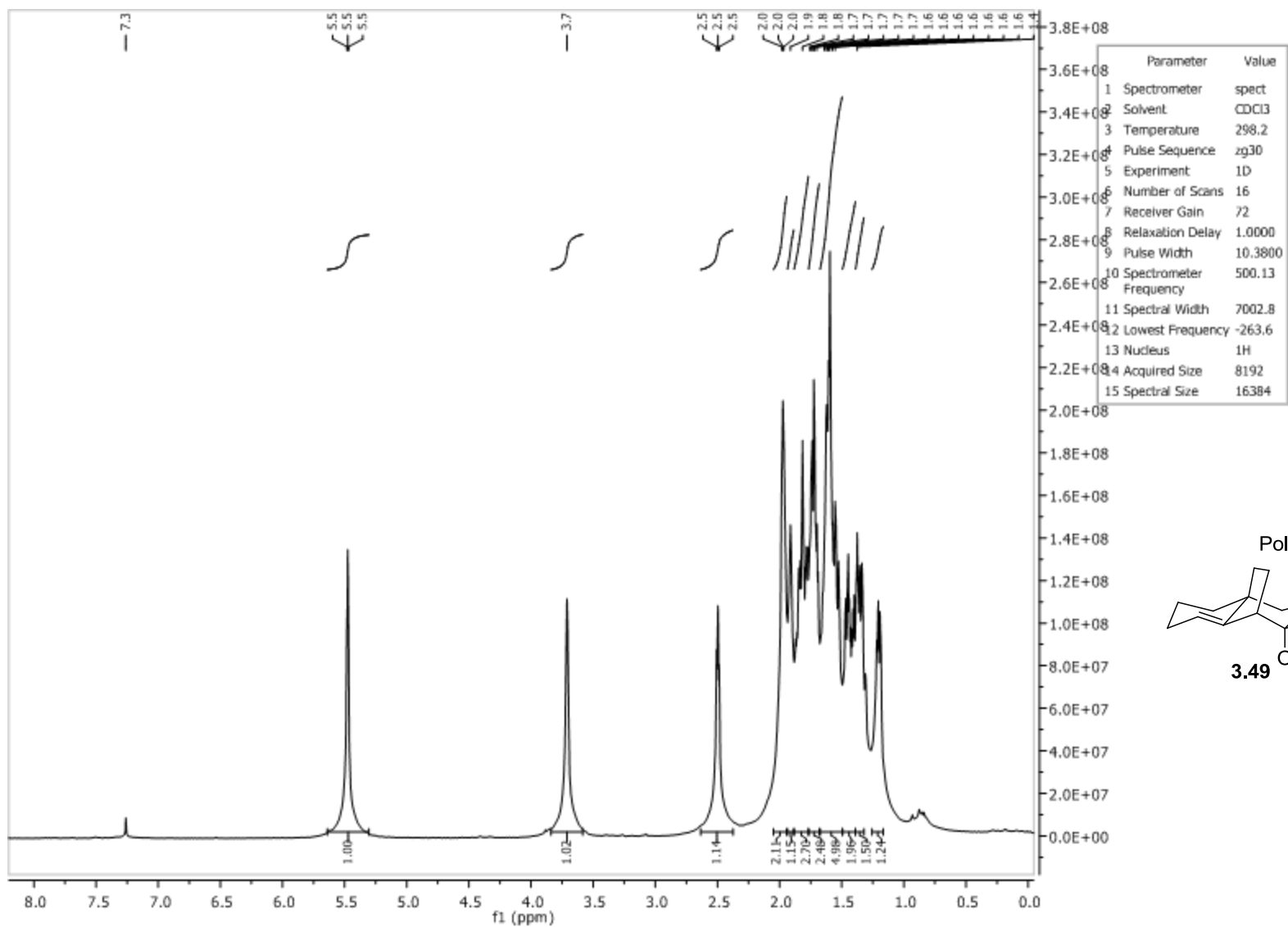
3.38

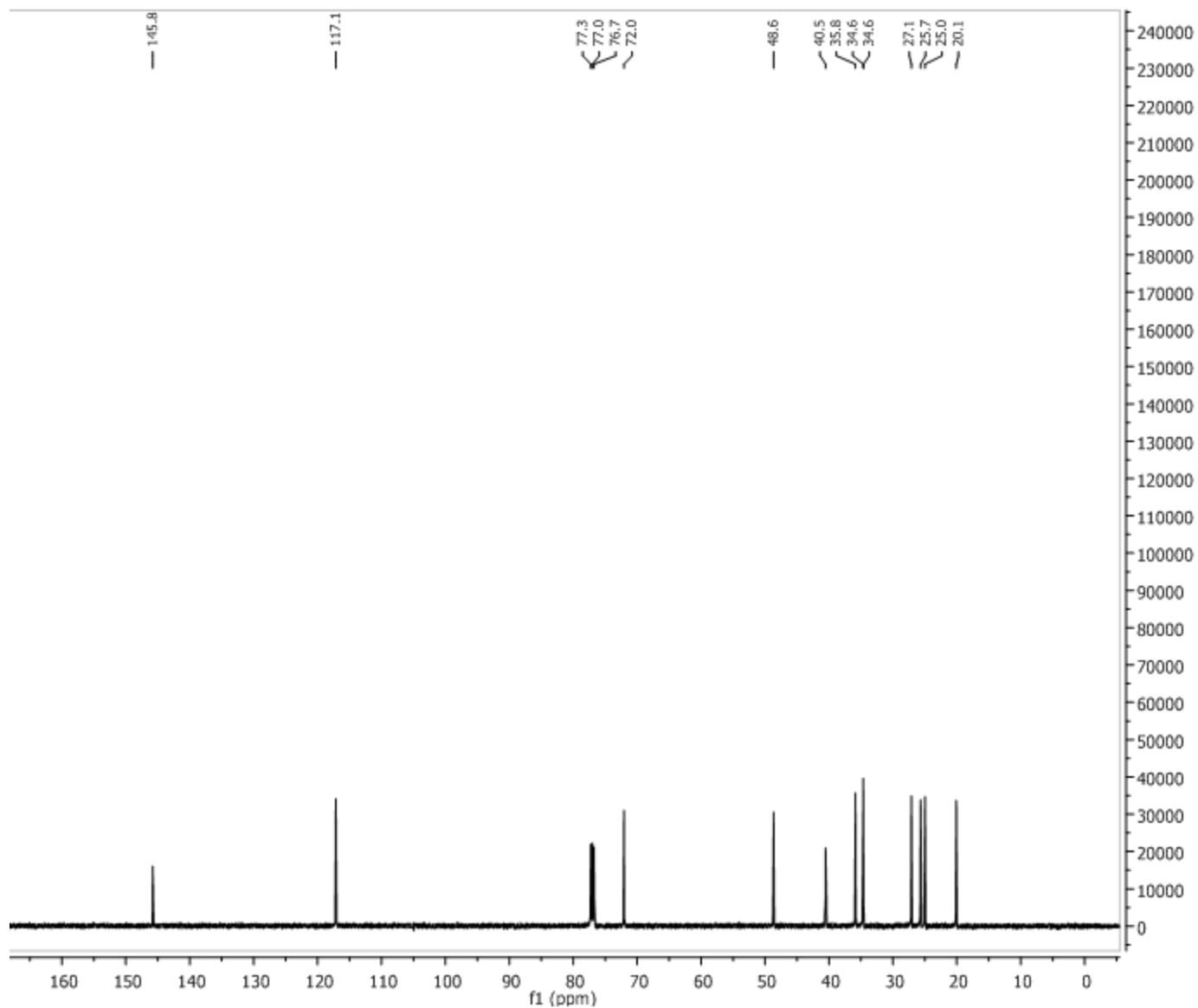


Parameter	Value
1 Spectrometer	spect
2 Solvent	CDCl3
3 Temperature	298.2
4 Pulse Sequence	zg30
5 Experiment	1D
6 Number of Scans	8
7 Receiver Gain	161
8 Relaxation Delay	1.0000
9 Pulse Width	10.2500
10 Acquisition Time	3.9846
11 Spectrometer Frequency	400.15
12 Spectral Width	8223.7
13 Lowest Frequency	-1640.8
14 Nucleus	1H
15 Acquired Size	32768
16 Spectral Size	65536

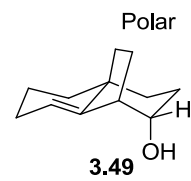


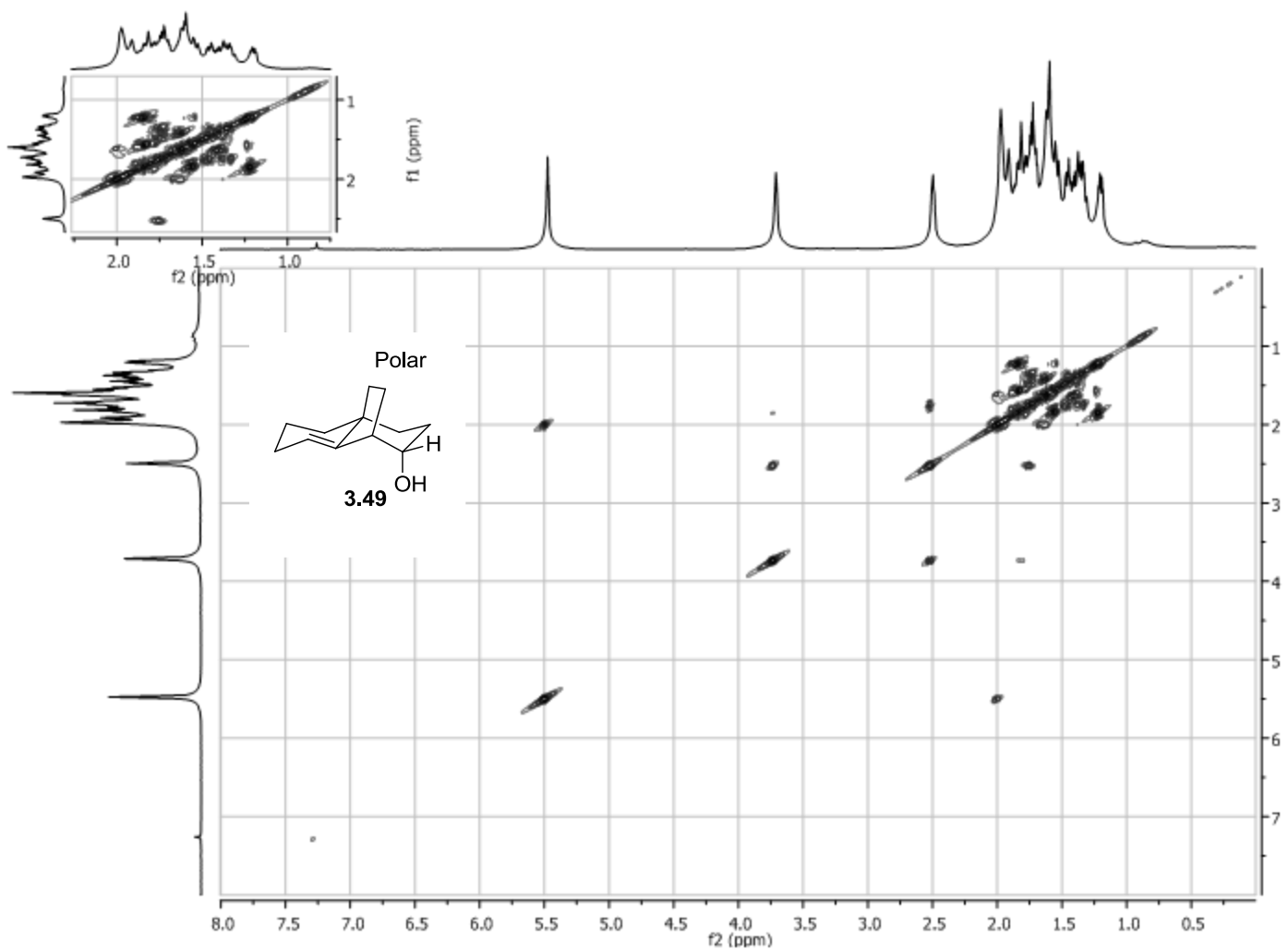


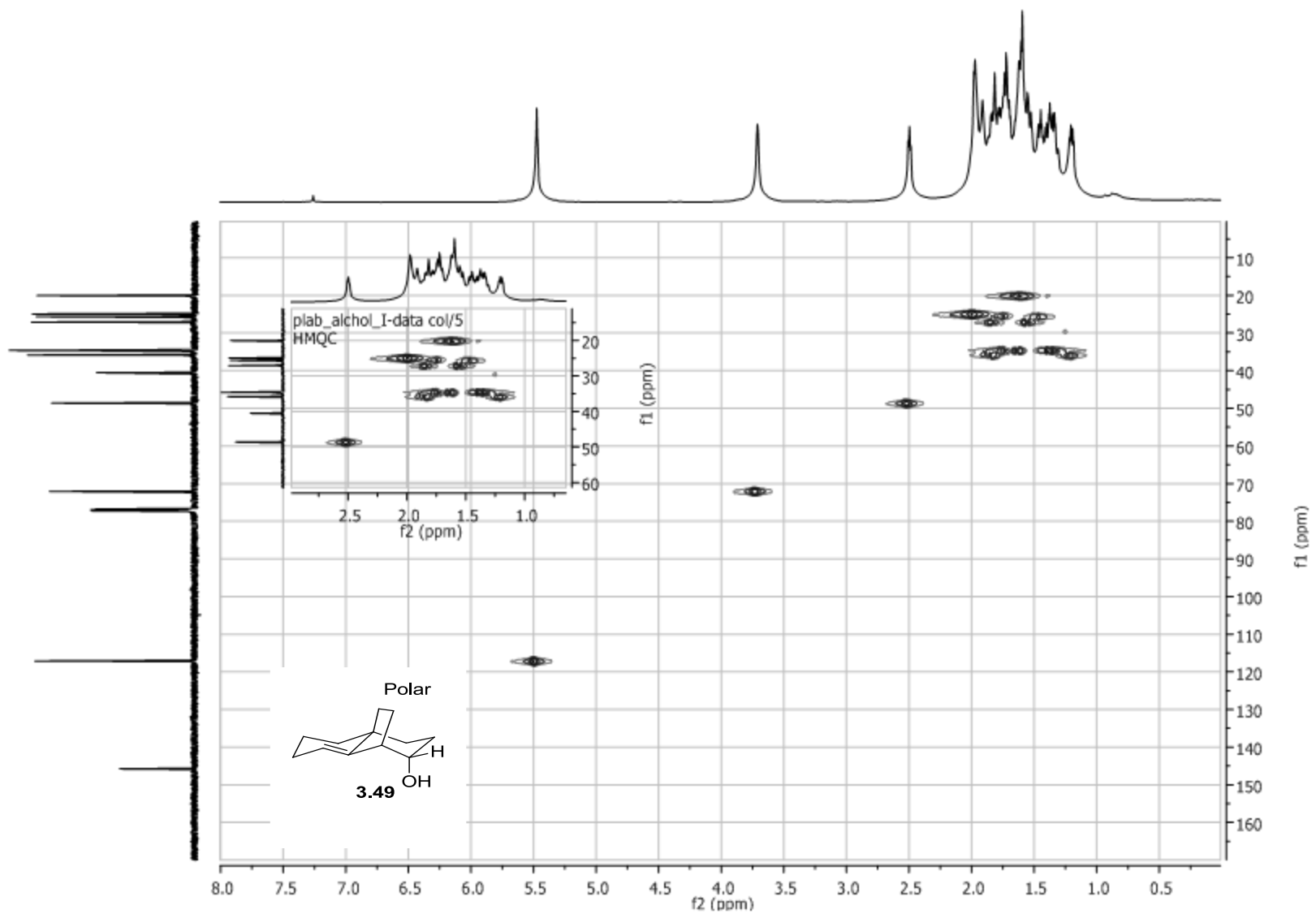


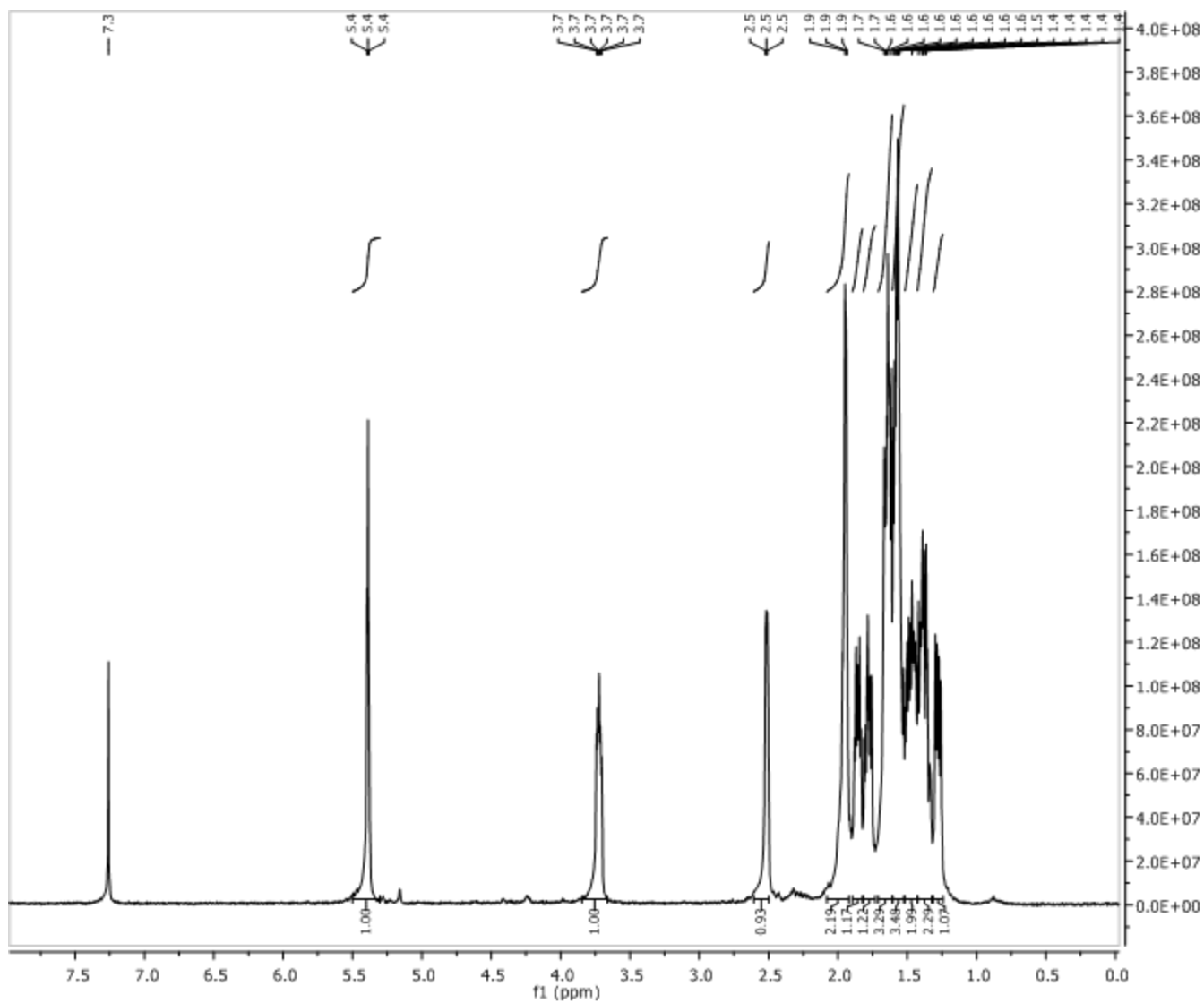


Parameter	Value
1 Spectrometer	spect
2 Solvent	CDCl3
3 Temperature	298.2
4 Pulse Sequence	zgpg30
5 Experiment	1D
6 Number of Scans	2048
7 Receiver Gain	9195
8 Relaxation Delay	3.0000
9 Pulse Width	9.0000
10 Spectrometer Frequency	125.77
11 Spectral Width	27777.8
12 Lowest Frequency	-693.2
13 Nucleus	13C
14 Acquired Size	32768
15 Spectral Size	65536

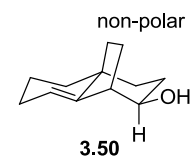


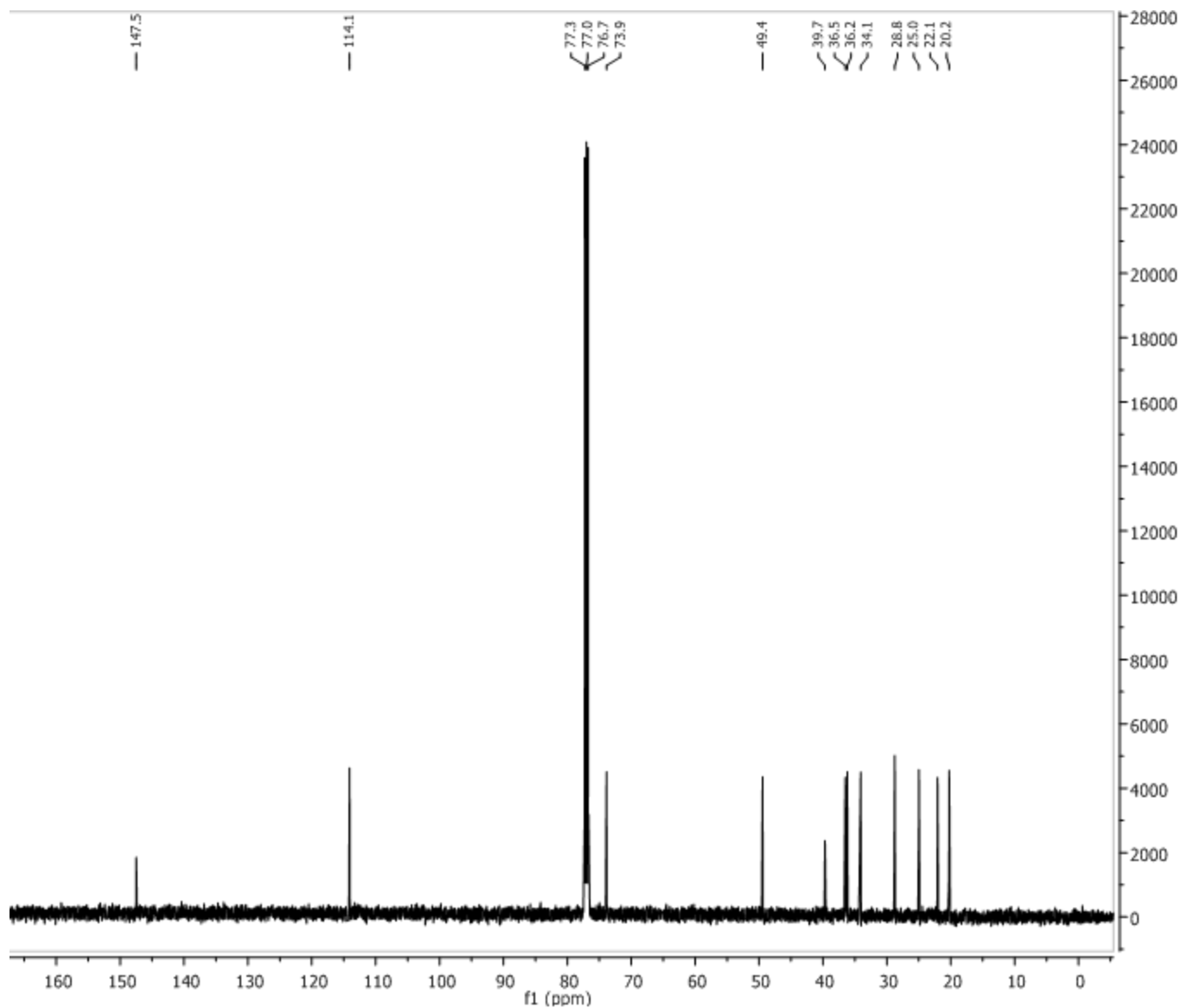




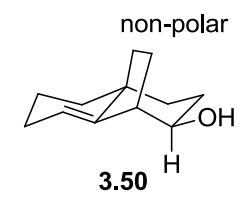


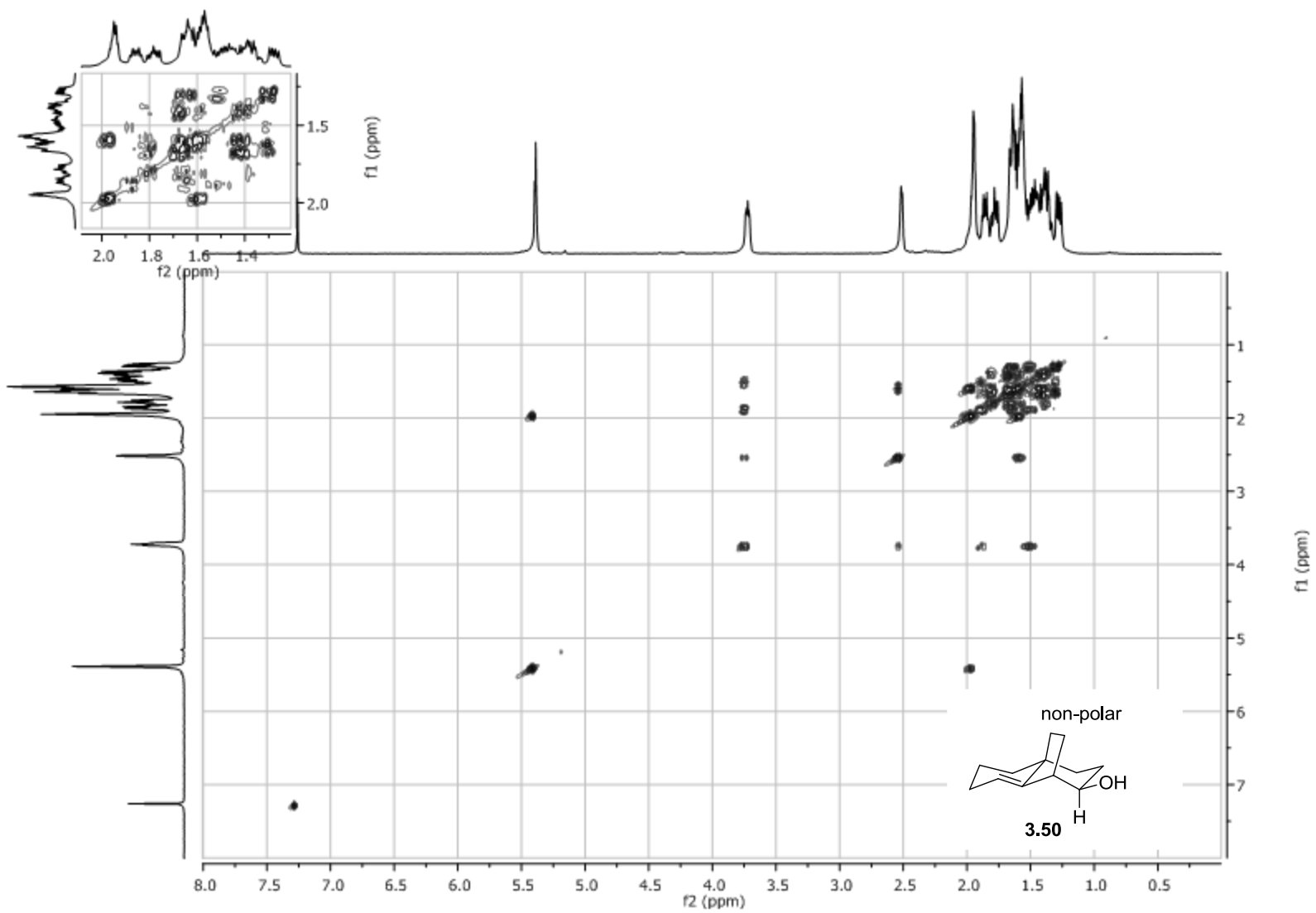
Parameter	Value
1 Spectrometer	spect
2 Solvent	CDCl3
3 Temperature	298.2
4 Pulse Sequence	zg30
5 Experiment	1D
6 Number of Scans	16
7 Receiver Gain	322
8 Relaxation Delay	1.0000
9 Pulse Width	10.3800
10 Spectrometer Frequency	500.13
11 Spectral Width	7002.8
12 Lowest Frequency	-264.1
13 Nucleus	1H
14 Acquired Size	8192
15 Spectral Size	16384

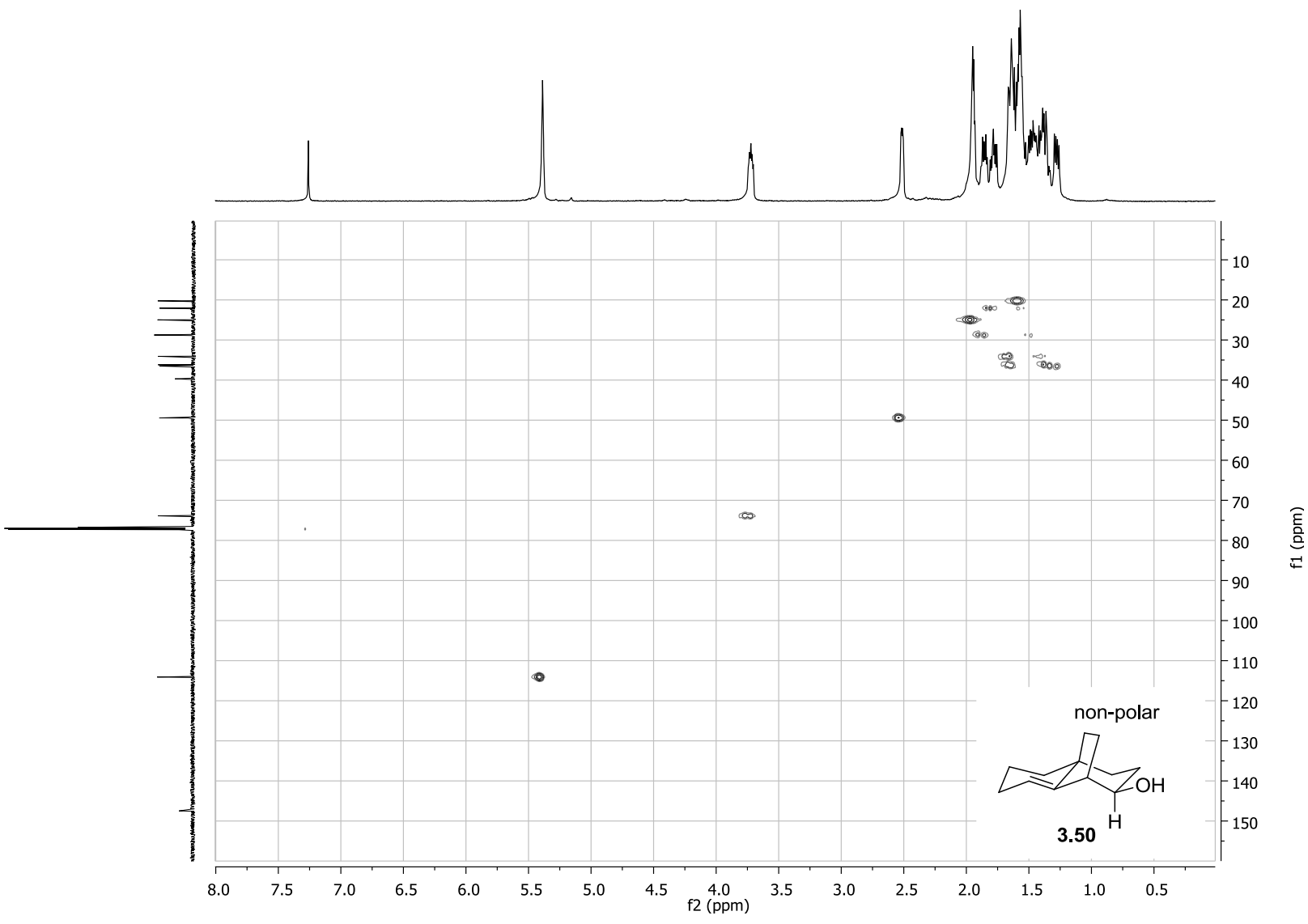


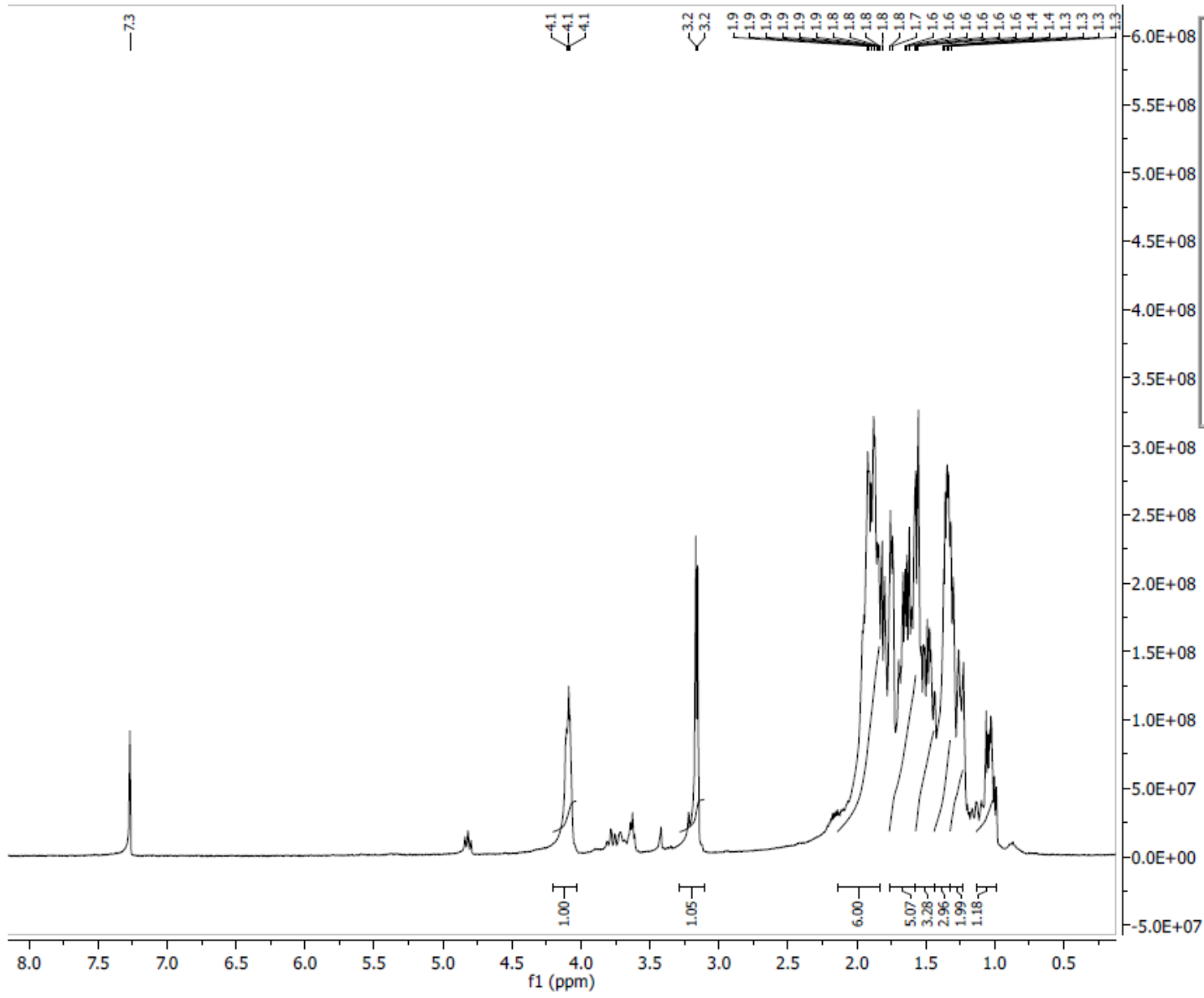


Parameter	Value
1 Spectrometer	spect
2 Solvent	CDCl3
3 Temperature	298.2
4 Pulse Sequence	zgpg30
5 Experiment	1D
6 Number of Scans	2048
7 Receiver Gain	9195
8 Relaxation Delay	3.0000
9 Pulse Width	9.0000
10 Spectrometer Frequency	125.76
11 Spectral Width	27777.8
12 Lowest Frequency	-683.9
13 Nucleus	13C
14 Acquired Size	32768
15 Spectral Size	65536

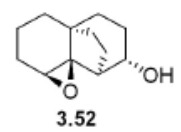


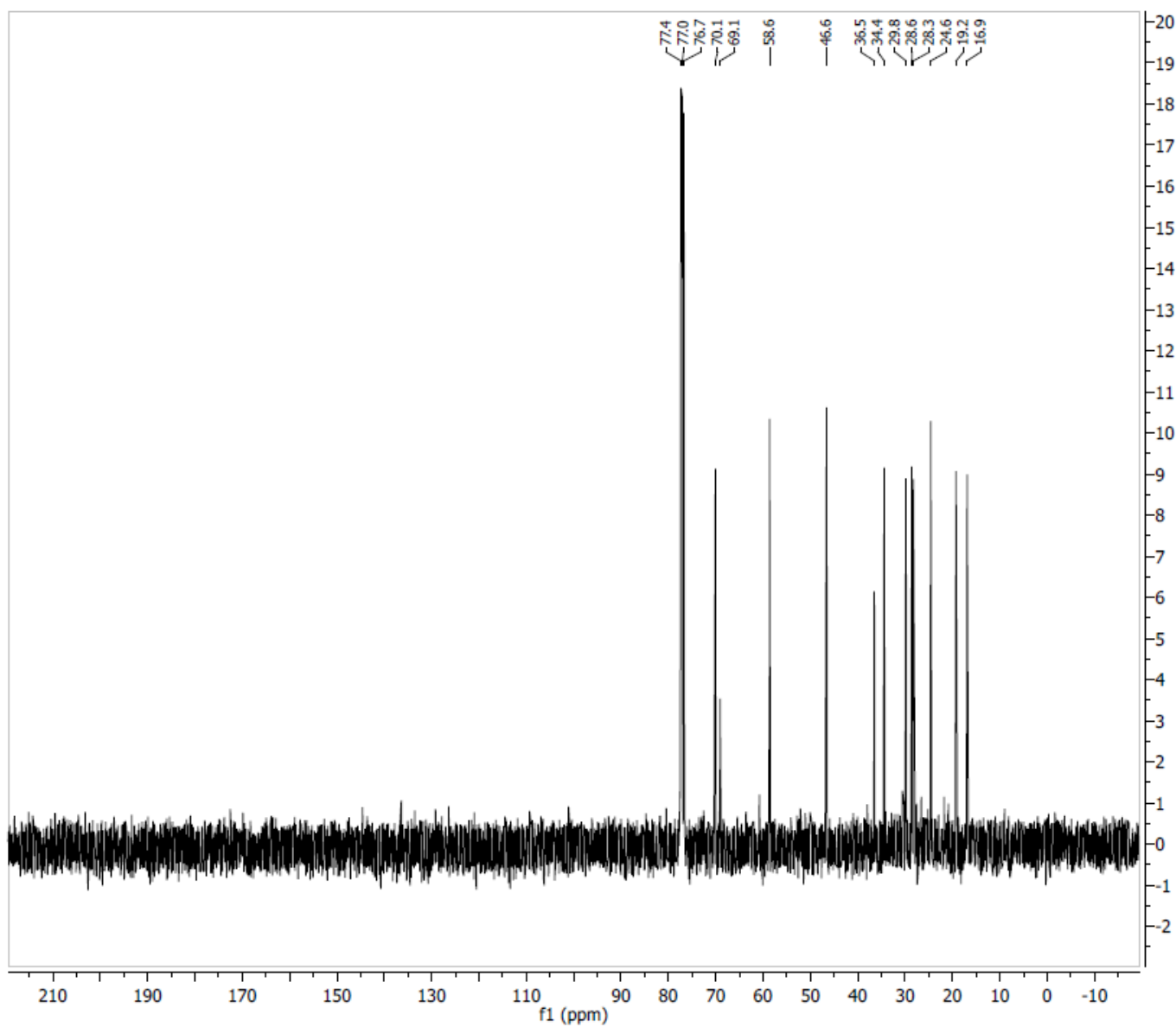




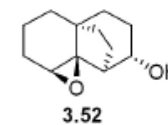


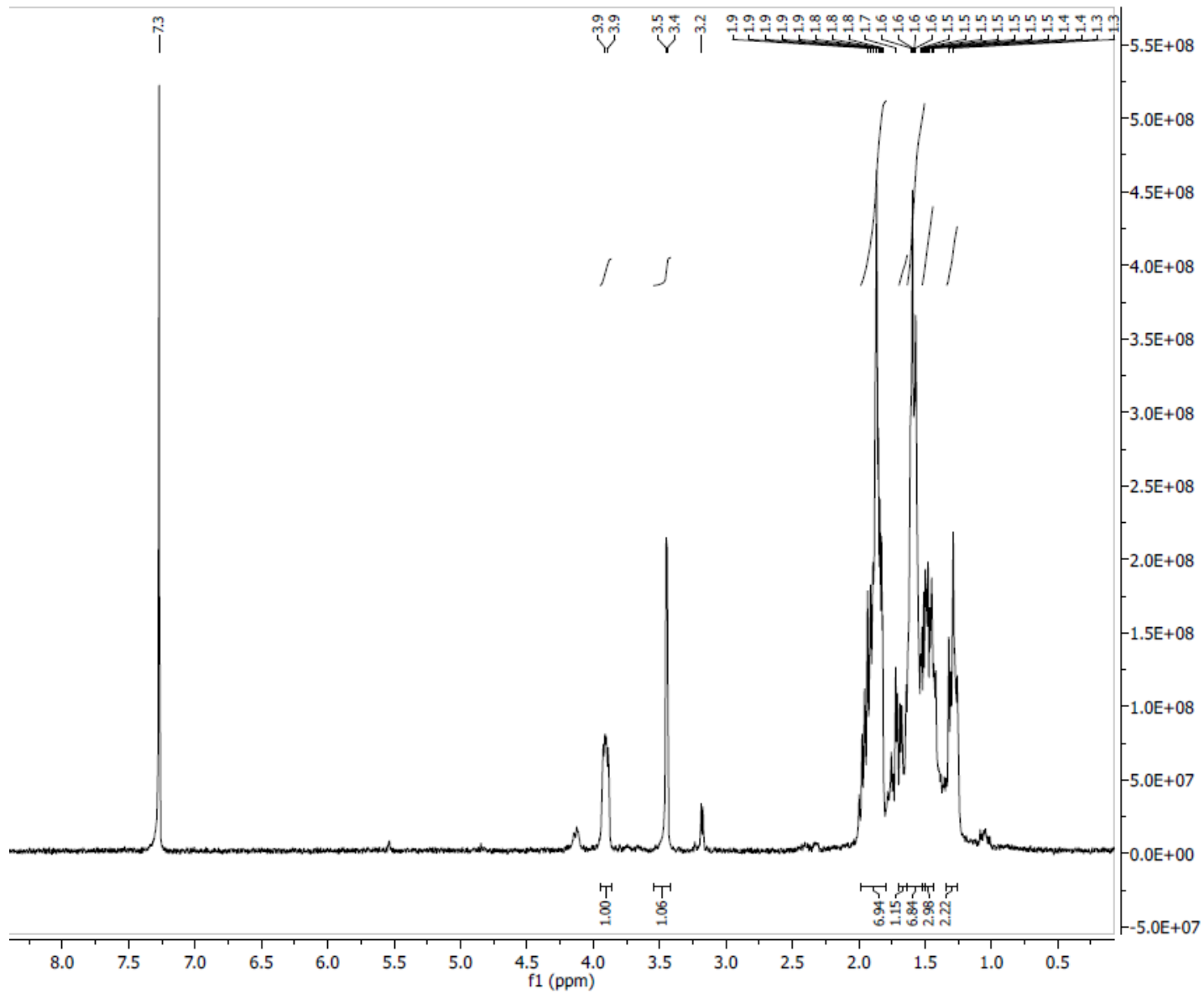
Parameter	Value
1 Spectrometer	spect
2 Solvent	CDCl3
3 Temperature	298.2
4 Pulse Sequence	zg30
5 Experiment	1D
6 Number of Scans	12
7 Receiver Gain	181
8 Relaxation Delay	1.0000
9 Pulse Width	10.2500
10 Acquisition Time	3.9846
11 Spectrometer Frequency	400.15
12 Spectral Width	8223.7
13 Lowest Frequency	-1640.8
14 Nucleus	1H
15 Acquired Size	32768
16 Spectral Size	32768



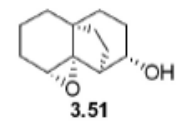


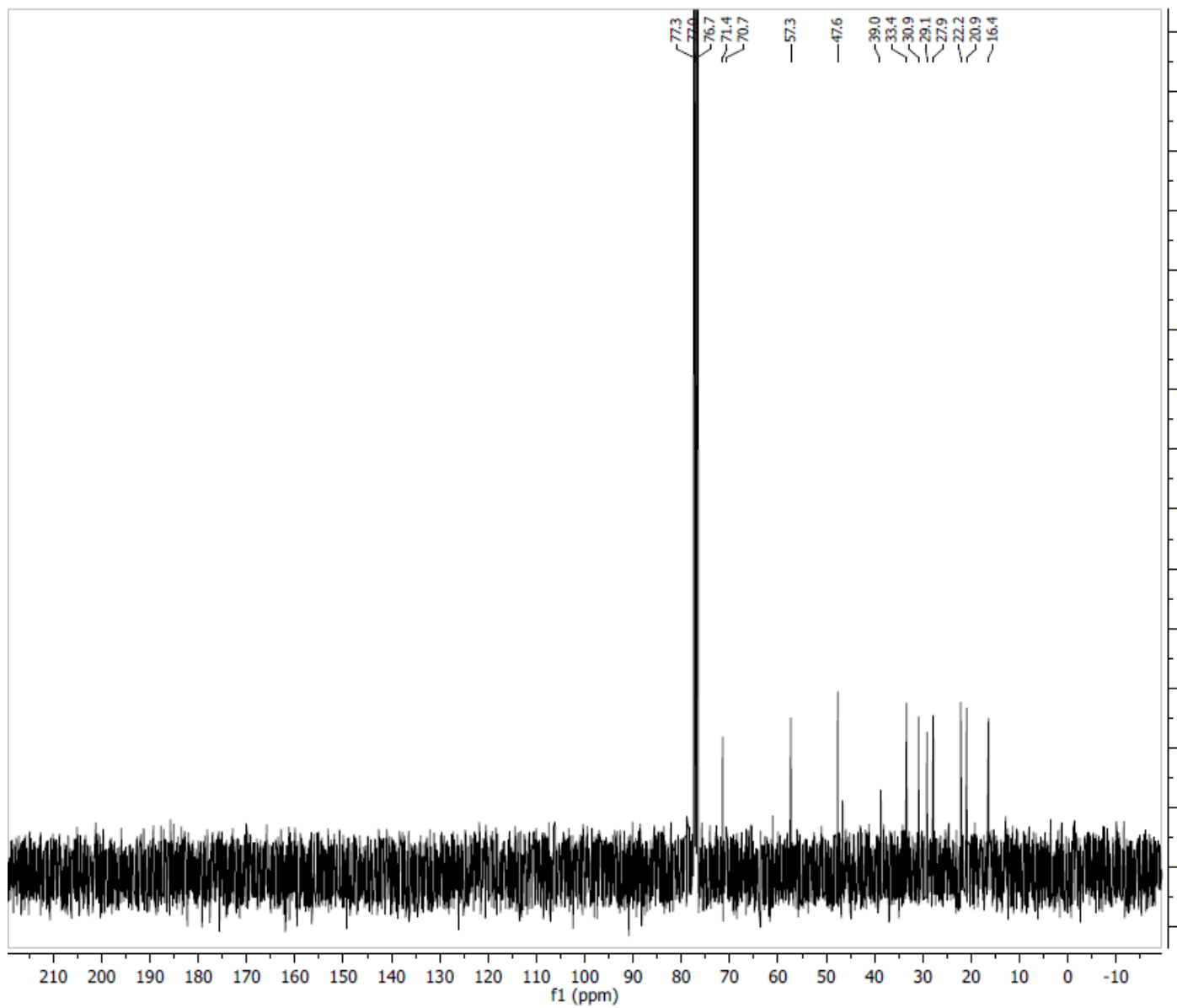
Parameter	Value
1 Spectrometer	spect
2 Solvent	CDCl3
3 Temperature	298.2
4 Pulse Sequence	zg30
5 Experiment	1D
6 Number of Scans	12
7 Receiver Gain	181
8 Relaxation Delay	1.0000
9 Pulse Width	10.2500
10 Acquisition Time	3.9846
11 Spectrometer Frequency	400.15
12 Spectral Width	8223.7
13 Lowest Frequency	-1640.8
14 Nucleus	1H
15 Acquired Size	32768
16 Spectral Size	32768



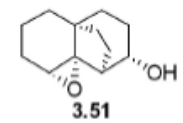


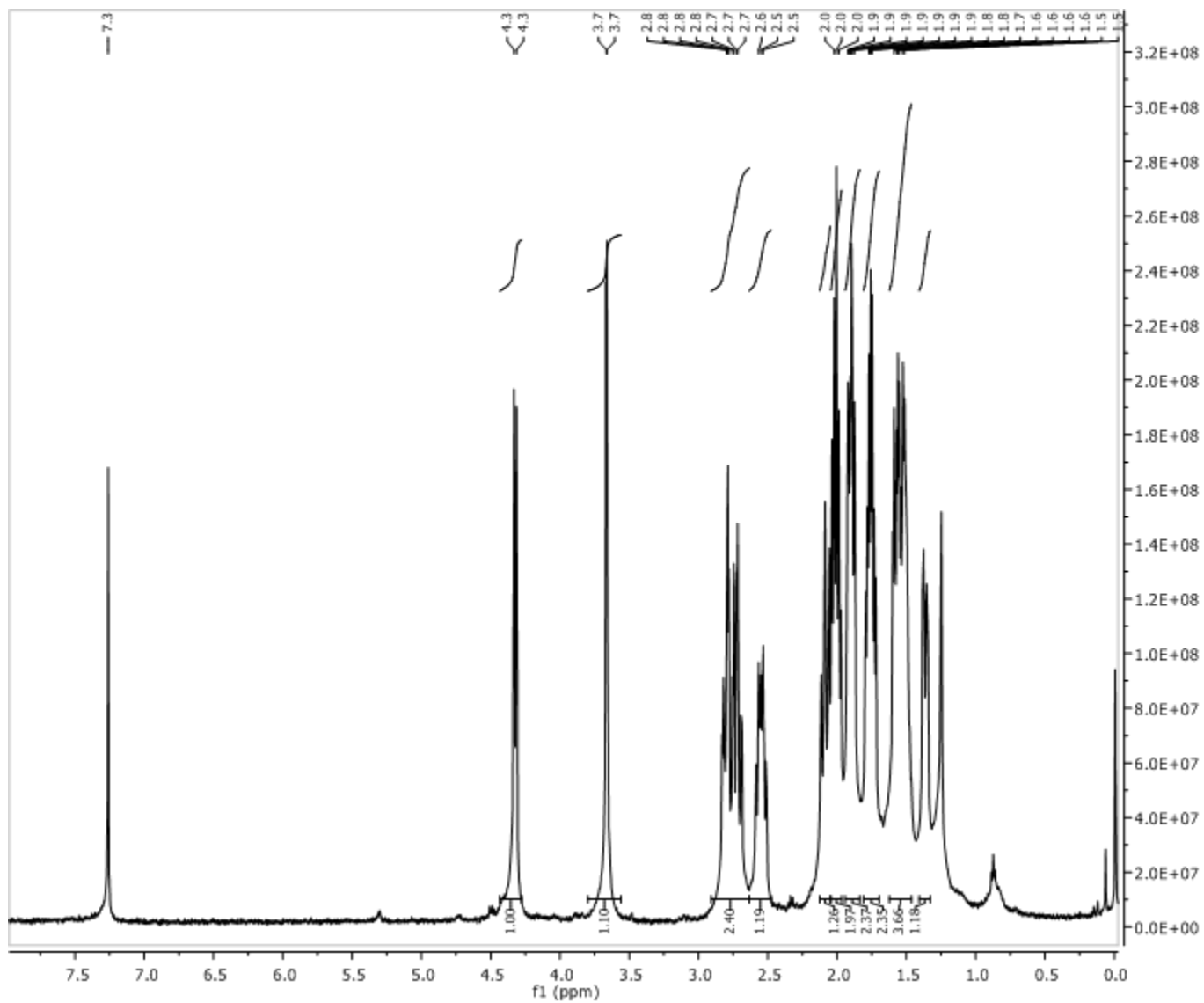
Parameter	Value
1 Spectrometer	spect
2 Solvent	CDCl3
3 Temperature	298.2
4 Pulse Sequence	zg30
5 Experiment	1D
6 Number of Scans	8
7 Receiver Gain	456
8 Relaxation Delay	1.0000
9 Pulse Width	10.2500
10 Acquisition Time	3.9846
11 Spectrometer Frequency	400.15
12 Spectral Width	8223.7
13 Lowest Frequency	-1640.8
14 Nucleus	1H
15 Acquired Size	32768
16 Spectral Size	32768



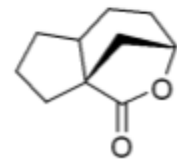


Parameter	Value
1 Spectrometer	spect
2 Solvent	CDCB
3 Temperature	298.2
4 Pulse Sequence	zgpg30
5 Experiment	1D
6 Number of Scans	512
7 Receiver Gain	32800
8 Relaxation Delay	2.0000
9 Pulse Width	10.0000
10 Acquisition Time	1.3631
11 Spectrometer Frequency	100.62
12 Spectral Width	24038.5
13 Lowest Frequency	-1957.9
14 Nucleus	¹³ C
15 Acquired Size	32768
16 Spectral Size	65536

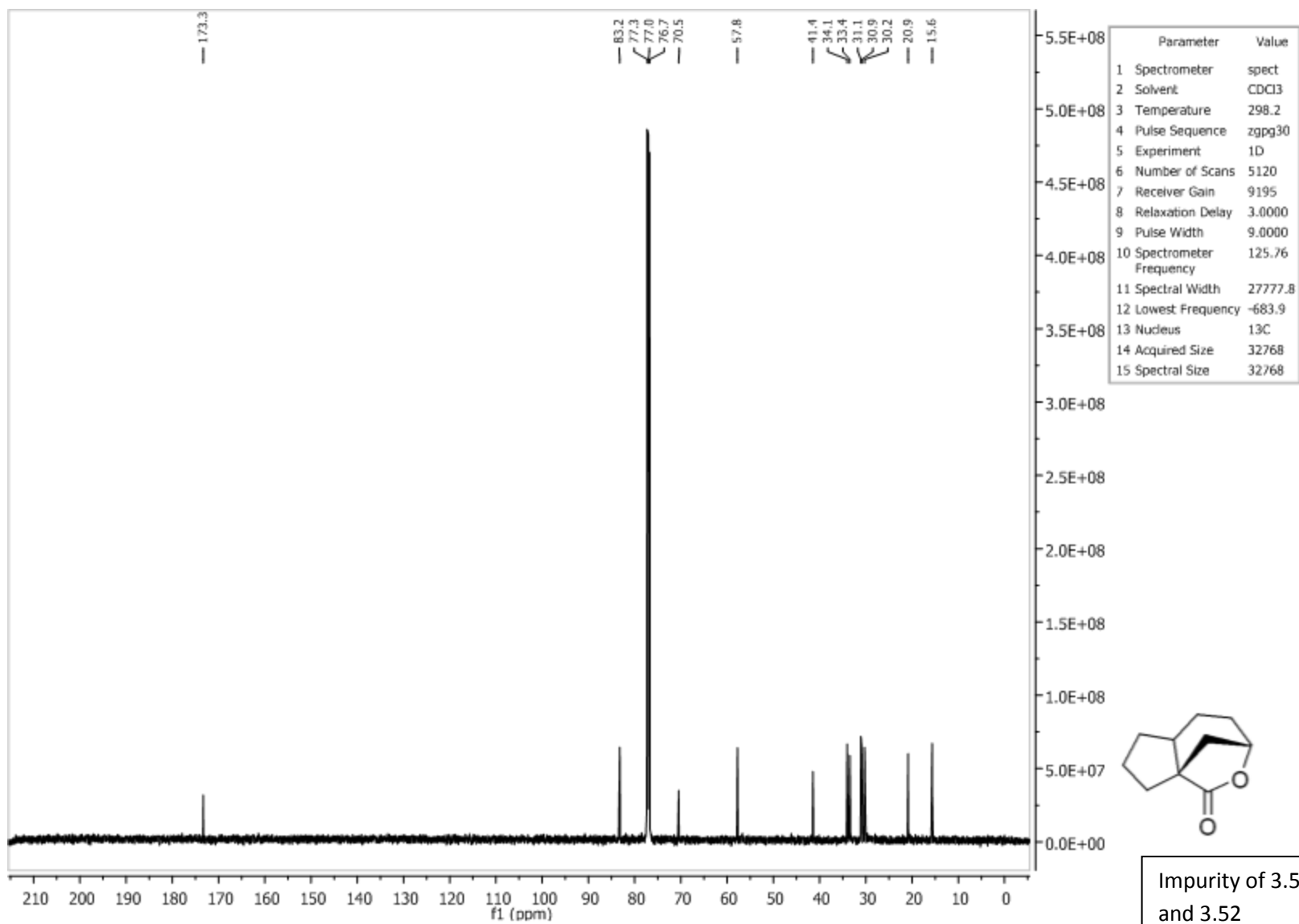


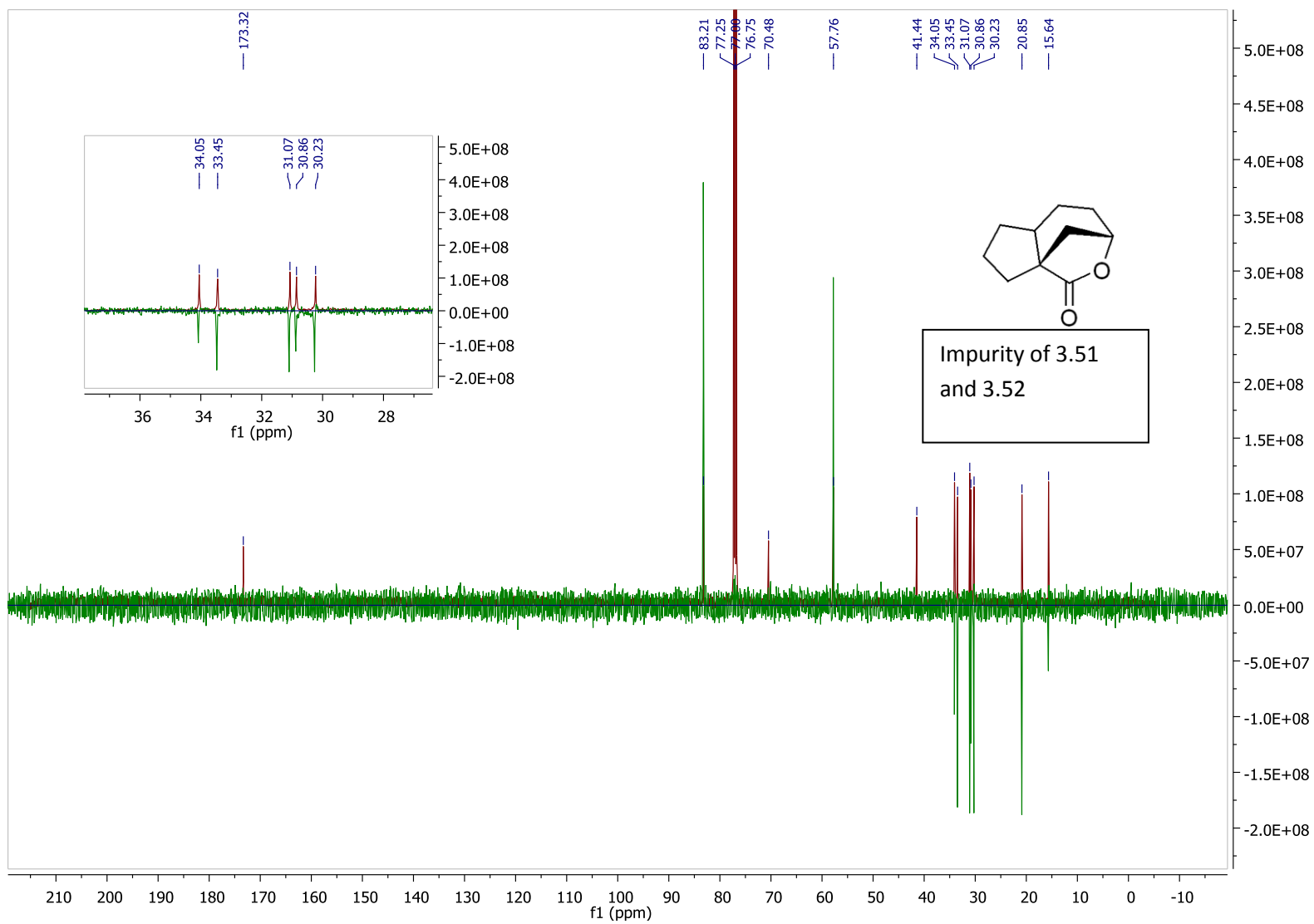


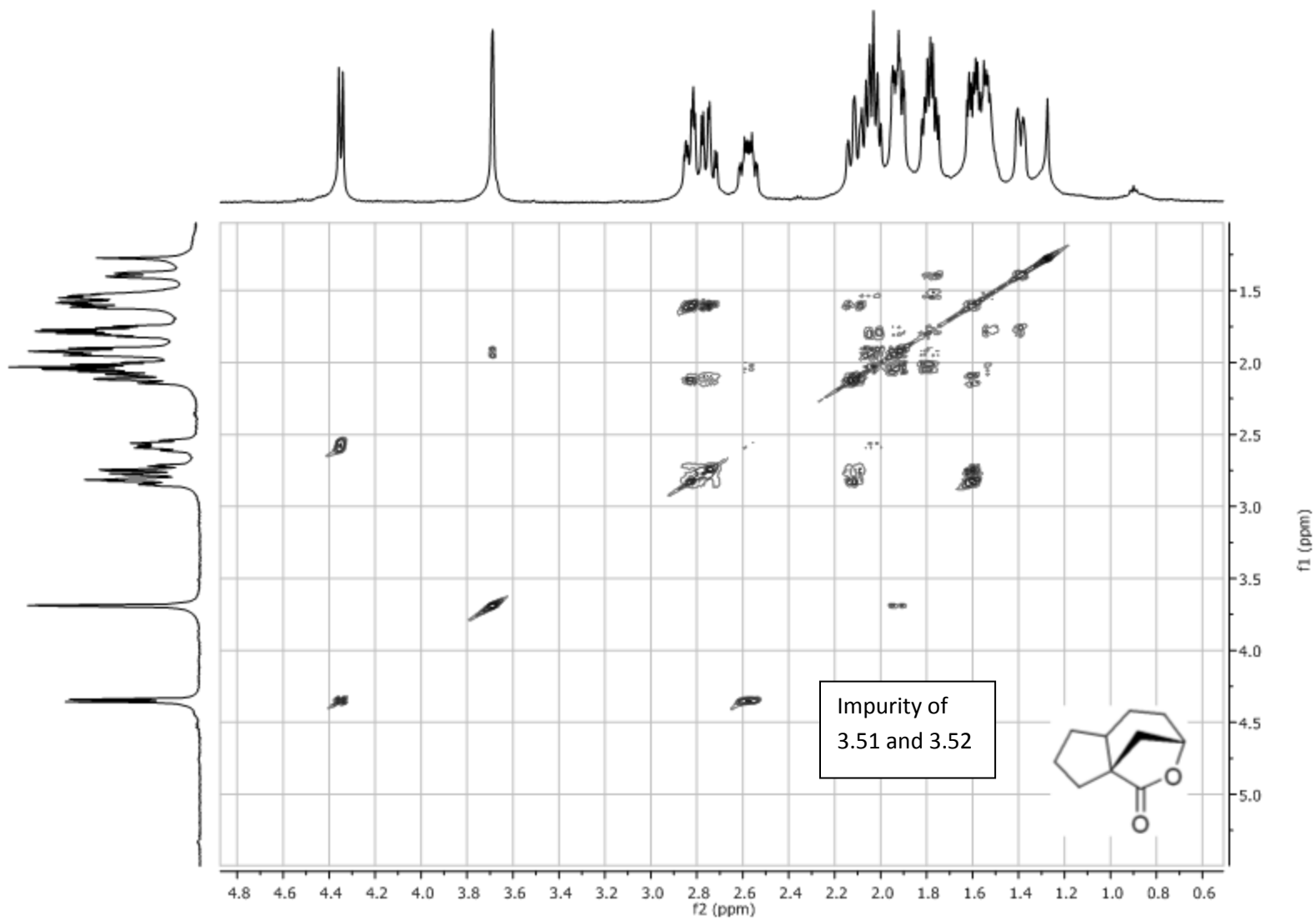
Parameter	Value
1 Spectrometer	spect
2 Solvent	CDCl3
3 Temperature	298.2
4 Pulse Sequence	zg30
5 Experiment	1D
6 Number of Scans	16
7 Receiver Gain	45
8 Relaxation Delay	1.0000
9 Pulse Width	10.3800
10 Spectrometer Frequency	500.13
11 Spectral Width	7002.8
12 Lowest Frequency	-250.6
13 Nucleus	1H
14 Acquired Size	8192
15 Spectral Size	16384

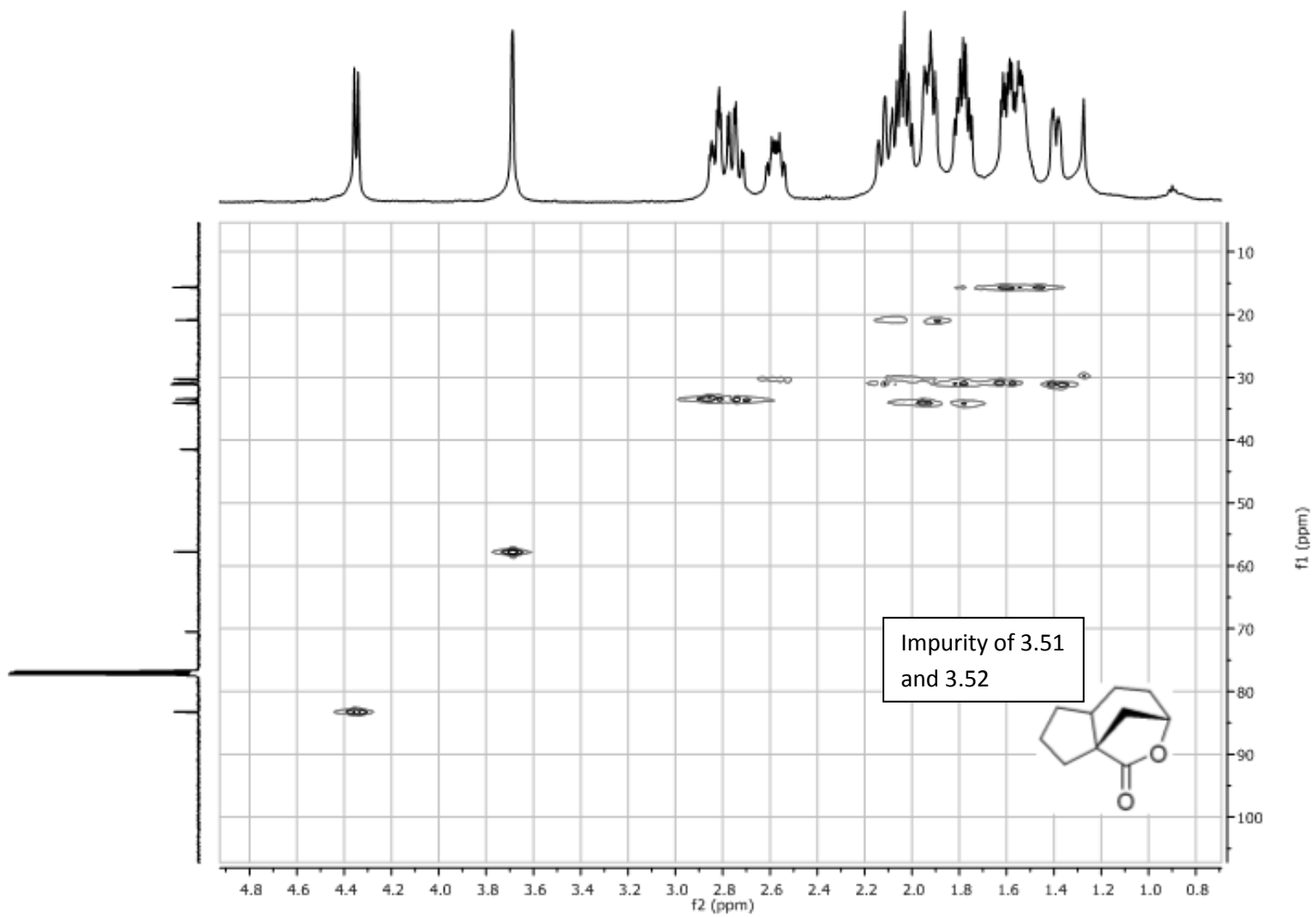


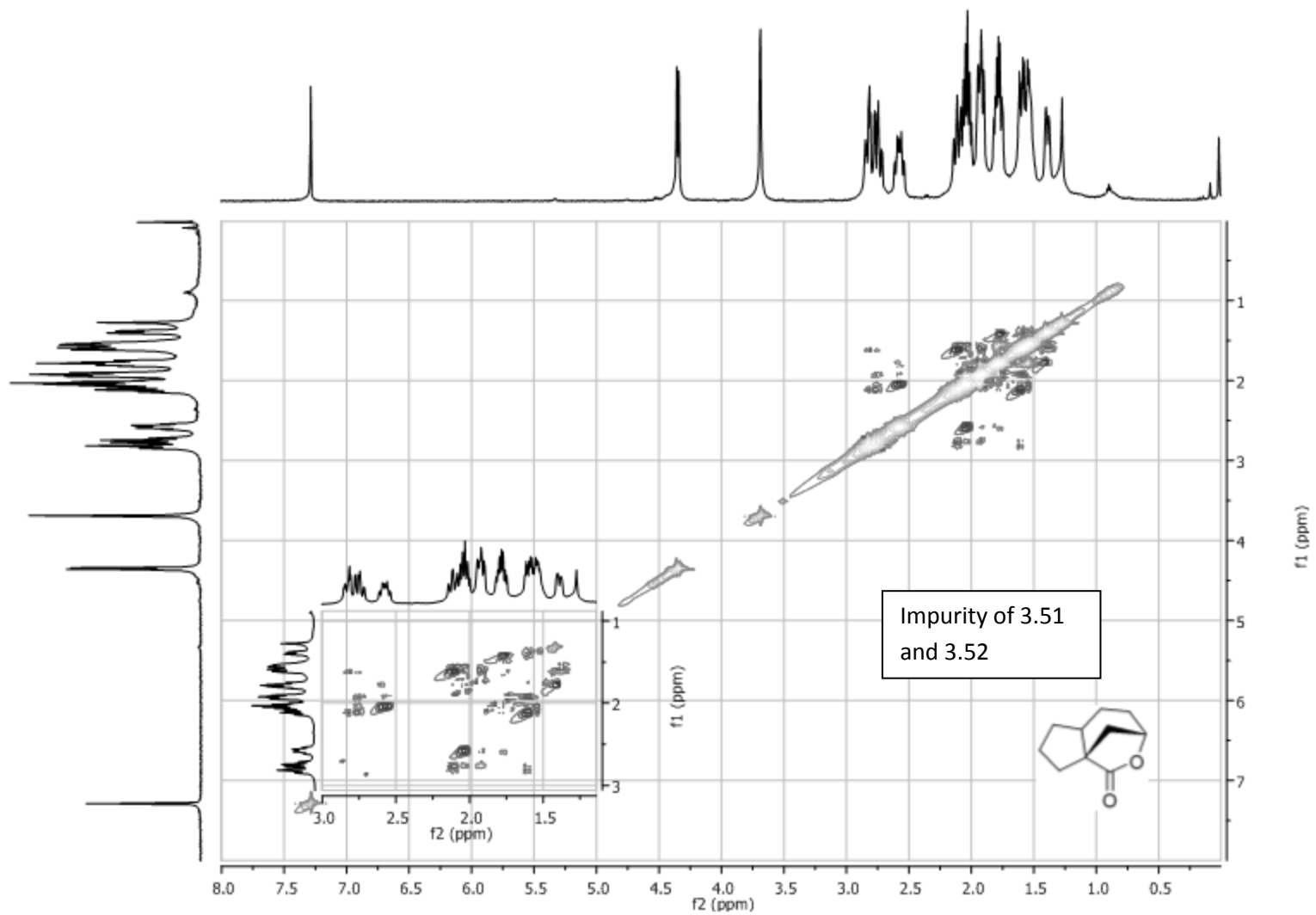
Impurity of 3.51 and 3.52

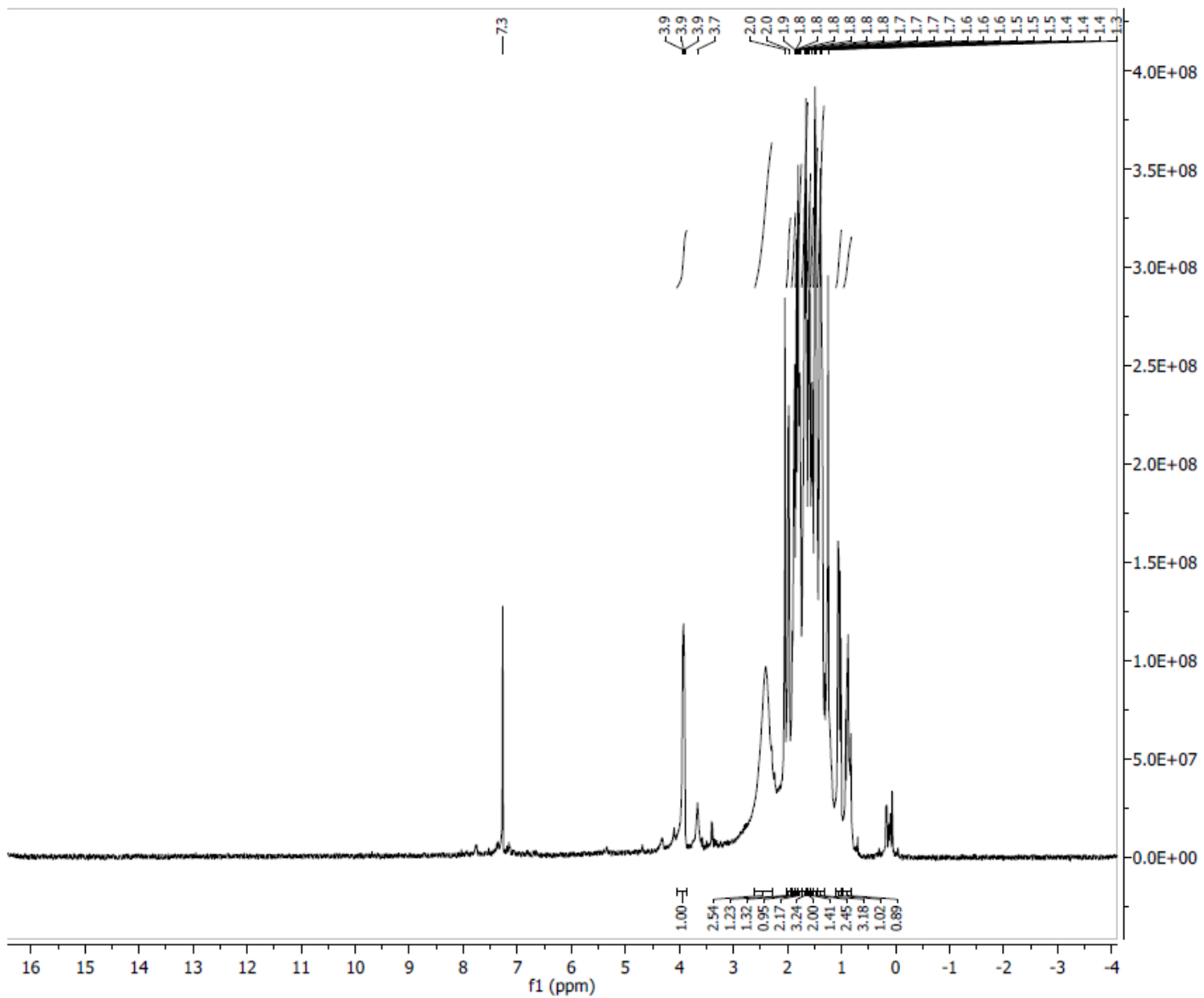




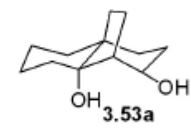


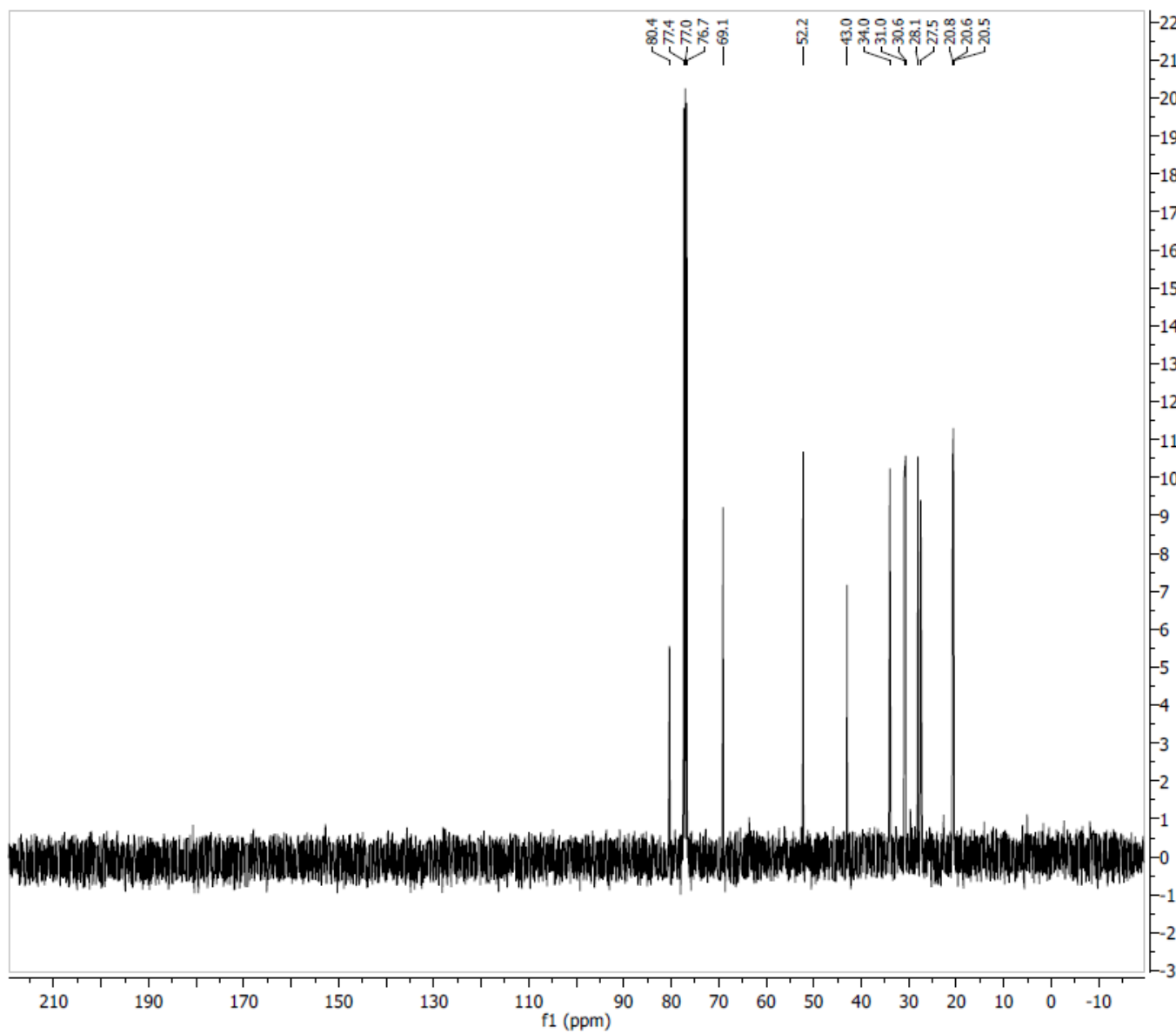




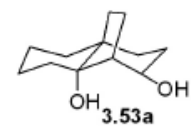


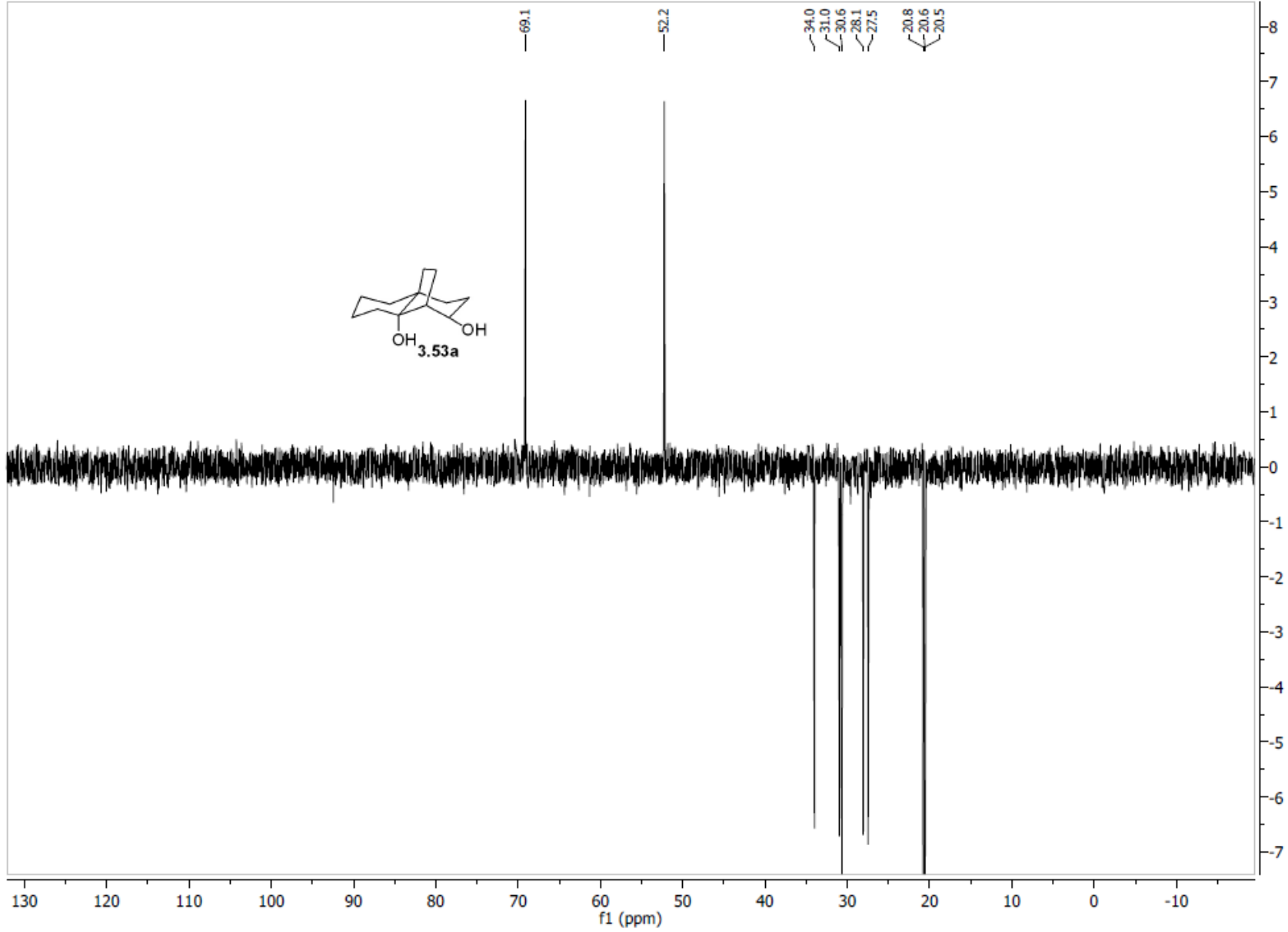
Parameter	Value
1 Spectrometer	spect
2 Solvent	CDCl3
3 Temperature	298.2
4 Pulse Sequence	zg30
5 Experiment	1D
6 Number of Scans	14
7 Receiver Gain	144
8 Relaxation Delay	1.0000
9 Pulse Width	10.2500
10 Acquisition Time	3.9846
11 Spectrometer Frequency	400.15
12 Spectral Width	8223.7
13 Lowest Frequency	-1640.8
14 Nucleus	1H
15 Acquired Size	32768
16 Spectral Size	32768

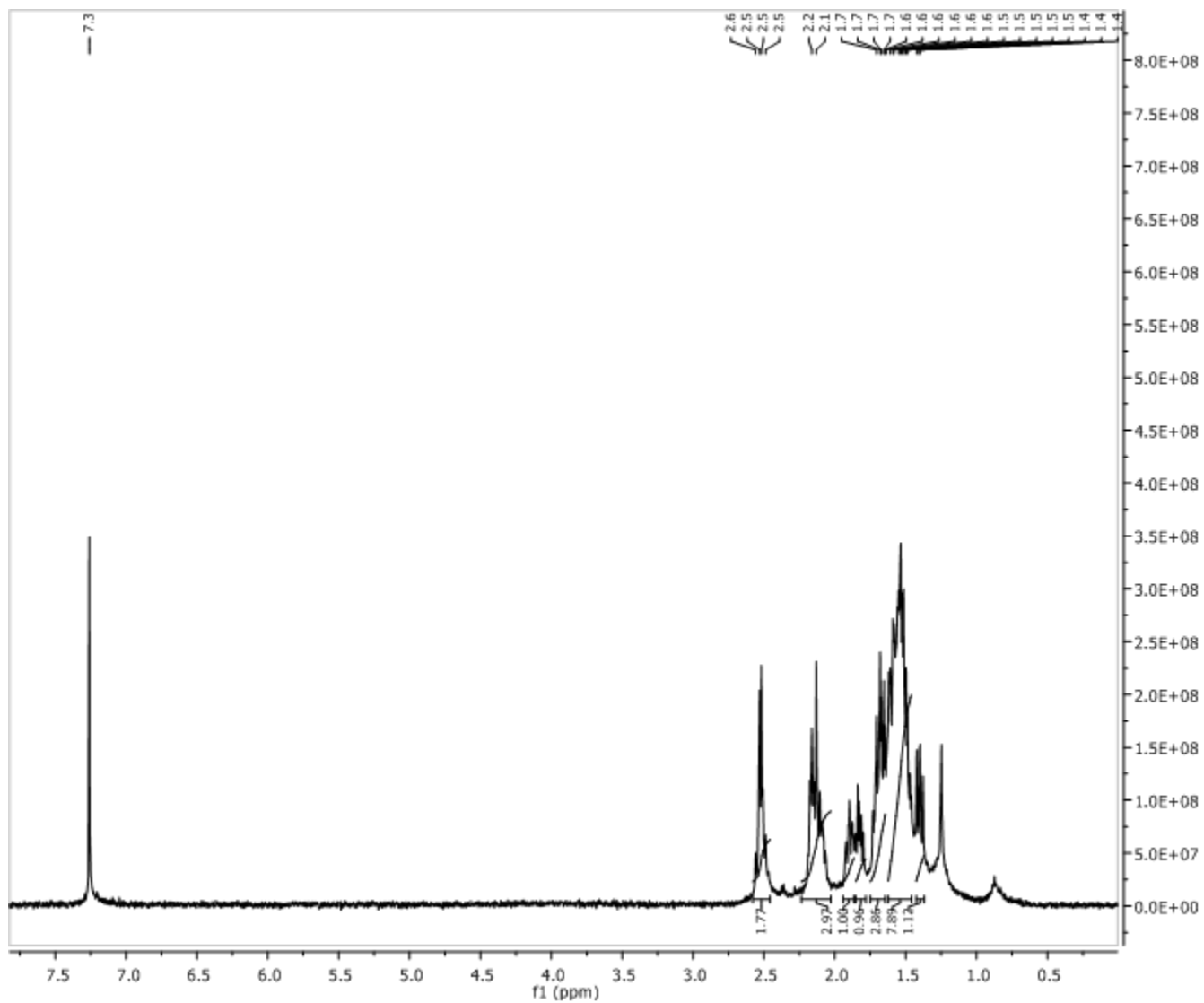




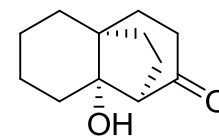
Parameter	Value
1 Spectrometer	spect
2 Solvent	CDCl3
3 Temperature	298.2
4 Pulse Sequence	zgpg30
5 Experiment	1D
6 Number of Scans	512
7 Receiver Gain	32800
8 Relaxation Delay	2.0000
9 Pulse Width	10.0000
10 Acquisition Time	1.3631
11 Spectrometer Frequency	100.62
12 Spectral Width	24038.5
13 Lowest Frequency	-1957.9
14 Nucleus	13C
15 Acquired Size	32768
16 Spectral Size	65536



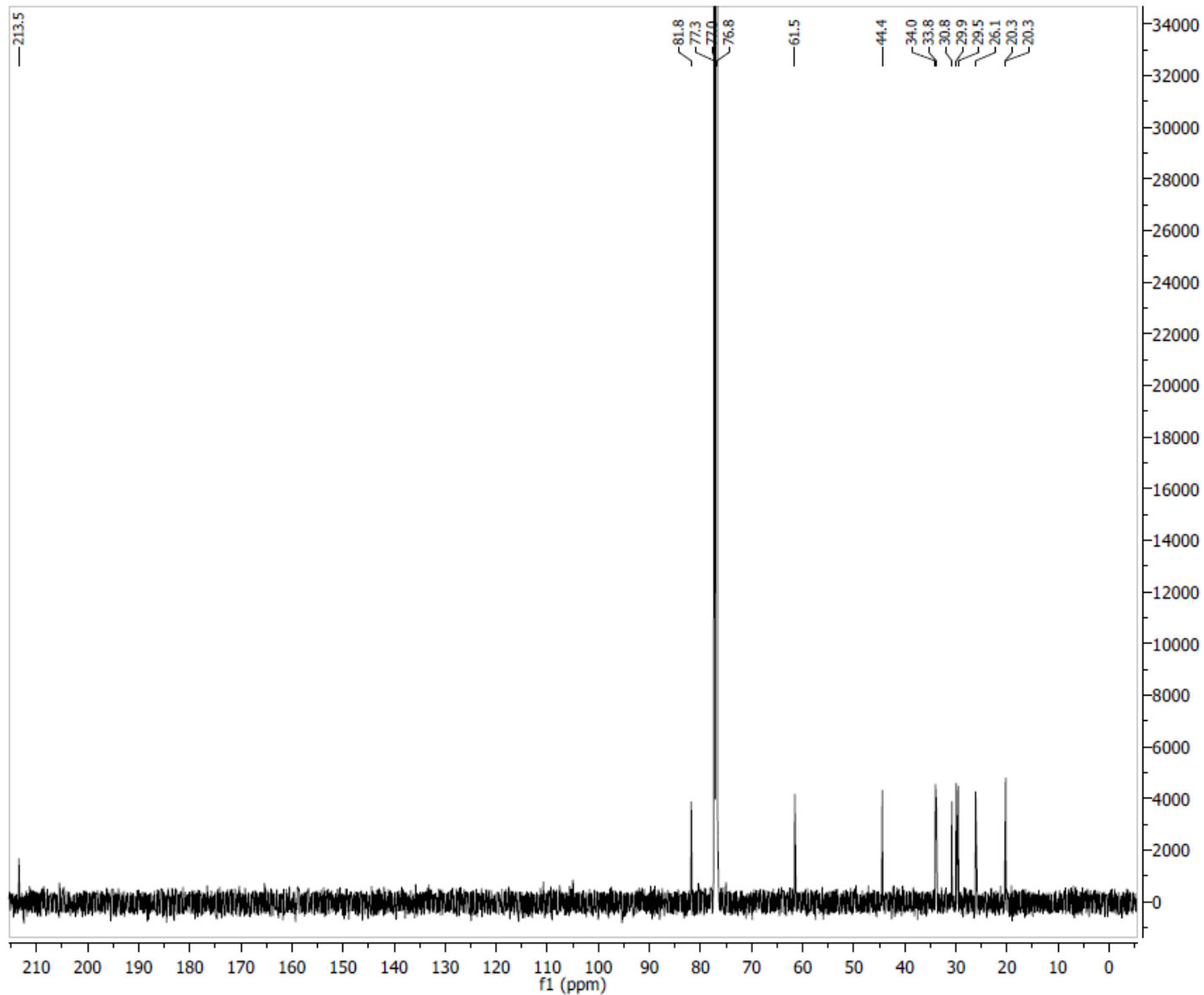




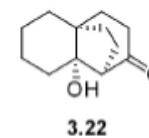
Parameter	Value
1 Spectrometer	spect
2 Solvent	CDCl3
3 Temperature	297.2
4 Pulse Sequence	zg30
5 Experiment	1D
6 Number of Scans	1
7 Receiver Gain	575
8 Relaxation Delay	1.0000
9 Pulse Width	11.0000
10 Spectrometer Frequency	500.13
11 Spectral Width	7002.8
12 Lowest Frequency	-264.6
13 Nucleus	1H
14 Acquired Size	8192
15 Spectral Size	16384

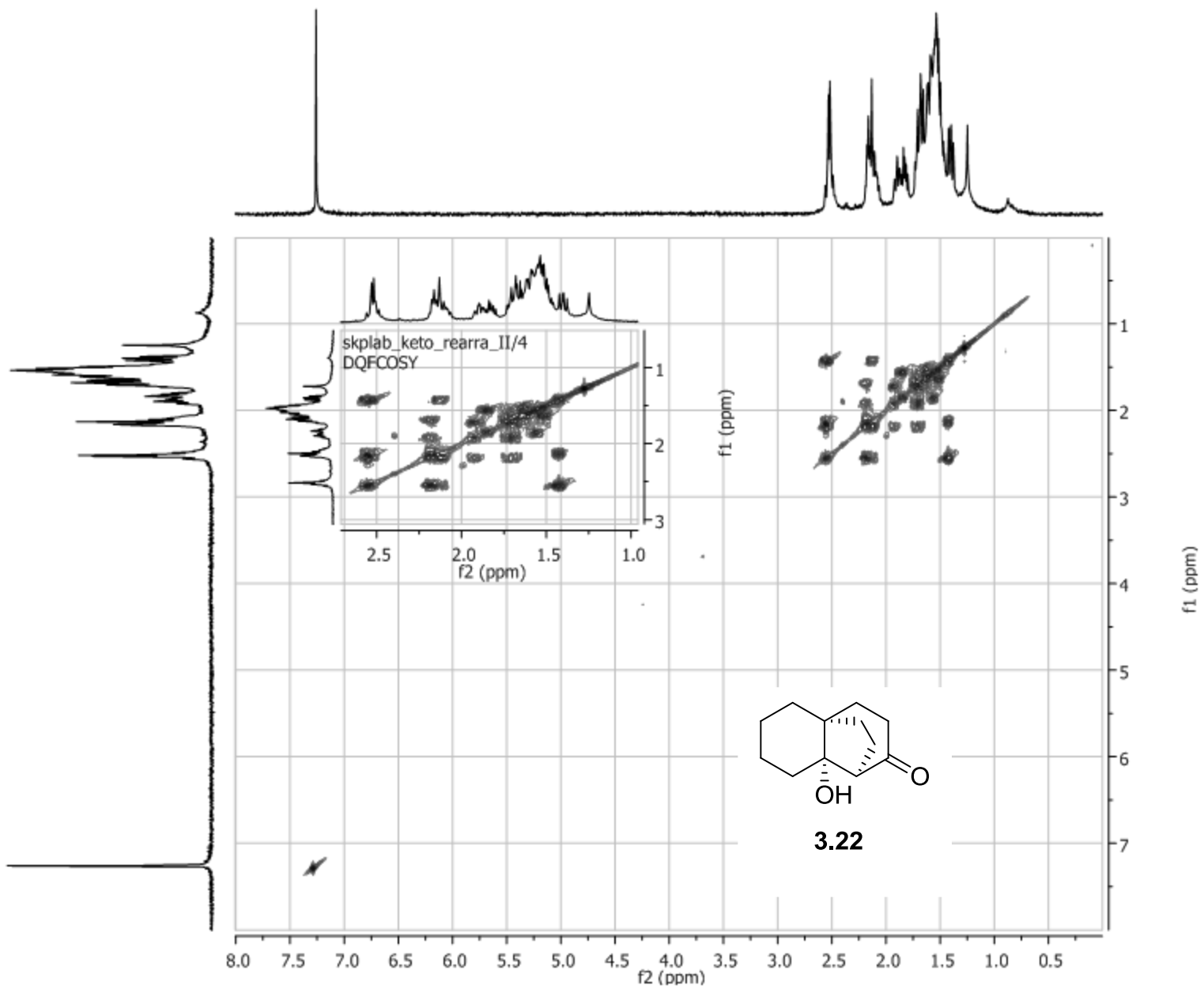


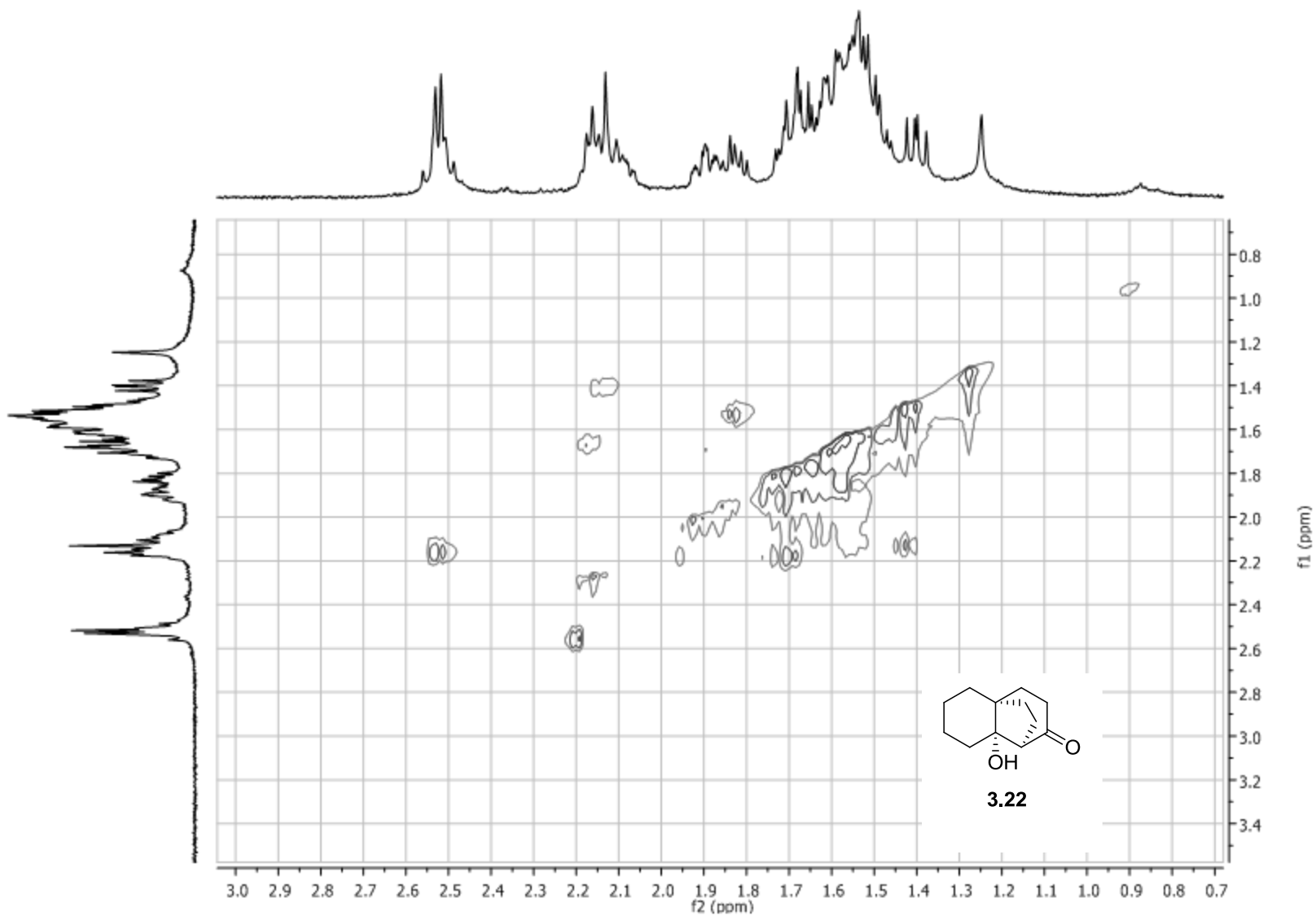
3.22

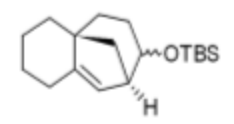
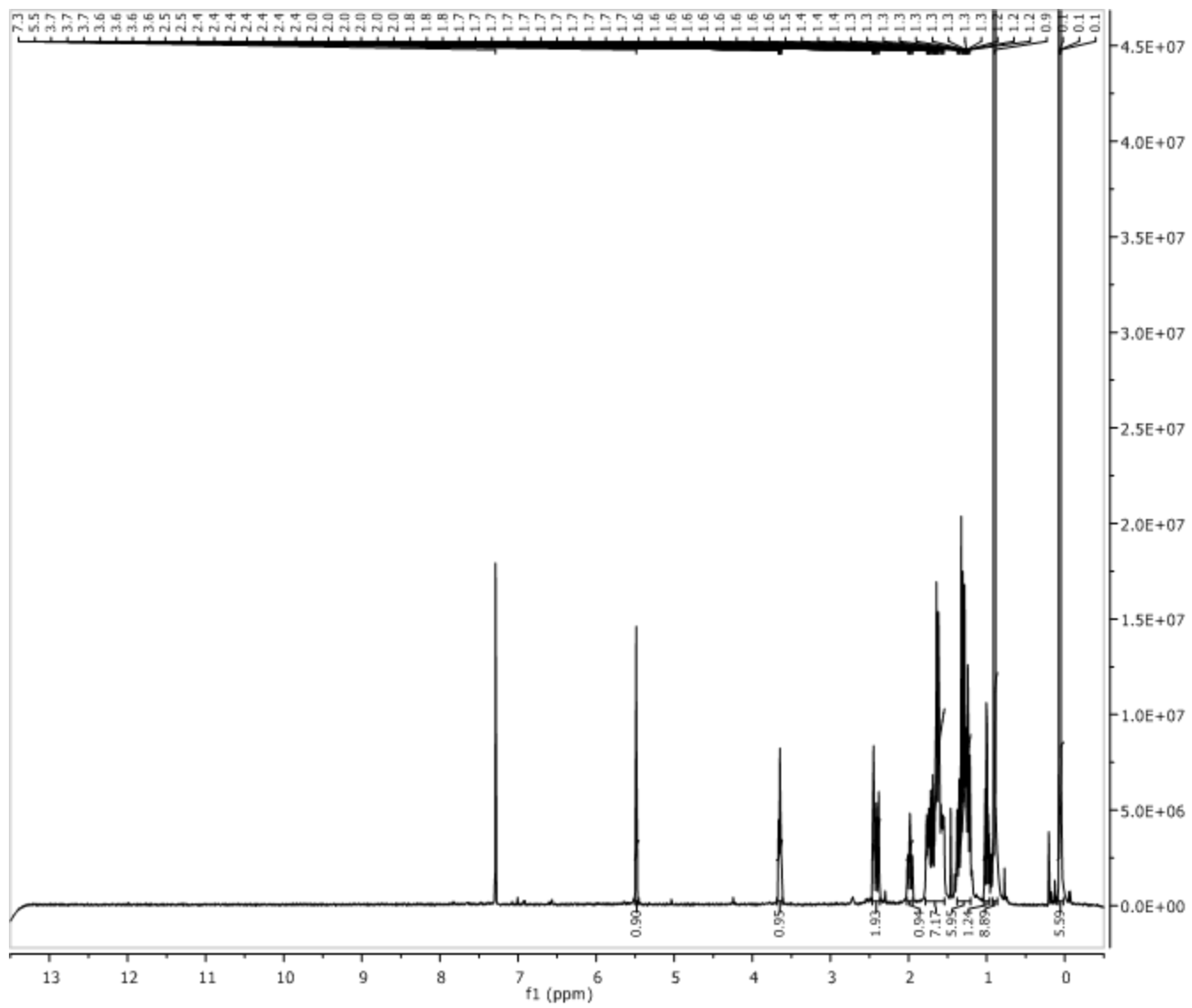


Parameter	Value
1 Spectrometer	spect
2 Solvent	CDCB
3 Temperature	297.2
4 Pulse Sequence	zgpg30
5 Experiment	1D
6 Number of Scans	5081
7 Receiver Gain	13004
8 Relaxation Delay	3.0000
9 Pulse Width	11.0000
10 Acquisition Time	1.1797
11 Spectrometer Frequency	125.76
12 Spectral Width	27777.8
13 Lowest Frequency	-683.9
14 Nucleus	13C
15 Acquired Size	32768
16 Spectral Size	65536

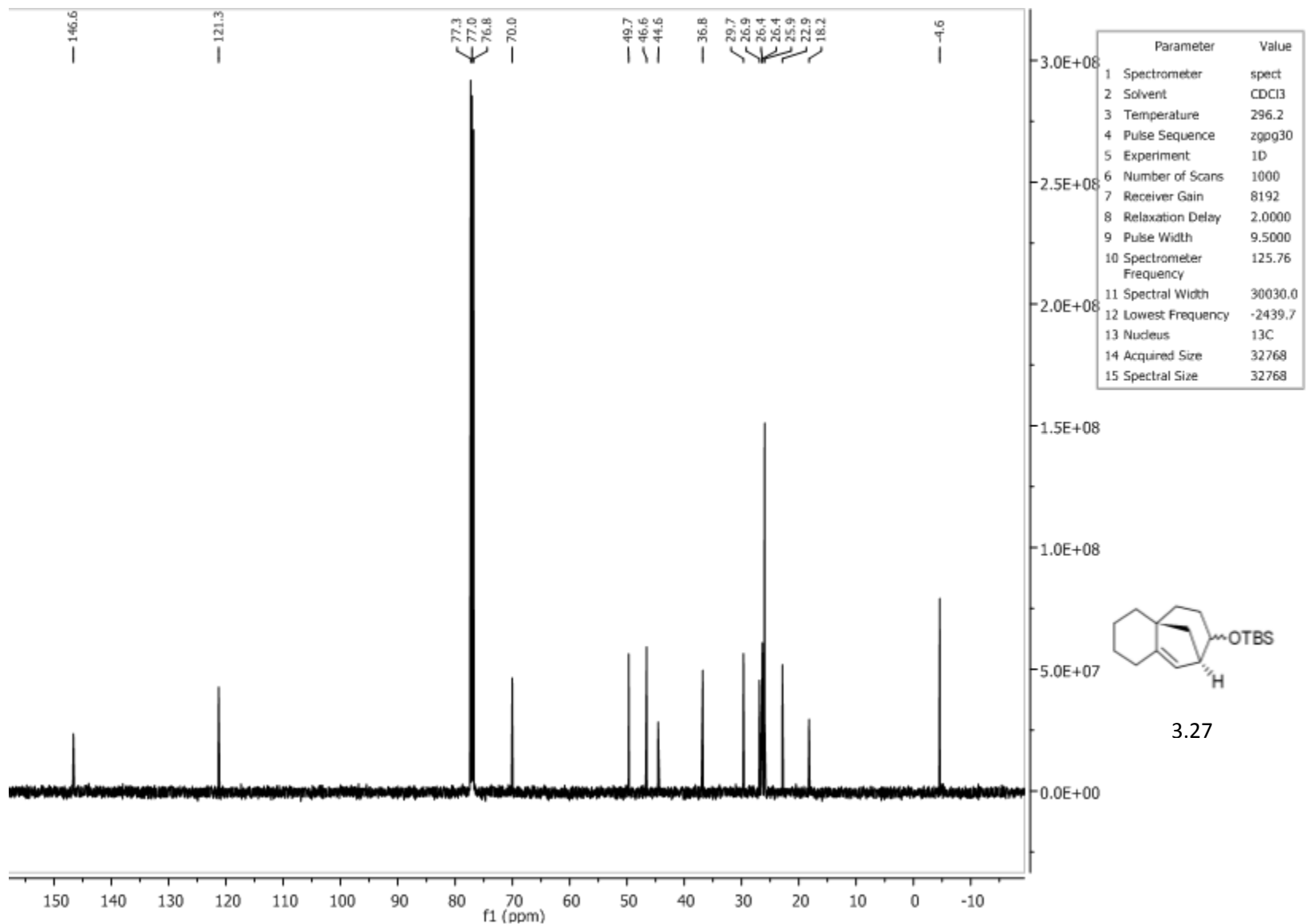


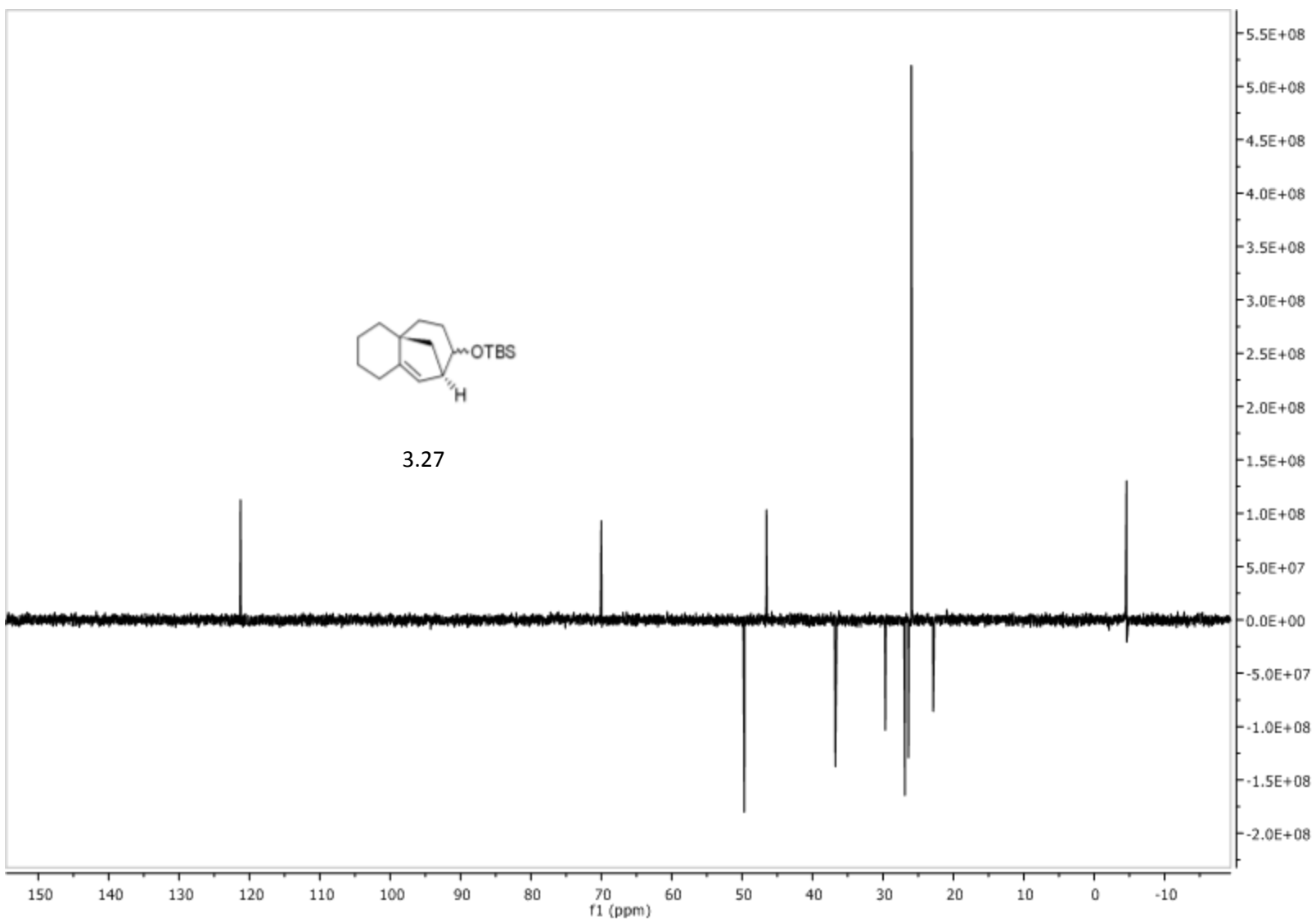


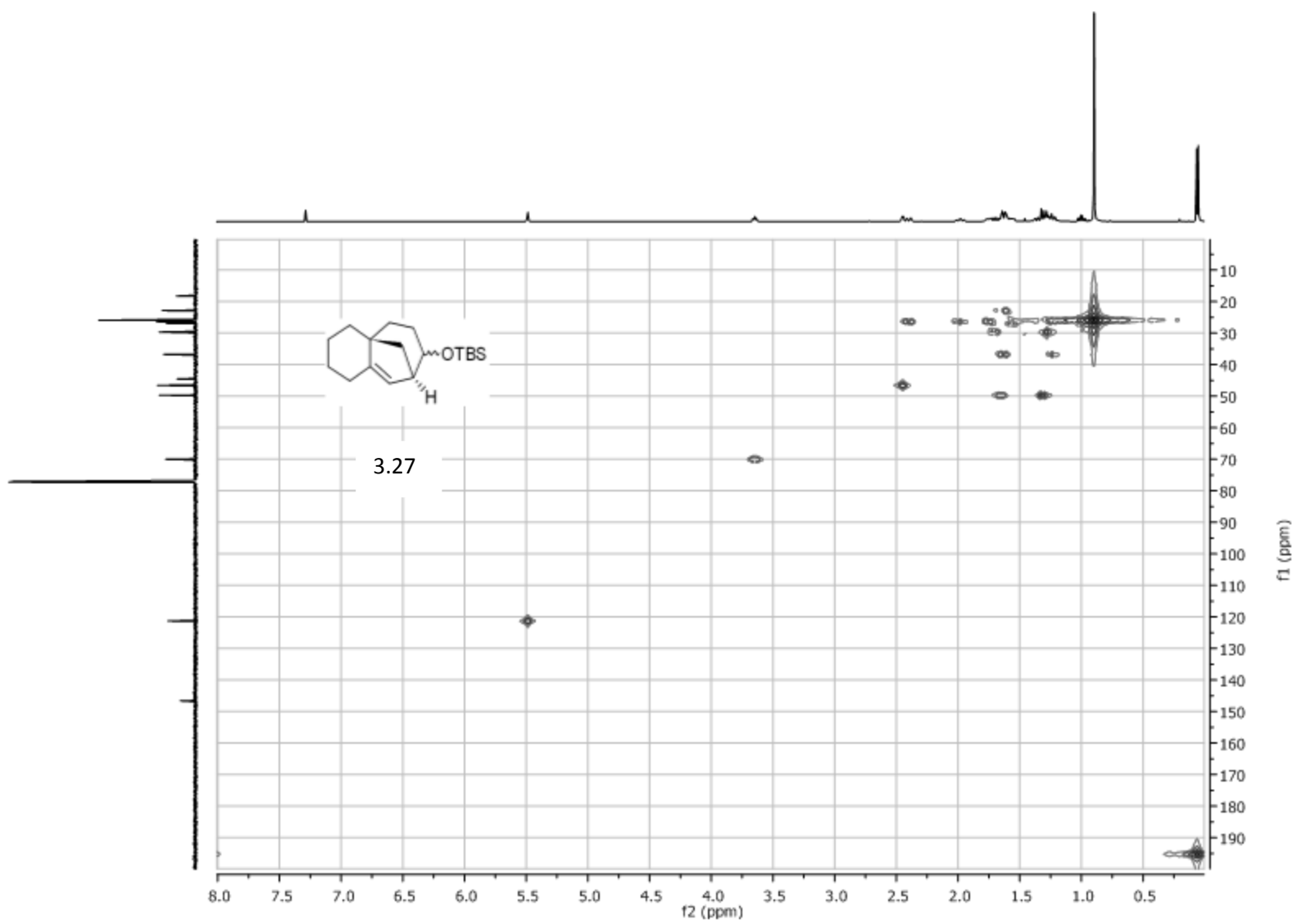


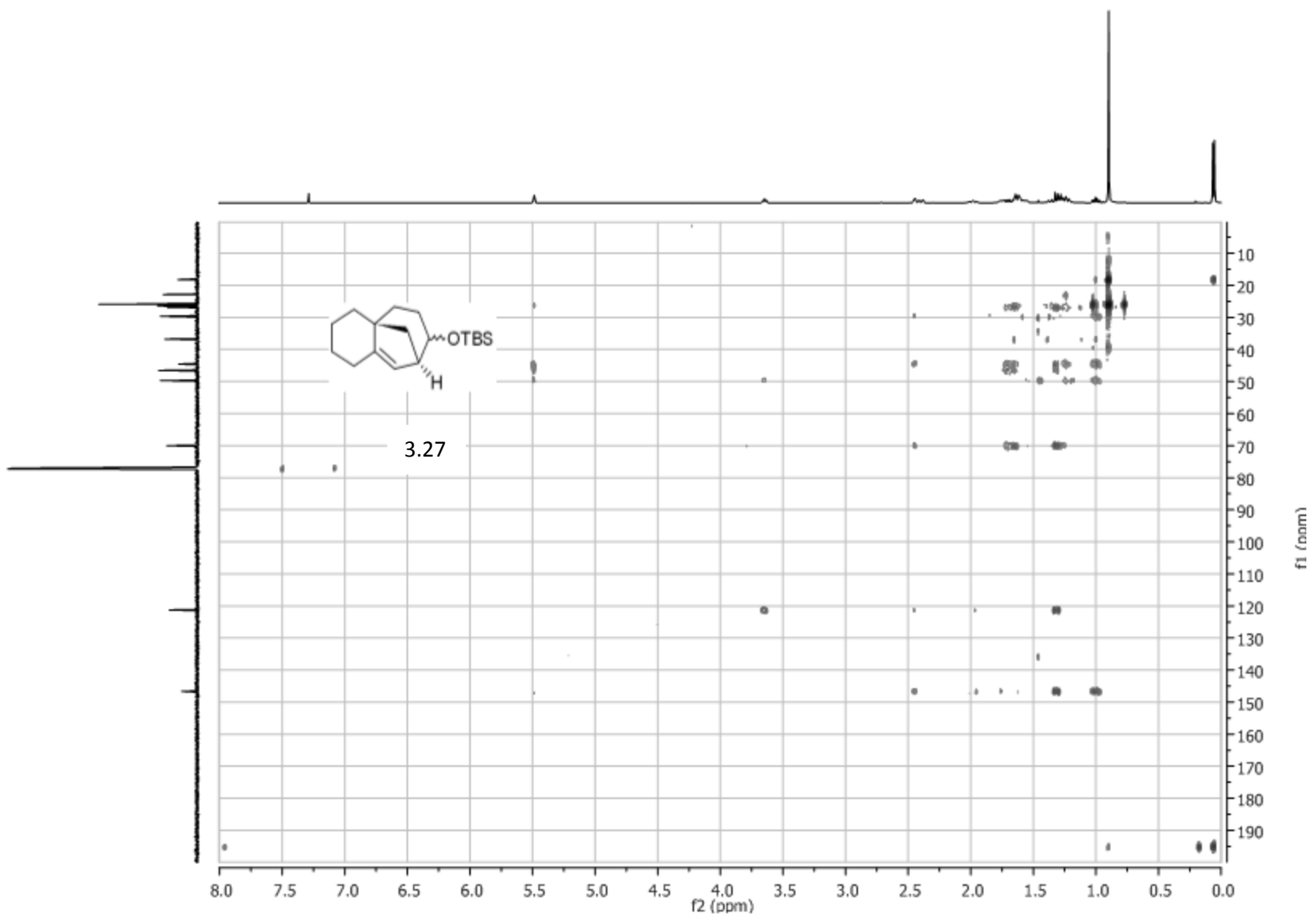


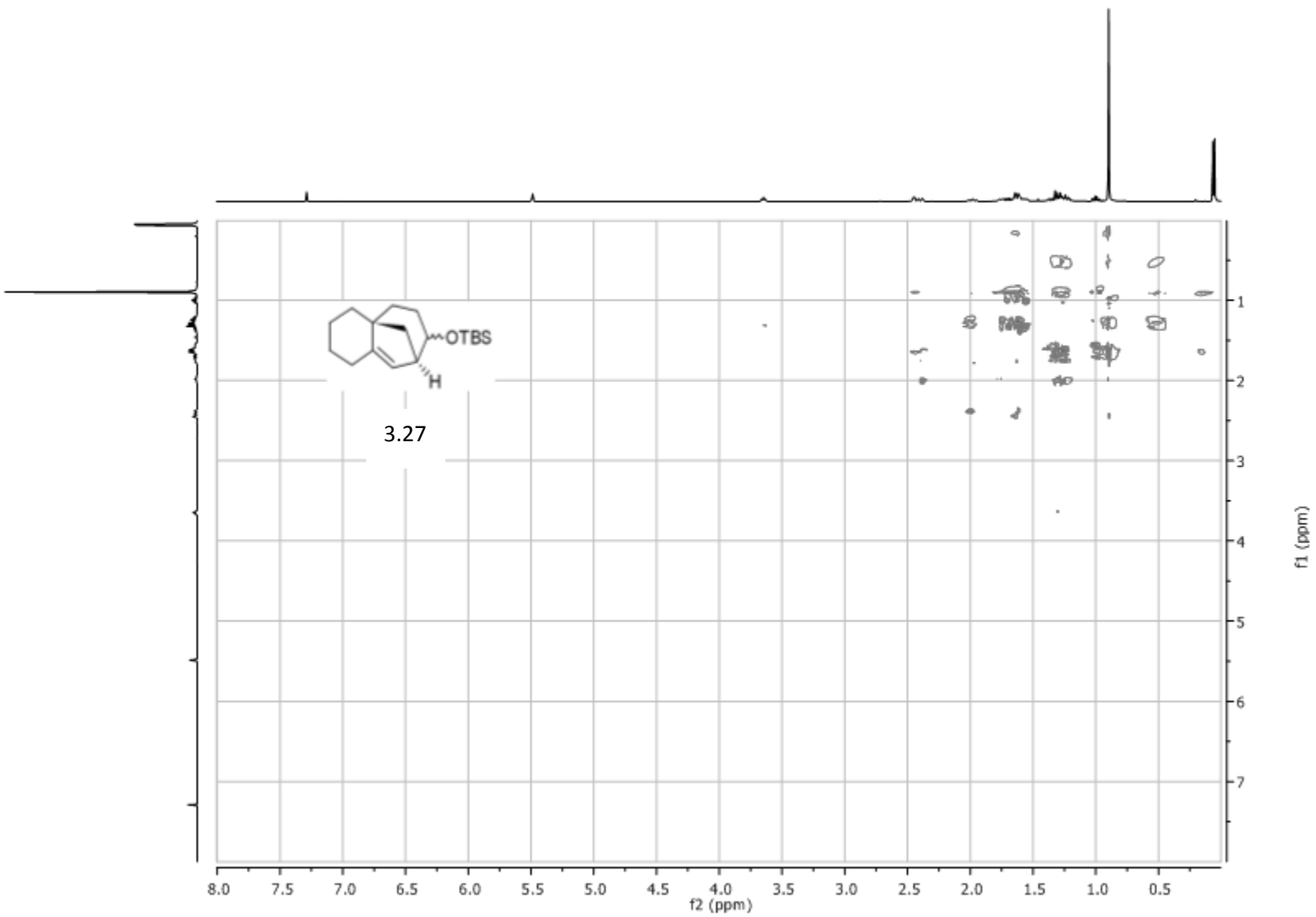
3.27

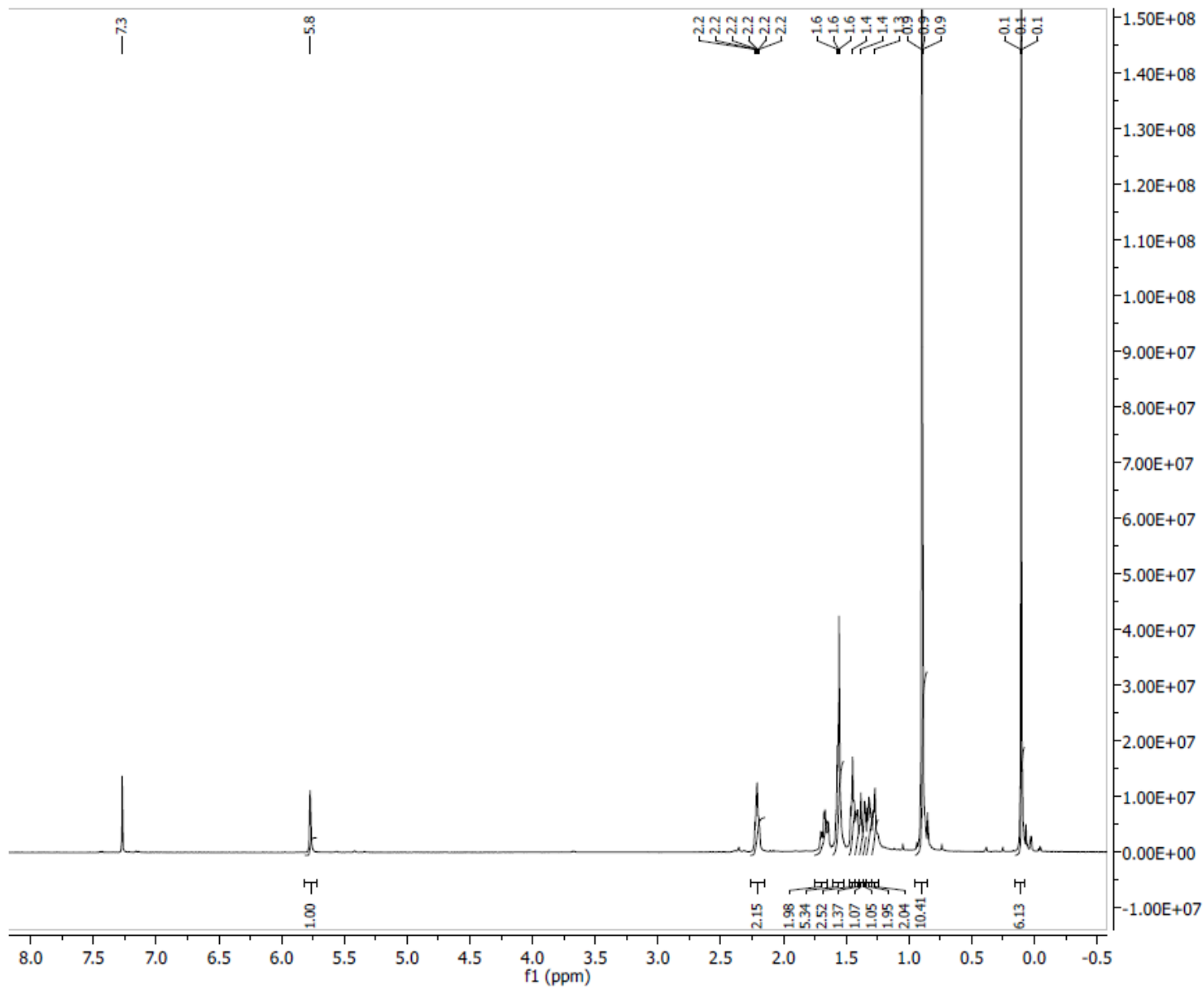




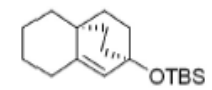




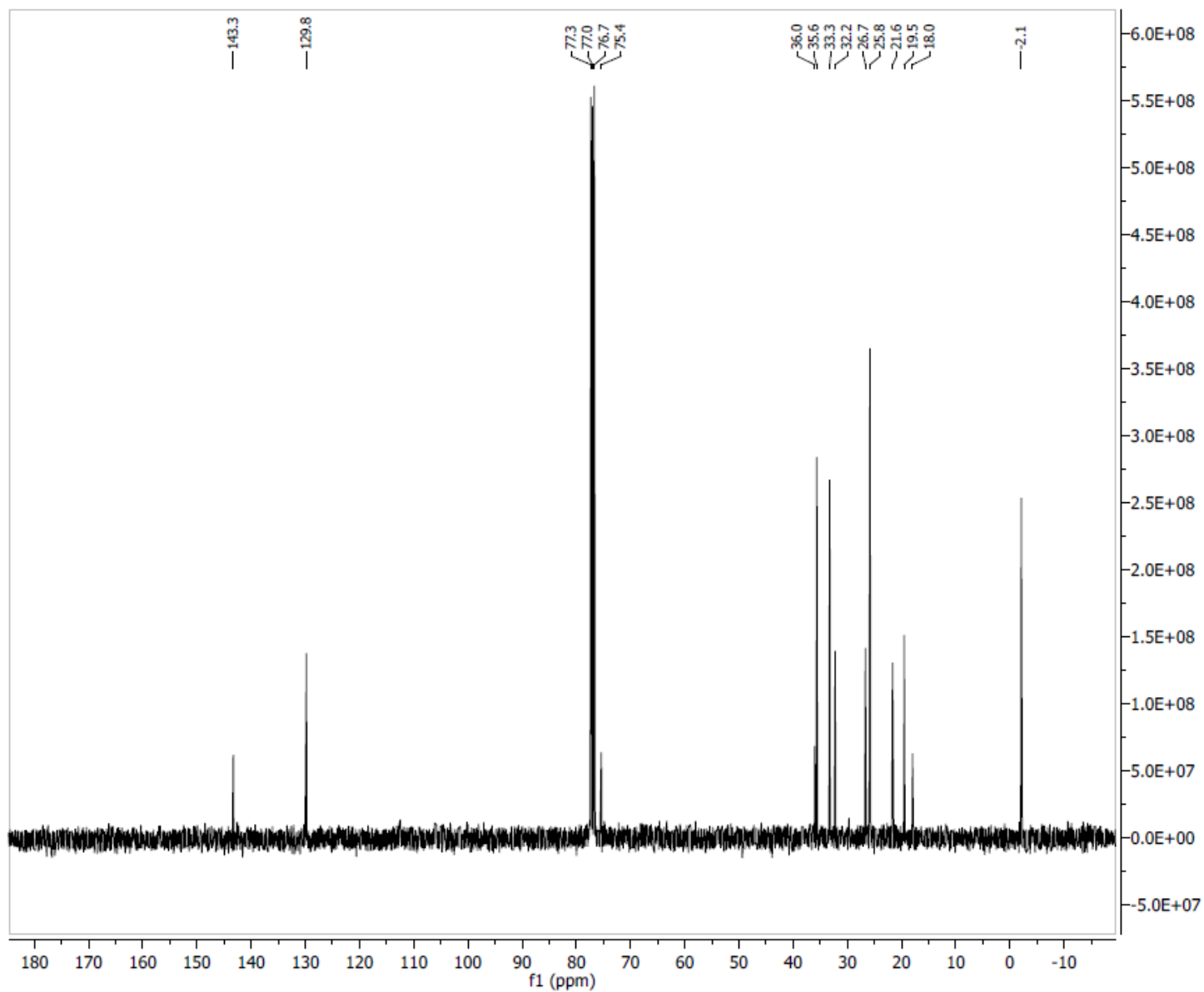




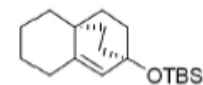
Parameter	Value
1 Spectrometer	spect
2 Solvent	CDCB3
3 Temperature	300.2
4 Pulse Sequence	zg30
5 Experiment	1D
6 Number of Scans	16
7 Receiver Gain	322
8 Relaxation Delay	1.0000
9 Pulse Width	10.0000
10 Acquisition Time	3.9846
11 Spectrometer Frequency	400.15
12 Spectral Width	8223.7
13 Lowest Frequency	-1640.8
14 Nucleus	1H
15 Acquired Size	32768
16 Spectral Size	32768



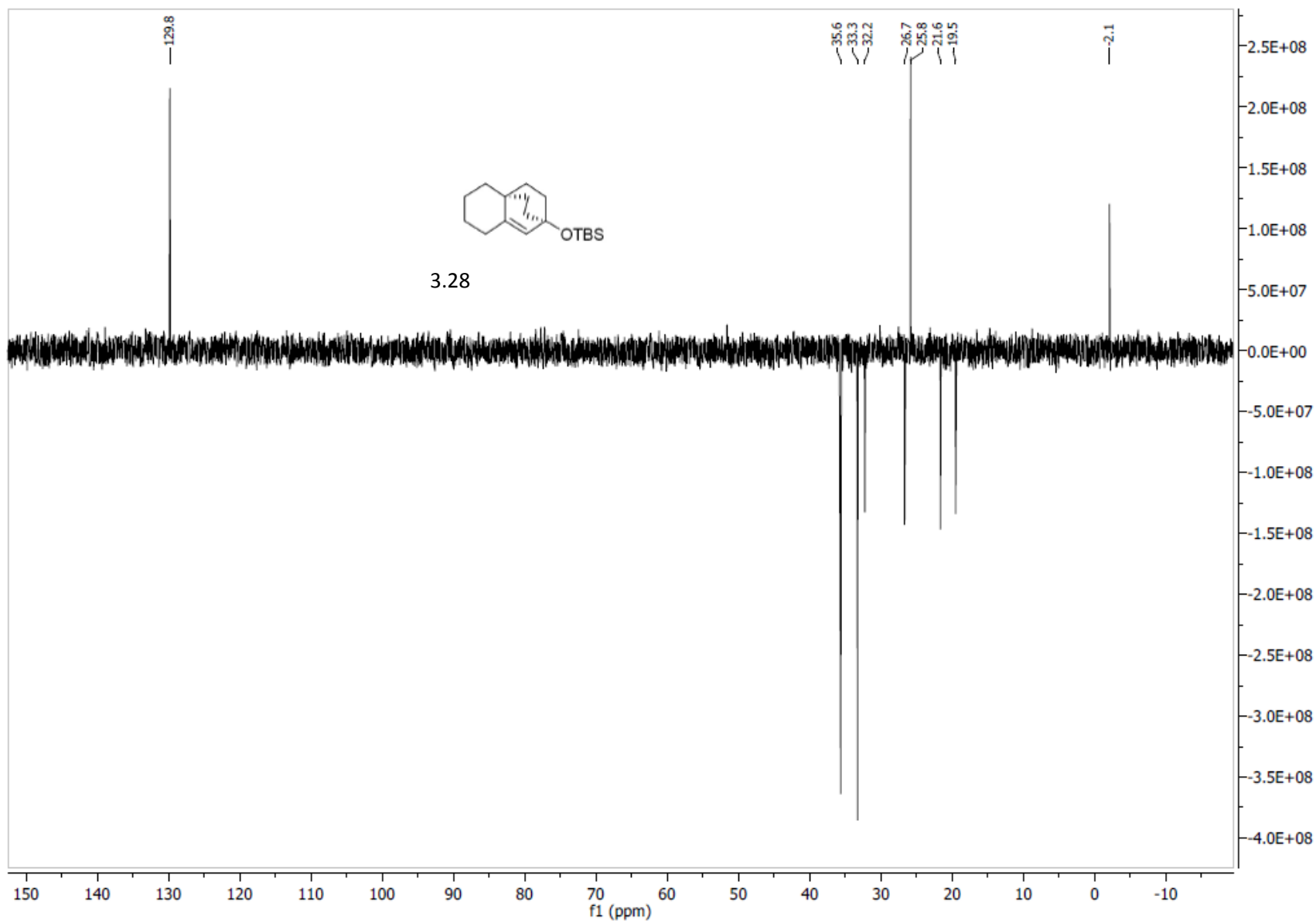
3.28

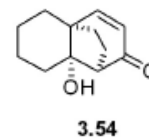
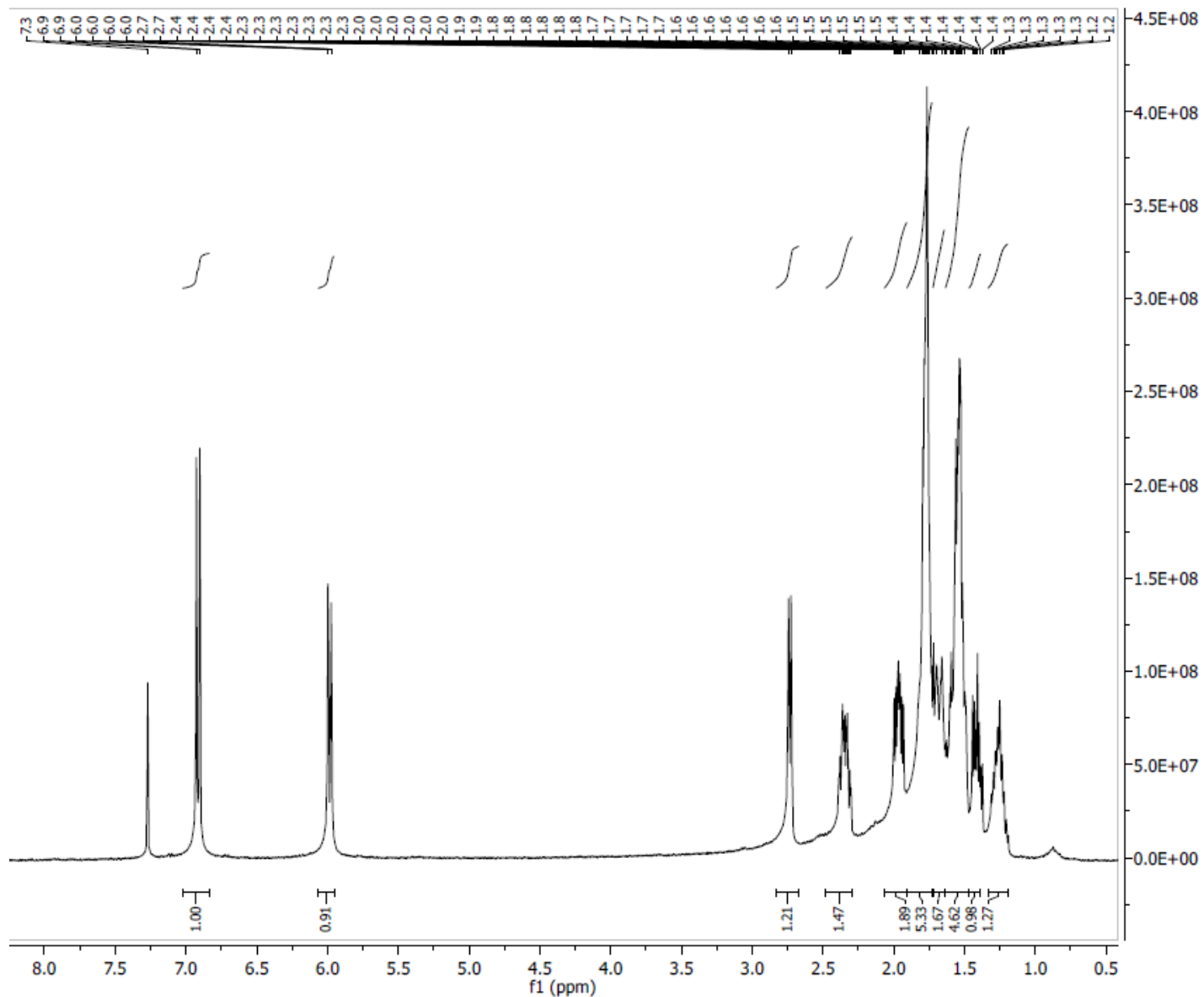


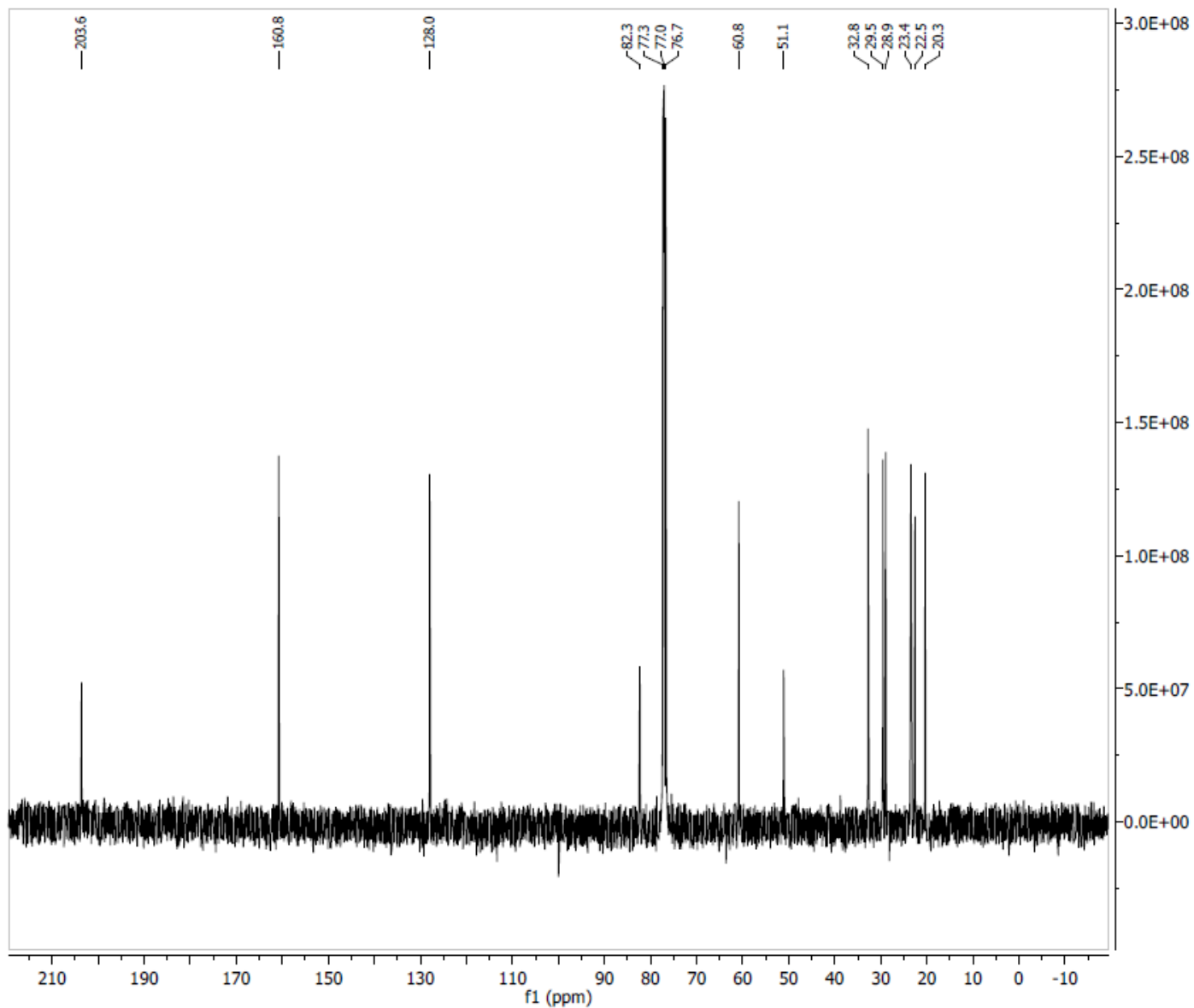
Parameter	Value
1 Spectrometer	spect
2 Solvent	CDCB
3 Temperature	300.2
4 Pulse Sequence	zgpg30
5 Experiment	1D
6 Number of Scans	1500
7 Receiver Gain	32800
8 Relaxation Delay	2.0000
9 Pulse Width	9.0000
10 Acquisition Time	1.3631
11 Spectrometer Frequency	100.62
12 Spectral Width	24038.5
13 Lowest Frequency	-1957.9
14 Nucleus	13C
15 Acquired Size	32768
16 Spectral Size	32768



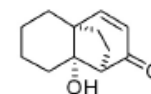
3.28



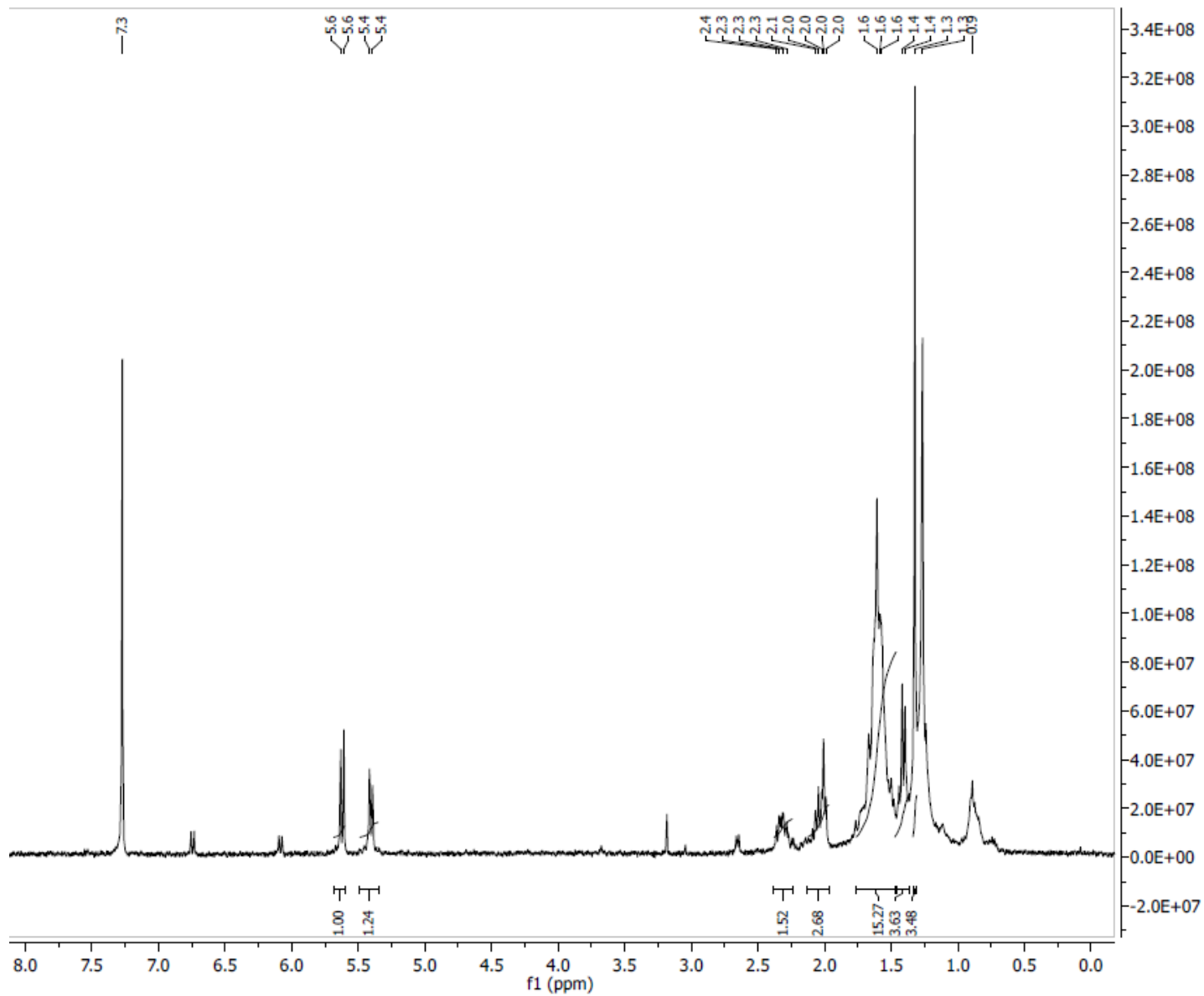




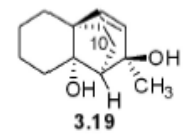
Parameter	Value
1 Spectrometer	spect
2 Solvent	CDCl3
3 Temperature	298.2
4 Pulse Sequence	zg30
5 Experiment	1D
6 Number of Scans	8
7 Receiver Gain	256
8 Relaxation Delay	1.0000
9 Pulse Width	10.2500
10 Acquisition Time	3.9846
11 Spectrometer Frequency	400.15
12 Spectral Width	8223.7
13 Lowest Frequency	-1640.8
14 Nucleus	1H
15 Acquired Size	32768
16 Spectral Size	32768

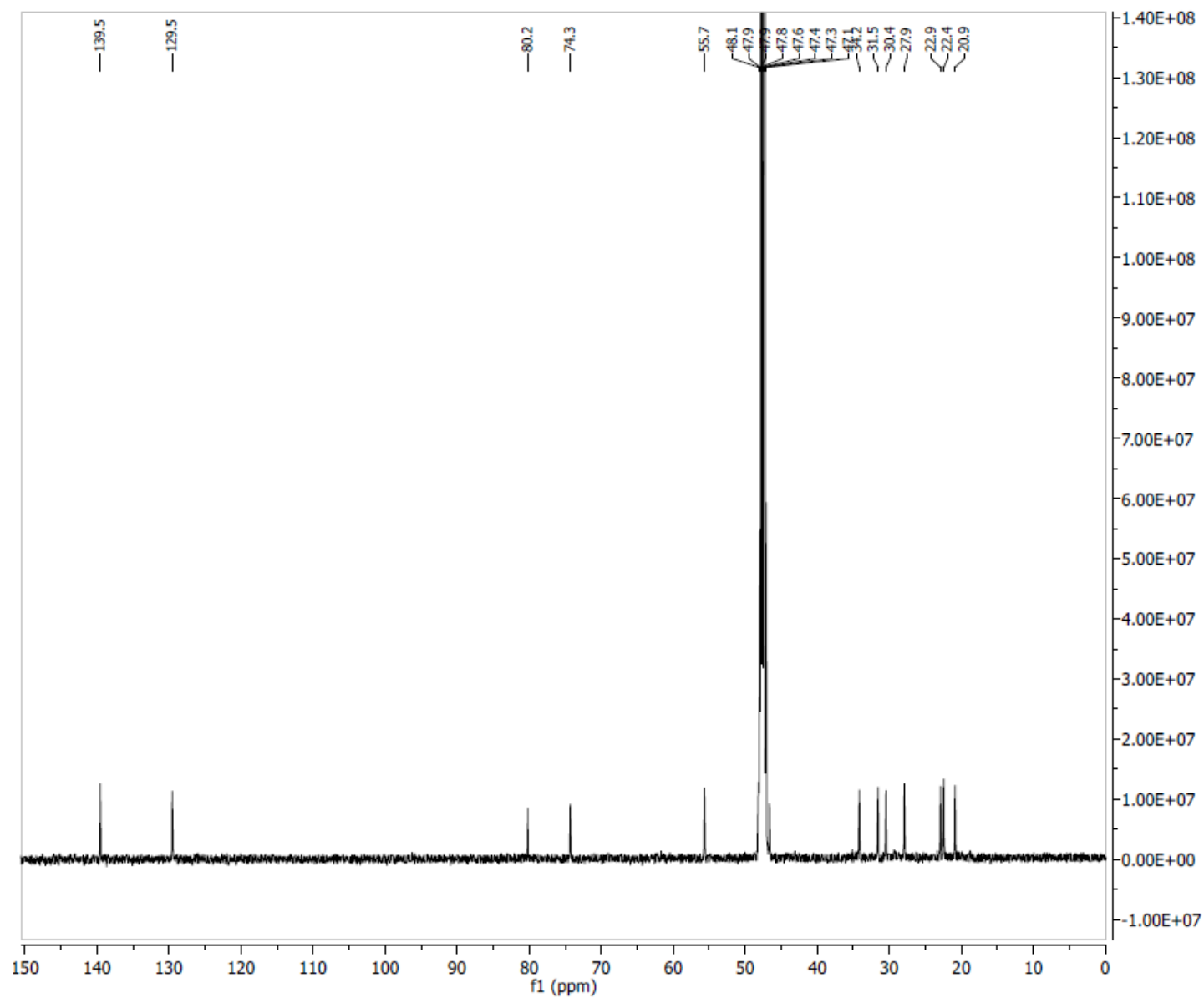


3.54

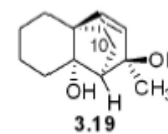


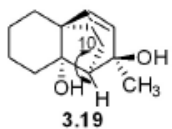
Parameter	Value
1 Spectrometer	spect
2 Solvent	CDCl3
3 Temperature	298.2
4 Pulse Sequence	zg30
5 Experiment	1D
6 Number of Scans	8
7 Receiver Gain	512
8 Relaxation Delay	1.0000
9 Pulse Width	10.2500
10 Acquisition Time	3.9846
11 Spectrometer Frequency	400.15
12 Spectral Width	8223.7
13 Lowest Frequency	-1640.8
14 Nucleus	1H
15 Acquired Size	32768
16 Spectral Size	32768



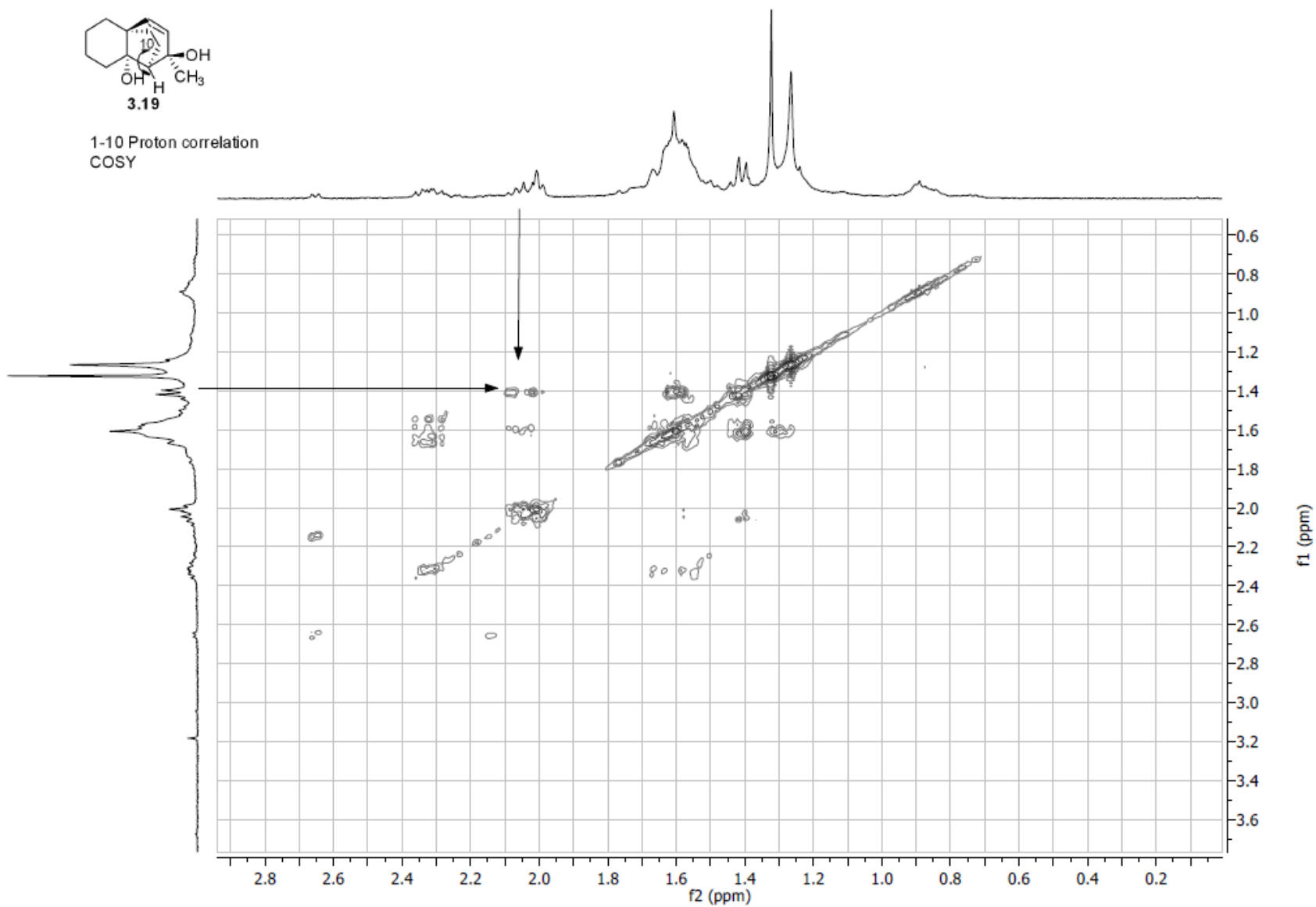


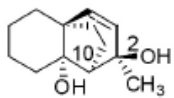
Parameter	Value
1 Spectrometer	spect
2 Solvent	MeOD
3 Temperature	298.2
4 Pulse Sequence	zgpg30
5 Experiment	1D
6 Number of Scans	6144
7 Receiver Gain	9195
8 Relaxation Delay	3.0000
9 Pulse Width	9.0000
10 Acquisition Time	1.1796
11 Spectrometer Frequency	125.76
12 Spectral Width	27777.8
13 Lowest Frequency	-683.9
14 Nucleus	13C
15 Acquired Size	32768
16 Spectral Size	32768





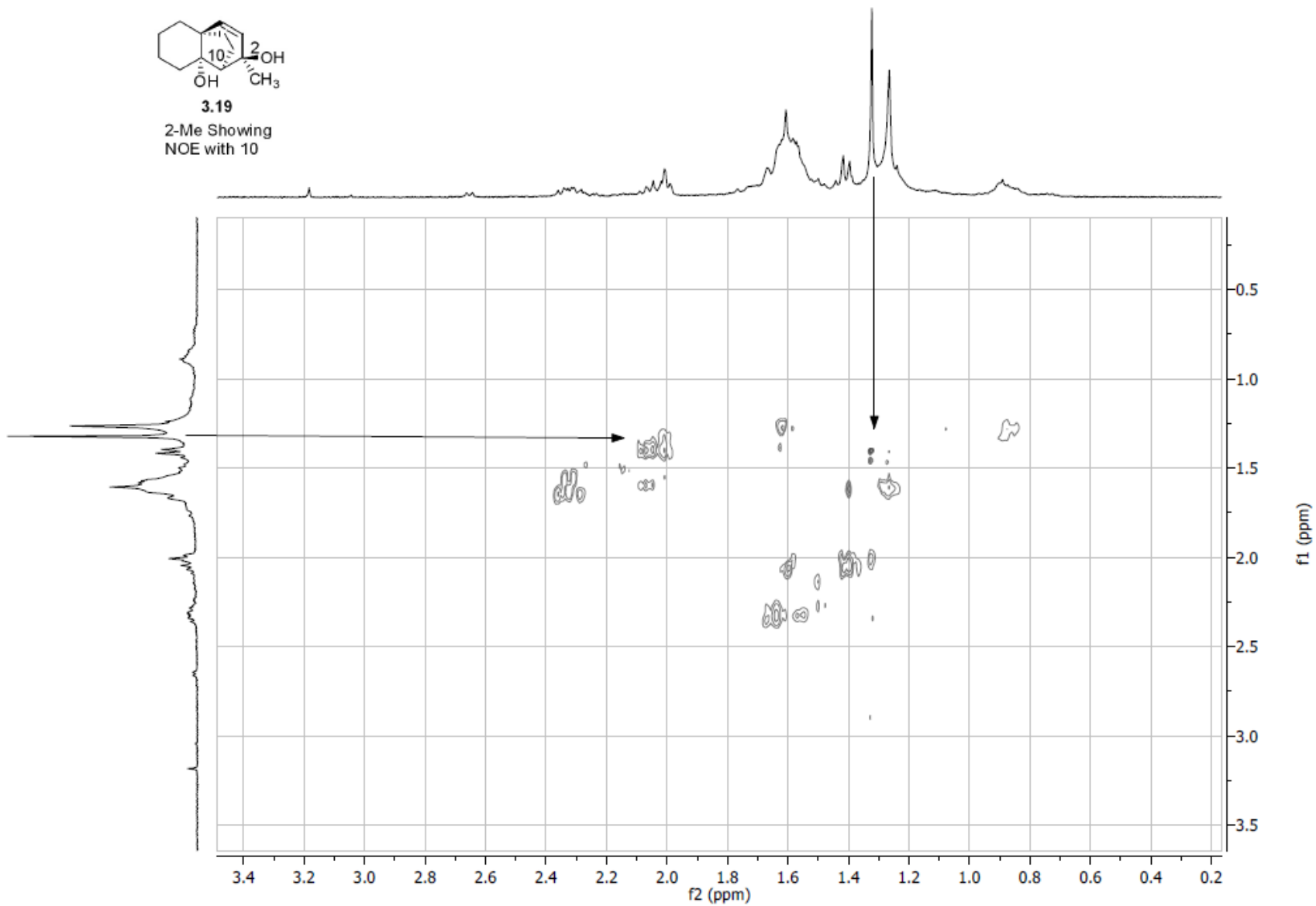
1-10 Proton correlation
COSY

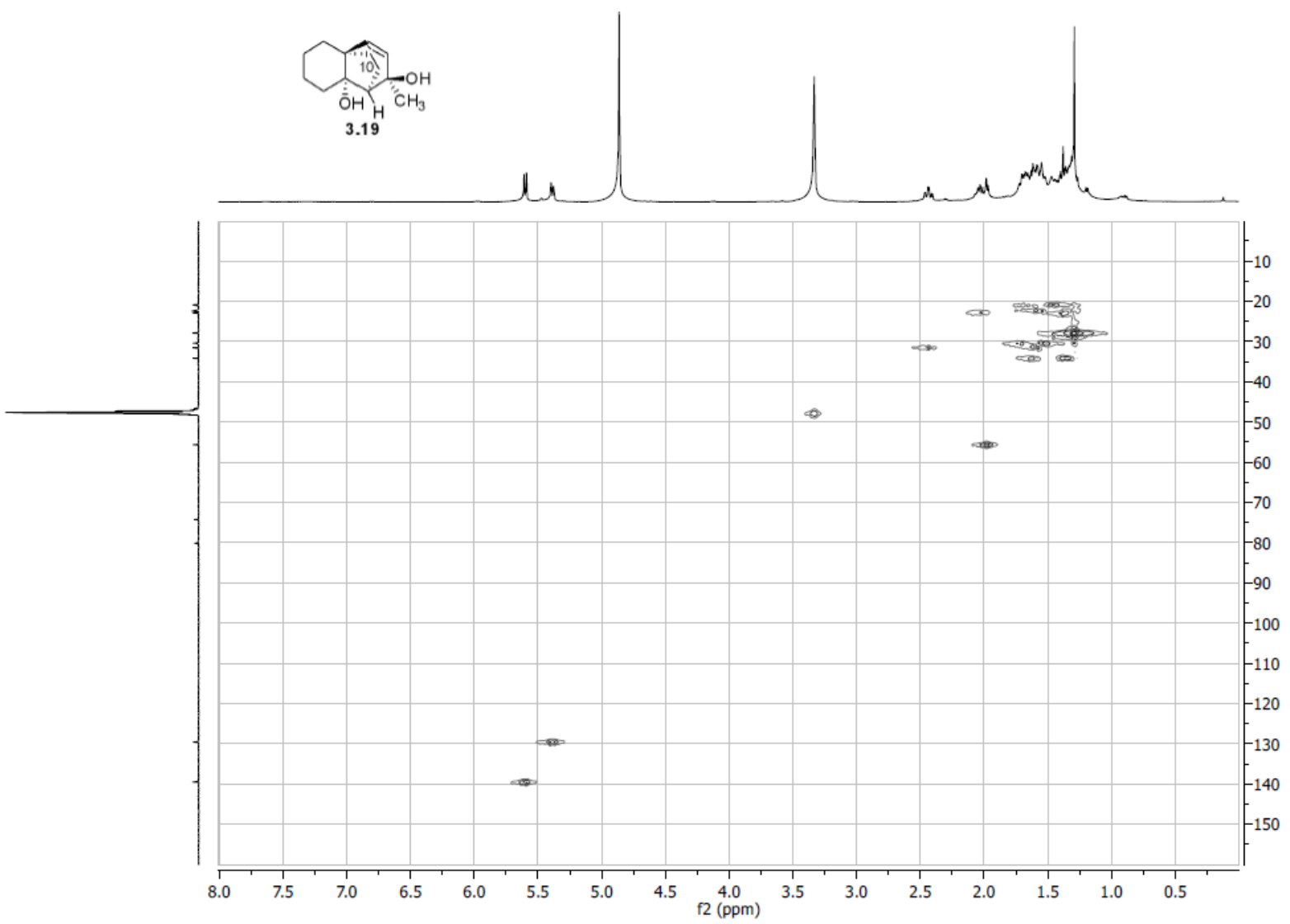
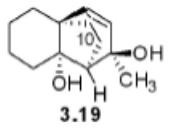




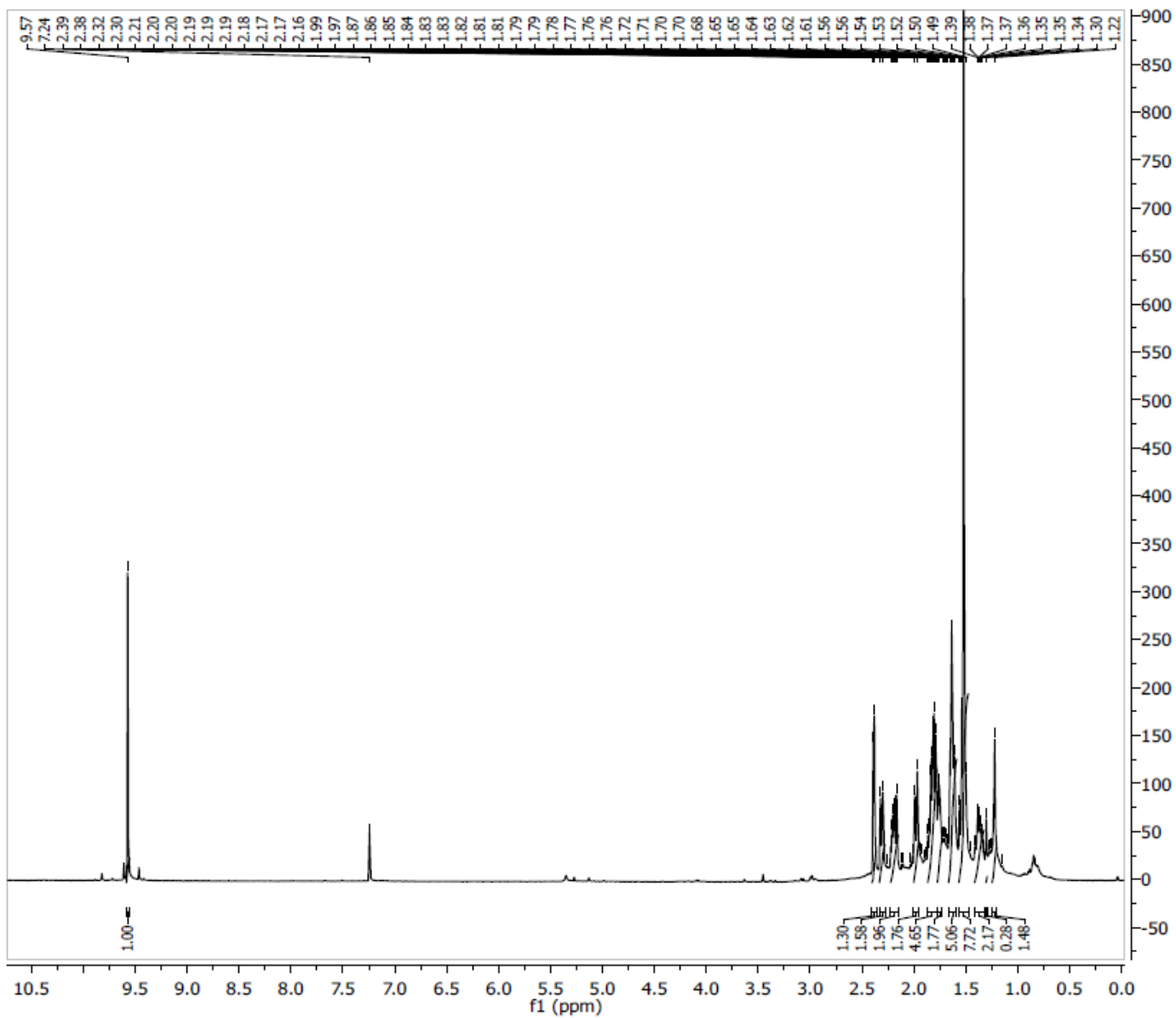
3.19

2-Me Showing
NOE with 10

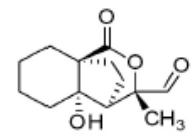




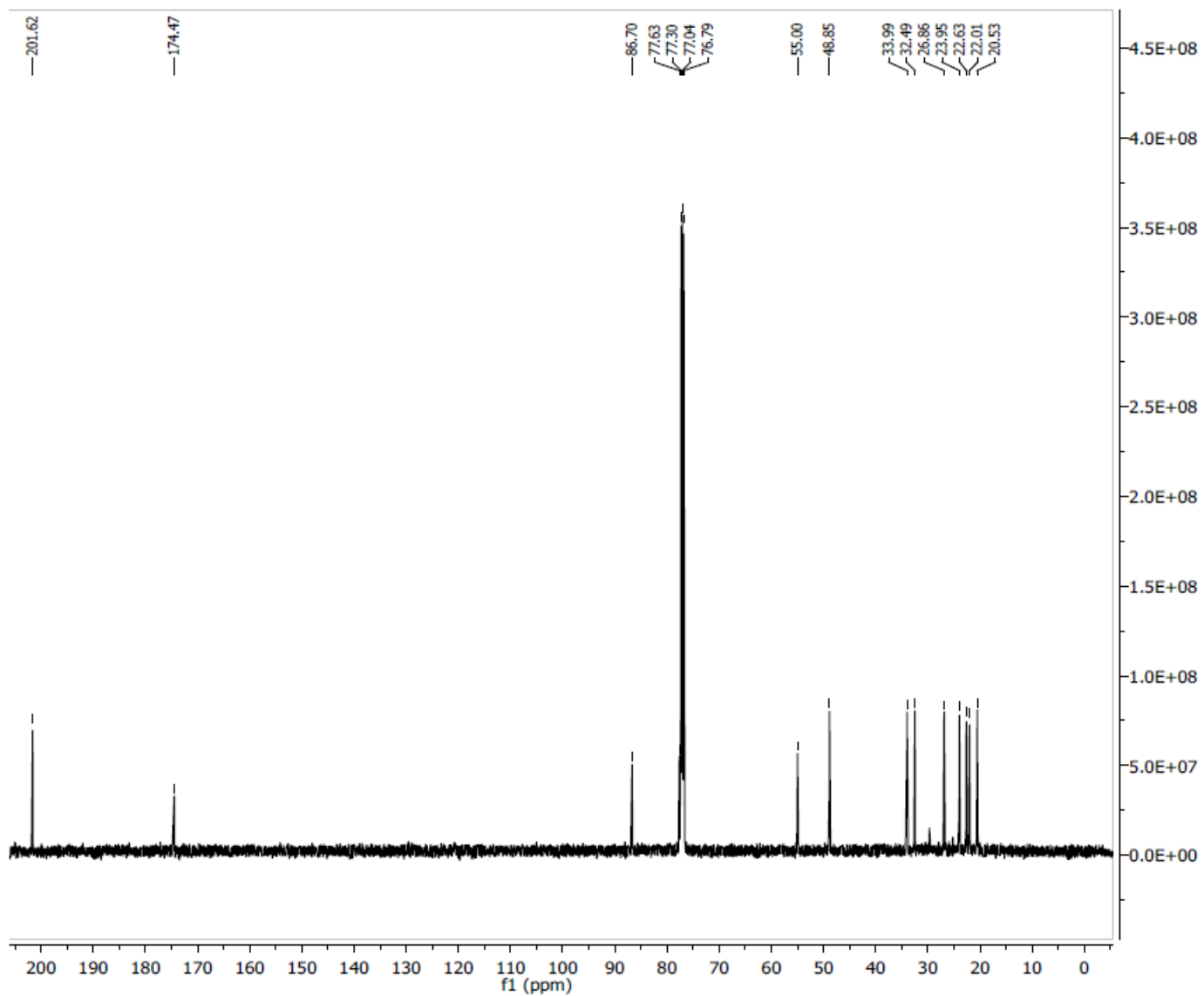
HMQC



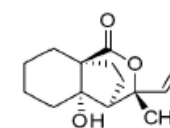
Parameter	Value
1 Origin	Varian
2 Site	
3 Spectrometer	inova
4 Solvent	cdcl3
5 Temperature	25.0
6 Pulse Sequence	s2pul
7 Experiment	1D
8 Number of Scans	32
9 Receiver Gain	30
10 Relaxation Delay	1.0000
11 Pulse Width	0.0000
12 Acquisition Time	2.0486
13 Acquisition Date	2010-11-11T08:25:37
14 Modification Date	2010-11-11T08:26:42
15 Spectrometer Frequency	599.89
16 Spectral Width	9598.1
17 Lowest Frequency	-1199.8
18 Nucleus	1H
19 Acquired Size	19663
20 Spectral Size	65536



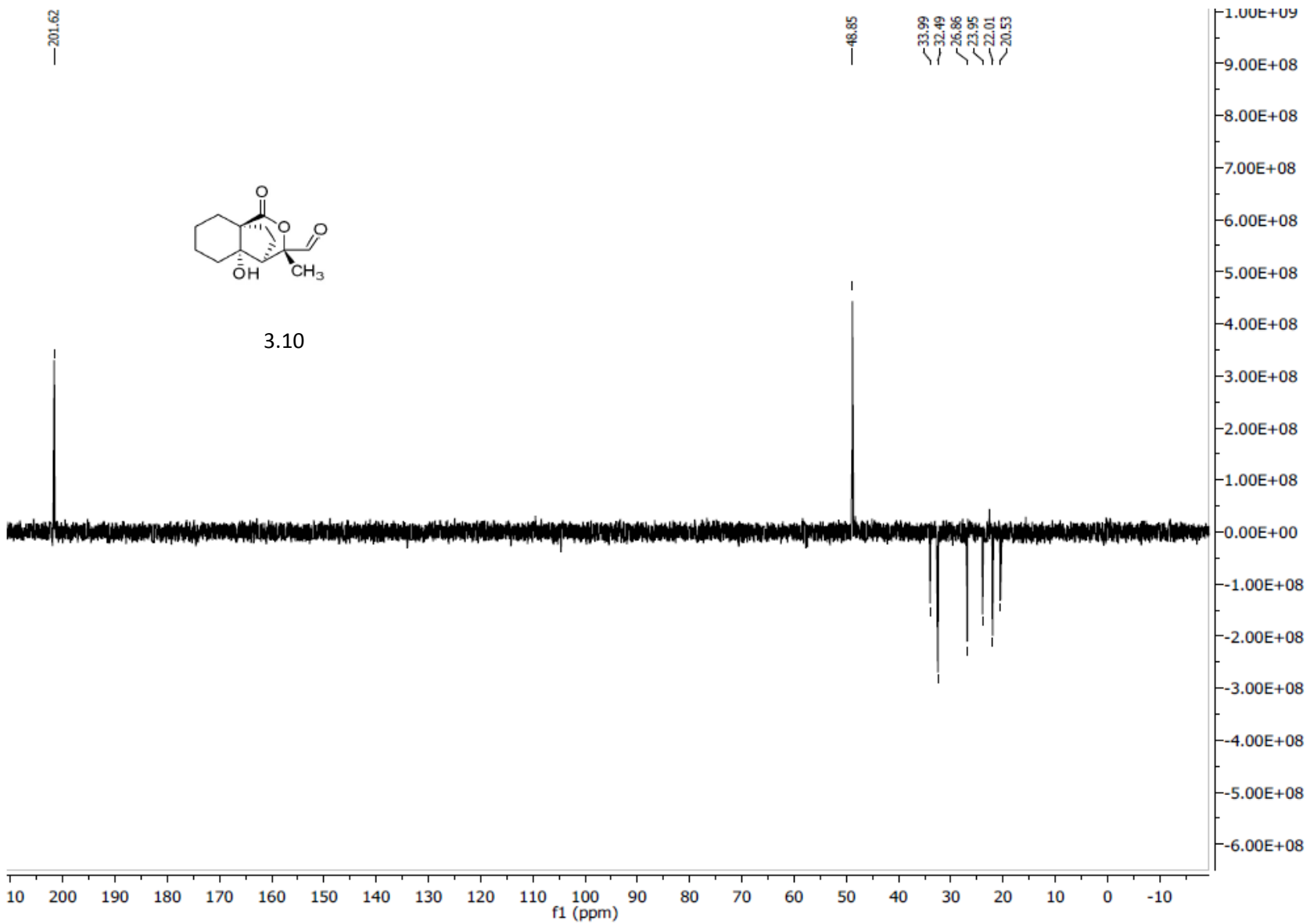
3.10

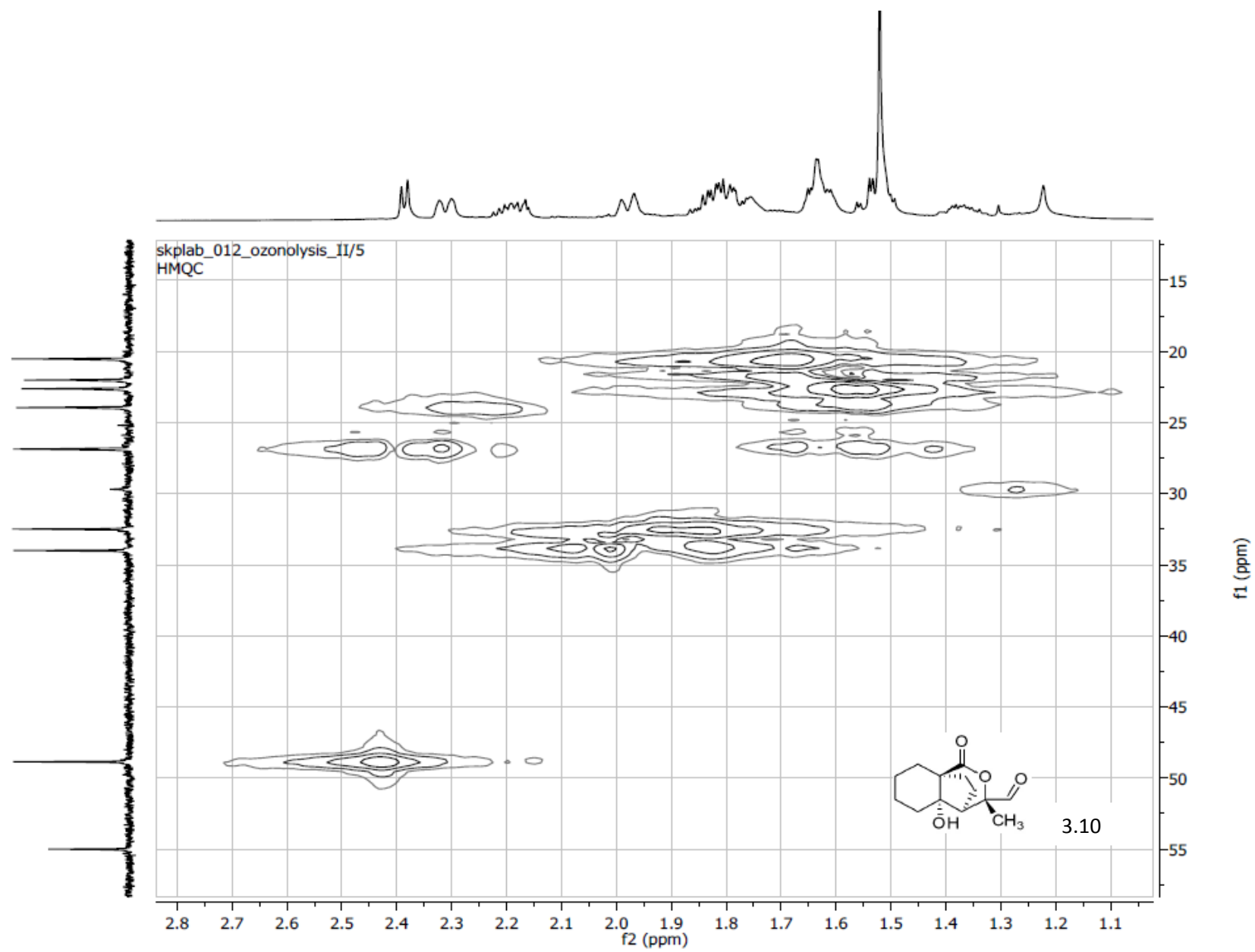


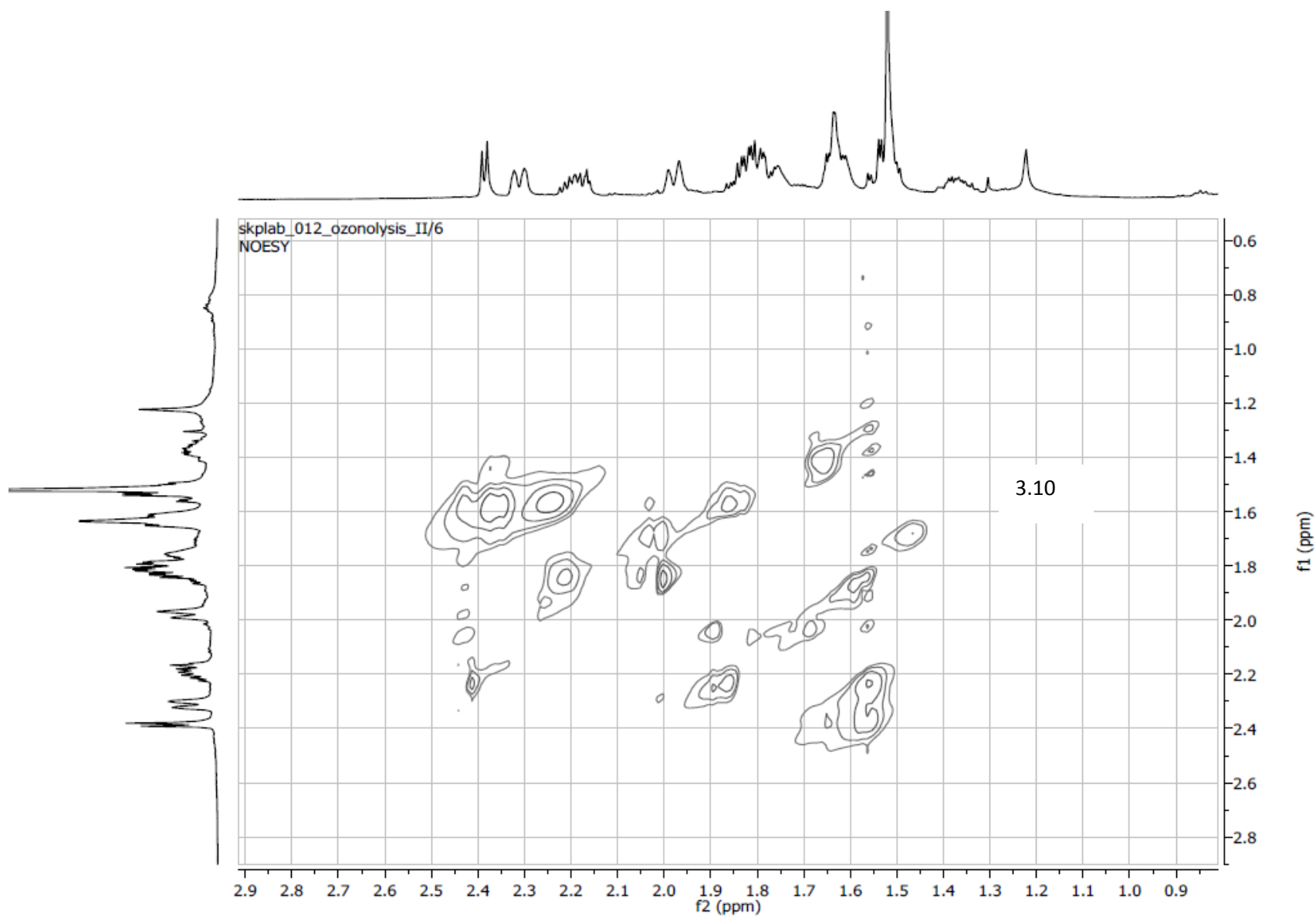
Parameter	Value
1 Spectrometer	spect
2 Solvent	CDCI3
3 Temperature	298.2
4 Pulse Sequence	zgpg30
5 Experiment	1D
6 Number of Scans	3072
7 Receiver Gain	7298
8 Relaxation Delay	3.0000
9 Pulse Width	9.0000
10 Spectrometer Frequency	125.76
11 Spectral Width	27777.8
12 Lowest Frequency	-683.9
13 Nucleus	13C
14 Acquired Size	32768
15 Spectral Size	32768

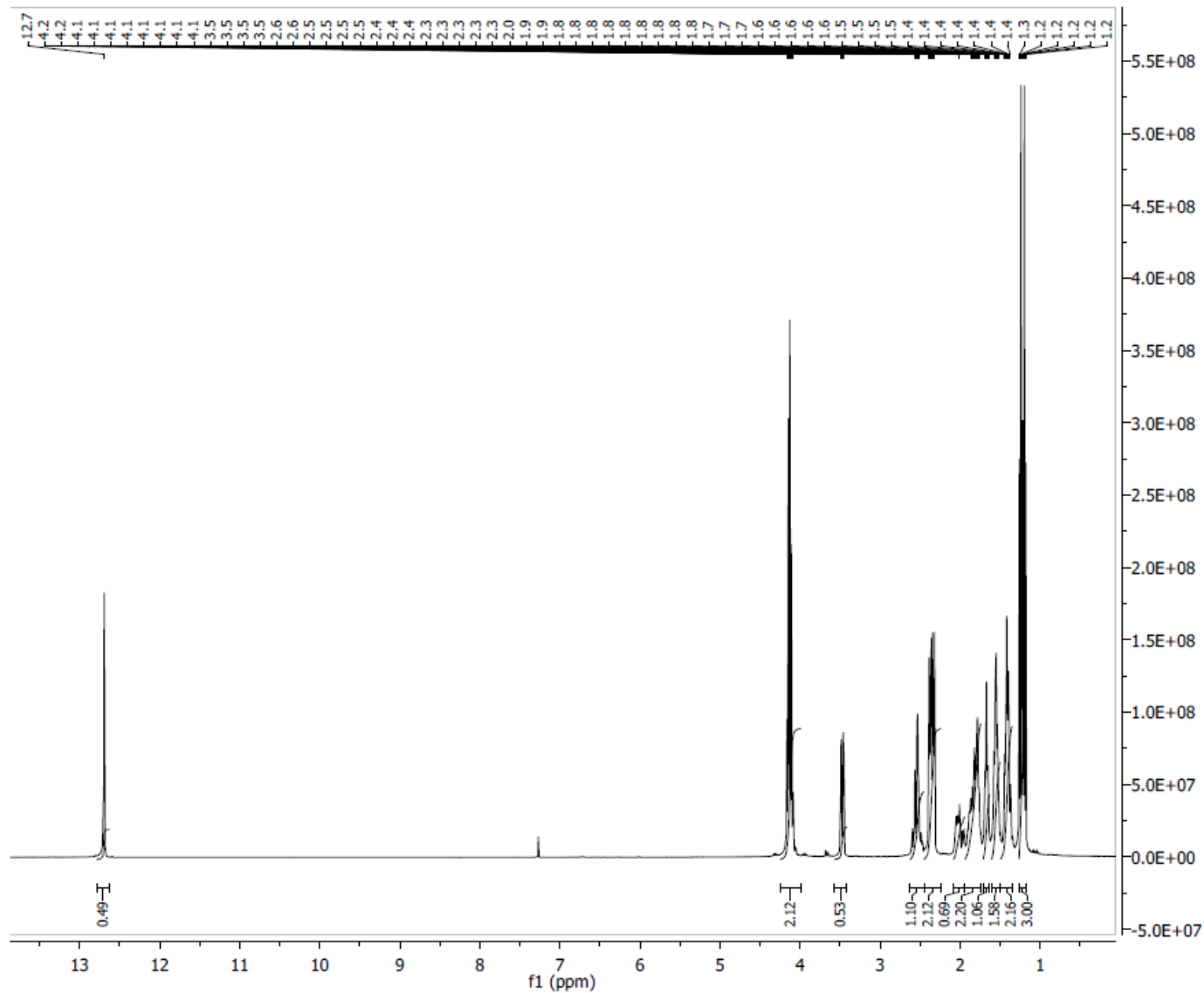


3.10

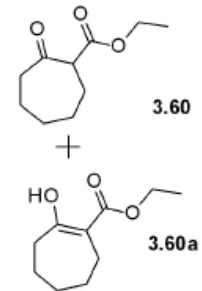


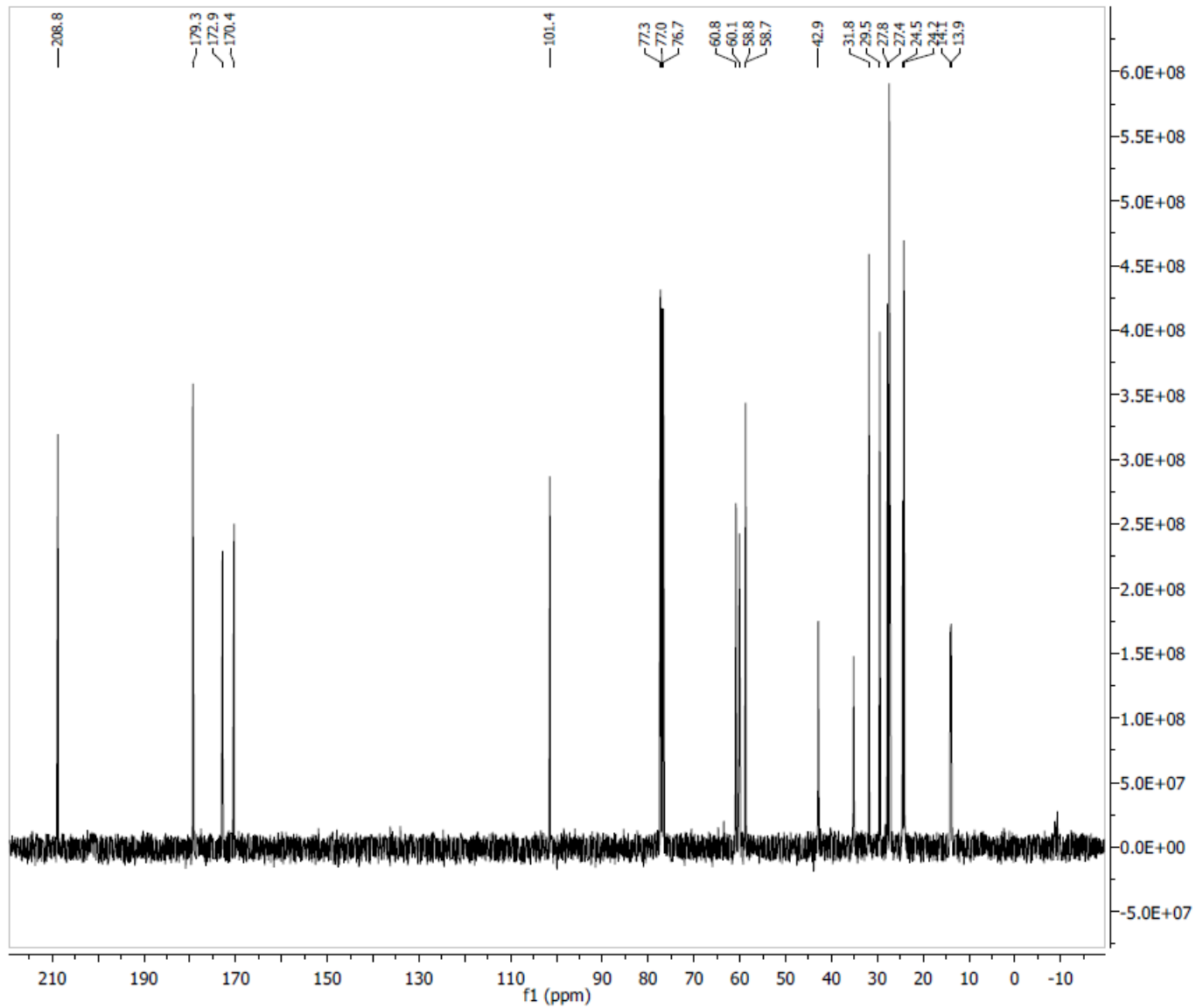




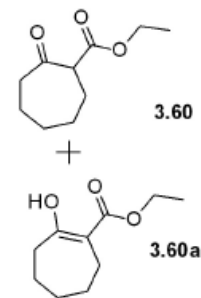


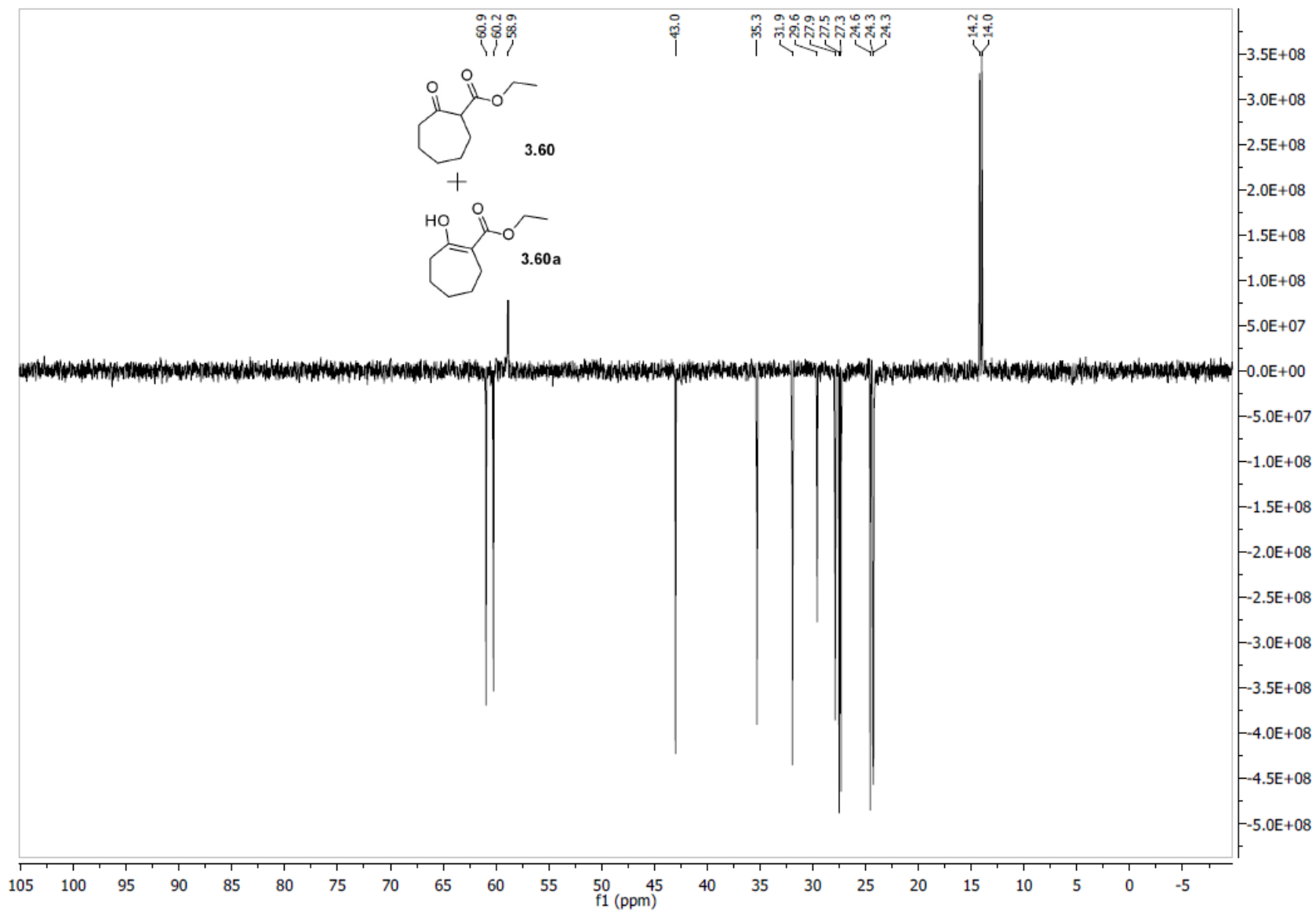
Parameter	Value
1 Spectrometer	
2 Solvent	
3 Temperature	
4 Pulse Sequence	
5 Experiment	1D
6 Number of Scans	
7 Receiver Gain	
8 Relaxation Delay	
9 Pulse Width	
10 Acquisition Time	nan
11 Spectrometer Frequency	400.15
12 Spectral Width	8223.7
13 Lowest Frequency	-1640.8
14 Nucleus	Unknown
15 Acquired Size	0
16 Spectral Size	32768

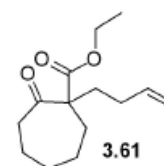
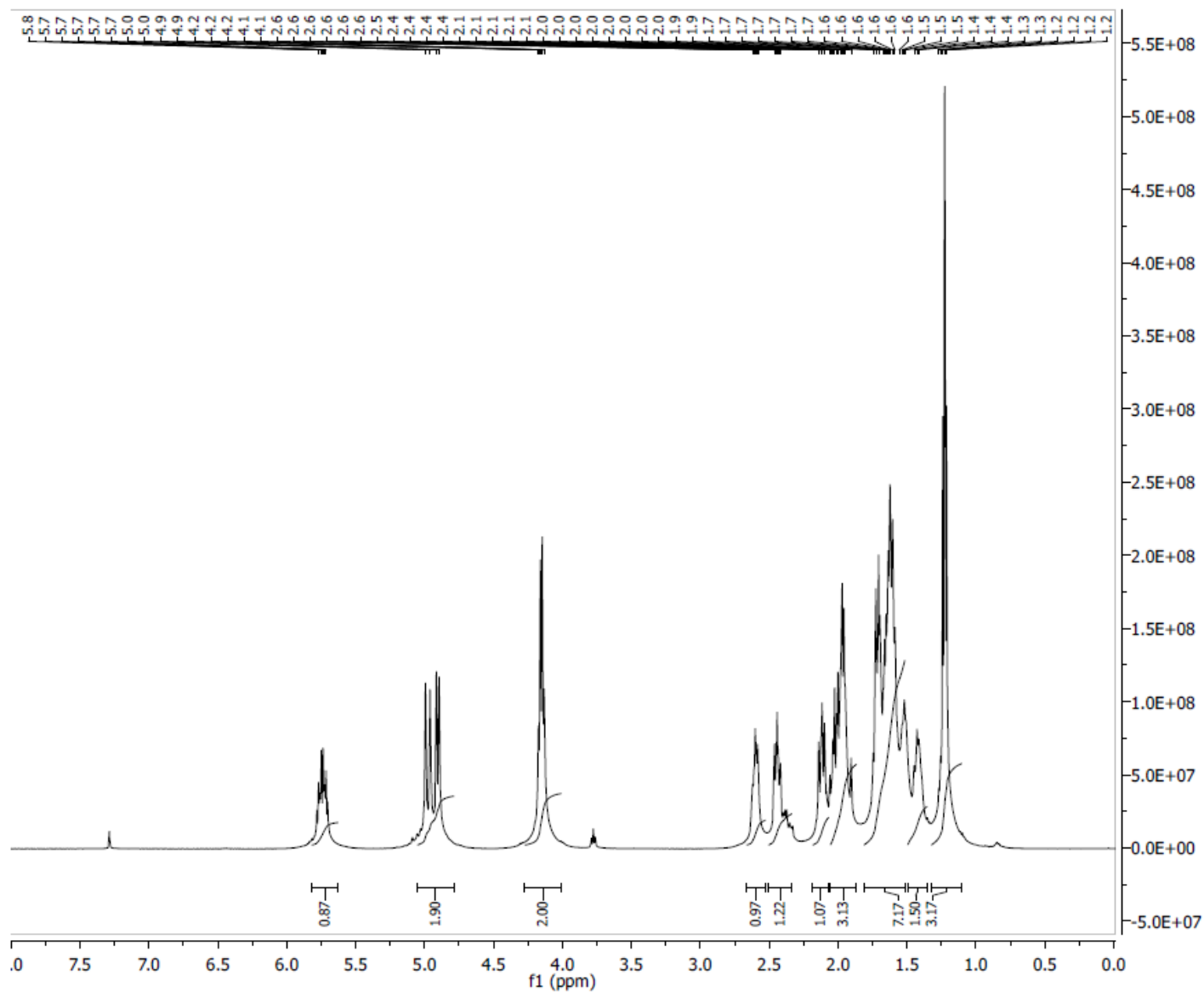


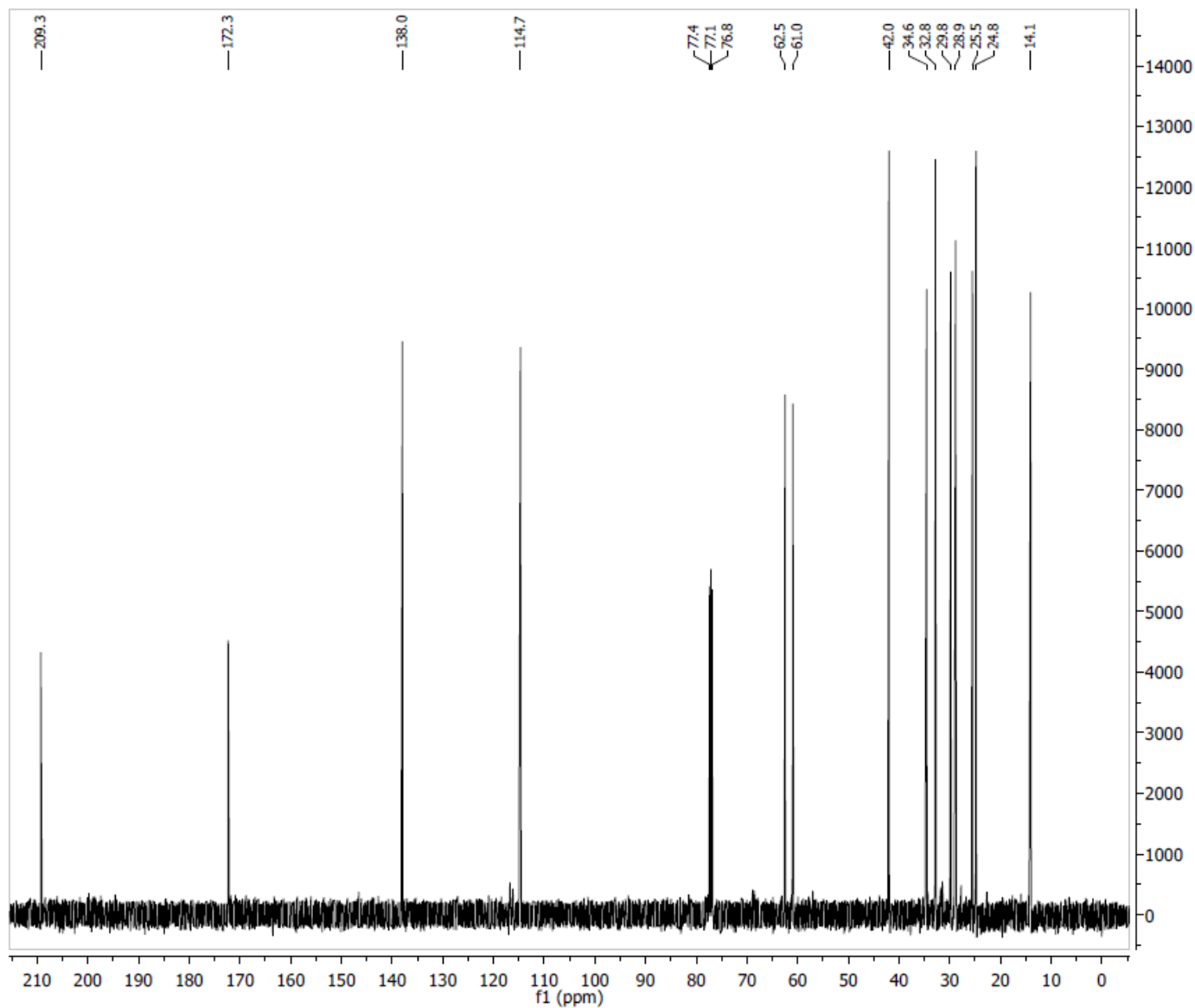


Parameter	Value
1 Spectrometer	
2 Solvent	
3 Temperature	
4 Pulse Sequence	
5 Experiment	1D
6 Number of Scans	
7 Receiver Gain	
8 Relaxation Delay	
9 Pulse Width	
10 Acquisition Time	nan
11 Spectrometer Frequency	100.62
12 Spectral Width	24038.5
13 Lowest Frequency	-1957.9
14 Nucleus	Unknown
15 Acquired Size	0
16 Spectral Size	32768

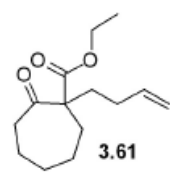


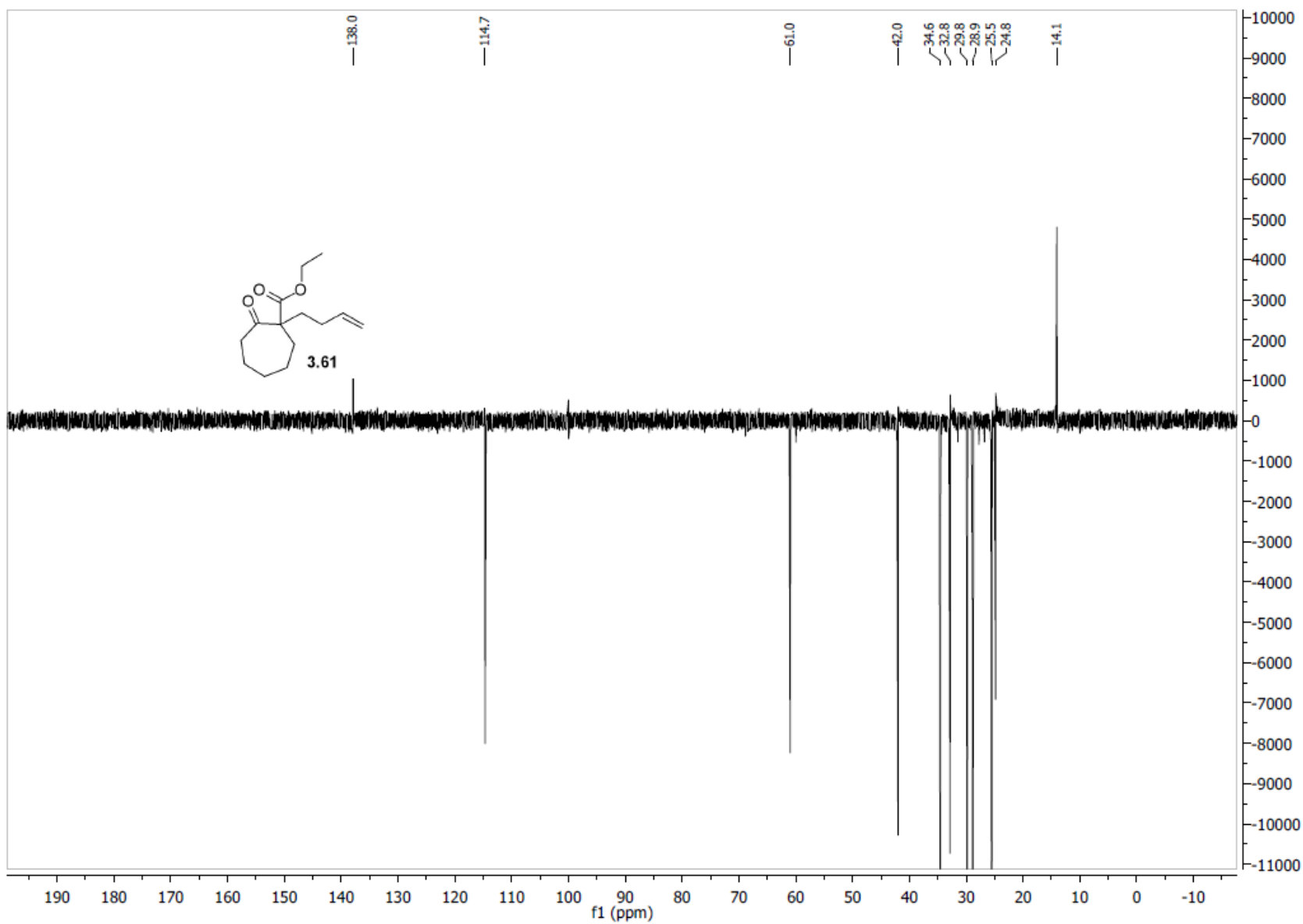


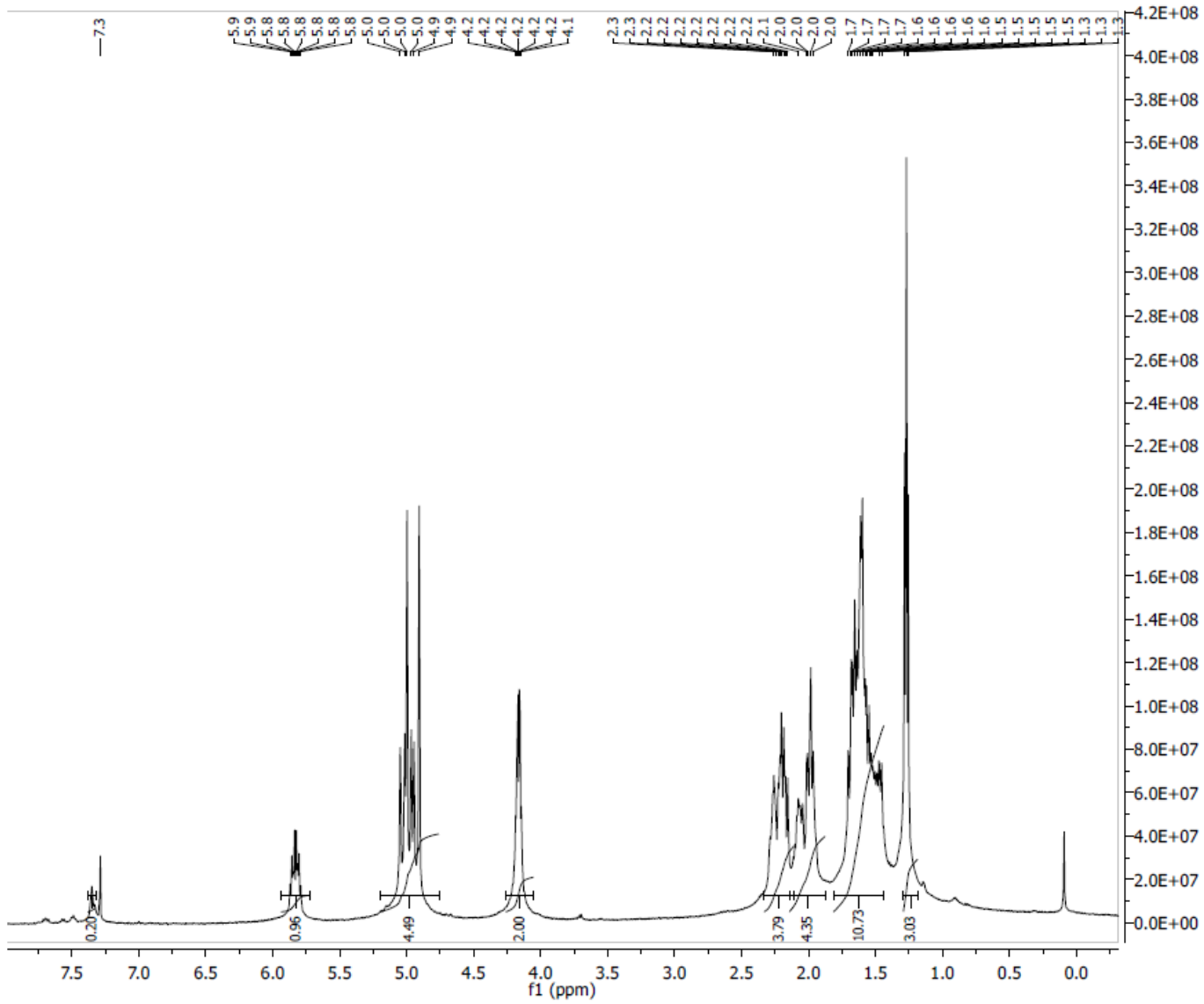




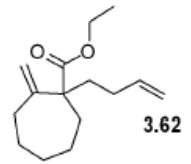
Parameter	Value
1 Spectrometer	spect
2 Solvent	CDCl3
3 Temperature	298.2
4 Pulse Sequence	zgpg30
5 Experiment	1D
6 Number of Scans	300
7 Receiver Gain	9195
8 Relaxation Delay	3.0000
9 Pulse Width	9.5000
10 Acquisition Time	1.1796
11 Spectrometer Frequency	125.77
12 Spectral Width	27777.8
13 Lowest Frequency	-683.9
14 Nucleus	13C
15 Acquired Size	32768
16 Spectral Size	65536

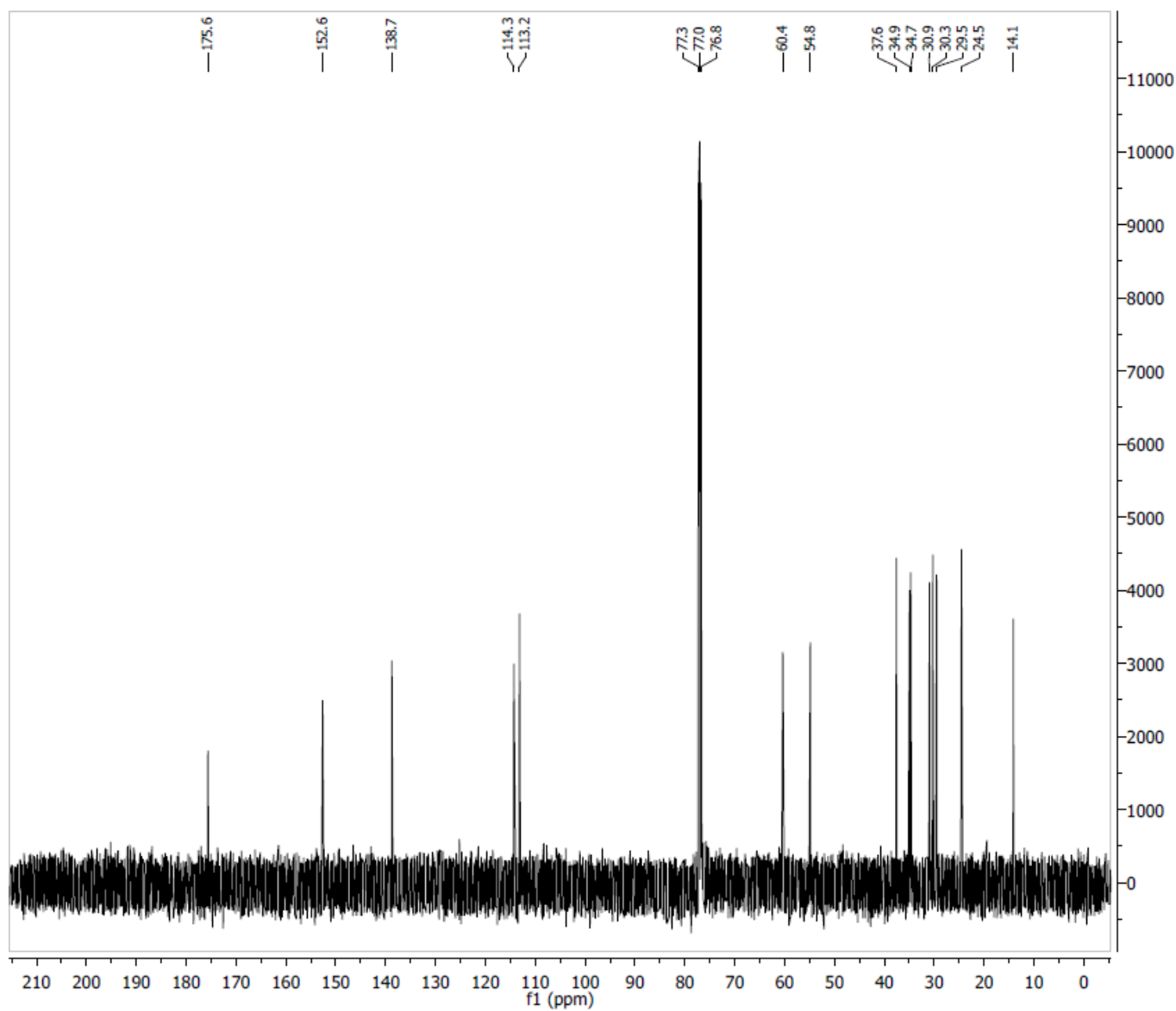




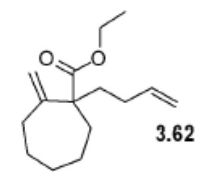


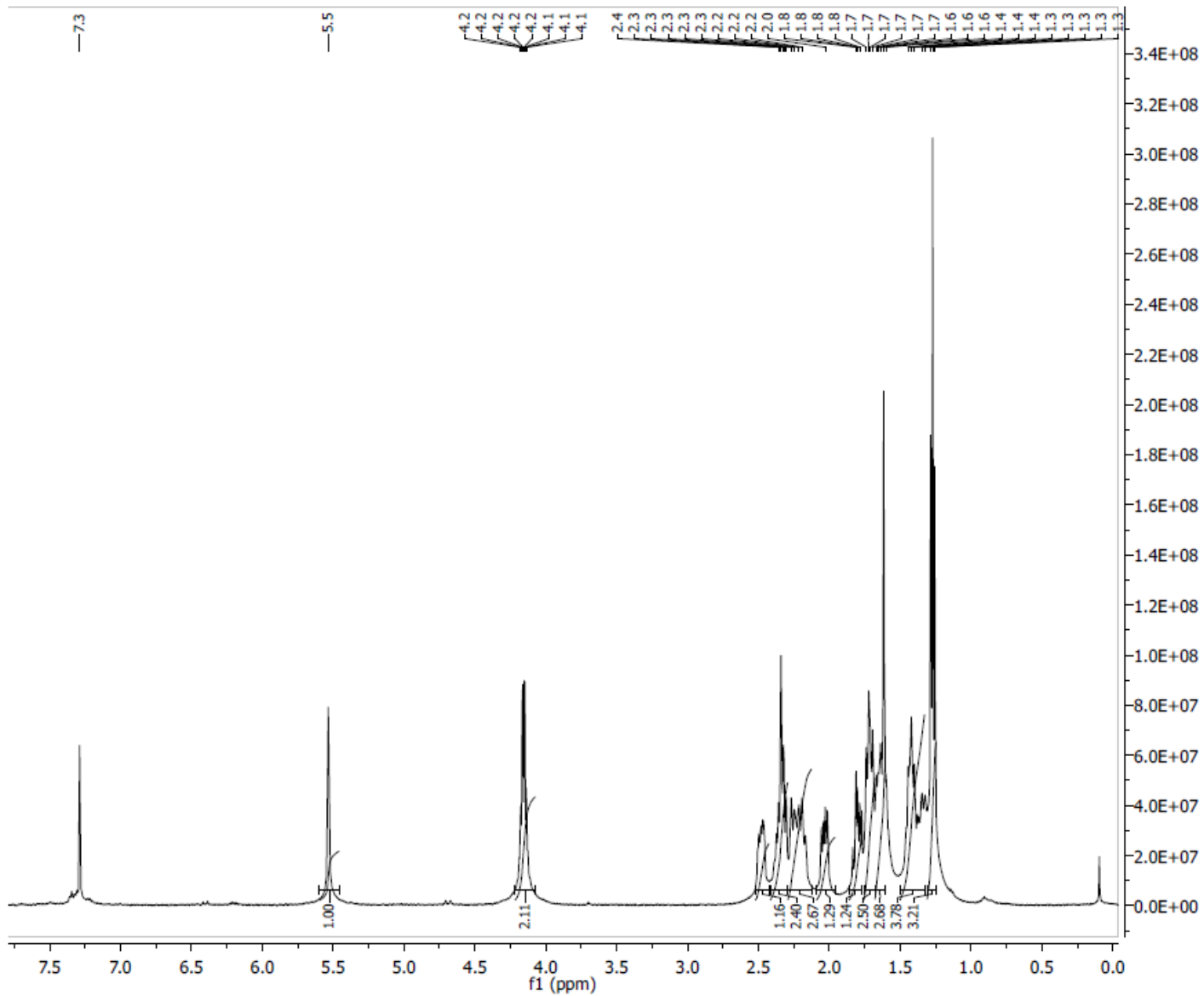
Parameter	Value
1 Spectrometer	spect
2 Solvent	CDCl3
3 Temperature	298.2
4 Pulse Sequence	zg30
5 Experiment	1D
6 Number of Scans	16
7 Receiver Gain	287
8 Relaxation Delay	1.0000
9 Pulse Width	11.0000
10 Acquisition Time	1.1698
11 Spectrometer	500.13
Frequency	
12 Spectral Width	7002.8
13 Lowest Frequency	-250.6
14 Nucleus	1H
15 Acquired Size	8192
16 Spectral Size	16384



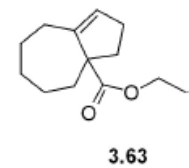


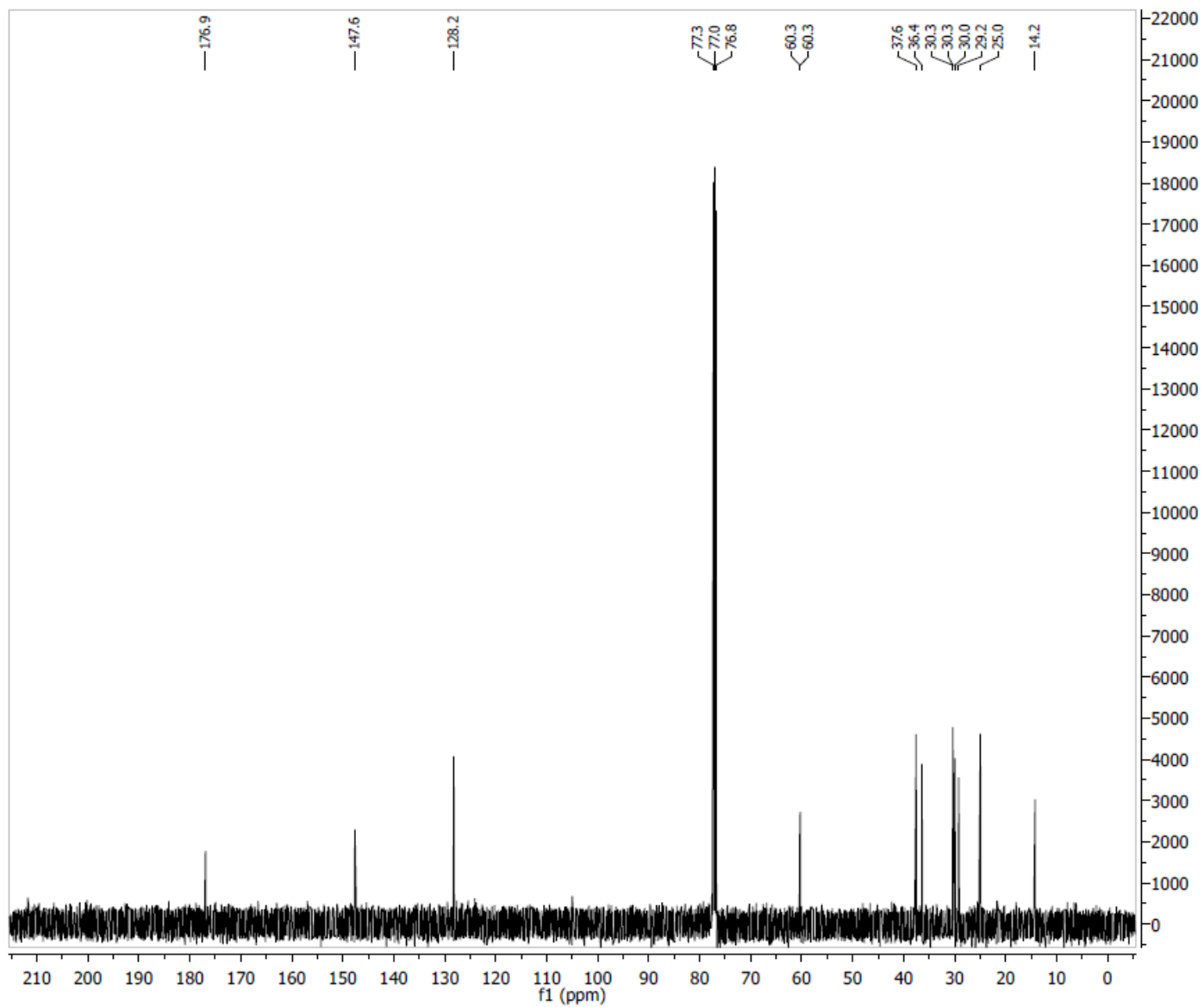
Parameter	Value
1 Spectrometer	spect
2 Solvent	CDCl3
3 Temperature	298.2
4 Pulse Sequence	zgpg30
5 Experiment	1D
6 Number of Scans	1024
7 Receiver Gain	9195
8 Relaxation Delay	3.0000
9 Pulse Width	9.5000
10 Acquisition Time	1.1796
11 Spectrometer Frequency	125.77
12 Spectral Width	27777.8
13 Lowest Frequency	-683.9
14 Nucleus	13C
15 Acquired Size	32768
16 Spectral Size	65536



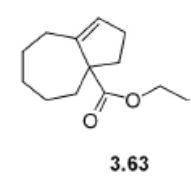


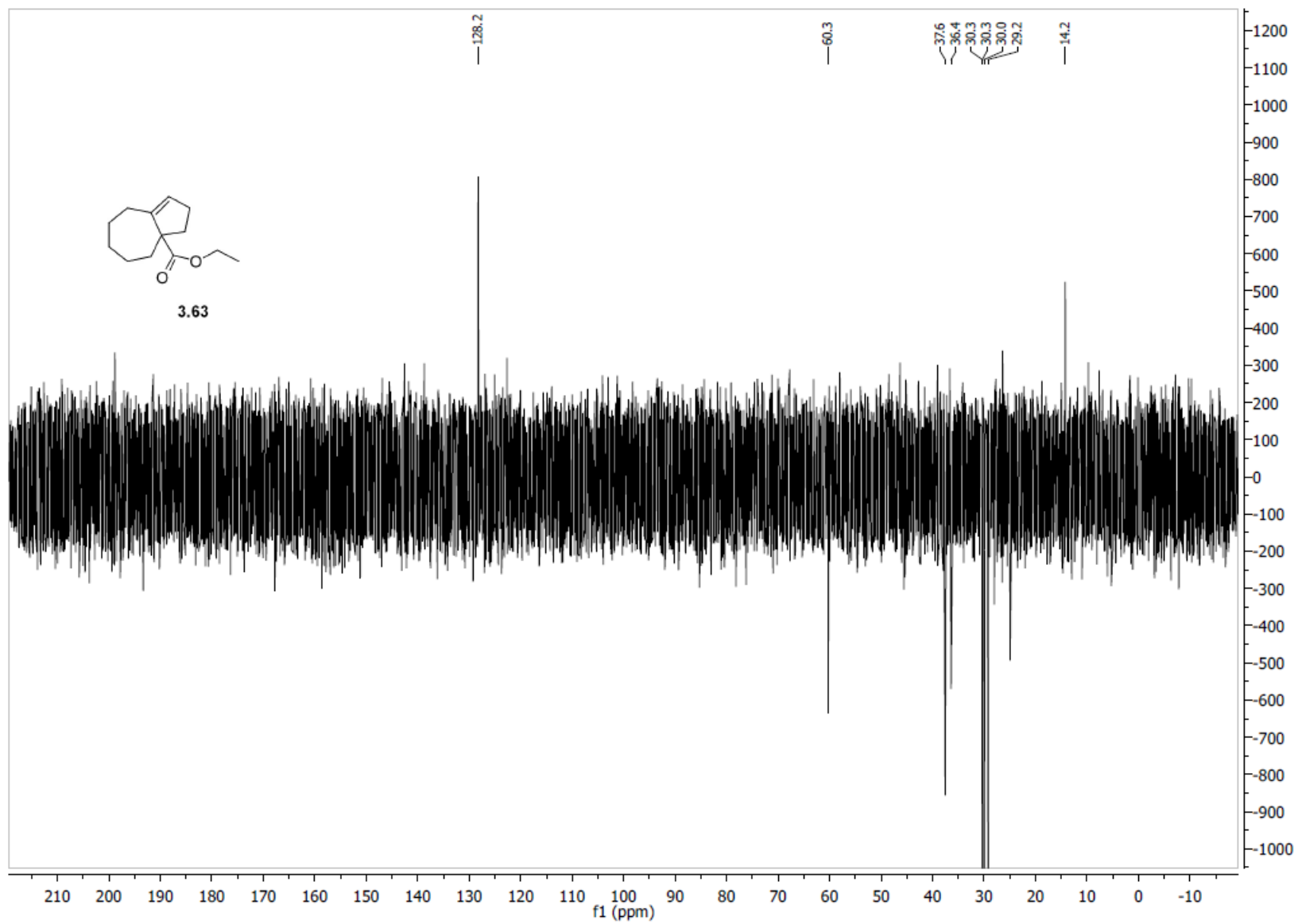
Parameter	Value
1 Spectrometer	spect
2 Solvent	CDCI3
3 Temperature	298.2
4 Pulse Sequence	zg30
5 Experiment	1D
6 Number of Scans	16
7 Receiver Gain	456
8 Relaxation Delay	1.0000
9 Pulse Width	11.0000
10 Acquisition Time	1.1698
11 Spectrometer Frequency	500.13
12 Spectral Width	7002.8
13 Lowest Frequency	-250.6
14 Nucleus	1H
15 Acquired Size	8192
16 Spectral Size	16384

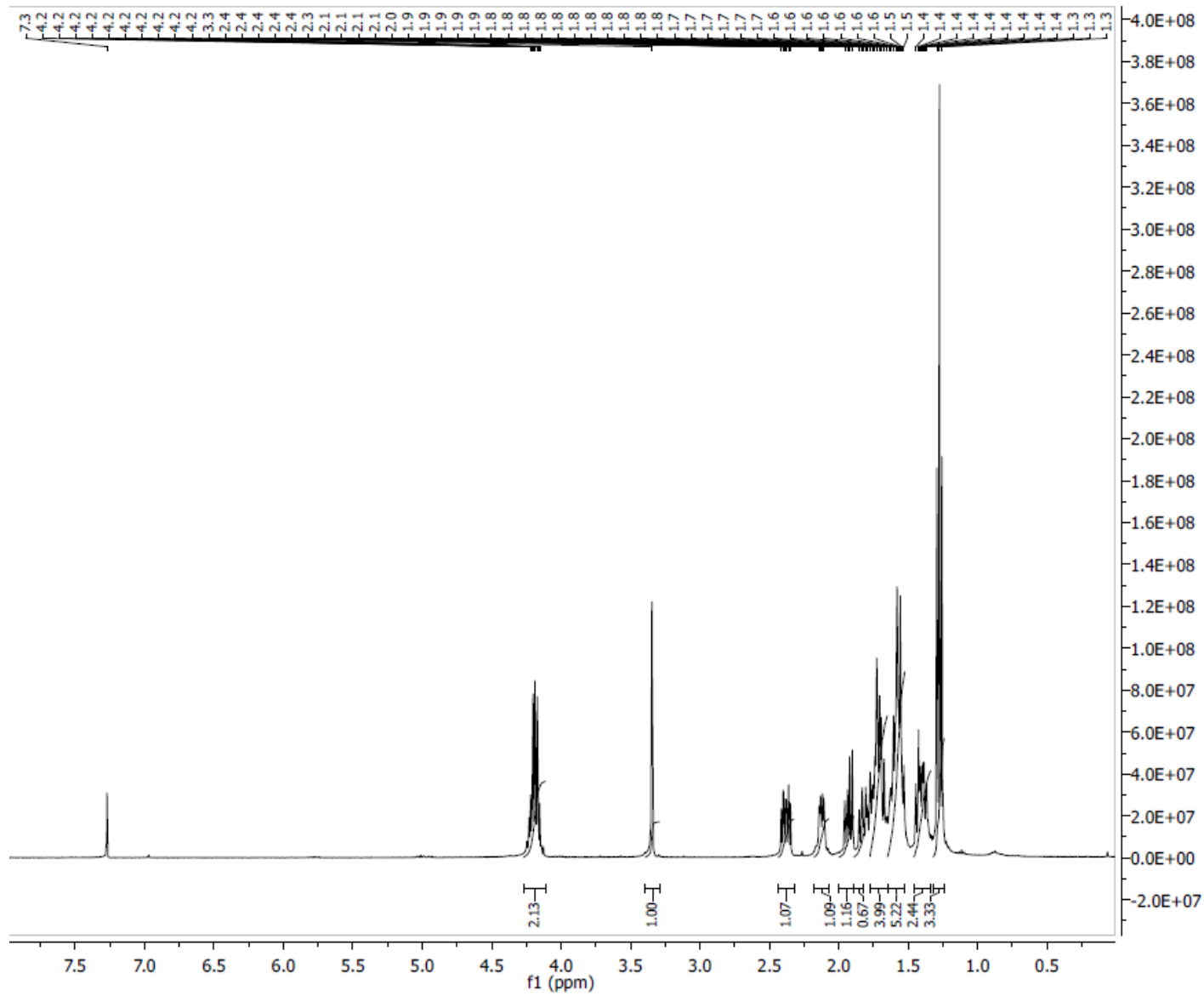




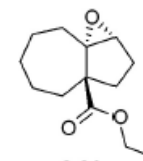
Parameter	Value
1 Spectrometer	spect
2 Solvent	CDCB
3 Temperature	298.2
4 Pulse Sequence	zgpg30
5 Experiment	1D
6 Number of Scans	1024
7 Receiver Gain	9195
8 Relaxation Delay	3.0000
9 Pulse Width	9.5000
10 Acquisition Time	1.1796
11 Spectrometer Frequency	125.77
12 Spectral Width	27777.8
13 Lowest Frequency	-683.9
14 Nucleus	13C
15 Acquired Size	32768
16 Spectral Size	65536



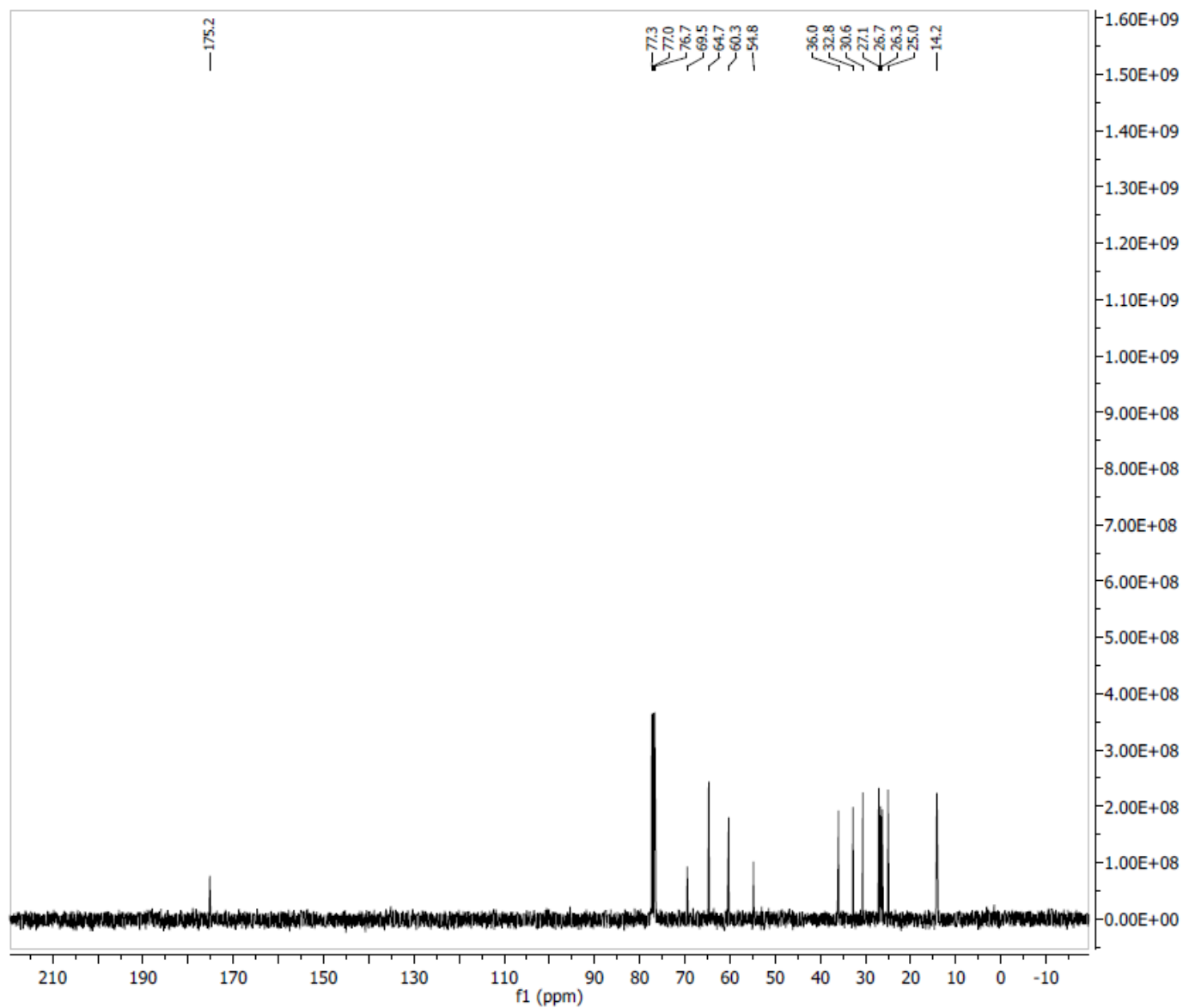




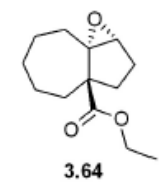
Parameter	Value
1 Spectrometer	spect
2 Solvent	CDCl3
3 Temperature	298.2
4 Pulse Sequence	zg30
5 Experiment	1D
6 Number of Scans	8
7 Receiver Gain	181
8 Relaxation Delay	1.0000
9 Pulse Width	10.2500
10 Acquisition Time	3.9846
11 Spectrometer Frequency	400.15
12 Spectral Width	8223.7
13 Lowest Frequency	-1640.8
14 Nucleus	1H
15 Acquired Size	32768
16 Spectral Size	32768

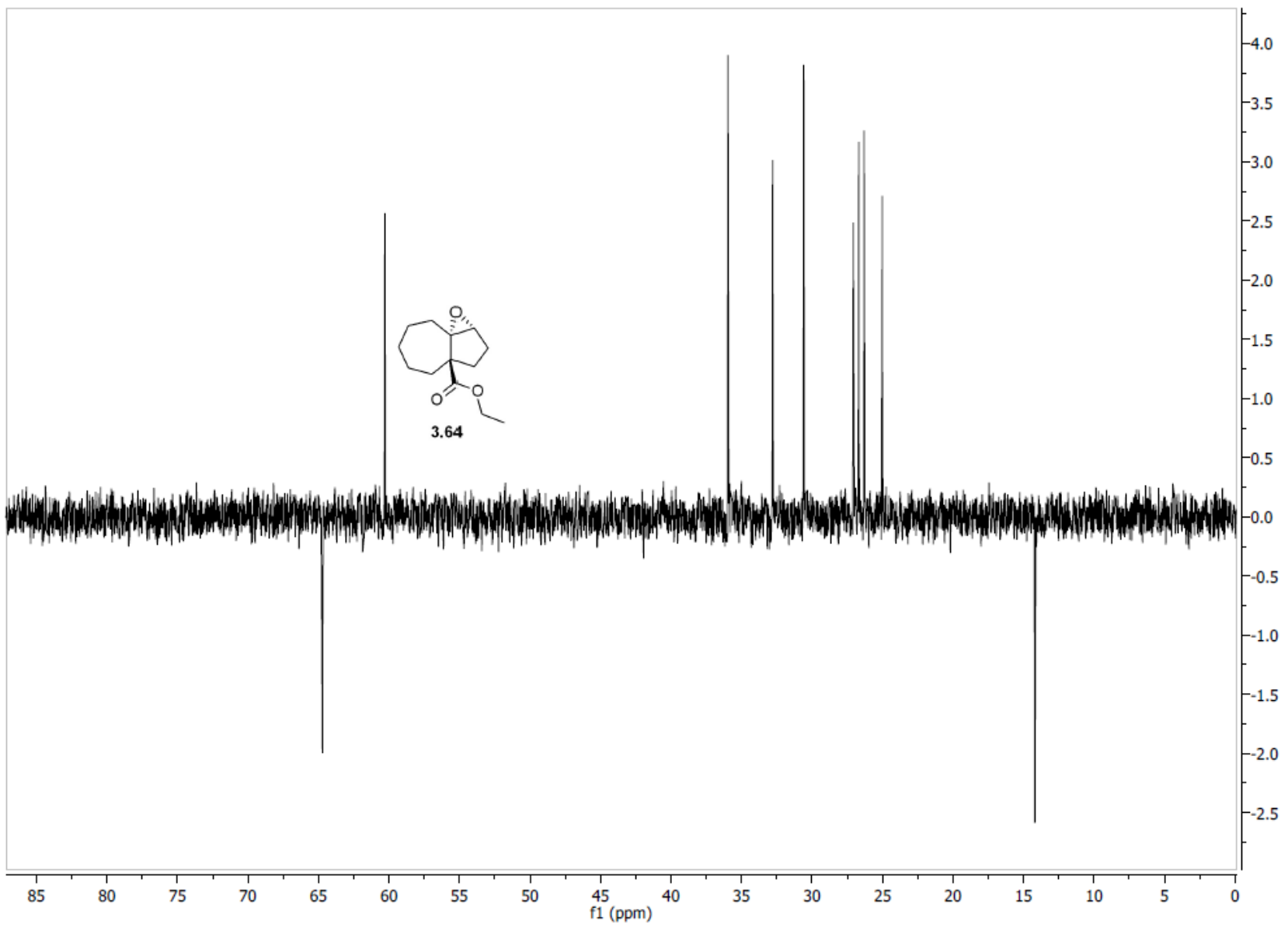


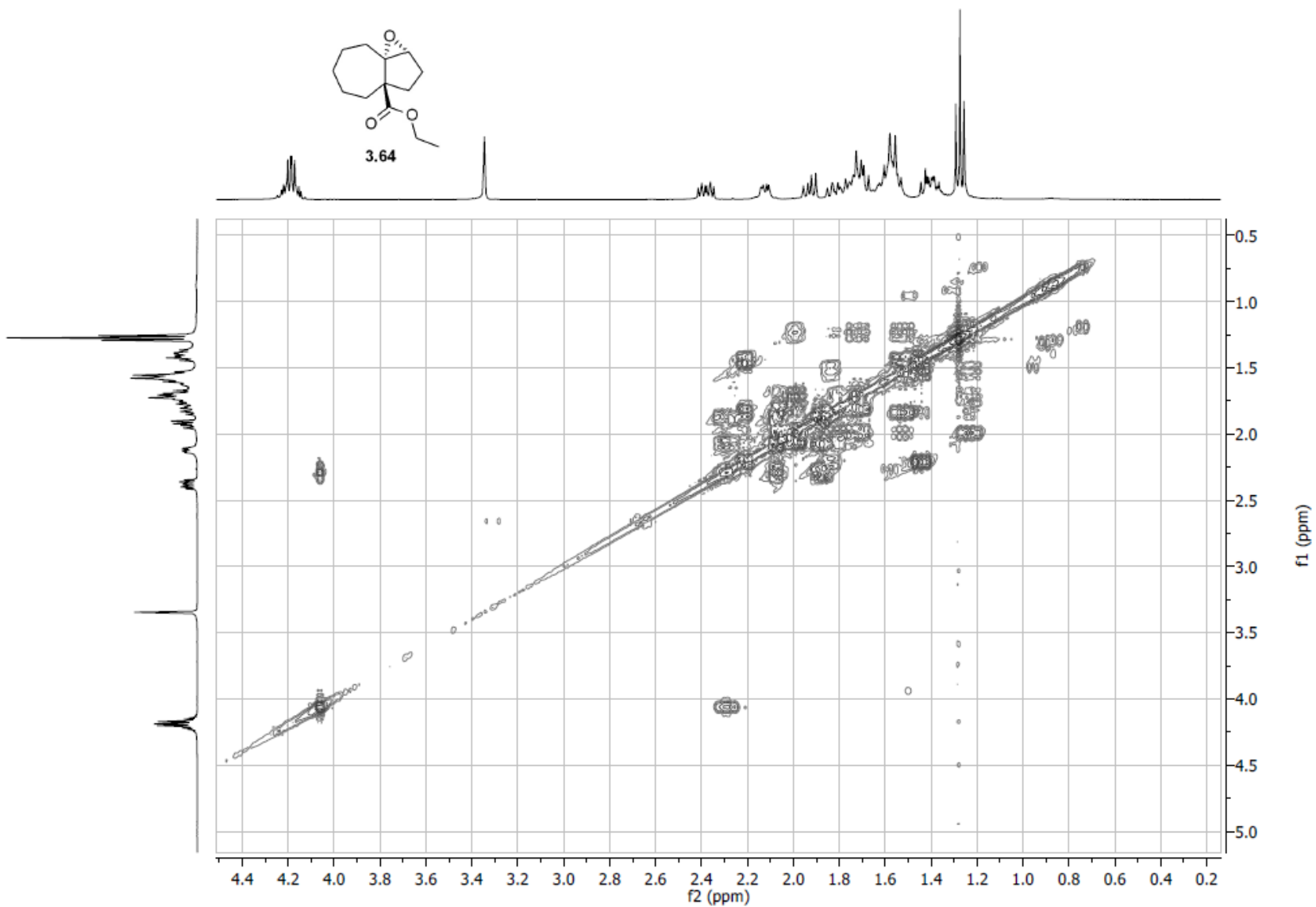
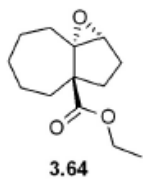
3.64

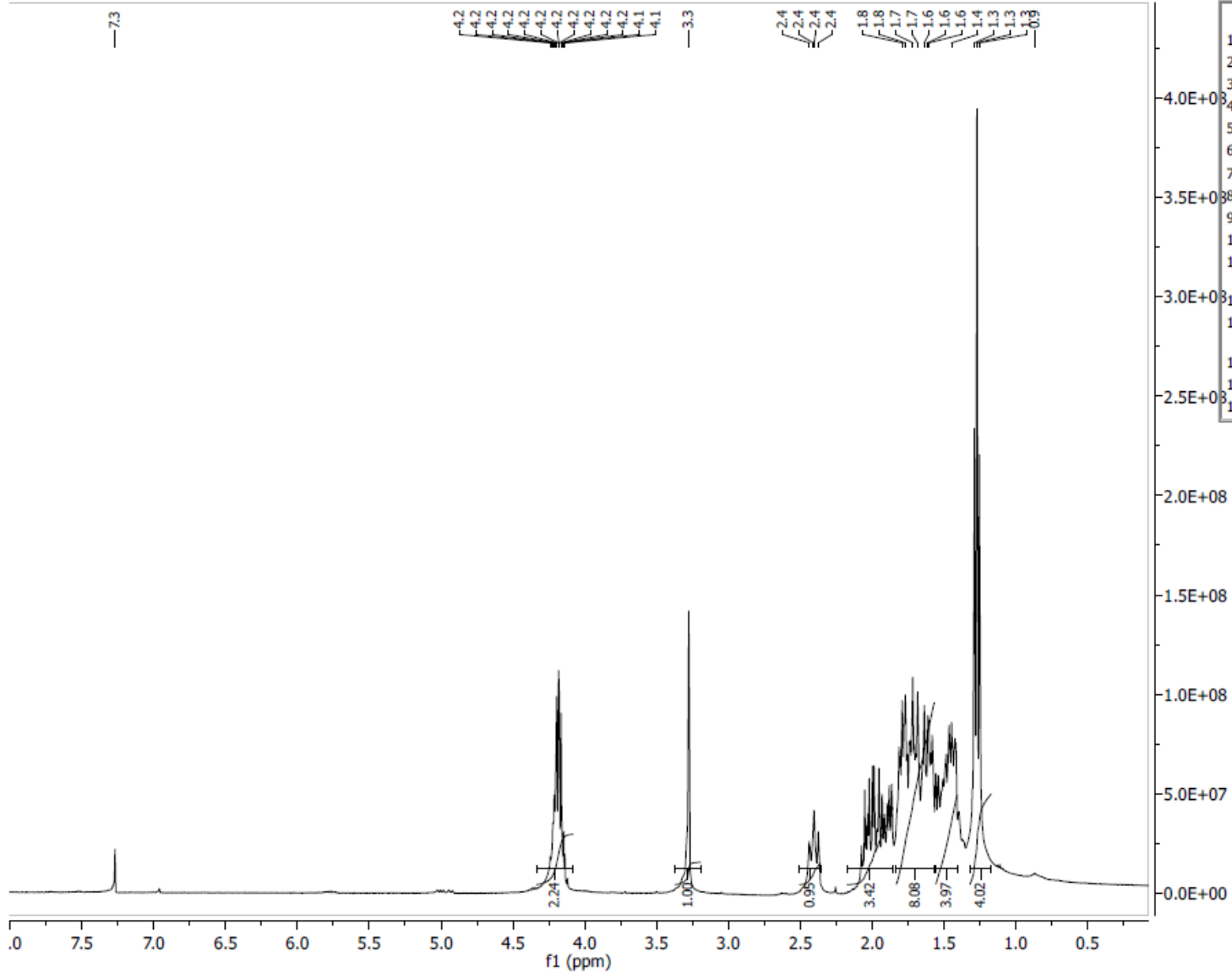


Parameter	Value
1 Spectrometer	spect
2 Solvent	CDCB
3 Temperature	298.2
4 Pulse Sequence	zgpg30
5 Experiment	1D
6 Number of Scans	223
7 Receiver Gain	32800
8 Relaxation Delay	2.0000
9 Pulse Width	11.1250
10 Acquisition Time	1.3631
11 Spectrometer Frequency	100.62
12 Spectral Width	24038.5
13 Lowest Frequency	-1957.9
14 Nucleus	¹³ C
15 Acquired Size	32768
16 Spectral Size	32768

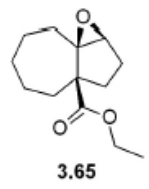


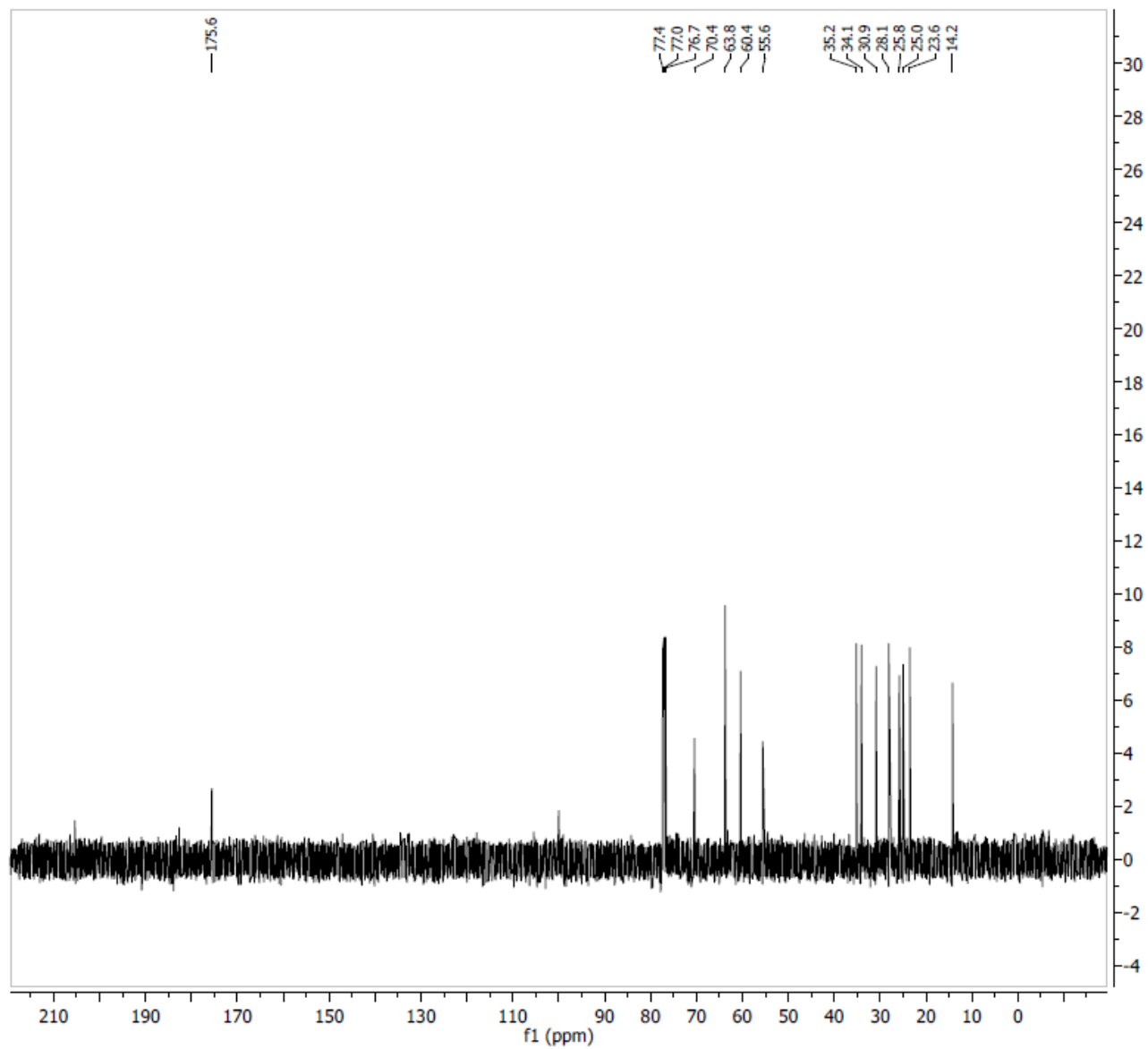




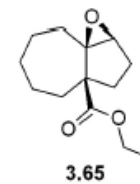


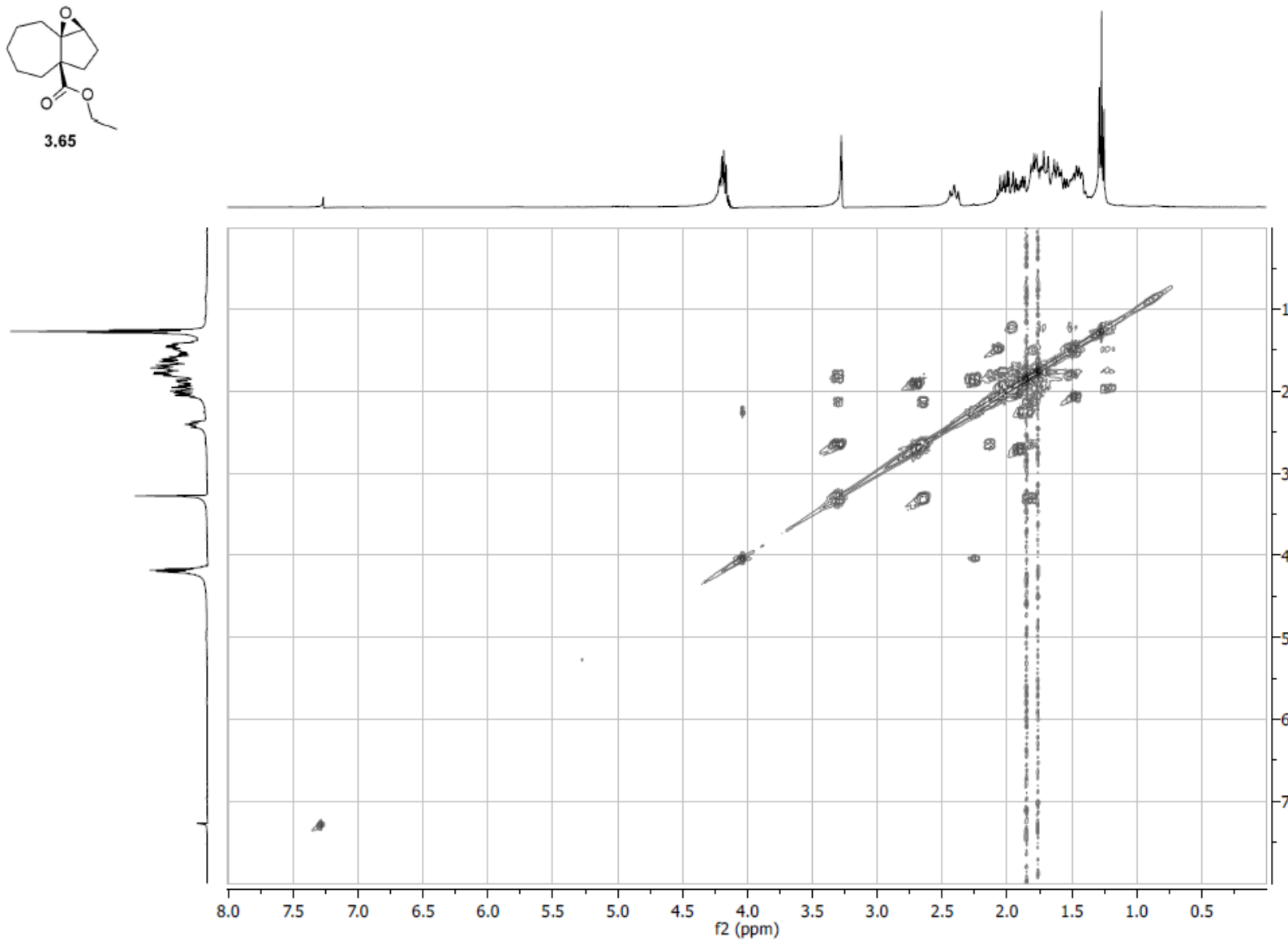
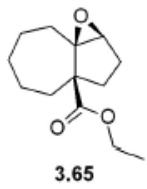
Parameter	Value
1 Spectrometer	spect
2 Solvent	CDCl3
3 Temperature	298.2
4 Pulse Sequence	zg30
5 Experiment	1D
6 Number of Scans	8
7 Receiver Gain	144
8 Relaxation Delay	1.0000
9 Pulse Width	10.2500
10 Acquisition Time	3.9846
11 Spectrometer Frequency	400.15
12 Spectral Width	8223.7
13 Lowest Frequency	-1640.8
14 Nucleus	1H
15 Acquired Size	32768
16 Spectral Size	32768





Parameter	Value
1 Spectrometer	spect
2 Solvent	CDCl3
3 Temperature	298.2
4 Pulse Sequence	zgpg30
5 Experiment	1D
6 Number of Scans	200
7 Receiver Gain	32800
8 Relaxation Delay	2.0000
9 Pulse Width	11.1250
10 Acquisition Time	1.3631
11 Spectrometer Frequency	100.63
12 Spectral Width	24038.5
13 Lowest Frequency	-1957.9
14 Nucleus	13C
15 Acquired Size	32768
16 Spectral Size	65536





CHAPTER 5
INTRODUCTION- CASPASE-1

Caspase-1-Introduction

Caspases represent a family of aspartate-specific cysteine dependent proteases involved in the biochemical mechanisms underlying proinflammatory cytokine maturation and cellular apoptosis. Initially, caspases' role in apoptosis was confirmed by studies performed on the nematode worm *Caenorhabditis elegans*. Yuan's research group showed CED-3 plays an important role in programmed cell death and more importantly, CED-3 is homologous to human protease caspase-1.⁶⁸ Subsequently, studies revealed that caspase-1 is more involved in maturation of inflammatory cytokines rather than in apoptosis. However, the finding of homology between CED-3 and human caspase-1 led to the discovery of large class of CED-3/caspase-1 like proteases in mammals as well as humans.⁶⁹

To date, 15 mammalian caspases have been identified out of which 12 are present in humans and have shown high phylogenetic conservation. Caspases play a crucial role in both apoptosis and inflammation. Inflammatory caspases are involved in maturation of cytokines, which in turn are responsible for several inflammatory disorders like rheumatoid arthritis, multiple sclerosis osteoarthritis and septic shock. Apoptotic caspases are involved in programmed cell death in multicellular organism and up-regulation (in Cancer) or down-regulation (stroke or myocardial infarction) of apoptosis is warranted in several disease states. Because of their important biological roles, these enzymes have been considered as good targets in drug discovery process.^{70, 71}

All the caspases share several common features like similarity in amino acid residues, structure and substrate specificity. They are expressed in cells as single chain zymogen 32-55 kDa comprising of three domains; N-terminal prodomain, large subunit domain and a small subunit domain.

The inactive enzyme has to be proteolytically activated to its active form which is believed to occur either via autoproteolysis, or via cleavage by other caspase or non-caspase proteases. The active form of the enzyme is a heterodimer that is made up of 2 large subunits 17-20 kDa (p20) and 2 small subunits (p10) 10-12 kDa. All of them have a cysteine residue in its active site, which acts as a nucleophile, and most importantly they share a stringent requirement for cleavage of their substrate after aspartic acid residue. The large and small subunits of human caspases have 29 amino acid residues in common. Seven of these residues play a pivotal role in substrate recognition and catalysis, while the remaining 22 residues are distributed throughout the protein. It can be speculated that these 22 conserved residues may help to maintain the structural integrity of active form of the enzyme.^{71, 72}

5.1 Classification of Caspases

Broadly, caspases can be divided into two categories based on their physiological functions: inflammatory and apoptotic caspases. Caspase 2, 3 and 6-10 are involved in the apoptotic processes; while caspase 1, 4, 5 and 12 are involved in maturation of cytokines, consequently leading to the inflammatory response. Classification based on phylogenetic analysis puts caspase into two major subfamilies caspase-1 type or the cell death gene CED type. Further they are subdivided based on the long (more than 90 amino acid residue) or short (20-30 amino acid residue) prodomain of the zymogen. Based on these criterion, mammalian caspases can be divided in to three subclasses; Inflammatory caspases with large prodomain (caspase 1, 4, 5, 12, 13 & 14), Initiator caspase with long prodomain additionally having a (DED) death effector domain (caspase 8 & 10) or a (CARD) caspase-recruitment domain (caspase 2 and 9) and the last class is effector caspase with a short prodomain (caspase 3, 6 & 7).⁷²⁻⁷⁴

5.2 Zymogen Activation

Zymogen activation (inactive procaspase) is tightly regulated and only occurs in response to specific stimuli. Activation of procaspase takes place by proteolytic cleavage of a pro-domain and separation of the large and small subunits of the active caspases. The cleavage is often carried out by other caspases/proteases, with scission taking place at two distinct sites, each containing aspartic acid residues (4 Asp containing peptide bonds). Most of the procaspases are less active than the caspases though the difference in the activity between the zymogen and its active form may vary. For example, procaspase 3 & 7 in 10,000 fold less active than caspase 3 & 7 while procaspase -9 is only 10 fold less active than caspase-9.⁷⁵ There are some differences in the mechanism of activation between inflammatory, effector and initiator caspases. The effector caspases (-3, -6 & -7)⁷⁶⁻⁷⁸ are homodimers, which are activated by proteolysis, liberating the active dimer from the prodomain. The initiator and inflammatory caspases are activated by “induced proximity model”, wherein the monomers are forced to dimerize and form multiprotein complexes.^{79, 80}

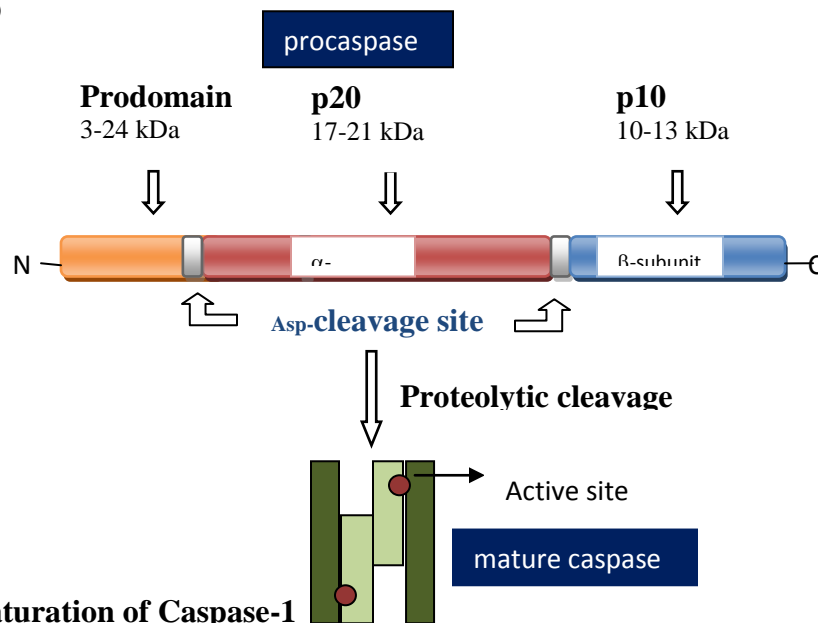


Figure 5.1: maturation of Caspase-1

5.3 Caspase-1 also known as interleukin 1 β -converting enzyme (ICE)

Caspase-1 also known as interleukin 1 β -converting enzyme (ICE) primarily localized in monocytes, is one of the most studied caspases by both industry as well as academia. ICE was the first human caspase to be identified in 1989 and was isolated in an effort to identify the enzyme responsible for maturation of interleukin-1 β (IL-1 β). ICE is known to cleave inactive IL-1 β 31 kDa precursor to its active form 17.5 kDa which is then secreted by monocytes and macrophages. Moreover, ICE is also involved in processing of IL-18 and IL-1 α . It has been established for years now that it plays a more prominent role in regulation of inflammatory progression and is less involved in apoptotic pathways. ^{69, 81}

5.4 Role of Caspase-1

Thornberry's research group ^{81, 82} identified the importance of ICE in maturation of cytokines. Activation of ICE leads to secretion of IL-1 β by macrophages following an attack by exogenous compounds either from bacteria or a virus. Interleukin-1 processing leads to myriad of events ranging from initiation of fever to induction of inflammatory response to cellular activities like proliferation, differentiation and apoptosis. Moreover, IL- β mediated induction of cyclooxygenase-2 in the central nervous system is responsible for pain and hypersensitivity reactions. Secretion of other interleukins IL-18 and IL-33 mediated by ICE, suggest that it is responsible for inflammatory processes as well as innate immunity. Gurcel *et.al*; ⁸³ suggested an additional role of ICE in fortification of the injured cells. Bacterial pore forming toxins trigger inflammasome (NALP3 and Ipaf) formation leading to activation of ICE, which in turn promotes lipid metabolism (via activation of sterol regulatory element binding protein) to repair the membrane damage. ⁸⁴

5.5 Activation of Caspase-1

ICE belongs to subclass of inflammatory caspases having a long N-terminal prodomain, which is likely to be involved in protein-protein interaction leading to activation of the caspase-1. The activation of ICE is very similar to that of initiator caspases. The N-terminal domain has a “caspase activation and recruitment domain” (CARD) motif which is responsible for inducing autocatalytic activation by bringing two or more proteins in very close proximity

Studies conducted on CASP-11-null mice indicate that caspase-11 is required for activation of caspase-1. The mice lacking of caspase-11 were unable to produce any IL- β , similar to the observation in case of ICE knockout mice.⁵⁵ Currently, no human analog of murine caspase-11 has been found. However, caspase-4 & 5 show considerable sequence homology to the murine caspase.^{85, 86} Moreover, studies have revealed upregulation of caspase-11 and caspase-5 in response to lipopolysaccharide (LPS) challenge, suggesting role of caspase-5 in activation of ICE.⁸⁷

Activation of ICE has been studied by many research groups and a few mechanisms have been put forward. Similar to other established caspase activation pathways, activation of ICE should involve some adaptor molecule capable of inducing autocatalytic proteolysis. This adaptor molecule should have a region that interacts with ICE, probably another CARD domain capable of interacting with the ICE pro-domain. Additionally, it is likely that it also possesses an oligomerization motif to facilitate caspase clustering.⁸⁸ To date, several CARD containing complexes have been shown to interact with CARD domain of procaspase-1, including Rip2/RICK/CARDIAK (CARD-containing IL-1 α -converting enzyme associated kinase),⁸⁹ (ICE protein activating factor) Ipaf/CARDI2/CLAN, ASC/PYCARD and NALP1 (inflammasome) complexes. Recent studies have shown that Rip2/RICK/CARDIAK complex is more involved in

activation of nuclear factor kappa-light-chain-enhancer of activated B cells complex (NF- κ B) and less involved with caspase-1.^{90, 91} Ipaf contains N-terminal CARD as well as multiple leucine rich repeats (LRR) at C-terminal, and it oligomerizes in the presence of procaspase-1. LRR motif is also found in toll receptor family and is implicated in pathogen recognition. This further confirms the role of Ipaf as a pathogen-recognizing molecule.⁹² Though Ipaf links with ICE are strong, studies at physiological concentration of Ipaf are yet to be published. Apoptosis-associated speck-like protein with a CARD (ASC) has also been implicated as an ICE adaptor. Bipartite ASC contains a CARD and a pyrin motif. Studies have shown that its CARD domain interacts with ICE.^{93, 94} Lastly, NALP-1 which contains pyrin and CARD recruits caspase-1 via ASC as well as caspase-5 through the CARD domain present in the C-terminus of NALP-1. Tschopp and associates suggested that NALP-1 induces the formation of caspase-1/caspase-5 complex called “inflammasome”. The inflammasome is composed of caspase-1, ASC and inflammasome component NALP1, NALP3 and Ipaf, which can sense foreign bodies (bacteria, virus) This model is widely accepted for caspase-1 activation, however, what triggers inflammasome activation is not completely clear yet.⁹⁵⁻⁹⁷

5.6. Structure of Caspase-1

Several crystal structures of caspase-1 enzyme bound to native ligand or inhibitor form have been published in protein data bank. Cleavage of procaspase (p45) at four Asp-Xaa bonds (Asp 103-ser104, Asp 119-Asn 120, Asp 297-Ser 298 and Asp 316-Ala317) gives active ICE, which is a tetramer comprising 2 large p20 subunits (residues 120-297) and 2 p10 small subunits (317-404 residues). Caspase is made up of six-stranded β sheets, forming the core of the enzyme. Five of them lie parallel to each other while one is antiparallel (1, 164-170; 2, 199-205; 3, 230-236; 4, 278-283 7, 327-331 and 8, 388-393 residues respectively). The core is surrounded by six α

helices which are roughly parallel to the beta sheet, and they prevent the core from water molecules. The last seven residues from p20 and the first residues from p10 form two other anti-parallel β -sheets (5, 291-297 and 6, 317-323). The tetramers two subunits align themselves in head-to-tail configuration with two identical active sites at the opposite end of the enzyme.^{81, 98, 99}

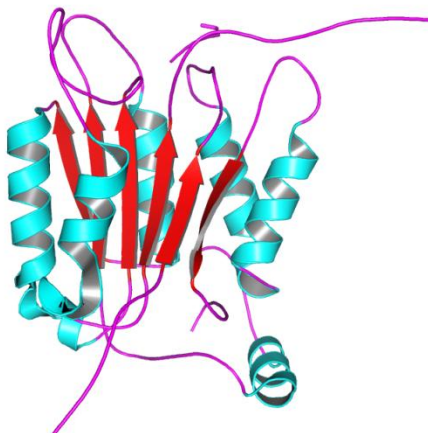


Figure 5.2. : Cartoon representation of caspase-1

5.7 Active site of Caspase-1

One of the pioneering studies in the field of ICE research by Thornberry associates, was the identification of tertiary protein structure of ICE and the ensuing discovery of the tetrapeptide; Ac-YVAD-CHO possessing potent ICE inhibitory activity.⁸¹ Later on, Wilson and Associates from Vertex Pharmaceuticals published x-ray crystal structures of ICE co-crystallized with tetrapeptide aldehyde inhibitor (acetyl-Tyr-Val-Ala-Asp-H). Cys 285 was confirmed as a nucleophile to which aldehyde is attached in covalent fashion.^{100, 101} Along with Cys 285, His 237 forms the catalytic diad in the active site. The analysis of enzyme-substrate complex reveals that both the large and small subunits are required for ICE activity. The inhibitor occupies S1-S4 subsite of ICE wherein S1 is present in p20 subunit while S2-S4 (Val 338 to Pro 343) is formed by residues from p10. Subunits p10 and p20 play role in recognition of aspartic acid of the

substrate (at S1 subsite) by contributing residues Arg 179 (p20) and Arg 341 (p10) for salt bridge interactions. Arg 179-Asp interaction seems to be more important based on hydrogen bonding distances. P1 carboxylate (Asp residue) is stabilized by Arg (179, 341) and Gln 283, while P2 and P3 are solvent exposed. P4 of the inhibitor (Tyrosine) makes hydrophobic interaction with residues His 342, Val 348 and Arg 383 in S4 subsite.^{81, 99, 101}

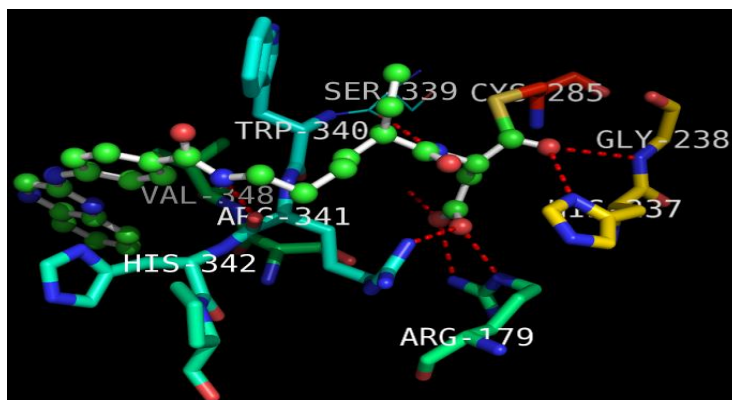


Figure 5.3.: cartoon depiction of caspase-1 active site with cysteine 285 covalently attached to the inhibitor

The Romanowski research lab carried out X-ray crystallographic studies on both ligand free and malonate-bound human caspase-1 in order to unravel the mechanism of substrate binding.¹⁰² The aim of this study was to investigate the conformational changes in active site upon binding of substrate to aspartate recognition site. The analysis of empty enzyme suggests that there is a major structural rearrangement in ligand free and ligand bound caspase-1, especially in three well defined regions; loop 2 (minor changes), loop 3 (most changes) and loop 4 (minor changes). Furthermore, the empty enzyme is not accessible to the substrate scaffold largely due to its closed (or partially closed) active site conformation. This is due to a major shifting of loop 3 (by 4.9 Å) of the p10 subunit occluding the catalytic cleft of ICE in the ligand-free form. Foremost

changes occur within the 15 residues of loop 3 containing critical residue Arg 341 of the P1 substrate recognition pocket. In the ligand free ICE the Arg 341 and Trp 340 is present on the surface. Binding of the aspartate containing ligand to the protein, transfers the Arg 341 from surface to S1 pocket and Trp 340 to S2 pocket of the ICE active site. In this transition of the loop 3, Arg 341 is rotated by 180 degrees from surface to oxyanion hole with proline 335 and 343 serving as pivot points. Romanowski et.al suggest that the binding of aspartate moiety of the substrate to S1 pocket is essential to bring about conformational change with subsequent opening of the active site which is now capable of catalysis.¹⁰²

5.8 Allosteric site in Caspase-1

Wells, Romanowski and associates by the aid of X-ray crystallography discovered an allosteric circuit in ICE.^{103, 104} In corroboration with their (Romanowski group) earlier¹⁰⁵ findings, they found that the protease exists in two distinct states: on-state/open state when the active site is occupied and an off-state/closed state when enzyme is not occupied. In this study, they found that there is allosteric binding site at the dimer interface, 15 Å away from the active site of the enzyme. More importantly, when the allosteric site is occupied by a synthetic small molecule the enzyme remains in off-state. Going from on-state to off-state of the enzyme, a network of 21 hydrogen bonds from nine side chain residues connecting the active and allosteric site, change partners. Out of these nine side chains, Arg286 and Glu390 form salt bridge interactions and are most crucial for retaining catalytic activity.^{104, 105}

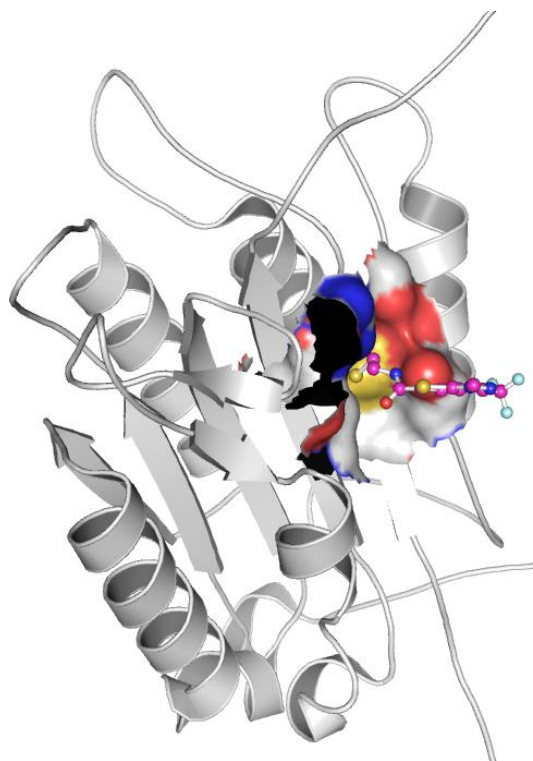


Figure 5.4: Allosteric site of Caspase-1

5.9. Catalytic mechanism of caspase-1 mediated hydrolysis of peptide bond

Mechanism of the cleavage of the peptide bond by caspases is similar to that of other cysteine proteases. The active site of the enzyme was confirmed by solving the crystal structure of the caspase-1 covalently bound to its inhibitor via the sulphhydryl group of the cysteine residue (Cys-285). The active site contains a catalytic dyad comprising of a cysteine 285¹⁰⁰ residue which acts as nucleophile and histidine 237 acting as a base. Both these residues are harbored in the p20 large subunit of the tetramer. The histidine residue not only enhances the nucleophilicity of cysteine residue in the active site but also activates water molecule which plays important role in hydrolysis of the peptide bond. The mechanism of hydrolysis is delineated in the figure 5.5. given below. The aspartic acid moiety in substrate is anchored by the Arg341 and Ser347 from p10 subunits, while Arg179 and Gln283 from p20 subunits. This helps orienting the carbonyl

group of the substrate so that it is easily accessible for the nucleophilic attack. The hydrolytic mechanism proceeds by attack of the Cys 285 on the electrophilic carbonyl group of the substrate molecule forming a tetrahedral intermediate. Two possible geometries are suggested for the tetrahedral intermediate of the substrate, one in which oxyanion hole is in contact with His 237 instead of Cys 285 and second one in which oxyanion hole is stabilized by Cys285 and Gly238. However, the tetrahedral intermediate stabilized by oxyanion hole formed by Cys285 and Gly238 is the more likely one. The tetrahedral transition state collapses, liberating the free amine and the acyl enzyme. The acyl-enzyme is then attacked by water molecule to give another tetrahedral intermediate, which subsequently disintegrates giving free acid and regenerating the Cys285 residue. Though the overall mechanism of hydrolysis of substrate is similar in all caspases; however, their catalytic activity varies among the family members.^{81, 100, 101}

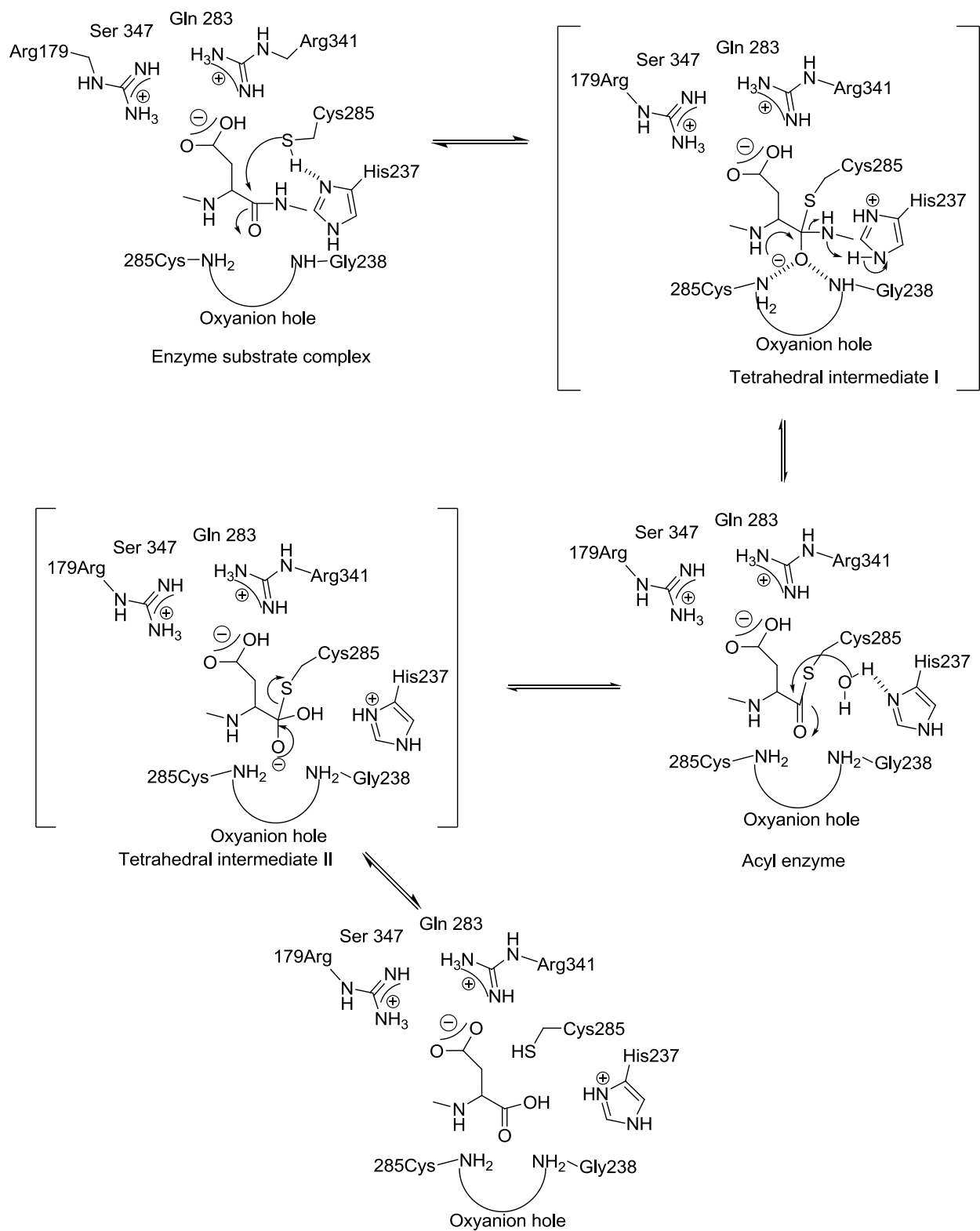


Figure 5.5.: Detailed Mechanism of hydrolysis of peptide bond catalyzed by Caspase-1

5.10. Caspase-1 and Diseases

5.10.1 Epilepsy and ICE

Selected anti-inflammatory drugs displayed anticonvulsant activity in epileptic syndromes that were unresponsive to classical second generation anti-epileptic drugs. This observation was the first indication of possibility of role of inflammation in epilepsy. Several studies showed fluctuations in cytokine levels in CSF and serum of epileptic patients. Moreover, epileptogenic brain specimens surgically removed from epileptic patients (drug-resistant epilepsy with differing origins) showed increased levels of proinflammatory cytokines (IL-1 β and IL-1 receptor type 1) in the glia, neurons and endothelial cell of the blood brain barrier. IL-1 β is induced in the brain following injuries like seizures. In control brains from normal patients, no such increase in cytokine levels was observed.¹⁰⁶⁻¹⁰⁸

Biochemical studies showed that IL-1 β activates Src family of tyrosine kinase which in turn phosphorylates NMDA receptors. This results in NMDA receptor mediated calcium influx in to the neurons.¹⁰⁹ The influx of calcium plays role in (over) excitation of neurons and seizures.¹¹⁰⁻¹¹²

The role of inflammatory mediators in the etiology of epilepsy was further confirmed by use of several animal models. The animal model studies resulted in three important findings

- 1) Pre-existing proinflammatory changes in the brain increased seizure susceptibility and treatment of animals with anti-inflammatory drugs blocked the proconvulsant effects
- 2) Inhibition of specific proinflammatory signals in the brain reduced frequency of seizures
- 3) Induced (chemically or electrically) seizures trigger a inflammatory response in the brain suggesting that recurrent seizures can induce proinflammatory mechanisms in brain

All of these taken together suggest that inflammatory molecules might be involved in the etiopathogenesis of epilepsy, and inhibition of the inflammatory processes can be a novel target in the treatment of epilepsy.^{108, 110-112}

ICE plays an important role in the maturation of IL-1 β , hence inhibitors of ICE may become an attractive in the treatment of epilepsy. Two molecules from the vertex (Pralnacasan-VX-740 and VX-765) were tested against inflammatory disorders. VX-765 demonstrated good anti-convulsant profile in rodents following systemic administration. It also reduced frequency and duration of seizure in mice, which were resistant to classical anti-convulsant drugs. Currently, VX-765 is in phase 2b clinical trial stage for treatment of seizures.^{113, 114}

5.10.2. ICE and multiple sclerosis

Multiple sclerosis is an immune-mediated demyelinating disease characterized by CNS white matter plaques. The neuropathological characteristic of the disease is the presence of inflammatory infiltrates containing few T cells within CNS. It is noted that TNF- α , IFN- γ , and IL-1 β are present in MS plaques. IL-1 β has also been shown to induce experimental autoimmune encephalomyelitis (EAE) in an MS animal model. Furlan and associates' findings suggest that the ICE mRNA blood levels are elevated and are at peak at the time of maximal EAE severity.¹¹⁵ Dowling *et.al.* established that there is marked up regulation of¹¹⁶ in MS plaques (acute as well as chronic). Moreover, ICE deficient mice demonstrated reduced EAE incidence. Similar results were obtained with pharmacological blockade of ICE in animal models. However, the ICE inhibitor only reduces EAE incidence in the preventive protocol and not in the therapeutic protocol, suggesting that ICE plays a crucial role in early stage of immune-mediated inflammatory process finally leading to EAE. All these results taken together indicate that the ICE plays a pivotal role in regulation of proinflammatory cytokines and inhibition of the ICE is a

potential therapeutic target for treatment of immune mediated inflammatory diseases.¹¹⁵

5.10.3. ICE and Rheumatoid Arthritis

Rheumatoid arthritis (RA) is a systemic chronic inflammatory disorder characterized by inflammation of various tissues. In RA patients, procytokines levels were higher in the synovial fluid (TNF- α , IL-1 β IL-6 and IL-18) from the joints irrespective of therapy. These cytokines are capable of inducing various inflammatory responses along with cartilage breakdown. ICE is known to play an important role in maturation of IL-1 β and IL-18, which are involved in mediation of RA. Researchers have demonstrated that ICE inhibitors were able to reduce the cytokine levels and subsequently alleviate symptoms of RA in animal models. Pralnacasan, an ICE inhibitor has shown to reduce cartilage damage and bone degradation in murine models. Pralnacasan initially showed promise in clinical trials against RA, however, was discontinued in phase IIb due to Pralnacasan induced liver fibrosis.¹¹⁷⁻¹¹⁹ Though ICE inhibitors have shown some potential in treatment of RA, safety in long term usage (required in treatment of inflammatory disease) is to yet to be assessed. In order to develop a successful ICE inhibitor for treatment of inflammatory disorders it is necessary to develop a very specific inhibitor of ICE with good safety profile.^{120, 121}

5.10.4. ICE and other diseases

ICE has been implicated in sepsis but the exact mechanism of involvement of ICE is not known. Pro IL-18 is processed by ICE to mature IL-18, which in turn induces TNF- α production and T-cell polarization. Moreover, reduction in apoptosis of neutrophils as seen in sepsis is mediated by production of IL-1 β . Both these observations suggest ICE inhibition might be a viable treatment

option of sepsis. ICE has also been implicated in neurodegenerative disorders like Huntington's disease, Alzheimer's disease and Parkinson's disease. Though the regulation of ICE along with other caspases (2, 3, 7 and 8) has been observed in many of such diseases, the exact role of ICE has yet to be elucidated.¹²²

5.11. Development of ICE inhibitors

ICE plays an important role in the maturation of proinflammatory cytokines, which in turn play a role in various immune mediated inflammatory disorders. Researchers over the years, utilizing ICE knockout animal models and ICE pharmacological inhibitors, have proved that it is possible to regulate cytokine levels by inhibition of ICE. ICE-deficient mice exhibit a shift in the transport of several proinflammatory cytokines like IL-1 β , IL-1 α , IL-6 and TNF- α . These studies clearly indicate that ICE inhibitors have great potential to be developed in drugs for use against several inflammatory disorders. Due to its high therapeutic potential, pharmaceutical companies have invested time and money in pursuing this target for treatment of immune mediated inflammatory disorders.^{123, 124}

ICE has been the most well studied inflammatory caspases. One of the pioneering studies in field of ICE research by Thornberry associates was the identification of the tertiary protein structure of ICE and ensuing discovery of the tetrapeptide Ac-YVAD-CHO possessing potent ICE inhibitory activity.¹⁰⁰ Later on, X-ray crystal structures of ICE co-crystallized with various inhibitors have been published. As a result of extensive structural studies over the years, precise pharmacophoric requirement of ICE inhibitors have been identified. The substrate can be divided in to four portions P1, P2, P3 and P4 (figure 5.6). Out of these requirements at P1 and P4 are very stringent, while wide ranges of substitutions are tolerated in P2 and P3.^{81, 122, 124, 125}

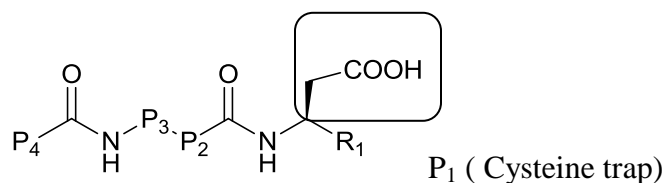


Figure 5.6.: Typical caspase-1 inhibitor

5.11.1 Substrate Specificity for caspase-1

Prerequisites for the substrates of ICE inhibitors are generally well accepted and are as follows:

- 1) Presence of L-Aspartic acid residue in the P1 site that emulates the cleavage site (Asp-Ala) of the pro form of IL-1 β . This distinctive feature confers specificity to caspases over other cysteine proteases (calpains, cathepsins etc) Additionally, the aspartate residue forms crucial salt bridge interactions with Arg179, Gln283 and Arg341 thus anchoring the ligand in appropriate orientation exposing the adjoining electrophilic warhead group to the nucleophilic Cys285.^{99, 100}
- 2) Presence of electrophilic warhead groups in the P1 site to which Cys285 forms a covalent bond. His237 stabilizes the oxyanion of the warhead group suggesting its involvement in the catalytic cascade. Depending upon the nature of substituent adjacent to the electrophilic center (usually carbonyl group) the inhibitor can be reversible or irreversible.^{123, 126}

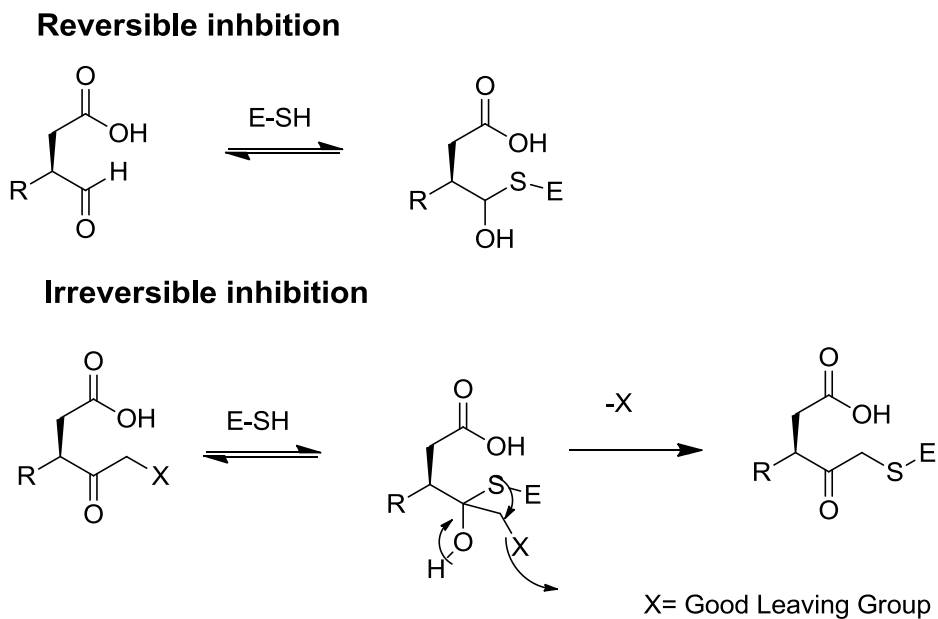


Figure 5.7.:Types of caspase-1 inhibitors

Variety of both reversible and irreversible warhead groups have been identified in an effort to optimize the potency, selectivity, cell permeability, safety and ADME properties of ICE inhibitors. Some examples of cysteine traps used in ICE inhibitor design are shown below. Bioisosteric replacement of acid group (e.g. sulphonamide) to improve cell permeability has also been reported. Presence of an additional hydrophobic P1' subsite adjacent to P1 has also been explored.¹²⁷ Till date, most successful cysteine trap is hemiacetal prodrug which is found in inhibitor in clinical trials (VX-740= Pralnacasan and VX-765)

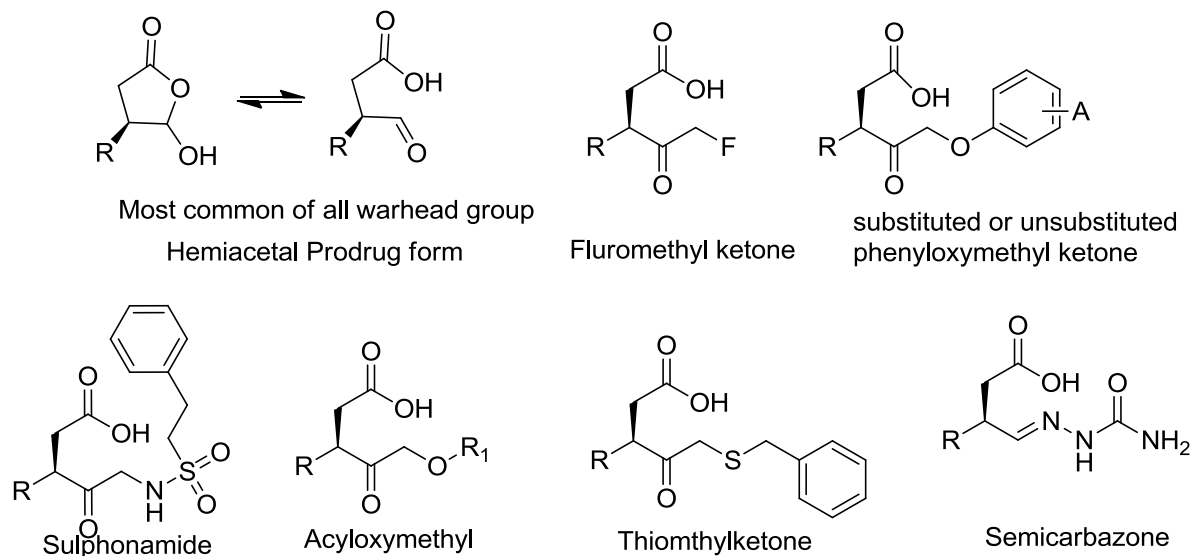


Figure 5.8.: Different warhead groups used in caspase-1 inhibitors

- 3) P2-P3 requirements are not very stringent and most of the variation is seen in the design of ICE inhibitors is in this region. Dolle and coworkers employed N-methyl scan of substrate amide (ICE inhibitor) to determine crucial H-bond interaction of the amides of the tetrapeptide (P₂-P₃ region) with caspase-1 active site. Dolle *et.al.* later¹²⁸ identified cyclic motifs that would retain these key hydrogen bonding interactions in P2-P3.^{129, 130}

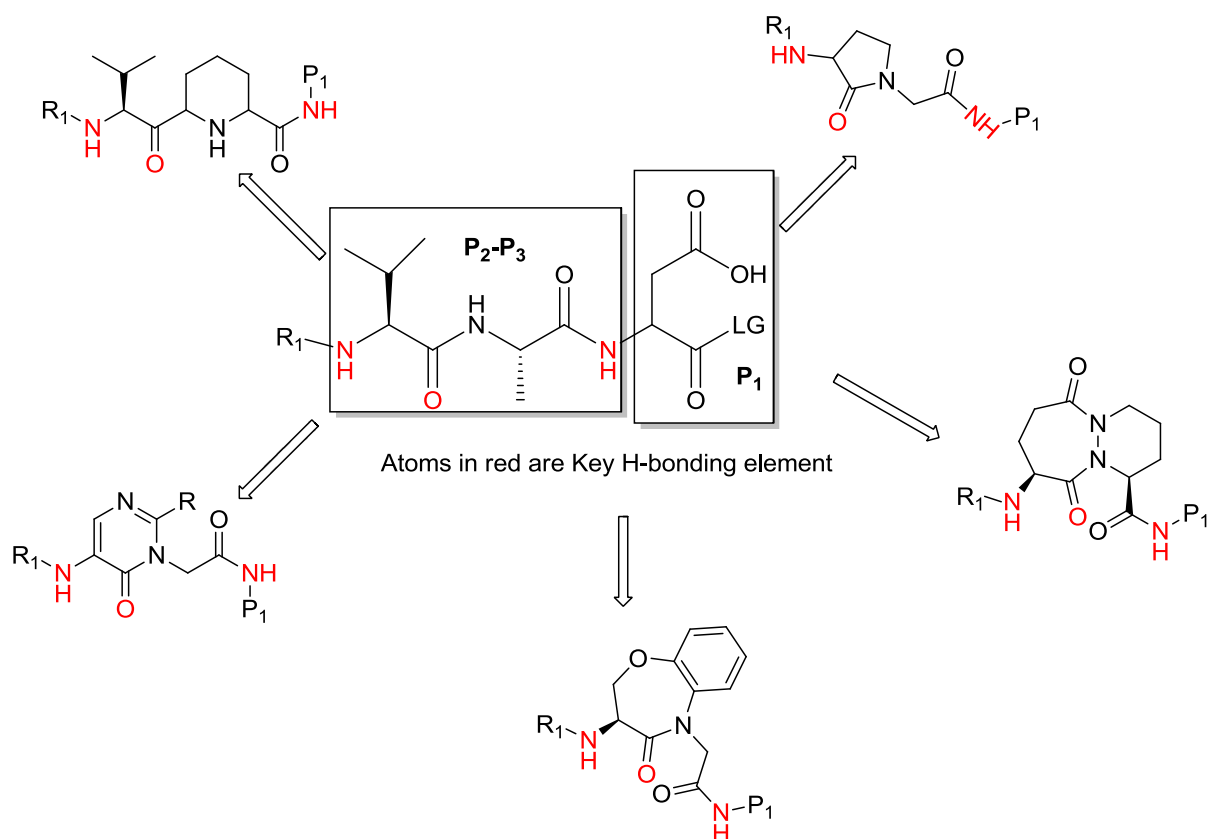


Figure 5.9.: Crucial hydrogen bonding interaction in P2-P3 region of caspase-1 inhibitor

Further optimizations on Pyridazinondiazepine scaffold led to the discovery of Vertex's molecule pralnacasan, which was first ICE inhibitor in clinical trial

- 4) Finally P4 requirement is very precise and is the determinant of specificity amongst different caspases (Karannevsky et.al). For caspase-1, hydrophobic aromatic groups are generally tolerated well.¹³¹

Figure 5.10. shows P1-P4 regions of Ac-YVAD-CHO inhibitor in the caspase-1 active site (S1-S4). All the crucial hydrogen bonding interactions are shown in green.

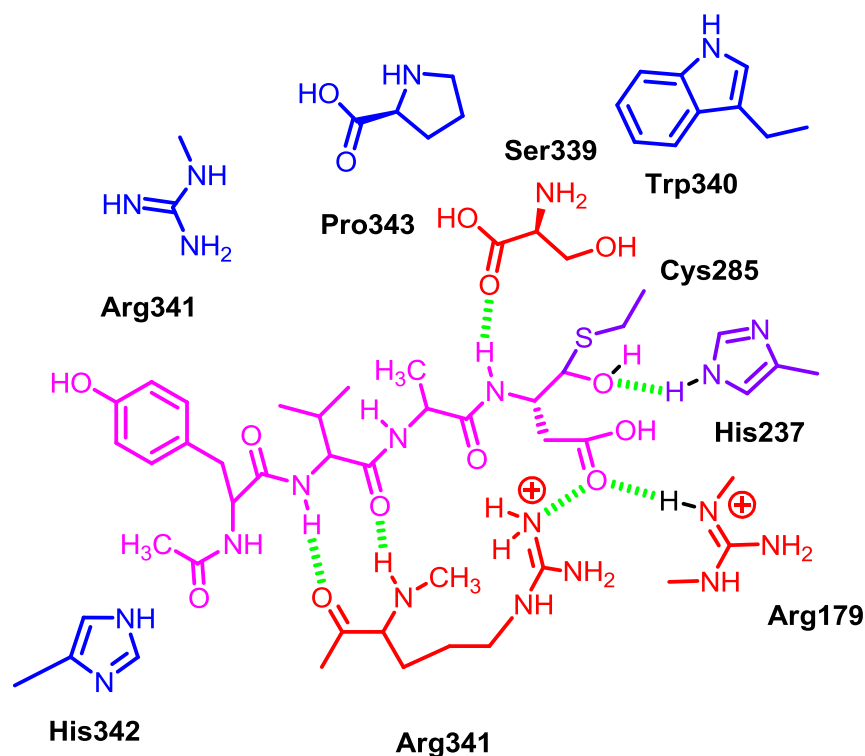


Figure 5.10.: Depiction of active site of Caspase-1 with bound inhibitor Ac-YVAD-CHO, as reported in the co-crystal structure.

5.12. Caspase-1 Inhibitors in literature

Using precise knowledge of the active site and crucial protein ligand interactions of ICE, many research groups, both from industry and academia have reported several ICE inhibitors till date. Especially with advent of Pralnacasan clinical trials (stopped at phase-II), and VX-765 clinical trials for treatment of drug resistant epilepsy (just cleared in Phase IIa and Phase IIb will start later in 2011) and psoriasis (completed phase II) have continued interest of scientist in development of novel ICE inhibitors for the treatment of immune mediated inflammatory diseases. Moreover, anakinra (Kineret®) that modulates IL-1 β levels is approved for the treatment of some inflammatory disorders further suggest need for development of new ICE

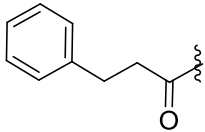
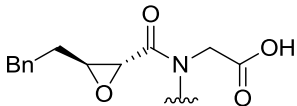
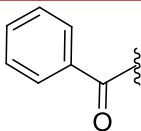
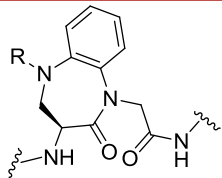
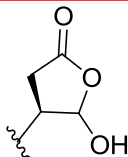
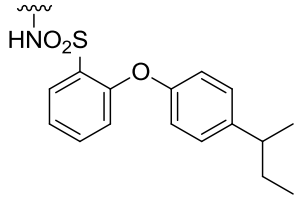
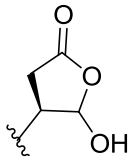
inhibitors. Review of inhibitors developed till date is summarized in table given below which suggests that peptidomimetic design is still favored. Recently, several approaches have been undertaken by proctor and gamble to simplify the peptidic scaffold (table 5.1) and to modulate pharmacokinetic properties of ICE inhibitors.

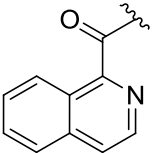
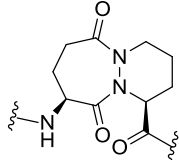
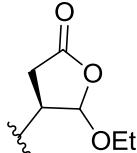
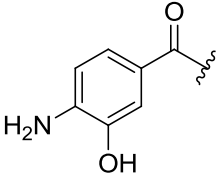
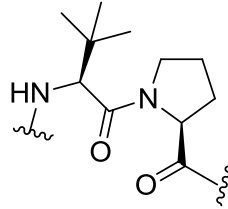
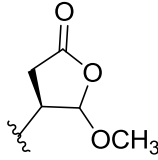
Several non-peptidic ICE inhibitors have been reported but none of them have been continued further in drug development program.¹³⁴

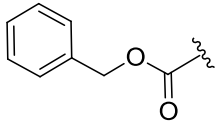
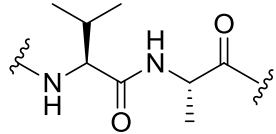
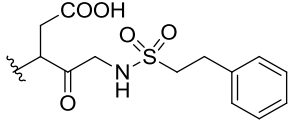
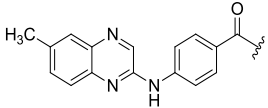
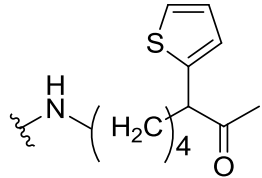
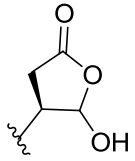
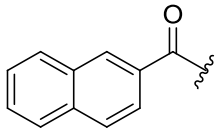
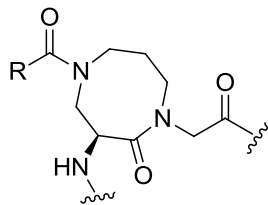
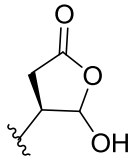
Problems associated with development of Caspase-1 inhibitors

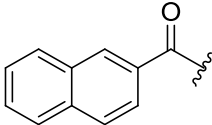
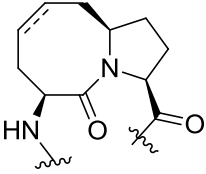
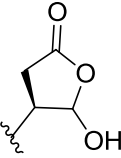
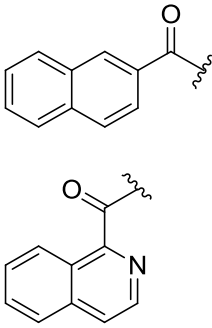
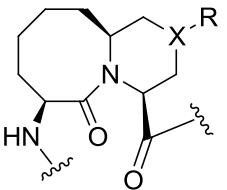
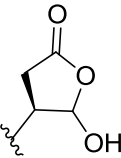
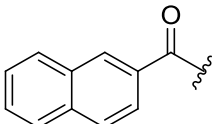
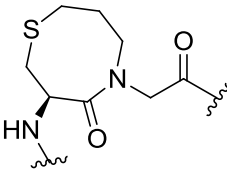
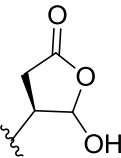
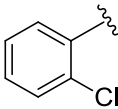
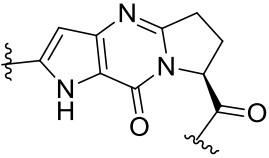
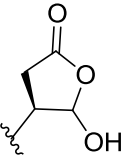
Even after several years of caspase-1 research, only two candidates (Pranlacasan and VX-765) have reached clinical trials. This clearly indicates that there are some problems associated with caspase-1 drug development. One of the major problems associated with ICE inhibitor development is obtaining specificity amongs several human cysteine proteases.^{134, 135}

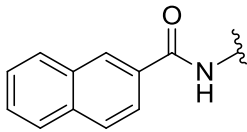
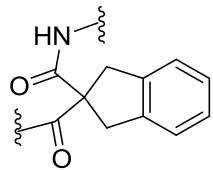
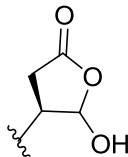
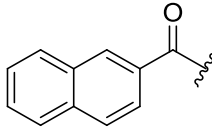
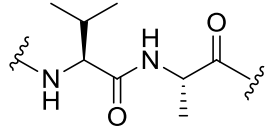
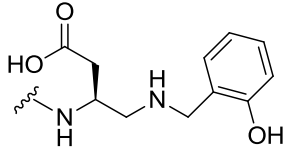
Table 5.1: Caspase-1 Inhibitors from literature

P4	P2-P3	P1	Notes	References
Ac-Y	VA	D-CHO	One of the first successful tetrapeptide with ICE-1 inhibition activity with IC-50 2-5 nM	81
	VA		Epoxide as Cysteine trap high caspase selectivity	136, 137
			Designed to explore P3 region ($K_i = 90$ nM)	138
None			Pfizer Diphenyl ether sulfonamide analog designed to increase potency via hydrophobic interaction. Identification of P1 prime hydrophobic pocket	139

			($K_i = 100 \text{ nM}$)	
			Pralnacasan-Vertex First ICE inhibitor to reach the clinical trials, however discontinued in phase IIb clinical trials for the treatment of Rheumatoid arthritis due to liver toxicity at high dose (IC50 5nM)	140
			VX-765-Vertex Vertex Pharmaceutical just completed phase II on treatment resistant patients using VX-765. Preliminary endpoint shows VX-765 to be Safe and tolerable. Secondary endpoint suggest need for longer duration phase IIb trails. VX-765 inhibits acute and chronic seizures in preclinical models that do not respond to standard anti-epileptic drugs.	140, 134

			<p>Pfizer</p> <p>P1 Sulfonamides analogs as ICE inhibitors, designed to enhance the potency via intramolecular hydrogen bonding ($K_i= 4 \text{ nM}$)</p>	<p>141</p>
			<p>Sunesis Pharmaceutical</p> <p>Disulfide tethering used to find reversible ICE inhibitor. Novel tricyclic molecular fragment recognized binding specifically to S4. Substitution of peptidomimetic P2-P3 region with thienyl alkyl ester ($K_i= 5 \text{ nM}$)</p>	<p>142</p>
			<p>Procter and Gamble Pharmaceutical</p> <p>Diazocan derivative, P2-P3 cyclic probe. R= Substituted Phenyl ring</p> <p>Most potent analog; R = Ph(3-OMe)</p> <p>10,000 fold selective over caspase 3 & 8</p>	<p>143</p>

			<p>Intended to increase cell permeability</p> <p>IC 50 1 nM, Whole cell assay (THP-1) 3 nM</p>	144
	 <p>x = O, N When X= N; R= SO₂Me, SO₂Ph</p>		<p>P & G Pharmaceutical</p> <p>8, 6 fused bicyclic peptidomimetic (P2-P3).</p> <p>Designed to maximize interactions at S2 pocket of the active site. IC50 of 1 nM. Most of the derivatives were 10,000 fold more selective than caspase 3 and 8</p> <p>Whole cell assay (THP-1) 46-100 nM</p>	145
			<p>P & G Pharmaceutical</p> <p>Monocyclic Thiazepine derivative with IC50 of 30 nM of most active compound in the series. 10,000 foldmore selective than caspase 3 and 8</p>	146
			<p>P & G Pharmaceutical</p> <p>Pyrrolopyrimidinone as dipeptide mimetic</p>	147

			<p>(P2-P3) IC₅₀=14 nM</p> <p>Whole cell assay (THP-1) 500nM 252 nM</p>	
			<p>P & G Pharmaceutical</p> <p>1-(2-acylhydrazinocarbonyl)-cycloalkyl</p> <p>carboxamide derivative as ICE inhibitor</p> <p>IC₅₀ = 30 nM Whole cell assay (THP-1)</p> <p>500nM</p>	148
			<p>First example of noncovalent potent selective</p> <p>ICE inhibitor. Replacement of electrophilic</p> <p>aldehyde by benzylamine. K_i = 47 nM</p>	149

CHAPTER 6

SYNTHESIS AND BIOLOGICAL EVALUATION OF BERKELEYAMIDE A AND ITS DERIVATIVES

6.1. Introduction

Caspase-1 inhibitors have been highly pursued by industry as well as academia due to their immense therapeutic potential. However, even after decades of painstaking research, only few candidates have reached clinical trials. Moreover, none of them have made it to the market yet. This suggests that there is a continuous need to search for novel ICE inhibitors for the possible treatment of inflammatory disorders due to their tremendous potential. Over the years, many natural products isolated from varied natural sources have served as leads in the drug discovery process. With that perspective, we decided to explore some natural product leads for development of ICE inhibitors.^{150, 151}

Recently, several interesting secondary metabolites have been isolated from rare microbes evolved in extreme ecosystems such as Berkeley Pit Lake system in Montana using bioactivity guided fractionation. These secondary metabolites have shown an array of biological activity, ranging from anticancer to antimicrobial activity. One such secondary metabolite, berkeleyamide A (**6.1**), was isolated from the fungi *Penicillium rubrum*. The fungus was one of the first microbes to be studied and was isolated from a water sample taken from 885 feet of the lake. Crude chloroform extracts inhibited caspase-1 and matrix metalloproteinase-3 (MMP-3) in low micromolar range. After extensive purification, isolation and subsequent structure elucidation (using techniques like IR, NMR 1D & 2D, HRMS) of several compounds, they discovered four new amides; berkeleyamide A, B, C and D. All these compounds were active against caspase-1 and MMP-3. berkeleyamide A exhibited greatest potency amongst all the novel compounds and inhibited both caspase-1 and MMP-3 with IC₅₀ of 330 nM.¹⁵²

6.2 Structure of Berkeleyamide A

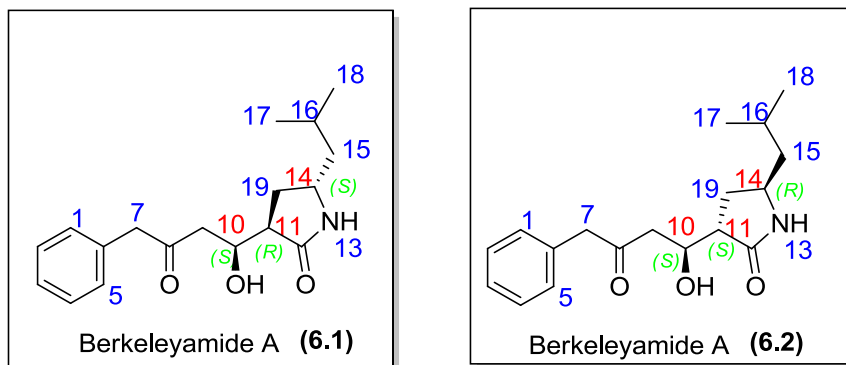
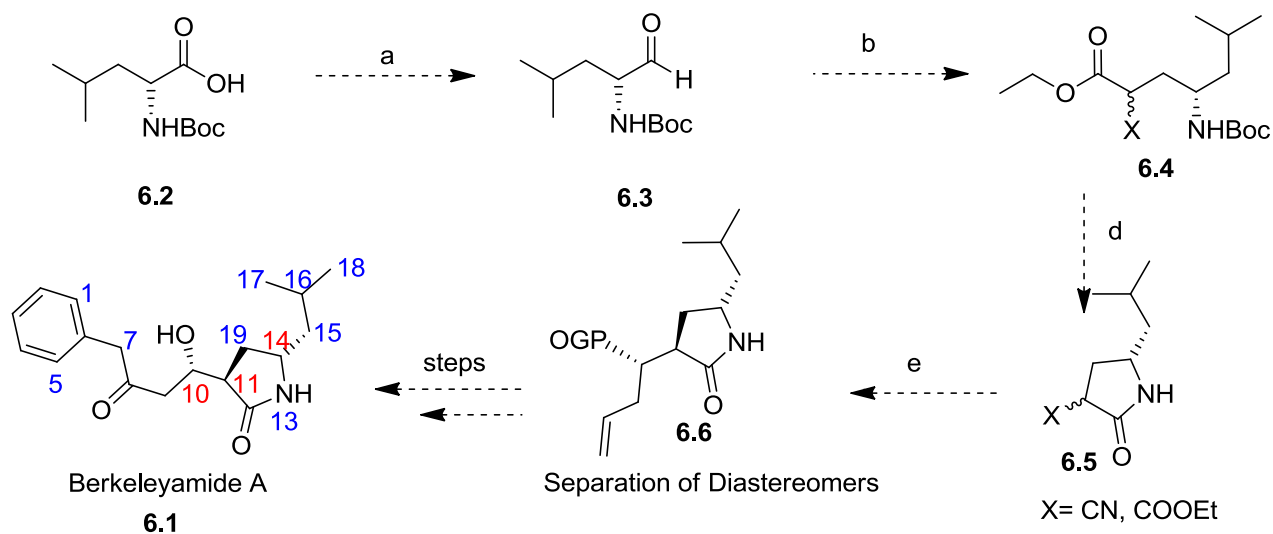


Figure 6.1. Possible diastereomers of berkeleyamide

The structure of berkeleyamide A was elucidated using detailed NMR studies. It has a core pyrrolidone scaffold with isobutyl chain substitution at 14-position, β -hydroxy-ketone side chain appended at 11 position and three stereogenic centers; C-10, C-11 and C-14. The absolute stereochemistry at C-10 was assigned as 10*S* using modified mosher ester analysis. There was ambiguity regarding the configuration of the C11 and C14 stereogenic centers at the time of isolation. However, it was known that they share a *trans* relationship, which was established by the use of NOESY 2D NMR studies. With this information at disposal, it is evident that berkeleyamide A can have either 10(*S*), 11(*R*) & 14 (*S*) absolute stereochemistry or 10(*S*), 11(*S*) and 14 (*R*). Intriguing biological properties and ambiguity of the absolute stereochemistry at C11 and C14 prompted us to initiate the total synthesis of **6.1**. The overall objective of this project was to accomplish the total synthesis of **6.1**, perform detailed structure activity relationship studies and apply structure based design approach in the quest of novel potent caspase-1 inhibitors based on **1** scaffold.¹⁵²

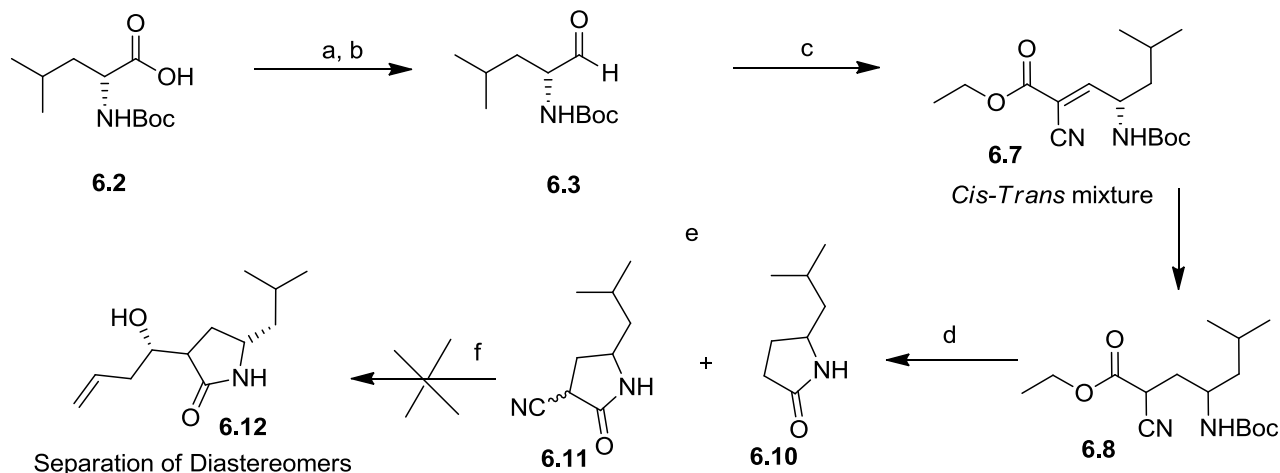
6.3. Route-1 proposed synthesis for berkeleyamide A

Berkeleyamide A has a disubstituted pyrrolidone scaffold with three stereogenic centers. Our proposed synthetic scheme is depicted in scheme 1, which relies on synthesis of the crucial pyrrolidone synthon followed by installation of the β -hydroxy ketone side chain. Assuming **1** is biosynthesized from naturally occurring *L*-leucine, it was logical to use commercially available Boc-*L*-Leucine for the construction of disubstituted pyrrolidone. The β -hydroxy ketone side chain can be appended by functional group manipulation of the X group. All the obtained diastereomers have been separated by either column chromatography or preparative HPLC.



Scheme 6.1: Proposed synthesis of berkeleyamide A

Proposed reactions a) synthesis of aldehyde b) Knoevenagel condensation and Hydrogenation d) one pot Boc-deprotection followed by cyclization e) Functional group manipulations



Scheme 6.2: Synthesis of disubstituted Pyrrolidone scaffold

Reagents and Conditions: a) N, O dimethylamine hydrochloride, N-methyl morpholine, EDCI DCM b) 2.4 M LAH in THF solution, THF c) Ethyl cyanoacetate, 10% Silica gel CHCl_3 d) 10% Pd/C, H_2 e) $\text{LaCl}_3 \cdot 7\text{H}_2\text{O}$ water:acetonitrile (9:1) f) Grignard, THF and then HCl

According to the retrosynthetic analysis of **6.1**, formation of pyrrolidone scaffold was the key step towards the total synthesis of this natural product. To achieve this objective, commercially available N-Boc-L-Leucine **6.2** was converted into Weinreb amide **6.3**, using standard peptide coupling conditions. Weinreb amide obtained (96%) was then subjected to reduction using lithium aluminium hydride (LAH) solution (2.4M) to give an aldehyde in 90% yield. The next crucial step in our scheme was homologation of the aldehyde fragment and we decided to employ Knoevenagel condensation for the same. Knoevenagel reaction is a modification of aldol reaction and involves a nucleophilic attack of active methylene group containing compound (like diethyl malonate or Meldrum's acid) on an aldehyde followed by subsequent dehydration to give a α,β -unsaturated compound. Having aldehyde in hand next step was Knoevenagel condensation of the aldehyde with diethyl malonate (active methylene

containing compound) in presence of an appropriate catalyst. Unfortunately, after exploring different reaction conditions for the Knoevenagel reaction, it did not proceed as anticipated. Given below (Table 6.1) is the summary of various reaction conditions and different catalysts. The failure of the reaction was attributed to the polymerization of the aldehyde *N*-Boc-*L*-Leucinal and may have been caused because of the inability of diethyl malonate to carry out the nucleophilic attack on the aldehyde. Hence diethyl malonate was replaced with more reactive ethyl cyanoacetate as an active methylene component of the Knoevenagel condensation. Accordingly, *N*-Boc-*L*-Leucinal was treated with catalytic amounts of piperidine acetate in presence of ethyl cyanoacetate in benzene to give the desired α, β unsaturated ester albeit with poor yields. After screening for several different catalysts, silica gel was found to be the best catalyst for the Knoevenagel condensation yielding approximately 70% of the required product.

Table 6.1: Different catalyst and reaction conditions for Knoevenagel reaction

Substrate	Catalyst	Reaction conditions	Results
Diethyl malonate	Piperidine acetate	Reflux in benzene using dean stark	No reaction
Diethyl malonate	p-Toluene sulfonic acid	Reflux in benzene using dean stark	No reaction
Diethyl malonate	Piperidine	Stirring at RT in ethyl acetate	No reaction
Diethyl malonate	Triphenyl phosphine	Stirring at RT in THF	No reaction
Diethyl malonate	<i>s</i> -Proline	Stirring at RT in ethanol	No reaction
Ethyl cyanoacetate	Piperidine	Stirring at RT in ethyl acetate	$\leq 20\%$ yield
Ethyl cyanoacetate	<i>s</i> -Proline	Stirring at RT in ethanol	$\leq 10\%$ yield
Ethyl cyanoacetate	Triphenylphosphine	Stirring at RT in THF	No reaction
Ethyl cyanoacetate	30% Silica	Stirring at RT in Ethyl acetate	55-70% yield

Once the Knoevenagel condensation condition was set, the next step in the proposed sequence was formation of the five membered lactam. Reduction of the α,β -unsaturated ester (*cis-trans*) using palladium over carbon catalyst and hydrogen under balloon pressure proceeded smoothly, furnishing a saturated γ -amino ester derivative. We envisioned one pot deprotection of Boc group followed by cyclization to form pyrrolidone scaffold from the saturated cyanoester **6.8**. Deprotection of the Boc group by either HCl or TFA required longer exposure times and resulted in incomplete conversion and/or product degradation. Alternatively, deprotection of the boc group in water using microwaves required only minutes for completion of the reaction. Upon exposure of ester **6.7** to microwaves at 100°C, two products were isolated; 5-isobutylpyrrolidin-2-one **6.9** and 5-isobutyl-2-oxopyrrolidine-3-carbonitrile **6.10**. When the reaction was carried out in the presence of catalytic amounts of mild Lewis acid like lanthanum chloride hepta-hydrate (Table 6.2), only 5-isobutyl-2-oxopyrrolidine-3-carbonitrile was isolated with moderate yields.

Table 6.2: Reaction conditions for cyclization (All reactions carried out in Microwave at normal absorption)

Catalyst	Reaction conditions	Temperature in °C	Ratio of 10:9		Overall Yield
			10	9	%
No catalyst	Water	100	50	50	40
No catalyst	Water:ACN (9:1)	100	50	50	38
No catalyst	ACN	60	NR	NR	-
ScOTf (10 mol %)	Water:ACN (9:1)	65	70	30	36
LaCl ₃ ·7H ₂ O (10 mol %)	Water:ACN (9:1)	65	90	10	53%
YbCl ₃ ·6H ₂ O (10 mol %)	Water:ACN (9:1)	65	80	20	41%

Though we were successful in synthesizing the disubstituted pyrrolidinone derivative, 5-isobutyl-2-oxopyrrolidine-3-carbonitrile was racemized (optical rotation and NMR). This was a minor setback in our progress, but we decided to move forward with racemic material and address this issue later.

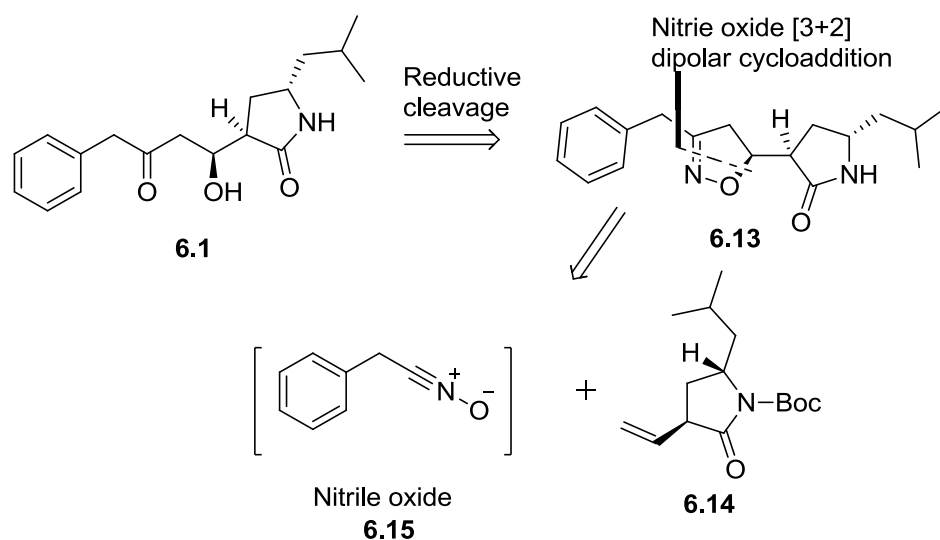
With the pyrrolidinone scaffold in hand, appending β -hydroxy ketone side chain was the final hurdle. According to our proposed synthetic route, either the cyano functional group of compound **6.10** can be subjected to grignard addition or the compound **6.9** can be subjected to an aldol type reaction. Grignard added to the cyano functional group was very sluggish and gave many inseparable products (needed HPLC purification). After several attempts, we were unable to homologate the cyano functional group. With this failure and earlier racemization problems we decided to switch to a more robust asymmetric route for synthesis of **6.1**.

6.4 Need for asymmetric route of synthesis of berkeleyamide A

We were simultaneously working on an asymmetric synthetic protocol, which would obviate the need for meticulous chromatographic separations of diastereomeric mixtures. The overall goal of this project was development of an efficient, enantioselective and scalable route for total synthesis of **6.1**. To achieve this specific objective, we designed an asymmetric route for the synthesis **6.1**, amenable for detailed structure activity relationship (SAR) studies and determination of absolute configuration of the natural product. Discussed below is our asymmetric route for synthesis of **6.1** and its diastereomers. We were also able to confirm the absolute configuration of the natural product to be 10*S*, 11*R*, 14*S*. This was in accordance with work simultaneously published by Brimble et al.¹⁵³

6.5 Prior work

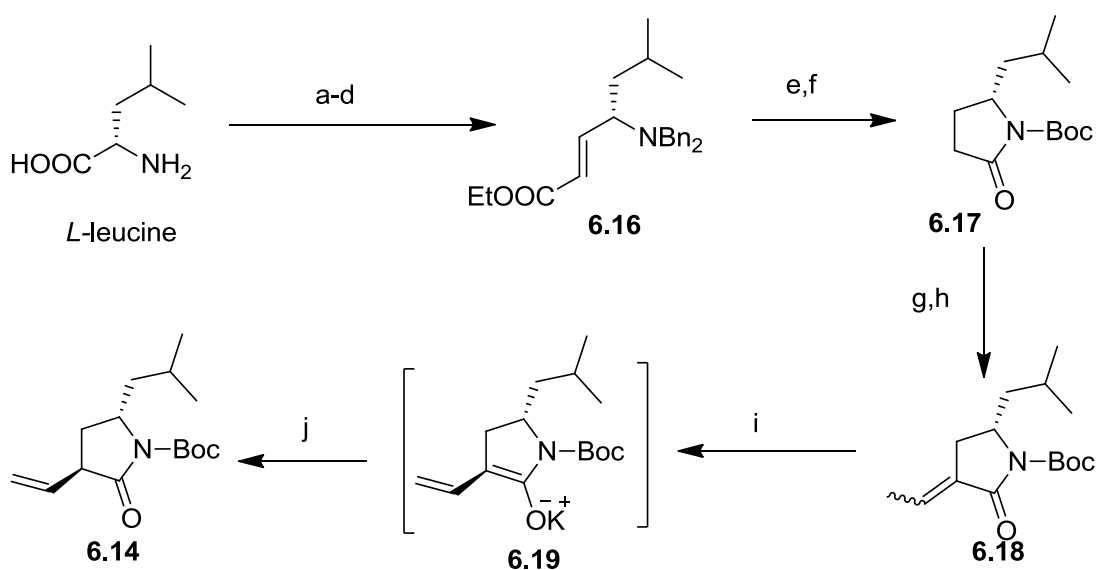
During the course of our work, Brimble and coworkers confirmed the absolute stereochemistry of **6.1** by co-eluting an authentic sample (obtained from Sterile et.al) and a synthetic sample in HPLC as 10*S*, 11*R*, 14*S*. Given below is their retrosynthetic scheme (Scheme 3), which relies on the application of a crucial [3+2]-dipolar cycloaddition towards completion of total synthesis of **6.1**. They visualized the formation of isoxazoline **6.13** by reaction between the dipolar nitrile oxide **6.15** and the dipolarophile chiral alkene **6.14**.



Scheme 6.3: Retrosynthetic analysis for berkeleyamide A by Brimble *et al*

Synthesis of chiral alkene **6.14** was carried out in 10 steps, starting from *L*-leucine. α,β -unsaturated ester **6.16** was synthesized from *L*-leucine in four steps in a straightforward manner. Reduction of the double bond and lactamization were carried out in one pot and the obtained lactam was protected by Boc group to give compound **6.17**. The lactam **6.17** was then subjected to alkylation with acetaldehyde followed by mesylation mediated dehydration to give internal alkene **6.18**. The internal alkene was then subjected to acid mediated kinetic protonation

to furnish the key chiral alkene. Next, they turn their attention toward the synthesis of nitrile oxide. Initial attempts of synthesis of **6.13** from nitroalkane failed due to homodimerization of nitrile oxide and isomerization of chiral alkene. Hence the authors decided to utilize dehydrohalogenation of a hydroxyiminoyl halide at lower temperatures for the synthesis of nitrile oxide.

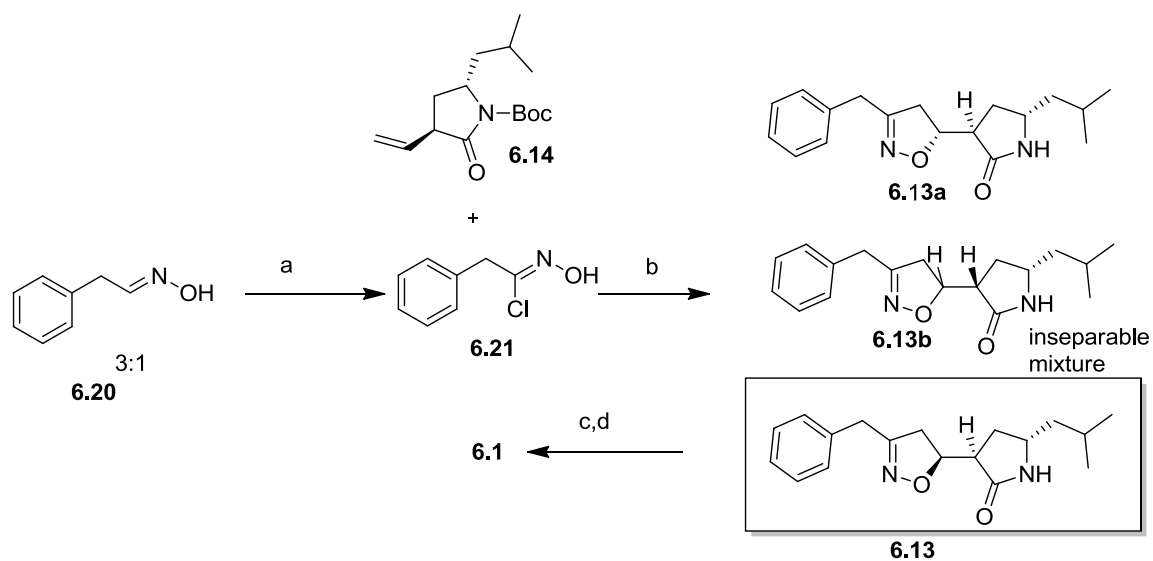


Scheme 6.4: synthesis of chiral alkene **6.14**

Reactions and conditions : a) NaBH_4 , H_2SO_4 , THF b) K_2CO_3 , BnBr c) Swern oxidation d) NaH, triethylphosphonoacetate e) $\text{Pd}(\text{OH})_2$, MeOH, AcOH f) $(\text{Boc})_2\text{O}$, DMAP g) LiHDMS, THF, Acetaldehyde g) MsCl, TEA then DBU i) KHMDS j) AcOH

Treatment of oxime **6.20** with N-cholorsuccinimide afforded iminoyl chloride **6.21** which on reaction with chiral alkene in the presence of a base gave mixtures of oxazoline cycloadduct products (**6.13**:**6.13a**:**6.13b**) in ratio 2.1:1:1 (2.1 is the required diastereomer and is shown in a

box, scheme). Berkeleyamide A was obtained from cycloadduct in two steps; molybdenum chloride mediated reductive cleavage of oxazoline scaffold and deprotection of group.¹⁵³

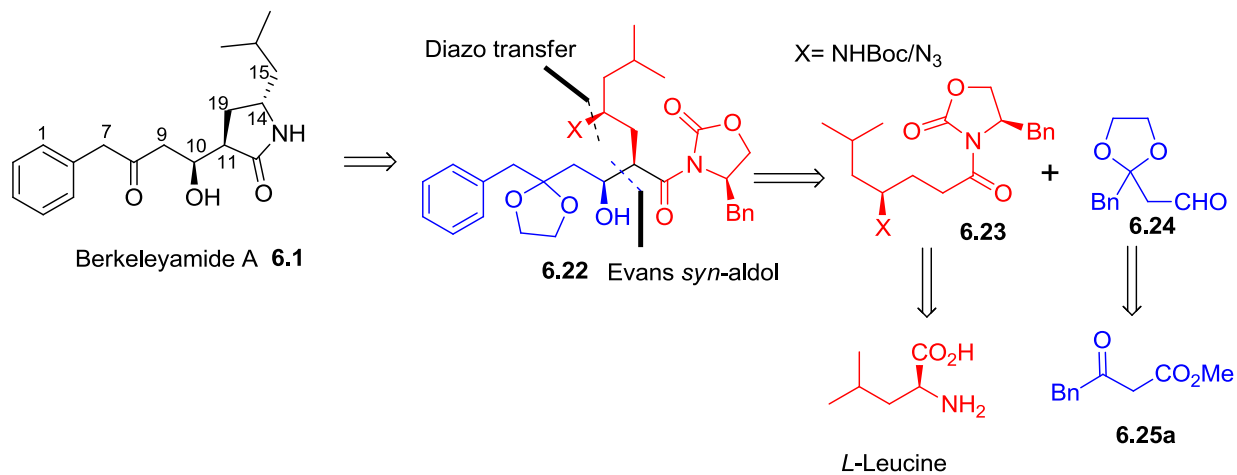


Schemes 6.5: Completion of synthesis of Berkeleyamide A by Brimble

Reagents and conditions: a) NCS, py, DCM b) TEA c) Mo(CO)₆, MeCN:H₂O d) TFA

Brimble and Associates completed the total synthesis of **6.1** in about 14 steps with 3 % overall yield. Their crucial cycloaddition reaction suffered from poor diastereoselectivity (2.1:1:1) and lower yield (~35%) of the required diastereomer. Though they confirmed the absolute stereochemistry of the molecule, their route is not amenable to scale up and SAR studies. This warrants development of asymmetric route, which is scalable and accessible for a structure activity relationship study.

6.6 Route-2 Total synthesis of Berkeleyamide A

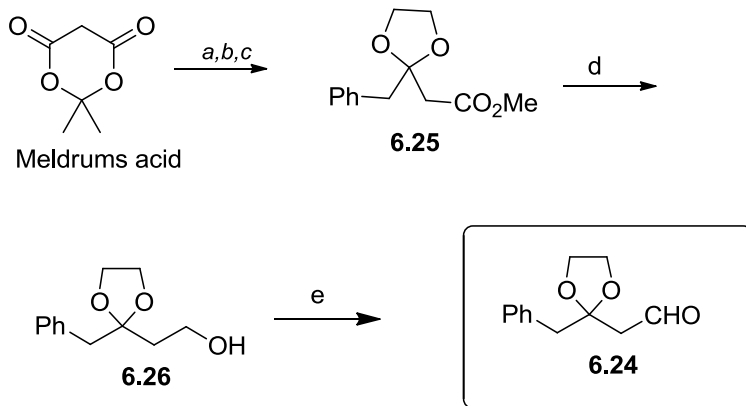


Scheme 6.6 : Route-2 retrosynthetic analysis of 6.1

We deliberated the use of a modular asymmetric synthetic approach for the synthesis of **6.1** and its diastereomers. Our plan was to employ Evans' aldol¹⁵⁴ reaction as a key step for C-C bond formation between chiral imide **6.23** (shown in red) and aldehyde **6.24** (shown in blue). The crucial asymmetric aldol reaction will facilitate the introduction of the required chirality at C10 and C11 (Scheme 6.6). As depicted in the retrosynthetic analysis, crucial *N*-acyl-4*R*-benzyl oxazolidin-2-one **6.23** was envisioned from *L*-leucine by assuming the natural *L*-configuration in the biosynthetic pathway. The other aldol coupling partner, aldehyde **6.24**, was envisioned from β-keto ester **6.25**, which can be made in two steps starting from meldrums acid. Our disconnection approach not only offered an enantioselective route to **6.1** but also presented us a flexible strategy to synthesize all possible diastereomers of **6.1**, for SAR studies, by simply incorporating either *L* or *D*-amino acid and adopting Evans' (*or*) non Evans' *syn/anti*-aldol synthetic approach.¹⁵⁵⁻¹⁵⁷

6.6.1 Synthesis of Aldehyde 6.24

As shown in Scheme 6.6, the aldehyde **6.24** was synthesized from commercially available Meldrum's acid. Meldrum's acid was converted to β -ketoester by typical acylation using phenyl acetylchloride followed by decarboxylative methanolysis.¹⁵⁸ The ketone functionality was then protected as the 1,3-dioxalane using 1,2-bis(trimethylsilyloxy)ethane and TMSOTf to give ketal **6.25**.¹⁵⁹ The corresponding ester was then converted to the required aldehyde **6.24** by a standard two step protocol; complete reduction of the ester to the alcohol by LAH followed by Dess-Martin-Periodinane mediated oxidation. We were able to synthesize the aldehyde **6.24** precursor alcohol **6.26** in multigram quantities with overall good yield.¹⁶⁰ However, unstable aldehyde (prone to oxidation to corresponding acid) was always prepared fresh before the aldol condensation reaction (scheme 6.7).

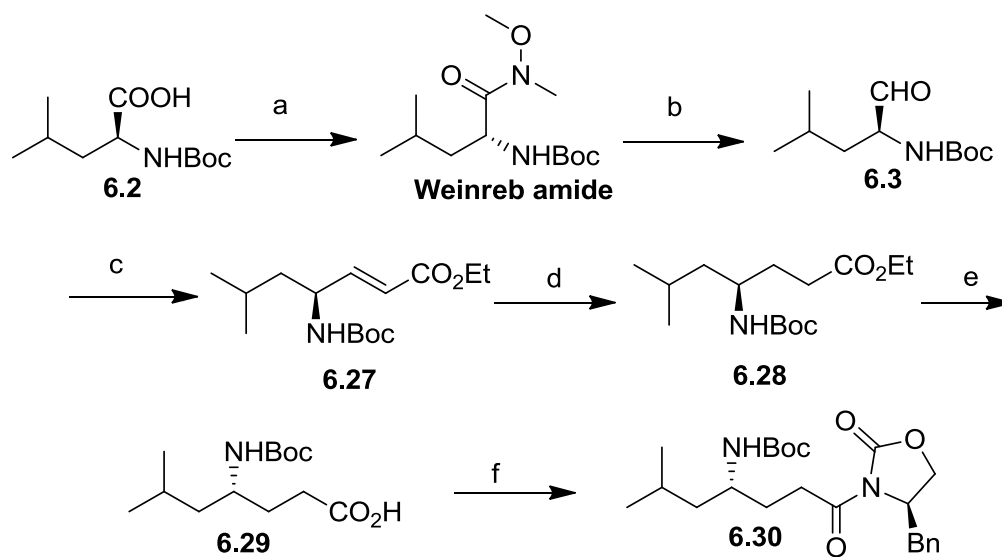


Scheme 6.7: Synthesis of aldehyde fragment 6.24

Reagents and Conditions: a) Phenylacetyl chloride, Pyridine, CH_2Cl_2 , 0°C -rt b) Methanol, reflux
c) 1,2-bis(trimethylsilyloxy)ethane, TMSOTf, CH_2Cl_2 , rt, 8h, 95%; d) 2.3M LiAlH_4 in THF, THF, 0°C -rt, 2h, 78%; e) Dess-Martin-Periodinane, CH_2Cl_2 , rt, 1h, 92%.

6.6.2 Synthesis of Chiral imide

Next, commercially available *N*-Boc-*L*-leucine was converted to *N*-Boc-*L*-leucinal **6.2** following a standard two-step protocol. Conversion of the *N*-Boc-*L*-leucine to mixed anhydride using isobutrylchlorformate and *N*-methyl morpholine and then transforming the mixed anhydride to weinreb amide by treating it with *N*,*O*-dimethylhydroxylamine hydrochloride. The weinreb amide formed was then converted to aldehyde using lithium aluminium hydride. The resulting aldehyde **6.2** was subjected to Horner-Wadsworth-Emmons (HWE) olefination using triethylphosphonoacetate and Lithium bis(trimethylsilyl)amide as base.^{161, 162} Due to known potential of α,β unsaturated ester **6.27** to undergo racemization, the ester was directly subjected to hydrogenation without purification. The α,β unsaturated ester was reduced using 5% palladium over carbon catalyst under hydrogen pressure of 20 psi to give aminoester **6.28** in 85% yield. Subsequent ester hydrolysis of **6.28** furnished γ -*N*-Boc-amino acid **6.29** in good yield. Large scale synthesis of **6.29** was achieved obviating the need for chromatographic purification. The free acid obtained was then converted to chiral imide using standard coupling protocol to give *N*-Boc chiral imide **6.30** (scheme 6.8).

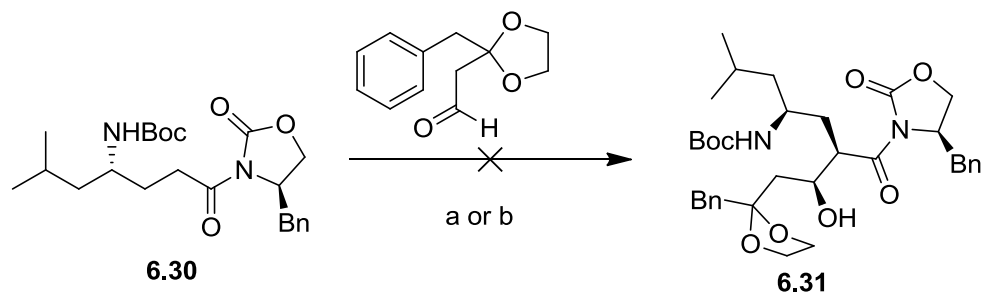


Scheme 6.8: Synthesis of γ -*N*-Boc-oxazolidinone fragment 6.30

Reagents and Conditions: a) (i) isobutrylchlorformate, *N*-methyl morpholine, -20°C (ii) *N*,*O*-dimethylhydroxylamine hydrochloride, CH_2Cl_2 , 0°C ; b) 2.3 M LAH in THF, Ether -20°C ; c) (i) Triethylphosphonoacetate, 1M LiHDMS in THF, THF, 0°C , **6.2**, -20 to 0°C , 0.5h; d) 5% Pd/C, H_2 , 20 psi, EtOAc, 1.5h, 85%; e) LiOH.H₂O, THF:MeOH:H₂O (9:2:1), rt, 2h, 79%; f) pivaloyl chloride, TEA, LiCl, 4(*R*)-benzyl-2-oxazolidinone, THF, -20°C -rt, 6h, 75%.

To carry out aldol reaction in asymmetric fashion, we envisaged use of Evans' aldol chemistry for installation of two stereogenic centers C10 and C11. However, our earlier attempts of an aldol reaction using chiral imide of *N*-boc γ -amino acid **6.29** and aldehyde fragment **6.24** failed to furnish any required product under standard Evans' aldol conditions; dibutylborontriflate and diisopropylethylamine (DIPEA)/ Triethylamine. Furthermore, our efforts of using titanium tetrachloride and DIPEA/Triethylamine in aldol reaction were also futile.¹⁵⁵

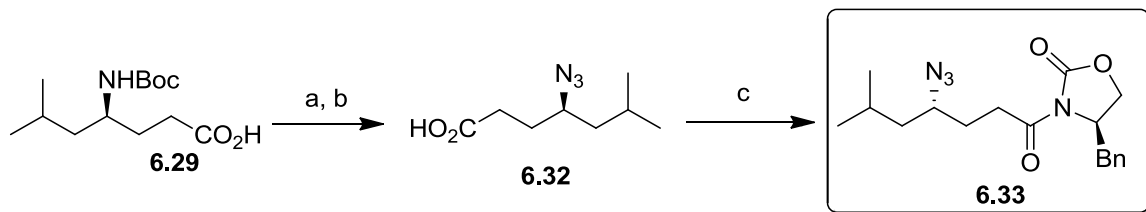
We attributed this failure of the aldol reaction due to presence of enolizable Boc (carbamate)¹⁶³ functionality in chiral imide .



Scheme 6.9 : Synthesis of aldol adduct **6.31**

Reagents and Conditions: a) i., Bu₂BOTf, Triethyl amine, DCM, -78 °C ii. Aldehyde **6.24** or b) i. TiCl₄, DIPEA, DCM, -78 °C ii. Aldehyde

The enolizable *N*-Boc carbamate functionality in **6.29** was then converted into the azide in unique two step protocol; Boc deprotection followed by azido transfer reaction using shelf stable imidazol-1-sulfonyl azide¹⁶⁴ to furnish γ -azido acid **6.32** in 77% yield. The azide transfer reagent was prepared according to the procedure reported in the literature. Reevaluation of the asymmetric aldol reaction using the chiral imide of **6.12** was then pursued. Accordingly, acid **6.18** was coupled with the 4(*R*)-benzyl-2-oxazolidinone chiral auxillary using a standard procedure in order to obtain the correct stereochemistry in the aldol reaction based on literature precedents.¹⁵⁴



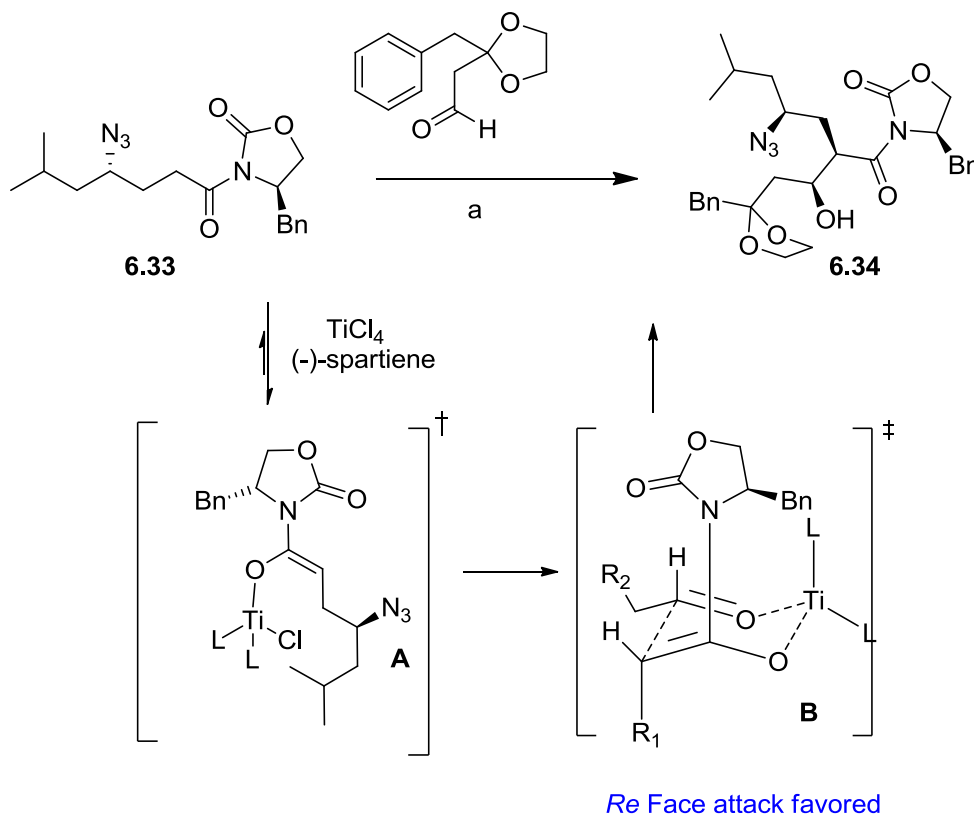
Scheme 6.10: Synthesis of Azido chiral imide derivative **6.33**

Reagents and conditions: a) 4.0M HCl in 1,4 dioxane, 0°C to rt, 12h; b) imidazol-1-sulfonyl azideHCl, K₂CO₃, CuSO₄·5H₂O, MeOH, rt, 14h, 77%; c) pivaloyl chloride, TEA, LiCl, 4(*R*)-benzyl-2-oxazolidinone, THF, -20°C-rt, 6h, 75%.

6.6.3 Asymmetric aldol reaction

With the required fragments **6.24** and **6.33** in hand, our plan was to use an asymmetric Evans' aldol reaction to couple these segments and to set the C10 and C11 stereochemistry. Evans' aldol reaction using standard conditions; dibutylboron triflate and TEA did not give any expected product. However, the asymmetric aldol reaction using a chiral imide derived from acid **6.32**, TiCl₄ and DIPEA gave the required aldol product, albeit with poor yield. To improve the yield further, two key features were taken in to consideration. First, the side product arising from the aldol reaction was a result of polymerization of aldehyde and second, in standard Evans' aldol protocol, usually more than two equivalents of aldehyde are used. With this in mind, Crimmin's modified aldol protocol, which uses only 1.0 equivalent of aldehyde and (-)-sparteine as base, was selected as the method of choice. As anticipated, the best conversion was achieved with Crimmin's modification of Evans' aldol protocol using (-)-sparteine as base. As shown Scheme 6.11, chiral imide **6.33** was treated with TiCl₄/(-)-sparteine to generate *Z*-enolate **A**, which was treated with aldehyde **6.24** to afford the aldol product **6.34**. One of the most significant feature of this reaction was that not only high yields were obtained, but more

importantly, exclusively single diastereomer was produced.¹⁶⁵ The (-)-sparteine is thought to serve as a bidentate ligand though exact role of this chiral base is not yet fully understood. It is however very clear that it does not play any role in chiral induction.



Scheme 6.11: Crimmin's Aldol protocol

Reactions and Conditions: a) TiCl_4 , (-)-sparteine, **6.24**, CH_2Cl_2 , 0°C , 3h, 74%

The stereochemical outcome of the aldol reaction can be rationalized using a Zimmerman-Traxler six membered chair-like transition state (Scheme 11). As anticipated, the facial selectivity of the aldehyde was directed by the chiral auxiliary of the enolate resulting in *re*-face attack to deliver Evans' *syn* aldol product. The absolute configuration of obtained alcohol was deduced using Mosher's method.

6.7 Mosher's method: Stereochemistry Assignment of C-10 hydroxy of aldol adduct

Determination of the absolute configuration of organic compounds is an important aspect for natural product chemist. Although there are several methods used to determine the absolute stereochemistry of organic molecules, Mosher's method, which uses 2-methoxy-2-phenyl-2-(trifluoromethyl)acetic acid (MTPA) esters has been extensively used, especially for secondary alcohols. The prototype protocol begins with the esterification of the secondary alcohol with the (*R*) and (*S*) enantiomers of MTPA followed by acquiring and comparing the NMR data for resulting diastereomers. One important thing to note is that MTPA is available in two forms: MTPA acid and MTPA acid chloride (MTPACl). Derivatization of the alcohol with the (*R*)-MTPA acid leads to the corresponding (*R*)-MTPA ester while the (*R*)-MTPA chloride leads to the (*S*)-MTPA ester. Mosher's approach depends on the anisotropic effects exerted by the aromatic ring on the substituents (L_1 and L_2). Mosher suggested that, in solution, the β C-H bond, carbonyl group of the ester and trifluoromethyl group of the MTPA ester derivative are in one plane (Figure 6.2). When the MTPA is placed in appropriate conformation as described by Mosher, the ^1H -NMR shift of L^1 of the (*R*)-MTPA ester show upfield signals relative to that of (*S*)-MTPA ester due to the diamagnetic effect of the phenyl ring. These differential shielding effects are represented as $\Delta\delta^{SR}$, calculated by measuring chemical shift differences between the certain protons in the (*S*)-MTPA ester and (*R*)-MTPA derivative. All the protons shielded in the (*R*)-MTPA have a positive $\Delta\delta^{SR}$ value, whereas those shielded in the (*S*)-MTPA derivative will have a negative $\Delta\delta^{SR}$ value. Based these values and postulated position of Mosher ester, the absolute configuration is determined.¹⁶⁶

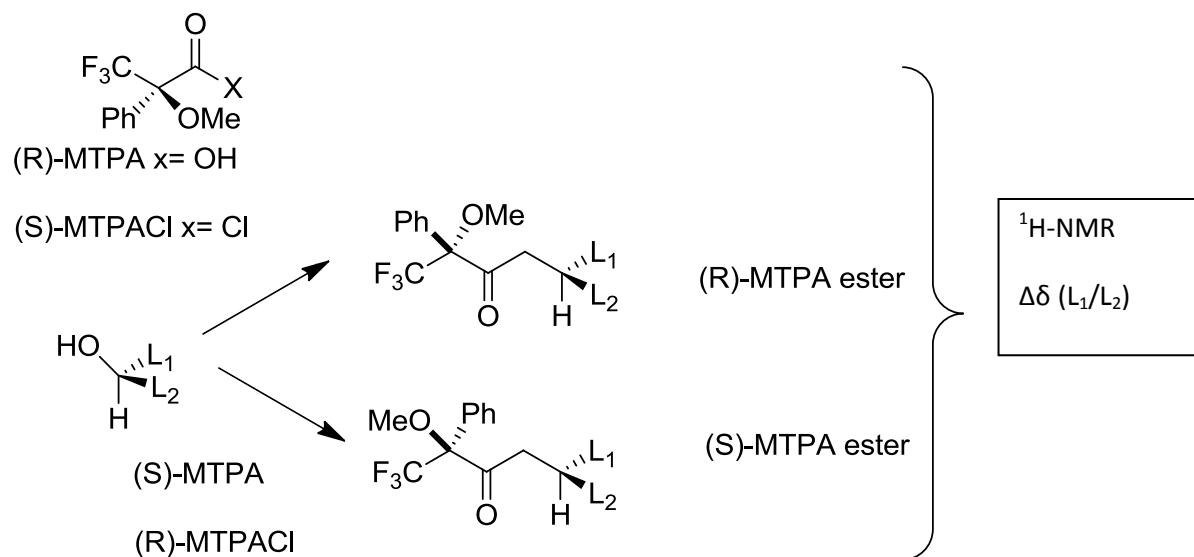
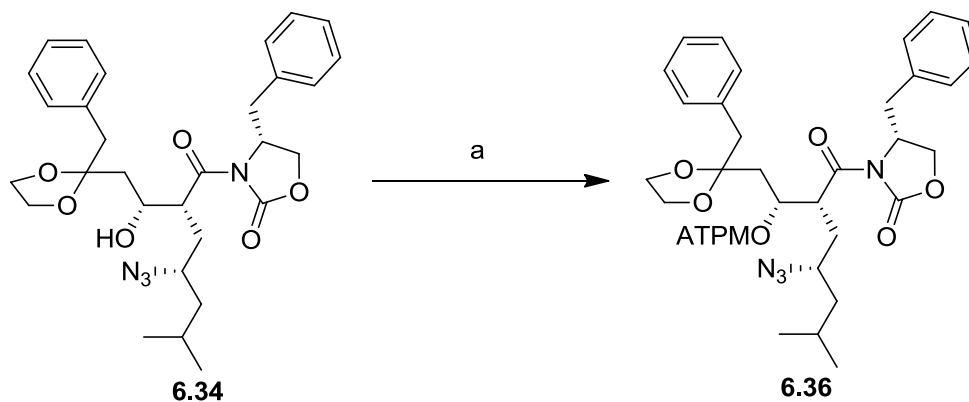


Figure 6.2. Configurational correlation model for (*R*)-MTPA and (*S*)-MTPA derivatives

The aldol adduct **6.34** was converted to (*R*) and (*S*) MTPA esters using (*S*) and (*R*) MTPACl respectively (scheme 11). ¹H-NMR spectra were recorded for both the diastereomers and differences in protons in ppm were calculated. Shown below in the figure 6.3.



Scheme 6.12: Mosher ester synthesis

Reactions and Conditions: a) (*R*)-MTPACl or (*S*)-MTPACl, DMAP, TEA, DCM, RT 30mins

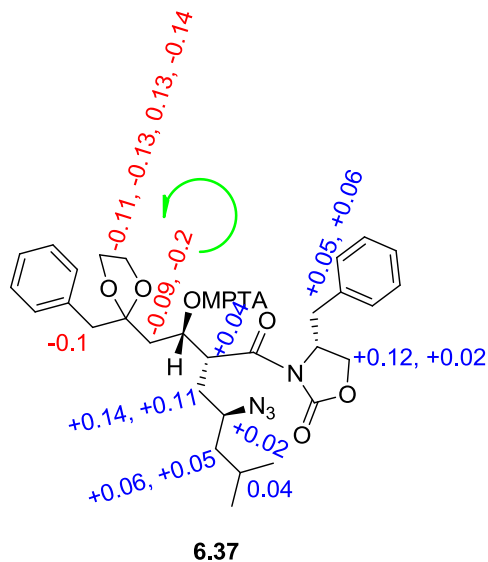
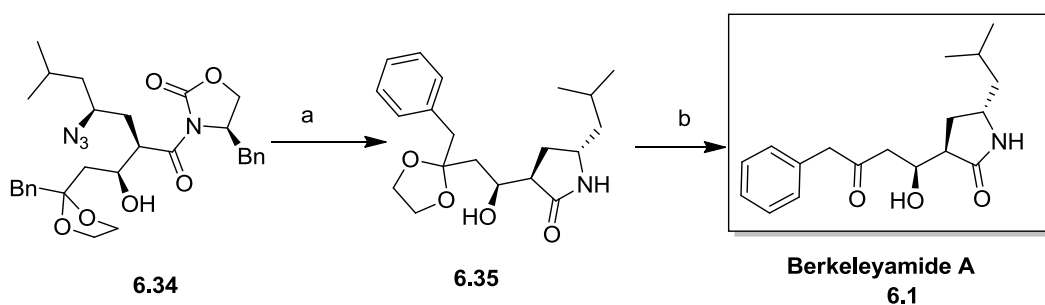


Figure 6.3: Mosher ester analysis confirming the *S*-configuration of the aldol adduct

The absolute configuration of the resulting alcohol at the C10 position was further confirmed by Mosher ester analysis to be *10S* as in the natural product **1**. Furthermore, the *syn* selectivity of the aldol product was confirmed by ^1H NMR analysis of Mosher ester derivatives (J_{10-11} , 2.95 Hz). With aldol product in hand total synthesis of berkeleyamide A was just couple of steps away.



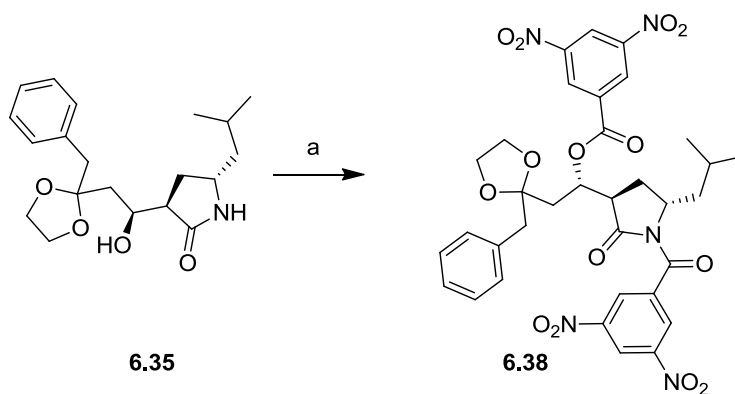
Scheme 6.13: Synthesis of **6.1**

Reactions and Conditions: a) 5% Pd/C, ammonium formate, MeOH, 1h, 85%; b) Pd(CH₃CN)₂Cl₂, acetone, H₂O, rt, 4h, 77%.

The transformation of the aldol adduct **6.34** into the natural product **6.1** required azide reduction, lactamization and ketal deprotection. Gratifyingly, after a few attempts, transfer hydrogenation using 5% Pd/C directly provided the lactam **6.35** in one pot from **6.34** in 85% yield. Moreover, chiral auxiliary was recovered without loss of its optical purity. Finally, ketal deprotection of **6.35** was then successfully achieved with Pd(CH₃CN)₂Cl₂ in moist acetone to yield (**6.1**) in 77% yield.¹⁶⁷ The ¹H NMR of our synthetic compound was in accordance with spectral details reported by isolation chemists further confirming the absolute configuration of **6.1** to be 10*S*, 11*R*, 14*S*. The spectral and other data of **6.1** were in full agreement with the reported data of the natural product. The 2D-NOESY correlations of **6.1** were also consistent as reported.

6.8 Crystal structure of berkeleyamide A derivative

Berkeleyamide A is liquid and hence has to be derivatized (in to solid) for X-ray crystal structure analysis. The absolute configuration of berkeleyamide A was further confirmed by derivatizing the ketal **6.35** in to di-dinitrobenzoyl derivative **6.38**. Single crystal was grown by slow evaporation of methanolic solution of **6.38** and analyzed using Bruker X-ray crystallography machine.



Scheme 6.14: Dinitrobenzoyl derivative of Ketal

Reagent and conditions a) 3,5 dinitrobenzoyl chloride, DMAP, TEA and DCM

Given below is the ORTEP diagram of X-ray crystal structure of derivative **6.38**,

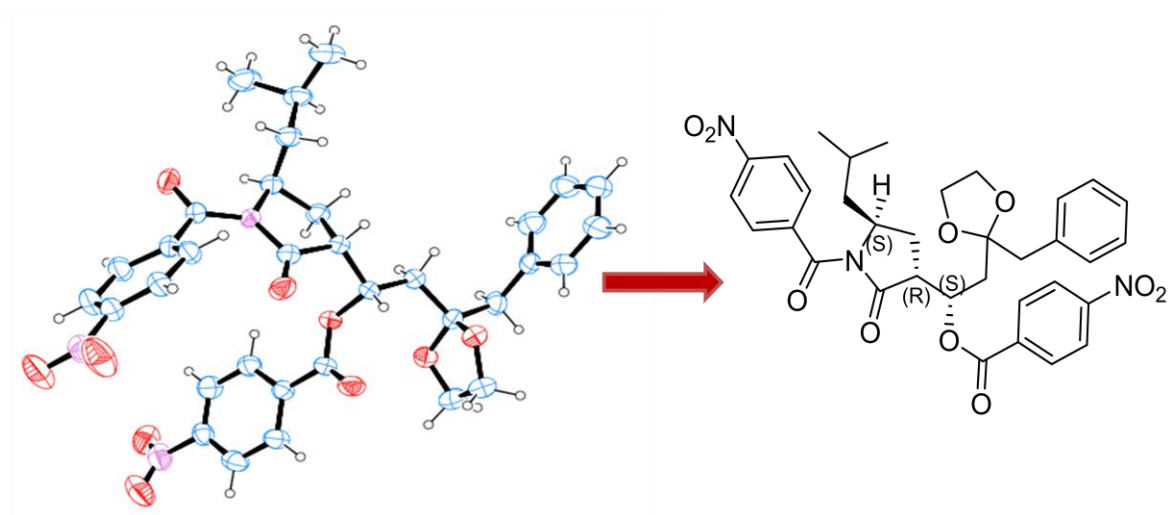


Figure 6.4: ORTEP representation of crystal structure of derivative of berkeleyamide A

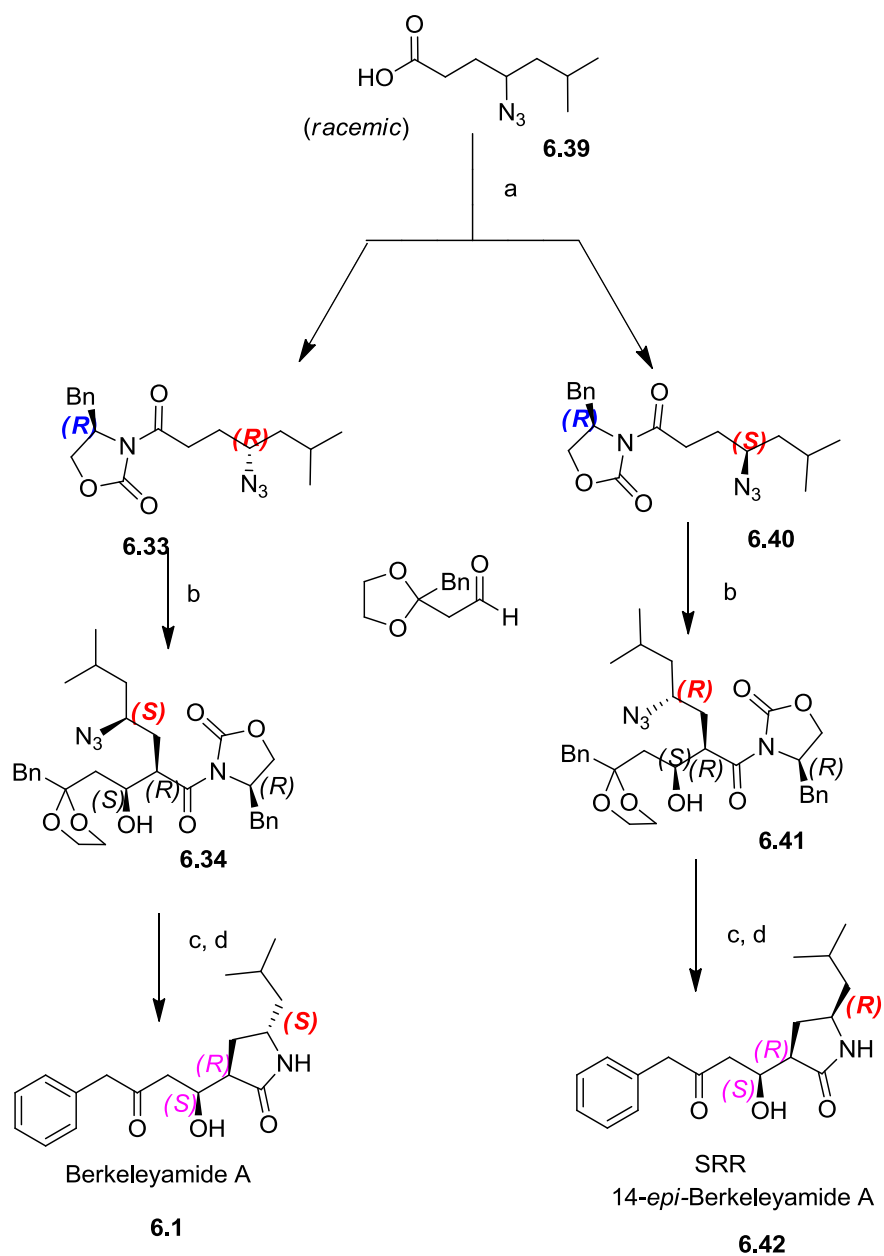
In summary, a concise synthesis of the caspase-1 inhibitor **1** has been achieved in 9 steps starting from *N*-Boc-*L*-leucinal with 18% overall yield. Our synthetic endeavor of **1** is very efficient, scalable and highly diastereoselective with the flexibility to develop various analogues

of the natural product. Using this modular approach, synthesis of remaining the diastereomers was carried out.

6.9 Synthesis of Diastereomers of berkeleyamide-A

In order to accomplish effective analoging, it is imperative to recognize the affinities of all the diastereomers of **6.1** towards ICE and subsequent identification of the most potent diastereomer. This not only confirms the role of chirality in affinity of the ligand towards the enzyme but also helps further to confirm the absolute configuration. Therefore, we proposed to synthesize all the possible diastereomers of the natural product and evaluate them for biological activity. As mentioned above, our approach is suitable for the synthesis of all the possible diastereomers of **6.1**. All the diastereomers can easily be obtained by either switching the chiral auxiliary from 4(*R*)-benzyl-2-oxazolidinone to 4(*S*)-benzyl-2-oxazolidinone or exchanging the starting precursor from *N*-Boc-*L*-leucine to *N*-Boc-*D*-leucine .

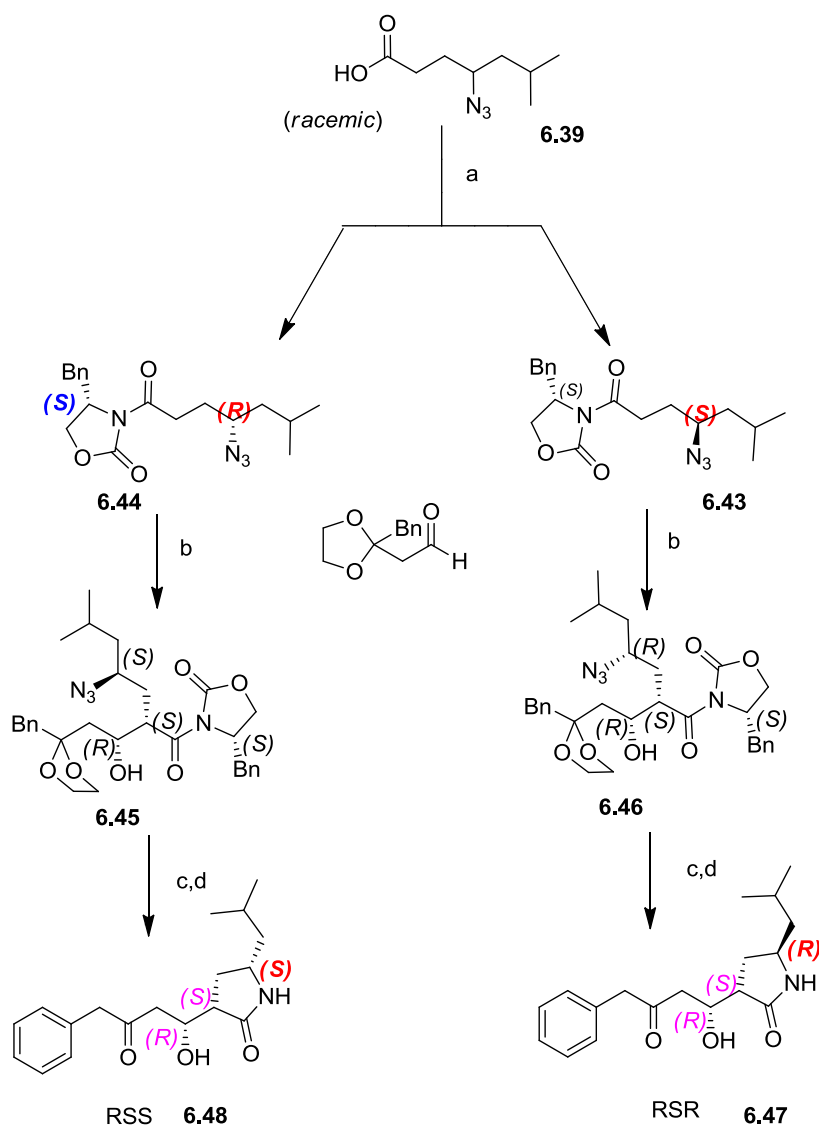
Instead of starting the synthesis with *N*-Boc-*D*-leucine, we decided to racemize Boc-*L*-leucine. After few initial attempts, we were able to achieve racemization by using longer reaction times at the HWE homologation step. After racemization of the *N*-Boc ester, all the steps in scheme were followed up until the γ -azido acid derivative (determined by optical rotation). The azido acid derivative was then coupled with 4(*R*)-benzyl-2-oxazolidinone to yield an inseparable mixture of chiral imides. The racemic mixture of chiral imides was then subjected to aldol reaction, giving rise to two aldol products, which were then easily separated using column chromatography. Both aldol products were then converted into berkeleyamide diastereomers by following lactmization and deketalization protocol.



Scheme 6.15: Synthesis of berkeleyamide A and its epimer; 6.42

Reactions and Conditions: a) pivaloyl chloride, TEA, LiCl, 4(*R*)-benzyl-2-oxazolidinone, THF, -20°C-rt, 6h, b) TiCl₄, (-)-sparteine, CH₂Cl₂, 0°C, 3h 60-70% overall yield (1:1 diastereomer yield) c) 5% Pd/C, ammonium formate, MeOH, 1h, 85%; d) Pd(CH₃CN)₂Cl₂, acetone, H₂O, rt, 4h, 77%.

Similarly, other diastereomers using 4(*S*)-benzyl-2-oxazolidinone chiral auxiliary and aldehyde were prepared.



Scheme 6.16: Synthesis of Diastereomers of berkeleyamide A

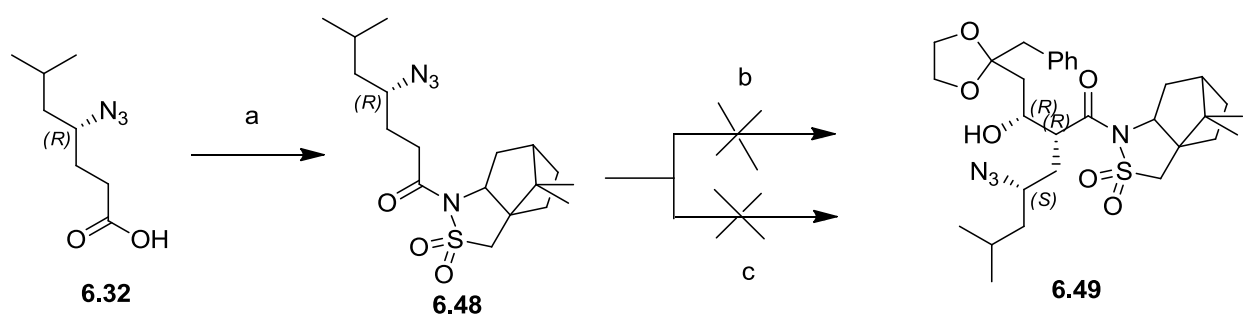
Reactions and Conditions: a) pivaloyl chloride, TEA, LiCl, 4(*R*)-benzyl-2-oxazolidinone, THF, -20°C-rt, 6h, b) TiCl₄, (-)-sparteine, CH₂Cl₂, 0°C, 3h 60-70% overall yield (1:1 diastereomer

yield) c) 5% Pd/C, ammonium formate, MeOH, 1h, 85%; d) Pd(CH₃CN)₂Cl₂, acetone, H₂O, rt, 4h, 77%.

6.10 Anti-aldol reaction

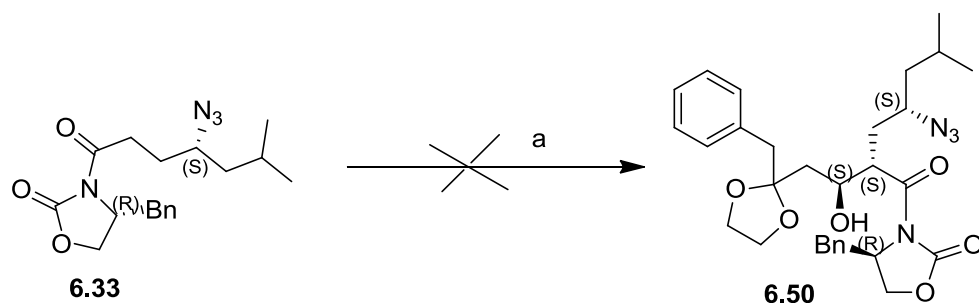
The synthesis of diastereomers arising from anti aldol reaction was very challenging. Initial attempts of applying modified Evans' anti aldol¹⁵⁶ protocol (scheme) as well as Oppolzer's anti aldol¹⁵⁷ methodology (scheme) were unsuccessful. In both the cases starting material we recovered at the end of the reaction.

Anti aldol reactions



Scheme 6.17: Oppolzer's protocol

Reactions and Conditions: a) Camphorsultam, PivCl, TEA, LiCl THF, 0°C to RT b) DIPEA TiCl₄, **6.24**, CH₂Cl₂, -78 °; c) Triethyl borane in 1 M hexanes, Trifluoro methanesulfonic acid (freshly distilled) 1 h, in DCM, DIPEA, -5°C 0.5 h and then **6.24** at -78 °C for 3 h. Reaction quenched by addition of extra DIPEA and phosphate buffer pH 7.0

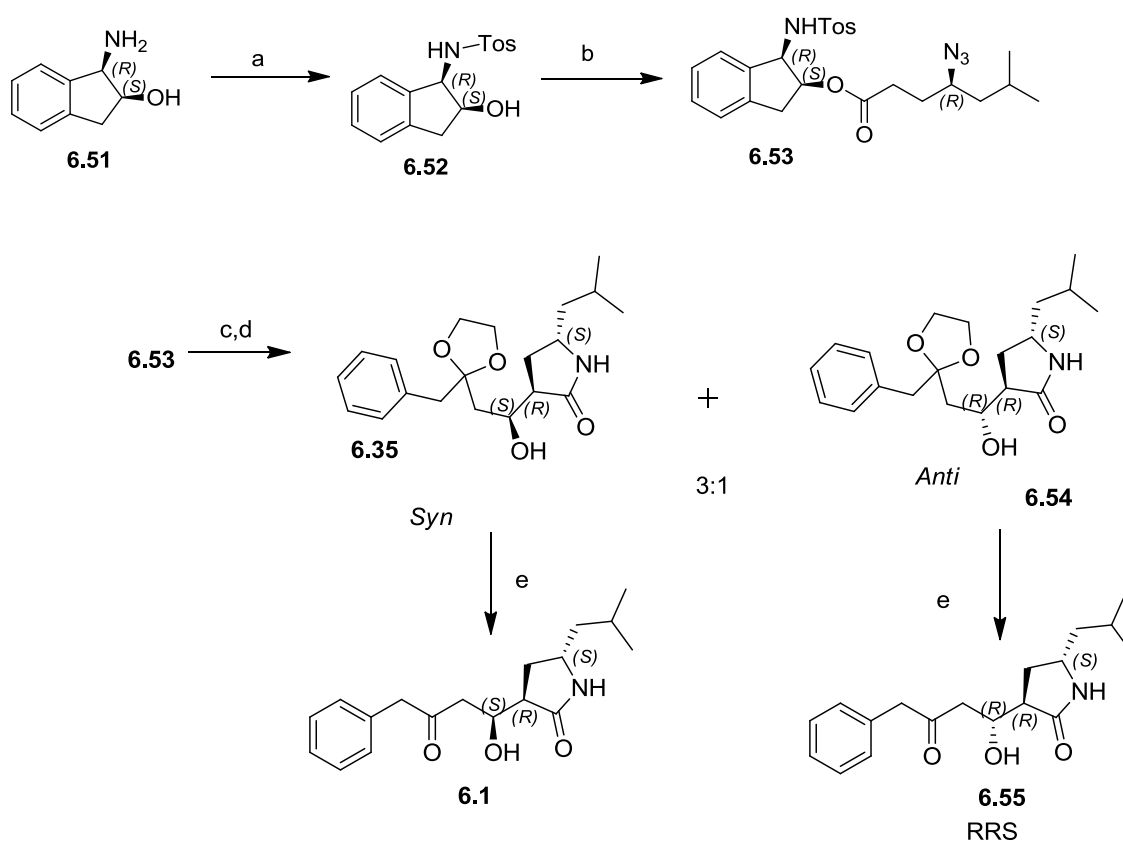


Scheme 6.18: Evans anti-aldol protocol

Reactions and Conditions: a) **6.24**, MgCl₂ 10 mol% TEA, TMSCl, NaSbF₆ 30 mol% in EtOAc, RT.

After a thorough literature search, we found that Ghosh's anti aldol reaction has wide applications and might work in our substrate. Delightfully, use of Ghosh's anti-aldol protocol¹⁶⁸ provided anti aldol product, albeit, with poor diastereoselectivity; 3:1 *syn* : *anti* product with a 70% yield. Ghosh's protocol uses of tosyl amino indanol as chiral auxiliary, TiCl₄ and Hunigs base, scheme 8. The anti-aldol formation can be rationalized by a six membered transition state Zimmerman-Traxler type model. Following are the assumptions for the formation of anti-aldol product 1) Chiral ester **6.53** on treatment with TiCl₄ forms *Z* enolate and formed enolate attacks the aldehyde on *Si*-face, 2) the titanium enolate forms a seven-membered metallocycle with a chair like conformation involving metal coordination with tosyl-amino functional group; 3) a second titanium metal is chelated to indanyloxy oxygen as well as to the aldehyde carbonyl forming another six-membered chair like transition state. Precomplexation of the aldehyde with TiCl₄ is necessary for the success of anti-aldol reaction, suggesting that there is involvement of two titanium metal in the transition state.

Though we were able to isolate the required anti-aldol product, the reaction suffered from poor diastereoselection. One of the reasons for the reduced diastereoselection is the presence of relatively large R¹ group which might not allow for the formation of the chair like seven membered ring and the Z-enolate formed attacks the aldehyde from *re*-face giving rise to majority of *syn*-aldol product.



Scheme 6.19: Synthesis of diastereomer of berkeleyamide using Ghosh's Methodology

Reactions and Conditions: a) *p*-toluenesulfonyl chloride, dimethylamino pyridine, Triethyl amine, DCM, 2h at RT 80% b) **6.32**, DCC, Triethylamine 10h RT c) TiCl_4 , *i*Pr₂NEt, 23 °C then **6.24** and TiCl_4 DCM, -78 °; d) 5% Pd/C, ammonium formate, MeOH, over night, 60%; (Note

Aldol product obtained was hard to characterize hence was immediately converted to respective ketals) e) $\text{Pd}(\text{CH}_3\text{CN})_2\text{Cl}_2$, acetone, H_2O , rt, 4h, 75%

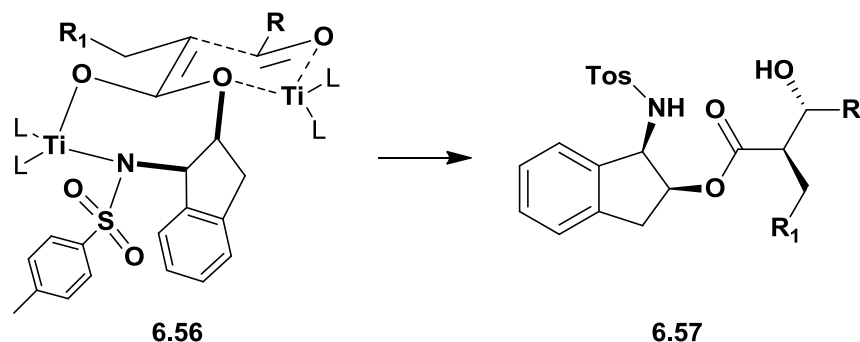


Figure 6.5: Rationale for anti-aldol product.

Overall, we were able to develop and implement a highly diastereoselective route for the total synthesis of berkeleyamide A and its diastereomers. All five diastereomers (including berkeleyamide A), along with azido acid and chiral imides were submitted for biological evaluation to our collaborators.

With total synthesis of the natural product and its diastereomer accomplished, our next aim was to design ICE inhibitors based on berkeleyamide scaffold. berkeleyamide was chosen as a lead as it was reported to inhibit ICE with IC_{50} of 300 nM. We conducted molecular modeling docking studies (disclosed in next section) in order to investigate the mode of binding of **6.1** and its diastereomers in ICE active site, while we were waiting on the biological results.

6.11 Design of Caspase-1 inhibitors based on berkeleyamide A scaffold

6.11.1 Background

ICE has been the most well studied inflammatory caspases and is key mediator of cytokines IL-1 β and IL-18 pathways. Due to its high therapeutic potential, pharmaceutical companies have pursued this target for treatment of immune mediated inflammatory disorders. One of the pioneering studies in field of ICE research by Thornberry associates was the identification of tertiary protein structure of ICE and ensuing discovery of the tetrapeptide Ac-YVAD-CHO possessing potent ICE inhibitory activity.⁸¹ Later on, a few x-ray crystal structures of ICE as well as ICE co-crystallized with various inhibitors have been published.¹³² With comprehensive knowledge of the active site and precise understanding protein-ligand interactions in ICE, structure based drug design seem to be a rational approach for design of novel inhibitors of ICE.

6.11.2 ICE active site –Quick Summary

Pro-ICE is activated to active ICE by assemblage of multiprotein complex called inflammasome. ICE in its active form is an oligomeric enzyme containing two subunits denoted p20 (residues 120-297) and p10 (residues 317-404). Prerequisites for the substrates of ICE inhibitors are generally well accepted and are as follows:

- 1) Presence of L-Aspartic acid residue in the P1 site. The aspartate residue forms crucial salt bridge interactions with Arg179, Gln283 and Arg341 thus anchoring the ligand in appropriate orientation exposing the adjoining electrophilic warhead group to the nucleophilic Cys285.
- 2) Presence of electrophilic warhead groups (aldehyde, ketone, haloketone, Michael acceptors, etc) in the P1 site to which Cys285 forms a covalent bond
- 3) P2-P3 requirements are not very stringent and that's where most of the variation is seen in the design of ICE inhibitors. However, it is necessary to retain certain hydrogen bonding interactions¹²⁸
- 4) Finally P4 requirement is very precise and is the determinant of specificity amongst different caspases. For caspase-1 large hydrophobic groups are generally tolerated well. Figure 4 shows P1-P4 regions of Ac-YVAD-CHO inhibitor in the caspase-1 active site.^{126,}

132, 133

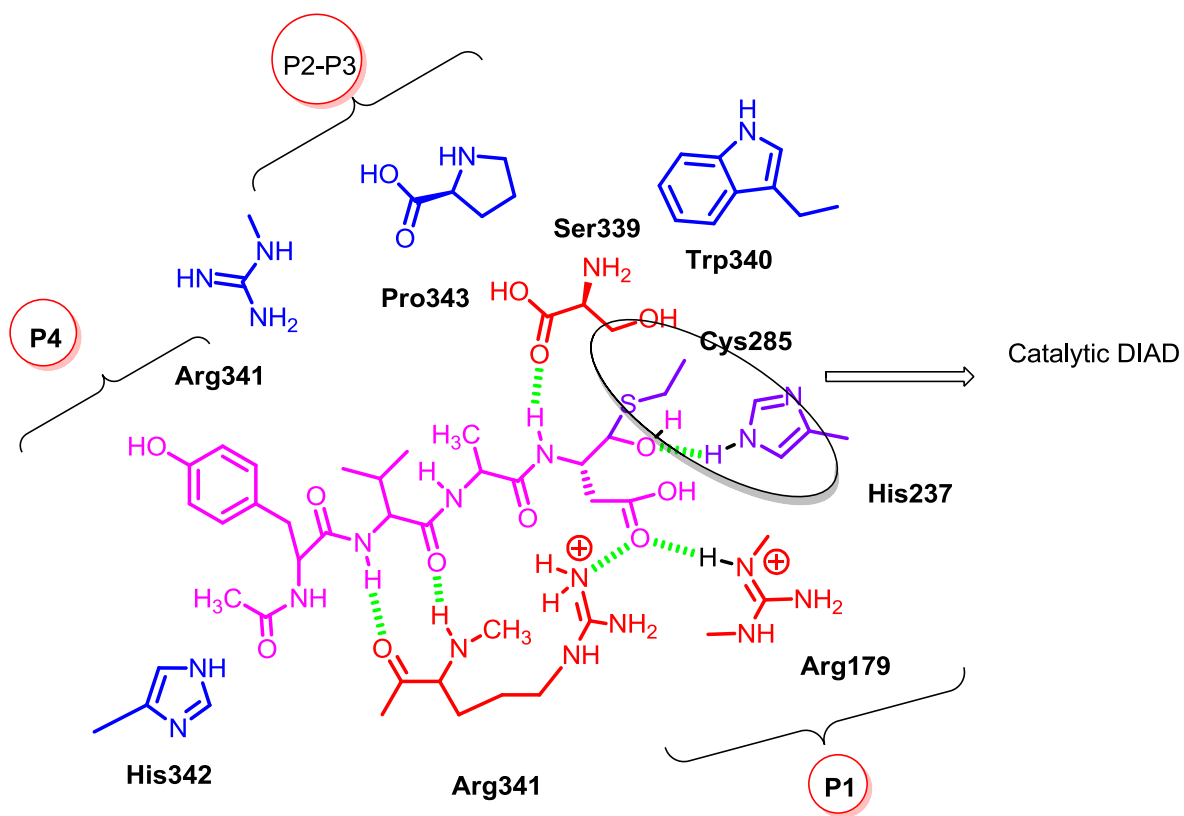


Figure 6.6: Depiction of active site residues of Caspase-1 with bound inhibitor Ac-YVAD-CHO, as reported in the co-crystal structure. Active site divided according to substrate specificity in P1, P2, P3 and P4. Catalytic diad; Cys285 and His237 are circled for clarity and are represented in magenta. All crucial hydrogen bonds are depicted in green.

6.11.3 Rational design of Caspase-1 inhibitor

With the pharmacophoric features essential for ICE inhibition well known and several crystal structures of ICE co-crystallized with ICE inhibitors available, we utilized a structure-based design approach for the design of ICE inhibitors based on berkeleyamide-A scaffold. Docking is one of the most important, versatile and widely used computational tools in structure-based drug design and development process. Molecular docking involves orientation of a ligand into the active site of the receptor, which in turn helps to elucidate crucial ligand-receptor interactions. Docking studies were performed in order to investigate the key protein-ligand interactions between ICE and **6.1**. Additionally, all the remaining seven diastereomers of **6.1** were also subjected to docking to examine effect of stereochemistry on the nature of protein-ligand interaction.¹³⁴

6.11.4 Molecular docking protocol

Docking studies were performed using Glide (Schrödinger) with extra-precision (XP) settings to predict the binding mode of **6.1** and its diastereomers in the active site of ICE. ICE enzyme (pdb code: 2HBQ)¹⁶⁹ along with co-crystallized inhibitor Z-VAD-FMK were retrieved from the protein data bank. Obtained enzyme was subjected to protein preparation using protein preparation wizard of Maestro. As a part of protein handling, all the water molecules were removed, hydrogen atoms were added and finally the enzyme was minimized using an OPLS2005 force-field. The second step of molecular docking is defining the active site by grid generation around the known bound ligand. The binding site was defined as the residues located within 12 Å distance of the bound ligand. A relatively larger active site was selected to check if there were any additional binding pockets around the active site. Once the grid was generated,

the next step was preparing the ligands that were to be docked into the active site. All the eight diastereomers of **6.1** were sketched using Maestro, visually inspected and minimized utilizing an OPLS2005 force-field from the macromodule of Schrodinger. Default settings were used for performing the docking of **6.1** and its diastereomers into the active site of 2HBQ. The final ligand poses were selected based on the Glide empirical docking scores (GlideScore) and E_{model} score.

6.11.5 Pose Validation

Pose validation study is one of the most important evaluation parameters in molecular docking studies as it validates the reproducibility of the binding pose of the native ligand. Pose validation was carried out in order to evaluate the performance of Glide. The native ligand Z-VAD-FMK was docked in 2HBQ active site using Glide. Glide was able to reproduce the binding pose of Z-VAD-FMK in the active site very similar to that in the crystal structure with excellent root mean squared deviation (RMSD) of 0.4. Ligplot depiction of Z-VAD-FMK in the ICE active site is shown below in figure 6.7. As projected, the aspartate moiety of the ligand in P1 shows salt bridge interactions with Arg179 and Arg341. The nucleophilic residue Cys285 is covalently bound to the warhead group and oxyanion thus formed is stabilized by Gln283 and His237. The P4 portion of the molecule is surrounded by hydrophobic amino acid residues, namely His, Trp Val and Pro. Moreover, all the crucial hydrogen bonding interactions of residues Arg341 and Ser339 with the ligand are retained.

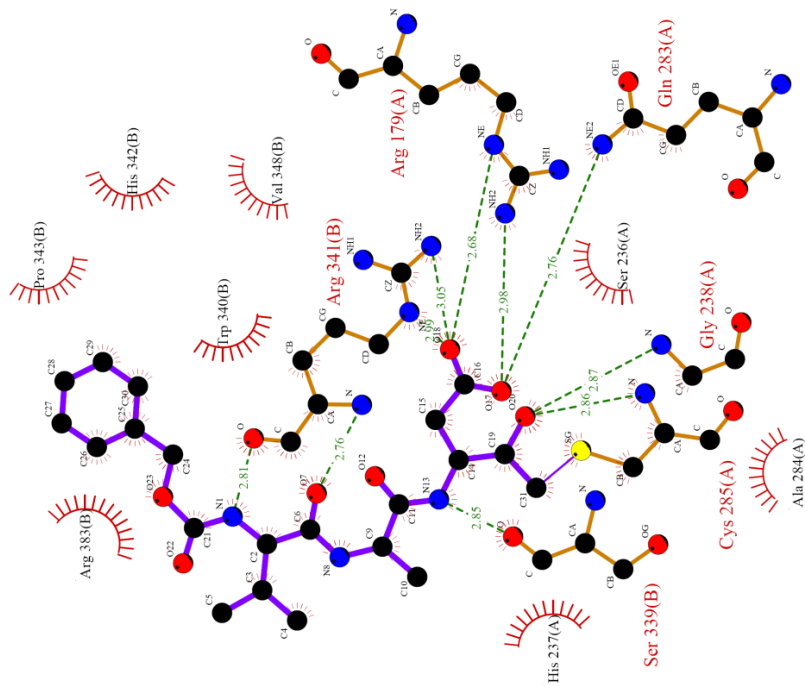


Figure 6.7: Ligplot depiction of Z-VAD-FMK in the Caspase-1 active site in the co-crystal structure 2HBQ.

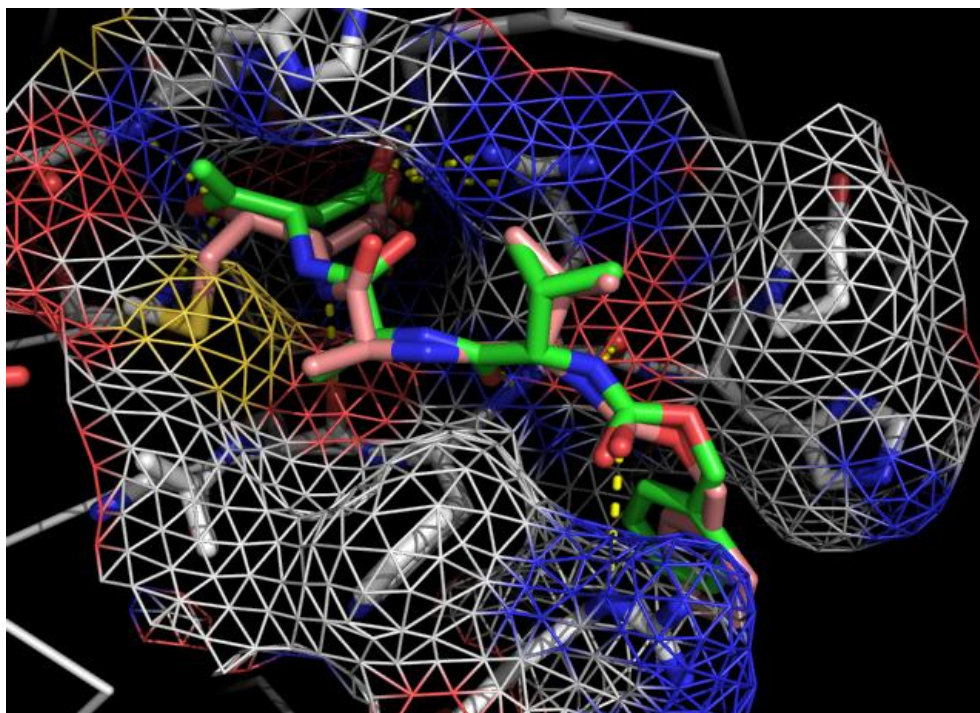


Figure 6.8: Pose validation studies. Ligand in green is the native ligand which was extracted and docked in the active site. Ligand in pink is the native ligand which is covalently attached to cysteine residue in the active site.

Once pose validation was completed, **6.1** was docked in similar fashion using Glide. Docking studies revealed that the **6.1** only partially occupied the ICE active site. The docking pose of **6.1** superimposed with native ligand Z-VAD-FMK in ICE active site is depicted in figure 6.8 given below. It can be clearly seen that the pyrrolidone scaffold of the molecule is occupying S2 site with the carbonyl of the lactam ring pointing towards the S3 pocket. The S1 pocket is not occupied, while S3 and S4 pockets of the enzyme are occupied by the β -hydroxy ketone moiety and the aromatic phenyl ring respectively. We then generated 10 docking poses of the naturally occurring diastereomer of **6.1**. The natural product, 8 out of ten times was docked in a similar fashion. Based on the insights from these docking studies, structural modifications will be

implemented in the design of inhibitors of ICE. Similarly seven diastereomers of the natural product were docked in the active site. It is important to note that six of them were docked differently from the natural product. Only the SSS diastereomer was docked in a similar fashion as the natural product, insinuating that the natural product and its epimer SSS might be the most active compounds. Overlay of docked **1** and the remaining diastereomers is shown below figure 6.9 (for clarity the active site residues are not shown).

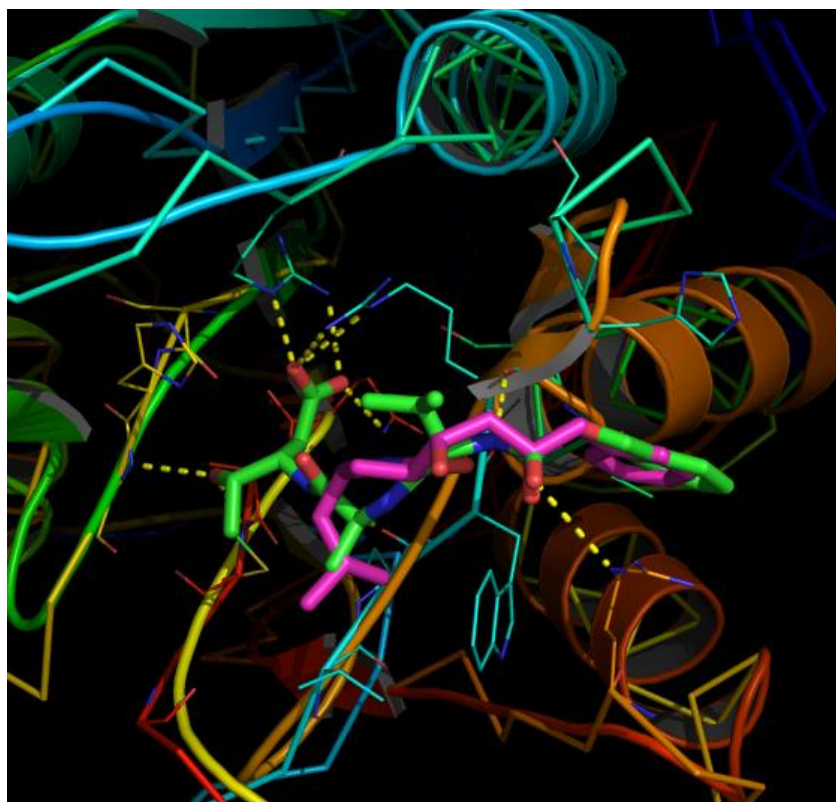


Figure 6.9: Overlay of **6.1** (docked in ICE active site) shown in magenta with Z-VAD-FMK shown in green in the ICE active site

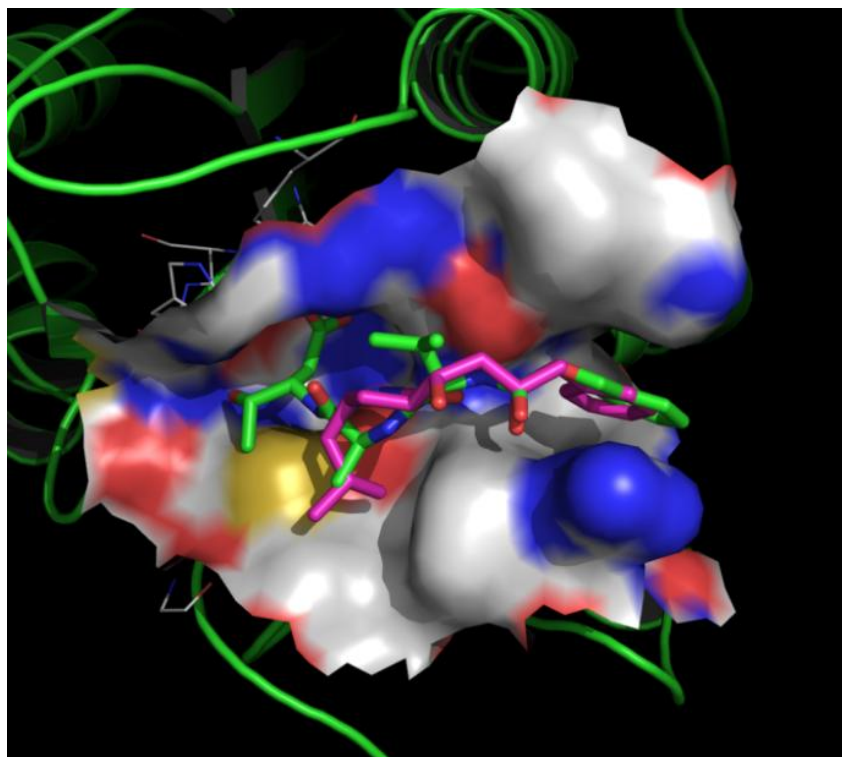


Figure 6.10: The overlay of **6.1** (magenta) and Z-VAD-FMK (green) in the active site of ICE. The active site is shown as van der Waals surface.

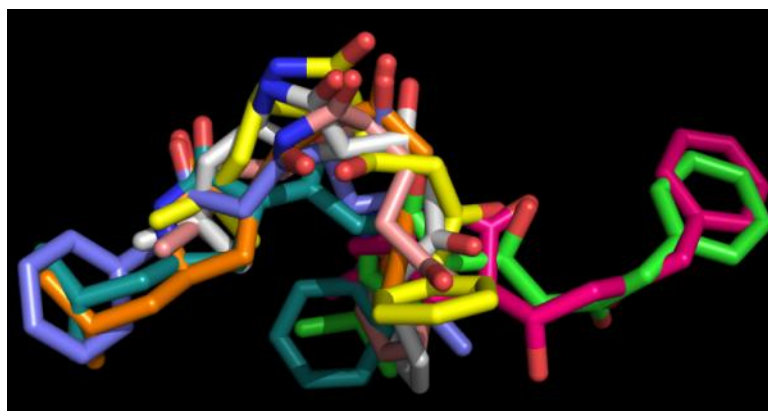


Figure 6.11: Overlay of all eight diastereomers docked in to the ICE active site. **6.1** is shown in green and SSS diastereomer is shown in magenta

6.12 Design of ICE inhibitors

We assumed that the natural product might be the most active diastereomer and applied rational design approach to **6.1** in the quest for novel ICE inhibitors. Based on our docking results and literature precedents for ICE inhibitors, we were intrigued by the fact that in spite of the natural product lacking the crucial P1 portion, berkeleyamide still showed potent caspase-1 inhibitory activity. We postulated that **6.1** exhibited ICE inhibitory activity by binding tightly to S2-S3 portion in the active site and occlude the entry of its natural substrate. Another hypothesis is that **6.1** may bind to allosteric site of the enzyme and modulate the conformation of the enzyme and its active site, making it inaccessible to its substrates. Figure 6.10 shows the overlay of the native inhibitor Z-VAD-FMK with Berkeleyamide A in the enzyme active site. From overlay it is pretty evident that **6.1** occupies mostly S2, S3 and S4 pocket while the crucial S1 pocket is only partially occupied.

This presents us with an opportunity to install an aspartic acid motif along with an electrophilic warhead via an appropriate linker. The aspartic acid residue will strongly anchor the molecule within the active site and help orient the electrophilic warhead group in close proximity to nucleophilic cysteine residue. To carry out this modification, we can take advantage of the free amide nitrogen in **6.1** molecule, type A derivatives. We also decided to substitute the phenyl end of the molecule with aspartic acid in case the ketone moiety functioned as the electrophilic warhead group type B derivatives. Other variations incorporated are deoxy-derivatives and ketone moiety protected as ketal to explore if these functional groups are essential of ICE activity. The designed derivatives of **6.1** are enlisted in the table 6.3 given below.

Table 6.3: Structures of proposed novel ICE inhibitors based on **1** scaffold

SJK 1		SJK 2	
SJK 3		SJK 4	
SJK 5		SJK 6	
SJK 7		SJK 8	
SJK 9		SJK 10	

Docking studies of the Designed molecules

Docking was carried out in a similar fashion as explained above. The enzyme was prepared by removing the water molecules and the native ligand. Hydrogen atoms were added and protein preparation wizard's protocol was followed for preparation of the protein. All the designed molecules were sketched using ligand builder module from Maestro. All the molecules were minimized and visually checked for correctness. Grid was generated around the active site (12Å) and all the molecules were docked in active site using docking protocol shown in figure 6.12.

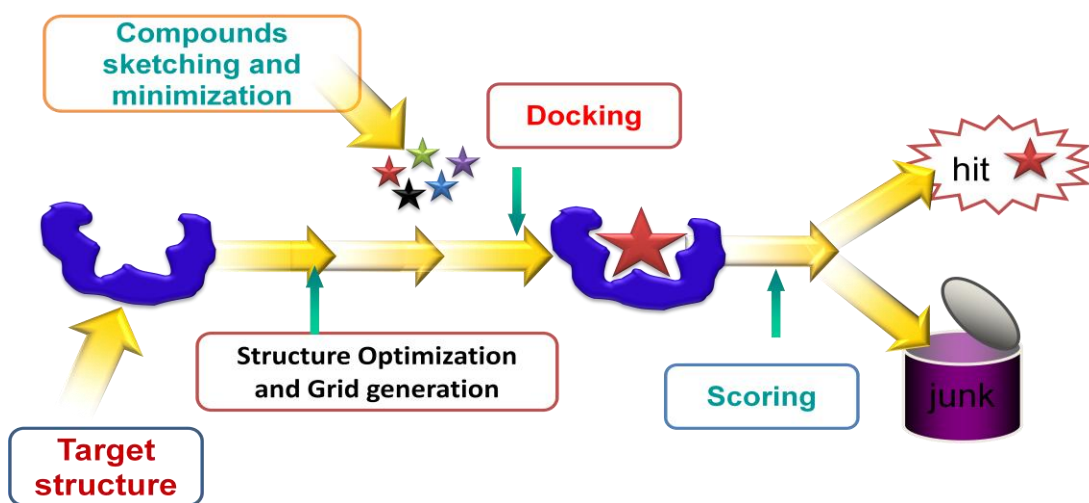


Figure 6.12: General protocol for docking

SJK-1 SJK-2, SJK-6 and SJK-7 had very good docking scores. It is important to note that SJK-1, SJK-2 and SJK-5 are prodrugs and their active form (free acid and aldehyde) was used for docking studies. All the above mentioned molecules occupied the S1 site of the enzyme and more importantly showed salt bridge interactions with Arg341 and Arg179. All these molecules also retained all the crucial hydrogen bonding interactions between Arg341 and Ser 339 require for ICE inhibitory activity. Given below in figure 6.13 is the overlay of the native ligand Z-

VAD-FMK shown in green and SJK-1 shown in magenta. It is evident from the figure 6.13 that both ligands are almost superimposed over each other in the active site. Moreover, the SJK-1 designed ligand retained all the crucial hydrogen bonding interactions: salt bridge interaction between aspartic acid residue and Arg341 and Arg179 as well as hydrogen bond interactions between residues Arg341 and Ser 339. It is also important to note that Cys285 is in proximity to the electrophilic aldehyde residue and the electrophilic war head group is oriented in such a way that is susceptible to attack by thiol functional group of cysteine residue.

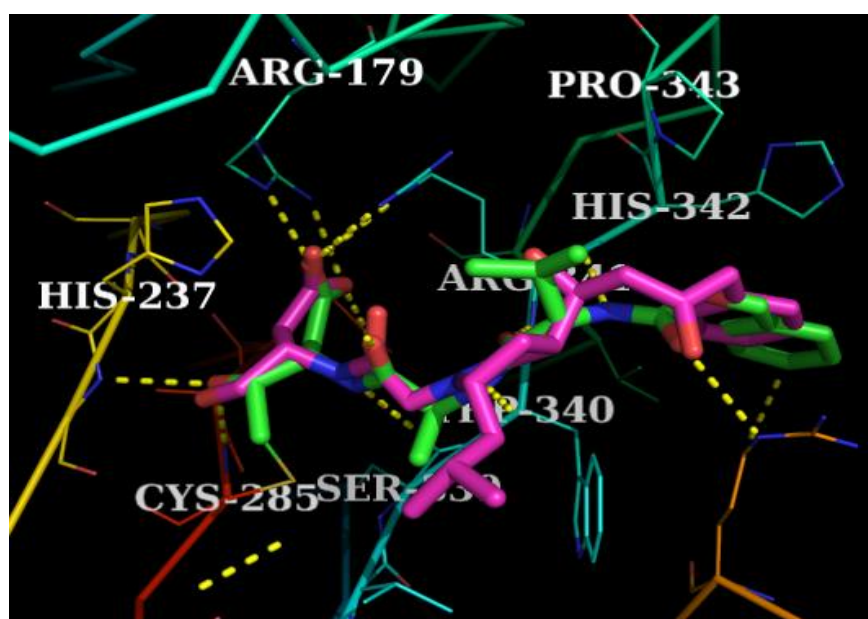


Figure 6.13: Overlay of SJK-2 (Magenta) and native ligand in Green in ICE active site shown as van der waals surface

Almost all the designed inhibitors occupied the active site of ICE except for the type B derivatives suggesting that type A derivative design is more appropriate. Shown below is the ligand interaction diagram (generated by using a script from Maestro) of the ICE active site and the ligand Z-VAD-FMK and ICE active site and SJK-1. Almost all the interactions, H-bond, π - π stacking interactions and even the solvent exposed areas of the both the ligands, are very

similar.

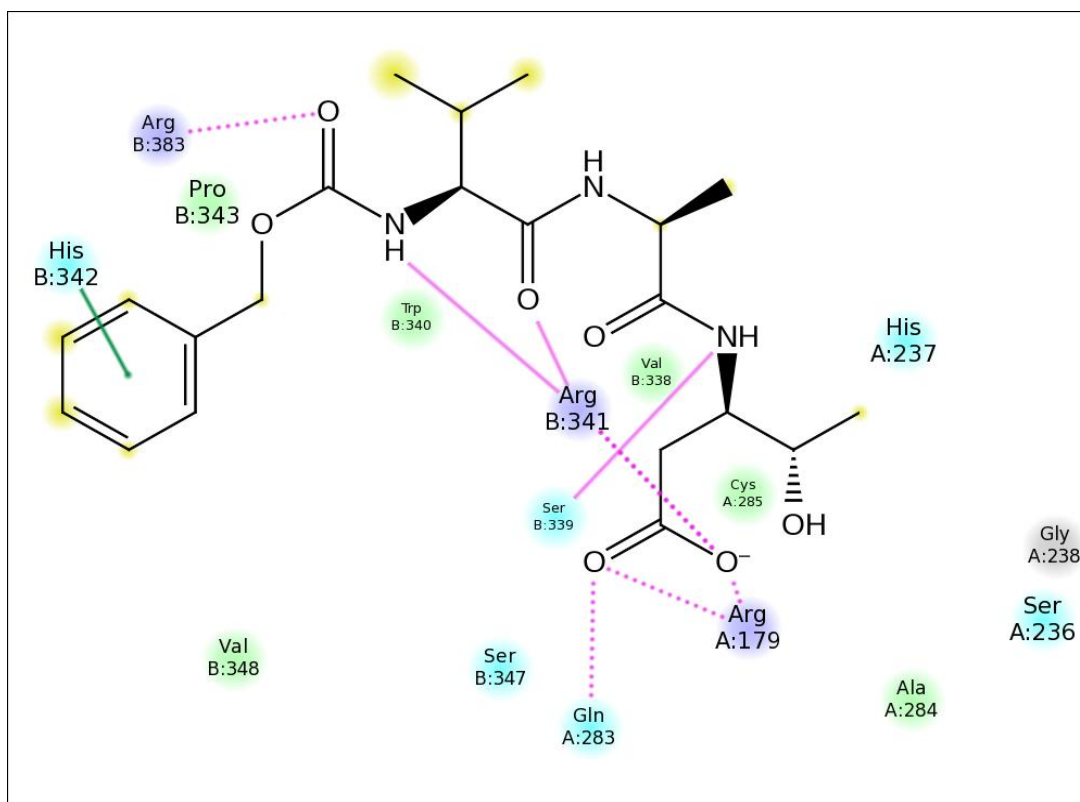


Figure 6.14: Ligand Interaction Diagram for native ligand Z-VAD-FMK in ICE active site.

Amino acid residue colors denote; Green= hydrophobic, Cyan = Polar; Red = negative charges, purple= positive charges. H-bond; solid lines for backbone interaction and dashed lines for side chain. π - π interaction is denoted by Green line. Solvent accessible surface area represented by yellow atom background. Text; small font is further while large font is close

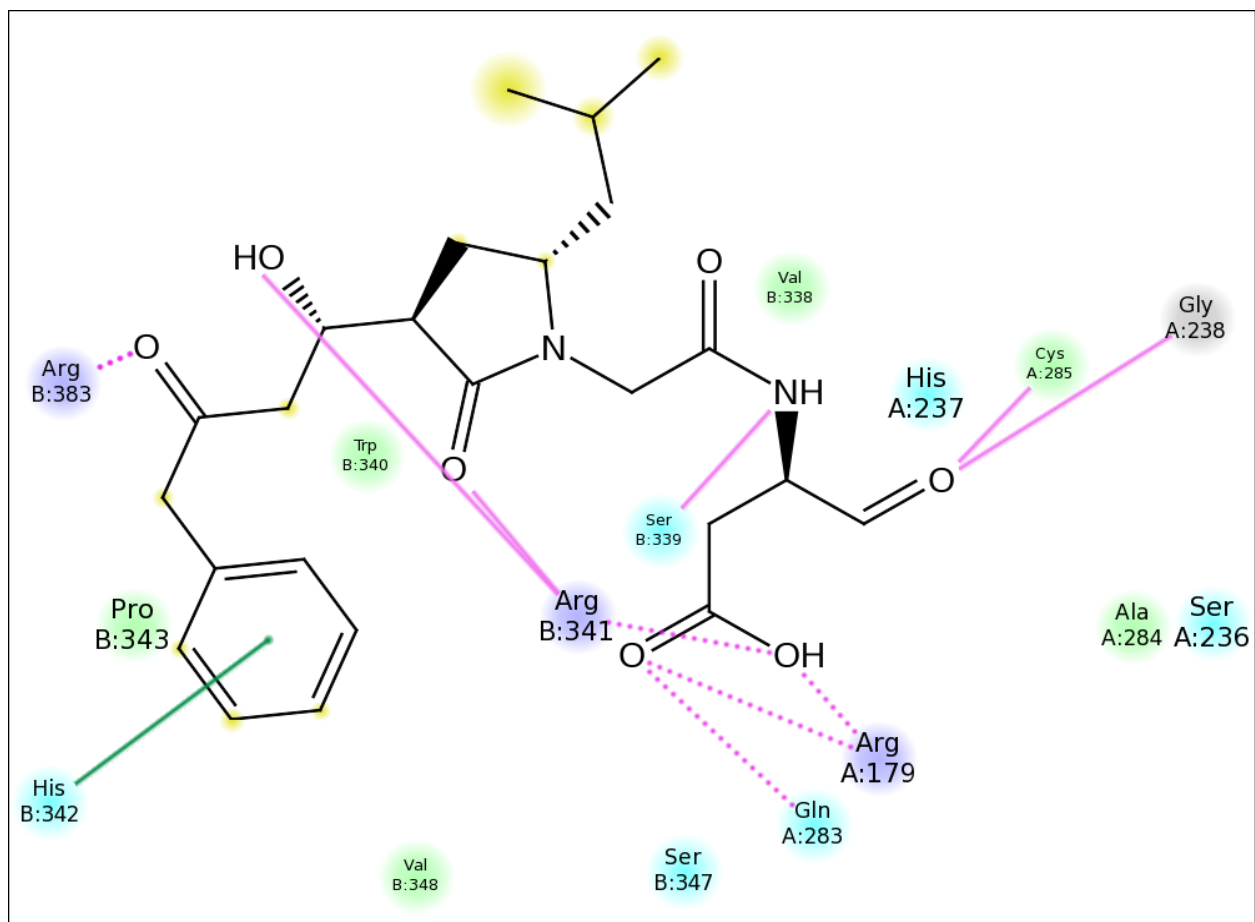


Figure 6.15: Ligand Interaction Diagram for SJK-1 in ICE active site.

Amino acid residue colors denote; Green= hydrophobic, Cyan = Polar; Red = negative charges, purple= positive charges. H-bond; solid lines for backbone interaction and dashed lines for side chain. π - π interaction is denoted by Green line. Solvent accessible surface area represented by yellow atom background. Text; small font is further while large font is close

In summary, our docking studies indicated that berkeleyamide A and its diastereomers only partially occupied the ICE active site. Moreover, the crucial S1 subsite containing the catalytic diad and the aspartic acid clamp (Arg179 and Arg341) were not occupied. According to our docking results (glide score and visual inspection), it seems that **1** and its diastereomers might have low affinity for the ICE active site. However, potent ICE inhibitory activity of berkeleyamide reported by Stierle and coworkers made this case very interesting.

6.13 Biological evaluation:

All the diastereomers, including berkeleyamide and some intermediates, were submitted for a caspase-1 inhibition assay. The assay was performed by our collaborators in CORE C facility at The University of Mississippi, under the guidance of Dr. Susan Manly. This is a fluorimetric assay performed using a commercially available 96 well-plate kit; BML-AK701' from EnzoLife sciences. The kit includes pure enzyme, buffers and a known inhibitor of caspase-1 as a reference standard: YVAD-CHO.

Principle of the Assay

The ICE Drug Discovery Kit contains a fluorogenic substrate (YVAD-AMC). Cleavage of the 7-amino-4-methylcoumarin (AMC) dye from the C-terminus of the peptide substrate by ICE shows increased fluorescence intensity, which is measured at 460 nm. Stronger the enzyme inhibition lesser would be the fluorescence intensity as compared to the blank.

Given below in table are the results obtained from this assay.

Table 6.4: Biological evaluation of berkeleyamide A and their derivatives against Caspase-1

Compound No.	Inhibition pmol/min
6.48	5.18
6.47	5.21
6.1	5.23
6.45	5.59
6.34	5.54
6.46	5.36
6.35	5.35
6.42	5.19
6.29	5.52
6.53	5.62
Blank	6.68
Ac-YVAD-CHO (control)	0.09

Unfortunately, none of the compounds submitted for the assay showed any activity against caspase-1. These results, though very surprising, are in accordance with our docking studies, which correctly predicted very weak affinity of these ligands with the ICE active. To eliminate any error in the assay, these assays were performed in triplicate. This also suggests neither **6.1** nor its diastereomer modulate ICE allosterically.

We also submitted our samples for anti-malarial, anti-leishmanial and anti-fungal activity.

Furthermore, we also evaluated their cytotoxic potential. None of the submitted compounds showed any potential anti-malarial, anti-leishmanial or anti-fungal activity (Table 6.5, 6.6 and 6.7 a&b) nor they were cytotoxic.

Table:6.5 Biological evaluation of berkeleyamide A and its derivatives : Anti-leishmanial Assay

Compound No.	Plate type	IC50 ($\mu\text{g/ml}$)	IC90 ($\mu\text{g/ml}$)
6.1	LEM Sec	NA	NA
6.48	LEM Sec	18	>40
6.47	LEM Sec	NA	NA
6.38	LEM Sec	NA	NA
6.45a(ketal of 6.48)	LEM Sec	NA	NA
6.46a(ketal of 6.47)	LEM Sec	NA	NA

Table 6.6: Biological evaluation of berkeleyamide A and its derivatives: Anti-Malarial Assay

Compound No.	IC50 ng/ml	S. I.	IC50 ng/ml	S. I.
6.1	NA	-	NA	-
6.48	NA	-	NA	-
6.47	NA	-	NA	-
6.38	NA	-	NA	-
6.45a(ketal of 6.48)	NA	-	NA	-
6.46a(ketal of 6.47)	NA	-	NA	-

Table 6.7a : Biological evaluation of berkeleyamide A and its derivatives : Anti-fungal Assay

Compound No.	Test Concentrations (µg/mL)	<i>C. albicans</i> IC ₅₀	<i>C. glabrata</i> IC ₅₀	<i>C. krusei</i> IC ₅₀	<i>A. fumigatus</i> IC ₅₀	<i>C. neoformans</i> IC ₅₀
6.1	20, 4.0, 0.8	-	-	-	-	-
6.48	20, 4.0, 0.8	-	-	-	-	-
6.47	20, 4.0, 0.8	-	-	-	-	-
6.38	20, 4.0, 0.8	-	-	-	-	-
6.45a(ketal of 6.48)	20, 4.0, 0.8	-	-	-	-	-
6.46a(ketal of 6.47)	20, 4.0, 0.8	-	-	-	-	-

Table 6.7b : Biological evaluation of berkeleyamide A and its derivatives : Anti-fungal Assay

Compound No.	Test Concentrations (µg/mL)	<i>S. aureus</i> IC ₅₀	MR S IC ₅₀	<i>E. coli</i> IC ₅₀	<i>P. aeruginosa</i> IC ₅₀	<i>M. intracellularis</i> IC ₅₀
6.1	20, 4.0, 0.8	-	-	-	-	-
6.48	20, 4.0, 0.8	-	-	-	-	-
6.47	20, 4.0, 0.8	-	-	-	-	-
6.38	20, 4.0, 0.8	-	-	-	-	-
6.45a(ketal of 6.48)	20, 4.0, 0.8	-	-	-	-	-
6.46a(ketal of 6.47)	20, 4.0, 0.8	-	-	-	-	-

Table 6.8: Standards used for Antifungal assay

Microorganism	Drug Control	IC ₅₀ (µg/ml)*	MIC (µg/ml)**
<i>Candida albicans</i> ATCC 90028 (Ca)	Amphotericin B	0.23	0.63
<i>Candida glabrata</i> ATCC 90030 (Cg)	Amphotericin B	0.23	0.63
<i>Candida krusei</i> ATCC 6258 (Ck)	Amphotericin B	0.68	1.25
<i>Aspergillus fumigatus</i> ATCC 90906 (Afu)	Amphotericin B	0.74	1.25
<i>Cryptococcus neoformans</i> ATCC 90113 (Cn)	Amphotericin B	0.19	0.63
<i>Staphylococcus aureus</i> ATCC 29213 (Sa)	Ciprofloxacin	0.10	0.50
Methicillin-resistant <i>S. aureus</i> ATCC 33591 (MRS)	Ciprofloxacin	0.09	0.25
<i>Escherichia coli</i> ATCC 35218 (Ec)	Ciprofloxacin	0.004	0.008
<i>Pseudomonas aeruginosa</i> ATCC 27853 (Pa)	Ciprofloxacin	0.078	1.000
<i>Mycobacterium intracellulare</i> ATCC 23068 (Mi)	Ciprofloxacin	0.56	1.00

*The concentration (mg/ml) that affords 50% inhibition of growth

**MIC (Minimum Inhibitory Concentration) is the lowest test concentration (mg/ml) that allows no detectable growth

Table 6.9: Biological evaluation of berkeleyamide A and its derivatives for Cytotoxicity Assay

Compound No.	TC50 ng/ml
6.1	NC
6.48	NC
6.47	NC
6.38	NC
6.45a(ketal of 6.48)	NC
6.46a(ketal of 6.47)	NC

6.14 Conclusion

In conclusion, we were able to develop and implement a highly diastereoselective route for total synthesis of berkeleyamide A. Asymmetric synthesis of the natural product was completed in a modular fashion in 9 steps, starting from *N*-Boc-Leucinal with an overall 18% yield. The salient feature of this route is that it is easily scalable and amenable to structural modifications for a structure activity relationship study. Furthermore, this route was successfully applied to the synthesis of four diastereomers (three *syn* and one *anti* with respect to stereogenic centers 10C and 11C).

After completion of the total synthesis of berkeleyamide A, we carried out molecular docking studies using GLIDE module of Schrodinger molecular modeling suite. Our docking studies indicated that berkeleyamide A and its diastereomers only partially occupied the ICE active site. Moreover, the crucial S1 subsite containing the catalytic diad and aspartic acid clamp (Arg179 and Arg341) was not engaged in salt bridge interactions with arginine residues. According to our docking results (glide score and visual inspection), we postulated that **6.1** and its diastereomers might have low affinity for ICE active site. However, potent ICE inhibitory activity of berkeleyamide reported by Stierle and coworkers made this case very interesting. We postulated that the natural product can either bind to an allosteric site or a distinct site in caspase-1 and exert its inhibitory effect.

Based on the literature precedent and our docking results, we designed novel ICE inhibitors based on a berkeleyamide scaffold and docked them in ICE active site. All the designed derivative showed better docking results than the natural product. Newly designed derivative containing the cysteine trap, occupied the S1 site in a similar fashion to reported ICE inhibitors. Moreover, the designed compounds also retained all crucial hydrogen bonding

interactions required for potent ICE inhibitory activity. Our docking results of the designed molecules indicate that they have good potential to be potent ICE inhibitors.

However, a major setback to our program was the biological results. We tested berkeleyamide A and its derivatives for ICE inhibitory activity and none of the compounds showed any significant activity. Moreover, we also tested these compounds for anti-fungal, anti-malarial and anti-leishmanial activity. Unfortunately, none of the tested derivatives, including the natural product, exhibited any significant activity.

Our biological evaluation of berkeleyamide A and its derivatives reveal that these compounds lacked caspase-1 inhibitory activity. One of the possible reason for the discrepancy in the activity reported by Steirle *et al* may be due to the presence of some impurity in the authentic sample, which possesses a high affinity for caspase-1. This is very unlikely, however, and an error in assaying the compounds cannot be completely ruled out.

The natural product and its derivatives did not exhibit any caspase-1 inhibitory activity, which was correctly predicted by our docking studies. This result validates our docking protocol to a certain extent. As our docking study indicated that newly designed molecules may show promising ICE inhibition, we plan on synthesizing and testing a short library our designed molecules.

CHAPTER 7
EXPERIMENTAL- BEREKELEYAMIDE A

General Experimental

^1H and ^{13}C NMR spectra were measured in CDCl_3 or C_6D_6 on Bruker 400 MHz (100 MHz) or 500 MHz (125 MHz) machines. Chemical shifts were reported in ppm downfield from tetramethylsilane (δ) as the internal standard and coupling constants are in hertz (Hz). Assignment of proton resonances were confirmed by correlated spectroscopy. IR spectra were recorded using a universal attenuated total reflection sampling accessory with a Zinc Selenide crystal on a Perkin-Elmer Spectrum 100 FT-IR spectrometer. The high-resolution mass spectra (HRMS) were recorded on a Micromass Q-ToF Micro mass spectrometer with lock spray source. Optical rotations were measured on an Autopol V automatic polarimeter, from Rudolph Research Analytical in a 1 dm or a 5 dm cell. Melting points were measured on an OptiMelt[®] V.1.061 (Stanford Research systems) instrument and were uncorrected. The reaction progress was monitored on precoated silica gel G or GP Analtech TLC plates. Spots were visualized under 254 nm UV light and/or by dipping the TLC plate into a solution of 2 ml anisaldehyde and 10 ml glacial acetic acid and 5 ml H_2SO_4 in 340 ml MeOH followed by heating with a hot gun. Column chromatography was performed with Dynamic Adsorbents Inc. silica gel 60 (230-400 mesh). All the solvents (hexane, ethyl acetate, CH_2Cl_2 , Et_2O) were distilled prior to use. All reactions were performed under an atmosphere of argon using oven-dried glassware and standard syringe/septa techniques. The solvents THF and Et_2O were distilled from sodium-benzophenone, toluene, cyclohexane, benzene from sodium. CH_2Cl_2 was dried over P_2O_5 . DMF, NEt_3 , $^i\text{Pr}_2\text{NH}$ and $^i\text{Pr}_2\text{NEt}$ and were distilled from CaH_2 .

(R)-tert-butyl (1-(methoxy(methyl)amino)-4-methyl-1-oxopentan-2-yl)carbamate (Weinreb Amide)

To a stirred solution of Boc-leucine (10.0 g, 43.2 mmol) in 150 ml anhydrous DCM was added N-Methylmorpholine (14.26 ml, 130 mmol) at -10°C. The reaction mixture was stirred for 30mins. After 30 mins stirring at -10°C, N,O dimethylhydroxylamine (5.06 g, 51.9 mmol), and EDC (9.95 g, 51.9 mmol) was added successively to give a yellow solution. The reaction mixture brought to RT over 1 hour and was stirred at this temperature for 2-3hrs. The reaction was monitored by TLC. After completion of the reaction 50.0 ml of water was added to quench the reaction. The organic layer was washed with 0.5N HCl, saturated NaHCO₃ followed by brine. The organic layer was dried over magnesium sulfate and then concentrated vacuum to furnish weinreb amide, which was carried forward into next reaction without purification. (10.9g, 92%) Colorless liquid; ν_{\max} 2958(s), 1715(s), $[\alpha]^{23}_{\text{D}}$ -23 (c =1.0 in methanol) ¹H NMR (500 MHz, CDCl₃) δ 9.58 (s, 1H), 5.03 (s, 1H), 4.23 (s, 1H), 1.81 – 1.72 (m, 1H), 1.65 (s, 2H), 1.50 – 1.38 (m, 11H), 0.96 (d, J = 6.5 Hz, 6H). ¹³C NMR (126 MHz, CDCl₃) δ 200.40, 155.57, 79.93, 77.25, 77.00, 76.75, 68.47, 58.33, 38.01, 28.20, 24.58, 23.01, 21.85.

N-tert-Butoxycarbonyl-L-leucinal (6.3)

To a stirred solution of weinreb amide (780 mg, 2.84 mmol) in a 25 mL round-bottomed flask in THF (10.0 ml) at to -78°C was charged LAH 1.0 M (2.84 ml, 2.84 mmol), very slowly. Resulting solution was stirred for 2.0 hrs at same temperature. After completion of reaction (monitored by TLC), a saturated solution of NaCl was added slowly followed by Rochelles salt. Reaction mixture was stirred vigorously for 30mins and the residue formed was filtered through celite. THF was concentrated to give oily residue which was further dissolve in ethyl acetate.

The organic layer was washed with brine, dried over magnesium sulfate and concentrated under vacuum to give crude **3**. The crude leucinal was purified by flash column chromatography using Hexanes:EtOAc (8:2). (520.0 mg, 85%). Colorless liquid; ν_{\max} 2958(s), 1735(s), 1700(b) $[\alpha]^{23}_{D}$ -45 (c = 1.0 in methanol) $^1\text{H NMR}$ (500 MHz, CDCl_3) δ 9.58 (s, 1H), 5.03 (s, 1H), 4.23 (s, 1H), 1.81 – 1.72 (m, 1H), 1.65 (s, 2H), 1.50 – 1.38 (m, 11H), 0.96 (d, $J = 6.5$ Hz, 6H). $^{13}\text{C NMR}$ (126 MHz, CDCl_3) δ 200.40, 155.57, 79.93, 77.25, 77.00, 76.75, 68.47, 58.33, 38.01, 28.20, 24.58, 23.01, 21.85.

General procedure for Knoevenagel reaction

In a 5 mL round-bottomed flask was charged **3** (50.0 mg, 0.232 mmol), Diethyl malonate (0.053 ml, 0.348 mmol), acetic acid (2.66 μl , 0.046 mmol) and Piperidine (4.60 μl , 0.046 mmol in Toluene (1.0 ml). The reaction mixture was stirred at RT for 1hr and then water was removed azeotropically using dean stark. Reaction was monitored by TLC. No new spot was observed after 5 hrs. Reaction was discontinued after 24 hrs due to considerable degradation.

(*S,E/Z*)-ethyl 4-((*tert*-butoxycarbonyl)amino)-2-cyano-6-methylhept-2-enoate (**6.7**)

In a 5.0 mL round-bottomed flask ethyl 2-cyanoacetate (228 mg, 1.061 mmol) was charged followed by *N*-Boc-Leucinal (100mg, 0.884 mmol) in Chloroform. To the resulting solution silica gel (106.0 mg, 1.768 mmol) was added as a catalyst. Reaction was stopped after no starting material was remaining; confirmed by TLC. After completion of reaction chloroform was evaporated to give silica impregnated compound which was further purified using flash column chromatography. (EtOAc:Hexanes 7.25:2.75) (161.0 mg, 58%) Yellow liquid; ν_{\max} 2878(s), 1715(s), 2200 (s); $^1\text{H NMR}$ (500 MHz, CDCl_3) δ 7.47 (s, 1H), 4.60 (s, 1H), 4.34 (dd, $J = 14.1$,

7.0 Hz, 2H), 1.71 (dt, $J = 19.8, 6.7$ Hz, 1H), 1.58 (dd, $J = 19.2, 11.2$ Hz, 2H), 1.52 – 1.41 (m, 10H), 1.38 (t, $J = 7.1$ Hz, 3H), 1.12 – 0.92 (m, 7H). ^{13}C NMR(126 MHz, CDCl_3) δ 163.19, 161.12, 154.85, 113.05, 108.78, 80.22, 77.25, 77.00, 76.75, 62.64, 50.12, 42.62, 28.31, 24.71, 22.88, 21.90, 14.04. LC MS ESI(M+1) 311.23 (Note: Spectra provided only for one of the geometrical isomer. Geometrical isomers *Cis* and *Trans* not separated and carried forward to next reaction without purification)

ethyl 4-((tert-butoxycarbonyl)amino)-2-cyano-6-methylheptanoate (6.8)

To a stirred solution of **7** (50.0mg, 0.161 mmol) in Ethyl acetate (2.0 ml) was carefully added Palladium 10% on carbon (17.14 mg, 0.161 mmol). A balloon of hydrogen gas was then used carry out the reduction under ballon pressure. The reaction was stirred 5-8 hrs and then filtered through celite. The ethyl acetate was recovered under vacuum and crude obtained was purified by column chromatography (EtOAc: Hexane 7:3) (39.0mg, 77%) Yellow liquid; ν_{max} 2878(s), 1745(s), 2210 (s) ^1H NMR (500 MHz, CDCl_3) δ 4.27 (d, $J = 9.0$ Hz, 1H), 4.12 (dd, $J = 13.1, 6.8$ Hz, 2H), 3.70 – 3.51 (m, 1H), 2.36 (t, $J = 7.6$ Hz, 2H), 1.90 – 1.80 (m, 1H), 1.71 – 1.55 (m, 2H), 1.42 (s, 8H), 1.25 (t, $J = 7.1$ Hz, 3H), 0.90 (d, $J = 6.5$ Hz, 6H). ^{13}C NMR (126 MHz, CDCl_3) δ 173.74, 155.61, 78.94, 77.31, 77.26, 77.06, 76.80, 60.38, 48.47, 45.15, 31.00, 28.39, 24.89, 22.99, 22.28, 14.21. LC MS ESI (M+Na) 335.30

5-isobutyl-2-oxopyrrolidine-3-carbonitrile and 5-isobutylpyrrolidin-2-one (6.10 and 6.11)

To a suspension of **8** (100.0mg, 0.320 mmol) in water:ACN (9:1) mixture was added Lanthanum chloride heptahydrate (0.320 mmol). The reaction mixture was place in a microwave tube and the solution was irradiated with microwave at normal absorption at 80°C. After 10 mins reaction was complete (starting material exhausted). Reaction mixture was extracted with EtOAc 5.0 ml

and organic layer was washed with brine. The organic layer was dried over magnesium sulfate and concentrated under vacuum. TLC showed presence of two products. Both these products were purified using column chromatography.

5-isobutyl-2-oxopyrrolidine-3-carbonitrile (6.11)

Thick oil solidifies on standing liquid film ; ν_{\max} 2242, 1689, ^1H NMR (400 MHz, CDCl_3) δ 6.76 (s, 1H), 3.80 – 3.69 (m, 1H), 3.57 – 3.46 (m, 1H), 2.77 – 2.65 (m, 1H), 2.11 – 1.95 (m, 1H), 1.77 – 1.63 (m, 2H), 1.63 – 1.52 (m, 1H), 1.43 (dd, $J = 13.7, 6.3$ Hz, 1H), 0.96 (d, $J = 6.5$ Hz, 6H) ^{13}C NMR (126 MHz, CDCl_3) δ 168.80, 116.96, 77.30, 77.04, 76.79, 51.39, 45.26, 33.51, 33.25, 25.27, 22.75, 22.34. LS-MS ESI- [M-H] 165.12

5-isobutylpyrrolidin-2-one (6.10)

Thick oil solidifies on standing liquid film ; ν_{\max} 2956, 1684.70 ^1H NMR (400 MHz, CDCl_3) δ 3.69 – 3.55 (m, 1H), 2.23 (ddd, $J = 7.9, 5.9, 3.8$ Hz, 1H), 2.18 – 2.08 (m, 1H), 1.61 (d, $J = 6.4$ Hz, 2H), 1.44 – 1.31 (m, 2H), 1.25 – 1.16 (m, 1H), 0.83 (dd, $J = 6.6, 3.2$ Hz, 6H). ^{13}C NMR (101 MHz, CDCl_3) δ 178.75, 77.47, 77.15, 76.84, 52.84, 45.90, 30.39, 28.30, 27.58, 25.02, 22.84, 22.32. LS-MS ESI- [M+H] 142.51

Methyl (2-benzyl-1,3-dioxolan-2-yl)acetate (6.25)

To a solution of **6.25a** beta-ketoester (8.0 g, 41.6 mmol) and 1,2-bis-[trimethylsilyl(oxy)]ethane (10.74 g, 52.0 mmol) in anhydrous dichloromethane (100 ml) was added TMSOTf (1.5 ml, 8.32 mmol) drop wise slowly at 0 °C. The mixture was allowed to warm to room temperature. After 8h, the reaction was quenched with TEA (1.2 ml, 8.54 mmol) and washed with 5% aqueous NaHCO_3 solution, water, brine, and dried over magnesium sulfate. The residue obtained after

concentration was used for next reaction without any further purification (9.3 g, 95%). Colorless liquid; ν_{\max} (CHCl₃)/cm⁻¹ 3031, 2953, 1736, 1436, 1205, 1095, 1032; ¹H NMR (400 MHz, CDCl₃) δ 7.36 – 7.22 (m, 5H), 3.99 – 3.89 (m, 2H), 3.80 – 3.69 (m, 2H), 3.73 (s, 3H), 3.13 (s, 2H), 2.67 (s, 2H); ¹³C NMR (126 MHz, CDCl₃) δ 169.99, 136.06, 130.77, 128.01, 126.60, 109.00, 65.28, 51.76, 43.77, 42.48; HRMS (ESI+) Calc. for C₁₃H₁₆O₄Na 259.0946; Found 259.0956.

2-(2-Benzyl-1,3-dioxolan-2-yl)ethanol (6.26)

To a solution of methyl (2-benzyl-1,3-dioxolan-2-yl)acetate (9.3 g, 39.4 mmol) in anhydrous THF (200 ml) was added 2.3M LiAlH₄ solution (18 ml, 41.6 mmol) drop wise at 0 °C. The mixture was allowed to room temperature. After 2h, excess of LiAlH₄ was quenched with EtOAc followed by saturated brine solution at 0 °C. The slurry obtained was passed through pad of celite and concentrated. The crude obtained was dissolved in ethyl acetate (100 ml) and washed with 1N HCl, water, brine, dried over magnesium sulfate and concentrated. The residue was purified on silica gel column chromatography (EtOAc:hexanes, 1:3) to afford pure alcohol product (6.4 g, 78%). Colorless liquid; ν_{\max} (CHCl₃)/cm⁻¹ 3432, 2956, 2886, 1121, 1030, 699; ¹H NMR (400 MHz, CDCl₃) δ 7.31 – 7.19 (m, 5H), 3.93 – 3.83 (m, 2H), 3.78 – 3.66 (m, 4H), 3.19 (s, 1H), 2.92 (s, 2H), 1.90 (t, *J* = 5.9 Hz, 2H); ¹³C NMR (101 MHz, CDCl₃) δ 136.29, 130.55, 128.01, 126.50, 111.42, 65.03, 58.36, 43.76, 39.21; HRMS (ESI+) Calc. for C₁₂H₁₆O₃Na 231.0997; Found 231.0991.

(2-Benzyl-1,3-dioxolan-2-yl)acetaldehyde (6.24): To a stirred solution of 2-(2-benzyl-1,3-dioxolan-2-yl)ethanol (1.0 g, 4.8 mmol) in dichloromethane (30 ml) was added Dess Martin

Periodinane (3.0 g, 7.2 mmol) portion wise at room temperature. After 1h, the mixture was concentrated, re-dissolved in ether and passed through celite. The residue obtained after concentration was purified by column chromatography using ether:hexanes (1:3) to afford **4** (0.91 g, 92%) as a colorless liquid; ν_{\max} (neat)/cm⁻¹ 3030, 2890, 1720, 1127, 1082, 1044; ¹H NMR (400 MHz, CDCl₃) δ 9.67 (t, J = 2.8 Hz, 1H), 7.37 – 7.15 (m, 5H), 3.95 – 3.86 (m, 2H), 3.84 – 3.75 (m, 2H), 2.96 (s, 2H), 2.63 (d, J = 2.8 Hz, 2H); ¹³C NMR (101 MHz, CDCl₃) δ 199.86, 135.57, 130.59, 128.13, 126.79, 109.20, 65.20, 50.78, 44.55.

Ethyl (2E,4S)-4-[(*tert*-butoxycarbonyl)amino]-6-methyl-hept-2-enoate (6.27): To a solution of triethyl phosphonoacetate (16.4 g, 73.0 mmol) in THF (200 ml) was added solution of 1.0 M NaHMDS (65.7 ml, 65.7 mmol) slowly at 0 °C. The resulting orange solution cooled to -20 °C and a solution of freshly prepared *N*-Boc-*L*-leucinal (15.72g, 73.0 mmol) in THF (50 ml) was added dropwise at the same temperature. After addition, the mixture was warmed to 0 °C and stirred under argon for additional 30 min and then quenched with saturated aqueous ammonium chloride solution at 0 °C. The organic layer was separated, concentrated, and the residue was dissolved in EtOAc (200 ml), washed with water and brine, dried over MgSO₄ and filtered. The filtrate was partially concentrated and subjected to reduction without further purification. As a pale yellow oil; $[\alpha]_{\text{D}}^{20}$ = -23 (c 1.50, MeOH); ν_{\max} (CHCl₃)/cm⁻¹ 3354, 2959, 1701, 1691, 1657, 1519, 1367, 1282, 1167, 1045; ¹H NMR (500 MHz, CDCl₃) δ 6.81 (dd, J = 15.4, 4.9 Hz, 1H), 5.90 (d, J = 15.6 Hz, 1H), 4.50 (d, J = 7.9 Hz, 1H), 4.32 (bs, 1H), 4.17 (q, J = 7.0 Hz, 2H), 1.67 (dt, J = 13.1, 6.5 Hz, 1H), 1.42 (s, 9H), 1.36 (m, 2H), 1.26 (t, J = 7.0 Hz, 3H), 0.91 (d, J = 6.6 Hz, 6H); ¹³C NMR (126 MHz, CDCl₃) δ 166.4, 155.0, 148.9, 120.4, 77.3, 60.4, 49.8, 43.8, 28.4, 24.7, 22.7, 14.2; HRMS (ESI⁺) Calc. for C₁₅H₂₇NO₄Na 308.1838; Found 308.1827.

Ethyl (4*R*)-4-[(*tert*-butoxycarbonyl)amino]-6-methylheptanoate (6.28): To the solution of **6.27** in EtOAc (100 ml) was added 5% Pd/C catalyst (1.0 g) and the reaction mixture stirred under H₂ atmosphere for 30 min at 20psi in Parr shaker. The catalyst was removed by filtration through a pad of Celite and the organic solvent was evaporated under reduced pressure. Then the crude obtained was purified by column chromatography using Et₂O:hexanes (1:5) to afford **6.28** (18.0 g, 85%) as colorless thick liquid; $[\alpha]_{D}^{20} = -6.20$ (*c* 1, MeOH); ν_{\max} (CHCl₃)/cm⁻¹ 3357, 2957, 1712, 1689, 1519, 1450, 1390, 1366, 1248, 1168, 1044, 1028; ¹H NMR (500 MHz, CDCl₃) δ 4.25 (d, *J* = 9.0 Hz, 1H), 4.10 (q, *J* = 6.8 Hz, 2H), 3.71 – 3.56 (m, 1H), 2.33 (t, *J* = 7.6 Hz, 2H), 1.80 (m, 1H), 1.58 (m, 2H), 1.40 (s, 9H), 1.28 (m, 2H), 1.23 (t, *J* = 6.8 Hz, 3H), 0.88 (d, *J* = 6.5 Hz, 6H); ¹³C NMR (126 MHz, CDCl₃) δ 173.7, 155.6, 78.9, 60.4, 48.5, 45.2, 31.0, 28.4, 24.9, 23.0, 22.3, 14.2; HRMS (ESI⁺) Calc. for C₁₅H₂₉NO₄Na 310.1994; Found 310.2002.

(4*R*)-4-[(*tert*-Butoxycarbonyl)amino]-6-methylheptanoic acid (6.29): To a solution of **6.28** (16.0 g, 55.7 mmol) in THF:MeOH (400 ml, 5:1) was added aqueous solution of 2M LiOH (84 ml, 168 mmol) at 0 °C. The reaction mixture was allowed to warm to room temperature and stirred for additional 2h. The mixture was concentrated to remove organic solvents, diluted with Et₂O (100 ml), separated the layers and the aqueous layer was carefully acidified with 1N HCl at 0 °C, extracted with methylene chloride (3x50 ml) and the combined organic layers were washed with brine, dried over MgSO₄ and concentrated to afford **6.29** as a white solid (11.46 g, 79%). M.p. 110-111 °C; $[\alpha]_{D}^{20} = -6.60$ (*c* 1.06, MeOH); ν_{\max} (neat)/cm⁻¹ 3331, 2948, 1709, 1657, 1534, 1454, 1394, 1365, 1276, 1253, 1167, 1116, 1026, 901, 872, 847; ¹H NMR (500 MHz, MeOD) δ 3.61 (bs, 1H), 2.33 (t, *J* = 7.5 Hz, 2H), 1.79 (ddd, *J* = 12.2, 8.1, 3.9 Hz, 1H), 1.72 – 1.63 (m, 1H),

1.63 – 1.51 (m, 1H), 1.46 (s, 9H), 1.42 – 1.33 (m, 1H), 1.28 – 1.18 (m, 1H), 0.99 – 0.87 (m, 6H); ^{13}C NMR (126 MHz, MeOD) δ 175.9, 156.9, 78.3, 44.3, 30.9, 30.2, 27.4, 24.7, 22.2, 21.1; HRMS (ESI⁺) Calc. for $\text{C}_{13}\text{H}_{26}\text{NO}_4$ 260.1862; Found 260.1856.

(4R)-4-Amino-6-methylheptanoic acid hydrochloride (6.29a): To a solution of **6.29** (10.24 g, 39.5 mmol) in anhydrous 1,4-dioxane (20 ml) was added 4M HCl in dioxane (50 ml, 200 mmol) at 0 °C. The reaction mixture was allowed to warm to room temperature and stirred for 12h under argon to yield thick slurry. The mixture was concentrated and resulting solid was dispersed in anhydrous ether and filtered under inert atmosphere to furnish **6.29a** as a white solid, m.p. 147-148 °C; $[\alpha]_{\text{D}}^{20} = -4.41$ (*c* 0.64, MeOH); ν_{max} (neat)/ cm^{-1} 2873, 1724, 1702, 1602, 1503, 1438, 1298, 1234, 1121, 896; ^1H NMR (400 MHz, D_2O) δ 3.35 – 3.26 (m, 1H), 2.46 (t, *J* = 7.5 Hz, 2H), 1.95 – 1.78 (m, 2H), 1.68 – 1.56 (m, 1H), 1.49 – 1.36 (m, 2H), 0.84 (dd, *J* = 6.5, 3.0 Hz, 6H); ^{13}C NMR (126 MHz, D_2O) δ 177.2, 49.5, 41.0, 29.6, 27.5, 23.8, 21.7, 21.2; HRMS (ESI⁺) Calc. for $\text{C}_8\text{H}_{18}\text{NO}_2$ 160.1338; Found 160.1342.

1H-imidazole-1-sulfonyl azide hydrochloride

Sulfuryl chloride (16.26 ml, 200 mmol) was added drop-wise to an ice-cooled suspension of sodium azide (13.00 g, 200 mmol) in MeCN (250 mL) and the mixture stirred overnight at room temperature. Imidazole (23.83 g, 350 mmol) was added to the ice-cooled mixture and the resulting slurry stirred for 3 h. at room temperature. The mixture was diluted with EtOAc (100mL) and H₂O (100mL) and the aqueous layer separated and discarded. The organic layer was washed with H₂O (10 mL) then saturated aqueous NaHCO₃ (2 × 15 mL), dried over

MgSO₄ and filtered. Concentration of the filtrate and flash chromatography (EtOAc/Hexanes, 1:3) gave **1** as a colourless liquid (0.62 g, 72%). IR ν_{\max} (film) 2168, 1379 and 1173 cm⁻¹ ¹H NMR (500 MHz, CDCl₃) δ = 7.1 (dd, 1 H, *J* = 0.7, 1.6 Hz, H-4), 7.35 (dd, 1 H, *J* = 1.4, 1.7 Hz, H-5), 7.96 (dd, 1 H, *J* = 0.8, 1.4 Hz,) ¹³C NMR (101 MHz, CDCl₃) δ = 117.3, 131.09, 136.7 HRMS (EI): *m/z* = 173.0013;

(4*R*)-4-azido-6-methylheptanoic acid (6.32): The reagent imidazole-1-sulfonyl azide hydrochloride (3.86 g, 18.40 mmol) was added to the suspension of **6.29a** (3.0 g, 15.33 mmol), potassium carbonate (7.84 g, 56.7 mmol) and copper(II) sulfate pentahydrate (0.380 g, 0.153 mmol) in 80 ml MeOH. After stirred for 14h, the resulting gray colored mixture was concentrated, diluted with water and adjusted the pH to 2 with conc. HCl at 0 °C. The resulting aqueous layer was extracted with ethyl acetate (3x30 ml) and the combined organic layer was washed with water, brine, dried over magnesium sulfate and concentrated. The residue was purified by column chromatography (hexanes: EtOAc, 9:1) to afford **6.32** (2.2 g, 77%) as a colorless liquid; $[\alpha]_{\text{D}}^{20} = +10.77$ (*c* 1.17, MeOH); ν_{\max} (neat)/cm⁻¹ 2959, 2873, 2097, 1707, 1416, 1369, 1267, 1245, 1172, 922; ¹H NMR (500 MHz, CDCl₃) δ 3.38 (ddd, *J* = 13.6, 8.9, 4.6 Hz, 1H), 2.51 (m, 2H), 1.98 (m, 1H), 1.75 (m, 2H), 1.52 (ddd, *J* = 14.4, 8.7, 5.9 Hz, 1H), 1.32 (m, 1H), 0.94 (d, *J* = 6.6 Hz, 6H); ¹³C NMR (126 MHz, CDCl₃) δ 178.7, 60.0, 43.3, 30.5, 29.5, 25.0, 22.9, 22.1; HRMS (ESI⁺) Calc. for C₈H₁₅N₃O₂ 186.1243; Found 186.1247.

4*R*)-3-[(4*R*)-4-azido-6-methylheptanoyl]-4-benzyl-1,3-oxazolidin-2-one (6.33): To a stirred solution of **6.32** (1.0 g, 5.4 mmol) in THF (40 ml) was added TEA (1.52 ml, 10.8 mmol) followed pivaloyl chloride (0.66 ml, 5.4 mmol) at -20 °C. After stirring for 2h, LiCl (275 mg, 6.48 mmol) and 4(*R*)-benzyl-oxazolidin-2-one (860 mg, 4.86 mmol) were added, the mixture

was allowed to warm to 0 °C and then to room temperature slowly and stirred for additional 4h. The mixture was concentrated and residue was partitioned between 5% aqueous KHSO₄ (20 ml) and ethyl acetate (50 ml). The organic layer was washed with 1M sodium bicarbonate (2x10 ml), brine (10 ml) and then dried over magnesium sulfate and concentrated. The residue was purified by column chromatography (EtOAc: hexanes, 3:17) to yield **6.33** (1.4 g, 75%) as a viscous liquid; $[\alpha]_{D}^{20} = -73.48$ (*c* 1.14, MeOH); ν_{\max} (neat)/cm⁻¹ 2958, 2097, 1777, 1698, 1454, 1386, 1351, 1210, 1106, 1050, 745, 701; ¹H NMR (400 MHz, CDCl₃) δ 7.32 (t, *J* = 7.2 Hz, 2H), 7.29 – 7.23 (m, 1H), 7.19 (d, *J* = 6.9 Hz, 2H), 4.67 (ddd, *J* = 10.7, 7.0, 3.2 Hz, 1H), 4.23 – 4.14 (m, 2H), 3.47 – 3.38 (m, 1H), 3.28 (dd, *J* = 13.4, 3.3 Hz, 1H), 3.14 – 2.98 (m, 2H), 2.77 (dd, *J* = 13.4, 9.5 Hz, 1H), 1.95 (dtd, *J* = 11.4, 7.5, 4.2 Hz, 1H), 1.79 (ddt, *J* = 20.2, 8.1, 6.1 Hz, 2H), 1.54 (ddd, *J* = 14.5, 8.8, 5.9 Hz, 1H), 1.34 (ddd, *J* = 13.7, 8.3, 5.2 Hz, 1H), 0.94 (dd, *J* = 6.6, 1.4 Hz, 6H); ¹³C NMR (101 MHz, CDCl₃) δ 172.5, 153.4, 135.3, 129.4, 128.9, 127.3, 66.3, 60.1, 55.1, 43.4, 37.8, 32.2, 29.1, 25.1, 22.9, 22.1; HRMS (ESI⁺) Calc. for C₁₈H₂₅N₄O₃ 345.1927; Found 345.1937.

(4R)-3-((2R,4S)-4-azido-2-((1S)-2-(2-benzyl-1,3-dioxolan-2-yl)-1-hydroxyethyl)-6-methylheptanoyl)-4-benzyl-1,3-oxazolidin-2-one (6.34): To a stirred solution of **6.33**(280 mg, 0.81 mmol) in dichloromethane (4 ml) was added freshly distilled TiCl₄ (94 μ l, 0.85 mmol) slowly at 0 °C. After 15 min, to this yellow suspension was added the (-)-sparteine (374 μ l, 1.6 mmol) drop wise to give a dark red solution, which was stirred for 1h at same temperature. Then a solution of **6.24** (184 mg, 0.89 mmol) in dichloromethane (2 ml) was added dropwise at 0 °C. After 2h, the mixture was quenched with half saturated aqueous solution of NH₄Cl. The organic layer was separated and aqueous layer was further extracted with dichloromethane. The

combined organic layer was washed with water, brine, dried over magnesium sulfate and concentrated. The residue was purified using column chromatography (hexanes:EtOAc, 3:1) to give the aldol product **6.34** (330 mg, 74%) as a colorless viscous liquid; $[\alpha]_{\text{D}}^{20} = -50.3$ (c 1.2, MeOH); ν_{max} (neat)/ cm^{-1} 3506, 2958, 2103, 1779, 1693, 1386, 1350, 1210, 1196, 1110, 702; ^1H NMR (500 MHz, CDCl_3) δ 7.34 (t, $J = 7.3$ Hz, 2H), 7.30 – 7.20 (m, 8H), 4.64 (ddd, $J = 10.2, 6.6, 3.0$ Hz, 1H), 4.28 (ddd, $J = 10.4, 5.3, 2.9$ Hz, 1H), 4.23 – 4.17 (m, 1H), 4.15 – 4.05 (m, 2H), 3.93 (dq, $J = 12.1, 6.9$ Hz, 2H), 3.75 (ddd, $J = 9.2, 4.8, 2.4$ Hz, 1H), 3.71 – 3.63 (m, 2H), 3.41 (dd, $J = 11.2, 6.1$ Hz, 1H), 3.35 (dd, $J = 13.3, 3.2$ Hz, 1H), 2.95 (q, $J = 13.9$ Hz, 2H), 2.69 (dd, $J = 13.2, 10.1$ Hz, 1H), 2.21 (ddd, $J = 14.2, 10.6, 3.7$ Hz, 1H), 1.85 (dd, $J = 11.0, 6.8$ Hz, 2H), 1.82 – 1.73 (m, 1H), 1.70 (ddd, $J = 14.1, 8.7, 2.8$ Hz, 1H), 1.55 (ddd, $J = 14.4, 8.4, 6.4$ Hz, 1H), 1.36 (ddd, $J = 13.7, 7.7, 5.7$ Hz, 1H), 0.93 (d, $J = 6.6$ Hz, 6H); ^{13}C NMR (126 MHz, CDCl_3) δ 173.9, 153.2, 135.9, 135.5, 130.7, 129.4, 129.0, 128.1, 127.3, 126.6, 111.4, 68.9, 65.9, 65.3, 64.9, 59.3, 55.7, 44.8, 43.8, 43.5, 40.6, 37.7, 32.1, 25.1, 22.7, 22.3; HRMS (ESI^+) Calc. for $\text{C}_{30}\text{H}_{39}\text{N}_4\text{O}_6$ 551.2870; Found 551.2875.

(1*S*,2*R*,4*S*)-4-azido-1-[(2-benzyl-1,3-dioxolan-2-yl)methyl]-2-[[*(4R)*-4-benzyl-2-oxo-1,3-oxazolidin-3-yl]carbonyl]-6-methylhept-2-yl(2*R*)-3,3,3-trifluoro-2-methoxy-2-phenylpropanoate [(*R*)-MTPA ester of (6.34**)]:** To a stirred solution of **6.34** (3 mg, 5.45 μmol), TEA (1.5 μl , 10.9 μmol) in anhydrous dichloromethane (1.7 ml) was added *S*-(-)- MTPA-Cl (1.4 mg, 0.054 mmol). After 30 min, the reaction mixture washed with water, brine, dried over magnesium sulfate and concentrated. The residue was purified by preparative TLC using hexanes: EtOAc (3:1) to afford *R*-MTPA ester of **2** (2.9 mg, 70%). ^1H NMR (400 MHz, CDCl_3) δ 7.59 (d, $J = 7.5$ Hz, 2H), 7.41 – 7.30 (m, 5H), 7.30 – 7.22 (m, 6H), 7.19 (d, $J = 7.2$ Hz, 2H), 5.75 – 5.68 (m, 1H), 4.58 – 4.49 (m, 1H), 4.27 (dt, $J = 10.4, 2.6$ Hz, 1H), 4.18 (t, $J = 8.2$ Hz,

1H), 4.15 – 4.09 (m, 1H), 3.95 (dd, $J = 13.4, 6.6$ Hz, 1H), 3.88 (dt, $J = 12.3, 6.1$ Hz, 1H), 3.73 (dd, $J = 12.2, 6.7$ Hz, 1H), 3.67 (t, $J = 6.6$ Hz, 1H), 3.53 (s, 3H), 3.31 – 3.23 (m, 2H), 2.90 (dd, $J = 33.3, 13.9$ Hz, 2H), 2.74 (dd, $J = 13.2, 9.9$ Hz, 1H), 2.17 (dd, $J = 15.4, 7.5$ Hz, 1H), 2.10 – 2.01 (m, 2H), 1.71 (tt, $J = 13.5, 6.9$ Hz, 1H), 1.58 (s, 1H), 1.53 – 1.44 (m, 1H), 1.44 – 1.35 (m, 1H), 1.32 – 1.23 (m, 2H), 0.92 (d, $J = 6.6$ Hz, 6H).

(1S,2R,4S)-4-azido-1-[(2-benzyl-1,3-dioxolan-2-yl)methyl]-2-[[[(4R)-4-benzyl-2-oxo-1,3-oxazolidin-3-yl]carbonyl]-6-methylheptyl(2S)-3,3,3-trifluoro-2-methoxy-2-

phenylpropanoate [(S)-MTPA ester of (6.34)]: Prepared as described above. ^1H NMR (400 MHz, CDCl_3) δ 7.58 – 7.53 (m, 2H), 7.40 – 7.31 (m, 5H), 7.30 – 7.18 (m, 8H), 5.80 (dd, $J = 5.7, 3.1$ Hz, 1H), 4.54 (t, $J = 8.5$ Hz, 1H), 4.30 (dd, $J = 16.8, 8.5$ Hz, 2H), 4.15 (dd, $J = 8.9, 2.1$ Hz, 1H), 3.83 (dd, $J = 12.7, 6.7$ Hz, 1H), 3.74 (dd, $J = 13.1, 6.7$ Hz, 1H), 3.64 – 3.56 (m, 4H), 3.52 (dd, $J = 12.6, 6.5$ Hz, 1H), 3.30 (dd, $J = 13.3, 3.1$ Hz, 2H), 2.88 – 2.75 (m, 3H), 2.24 – 2.14 (m, 1H), 1.98 (d, $J = 6.3$ Hz, 2H), 1.82 – 1.69 (m, 1H), 1.52 (ddd, $J = 16.3, 13.7, 4.9$ Hz, 2H), 1.39 – 1.29 (m, 2H), 0.94 (d, $J = 6.6$ Hz, 6H).

(3R,5S)-3-[(1S)-2-(2-benzyl-1,3-dioxolan-2-yl)-1-hydroxyethyl]-5-isobutylpyrrolidin-2-one

(6.35): To a solution of **6.34** (160 mg, 0.291 mmol) in MeOH (15 ml) was added ammonium formate (366 mg, 5.81 mmol), 5% Pd/C (60 mg) and stirred for 1h at room temperature. The mixture was concentrated and residue dissolved in ethyl acetate, washed with water, brine, dried over magnesium sulfate, and concentrated. The residue was purified by column chromatography (isopropanol: hexanes, 1:9) to afford **6.35** (86 mg, 85%) as a colorless viscous liquid; $[\alpha]_{\text{D}}^{20} = -11.4$ (c 0.35, MeOH); ν_{max} (CHCl_3)/ cm^{-1} 3224, 2925, 2954, 1687, 1454, 1269, 1128, 1030, 820,

735; ^1H NMR (500 MHz, CDCl_3) δ 7.30 – 7.20 (m, 5H), 6.04 (s, 1H), 4.44 (d, $J = 9.7$ Hz, 1H), 4.00 – 3.91 (m, 2H), 3.77 – 3.63 (m, 3H), 2.96 (dd, $J = 30.2, 13.9$ Hz, 2H), 2.36 (dd, $J = 15.2, 6.5$ Hz, 2H), 1.82 (dt, $J = 14.6, 12.2$ Hz, 2H), 1.71 – 1.64 (m, 1H), 1.64 – 1.55 (m, 1H), 1.43 – 1.35 (m, 1H), 1.32 – 1.23 (m, 1H), 0.91 (d, $J = 6.6$ Hz, 6H); ^{13}C NMR (126 MHz, CDCl_3) δ 177.7, 136.1, 130.6, 128.1, 126.6, 111.5, 66.5, 65.3, 65.0, 51.0, 46.5, 46.4, 43.9, 41.7, 27.7, 25.3, 22.9, 22.4; HRMS (ESI^+) Calc. for $\text{C}_{20}\text{H}_{30}\text{NO}_4$ 348.2175; Found 348.2176.

(-)-Berkeleyamide A (6.1): To a solution of **6.35** (23 mg, 0.066 mmol) in acetone (0.5 ml) and water (24 μl , 1.3 mmol) was added *bis* (acetonitrile) dichloropalladium (II) (3.43 mg, 0.013 mmol). The mixture was stirred for 4h and concentrated. The residue was purified by column chromatography (isopropanol: hexanes, 1:9) to afford **6.1** (15 mg, 77%) as a colorless viscous liquid; $[\alpha]_{\text{D}}^{20} = -34.2$ (c 0.48, MeOH), $[\alpha]_{\text{D}}^{20} = -31.1$ (c 0.11, MeOH); ν_{max} (CHCl_3)/ cm^{-1} 3257, 2955, 2927, 1704, 1686, 1454, 1367, 1271, 1077, 1030, 734; ^1H NMR (400 MHz, CDCl_3) δ 7.33 (t, $J = 7.2$, 3H), 7.30 – 7.24 (m, 1H), 7.24 – 7.17 (d, 2H), 6.11 (s, 1H), 4.37 (ddd, $J = 8.8, 5.3, 3.4$, 1H), 3.74 (s, 2H), 3.65 (td, $J = 11.9, 7.7$, 1H), 3.12 (s, 1H), 2.85 (dd, $J = 17.3, 3.2$, 1H), 2.71 (dd, $J = 17.3, 8.9$, 1H), 2.52 – 2.42 (m, 1H), 2.31 (dt, $J = 13.0, 7.6$, 1H), 1.72 (ddd, $J = 13.2, 9.3, 4.2$, 1H), 1.60 (td, $J = 13.4, 6.6$, 1H), 1.44 – 1.34 (m, 1H), 1.28 (dt, $J = 13.7, 7.0$, 1H), 0.91 (d, $J = 6.6$, 6H); ^{13}C NMR (101 MHz, CDCl_3) δ 208.5, 177.2, 133.6, 129.5, 128.7, 127.1, 66.9, 50.8, 50.7, 46.4, 46.1, 45.5, 28.8, 25.3, 22.8, 22.3; HRMS (ESI^+) Calc. for $\text{C}_{18}\text{H}_{26}\text{NO}_3$ 304.1913; Found 304.1902.

(S)-3-((2S,4S)-4-azido-2-((R)-2-(2-benzyl-1,3-dioxolan-2-yl)-1-hydroxyethyl)-6-methylheptanoyl)-4-benzyloxazolidin-2-one (6.45) and **(S)-3-((2S,4R)-4-azido-2-((R)-2-(2-benzyl-1,3-dioxolan-2-yl)-1-hydroxyethyl)-6-methylheptanoyl)-4-benzyloxazolidin-2-one (6.46)**:

To a stirred solution of 6.44+6.43 (100.0 mg, 0.290 mmol) in dichloromethane (4 ml) was added freshly distilled TiCl₄ (33.6 μ l, 0.305 mmol) slowly at 0 °C. After 15 min, to this yellow suspension was added the (-) Sparteine (167 μ l, 0.726 mmol) drop wise to give a dark red solution, which was stirred for 1h at same temperature. Then a solution of **6.24** 2-(2-benzyl-1,3-dioxolan-2-yl)acetaldehyde (65.9 mg, 0.319 mmol) in dichloromethane (2 ml) was added dropwise at 0 °C. After 2h, the mixture was quenched with half saturated aqueous solution of NH₄Cl. The organic layer was separated and aqueous layer was further extracted with dichloromethane. The combined organic layer was washed with water, brine, dried over magnesium sulfate and concentrated. The residue was purified using column chromatography (hexanes:EtOAc, 3:1) to give the mixture of aldol products Aldol **6.45** (48.0 mg, 0.087 mmol, 30.0 % yield) and Aldol **6.46** (53.0mg, 0.096 mmol, 33.1 % yield) as a colorless viscous liquid

(S)-3-((2S,4S)-4-azido-2-((R)-2-(2-benzyl-1,3-dioxolan-2-yl)-1-hydroxyethyl)-6-methylheptanoyl)-4-benzyloxazolidin-2-one (6.45)

$[\alpha]_D^{20} = 30.3$ (*c* 1.0, MeOH); ν_{\max} (neat)/cm⁻¹ 3500, 2955, 2100, 1769, 1683, 1350, 1210, 730 ¹H NMR (500 MHz, CDCl₃) δ 7.37 (t, *J* = 7.3 Hz, 2H), 7.29 (dd, *J* = 13.2, 6.8 Hz, 6H), 7.26 – 7.21 (m, 2H), 4.57 (td, *J* = 7.7, 2.4 Hz, 1H), 4.32 – 4.26 (m, 1H), 4.19 – 4.08 (m, 2H), 4.05 (dd, *J* = 16.2, 8.2 Hz, 1H), 4.01 – 3.94 (m, 2H), 3.88 – 3.78 (m, 2H), 3.78 – 3.70 (m, 1H), 3.52 – 3.41 (m, 2H), 2.97 (s, 2H), 2.66 (dd, *J* = 13.1, 10.8 Hz, 1H), 2.06 – 1.99 (m, 1H), 1.98 – 1.72 (m, 4H),

1.57 (ddd, $J = 14.4, 9.0, 5.7$ Hz, 1H), 1.38 (ddd, $J = 13.7, 8.5, 5.0$ Hz, 1H), 1.28 (t, $J = 7.1$ Hz, 1H), 0.96 (d, $J = 6.5$ Hz, 6H). ^{13}C NMR (126 MHz, CDCl_3) δ 174.30, 153.47, 135.94, 135.77, 130.64, 129.48, 128.98, 128.10, 127.26, 126.66, 111.43, 77.41, 77.15, 76.90, 69.56, 65.83, 65.28, 64.91, 60.41, 55.98, 46.30, 43.76, 43.68, 40.04, 37.17, 34.02, 25.04, 23.03, 22.07, 14.24. (ESI⁺) for $\text{C}_{30}\text{H}_{39}\text{N}_4\text{O}_6 = 551.30$

(S)-3-((2S,4R)-4-azido-2-((R)-2-(2-benzyl-1,3-dioxolan-2-yl)-1-hydroxyethyl)-6-methylheptanoyl)-4-benzyloxazolidin-2-one (6.46):

$[\alpha]_{\text{D}}^{20} = 30.3$ (c 1.6, MeOH); ν_{max} (neat)/ cm^{-1} 3506, 2958, 2103, 1779, 1693, 1386, 1350, 1210, ^1H NMR (500 MHz, CDCl_3) δ 7.40 – 7.35 (m, 2H), 7.34 – 7.23 (m, 9H), 5.31 (s, 1H), 4.76 – 4.56 (m, 1H), 4.31 (dd, $J = 10.3, 2.7$ Hz, 1H), 4.27 – 4.22 (m, 1H), 4.19 – 4.08 (m, 2H), 4.02 – 3.91 (m, 2H), 3.83 – 3.77 (m, 1H), 3.76 – 3.68 (m, 2H), 3.49 – 3.41 (m, 1H), 3.38 (dd, $J = 13.2, 2.9$ Hz, 1H), 2.98 (q, $J = 13.9$ Hz, 2H), 2.73 (dd, $J = 13.1, 10.2$ Hz, 1H), 2.25 (ddd, $J = 14.1, 10.7, 3.5$ Hz, 1H), 1.88 (dd, $J = 10.8, 7.0$ Hz, 2H), 1.84 – 1.77 (m, 1H), 1.76 – 1.71 (m, 1H), 1.63 – 1.52 (m, 1H), 1.43 – 1.36 (m, 1H), 0.96 (d, $J = 6.6$ Hz, 7H) ^{13}C NMR (126 MHz, CDCl_3) δ 173.86, 153.19, 135.92, 135.50, 130.68, 129.45, 129.01, 128.10, 127.35, 126.65, 111.43, 77.40, 77.15, 76.89, 68.92, 65.87, 65.35, 64.92, 59.27, 55.68, 44.70, 43.79, 43.50, 40.54, 37.70, 32.08, 25.08, 22.77, 22.30. (ESI⁺) for $\text{C}_{30}\text{H}_{39}\text{N}_4\text{O}_6 = 551.29$

(R)-3-((2R,4R)-4-azido-2-((S)-2-(2-benzyl-1,3-dioxolan-2-yl)-1-hydroxyethyl)-6-methylheptanoyl)-4-benzyloxazolidin-2-one (6.41)

$[\alpha]_{\text{D}}^{20} = -40.3$ (c 1.9, MeOH); ν_{max} (neat)/ cm^{-1} 3516, 2948, 2113, 1778, 1693, 1386; ^1H NMR (500 MHz, CDCl_3) δ 7.37 (t, $J = 7.3$ Hz, 2H), 7.29 (dd, $J = 13.4, 7.1$ Hz, 6H), 7.25 – 7.20 (m, 1H), 4.57 (td, $J = 7.7, 2.5$ Hz, 1H), 4.30 (ddd, $J = 9.7, 6.7, 2.8$ Hz, 1H), 4.19 – 4.09 (m, 2H), 4.06

(d, $J = 8.0$ Hz, 1H), 4.04 – 3.91 (m, 3H), 3.89 – 3.66 (m, 3H), 3.57 – 3.37 (m, 2H), 2.97 (s, 2H), 2.66 (dd, $J = 13.1, 10.8$ Hz, 1H), 2.06 – 1.70 (m, 6H), 1.57 (ddd, $J = 14.3, 8.9, 5.7$ Hz, 1H), 1.38 (ddd, $J = 13.7, 8.4, 5.0$ Hz, 1H), 1.29 (dd, $J = 8.3, 5.9$ Hz, 1H), 1.05 – 0.84 (m, 6H). ^{13}C NMR (126 MHz, CDCl_3) δ 174.30, 153.44, 135.95, 135.78, 130.63, 129.45, 128.97, 128.08, 127.24, 126.64, 111.43, 77.35, 77.09, 76.84, 69.56, 65.83, 65.26, 64.90, 60.40, 55.96, 46.31, 43.78, 43.70, 40.11, 37.21, 34.02, 25.05, 23.00, 22.07. (ESI^+) $\text{C}_{30}\text{H}_{39}\text{N}_4\text{O}_6 = 551.28$.

(3S,5S)-3-((R)-1-hydroxy-3-oxo-4-phenylbutyl)-5-isobutylpyrrolidin-2-one (6.48)

To a solution of Ketal 6.48a (18.0 mg, 0.052 mmol) in acetone (0.5 ml) and Water (12.13 μl , 0.673 mmol) was added *bis* (acetonitrile) dichloropalladium (II) (2.06 mg, 0.008 mmol). The mixture was stirred for 4h and concentrated. The residue was purified by column chromatography (isopropanol: hexanes, 1:9) to afford Isomer I_RSS_6.48 (10.0mg, 0.033 mmol, 63.6 % yield) as a colorless viscous liquid ; $[\alpha]_D^{20} = -33.2$ (c 0.7, MeOH), ν_{max} (CHCl_3)/ cm^{-1} 3250, 2965, 2917, 1700, 1687, 1360, 1201; ^1H NMR (500 MHz, CDCl_3) δ 7.35 (t, $J = 7.3$ Hz, 2H), 7.29 (t, $J = 7.3$ Hz, 2H), 7.22 (d, $J = 7.1$ Hz, 2H), 6.26 (s, 1H), 4.43 (d, $J = 3.5$ Hz, 1H), 3.83 – 3.72 (m, 3H), 3.61 (dt, $J = 14.0, 6.7$ Hz, 2H), 3.48 (d, $J = 2.2$ Hz, 1H), 2.88 (dd, $J = 17.1, 3.4$ Hz, 1H), 2.73 (dd, $J = 17.1, 8.9$ Hz, 1H), 2.52 (ddd, $J = 10.6, 9.0, 5.1$ Hz, 1H), 2.20 (ddd, $J = 12.6, 8.6, 6.8$ Hz, 1H), 1.74 – 1.59 (m, 3H), 1.47 (dt, $J = 13.9, 7.0$ Hz, 2H), 1.39 – 1.32 (m, 2H), 0.94 (d, $J = 2.3$ Hz, 3H), 0.93 (d, $J = 2.3$ Hz, 4H). ^{13}C NMR (126 MHz, CDCl_3) δ 208.45, 177.09, 133.69, 129.52, 128.77, 127.16, 77.30, 77.05, 76.79, 66.36, 50.68, 50.62, 46.84, 46.41, 45.81, 29.69, 25.32, 22.72, 22.59. ESI^+ (M+Na) $\text{C}_{18}\text{H}_{25}\text{NNaO}_3$ 326.18

(3S,5R)-3-((R)-1-hydroxy-3-oxo-4-phenylbutyl)-5-isobutylpyrrolidin-2-one (6.47)

To a solution of **6.47a** (24.00 mg, 0.069 mmol) in acetone (0.5 ml) and Water (16.18 μ l, 0.898 mmol) was added *bis* (acetonitrile) dichloropalladium (II) (2.69 mg, 0.010 mmol). The mixture was stirred for 4h and concentrated. The residue was purified by column chromatography (isopropanol: hexanes, 1:9) to afford (3S,5R)-3-((R)-1-hydroxy-3-oxo-4-phenylbutyl)-5-isobutylpyrrolidin-2-one (16.0 mg, 0.053 mmol, 76 % yield) **6.47** as a colorless viscous liquid (solidifies after few weeks) ; $[\alpha]_{\text{D}}^{20} = +34.2$ (*c* 0.9); ν_{max} (CHCl₃)/cm⁻¹ 3259, 2945, 2927, 1701, 1686, 1455, 1364, 1270, 1077, 1030, 734; ¹H NMR (500 MHz, CDCl₃) δ 7.64 – 6.83 (m, 42H), 6.51 (s, 8H), 4.42 (s, 7H), 3.76 (s, 14H), 3.67 (d, *J* = 11.4 Hz, 17H), 2.85 (d, *J* = 3.2 Hz, 2H), 2.83 – 2.58 (m, 12H), 2.58 – 2.10 (m, 16H), 1.98 (s, 2H), 1.72 (ddd, *J* = 13.1, 9.4, 4.0 Hz, 6H), 1.67 – 1.19 (m, 28H), 0.97 (s, 3H), 0.93 (d, *J* = 6.6 Hz, 46H). ¹³C NMR (126 MHz, CDCl₃) δ 208.65, 177.52, 133.67, 129.52, 128.77, 127.16, 77.32, 77.07, 76.81, 66.69, 50.76, 50.69, 46.47, 46.09, 45.61, 28.57, 25.23, 22.92, 22.32. ESI (M+1) 304.19

(3R,5R)-3-((S)-1-hydroxy-3-oxo-4-phenylbutyl)-5-isobutylpyrrolidin-2-one (6.42)

Procedure same as for compound **6.47**

$[\alpha]_{\text{D}}^{20} = +39.1$ (*c* 2.0, MeOH) ν_{max} (CHCl₃)/cm⁻¹ 3247, 2907, 1700, 1682, 1454, ¹H NMR (500 MHz, CDCl₃) δ 7.37 (t, *J* = 7.3 Hz, 2H), 7.29 (dd, *J* = 13.4, 7.1 Hz, 6H), 7.25 – 7.20 (m, 1H), 4.57 (td, *J* = 7.7, 2.5 Hz, 1H), 4.30 (ddd, *J* = 9.7, 6.7, 2.8 Hz, 1H), 4.19 – 4.09 (m, 2H), 4.06 (d, *J* = 8.0 Hz, 1H), 4.04 – 3.91 (m, 3H), 3.89 – 3.66 (m, 3H), 3.57 – 3.37 (m, 2H), 2.97 (s, 2H), 2.66 (dd, *J* = 13.1, 10.8 Hz, 1H), 2.06 – 1.70 (m, 6H), 1.57 (ddd, *J* = 14.3, 8.9, 5.7 Hz, 1H), 1.38 (ddd, *J* = 13.7, 8.4, 5.0 Hz, 1H), 1.29 (dd, *J* = 8.3, 5.9 Hz, 1H), 1.05 – 0.84 (m, 6H). ¹³C NMR (126 MHz, CDCl₃) δ 174.30, 153.44, 135.95, 135.78, 130.63, 129.45, 128.97, 128.08, 127.24, 126.64,

111.43, 77.35, 77.09, 76.84, 69.56, 65.83, 65.26, 64.90, 60.40, 55.96, 46.31, 43.78, 43.70, 40.11, 37.21, 34.02, 25.05, 23.00, 22.07. ESI (M+1) 304.19

N-((1R,2S)-2-hydroxy-2,3-dihydro-1H-inden-1-yl)-4-methylbenzenesulfonamide (6.52)

To a stirred suspension of 1R, 2S-cis-amioindan-2-ol, p-toluenesulfonyl chloride and DMAP in DCM was added TEA. After stirring for 2 h at 23 °C, the resulting solution was washed with water, brine and was dried over anhydrous magnesium sulfate. Solvent was reduced under vacuum to afford crude product. The crude was purified using column chromatography over silica gel (4:6 EtOAc:Hexanes) to give p-toluenesulfonamide cream colored solid obtained (m.p. 130-133) ¹H NMR (400 MHz, CDCl₃) δ 7.88 (d, *J* = 8.3 Hz, 2H), 7.36 (d, *J* = 8.0 Hz, 2H), 7.20 (dt, *J* = 19.0, 7.1 Hz, 2H), 7.09 (d, *J* = 7.3 Hz, 1H), 5.26 (d, *J* = 9.1 Hz, 1H), 4.70 (dd, *J* = 9.1, 4.8 Hz, 1H), 4.34 (dd, *J* = 4.9, 3.5 Hz, 1H), 3.06 (dd, *J* = 16.7, 5.1 Hz, 1H), 2.89 (d, *J* = 16.6 Hz, 1H), 2.46 (s, 3H), 1.78 – 1.63 (m, 1H). ¹³C NMR (101 MHz, CDCl₃) δ 143.79, 139.48, 137.57, 129.87, 128.51, 127.26, 127.20, 125.35, 124.56, 77.36, 77.05, 76.73, 72.84, 61.31, 39.29, 21.59.

(R)-(1R,2S)-1-(4-methylphenylsulfonamido)-2,3-dihydro-1H-inden-2-yl 4-azido-6-methylheptanoate (6.53)

To a stirred solution of N-tosyl-1-aminoindan-2-ol (213 mg, 0.702 mmol), DMAP (42.9 mg, 0.351 mmol) and (R)-4-azido-6-methylheptanoic acid (130.0 mg, 0.702 mmol) in DCM was added DCC (217 mg, 1.053 mmol) . The resulting slurry was stirred at 23°C for 18h. The slurry was filtered through pad of celite and concentrated to afford residue which was purified by silica gel chromatography to yield ester 91% yield ν_{\max} (CHCl₃)/cm⁻¹ 3278, 2957, 2100, 1737, 1336 ¹H NMR (400 MHz, CDCl₃) δ 7.83 (d, *J* = 8.2 Hz, 2H), 7.34 (d, *J* = 8.2 Hz, 2H), 7.25 (dd, *J* = 12.3,

3.4 Hz, 3H), 7.18 (d, $J = 6.1$ Hz, 1H), 5.20 (t, $J = 4.6$ Hz, 2H), 4.99 (dd, $J = 10.1, 5.2$ Hz, 1H), 3.31 (dt, $J = 8.8, 4.3$ Hz, 1H), 3.11 (dd, $J = 17.3, 4.9$ Hz, 1H), 2.92 (d, $J = 17.3$ Hz, 1H), 2.46 (s, 3H), 2.32 (t, $J = 7.4$ Hz, 2H), 1.85 – 1.71 (m, 3H), 1.65 (dt, $J = 14.3, 7.3$ Hz, 1H), 1.53 – 1.44 (m, 1H), 1.27 (ddd, $J = 13.5, 8.2, 5.3$ Hz, 2H), 0.93 (dd, $J = 6.6, 1.9$ Hz, 6H). ^{13}C NMR (101 MHz, CDCl_3) δ 171.91, 143.83, 139.58, 138.54, 137.87, 129.87, 128.69, 127.46, 126.99, 125.03, 124.24, 77.33, 77.02, 76.70, 75.03, 59.94, 59.51, 43.24, 37.37, 30.58, 29.49, 24.99, 22.84, 22.07, 21.57.

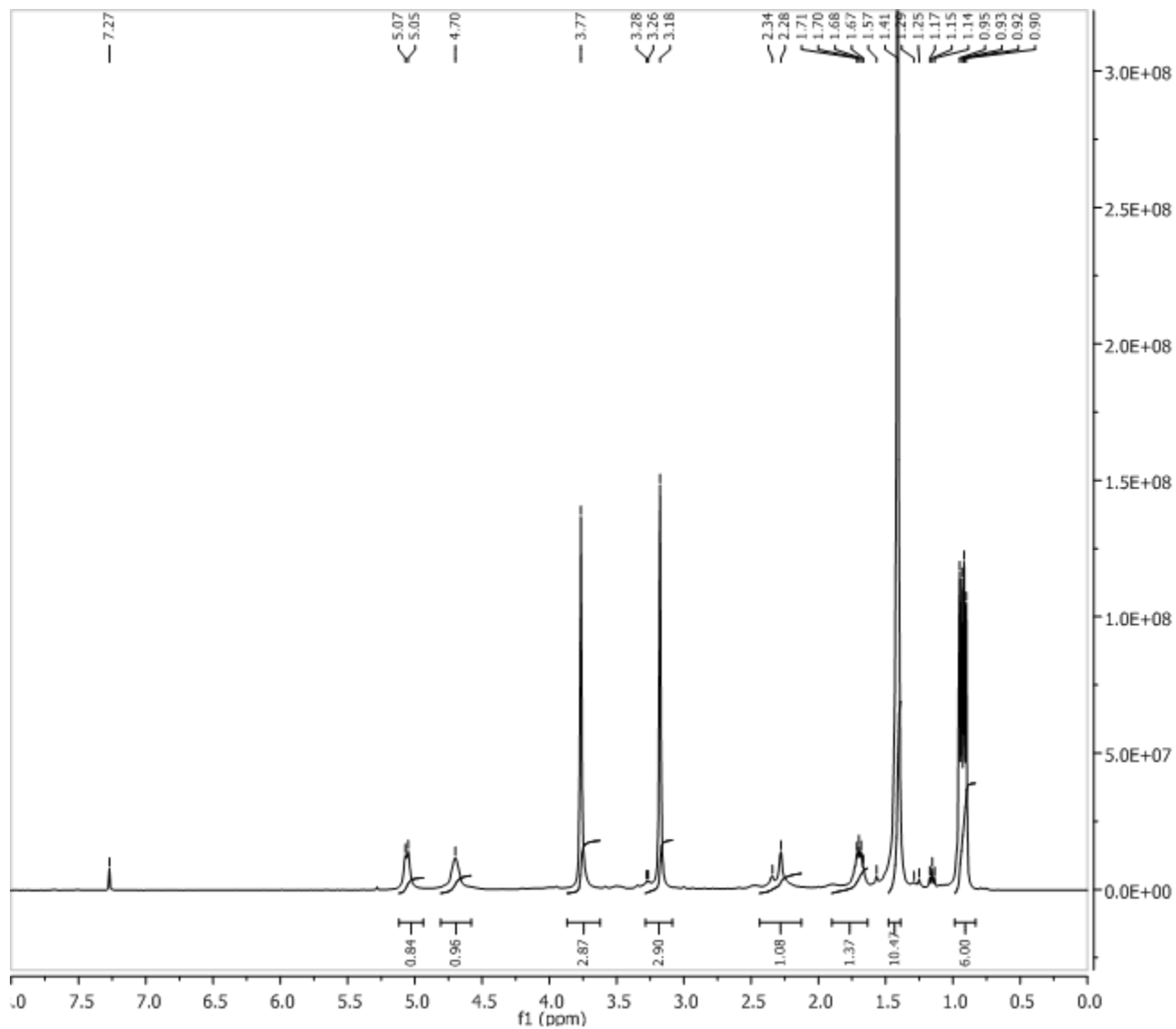
(3R,5S)-3-((R)-2-(2-benzyl-1,3-dioxolan-2-yl)-1-hydroxyethyl)-5-isobutylpyrrolidin-2-one
(6.54)

To a stirred solution of Tos Aminoidanol aux Azido acid (127.0 mg, 0.270 mmol) in dry CH_2Cl_2 was added 1M TiCl_4 (35.7 μl , 0.324 mmol) CH_2Cl_2 solution dropwise under argon at 0 $^\circ\text{C}$. The resulting solution was allowed to warm to 24 $^\circ\text{C}$ and stirred for another 15-20 mins. DIPEA (179 μl , 1.026 mmol) was added in a dropwise fashion to this solution at the same temperature, giving brown color solution. After stirring for additional 1 hr at 24 $^\circ\text{C}$, the resulting solution was taken in a syringe and was added very slowly using a syringe pump over 15mins into a solution of 2-(2-benzyl-1,3-dioxolan-2-yl)acetaldehyde (120 mg, 0.580 mmol) and TiCl_4 (8.93 μl , 0.081 mmol) at -78 $^\circ\text{C}$. The reaction mixture was stirred at -78 $^\circ\text{C}$ for 1hr and then quenched by addition of ammonium chloride solution. The layers were separated and the aqueous layer was washed with 10.0ml of DCM. Combined organic layers were washed with brine and then dried over magnesium sulfate to furnish crude aldol products. The crude products were separated using column chromatography (hexanes:EtoAc 7:3) The aldol product obtained were immediately cyclized using same procedure as in **6.47** $[\alpha]_{\text{D}}^{20} = -12.4$ (c 0.85, MeOH); ν_{max} (CHCl_3)/ cm^{-1}

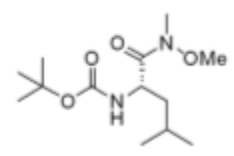
3222, 2929, 2954, 1689, 1454, 1269; ^1H NMR (500 MHz, CDCl_3) δ 7.47 – 7.18 (m, 6H), 6.54 (s, 1H), 4.37 (s, 1H), 4.14 (dd, $J = 9.3, 6.2$ Hz, 1H), 3.94 (s, 2H), 3.69 (dd, $J = 17.4, 6.6$ Hz, 3H), 3.02 (q, $J = 14.0$ Hz, 2H), 2.51 (dd, $J = 15.8, 6.8$ Hz, 1H), 2.21 – 2.02 (m, 2H), 1.88 – 1.77 (m, 2H), 1.70 – 1.56 (m, 1H), 1.46 – 1.36 (m, 1H), 1.35 – 1.22 (m, 2H), 0.93 (d, $J = 6.5$ Hz, 6H). ^{13}C NMR (126 MHz, CDCl_3) δ 178.36, 136.32, 130.75, 127.94, 126.42, 111.19, 77.31, 77.05, 76.80, 69.38, 65.32, 64.94, 50.83, 46.09, 45.22, 43.99, 41.46, 30.98, 25.26, 22.97, 22.23. HRMS (ESI^+) Calc. for $\text{C}_{18}\text{H}_{26}\text{NO}_3\text{Na}$ 370.1994; Found 370.2002.

(3R,5S)-3-((R)-1-hydroxy-3-oxo-4-phenylbutyl)-5-isobutylpyrrolidin-2-one (6.55)

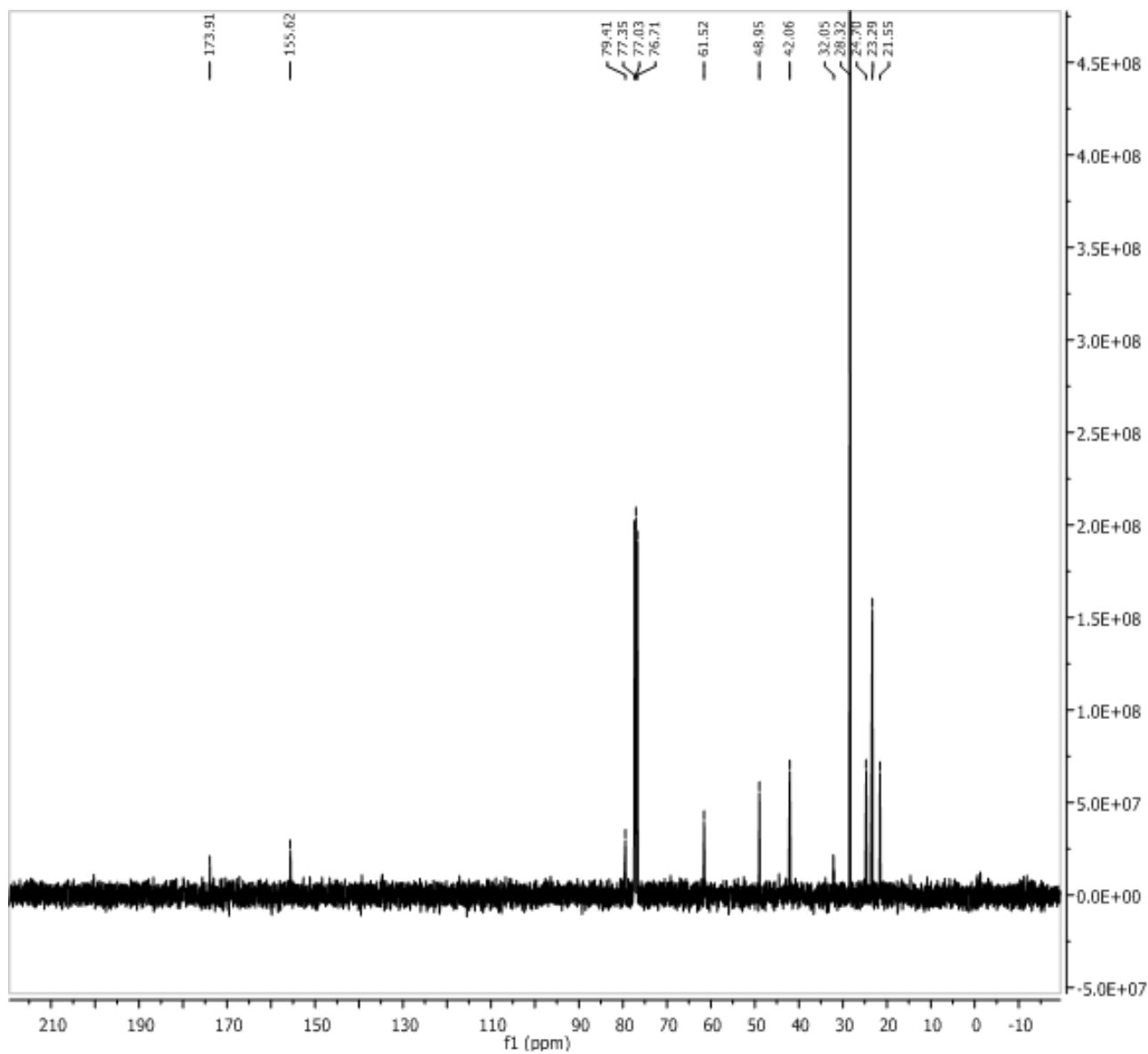
$[\alpha]_{\text{D}}^{20} = -40.1$ (c 0.5, MeOH) ^1H NMR (500 MHz, CDCl_3) δ 7.36 (d, $J = 7.1$ Hz, 1H), 7.35 – 7.27 (m, 3H), 7.23 (d, $J = 7.1$ Hz, 2H), 6.20 (s, 1H), 4.22 (s, 1H), 3.82 (s, 2H), 3.68 (s, 1H), 2.86 (dd, $J = 16.2, 8.5$ Hz, 1H), 2.74 – 2.64 (m, 1H), 2.51 (d, $J = 7.8$ Hz, 2H), 2.13 – 2.02 (m, 1H), 1.85 (d, $J = 9.4$ Hz, 1H), 1.69 – 1.56 (m, 1H), 1.47 – 1.37 (m, 1H), 1.30 (dd, $J = 14.9, 8.7$ Hz, 2H), 0.94 (d, $J = 6.6$ Hz, 6H). ^{13}C NMR (126 MHz, CDCl_3) δ 208.05, 178.52, 133.99, 129.80, 128.81, 127.03, 69.86, 51.34, 51.06, 46.32, 45.73, 45.39, 44.18, 30.76, 25.31, 23.11, 22.12. HRMS (ESI^+) Calc. for $\text{C}_{18}\text{H}_{26}\text{NO}_3\text{Na}$ 326.1732; Found 326.1726.



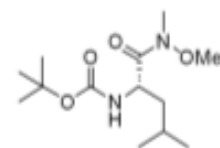
Parameter	Value
1 Spectrometer	spect
2 Solvent	CDCl3
3 Temperature	300.2
4 Pulse Sequence	zg30
5 Experiment	1D
6 Number of Scans	8
7 Receiver Gain	114
8 Relaxation Delay	1.0000
9 Pulse Width	10.0000
10 Spectrometer Frequency	400.15
11 Spectral Width	8223.7
12 Lowest Frequency	-1640.8
13 Nucleus	1H
14 Acquired Size	32768
15 Spectral Size	32768



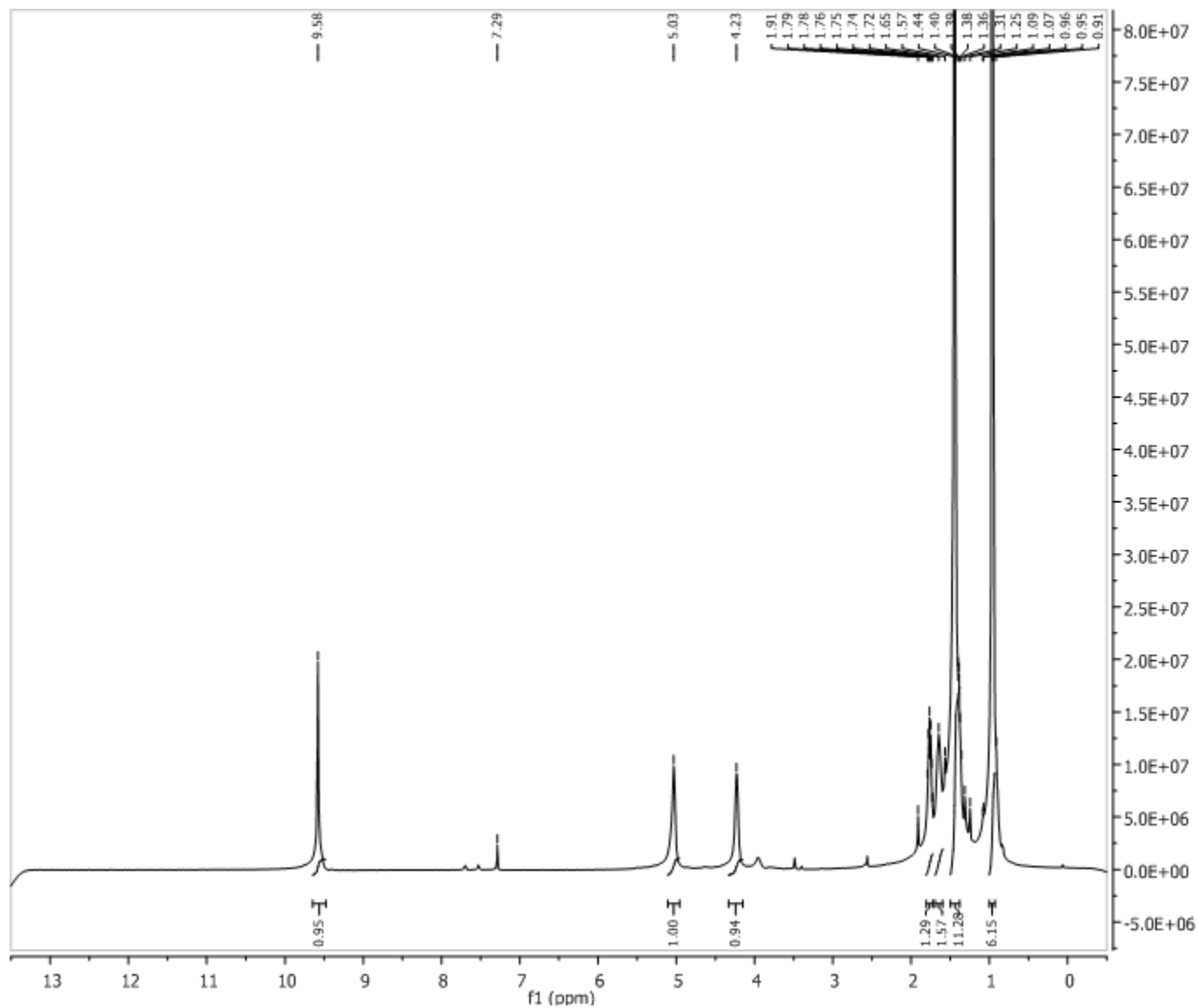
Weinreb Amide



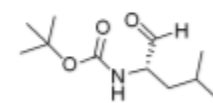
Parameter	Value
1 Spectrometer	spect
2 Solvent	CDCl3
3 Temperature	300.2
4 Pulse Sequence	zgpg30
5 Experiment	1D
6 Number of Scans	250
7 Receiver Gain	32800
8 Relaxation Delay	2.0000
9 Pulse Width	9.0000
10 Spectrometer Frequency	100.62
11 Spectral Width	24038.5
12 Lowest Frequency	-1957.9
13 Nucleus	13C
14 Acquired Size	32768
15 Spectral Size	32768



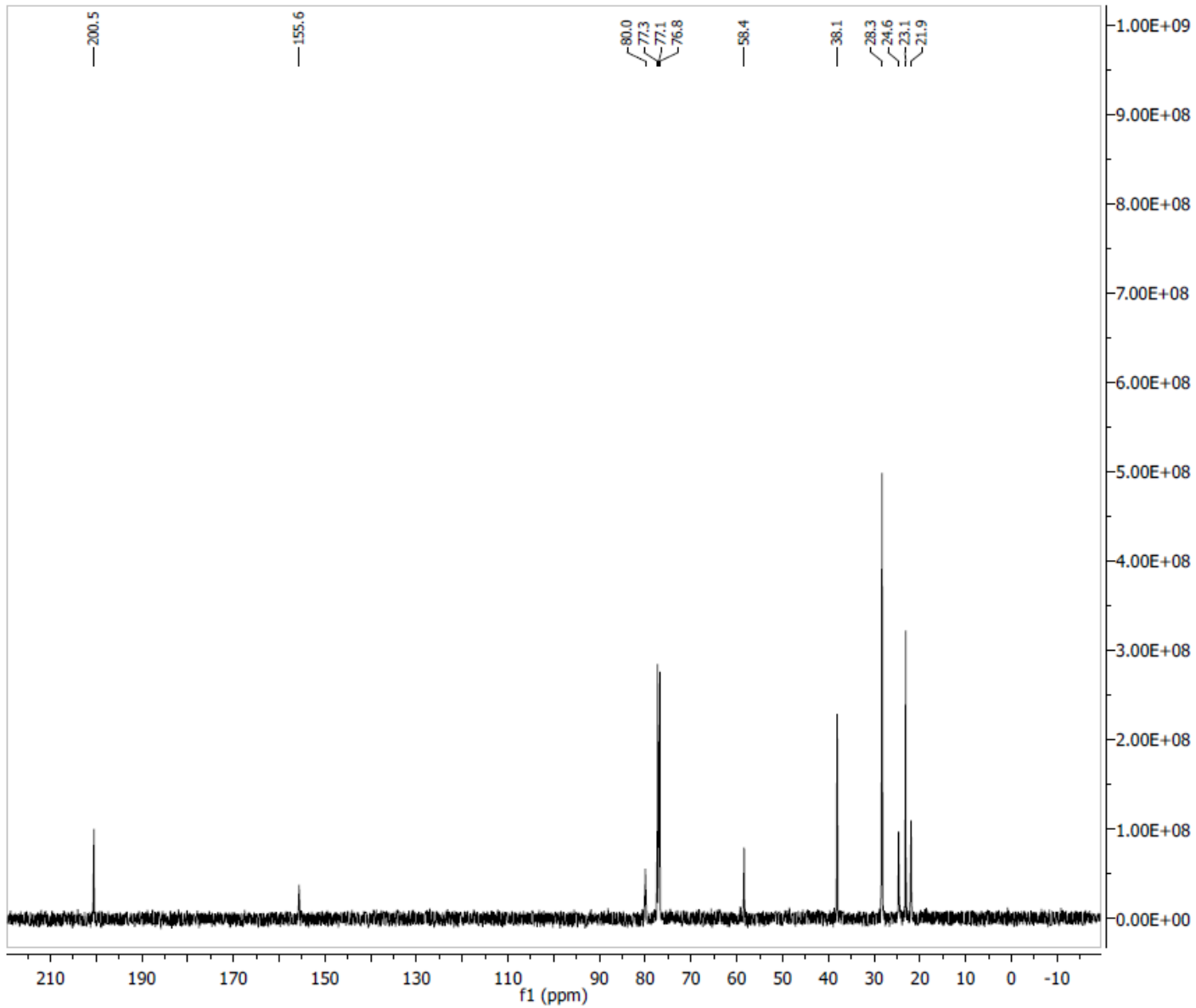
Weinreb
Amide



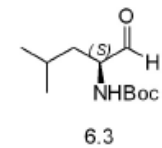
Parameter	Value
1 Spectrometer	spect
2 Solvent	CDCl3
3 Temperature	296.2
4 Pulse Sequence	zg30
5 Experiment	1D
6 Number of Scans	16
7 Receiver Gain	90
8 Relaxation Delay	1.0000
9 Pulse Width	11.0000
10 Spectrometer Frequency	500.13
11 Spectral Width	7002.8
12 Lowest Frequency	-250.6
13 Nucleus	1H
14 Acquired Size	8192
15 Spectral Size	16384

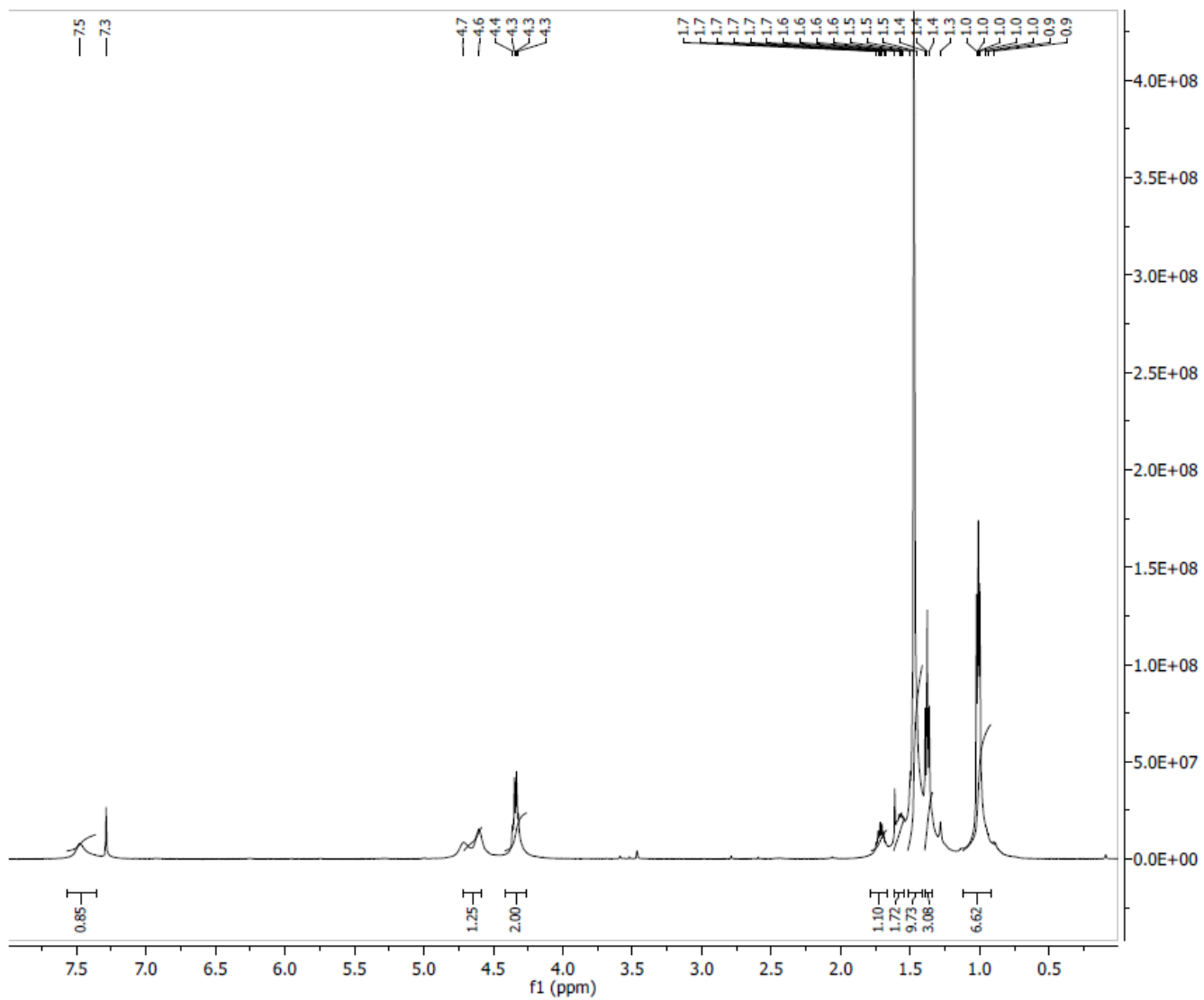


6.3

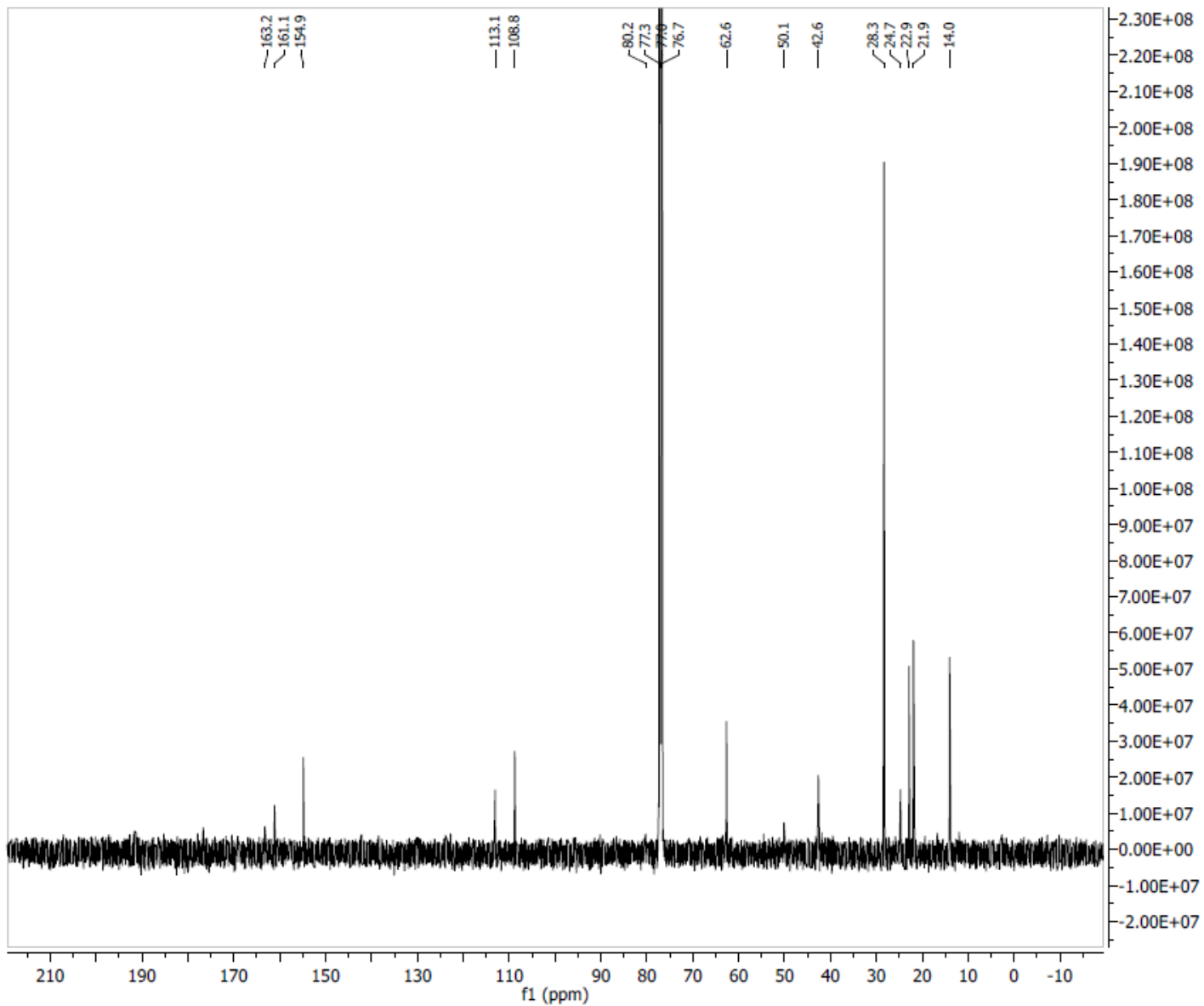


Parameter	Value
1 Spectrometer	spect
2 Solvent	CDCl3
3 Temperature	296.2
4 Pulse Sequence	zgpg30
5 Experiment	1D
6 Number of Scans	301
7 Receiver Gain	11585
8 Relaxation Delay	2.0000
9 Pulse Width	9.5000
10 Acquisition Time	1.0912
11 Spectrometer Frequency	125.76
12 Spectral Width	30030.0
13 Lowest Frequency	-2439.7
14 Nucleus	13C
15 Acquired Size	32768
16 Spectral Size	32768

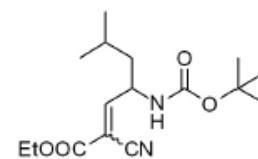




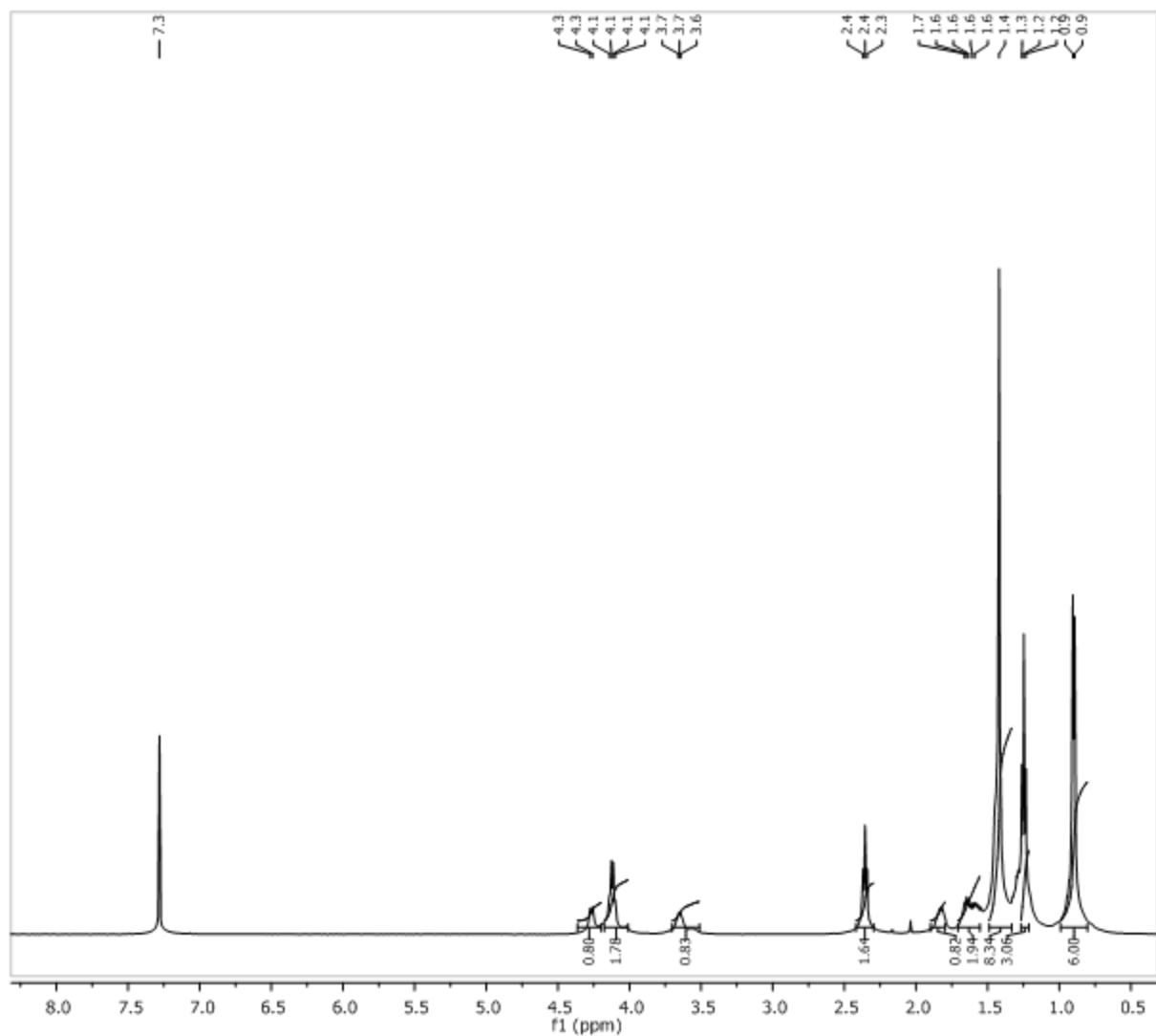
Parameter	Value
1 Spectrometer	spect
2 Solvent	CDCl3
3 Temperature	303.2
4 Pulse Sequence	zg30
5 Experiment	1D
6 Number of Scans	32
7 Receiver Gain	362
8 Relaxation Delay	1.0000
9 Pulse Width	11.0000
10 Acquisition Time	1.1699
11 Spectrometer Frequency	500.13
12 Spectral Width	7002.8
13 Lowest Frequency	-250.6
14 Nucleus	1H
15 Acquired Size	8192
16 Spectral Size	16384



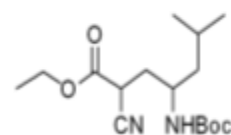
Parameter	Value
1 Spectrometer	spect
2 Solvent	CDCI3
3 Temperature	303.2
4 Pulse Sequence	zgpg30
5 Experiment	1D
6 Number of Scans	2048
7 Receiver Gain	9195
8 Relaxation Delay	3.0000
9 Pulse Width	9.5000
10 Acquisition Time	1.0912
11 Spectrometer Frequency	125.76
12 Spectral Width	30030.0
13 Lowest Frequency	-2439.7
14 Nucleus	13C
15 Acquired Size	32768
16 Spectral Size	32768



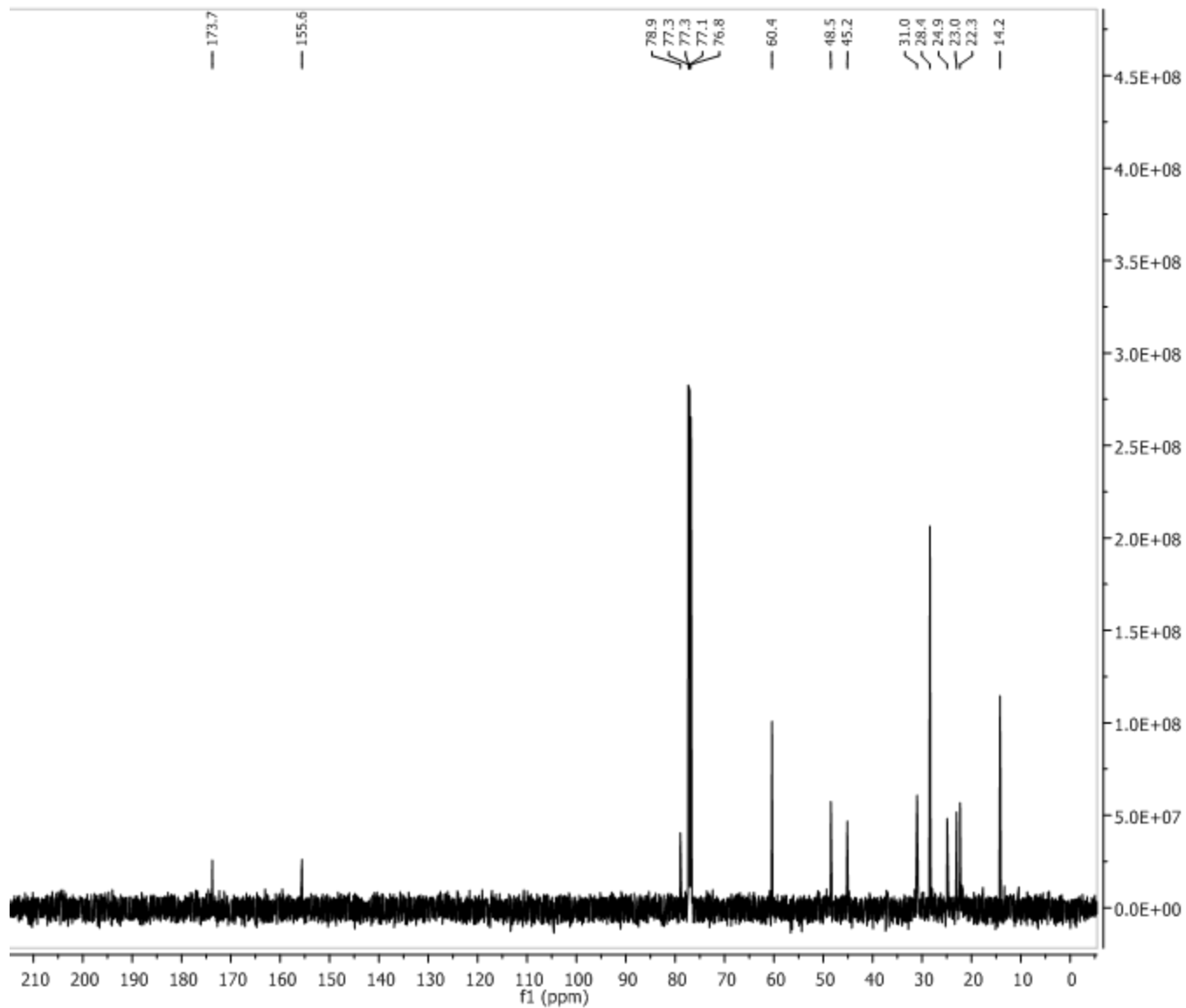
6.7



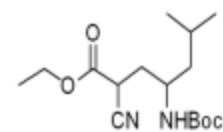
Parameter	Value
1 Spectrometer	spect
2 Solvent	CDCl3
3 Temperature	293.2
4 Pulse Sequence	zg30
5 Experiment	1D
6 Number of Scans	8
7 Receiver Gain	114
8 Relaxation Delay	1.0000
9 Pulse Width	11.0000
10 Acquisition Time	1.1698
11 Spectrometer Frequency	500.13
12 Spectral Width	7002.8
13 Lowest Frequency	-250.6
14 Nucleus	1H
15 Acquired Size	8192
16 Spectral Size	16384



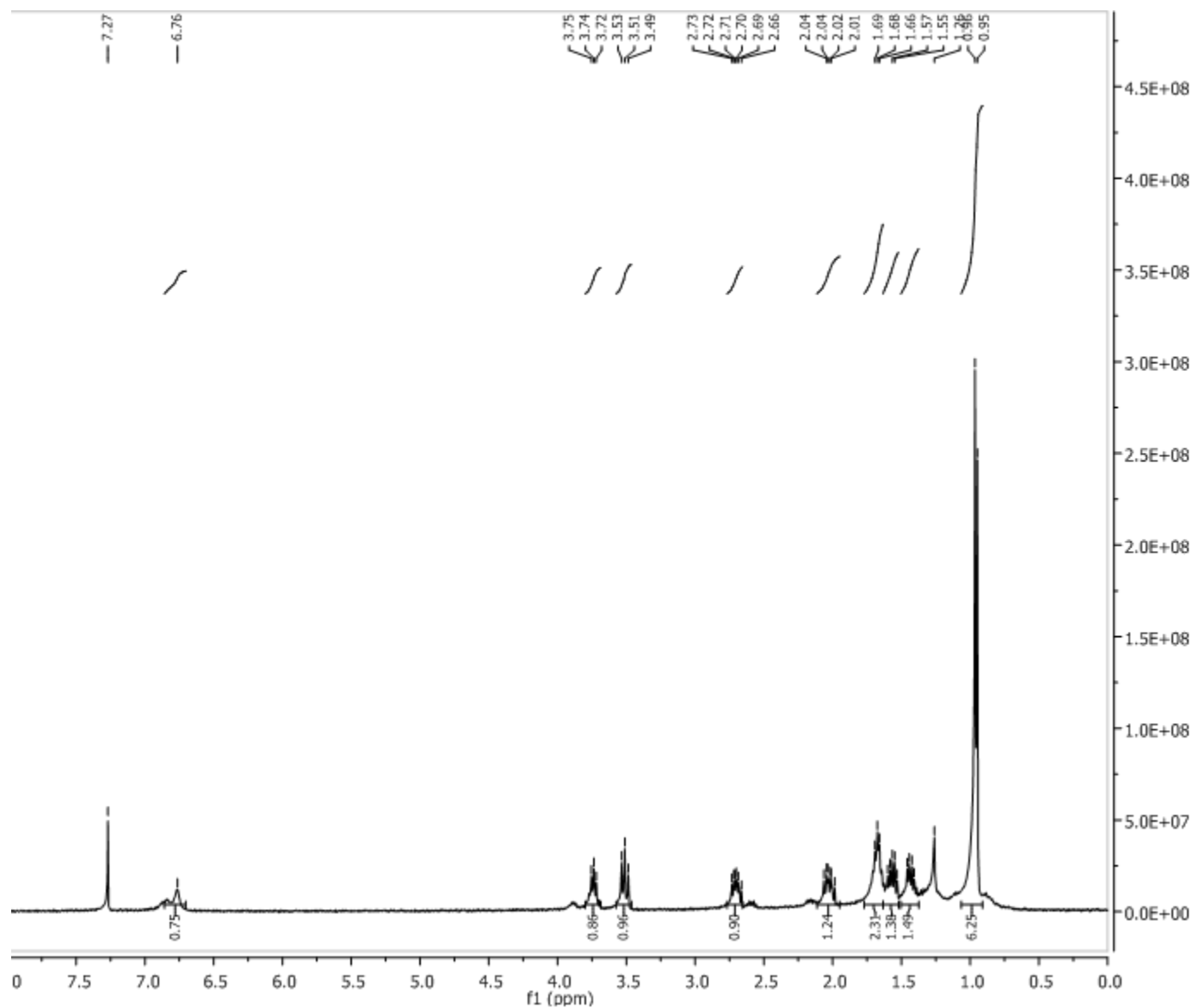
6.8
(racemic)



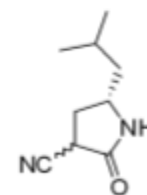
Parameter	Value
1 Spectrometer	spect
2 Solvent	CDCl3
3 Temperature	293.2
4 Pulse Sequence	zgpg30
5 Experiment	1D
6 Number of Scans	152
7 Receiver Gain	9195
8 Relaxation Delay	3.0000
9 Pulse Width	9.5000
10 Acquisition Time	1.1796
11 Spectrometer Frequency	125.76
12 Spectral Width	27777.8
13 Lowest Frequency	-683.9
14 Nucleus	13C
15 Acquired Size	32768
16 Spectral Size	32768



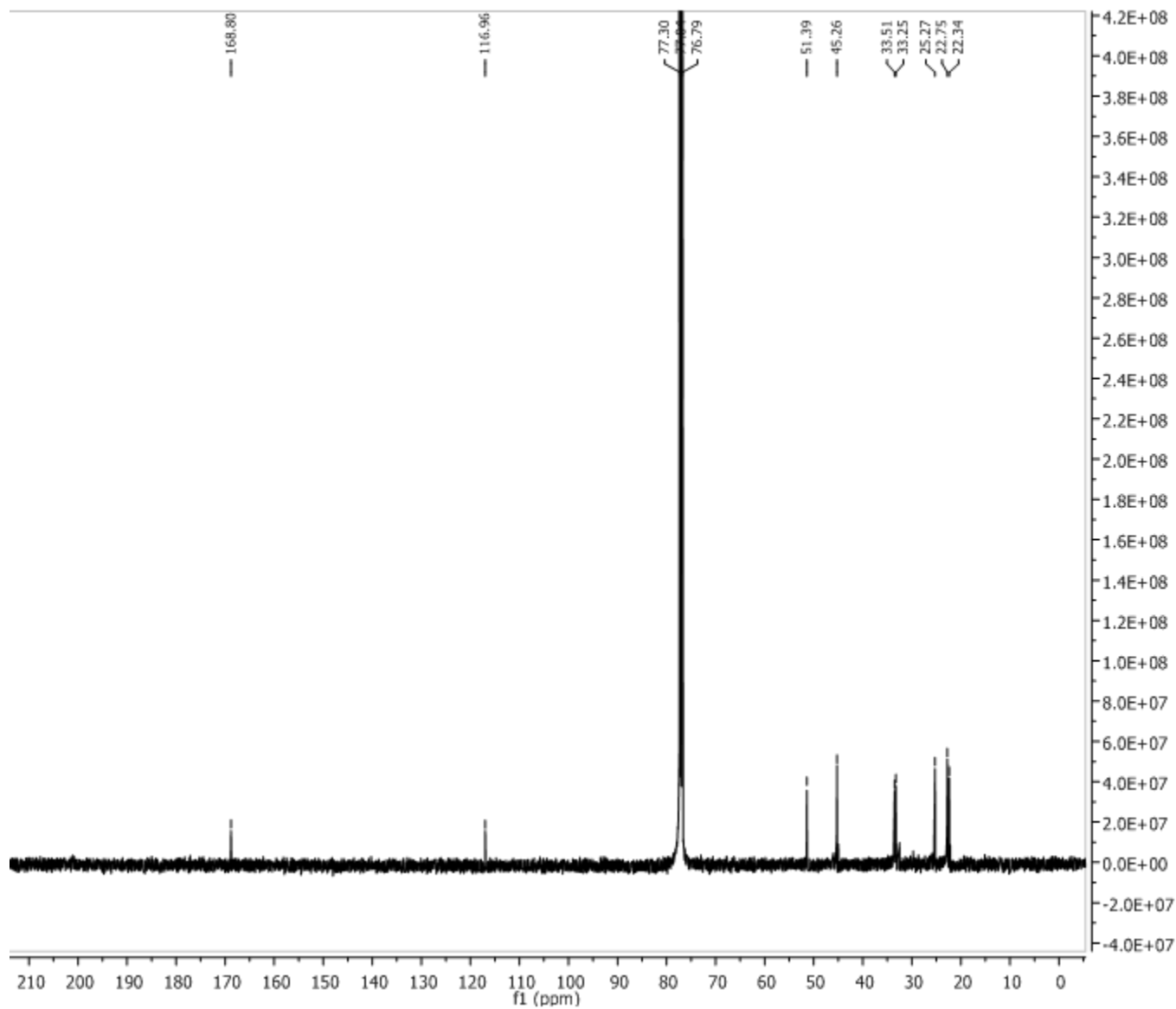
6.8



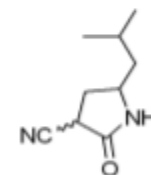
Parameter	Value
1 Spectrometer	spect
2 Solvent	CDCl3
3 Temperature	298.2
4 Pulse Sequence	zg30
5 Experiment	1D
6 Number of Scans	8
7 Receiver Gain	575
8 Relaxation Delay	1.0000
9 Pulse Width	10.0000
10 Spectrometer	400.15
Frequency	
11 Spectral Width	8223.7
12 Lowest	-1640.8
Frequency	
13 Nucleus	1H
14 Acquired Size	32768
15 Spectral Size	32768



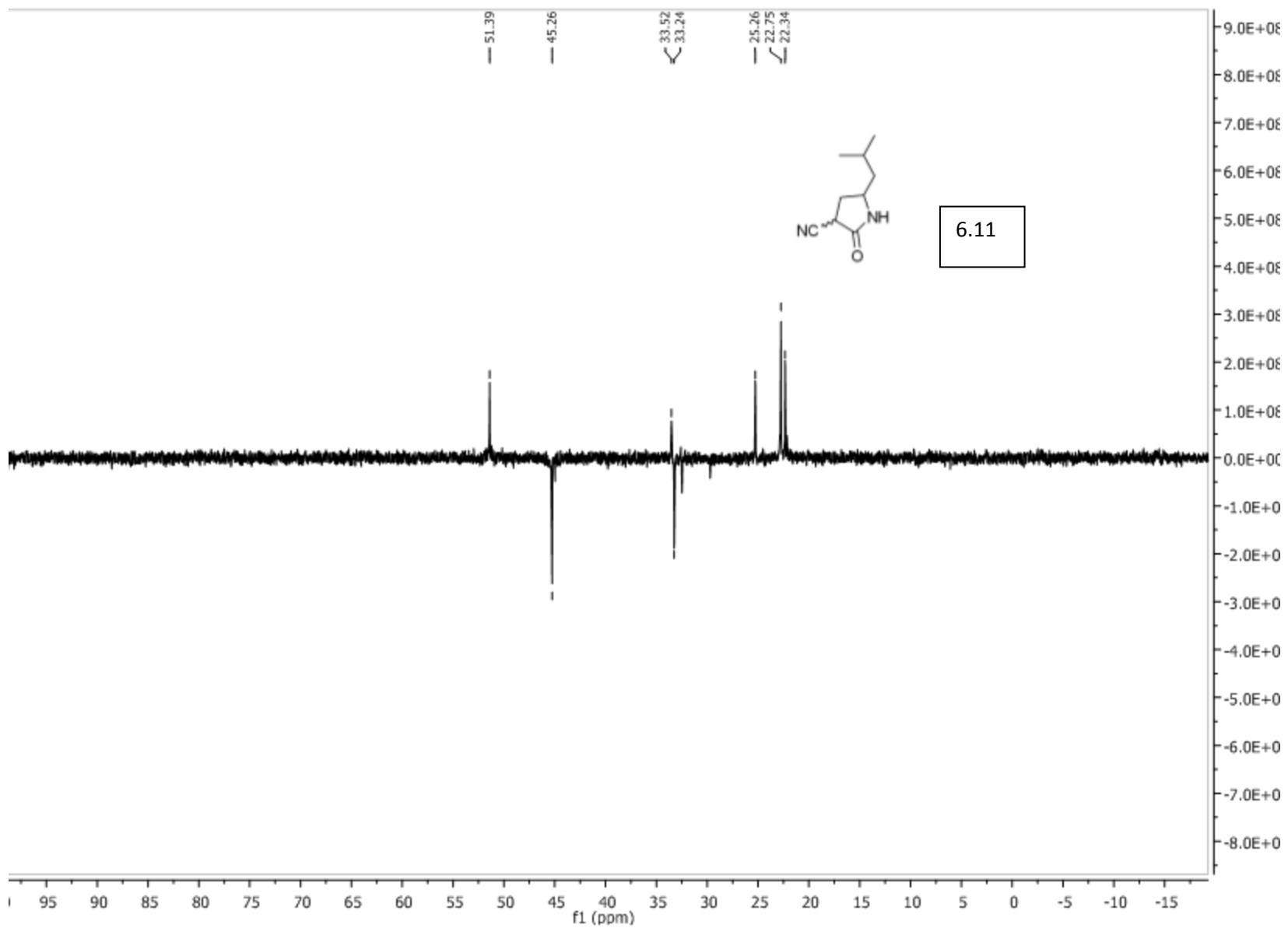
6.11
(racemic)

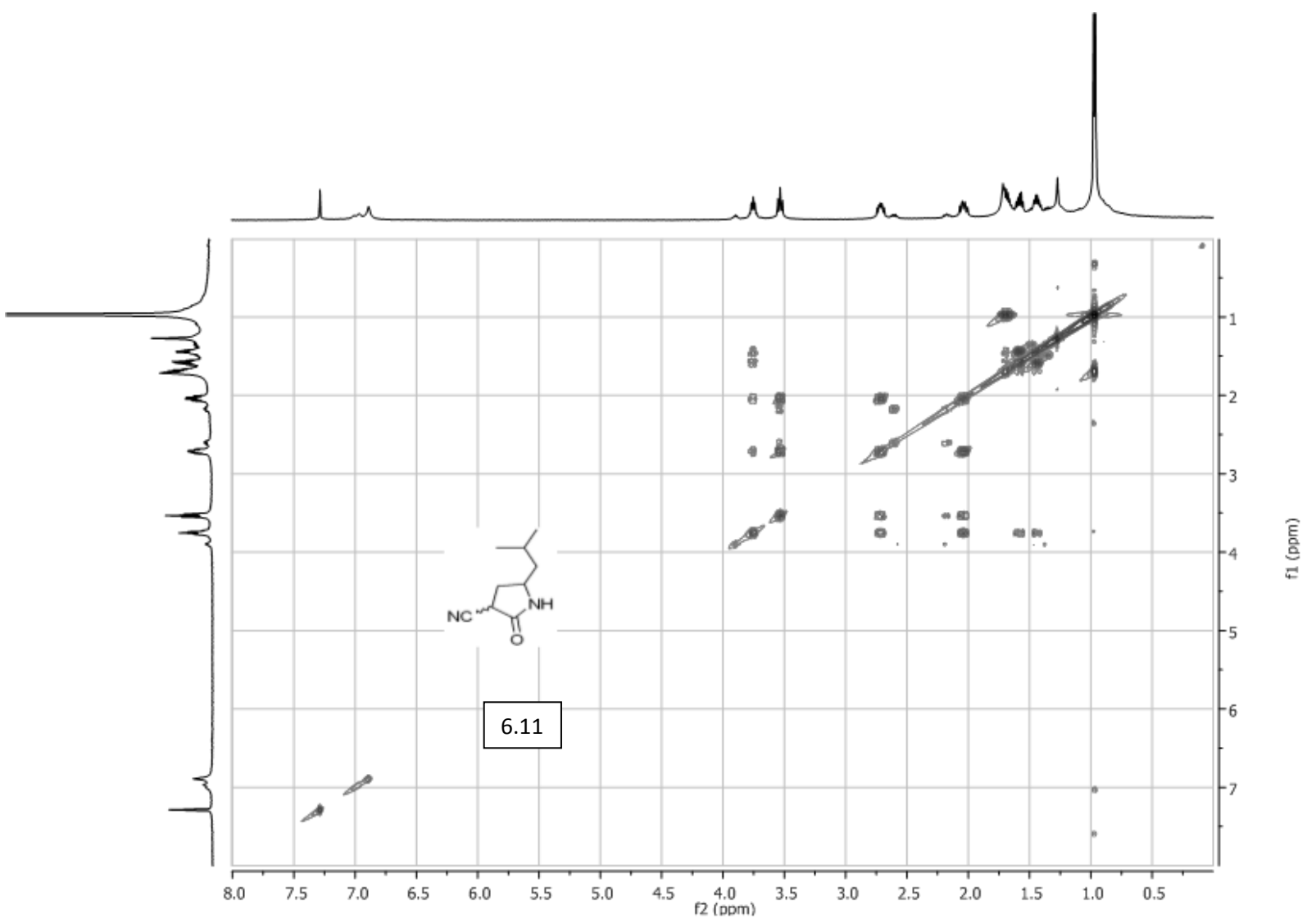


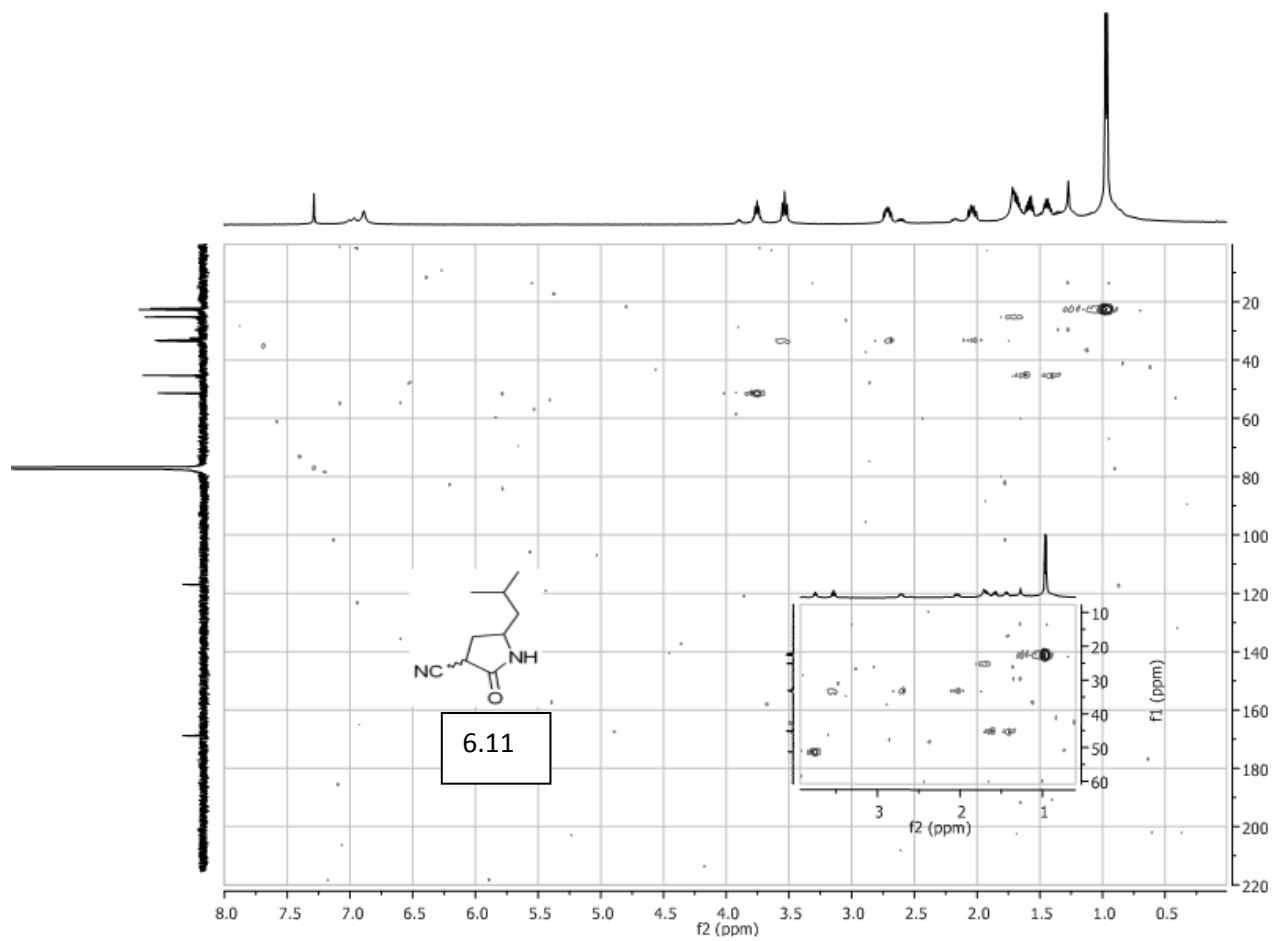
Parameter	Value
1 Spectrometer	spect
2 Solvent	CDCl3
3 Temperature	295.2
4 Pulse Sequence	zgpg30
5 Experiment	1D
6 Number of Scans	7200
7 Receiver Gain	10321
8 Relaxation Delay	3.0000
9 Pulse Width	9.5000
10 Spectrometer Frequency	125.76
11 Spectral Width	27777.8
12 Lowest Frequency	-683.9
13 Nucleus	13C
14 Acquired Size	32768
15 Spectral Size	32768



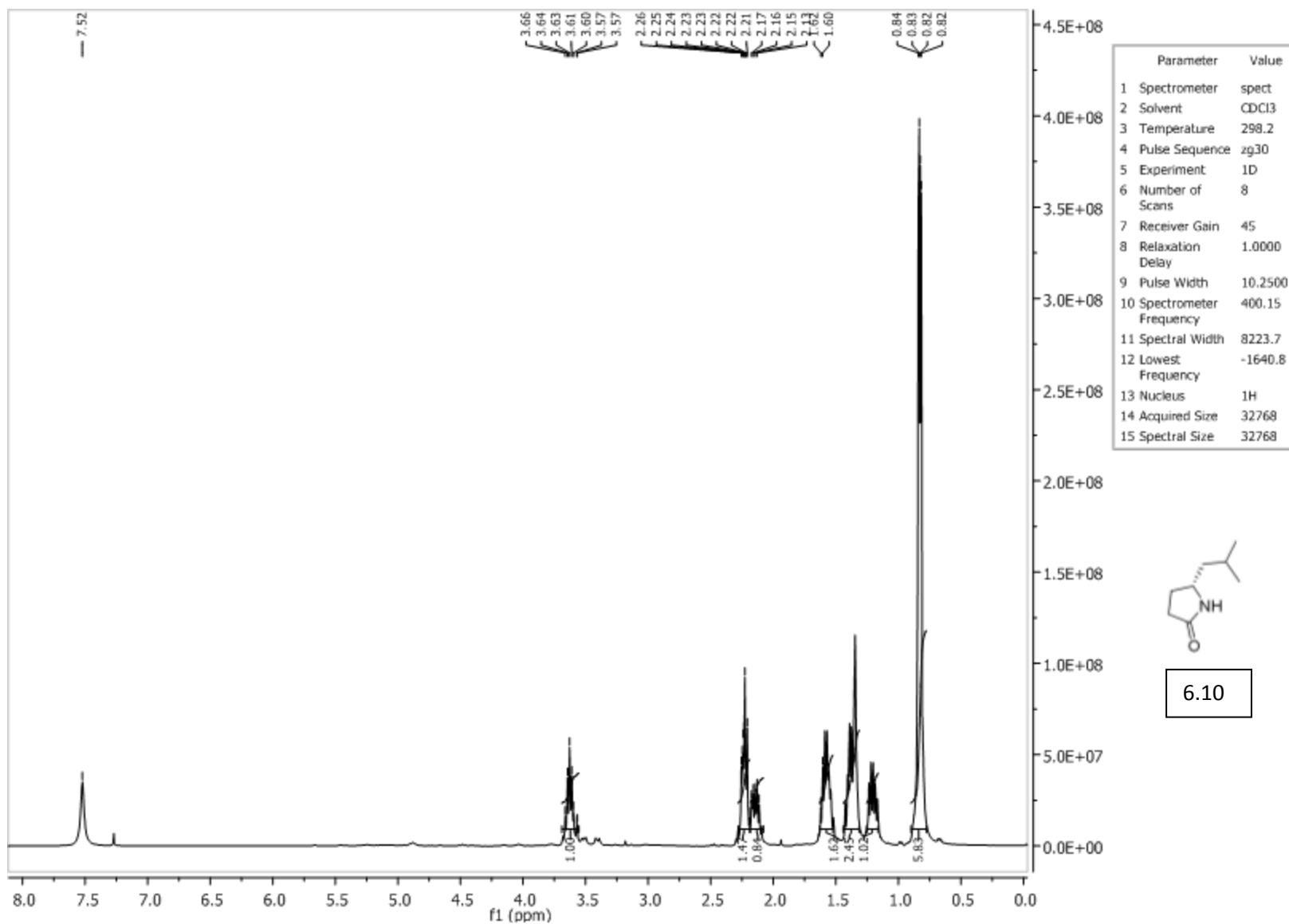
6.11

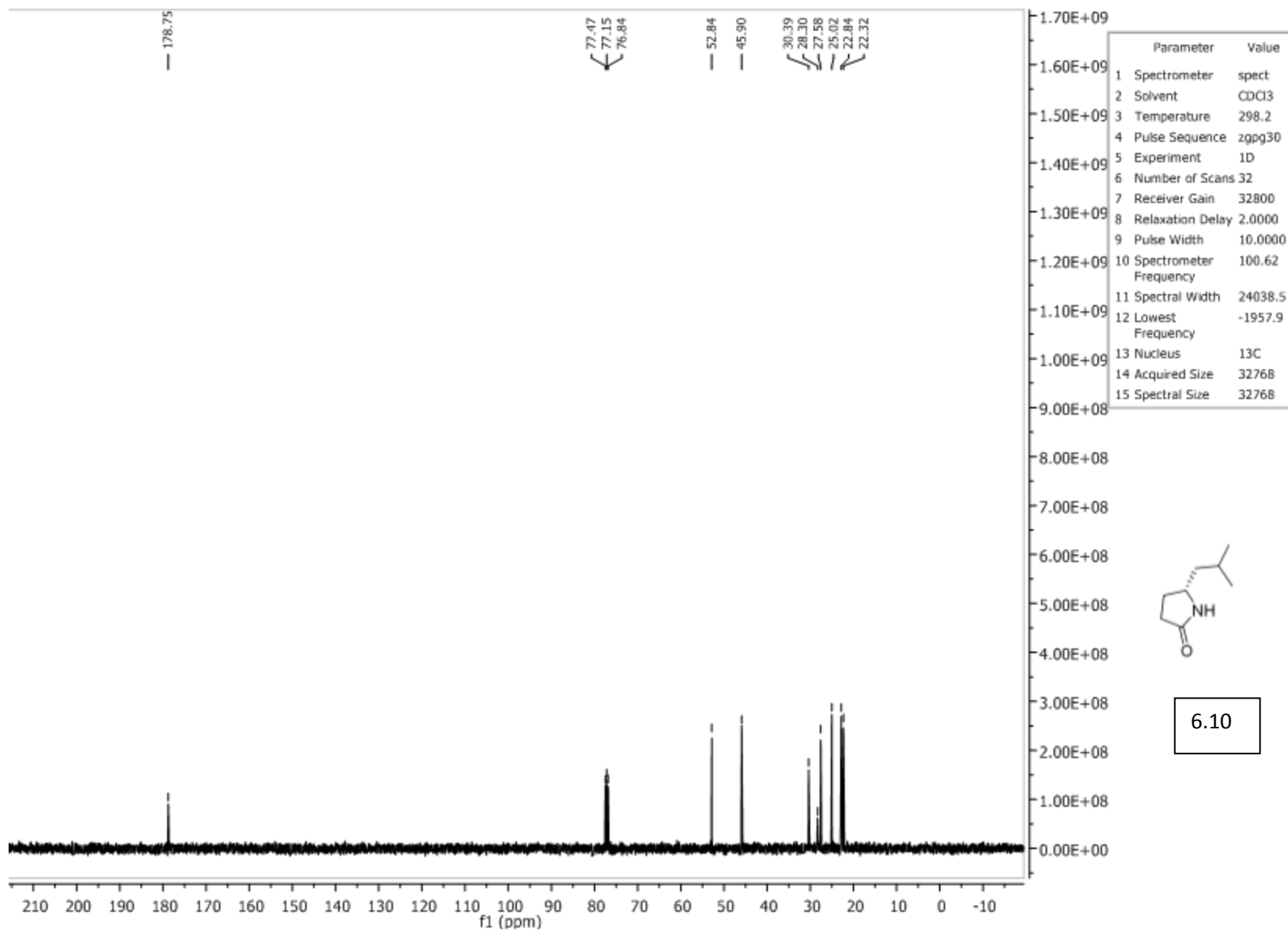


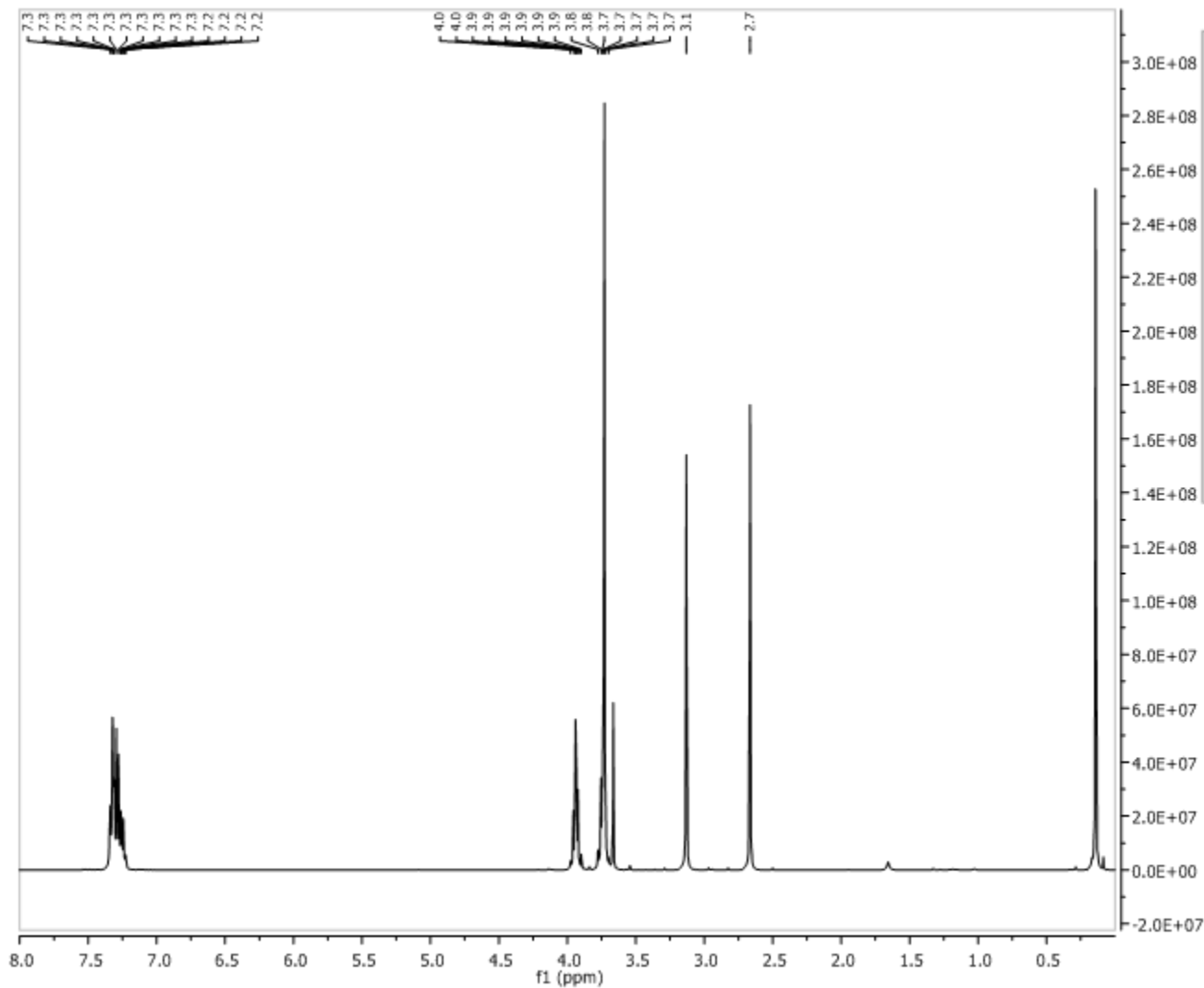




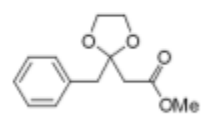
HMQC



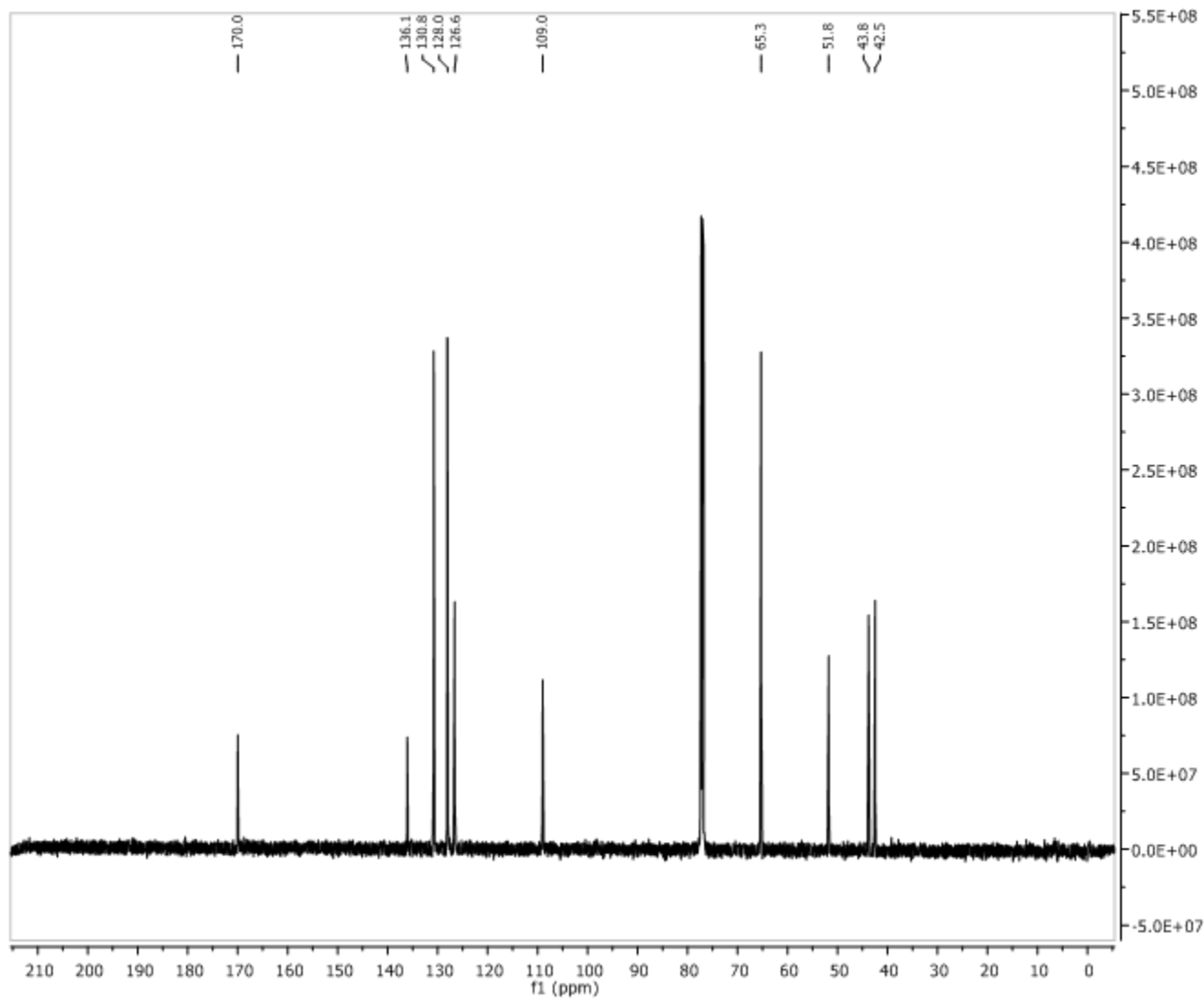




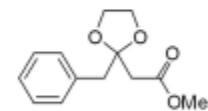
Parameter	Value
1 Data File Name	D:/ 122109/ 1/ pdata/ 1/ 1r
2 Spectrometer	spect
3 Solvent	CDCl3
4 Temperature	298.2
5 Pulse Sequence	zg30
6 Experiment	1D
7 Number of Scans	8
8 Receiver Gain	90
9 Relaxation Delay	1.0000
10 Pulse Width	11.5000
11 Acquisition Time	5.1118
12 Spectrometer Frequency	400.17
13 Spectral Width	6410.3
14 Lowest Frequency	-733.9
15 Nucleus	1H
16 Acquired Size	32768
17 Spectral Size	32768



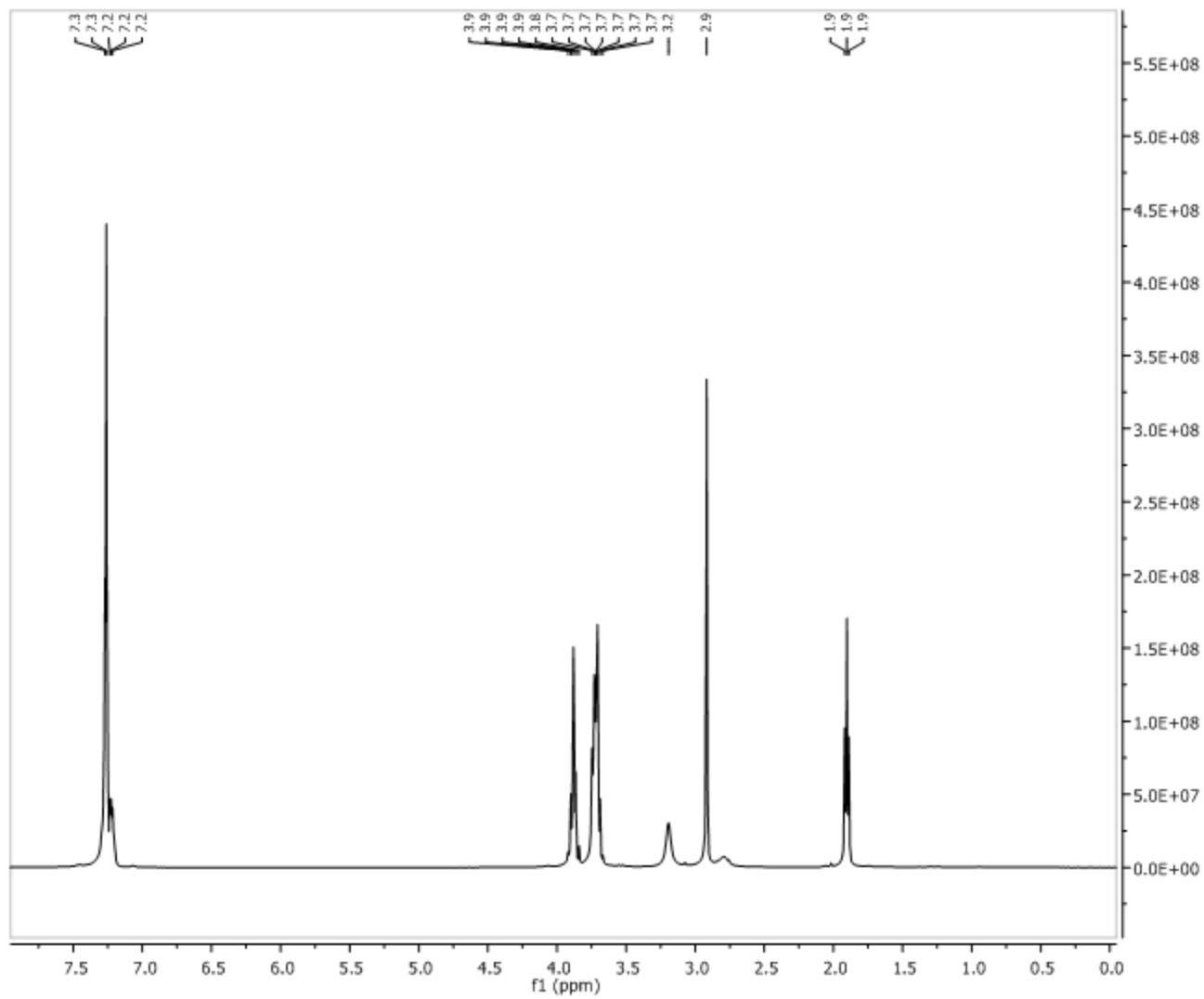
6.25



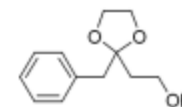
Parameter	Value
1 Spectrometer	spect
2 Solvent	CDCl3
3 Temperature	298.2
4 Pulse Sequence	zgpg30
5 Experiment	1D
6 Number of Scans	2000
7 Receiver Gain	6502
8 Relaxation Delay	3.0000
9 Pulse Width	9.5000
10 Acquisition Time	1.1797
11 Spectrometer Frequency	125.76
12 Spectral Width	27777.8
13 Lowest Frequency	-683.9
14 Nucleus	13C
15 Acquired Size	32768
16 Spectral Size	32768



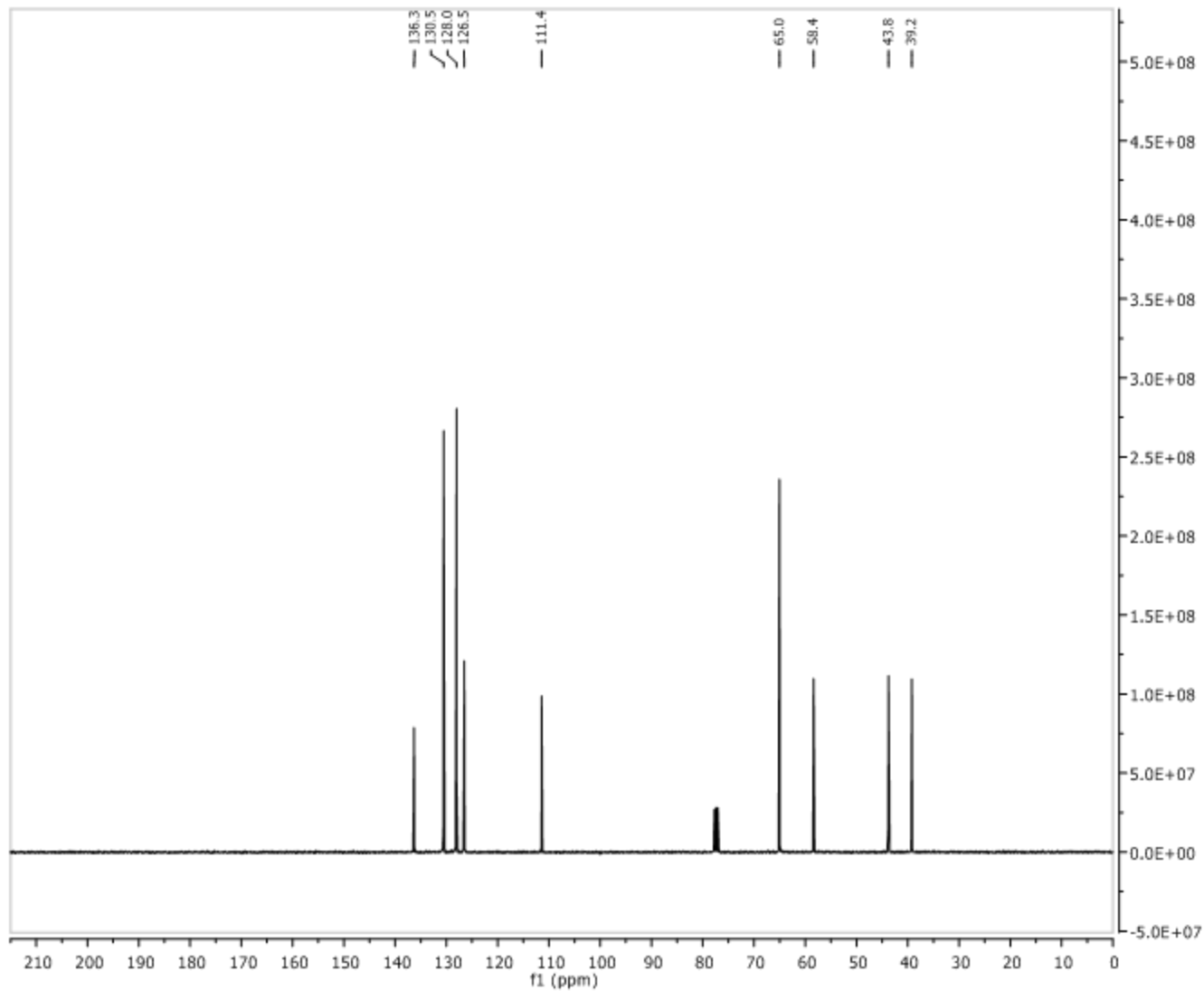
6.25



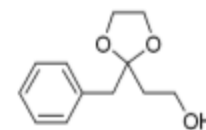
Parameter	Value
1 Spectrometer	spect
2 Solvent	CDCl3
3 Temperature	298.2
4 Pulse Sequence	zg30
5 Experiment	1D
6 Number of Scans	4
7 Receiver Gain	20
8 Relaxation Delay	1.0000
9 Pulse Width	10.0000
10 Acquisition Time	3.9846
11 Spectrometer Frequency	400.15
12 Spectral Width	8223.7
13 Lowest Frequency	-1632.3
14 Nucleus	1H
15 Acquired Size	32768
16 Spectral Size	32768



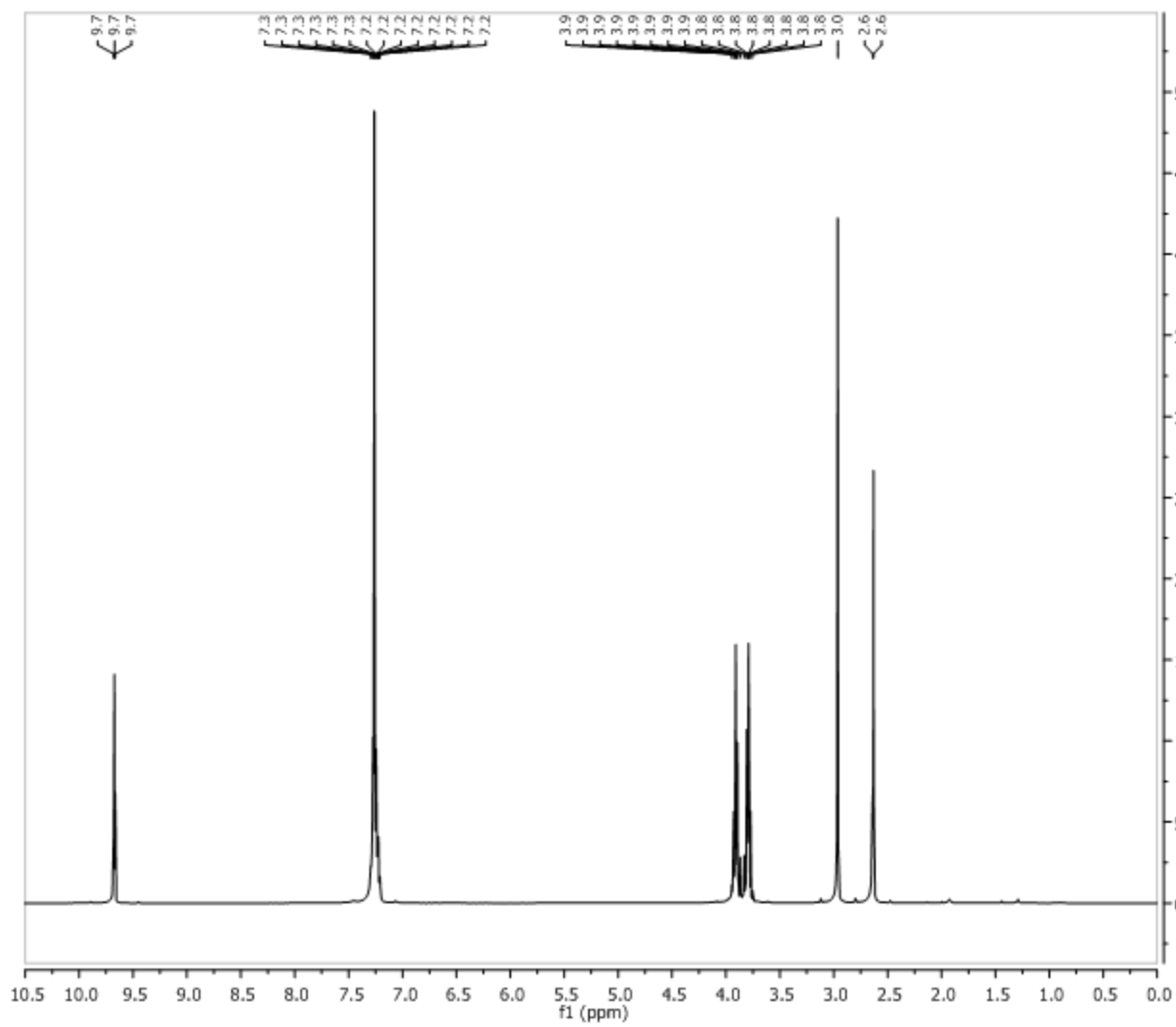
6.26



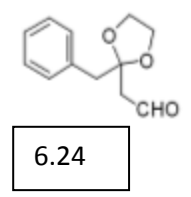
Parameter	Value
1 Spectrometer	spect
2 Solvent	CDCl3
3 Temperature	298.2
4 Pulse Sequence	zgpg30
5 Experiment	1D
6 Number of Scans	512
7 Receiver Gain	32800
8 Relaxation Delay	2.0000
9 Pulse Width	11.1250
10 Acquisition Time	1.3631
11 Spectrometer Frequency	100.62
12 Spectral Width	24038.5
13 Lowest Frequency	-1957.9
14 Nucleus	13C
15 Acquired Size	32768
16 Spectral Size	32768

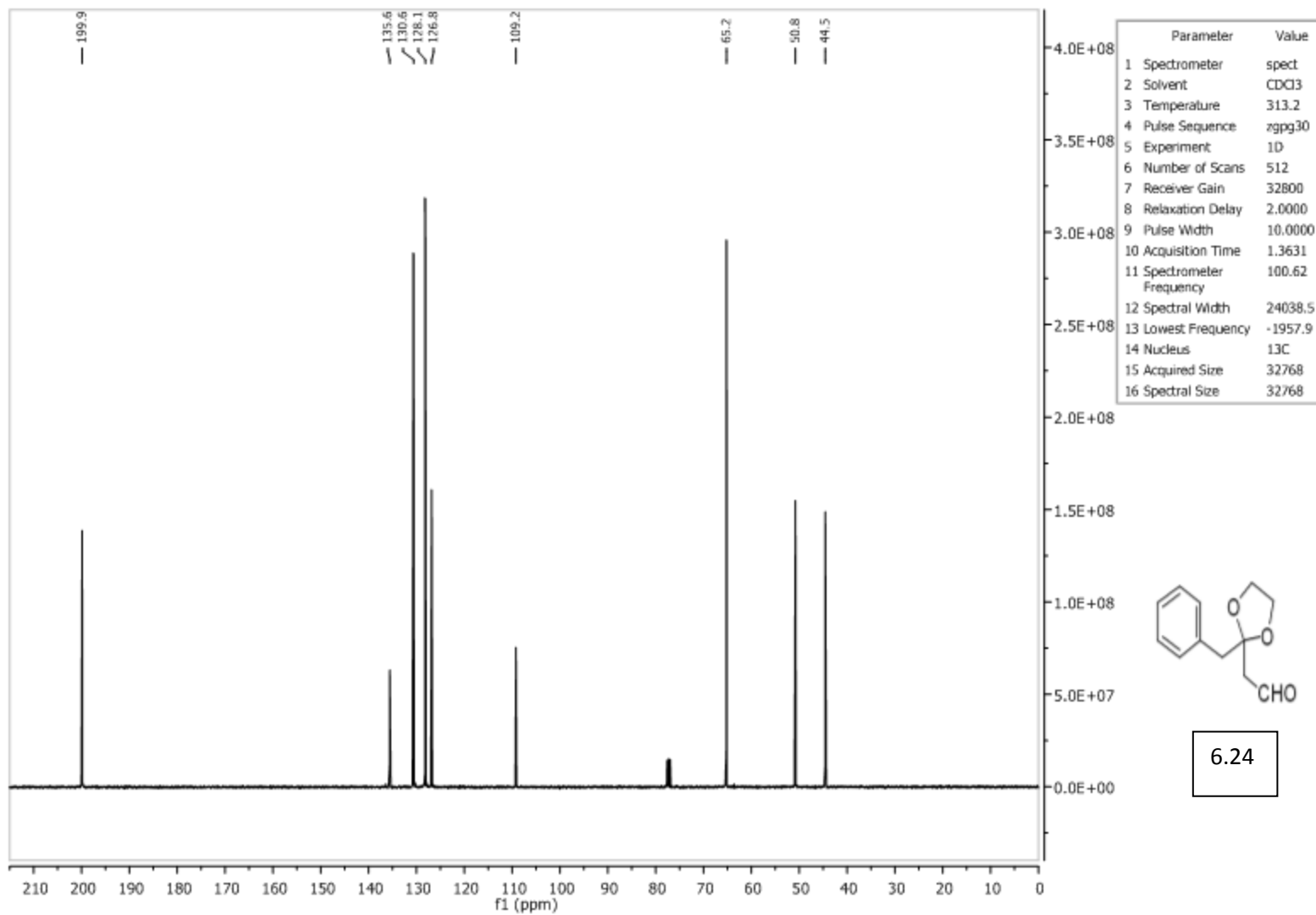


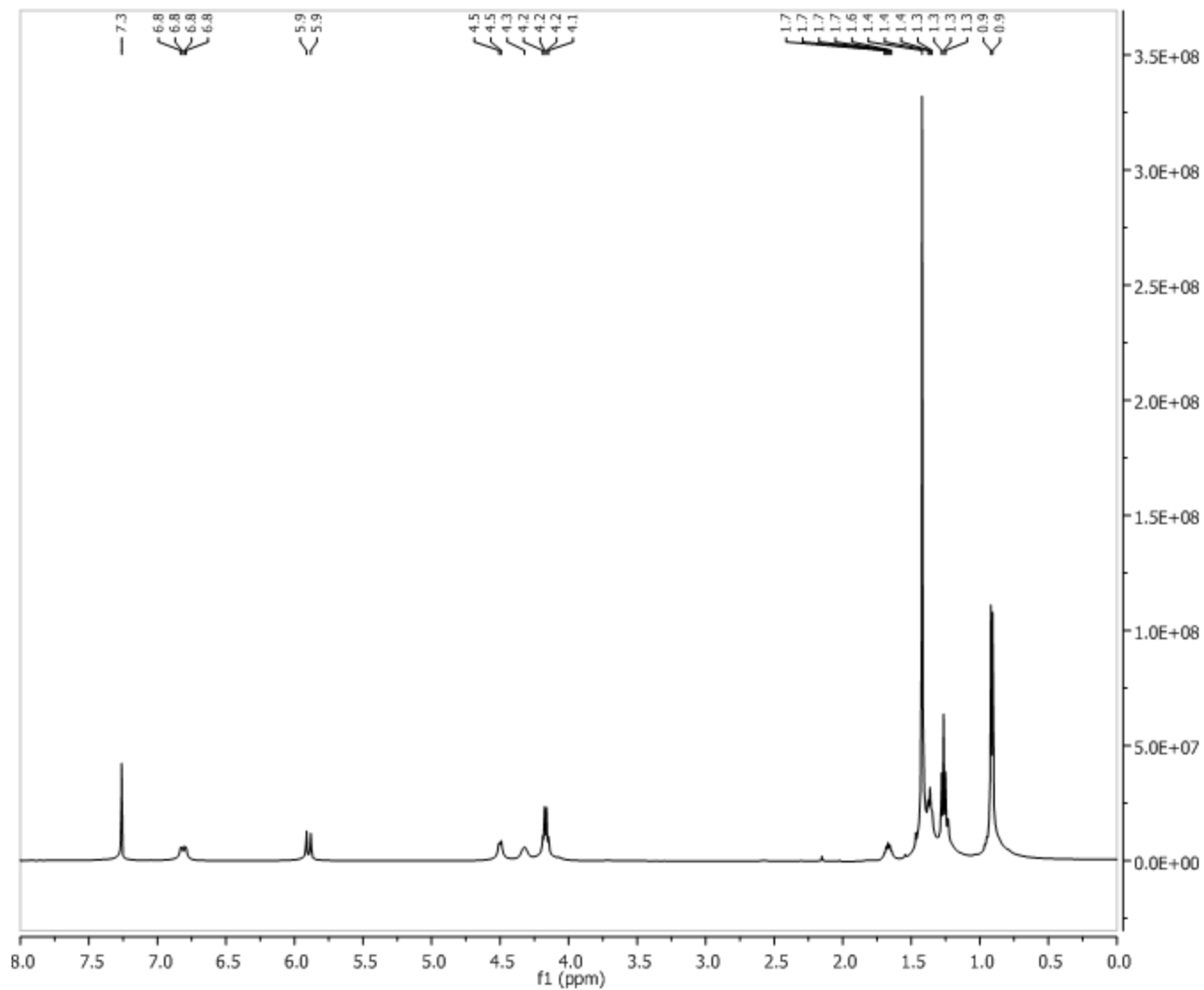
6.26



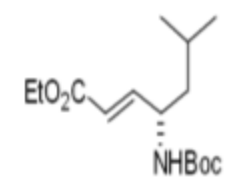
Parameter	Value
1 Spectrometer	spect
2 Solvent	CDCl3
3 Temperature	313.2
4 Pulse Sequence	zg30
5 Experiment	1D
6 Number of Scans	4
7 Receiver Gain	45
8 Relaxation Delay	1.0000
9 Pulse Width	10.2500
10 Acquisition Time	3.9846
11 Spectrometer Frequency	400.15
12 Spectral Width	8223.7
13 Lowest Frequency	-1640.0
14 Nucleus	1H
15 Acquired Size	32768
16 Spectral Size	32768



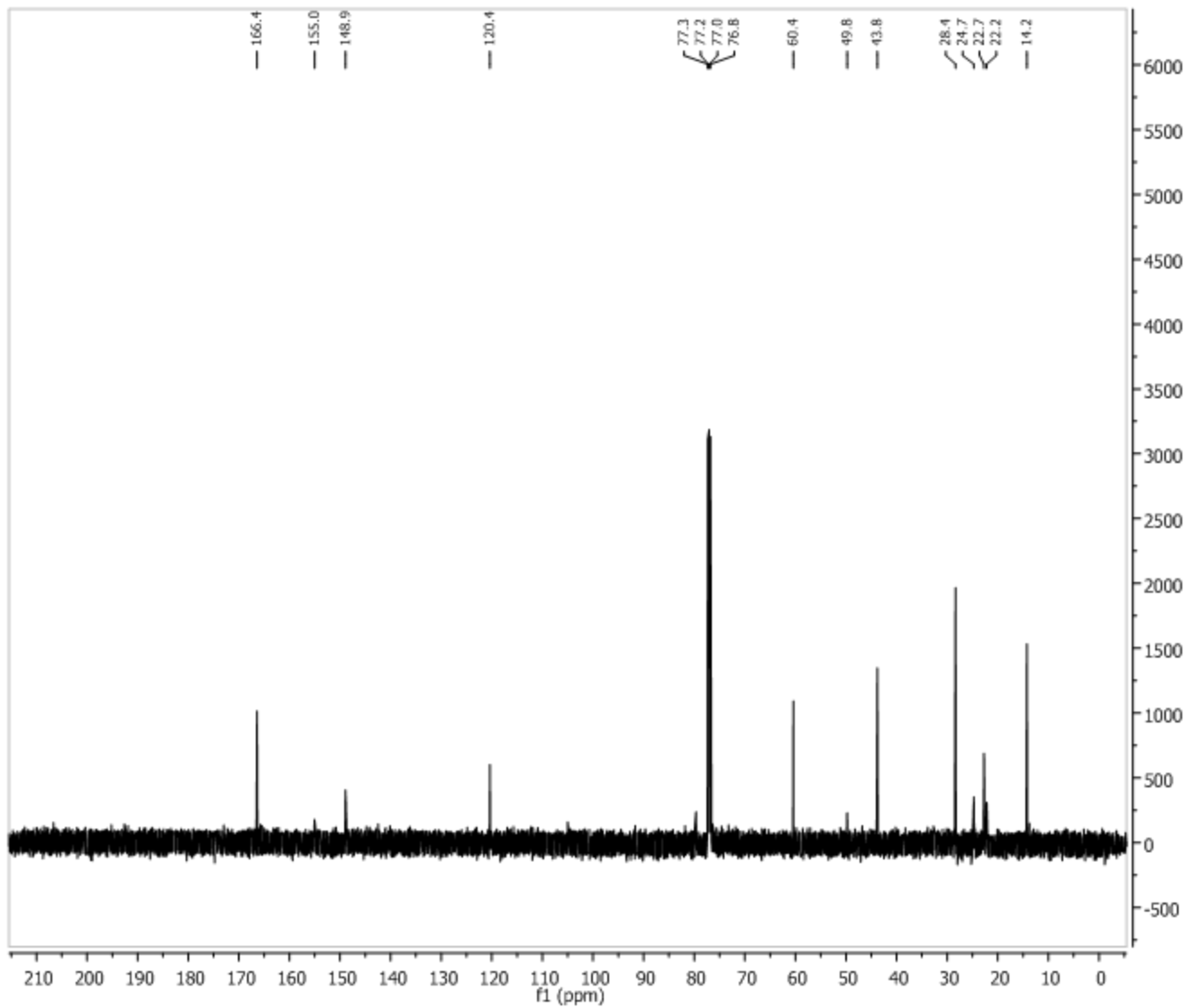




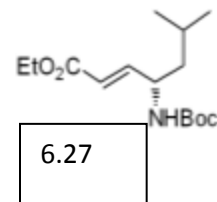
Parameter	Value
1 Spectrometer	spect
2 Solvent	CDCl3
3 Temperature	293.2
4 Pulse Sequence	zg30
5 Experiment	1D
6 Number of Scans	16
7 Receiver Gain	144
8 Relaxation Delay	1.0000
9 Pulse Width	11.0000
10 Acquisition Time	1.1698
11 Spectrometer Frequency	500.13
12 Spectral Width	7002.8
13 Lowest Frequency	-264.1
14 Nucleus	1H
15 Acquired Size	8192
16 Spectral Size	16384

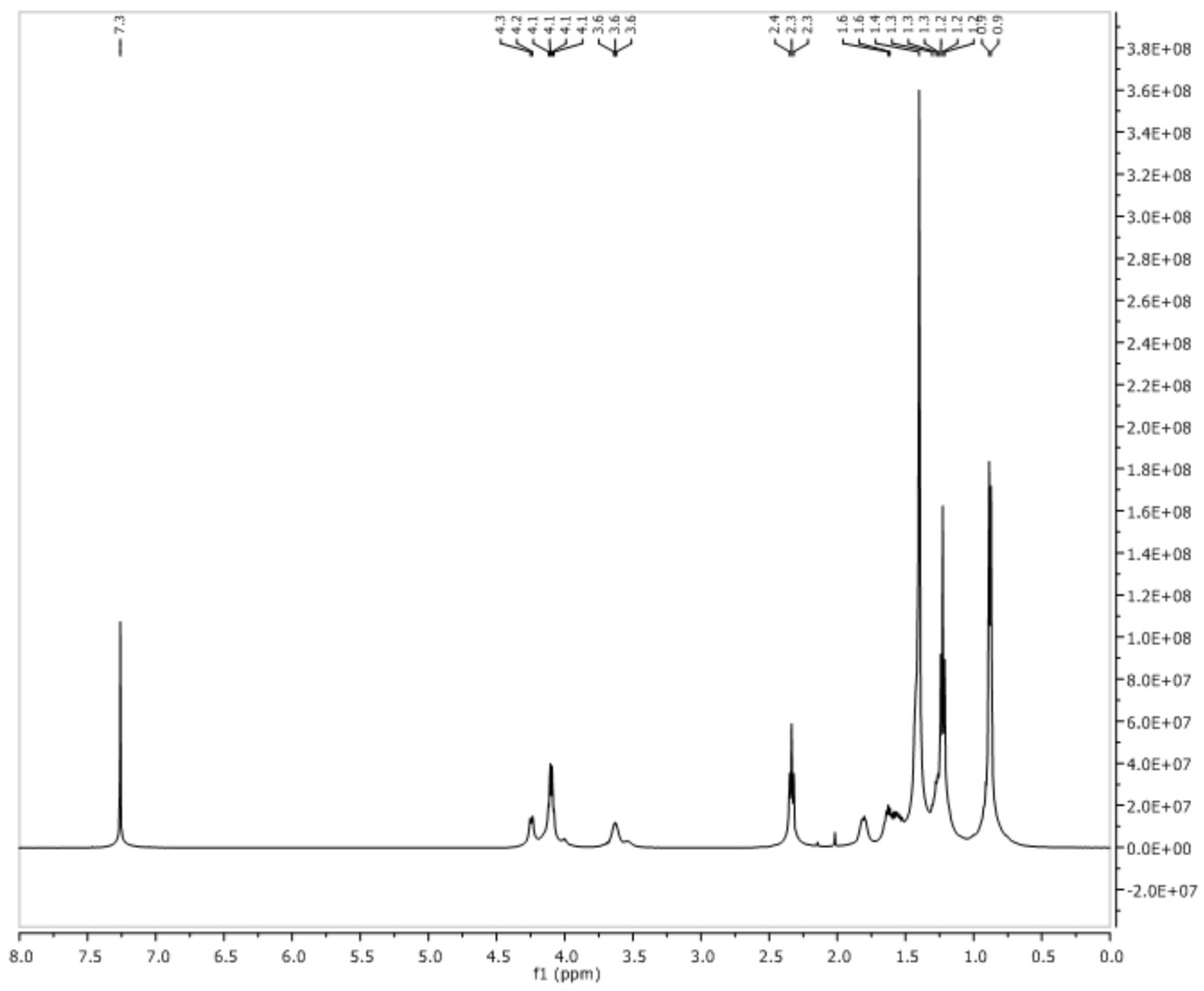


6.27

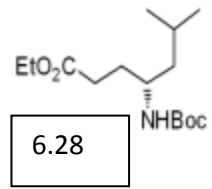


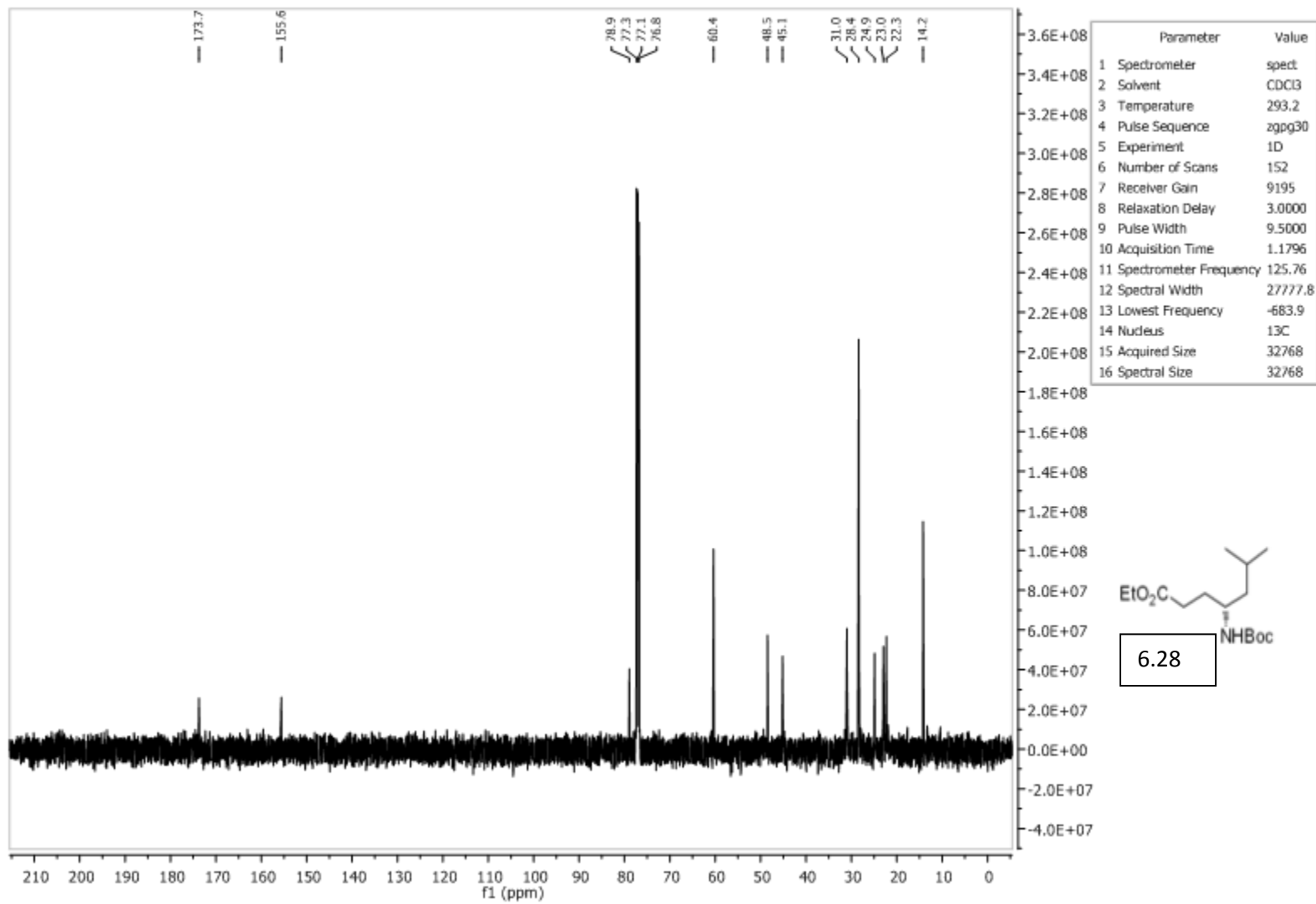
Parameter	Value
1 Spectrometer	spect
2 Solvent	CDCl3
3 Temperature	293.2
4 Pulse Sequence	zgpg30
5 Experiment	1D
6 Number of Scans	500
7 Receiver Gain	2896
8 Relaxation Delay	3.0000
9 Pulse Width	9.5000
10 Acquisition Time	1.1796
11 Spectrometer Frequency	125.77
12 Spectral Width	27777.8
13 Lowest Frequency	-683.9
14 Nucleus	13C
15 Acquired Size	32768
16 Spectral Size	65536

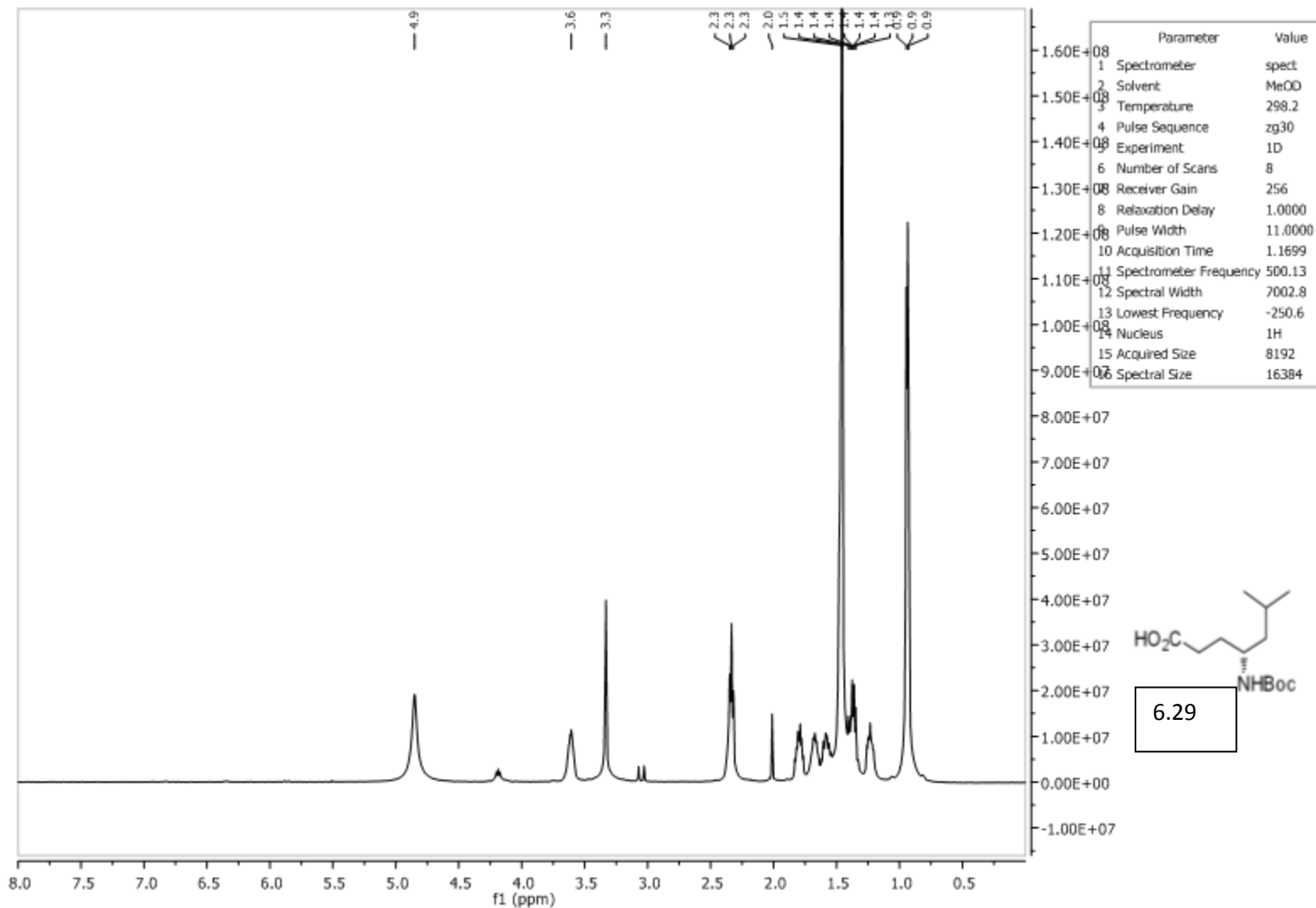


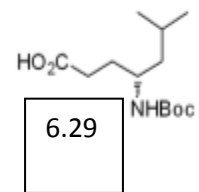
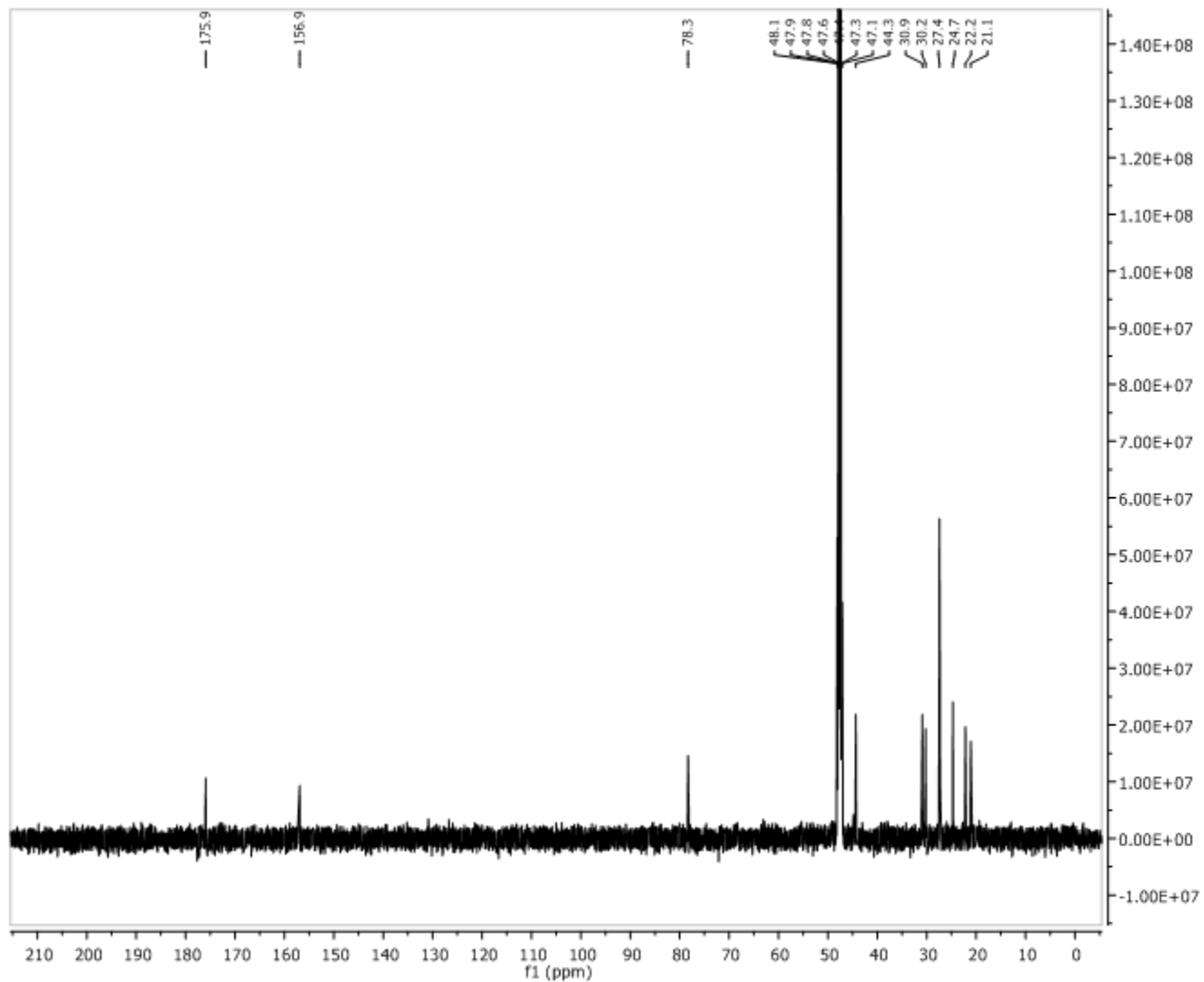


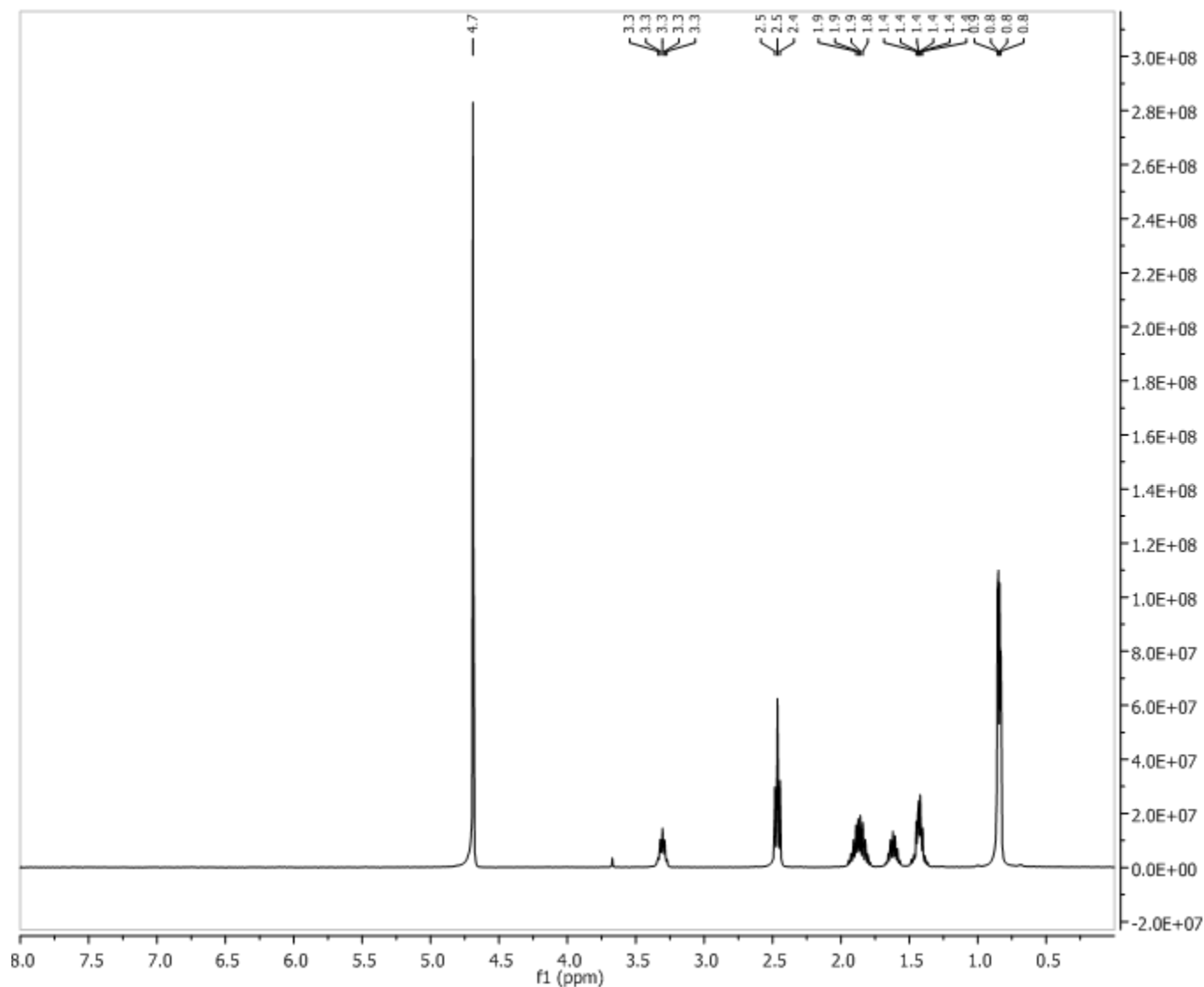
Parameter	Value
1 Spectrometer	spect
2 Solvent	CDCl3
3 Temperature	293.2
4 Pulse Sequence	zg30
5 Experiment	1D
6 Number of Scans	8
7 Receiver Gain	114
8 Relaxation Delay	1.0000
9 Pulse Width	11.0000
10 Acquisition Time	1.1698
11 Spectrometer Frequency	500.13
12 Spectral Width	7002.8
13 Lowest Frequency	-264.1
14 Nucleus	1H
15 Acquired Size	8192
16 Spectral Size	16384



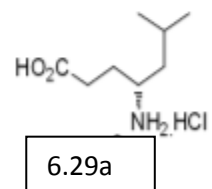


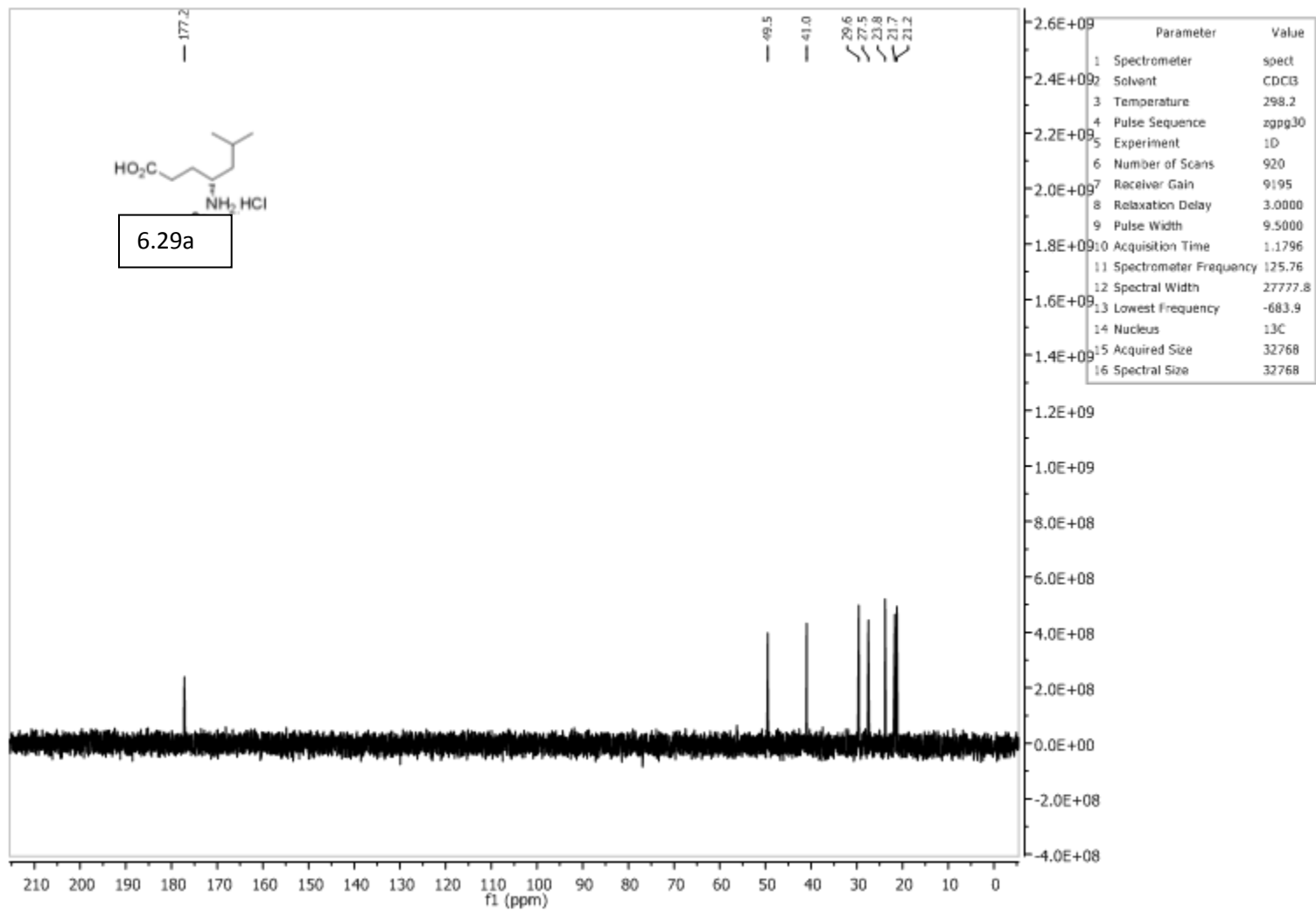


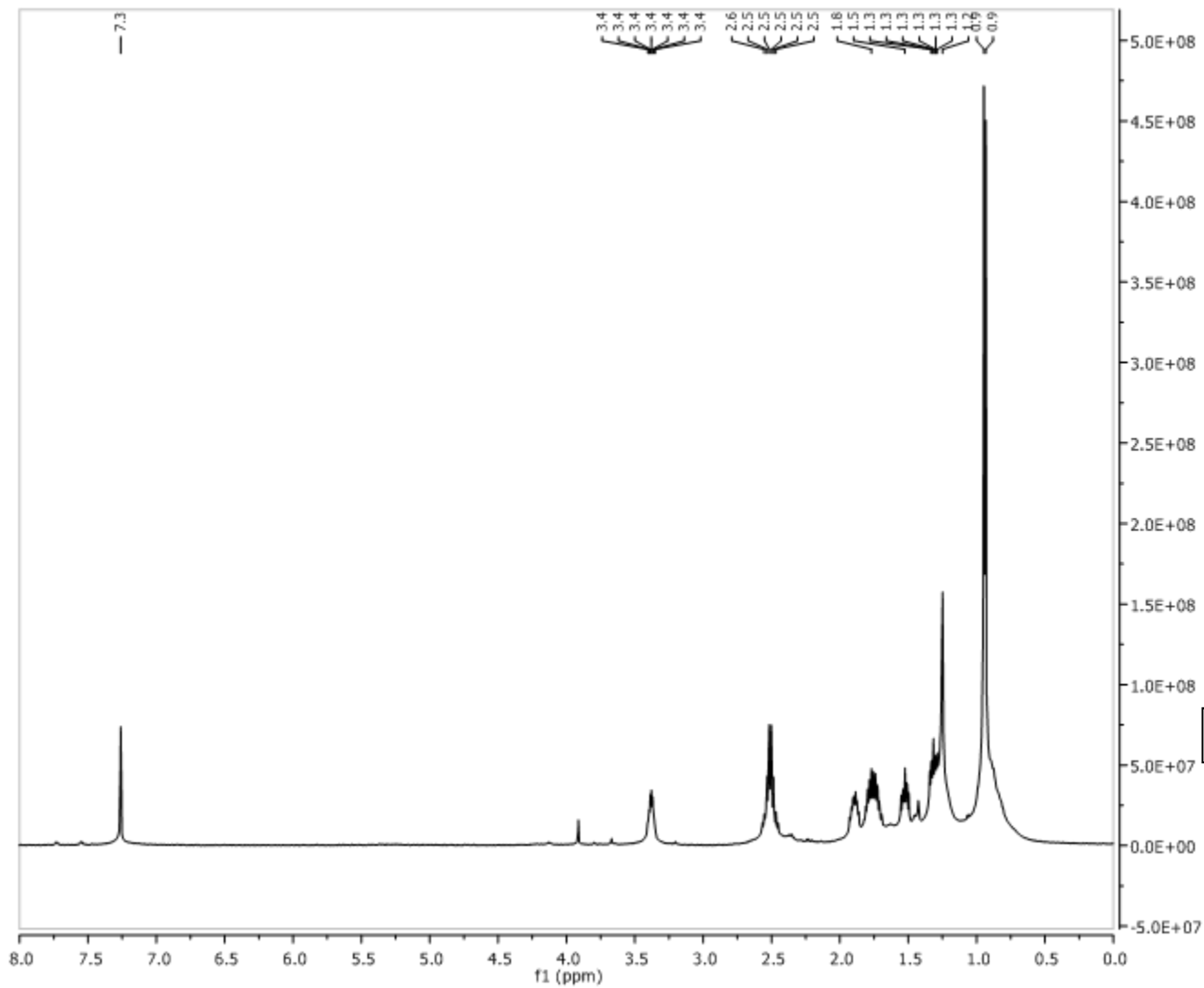




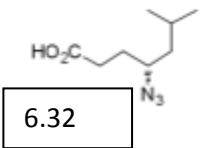
Parameter	Value
1 Spectrometer	spect
2 Solvent	D2O
3 Temperature	298.2
4 Pulse Sequence	zg30
5 Experiment	1D
6 Number of Scans	8
7 Receiver Gain	362
8 Relaxation Delay	1.0000
9 Pulse Width	10.2500
10 Acquisition Time	3.9846
11 Spectrometer Frequency	400.15
12 Spectral Width	8223.7
13 Lowest Frequency	-1640.8
14 Nucleus	1H
15 Acquired Size	32768
16 Spectral Size	32768

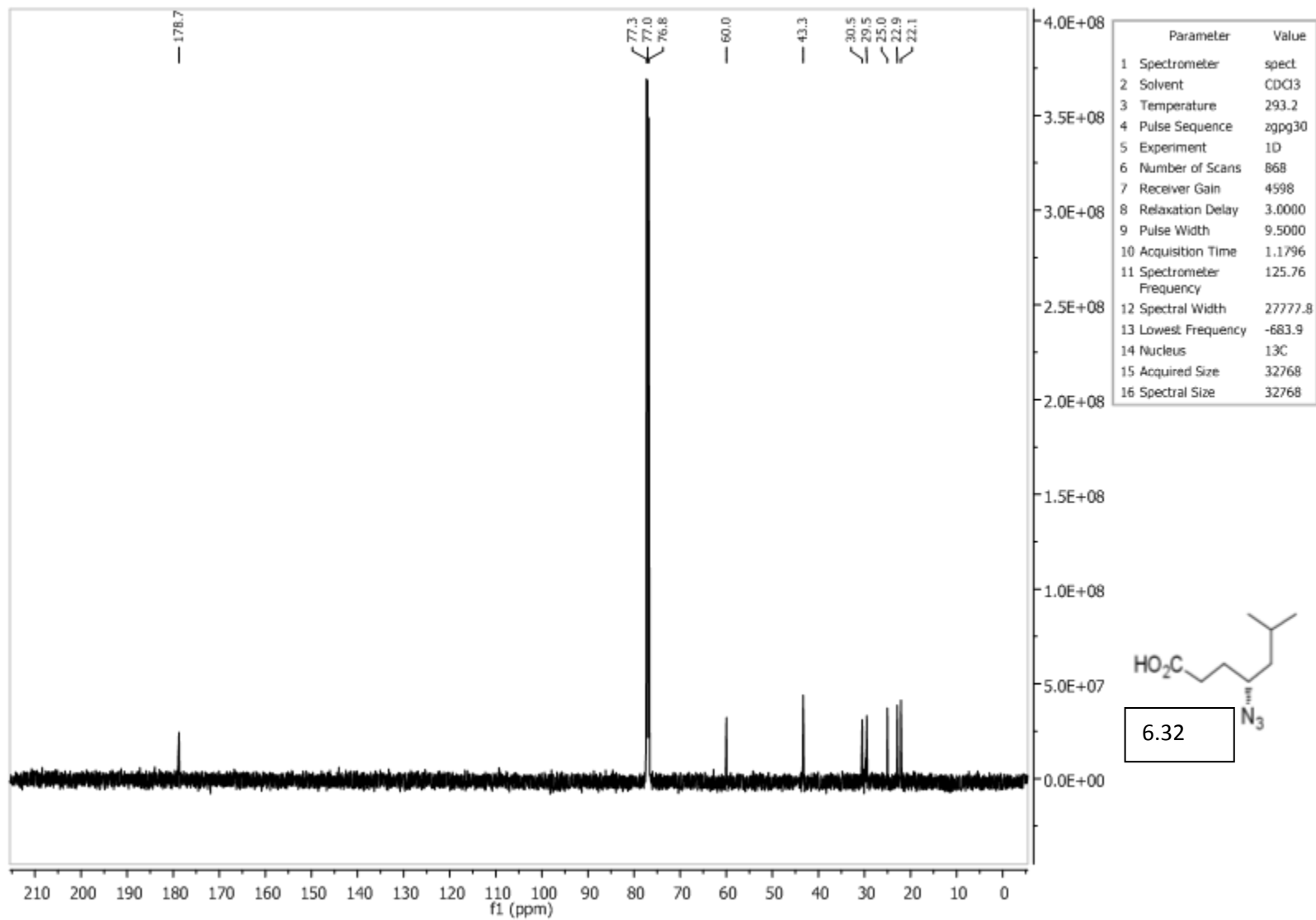


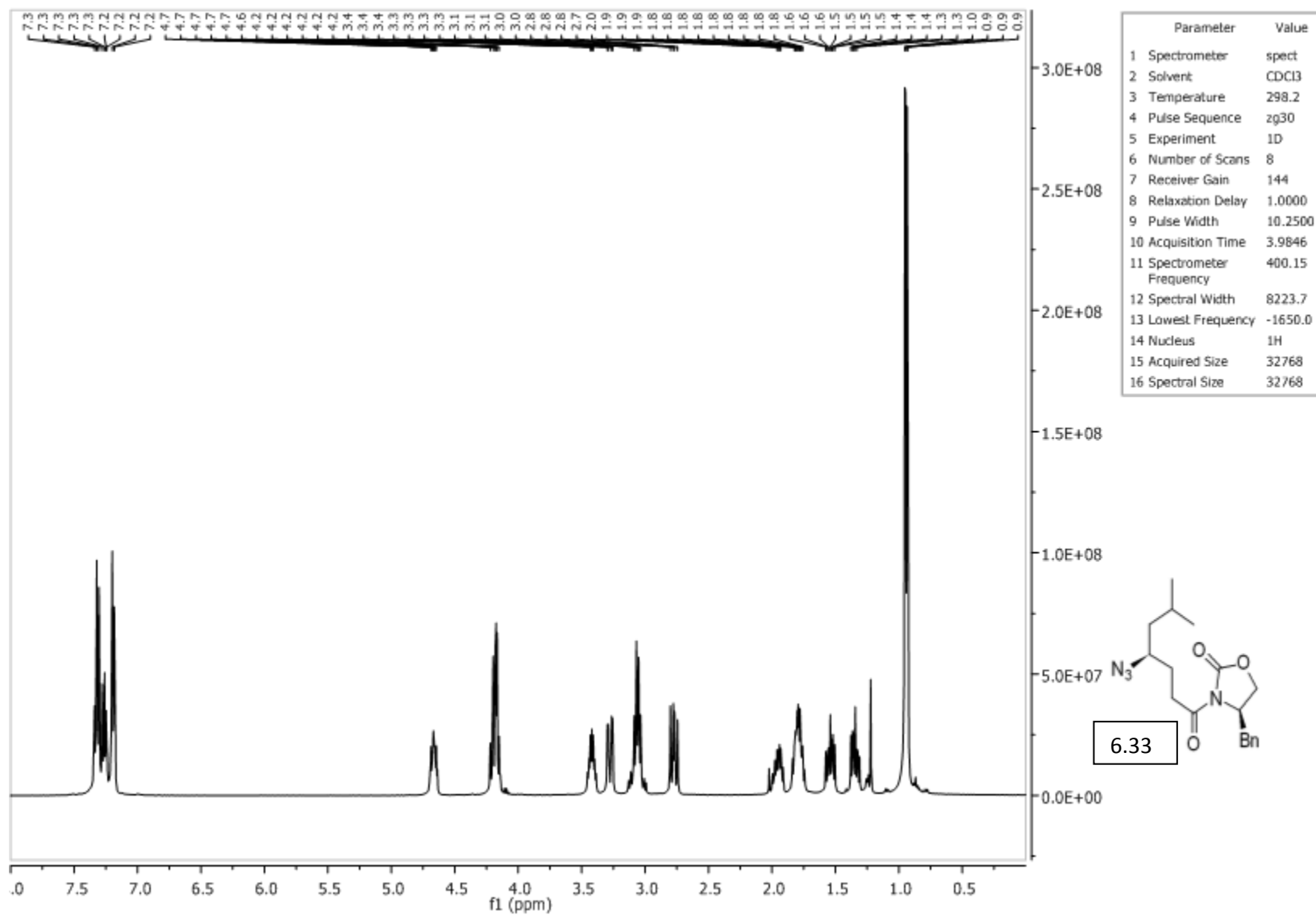


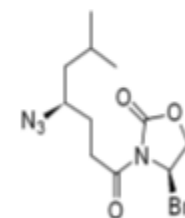
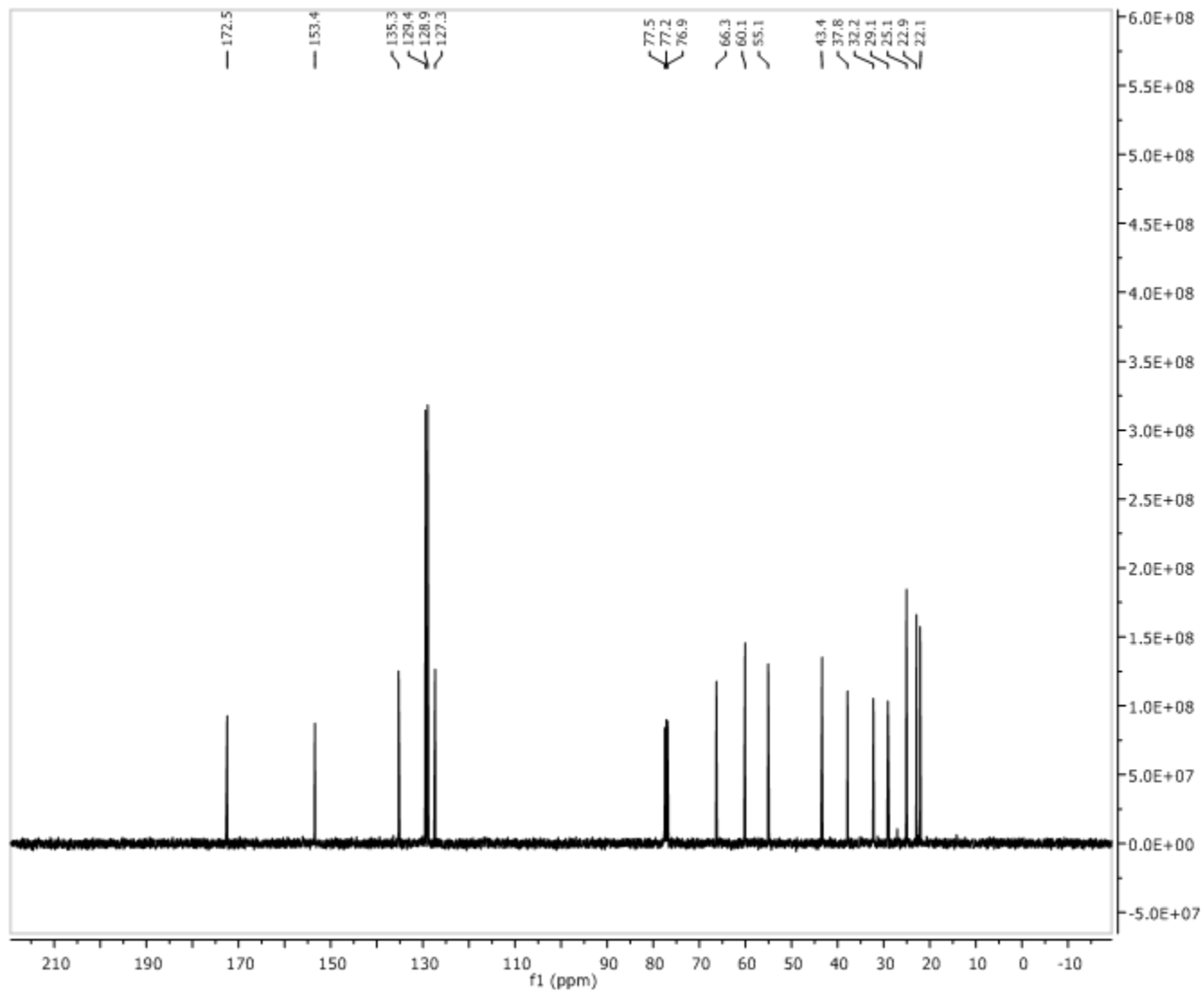


Parameter	Value
1 Spectrometer	spect
2 Solvent	CDCl3
3 Temperature	292.2
4 Pulse Sequence	zg30
5 Experiment	1D
6 Number of Scans	16
7 Receiver Gain	456
8 Relaxation Delay	1.0000
9 Pulse Width	11.0000
10 Acquisition Time	1.1698
11 Spectrometer Frequency	500.13
12 Spectral Width	7002.8
13 Lowest Frequency	-264.1
14 Nucleus	1H
15 Acquired Size	8192
16 Spectral Size	16384

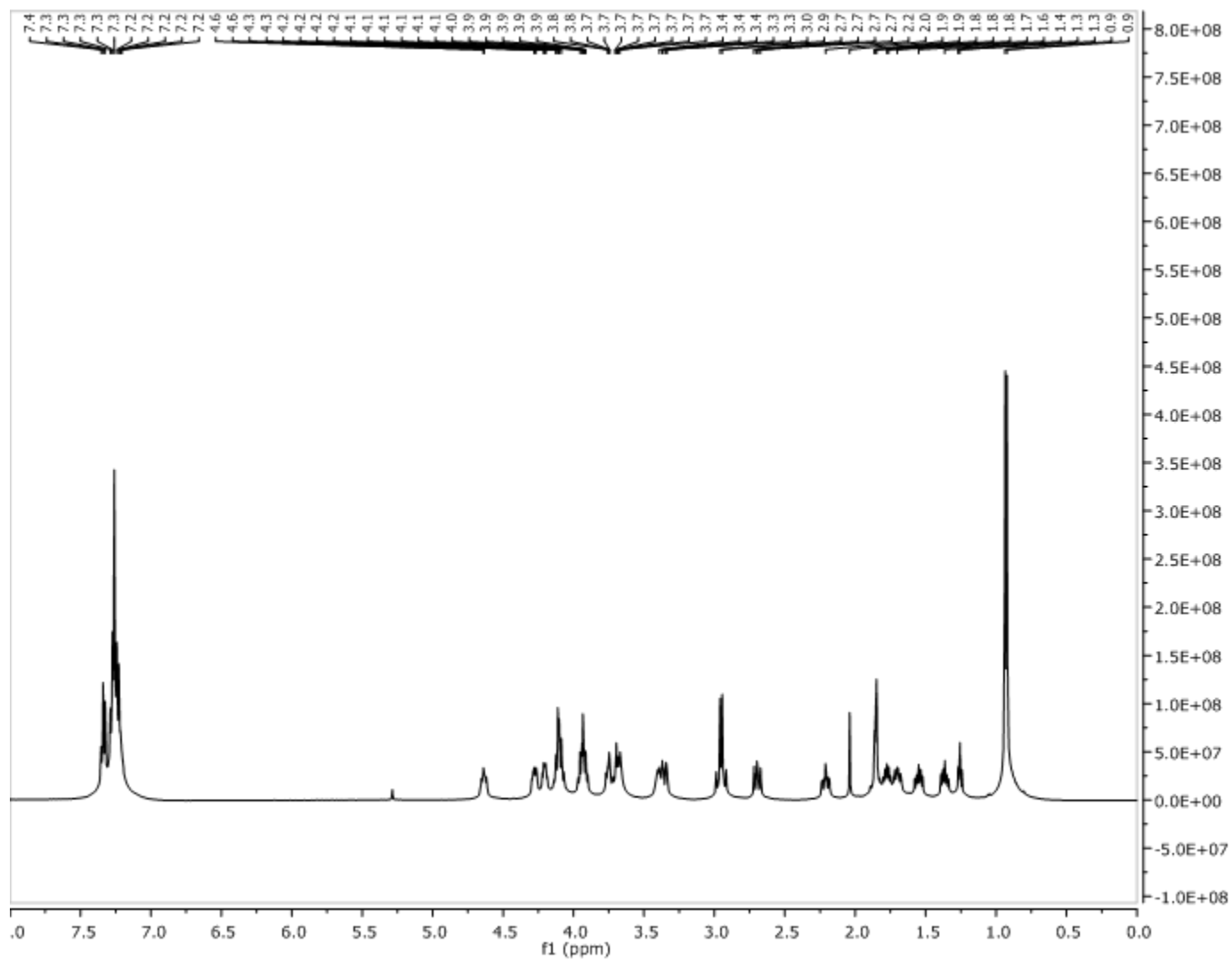




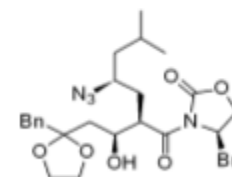




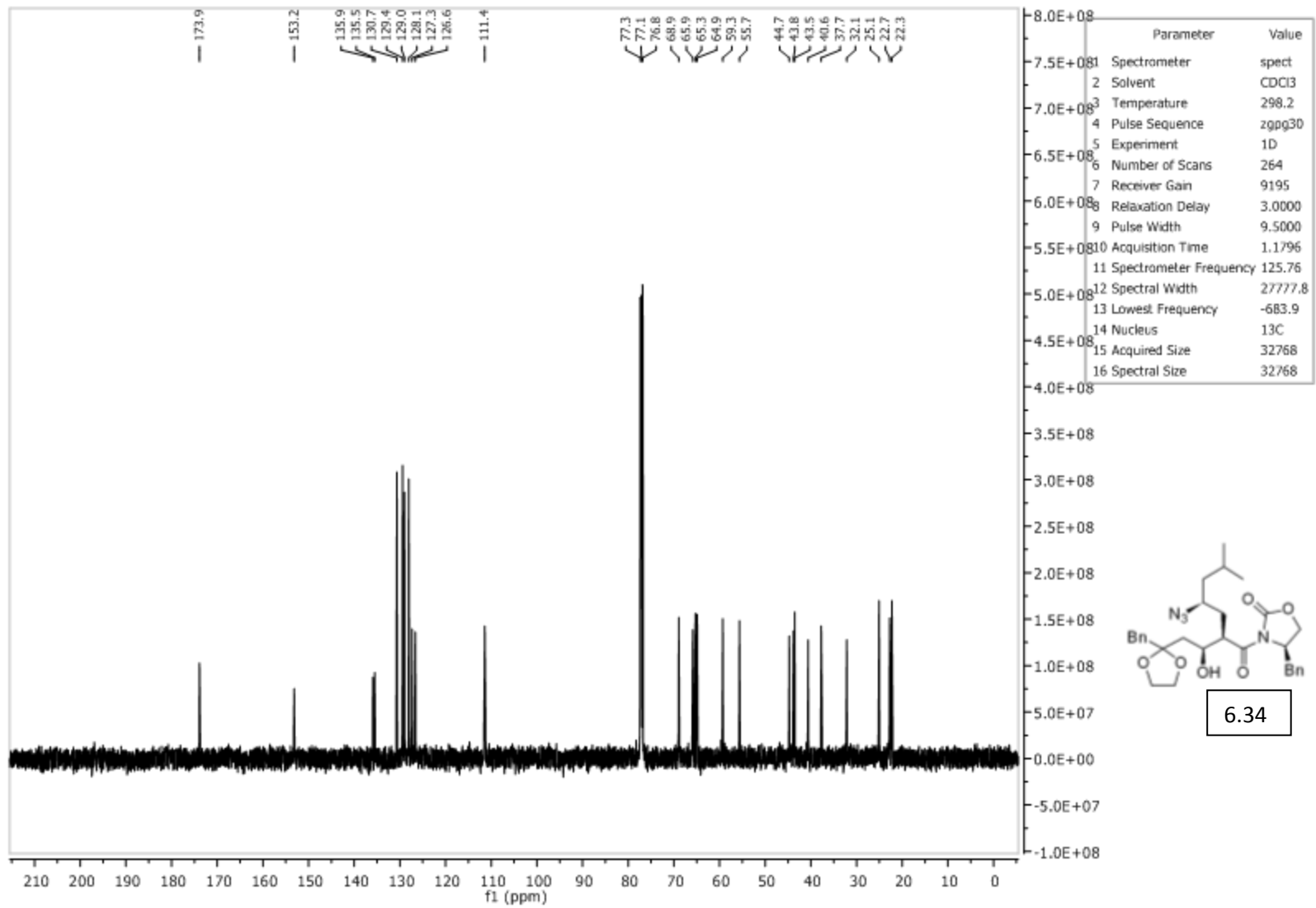
6.33

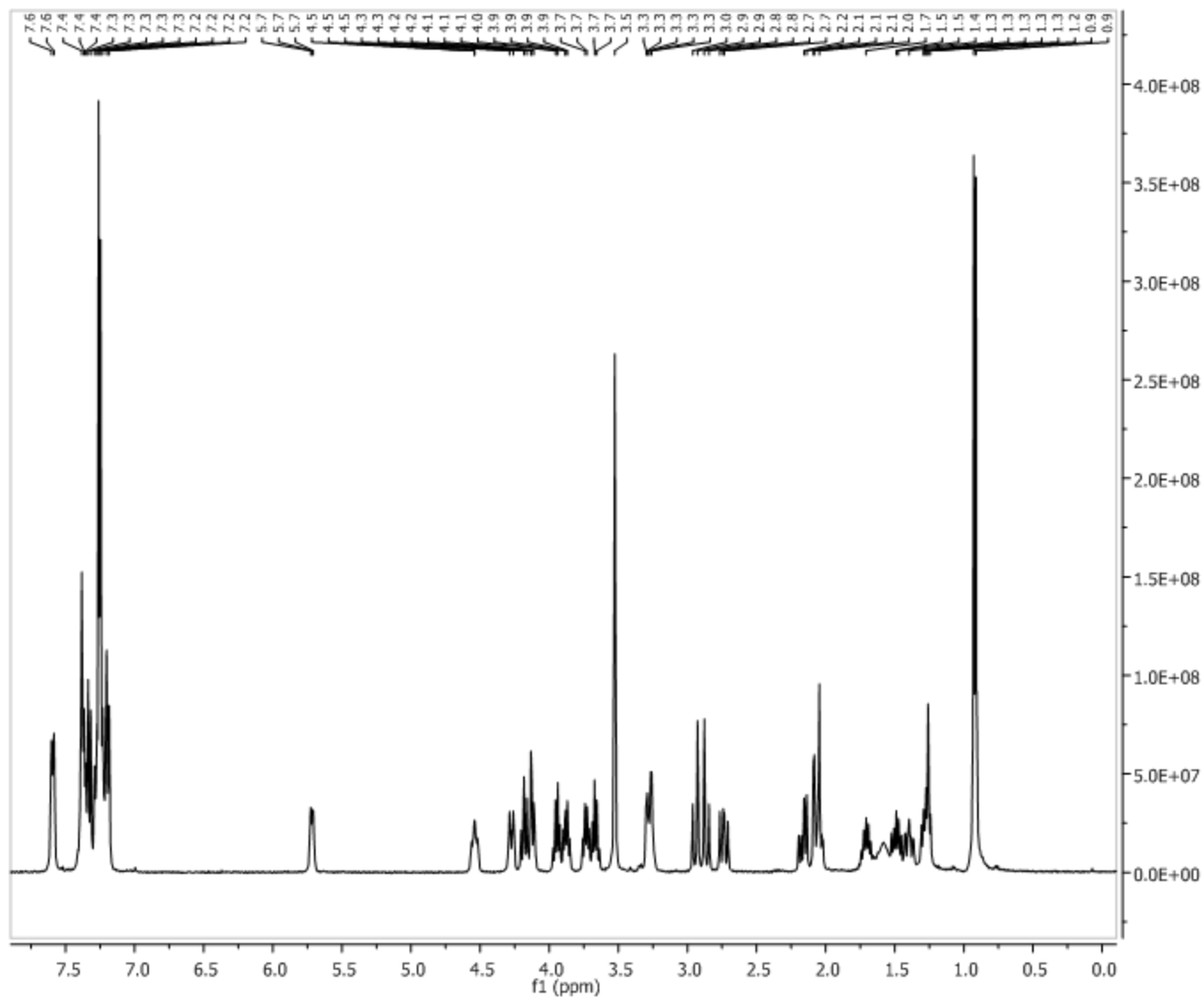


Parameter	Value
1 Spectrometer	spect
2 Solvent	CDCl3
3 Temperature	298.2
4 Pulse Sequence	zg30
5 Experiment	1D
6 Number of Scans	8
7 Receiver Gain	128
8 Relaxation Delay	1.0000
9 Pulse Width	11.0000
10 Acquisition Time	1.1699
11 Spectrometer Frequency	500.13
12 Spectral Width	7002.8
13 Lowest Frequency	-265.6
14 Nucleus	¹ H
15 Acquired Size	8192
16 Spectral Size	16384

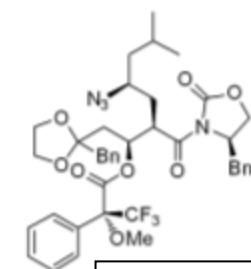


6.34

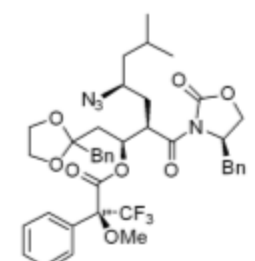
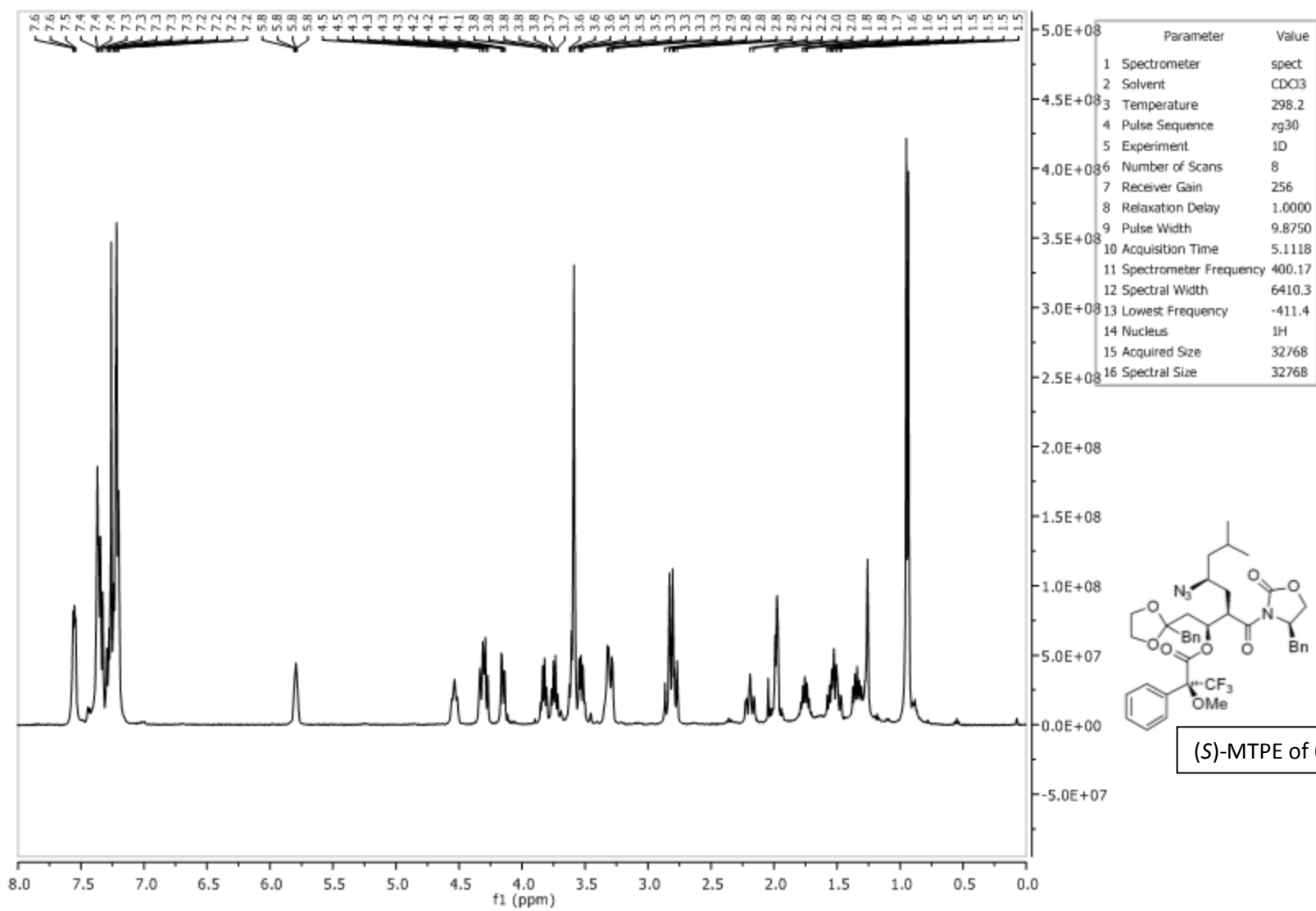




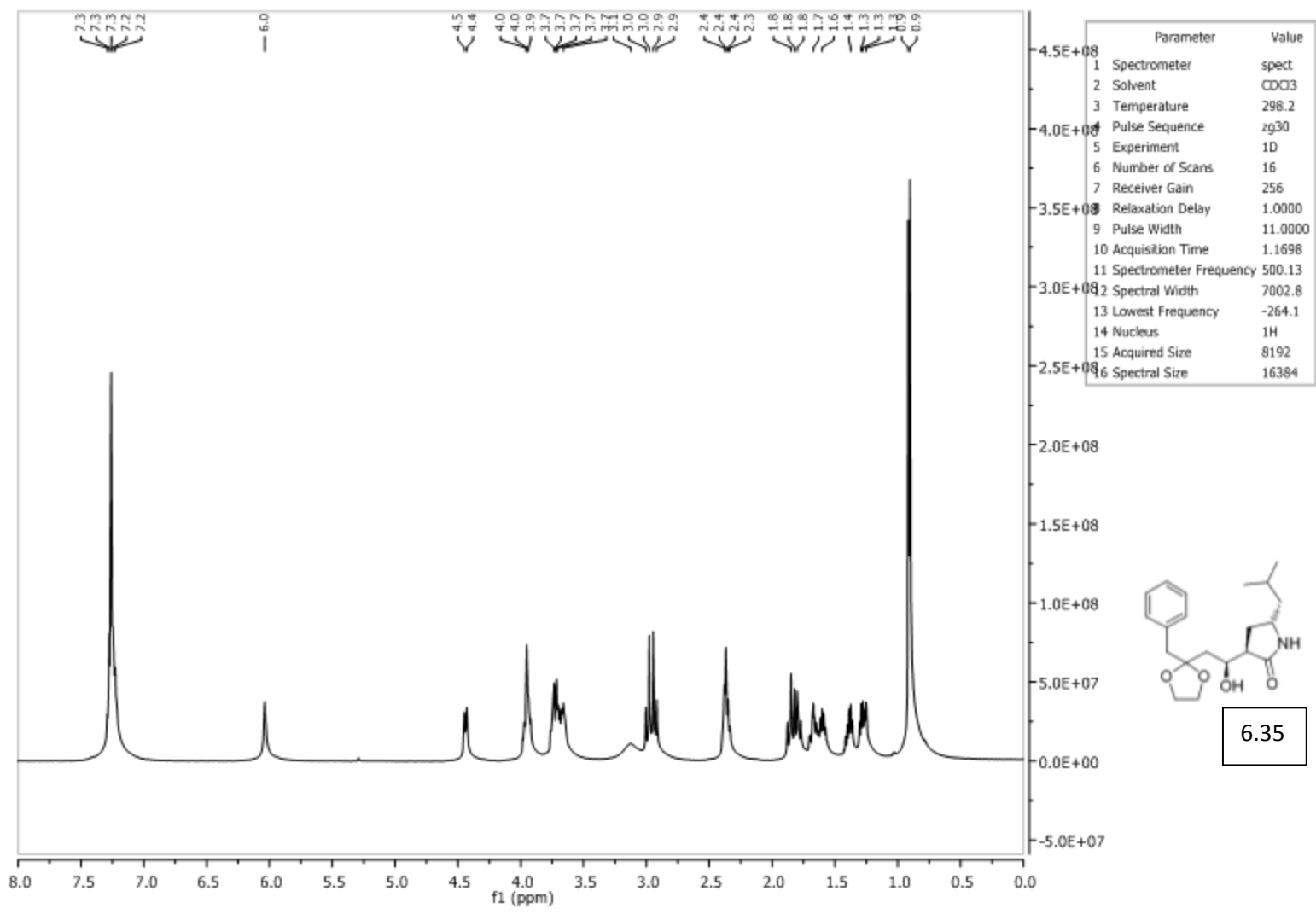
Parameter	Value
1 Spectrometer	spect
2 Solvent	CDCl3
3 Temperature	298.2
4 Pulse Sequence	zg30
5 Experiment	1D
6 Number of Scans	8
7 Receiver Gain	256
8 Relaxation Delay	1.0000
9 Pulse Width	9.8750
10 Acquisition Time	5.1118
11 Spectrometer Frequency	400.17
12 Spectral Width	6410.3
13 Lowest Frequency	-411.4
14 Nucleus	1H
15 Acquired Size	32768
16 Spectral Size	32768

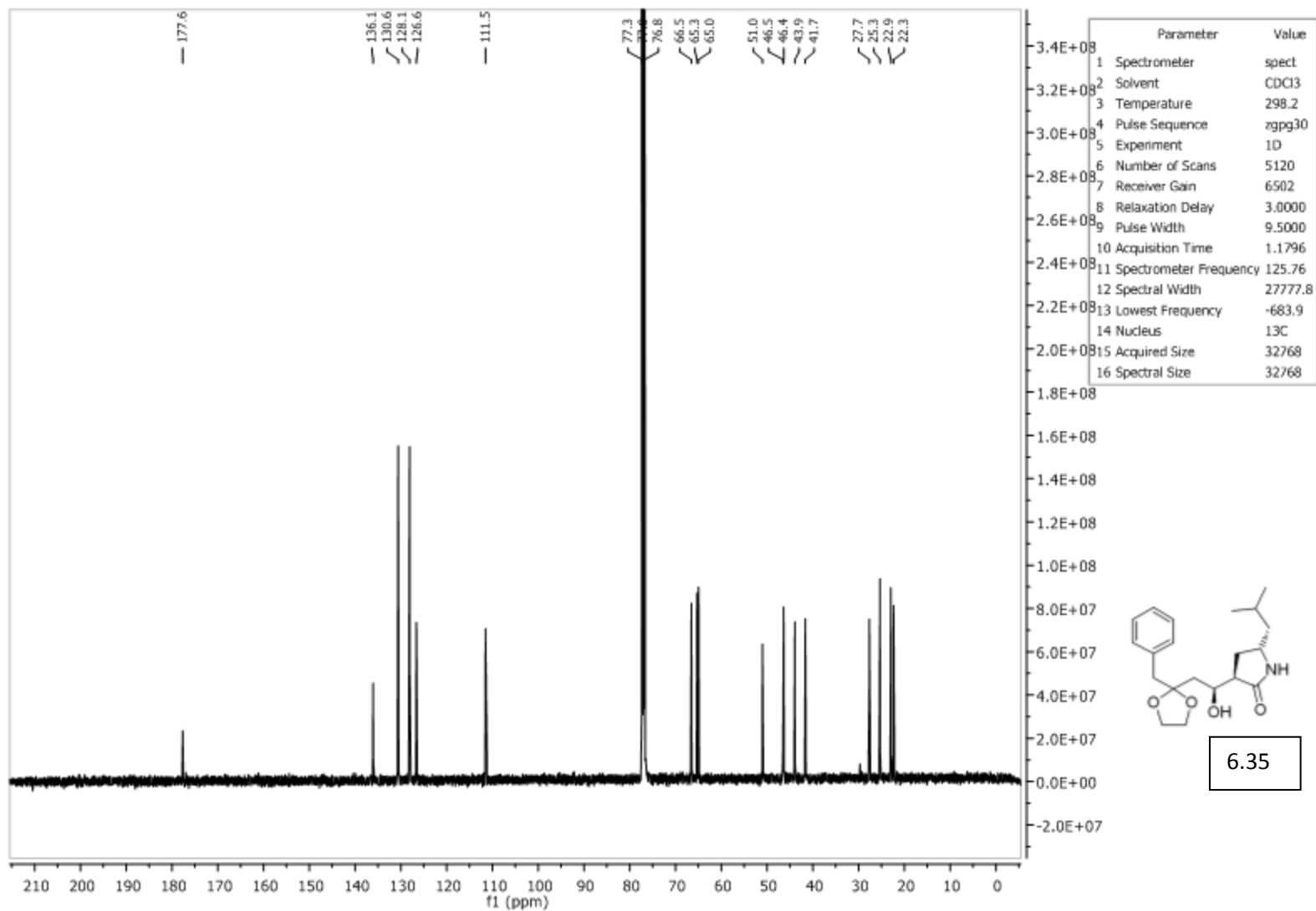


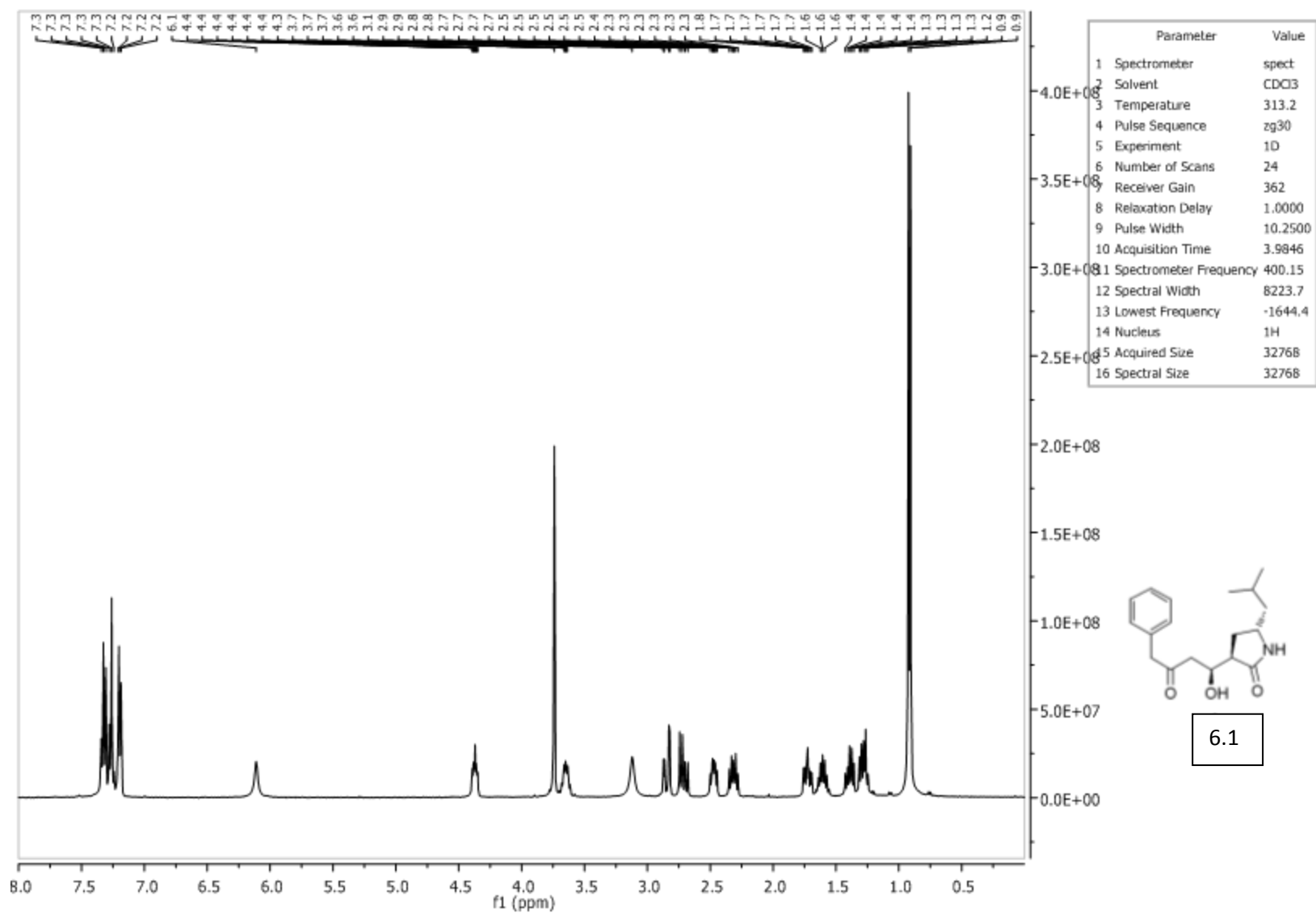
(R)-MTPE of 6.34

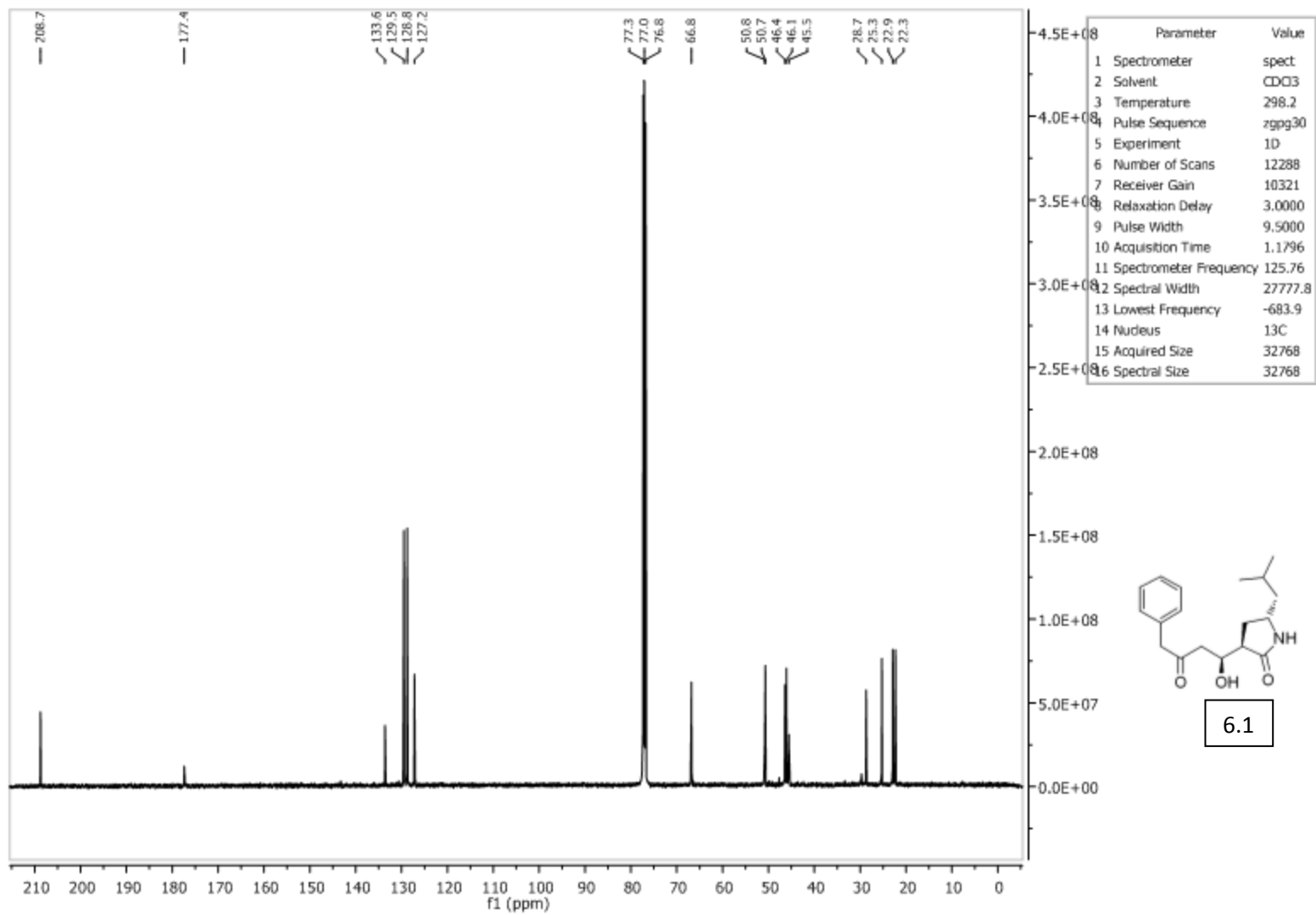


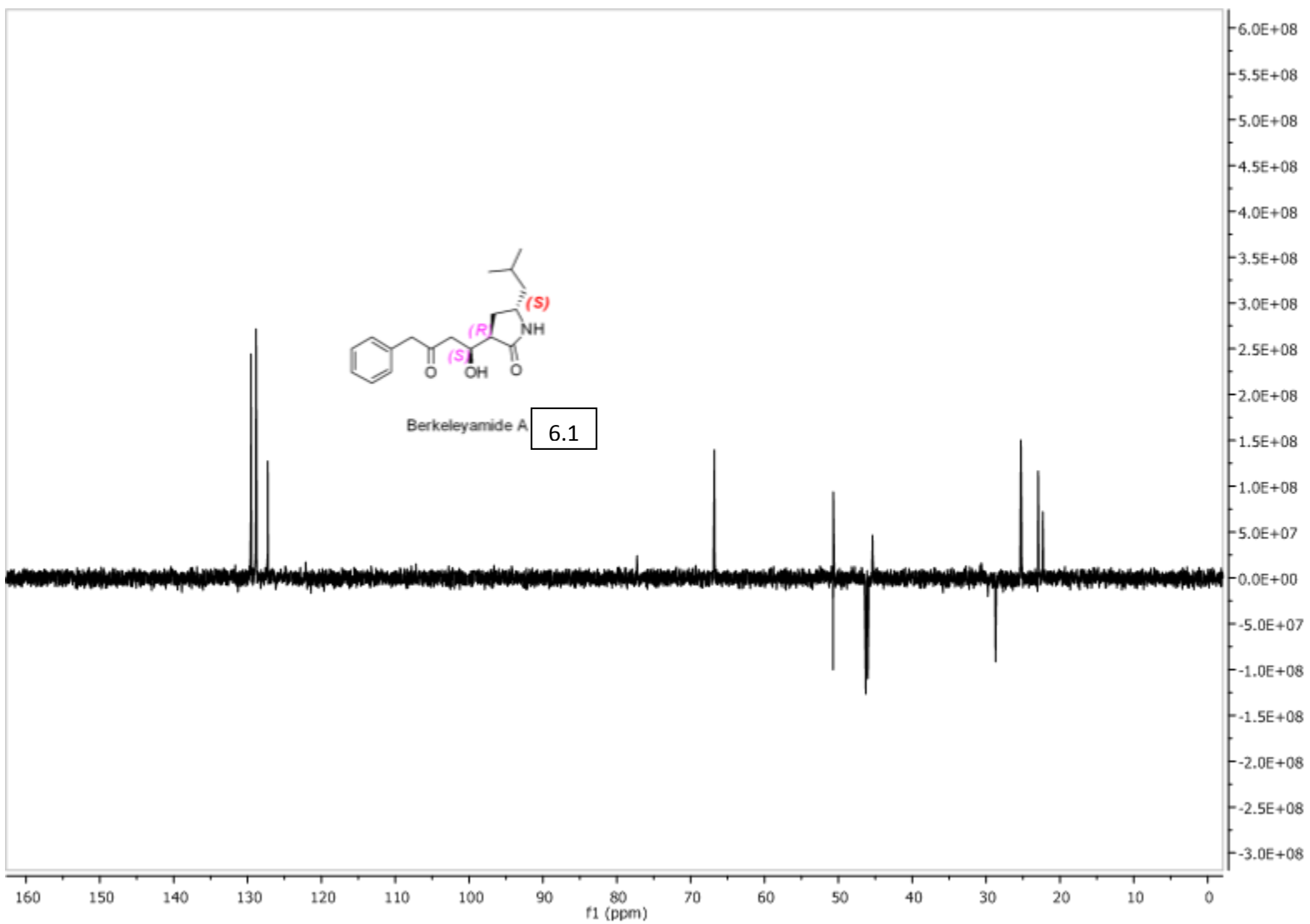
(S)-MTPE of 6.34

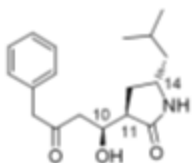




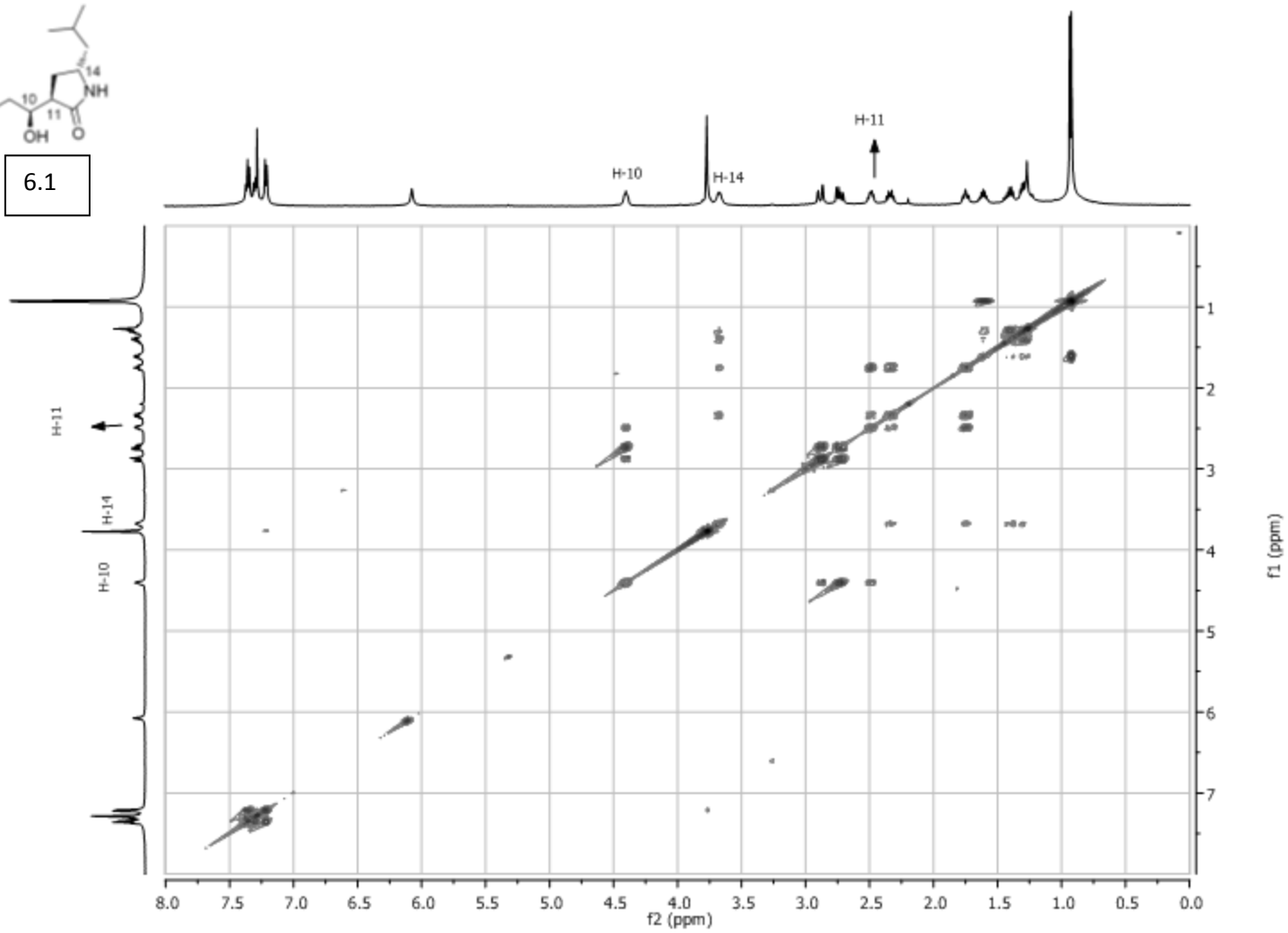


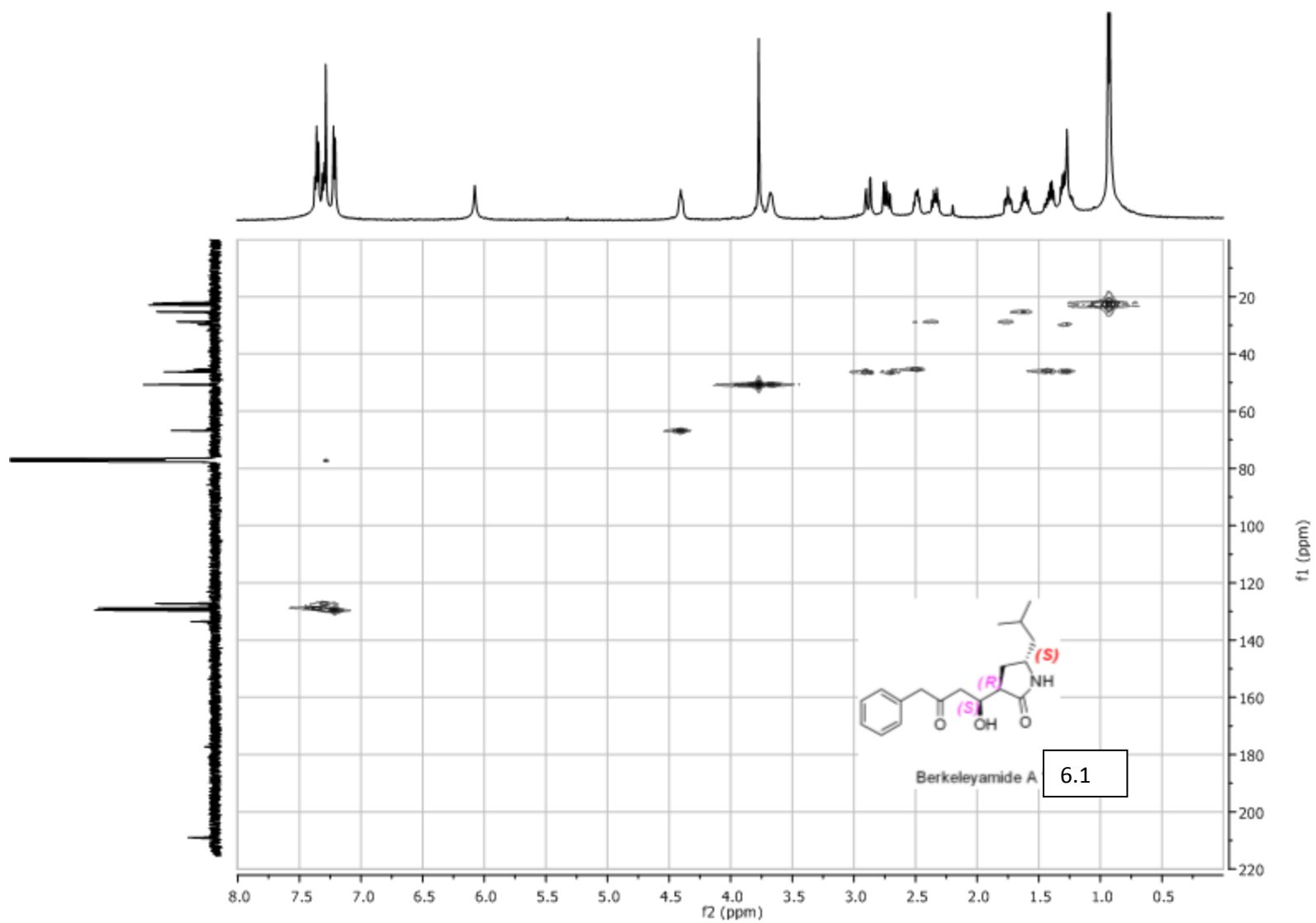


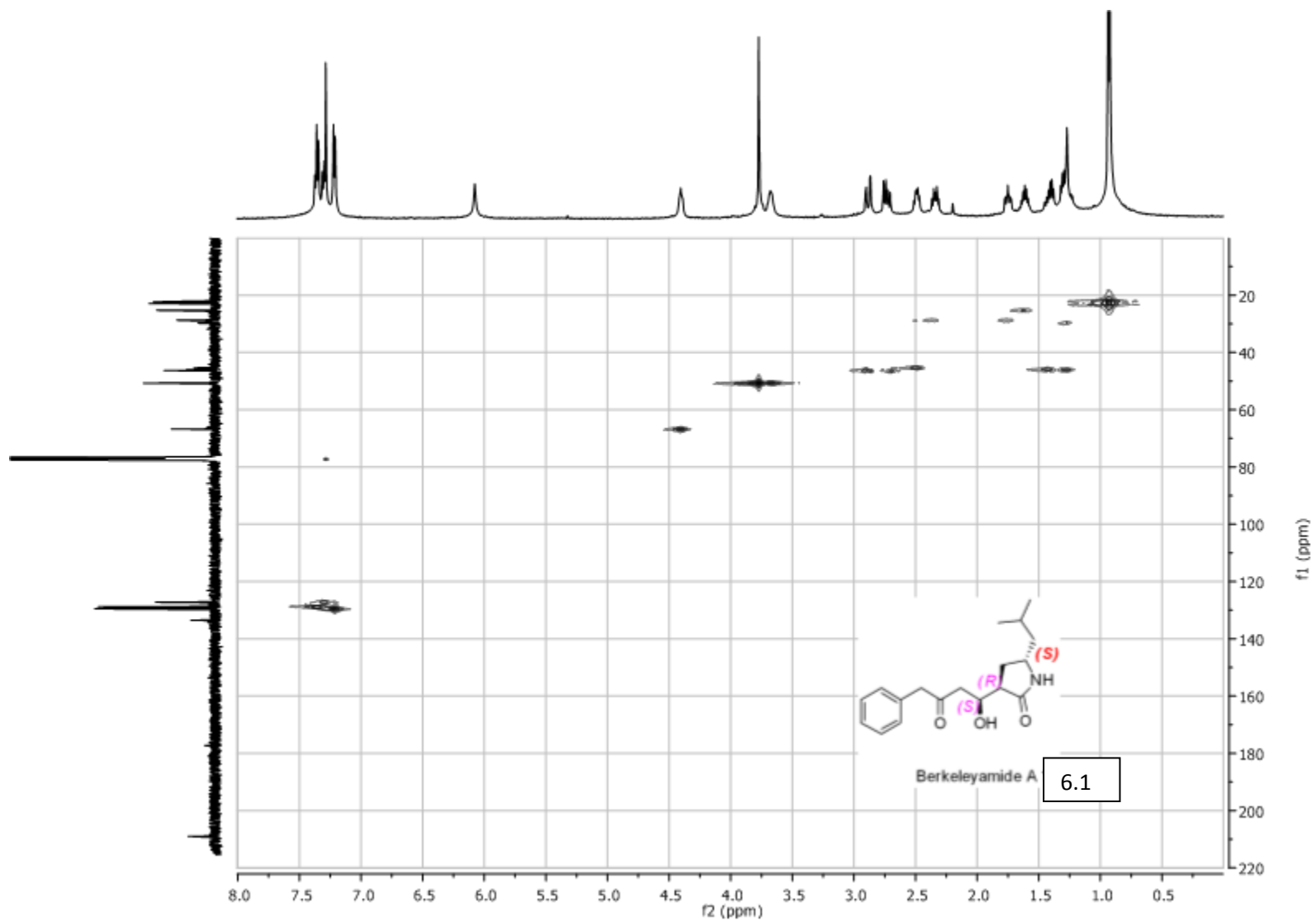


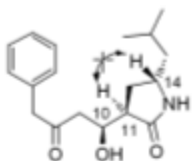


6.1



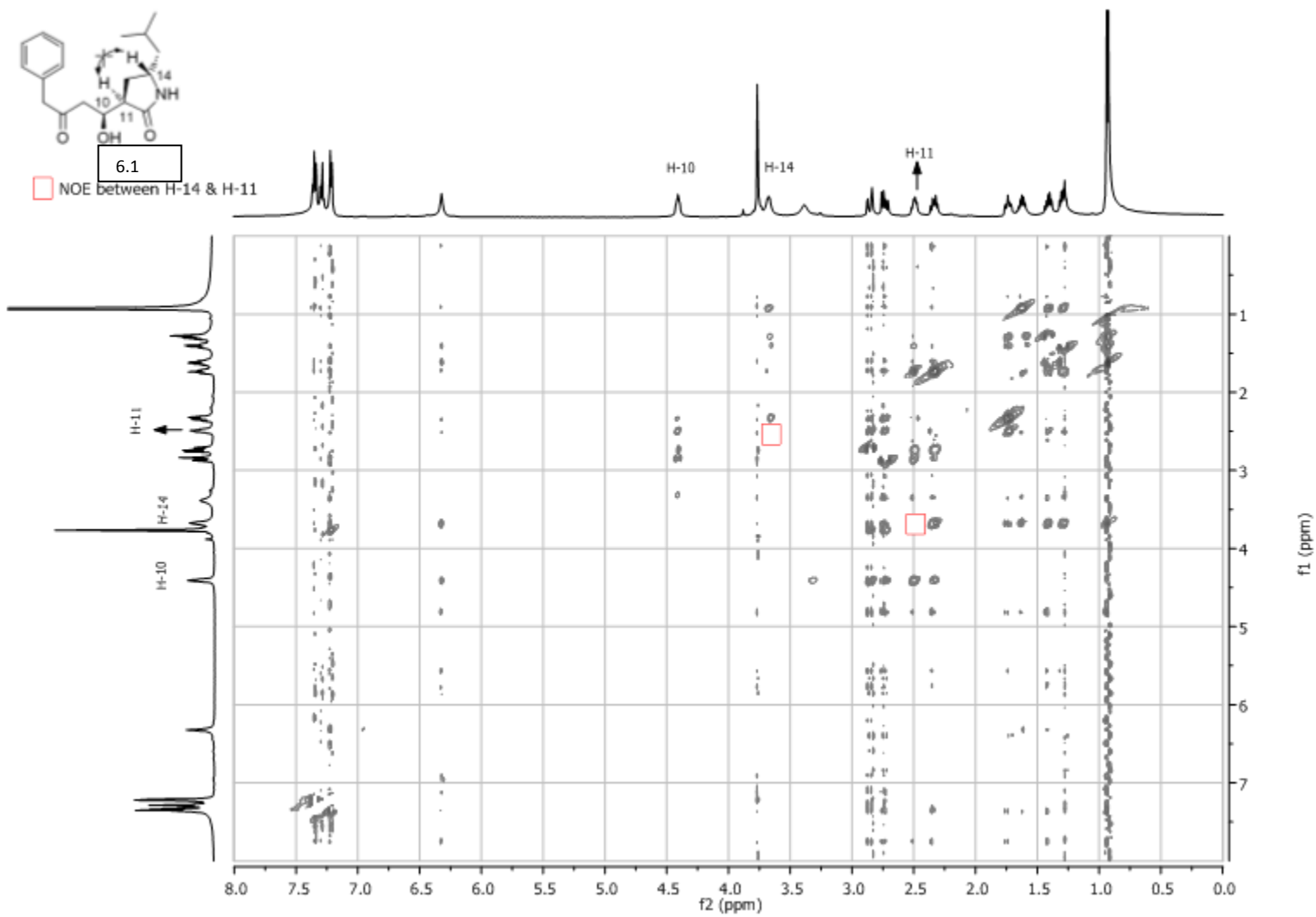


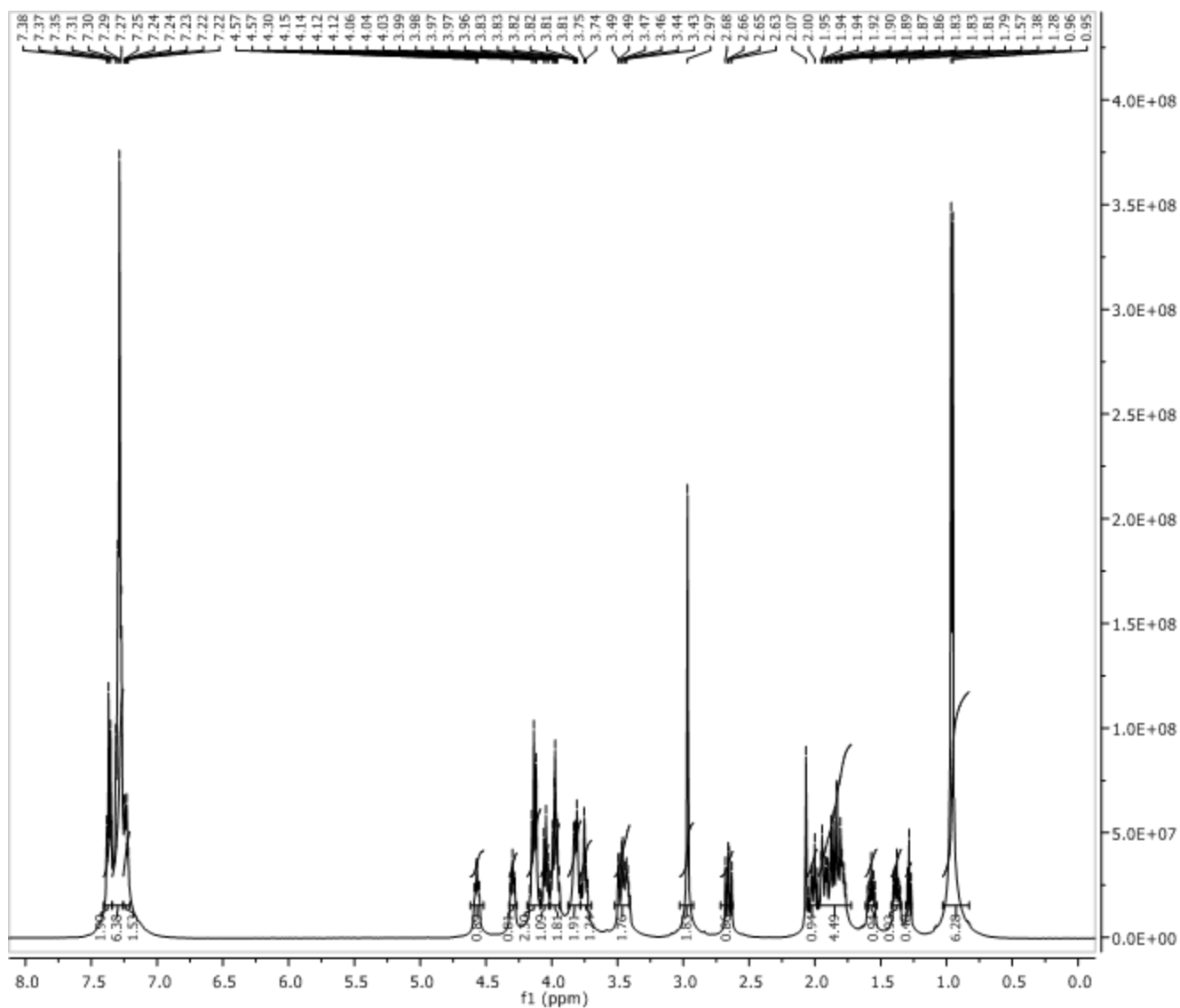




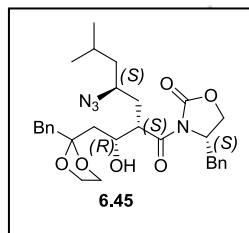
6.1

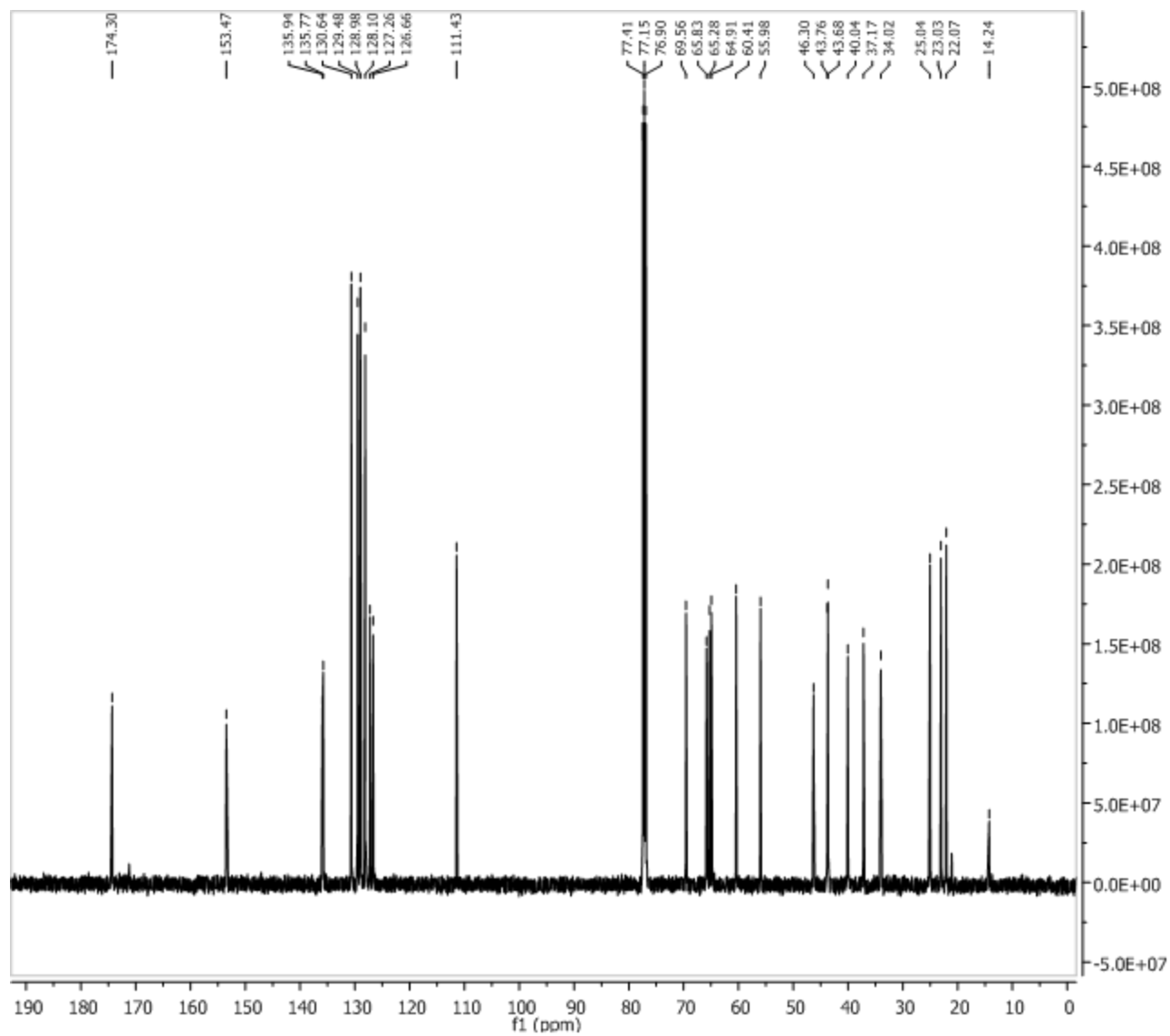
NOE between H-14 & H-11



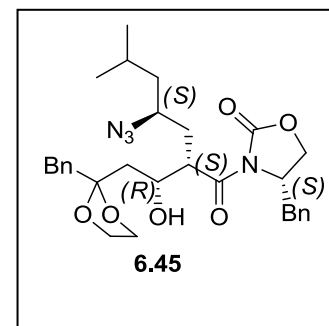


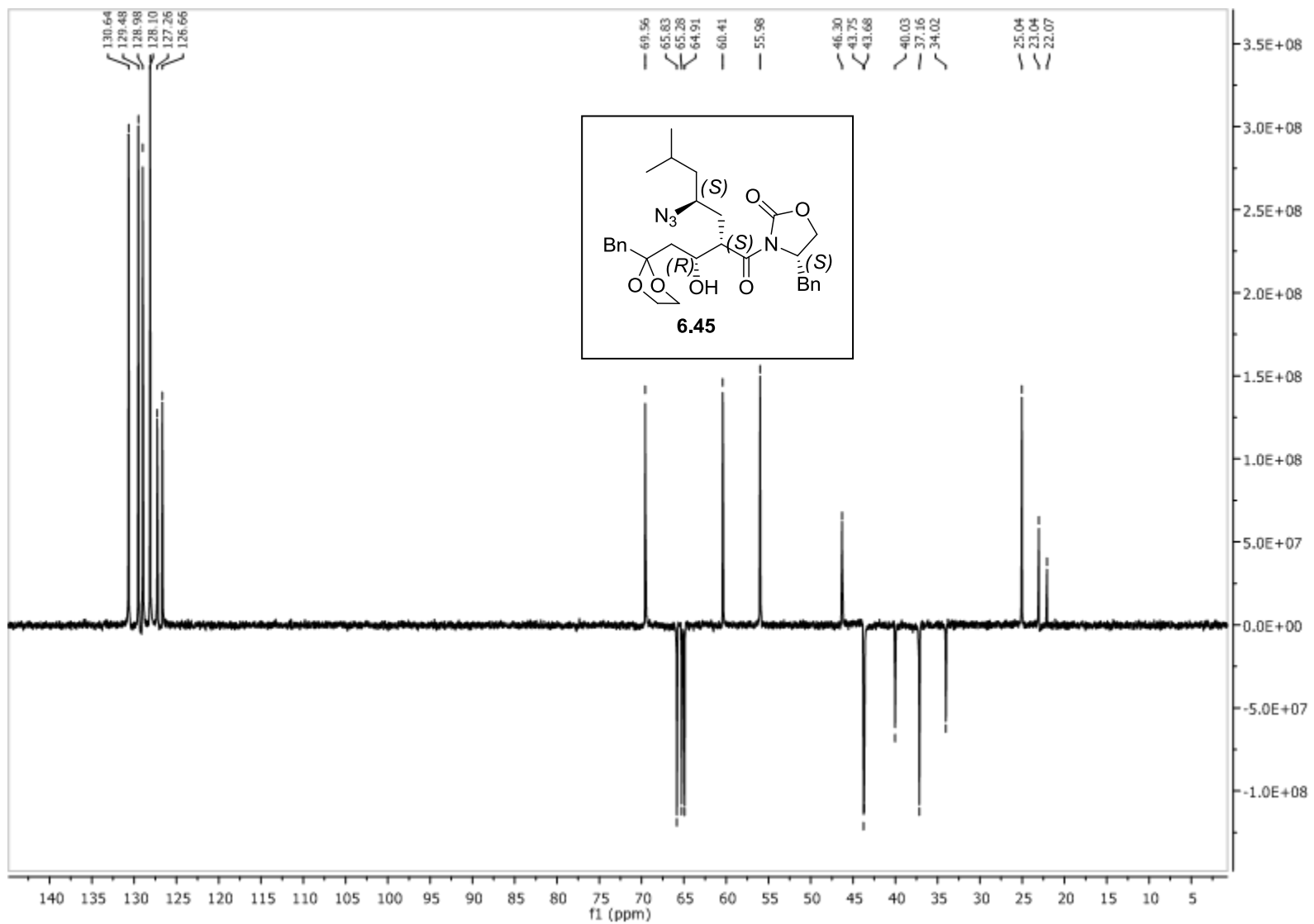
Parameter	Value
1 Spectrometer	spect
2 Solvent	CDCl3
3 Temperature	292.2
4 Pulse Sequence	zg30
5 Experiment	1D
6 Number of Scans	16
7 Receiver Gain	102
8 Relaxation Delay	1.0000
9 Pulse Width	11.0000
10 Spectrometer Frequency	500.13
11 Spectral Width	7002.8
12 Lowest Frequency	-250.6
13 Nucleus	1H
14 Acquired Size	8192
15 Spectral Size	16384

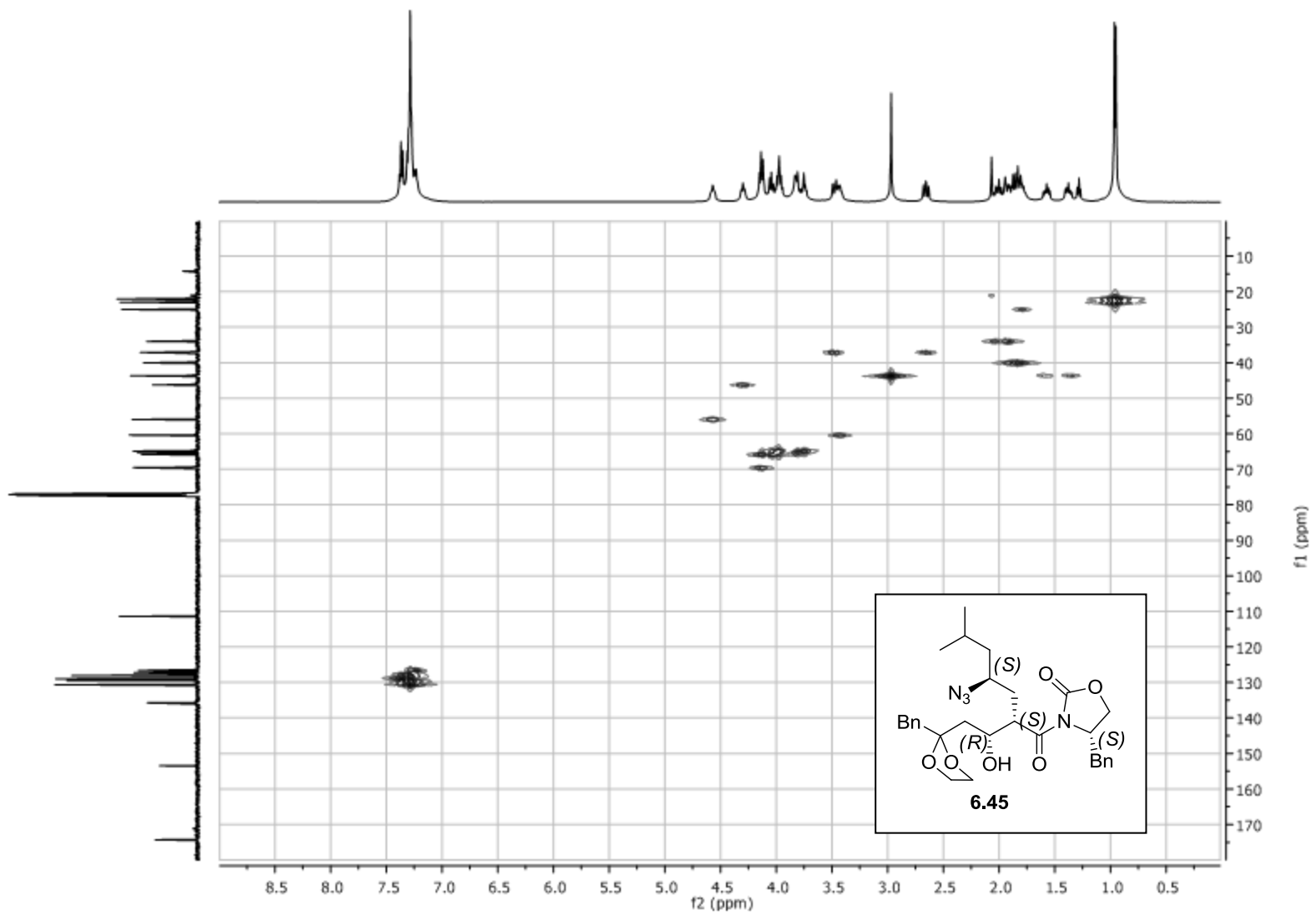


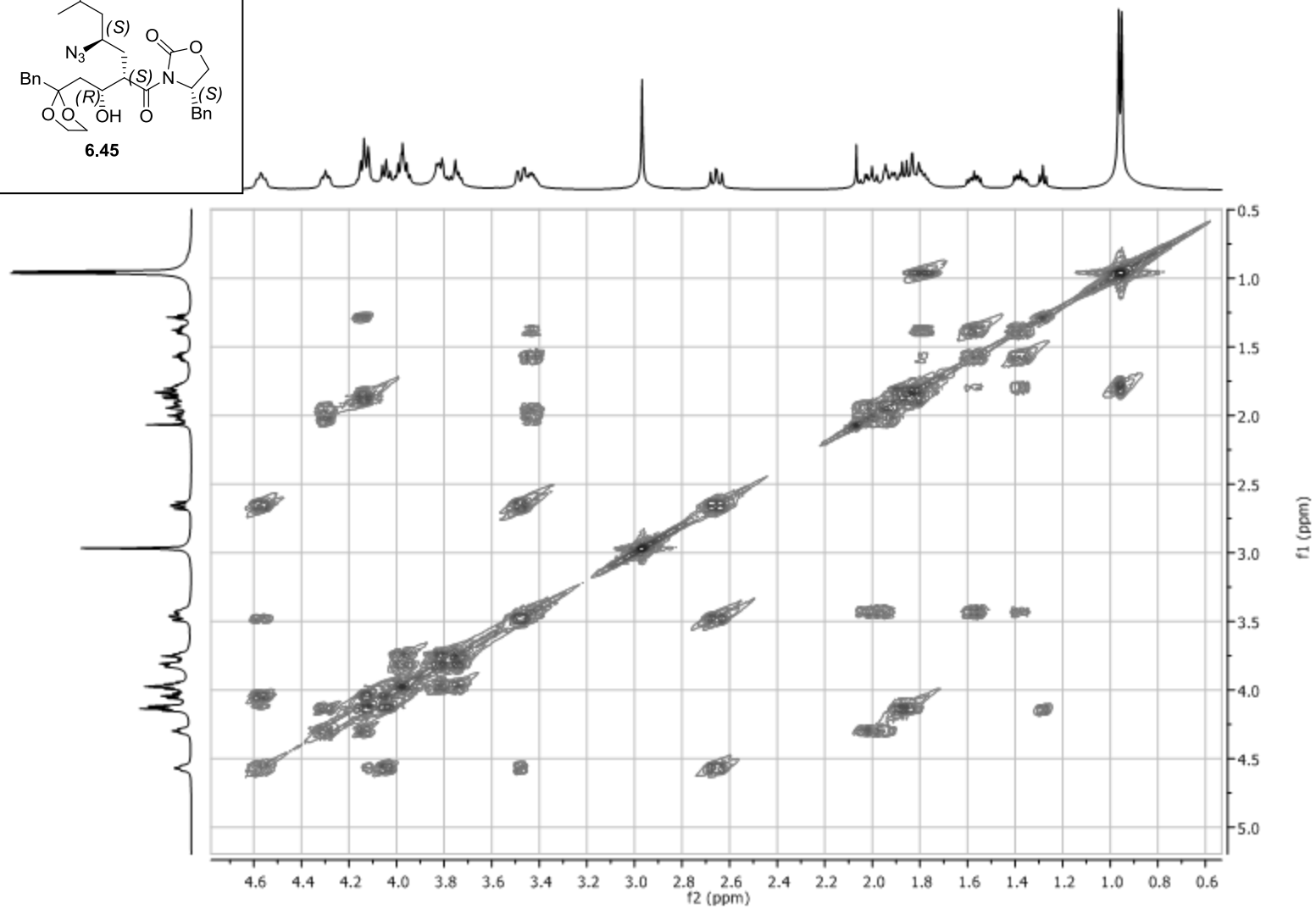
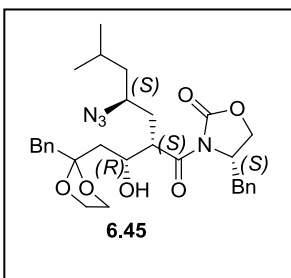


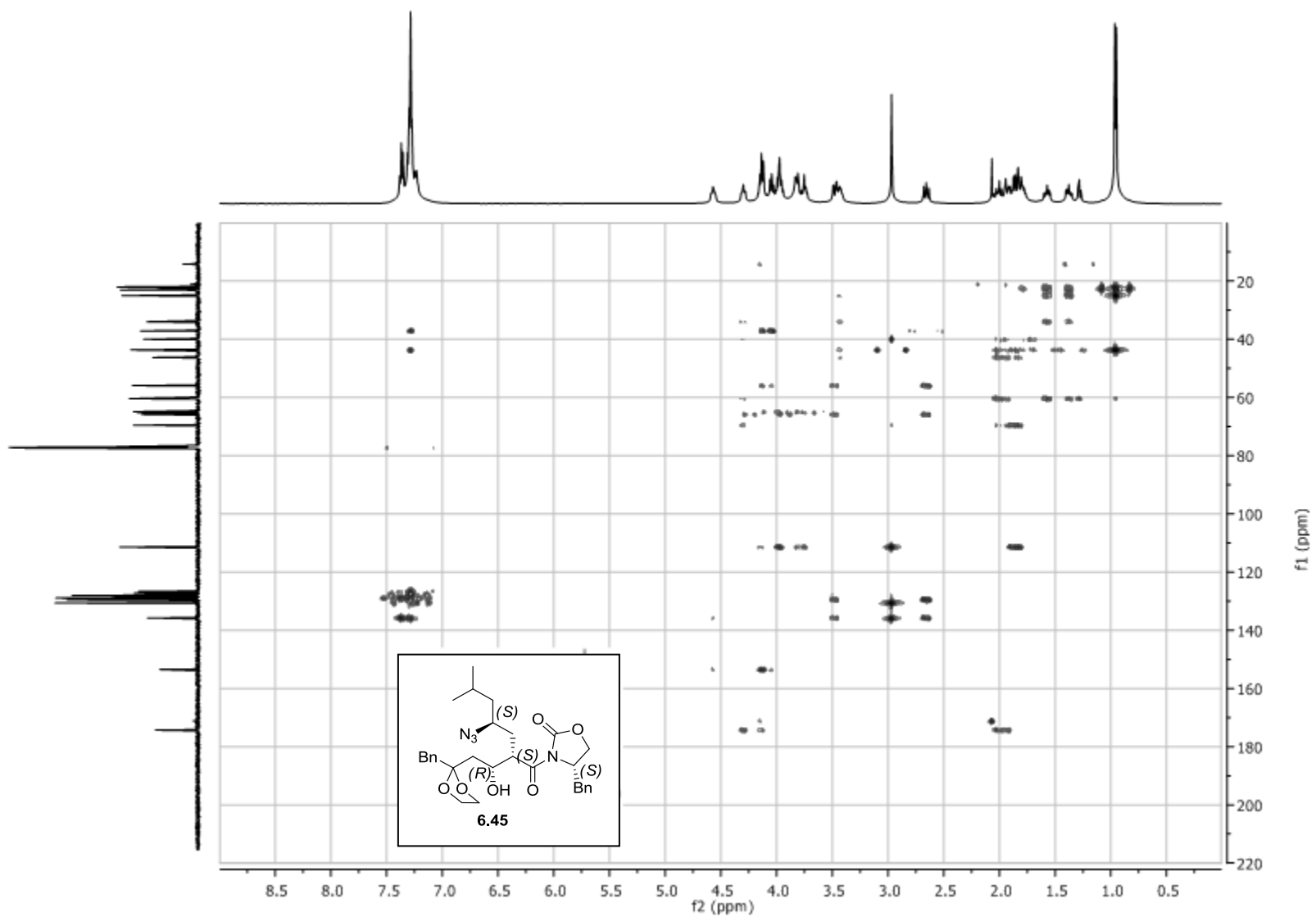
Parameter	Value
1 Spectrometer	spect
2 Solvent	CDCl3
3 Temperature	292.2
4 Pulse Sequence	zgpg30
5 Experiment	1D
6 Number of Scans	1024
7 Receiver Gain	9195
8 Relaxation Delay	3.0000
9 Pulse Width	9.5000
10 Spectrometer Frequency	125.76
11 Spectral Width	27777.8
12 Lowest Frequency	-683.9
13 Nucleus	13C
14 Acquired Size	32768
15 Spectral Size	32768

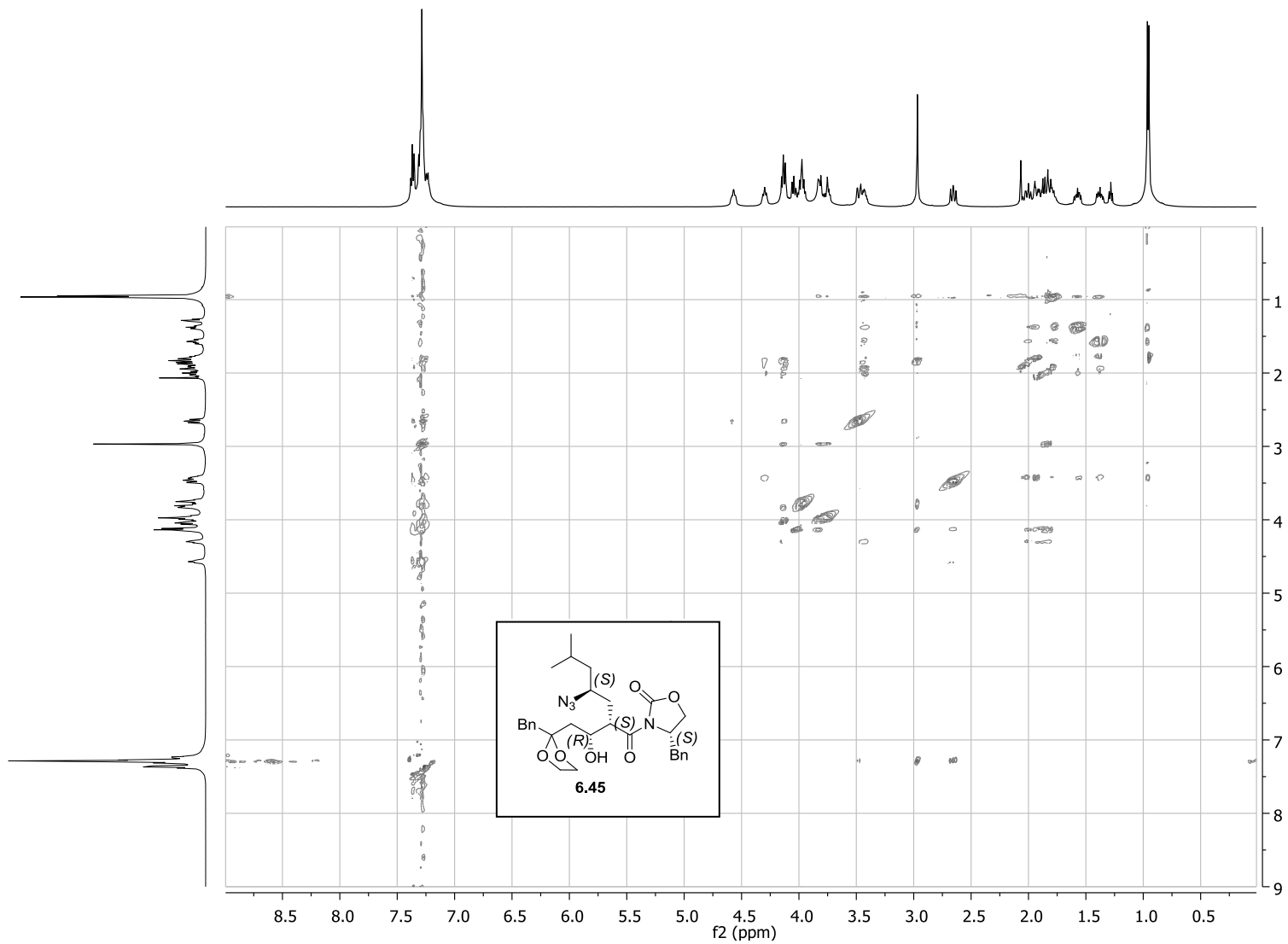


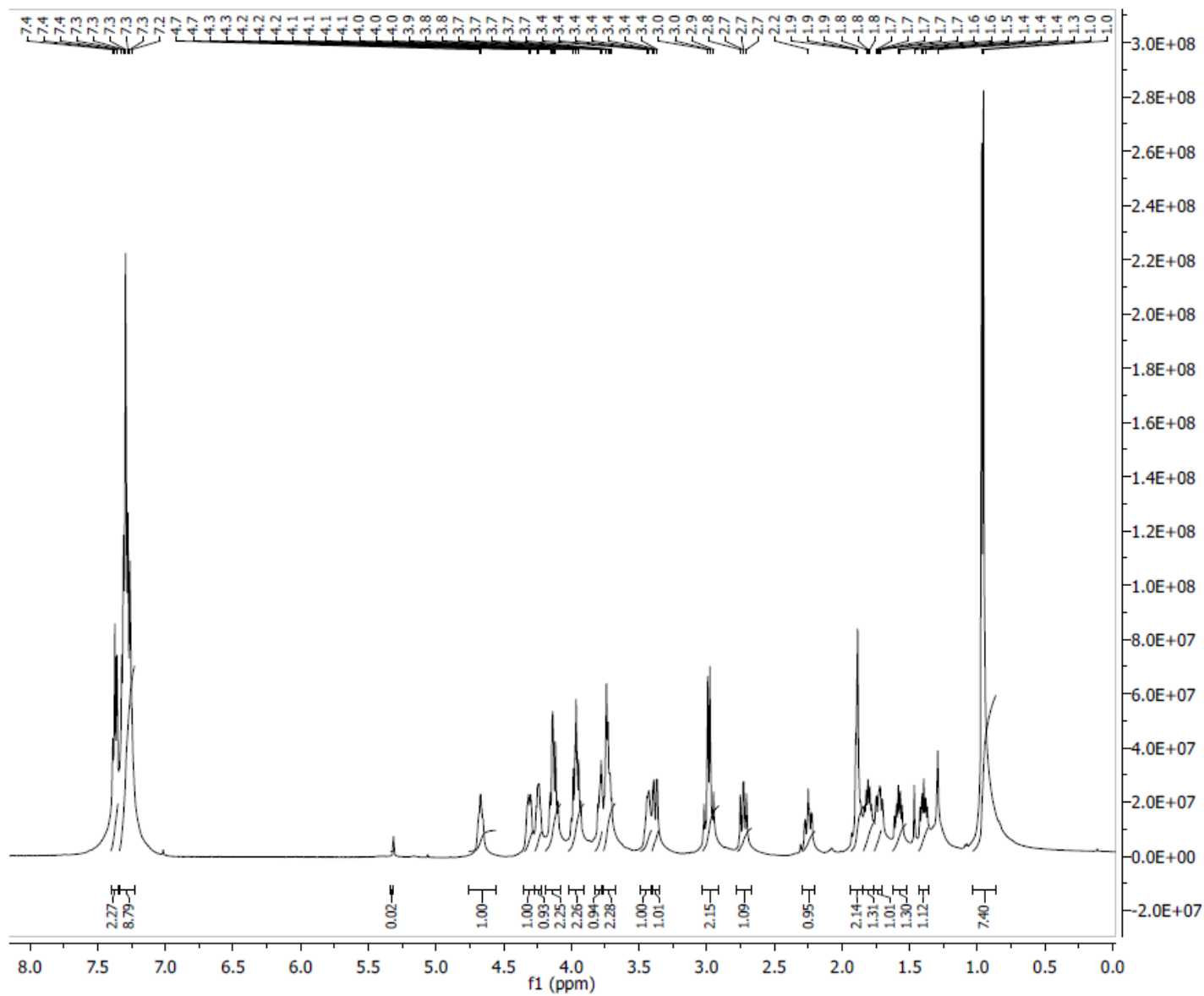




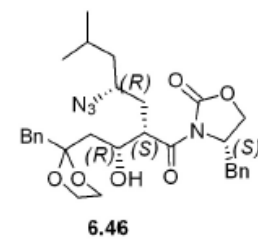


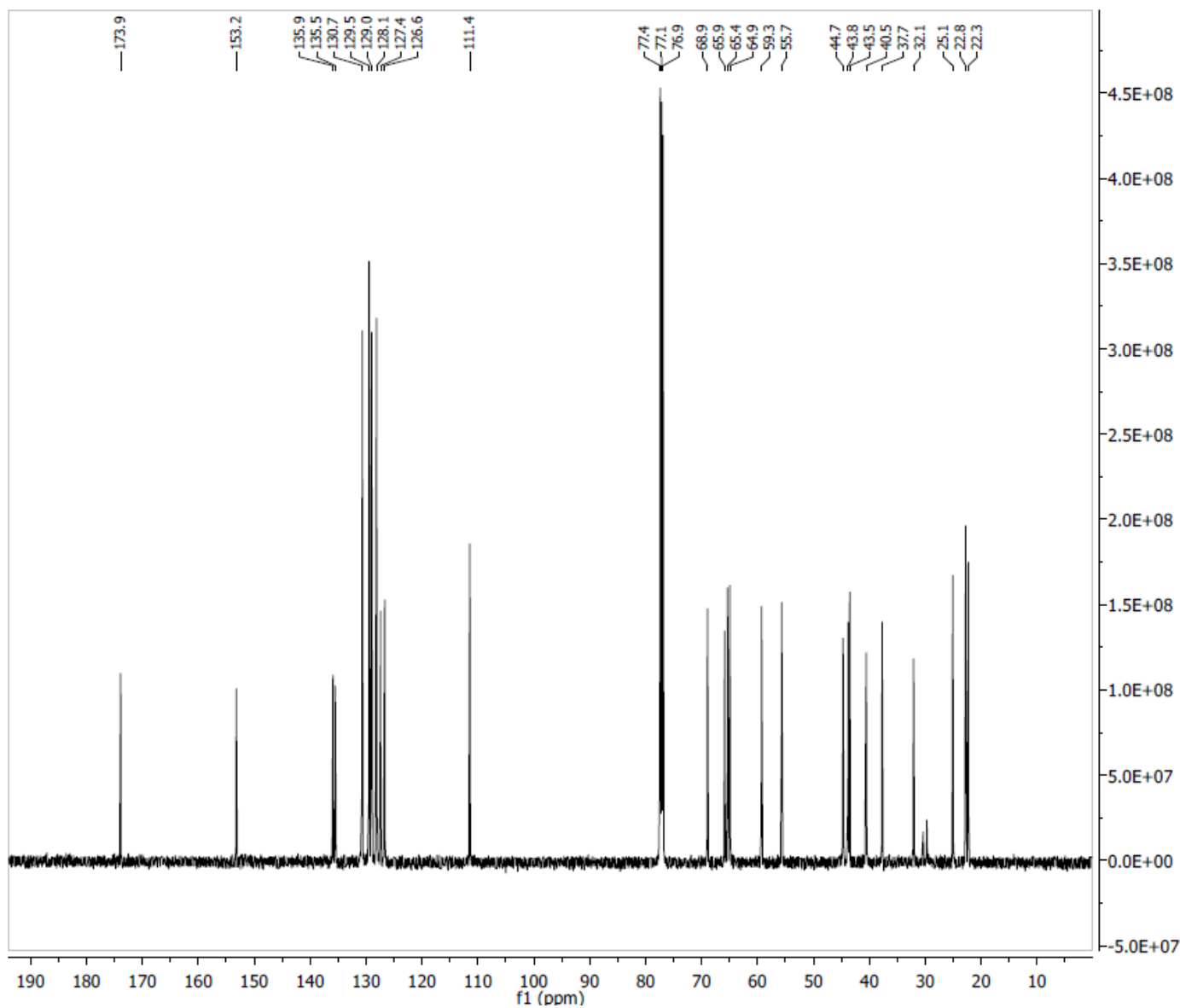




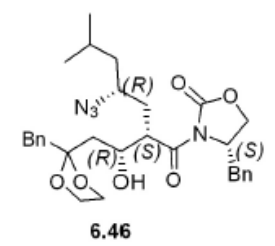


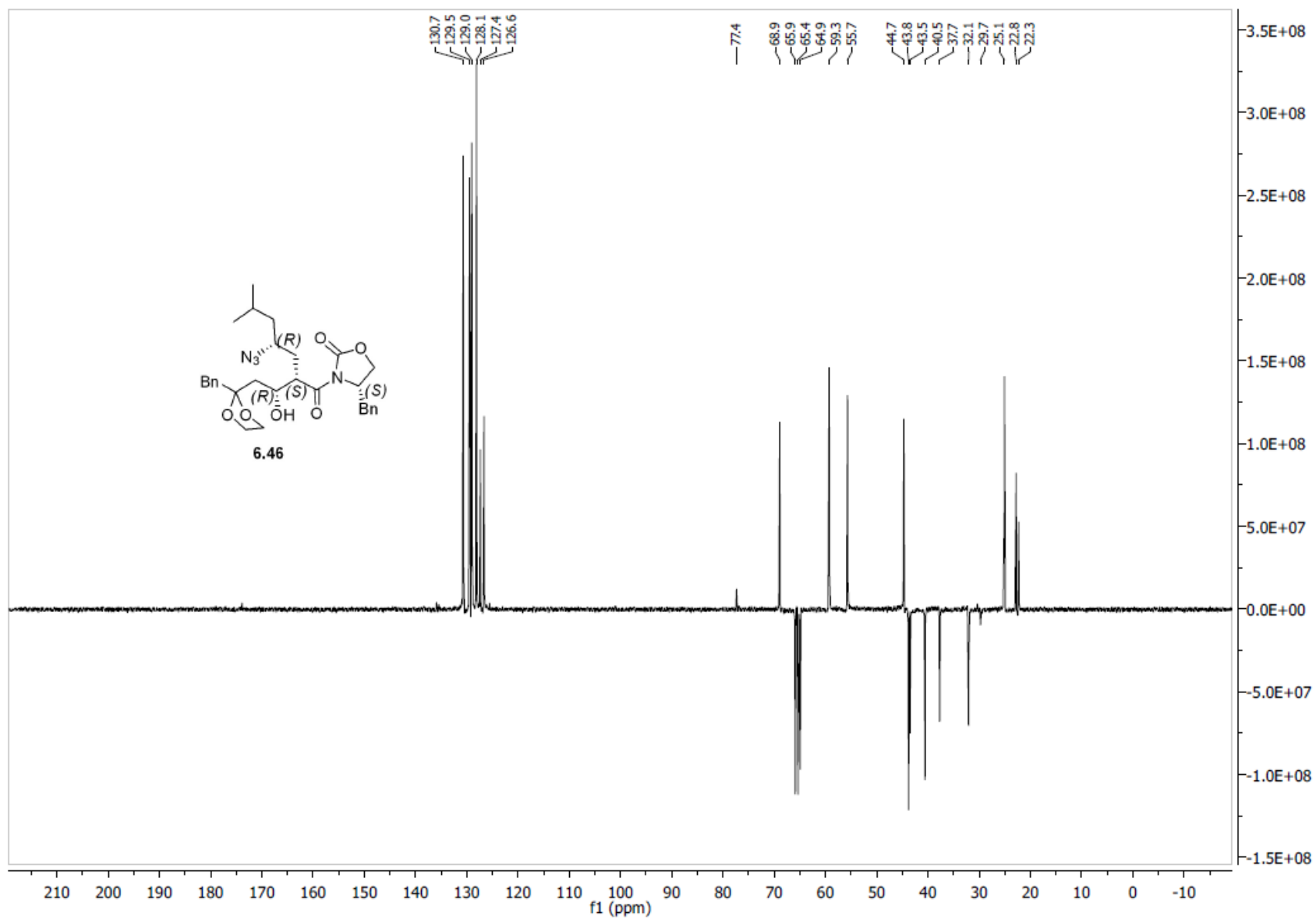
Parameter	Value
1 Spectrometer	spect
2 Solvent	CDCB
3 Temperature	292.2
4 Pulse Sequence	zg30
5 Experiment	1D
6 Number of Scans	16
7 Receiver Gain	72
8 Relaxation Delay	1.0000
9 Pulse Width	11.0000
10 Acquisition Time	1.1699
11 Spectrometer Frequency	500.13
12 Spectral Width	7002.8
13 Lowest Frequency	-250.6
14 Nucleus	1H
15 Acquired Size	8192
16 Spectral Size	16384

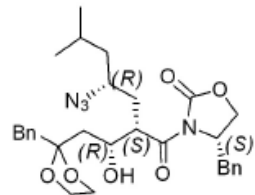




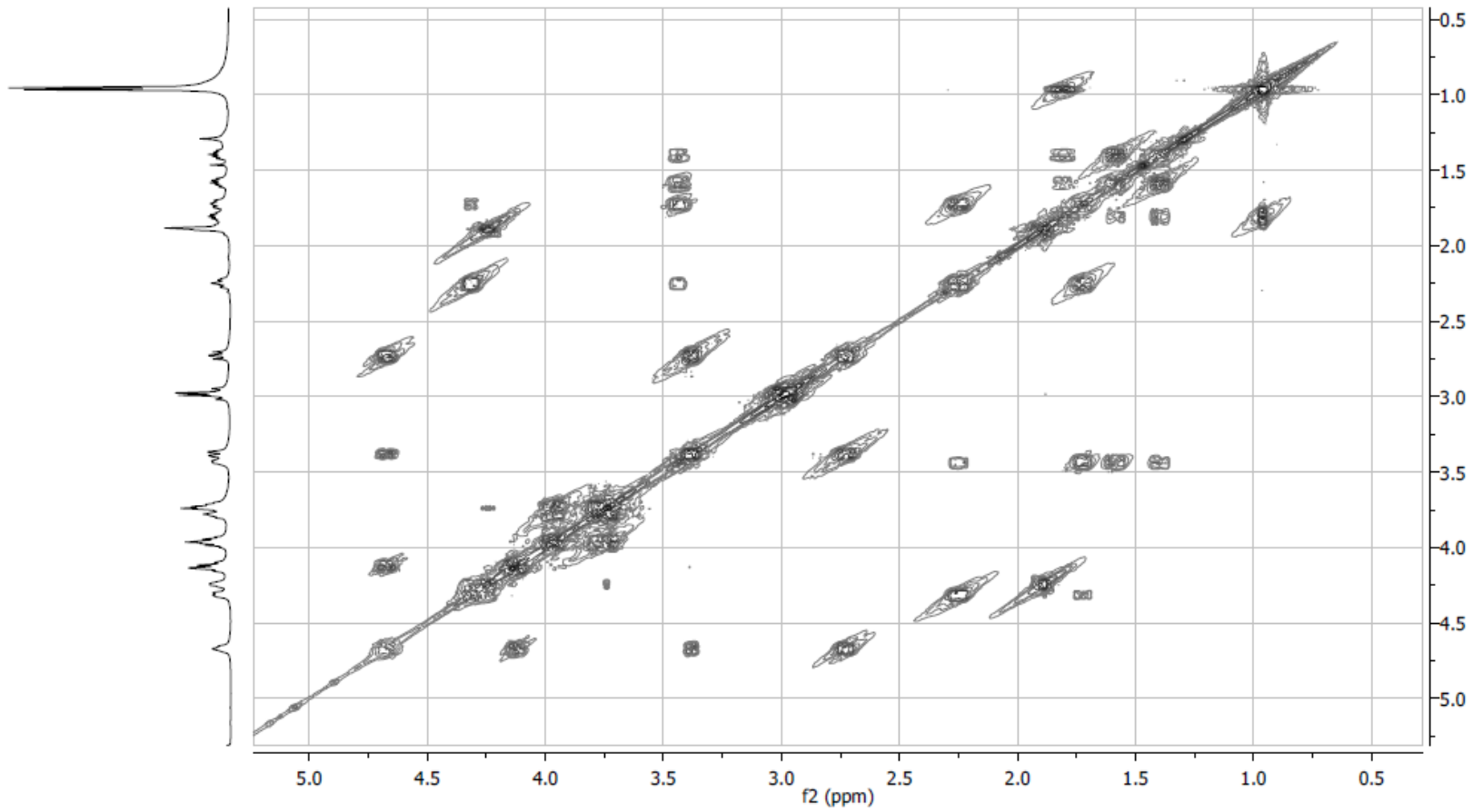
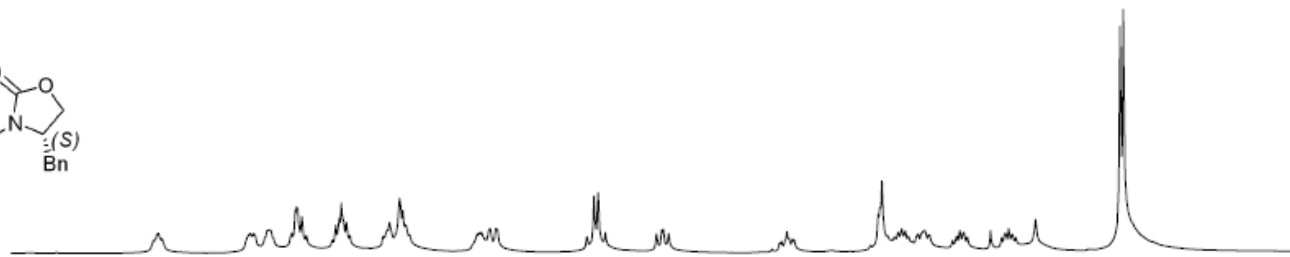
Parameter	Value
1 Spectrometer	spect
2 Solvent	CDCl3
3 Temperature	292.2
4 Pulse Sequence	zgpg30
5 Experiment	1D
6 Number of Scans	2000
7 Receiver Gain	10321
8 Relaxation Delay	3.0000
9 Pulse Width	9.5000
10 Acquisition Time	1.1797
11 Spectrometer Frequency	125.76
12 Spectral Width	27777.8
13 Lowest Frequency	-683.9
14 Nucleus	13C
15 Acquired Size	32768
16 Spectral Size	32768







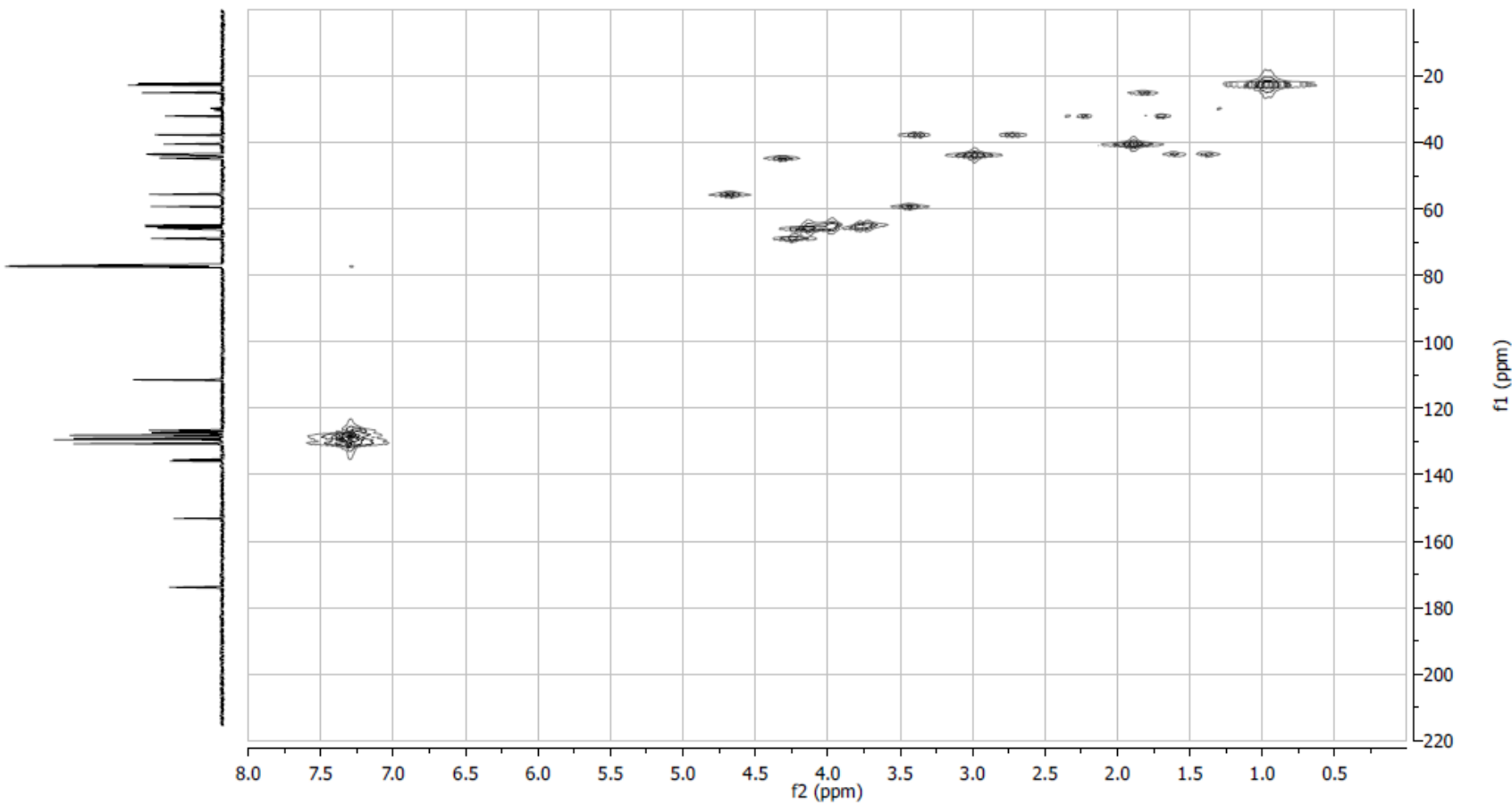
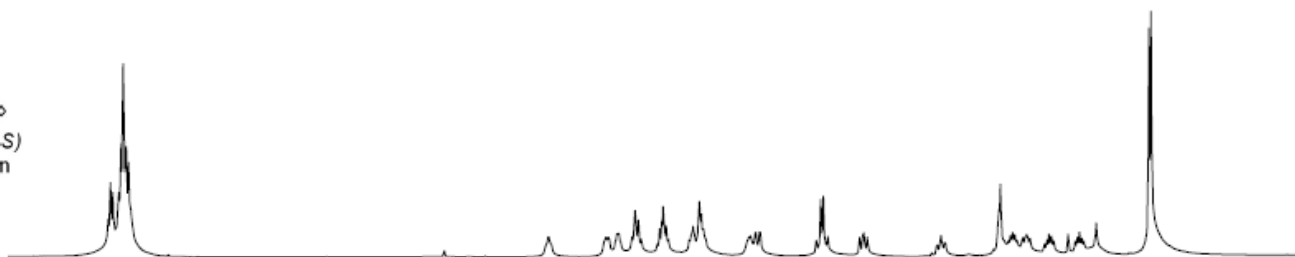
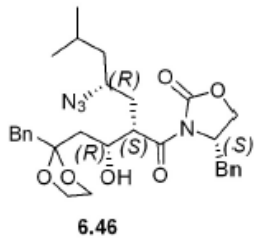
6.46

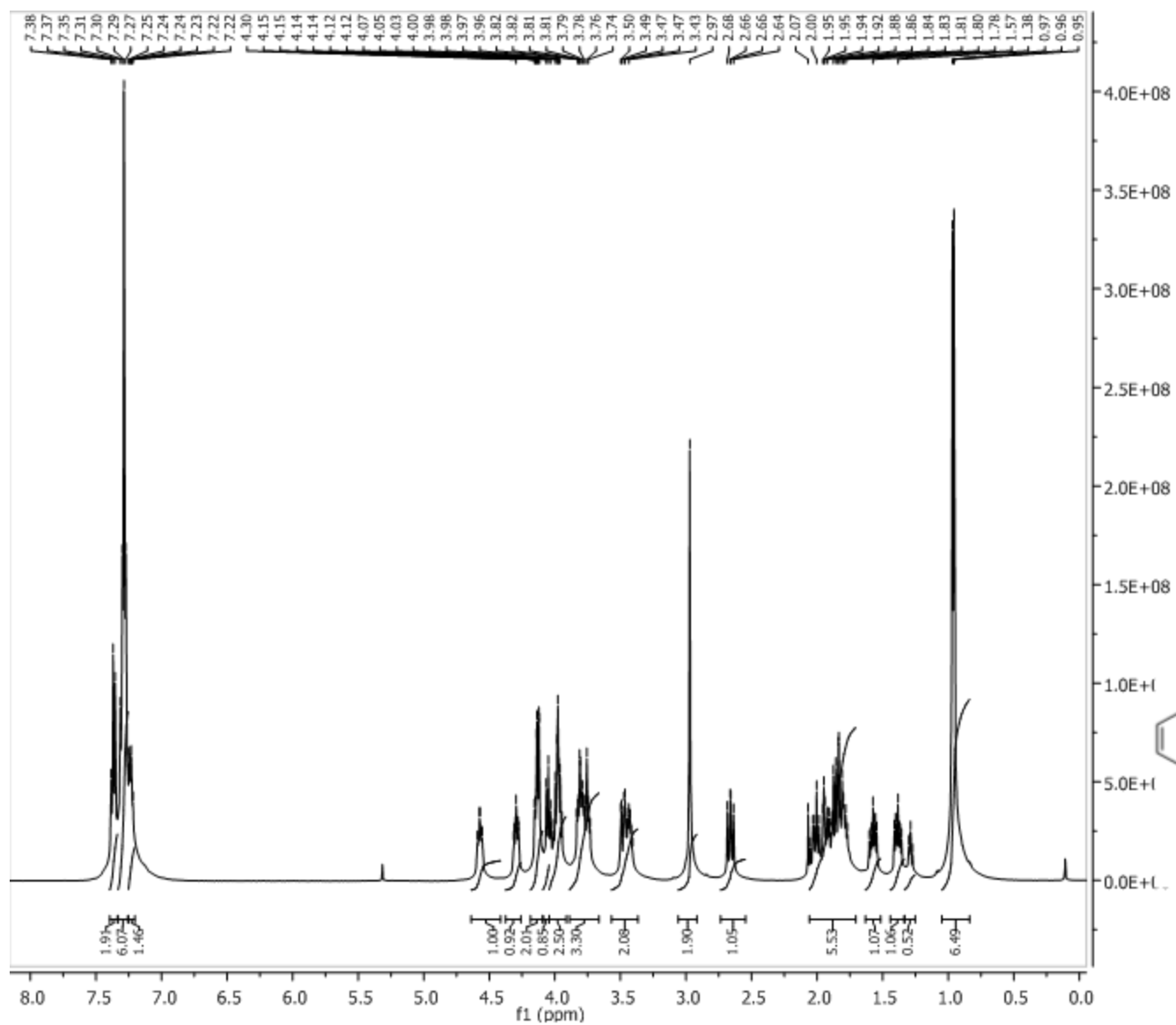


f1 (ppm)

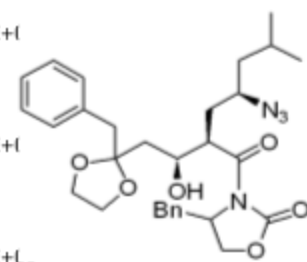
336

f2 (ppm)

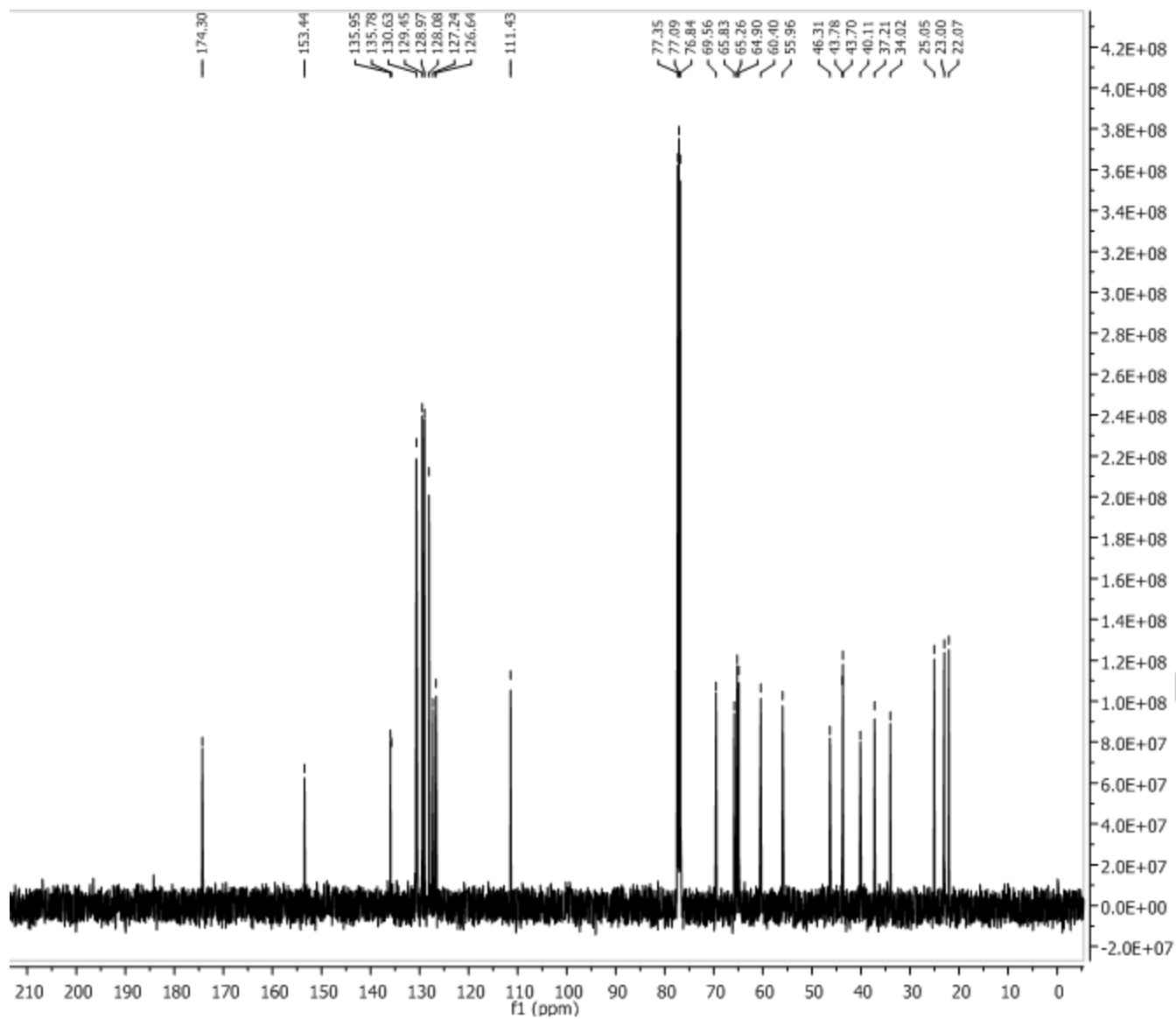




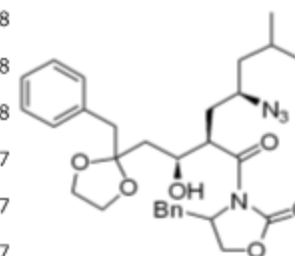
Parameter	Value
1 Spectrometer	spect
2 Solvent	CDCl3
3 Temperature	298.2
4 Pulse Sequence	zg30
5 Experiment	1D
6 Number of Scans	16
7 Receiver Gain	114
8 Relaxation Delay	1.0000
9 Pulse Width	11.0000
10 Spectrometer Frequency	500.13
11 Spectral Width	7002.8
12 Lowest Frequency	-250.6
13 Nucleus	1H
14 Acquired Size	8192
15 Spectral Size	16384



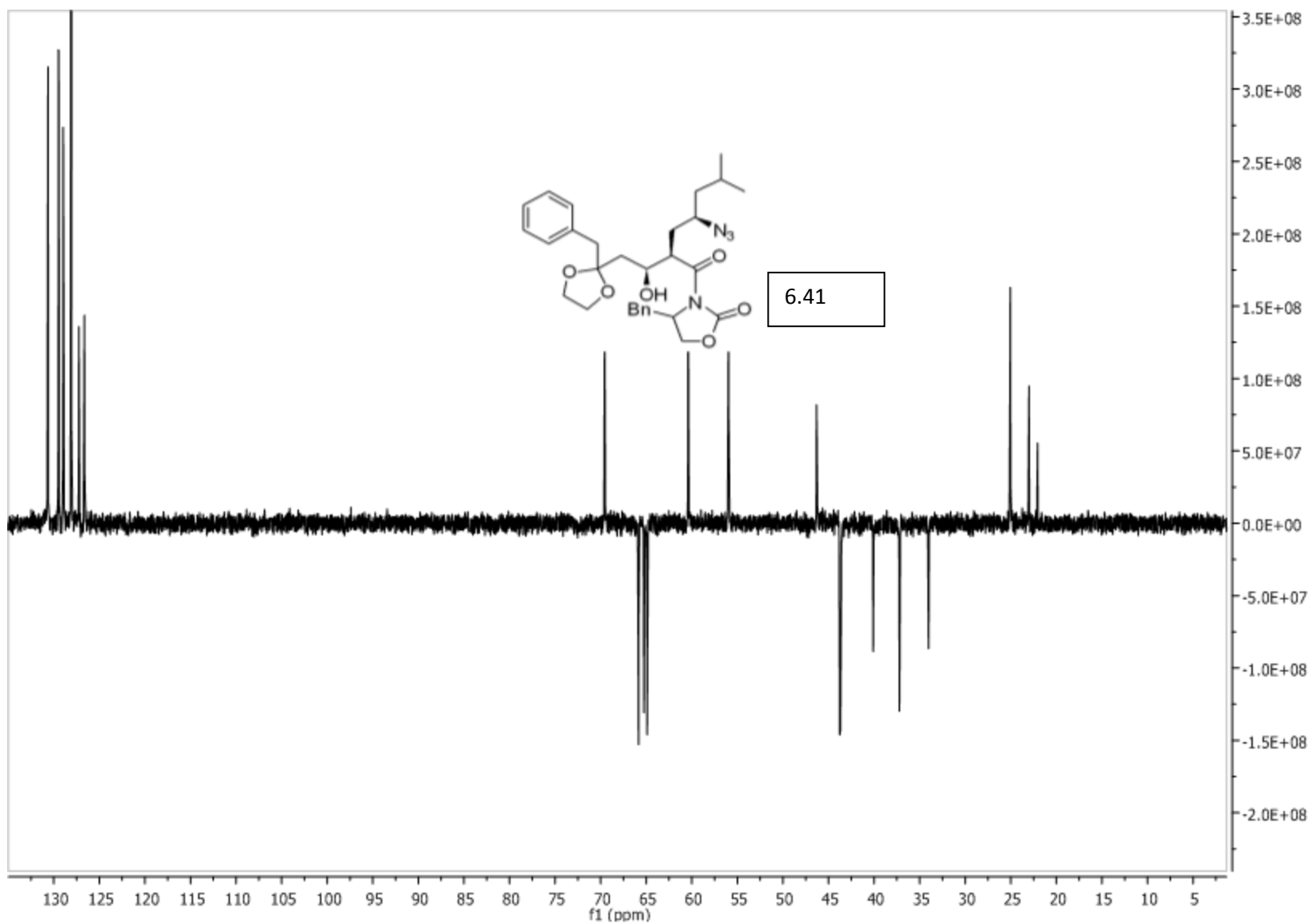
6.41

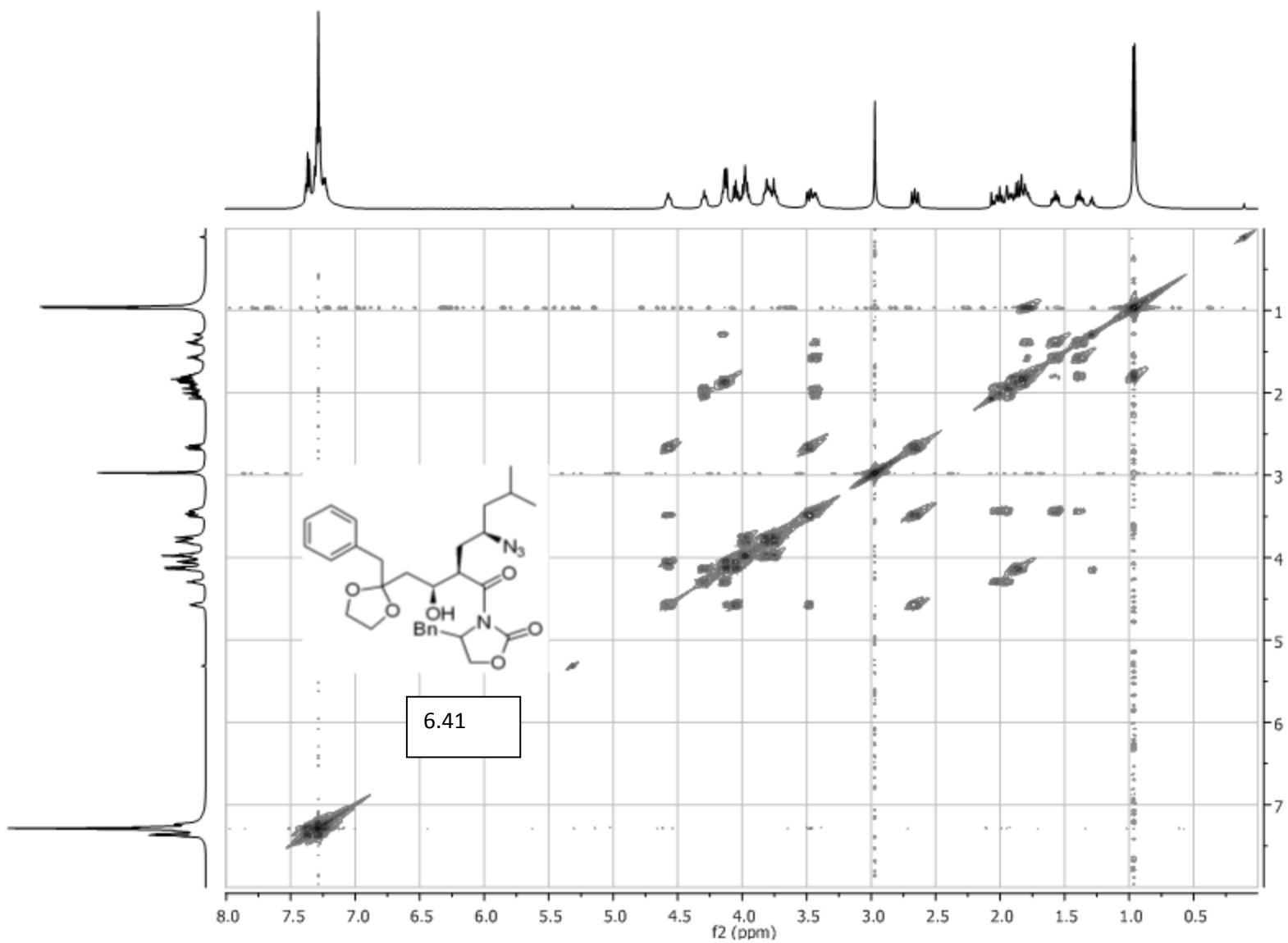


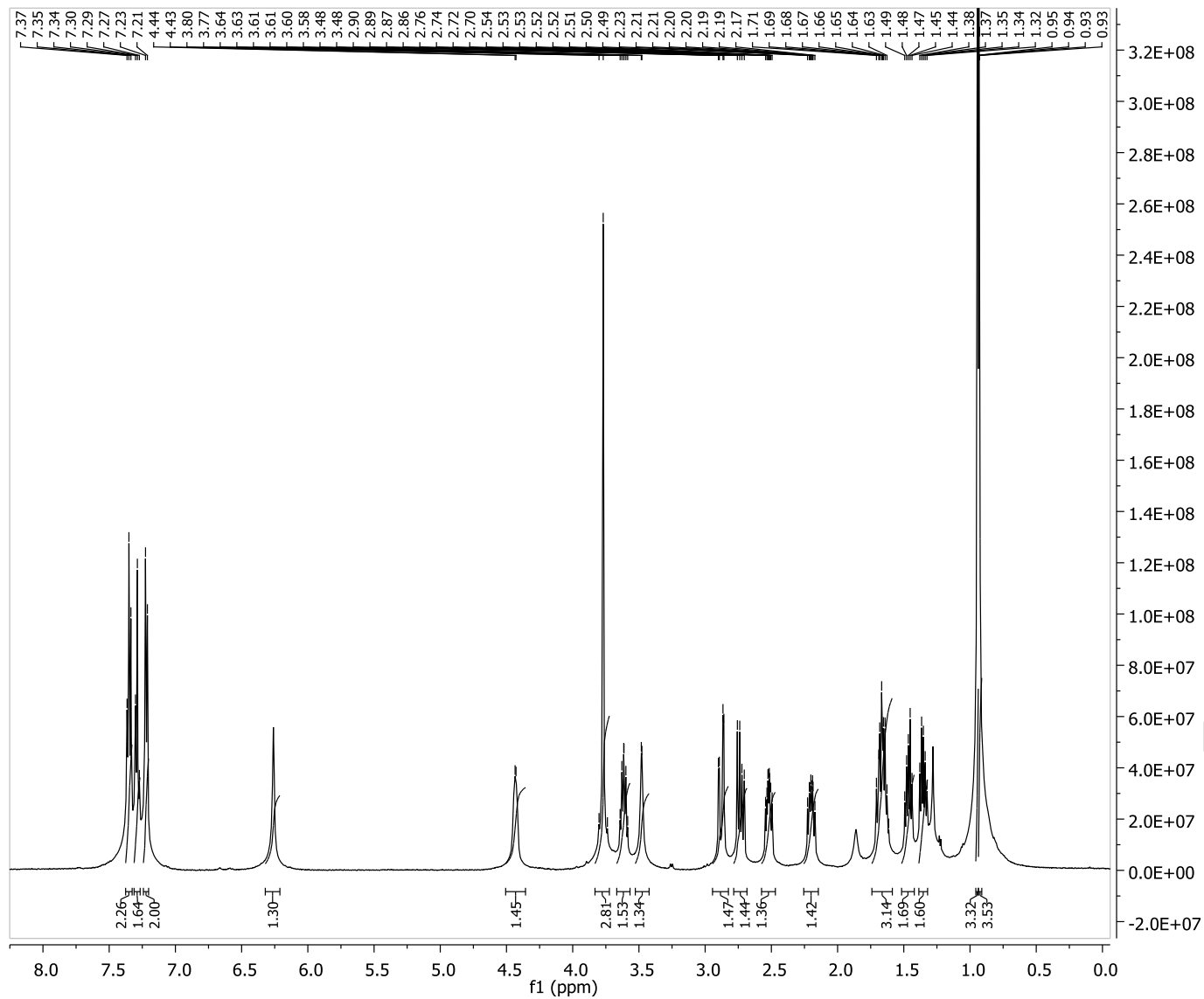
Parameter	Value
1 Spectrometer	spect
2 Solvent	CDCl3
3 Temperature	298.2
4 Pulse Sequence	zgpg30
5 Experiment	1D
6 Number of Scans	200
7 Receiver Gain	9195
8 Relaxation Delay	3.0000
9 Pulse Width	9.5000
10 Spectrometer Frequency	125.76
11 Spectral Width	27777.8
12 Lowest Frequency	-683.9
13 Nucleus	13C
14 Acquired Size	32768
15 Spectral Size	32768



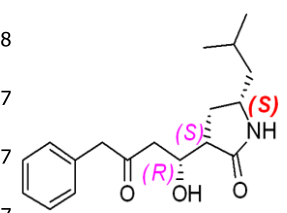
6.41



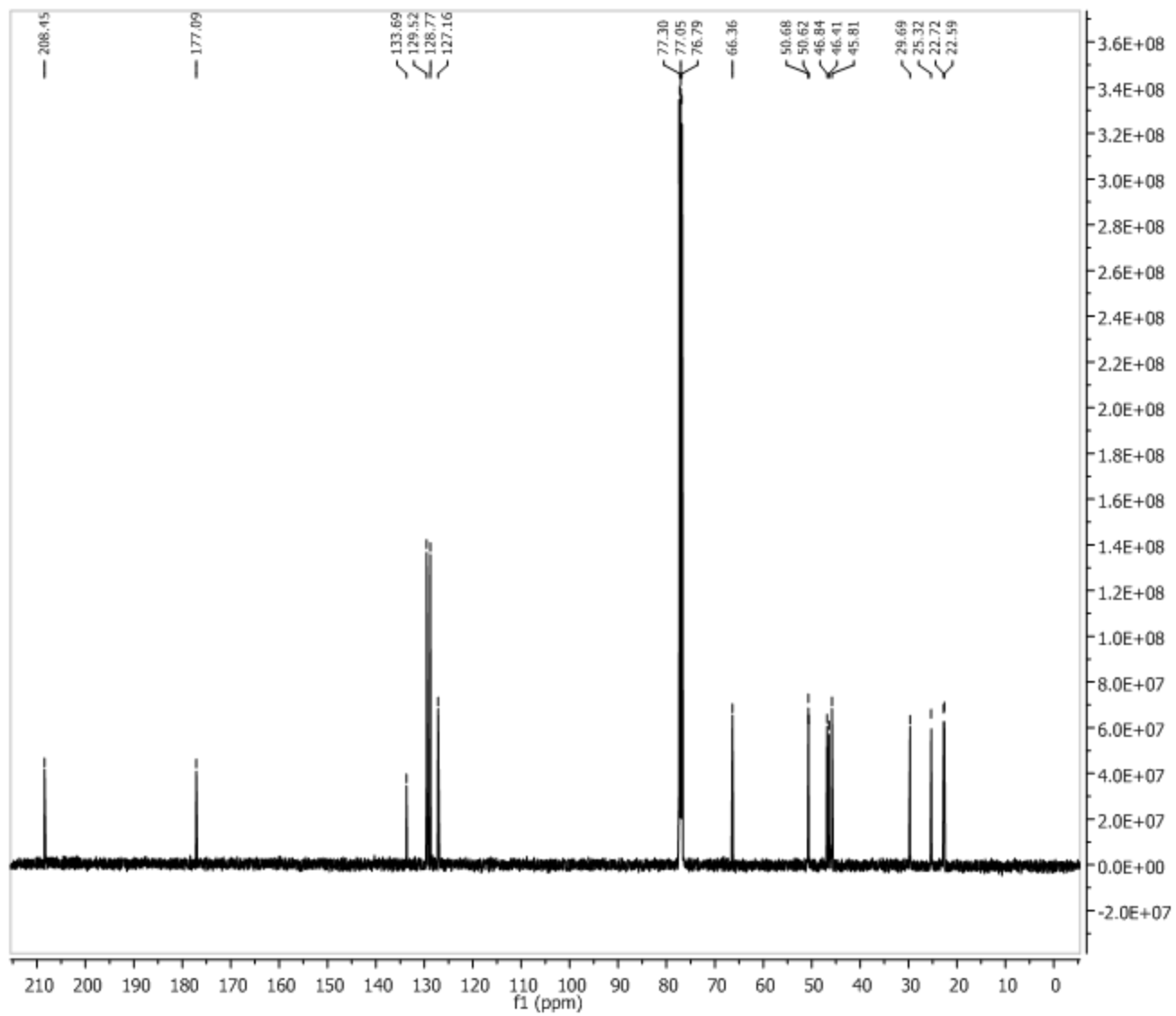




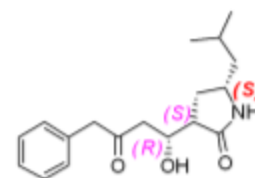
Parameter	Value
1 Spectrometer	spect
2 Solvent	CDCI3
3 Temperature	298.2
4 Pulse Sequence	zg30
5 Experiment	1D
6 Number of Scans	16
7 Receiver Gain	256
8 Relaxation Delay	1.0000
9 Pulse Width	11.0000
10 Spectrometer Frequency	500.13
11 Spectral Width	7002.8
12 Lowest Frequency	-250.6
13 Nucleus	1H
14 Acquired Size	8192
15 Spectral Size	16384



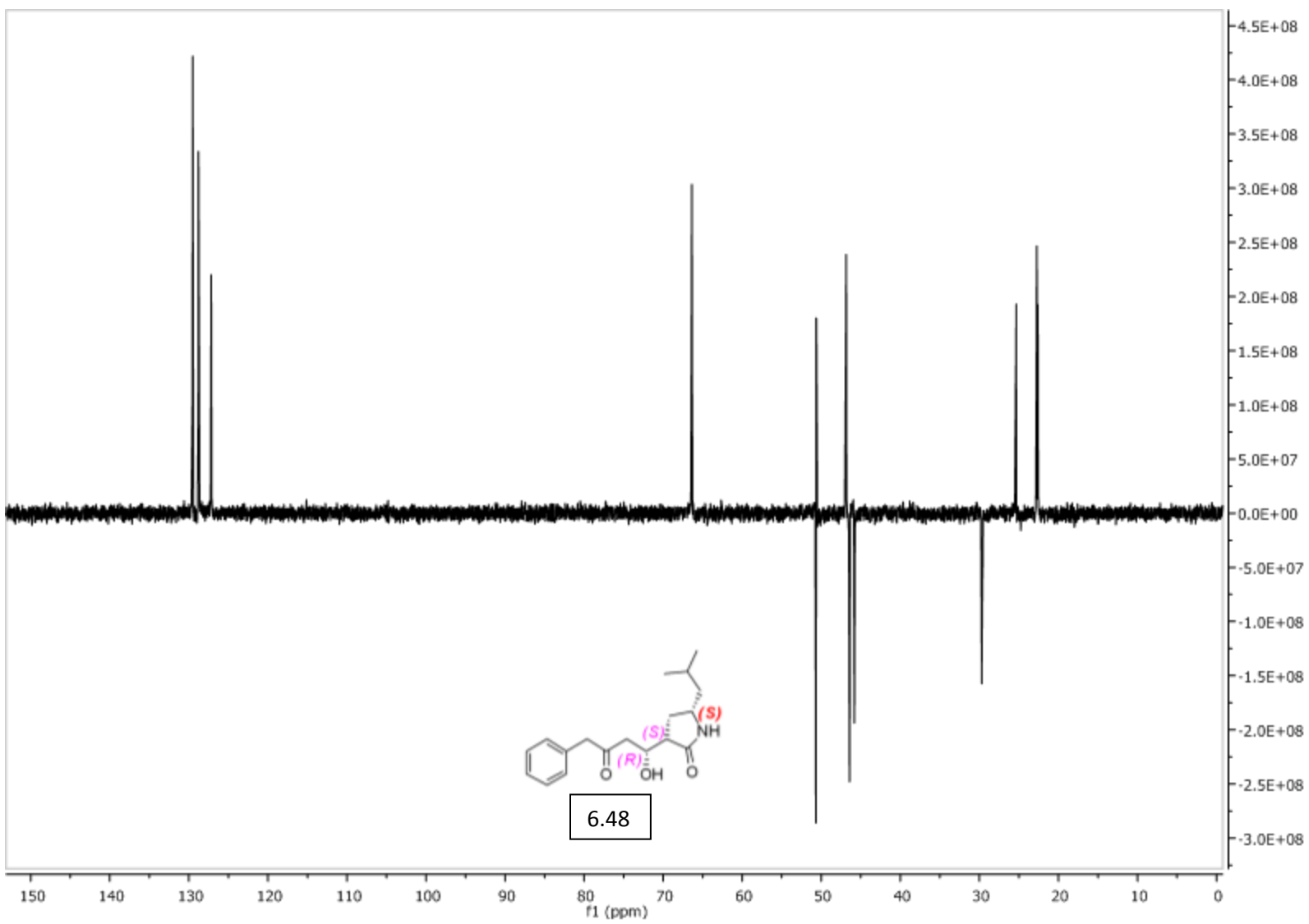
6.48

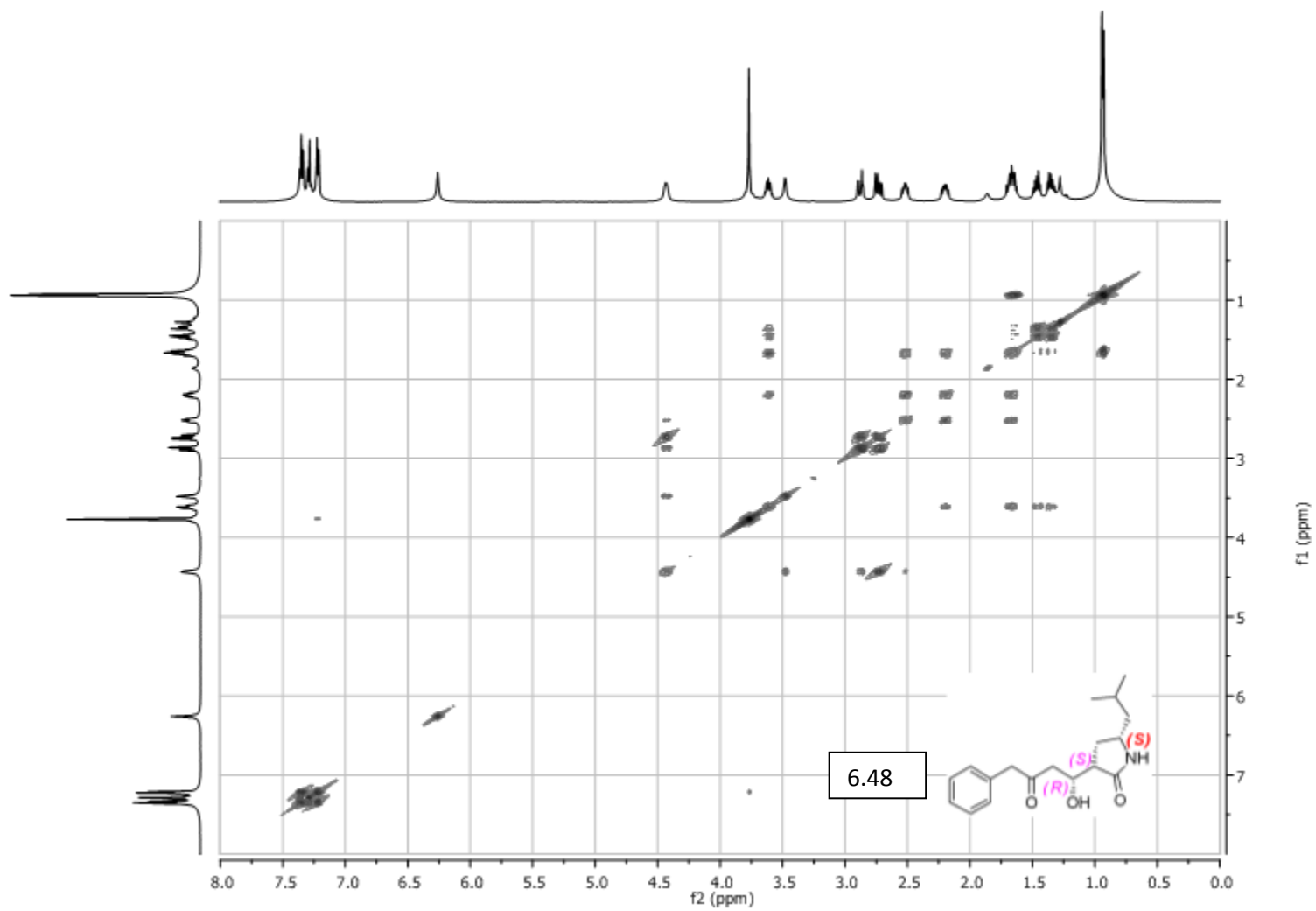


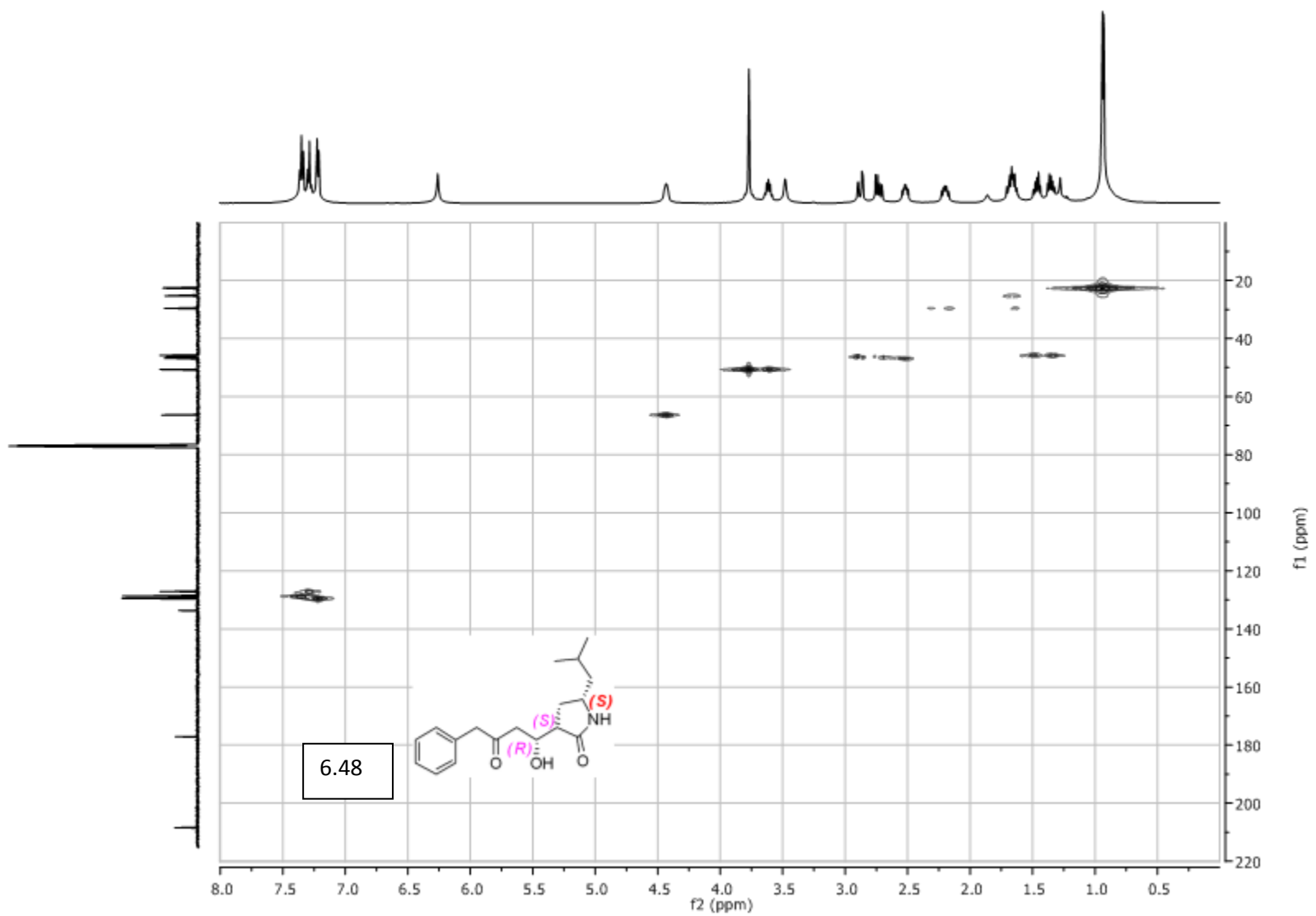
Parameter	Value
1 Spectrometer	spect
2 Solvent	CDCl3
3 Temperature	298.2
4 Pulse Sequence	zgpg30
5 Experiment	1D
6 Number of Scans	2000
7 Receiver Gain	6502
8 Relaxation Delay	3.0000
9 Pulse Width	9.5000
10 Spectrometer Frequency	125.76
11 Spectral Width	27777.8
12 Lowest Frequency	-683.9
13 Nucleus	13C
14 Acquired Size	32768
15 Spectral Size	32768

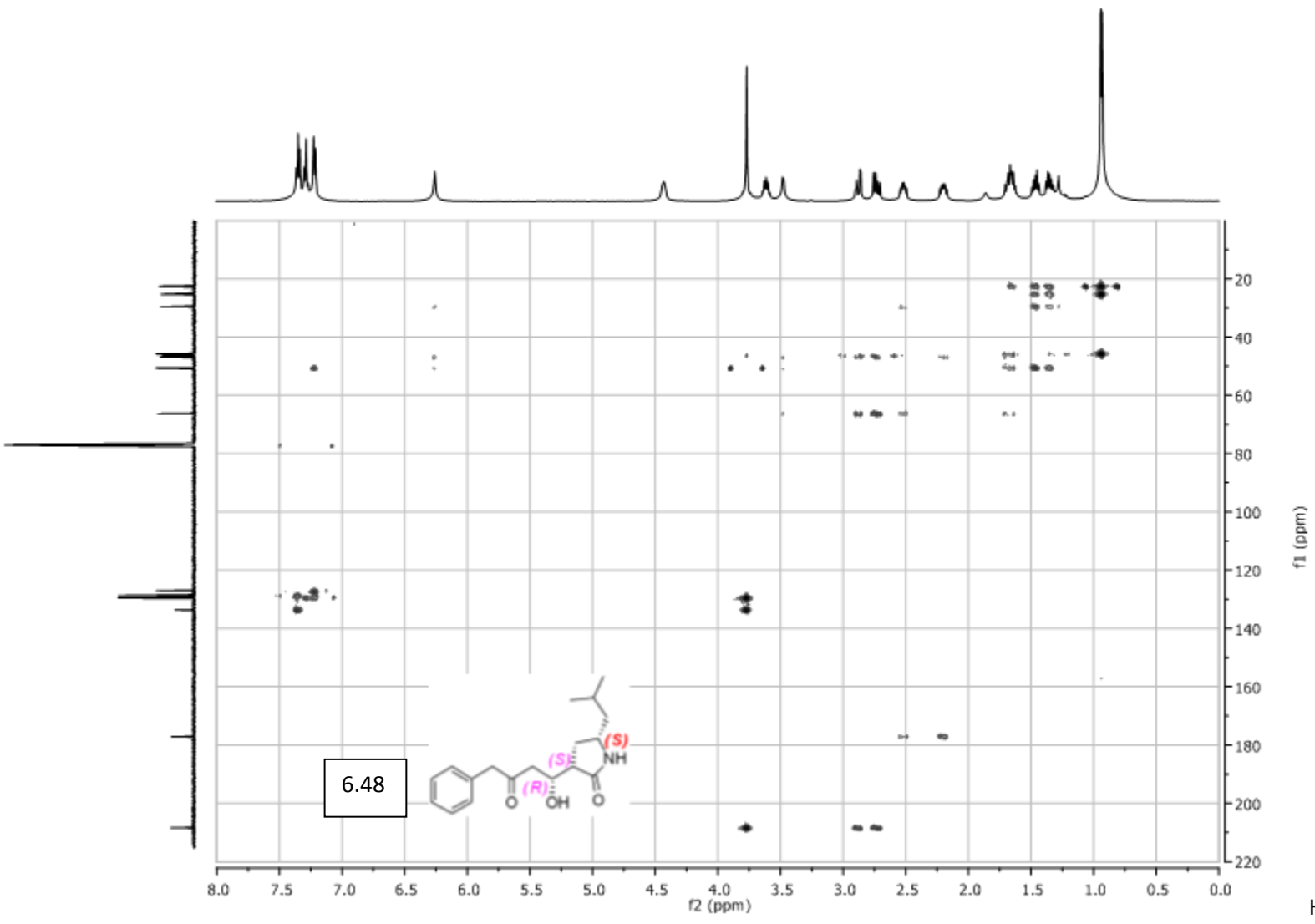


6.48



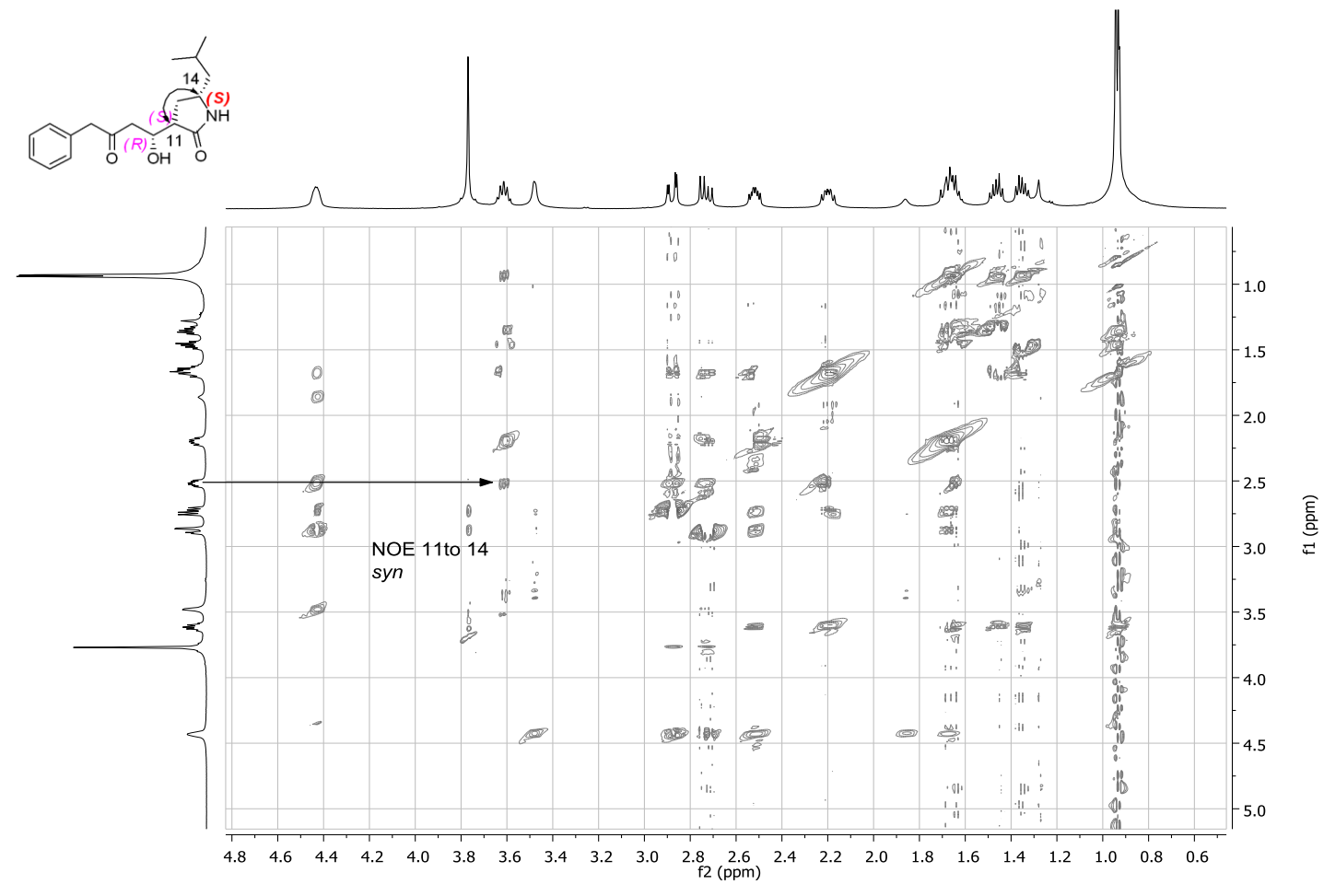
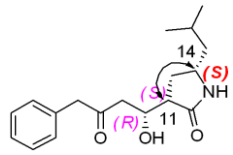




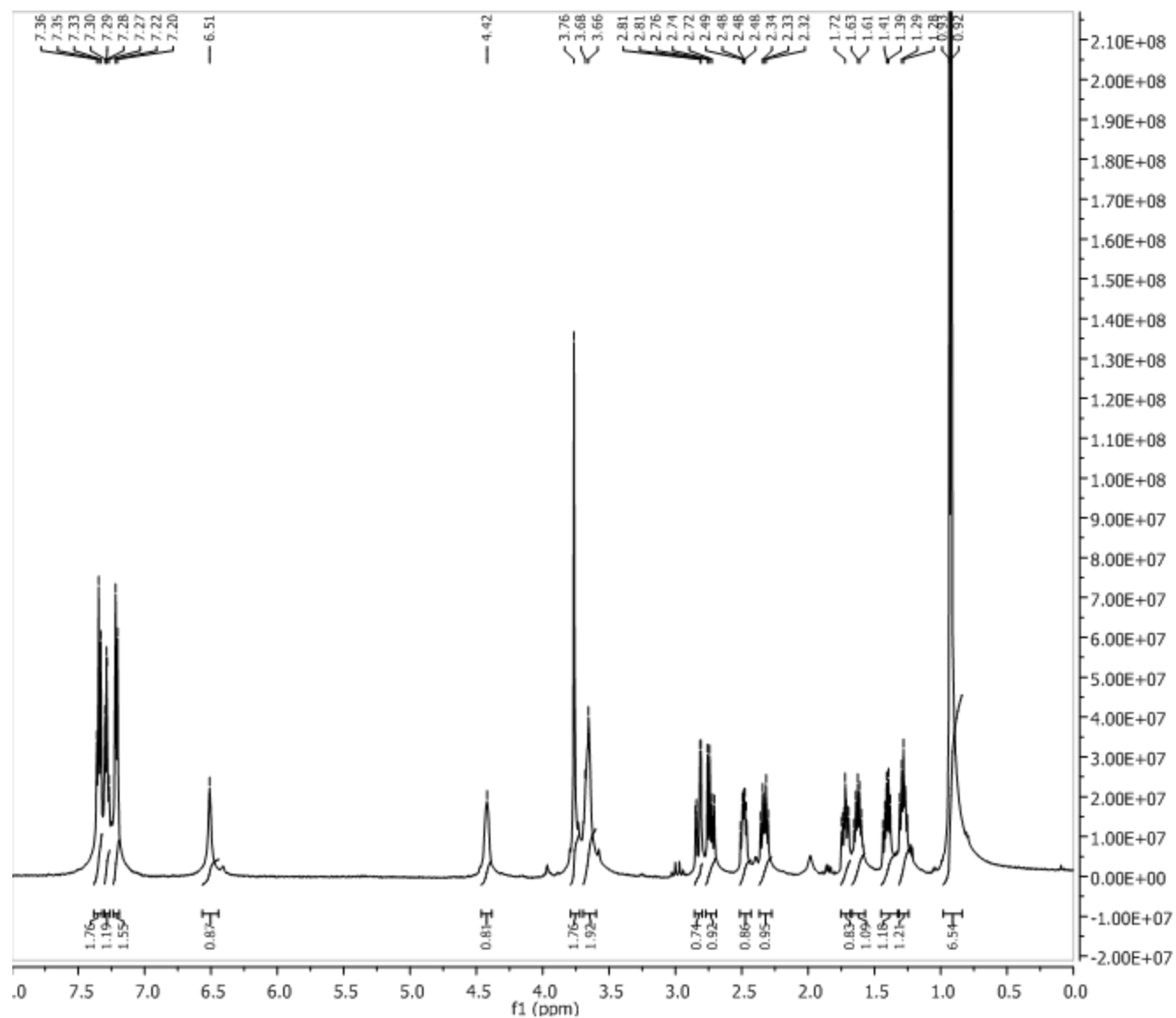


HMBC

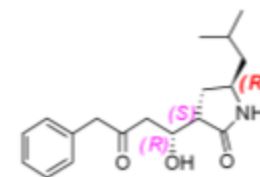
6.48



NOESY

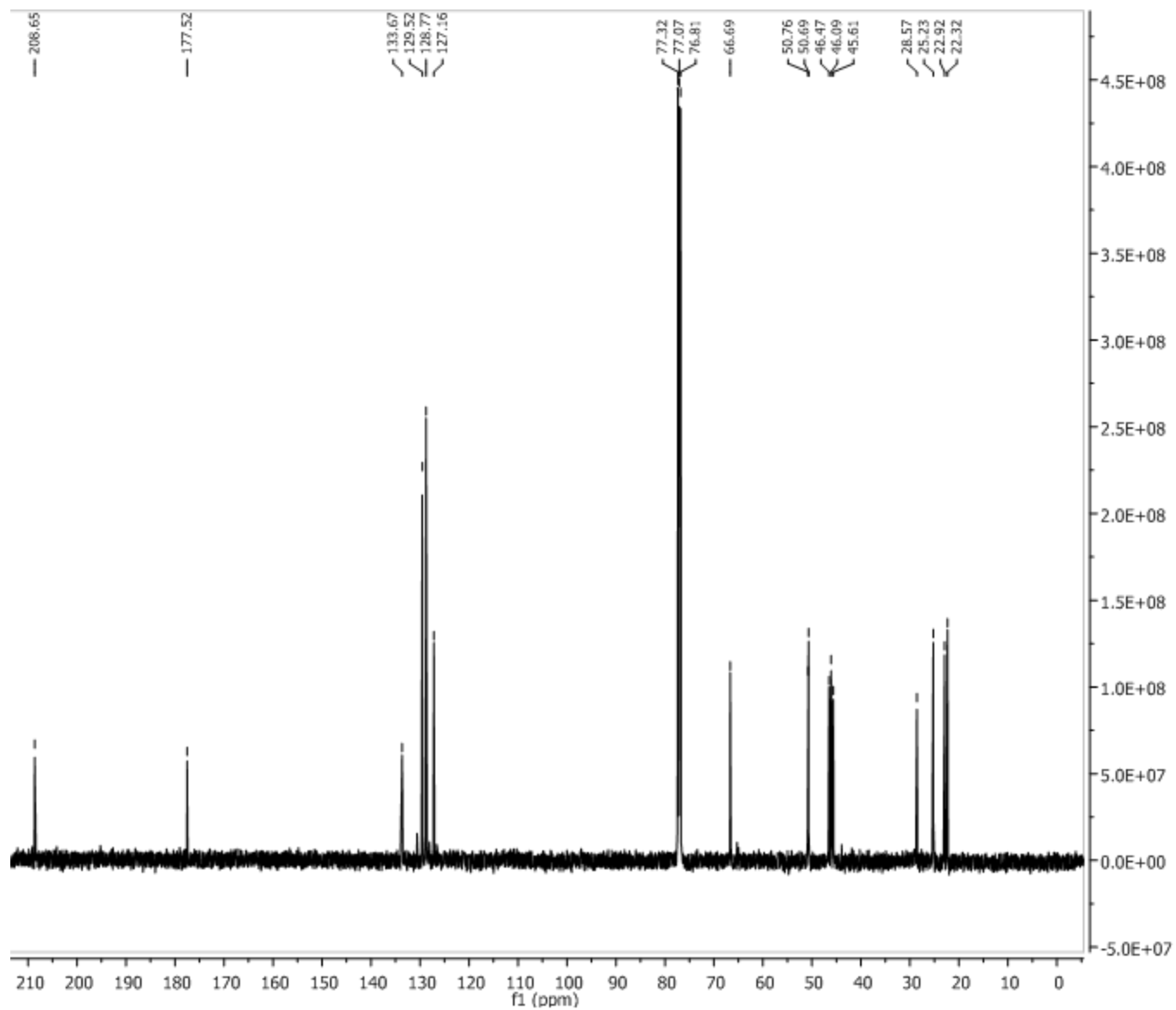


Parameter	Value
1 Spectrometer	spect
2 Solvent	CDCl3
3 Temperature	298.2
4 Pulse Sequence	zg30
5 Experiment	1D
6 Number of Scans	2
7 Receiver Gain	181
8 Relaxation Delay	1.0000
9 Pulse Width	11.0000
10 Spectrometer Frequency	500.13
11 Spectral Width	7002.8
12 Lowest Frequency	-250.6
13 Nucleus	1H
14 Acquired Size	8192
15 Spectral Size	16384

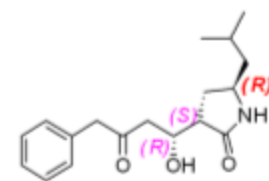


RSR

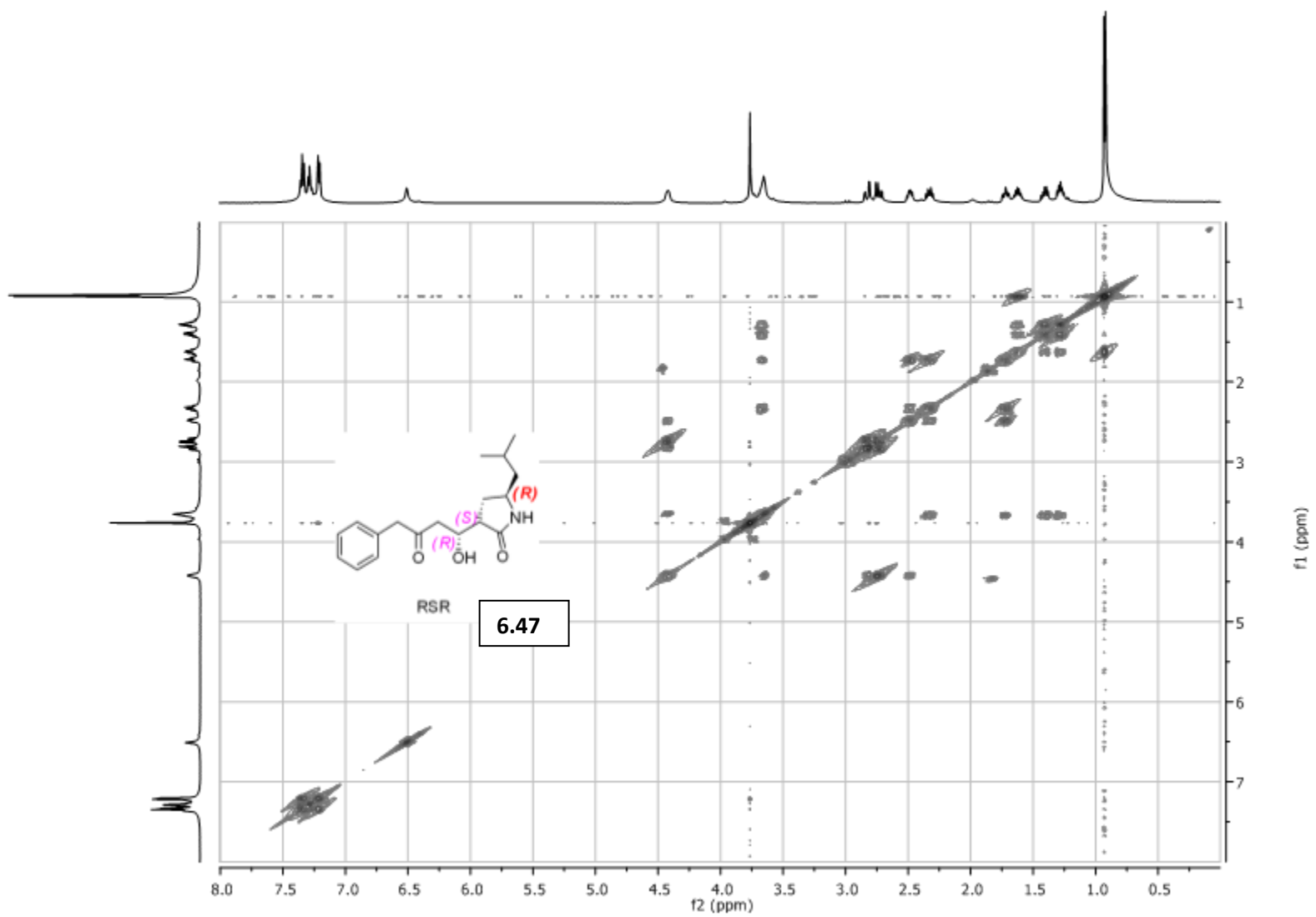
6.47

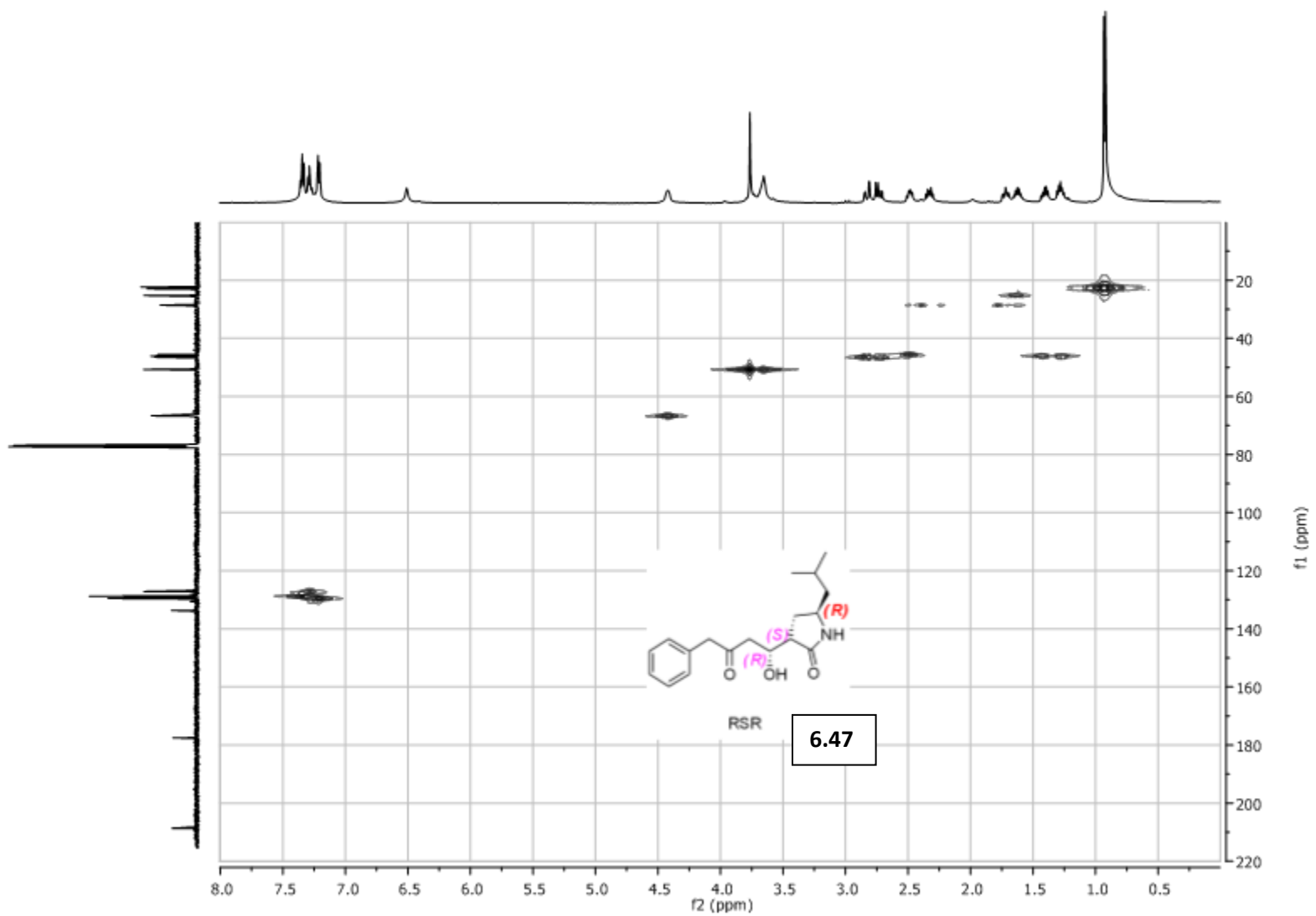


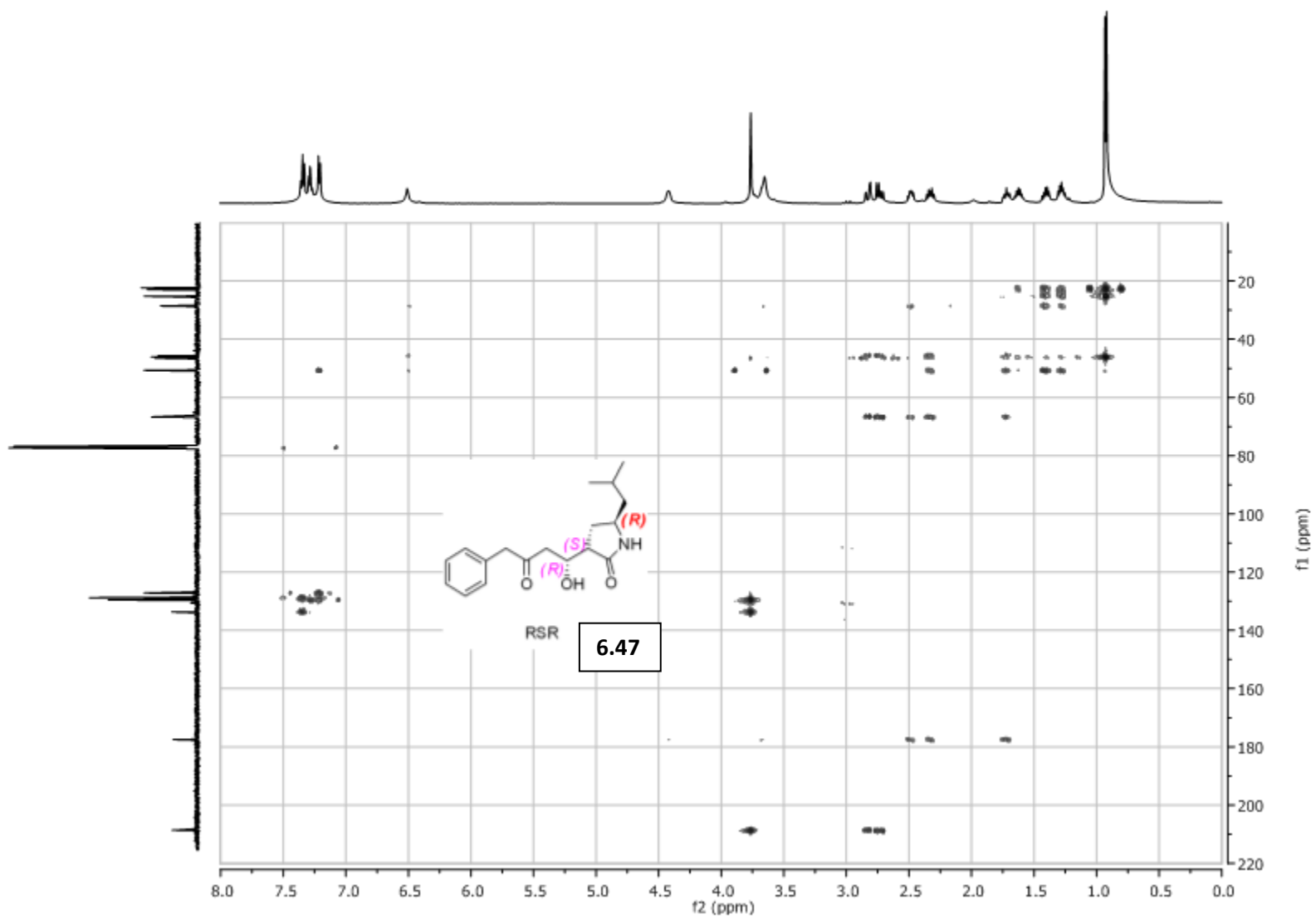
Parameter	Value
1 Spectrometer	spect
2 Solvent	CDCl3
3 Temperature	298.2
4 Pulse Sequence	zgpg30
5 Experiment	1D
6 Number of Scans	980
7 Receiver Gain	9195
8 Relaxation Delay	3.0000
9 Pulse Width	9.5000
10 Spectrometer Frequency	125.76
11 Spectral Width	27777.8
12 Lowest Frequency	-683.9
13 Nucleus	13C
14 Acquired Size	32768
15 Spectral Size	32768



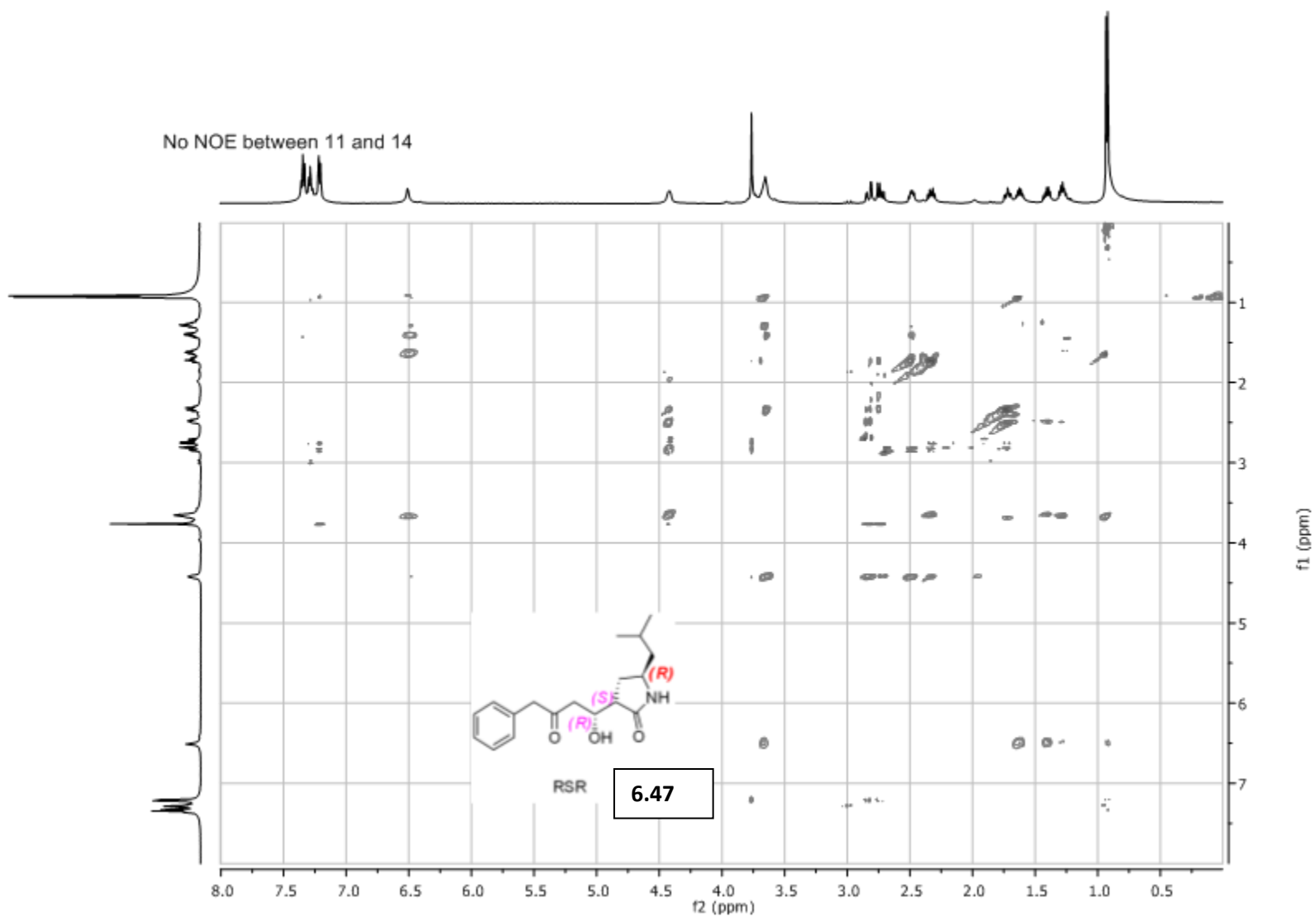
RSR 6.47

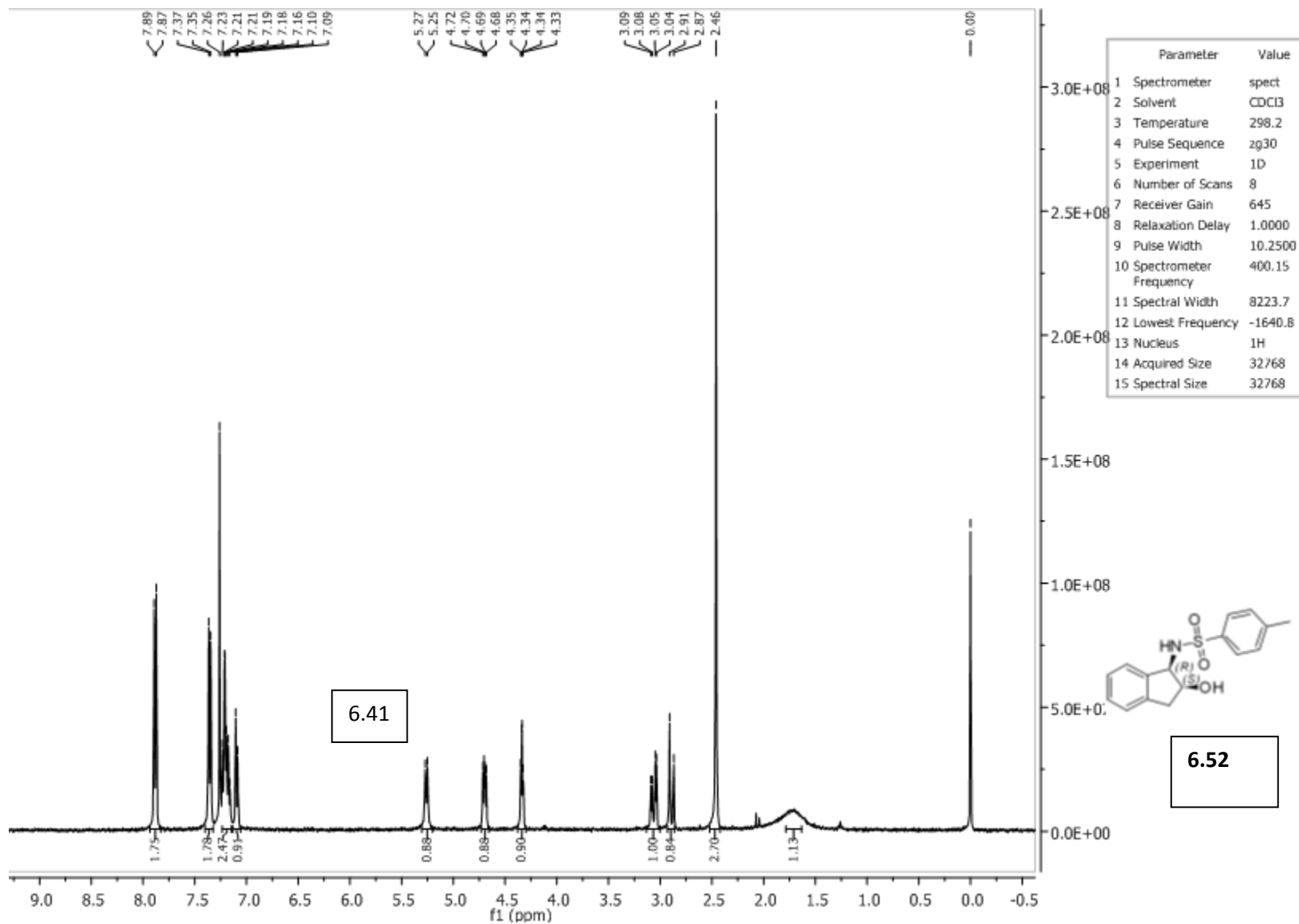


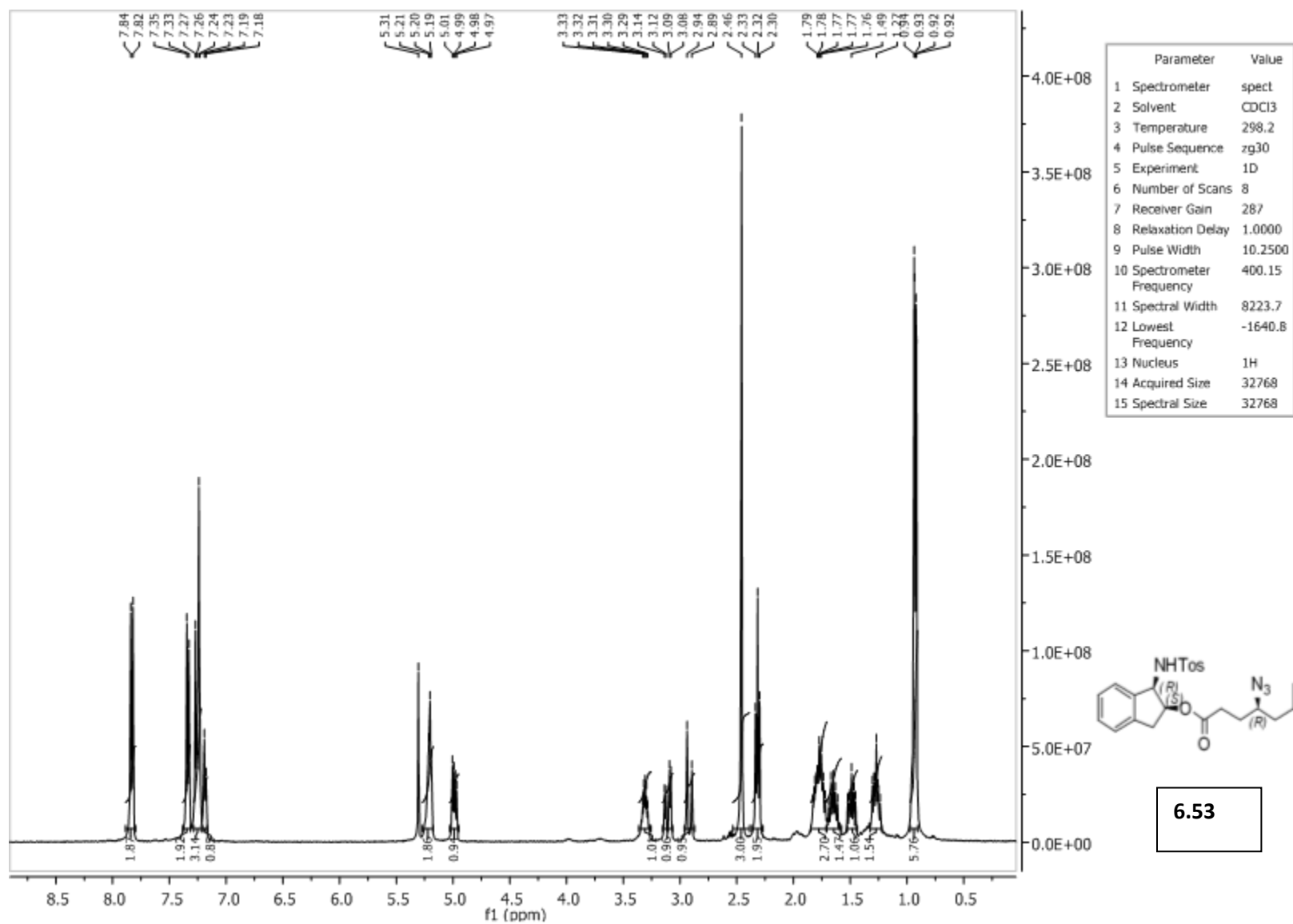


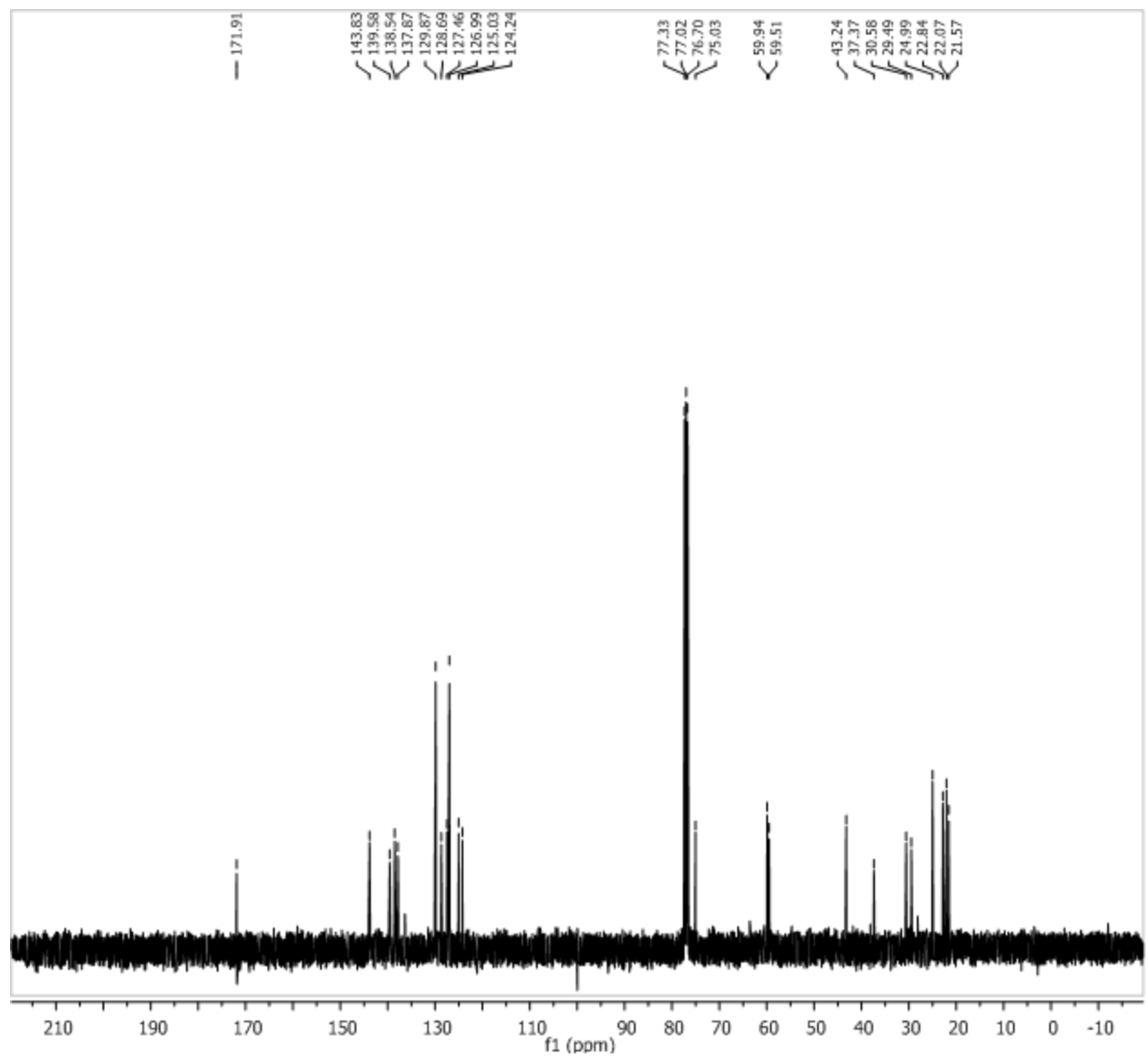


No NOE between 11 and 14

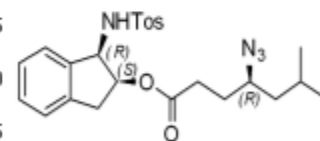




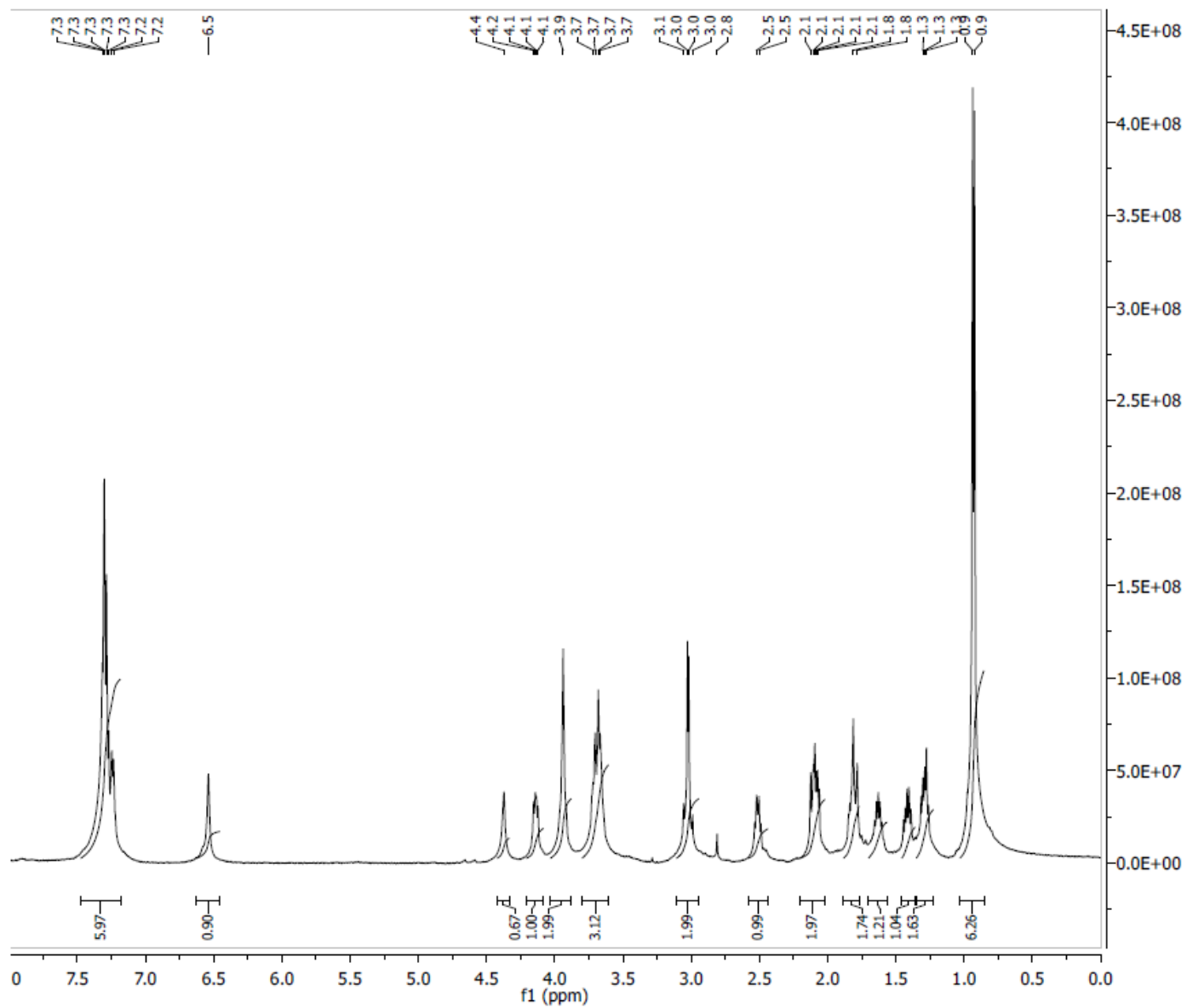




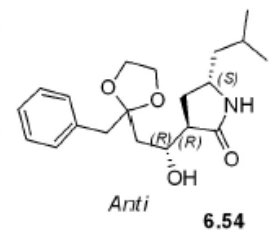
Parameter	Value
1 Spectrometer	spect
2 Author	
3 Solvent	CDCl3
4 Temperature	298.2
5 Pulse Sequence	zgpg30
6 Experiment	1D
7 Number of Scans	1024
8 Receiver Gain	32800
9 Relaxation Delay	2.0000
10 Pulse Width	10.0000
11 Spectrometer Frequency	100.63
12 Spectral Width	24038.5
13 Lowest Frequency	-1957.9
14 Nucleus	13C
15 Acquired Size	32768
16 Spectral Size	65536

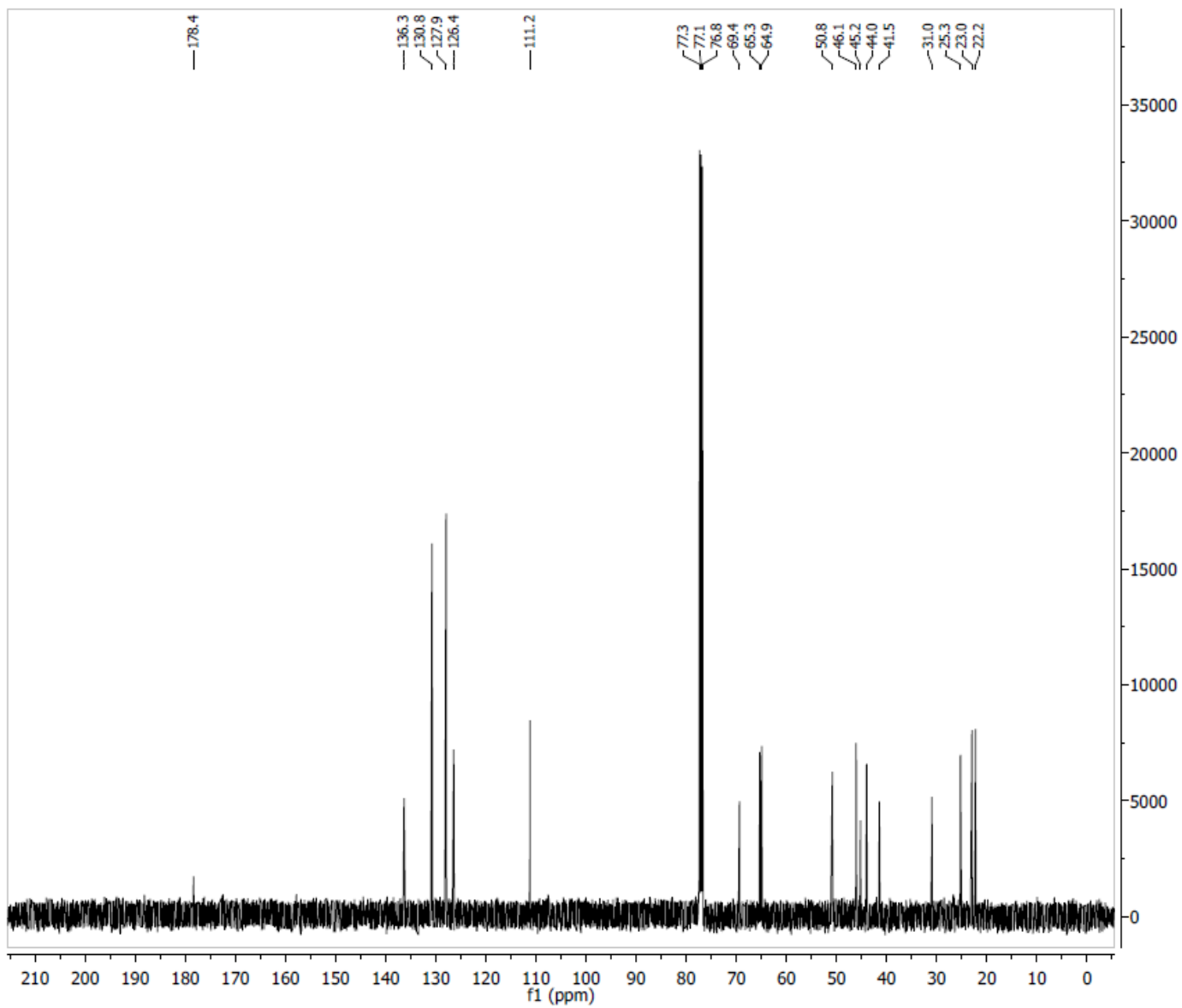


6.53

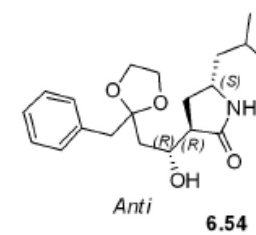


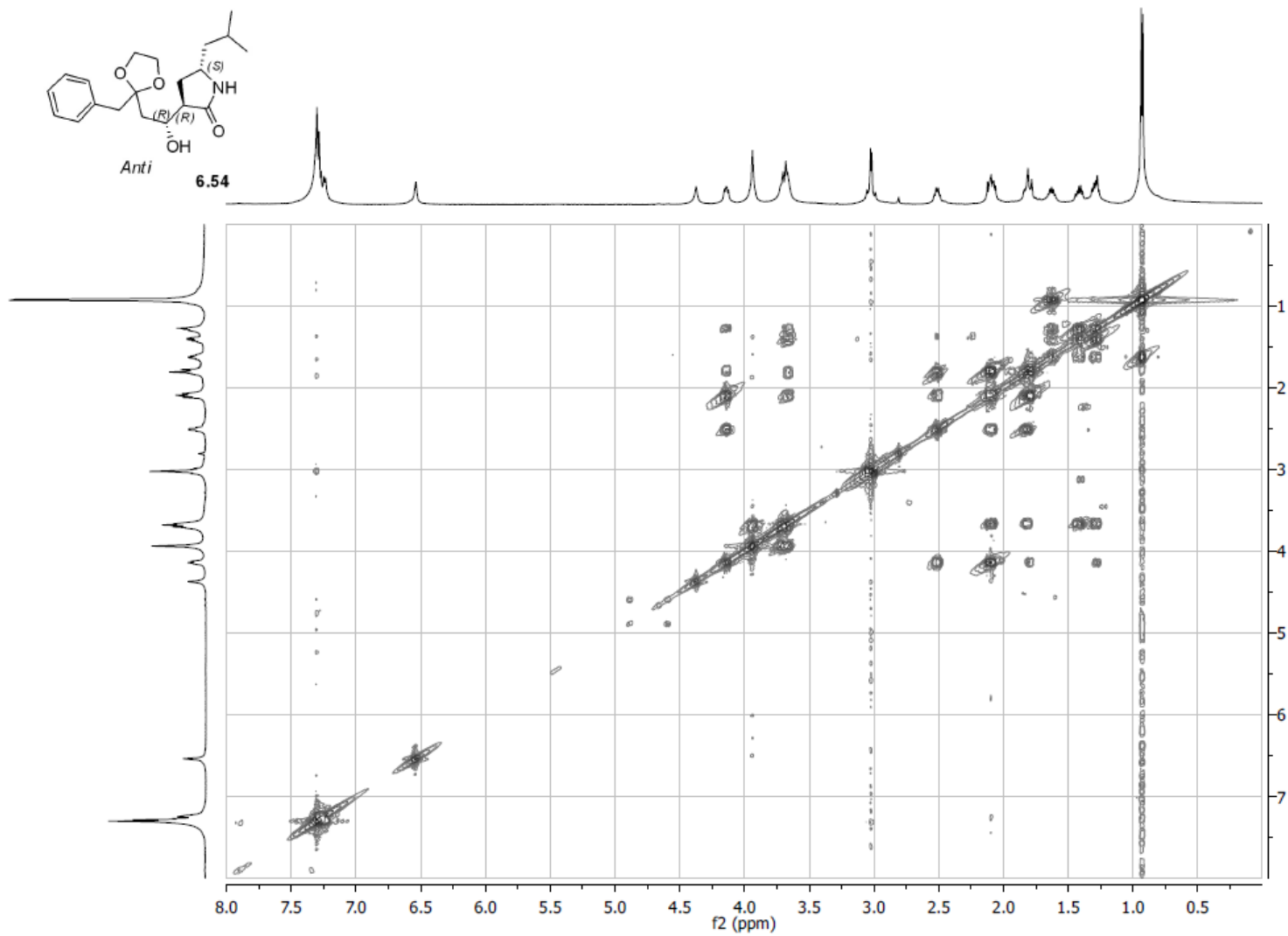
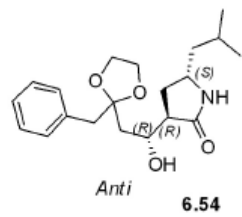
Parameter	Value
1 Spectrometer	spect
2 Solvent	CDCl3
3 Temperature	298.2
4 Pulse Sequence	zg30
5 Experiment	1D
6 Number of Scans	4
7 Receiver Gain	256
8 Relaxation Delay	1.0000
9 Pulse Width	10.3800
10 Acquisition Time	1.1698
11 Spectrometer Frequency	500.13
12 Spectral Width	7002.8
13 Lowest Frequency	-250.6
14 Nucleus	1H
15 Acquired Size	8192
16 Spectral Size	16384



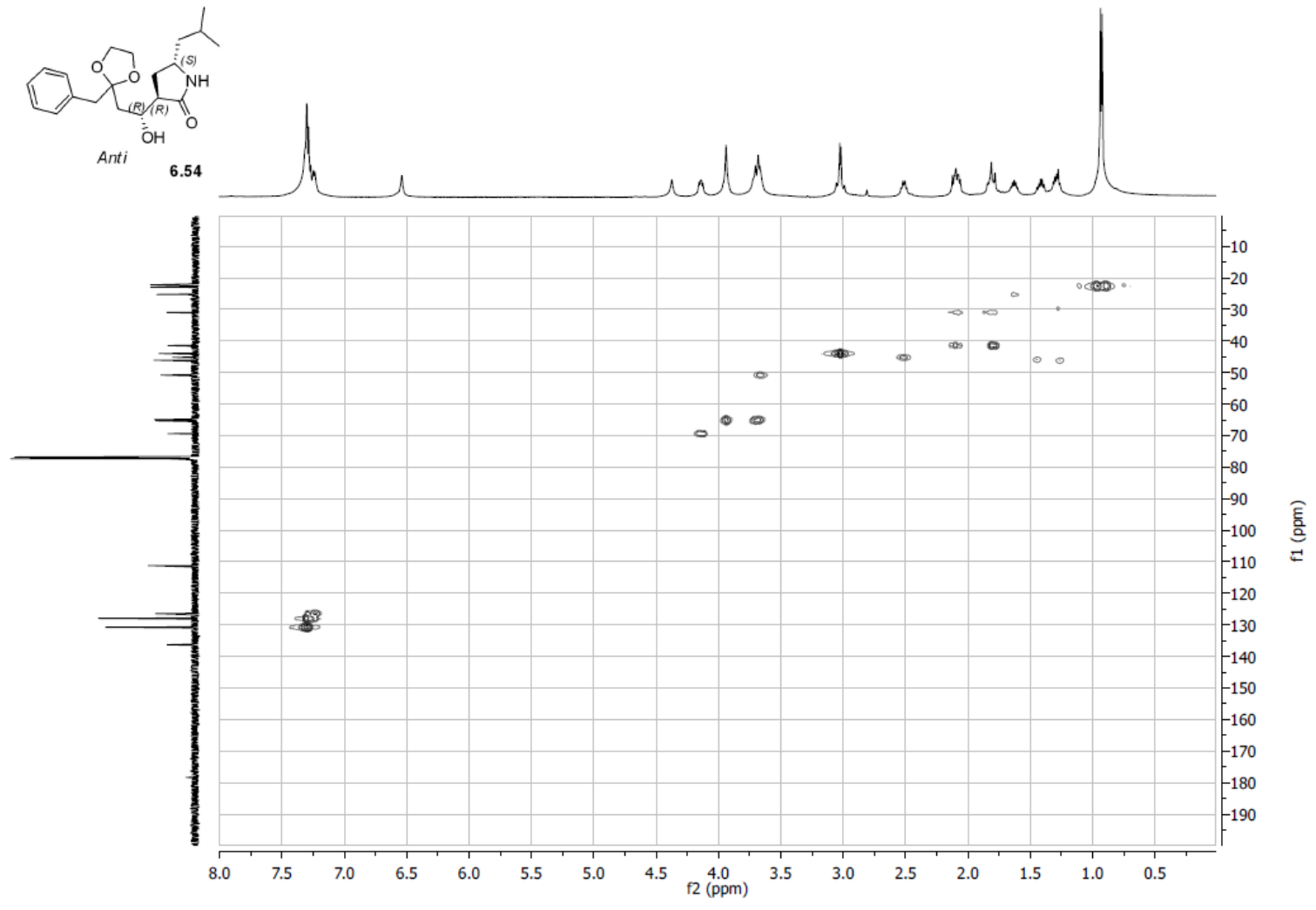
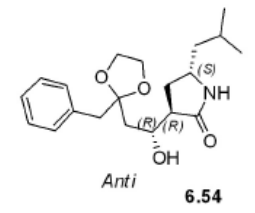


Parameter	Value
1 Spectrometer	spect
2 Solvent	CDCl3
3 Temperature	298.2
4 Pulse Sequence	zgpg30
5 Experiment	1D
6 Number of Scans	2048
7 Receiver Gain	9195
8 Relaxation Delay	3.0000
9 Pulse Width	9.0000
10 Acquisition Time	1.1796
11 Spectrometer Frequency	125.77
12 Spectral Width	27777.8
13 Lowest Frequency	-683.9
14 Nucleus	13C
15 Acquired Size	32768
16 Spectral Size	65536



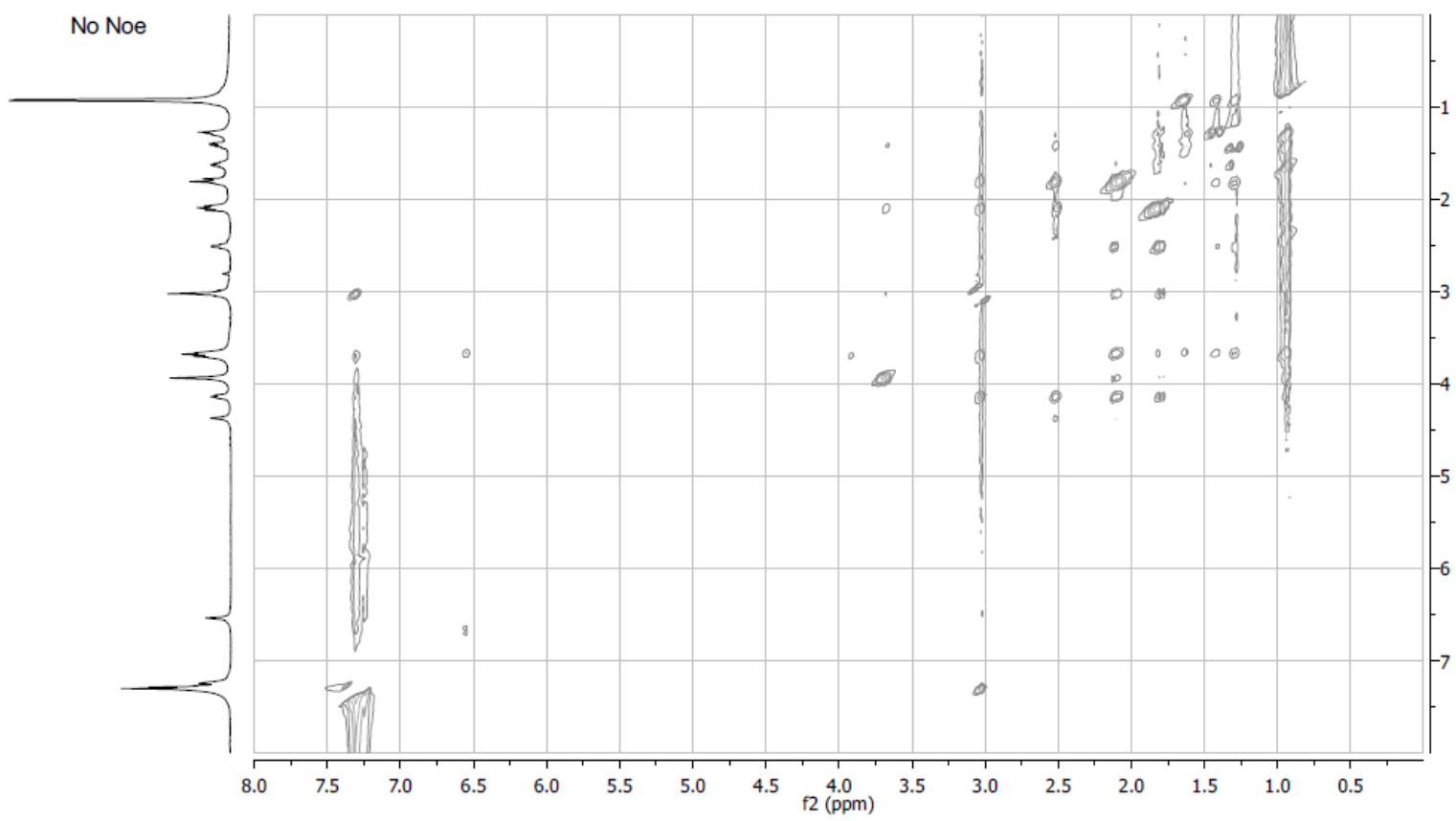
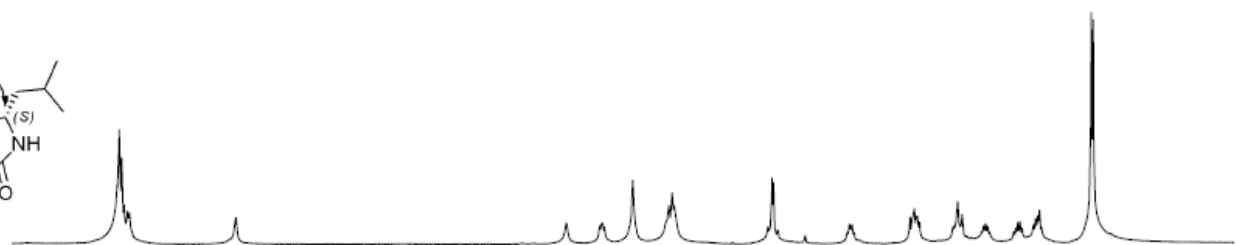
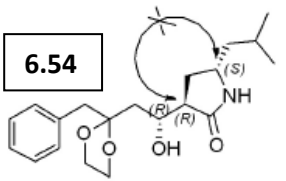


COSY

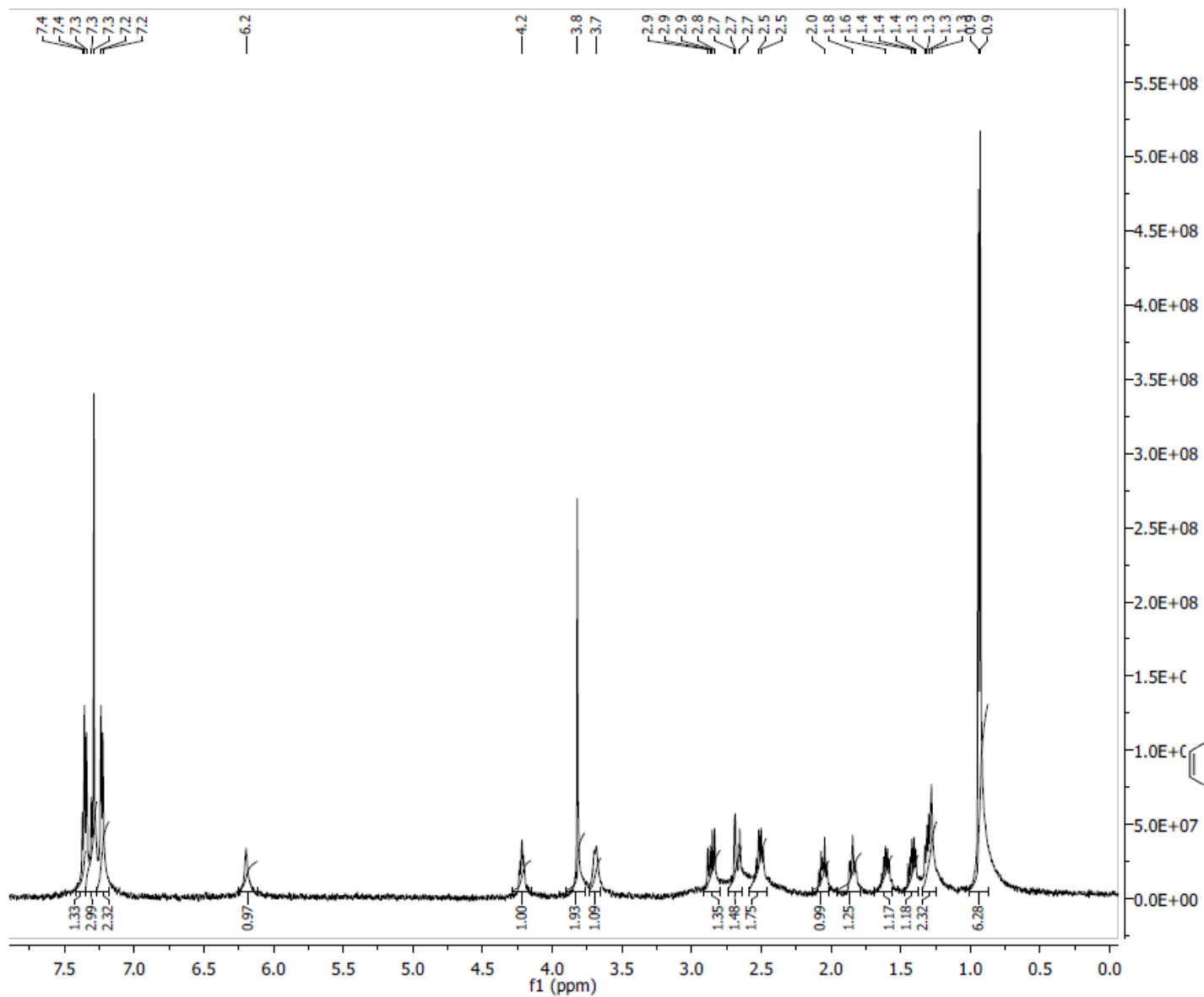


HMBC

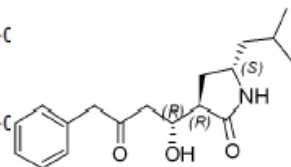
6.54



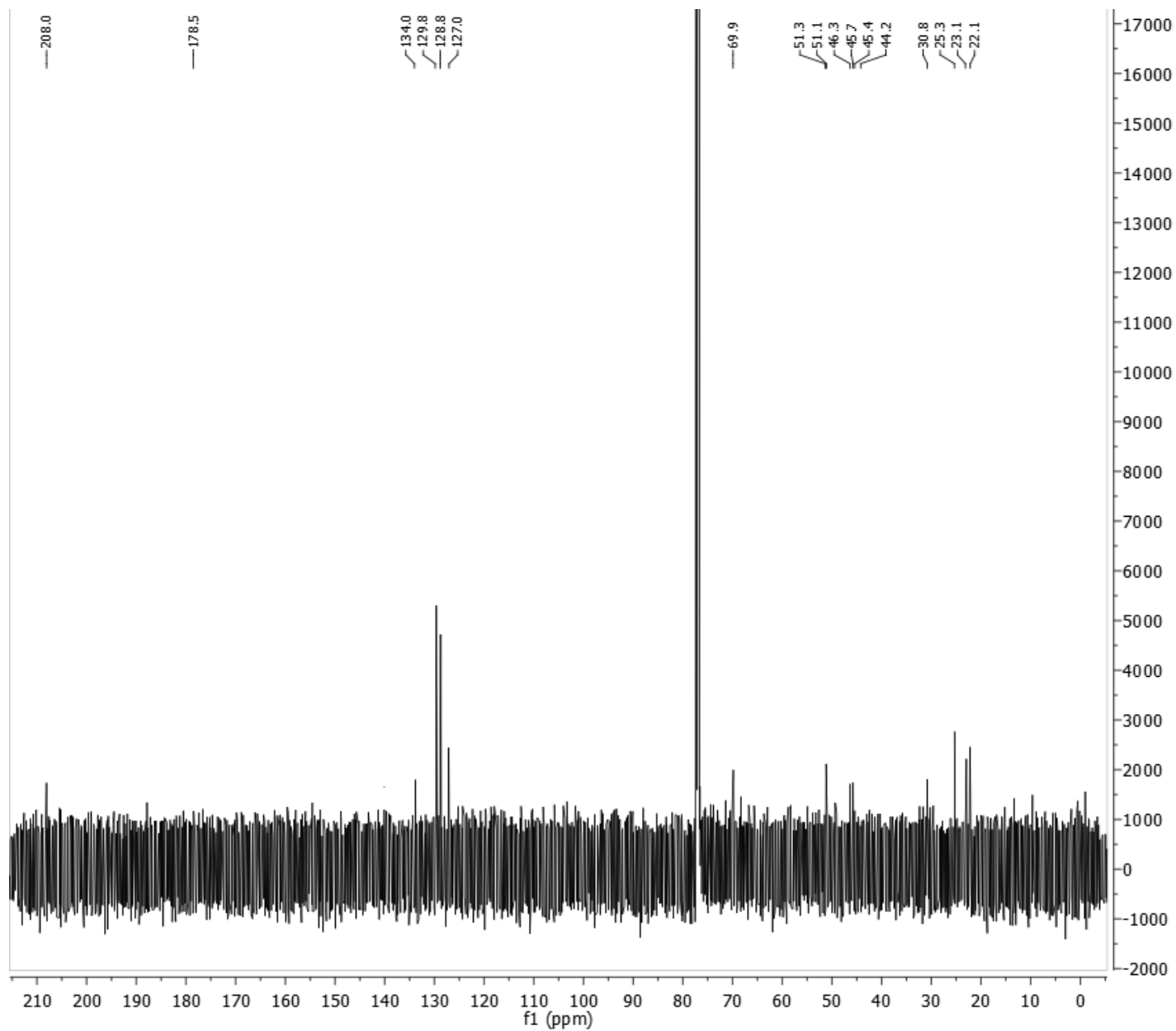
NOESY



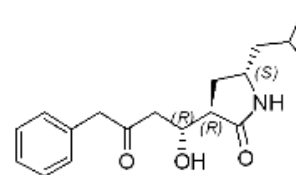
Parameter	Value
1 Spectrometer	spect
2 Solvent	CDCl3
3 Temperature	297.2
4 Pulse Sequence	zg30
5 Experiment	1D
6 Number of Scans	32
7 Receiver Gain	813
8 Relaxation Delay	1.0000
9 Pulse Width	11.0000
10 Acquisition Time	1.1699
11 Spectrometer Frequency	500.13
12 Spectral Width	7002.8
13 Lowest Frequency	-250.6
14 Nucleus	1H
15 Acquired Size	8192
16 Spectral Size	16384



6.55



Parameter	Value
1 Spectrometer	spect
2 Solvent	CDCl3
3 Temperature	297.2
4 Pulse Sequence	zgpg30
5 Experiment	1D
6 Number of Scans	3072
7 Receiver Gain	11585
8 Relaxation Delay	3.0000
9 Pulse Width	11.0000
10 Acquisition Time	1.1796
11 Spectrometer Frequency	125.77
12 Spectral Width	27777.8
13 Lowest Frequency	-683.9
14 Nucleus	13C
15 Acquired Size	32768
16 Spectral Size	65536



6.55

CHAPTER 8
BIBLIOGRAPHY

Bibliography

1. Cancer Facts and Figures. *American Cancer Society* **2009**.
2. Cragg, G. M.; Grothaus, P. G.; Newman, D. J. Impact of natural products on developing new anti-cancer agents. *Chem Rev* **2009**, 109, 3012-43.
3. Mukherjee, A. K.; Basu, S.; Sarkar, N.; Ghosh, A. C. Advances in cancer therapy with plant based natural products. *Curr Med Chem* **2001**, 8, 1467-86.
4. Wilson, R. M.; Danishefsky, S. J. Small molecule natural products in the discovery of therapeutic agents: the synthesis connection. *J Org Chem* **2006**, 71, 8329-51.
5. J. X. Wu; Hu, S.; Yang, G. L. *Chin.J.Dermatology* **1960**, 8, 18-25.
6. Chiu, P.; Leung Lai, T.; Ko Ben, C. B. Pseudolaric acids: isolation, bioactivity and synthetic studies. *Nat Prod Rep* 27, 1066-83.
7. Yang, S.-P.; Wu, Y.; Yue, J.-M. Five New Diterpenoids from *Pseudolarix kaempferi*. *J. Nat. Prod.* **2002**, 65, 1041-1044.
8. Han, Q.-B.; Yip, Y.-K.; Yang, N.-Y.; Wong, L.; Qiao, C.-F.; Song, J.-Z.; Yiu, H.; Xu, H.-X. Rapid analysis of pseudolaric acids in Cortex *Pseudolaricis* and related medicinal products by high performance liquid chromatography. *Talanta* **2007**, 73, 757-763.
9. Zhou, B. N.; Ying, B. P.; Song, G. Q.; Chen, Z. X.; Han, J.; Yan, Y. F. Pseudolaric Acids from *Pseudolarix kaempferi*. *Planta Med* **1983**, 47, 35-8.
10. Li, Z.; Pan, D.; Hu, C.; Wu, Q.; Yang, S.; Xu, G. Studies on the novel diterpenic constituents of Tu Jin Pi. I. Determination of chemical structures of pseudolaric acid A and pseudolaric acid B. *Huaxue Xuebao* **1982**, 40, 447-57.
11. Yang, S.-P.; Wu, Y.; Yue, J.-M. Five new diterpenoids from *Pseudolarix kaempferi*. *J Nat Prod* **2002**, 65, 1041-4.

12. Yang, S.-P.; Dong, L.; Wang, Y.; Wu, Y.; Yue, J.-M. Antifungal diterpenoids of *Pseudolarix kaempferi*, and their structure-activity relationship study. *Bioorg Med Chem* **2003**, *11*, 4577-84.
13. Li, Z.; Chen, K.; Pan, D.; Xu, G. New diterpenic constituents of Tu-Jin-Pi. III. Isolation and identification of pseudolaric acid A- β -D-glucoside and pseudolaric acid B- β -D-glucoside. *Huaxue Xuebao* **1985**, *43*, 786-8.
14. Liu, P.; Guo, H.; Wang, W.; Zhang, J.; Li, N.; Han, J.; Zhou, J.; Hu, Y.; Zhang, T.; Liu, Z.; Guo, D. Cytotoxic Diterpenoids from the Bark of *Pseudolarix kaempferi* and Their Structure-Activity Relationships. *J. Nat. Prod.* **2007**, *70*, 533-537.
15. Li, Z. L.; Pan, D. J.; Hu, C. Q.; Wu, Q. L.; Xu, G. Y.; Zhou, B. N.; Yin, B. P.; Sun, G. J.; Chen, Z. X.; et al. Studies on the antifungal constituents of tu jin pi. The structures of novel diterpenoids, pseudolaric acid A, B, C and C2. *Chem. Nat. Prod., Proc. Sino-Am. Symp.* **1982**, 150-5.
16. Li, Z.; Pan, D.; Wu, Q.; Xu, G. Studies on the novel diterpenic constituents of Tu-Jin-Pi. II. Identification of pseudolaric acid C2 and structural correlations of pseudolaric acid A, B, C and C2. *Huaxue Xuebao* **1982**, *40*, 757-61.
17. Liu, P.; Guo, H.; Tian, Y.; Wang, Q.; Guo, D. Benzoic acid allopyranosides from the bark of *Pseudolarix kaempferi*. *Phytochemistry* **2006**, *67*, 1395-8.
18. Zhou, B. N. The chemistry and bioactivities of some natural products from Chinese herbs. *Proc. Phytochem. Soc. Eur.* **1995**, *37*, 313-34.
19. Ying, B.; Yu, H.; Han, J. Study on the NMR spectra of pseudolaric acid B. *Youji Huaxue* **1988**, *8*, 273-5.

20. Yu, H.; Song, G. Determination of relative signs of scalar coupling constants in pseudolaric acid derivatives by proton COSY-45. *Huaxue Xuebao* **1988**, 46, 76-7.
21. Yao J.X.; Lin, X. Y. *Acta Chim Sin (Engl Ed)* **1982**, 40, 385-393.
22. Hamburger, M. O.; Shieh, H. L.; Zhou, B. N.; Pezzuto, J. M.; Cordell, G. A. Pseudolaric acid B: NMR assignments, conformational analysis and cytotoxicity. *Magn. Reson. Chem.* **1989**, 27, 1025-30.
23. Geng, Z.; Chen, B.; Chiu, P. Total synthesis of pseudolaric acid A. *Angew. Chem., Int. Ed.* **2006**, 45, 6197-6201.
24. Trost, B. M.; Waser, J.; Meyer, A. Total Synthesis of (-)-Pseudolaric Acid B. *J. Am. Chem. Soc.* **2007**, 129, 14556-14557.
25. Li, E.; Clark, A. M.; Hufford, C. D. Antifungal evaluation of pseudolaric acid B, a major constituent of *Pseudolarix kaempferi*. *J. Nat. Prod.* **1995**, 58, 57-67.
26. Jardat, M. S.; Noonan, D. J.; Wu, B.; Avery, M. A.; Feller, D. R. Pseudolaric acid analogs as a new class of peroxisome proliferator-activated receptor agonists. *Planta Med.* **2002**, 68, 667-671.
27. Zhang, Y.; Lu, R.; Yan, A. Inhibition of ova fertilizability by pseudolaric acid B in hamster. *Zhongguo Yaoli Xuebao* **1990**, 11, 60-2.
28. Pan, D. J.; Li, Z. L.; Hu, C. Q.; Chen, K.; Chang, J. J.; Lee, K. H. The cytotoxic principles of *Pseudolarix kaempferi*: pseudolaric acid-A and -B and related derivatives. *Planta Med* **1990**, 56, 383-5.
29. Ding, J.; Zhen, Y.; Tong, Y.; Yue, J.; Xiao, D. Novel anti-angiogenetic agents developing in China. *Gan To Kagaku Ryoho* **2002**, 29 Suppl 1, 59-66.

30. Li, M.-H.; Miao, Z.-H.; Tan, W.-F.; Yue, J.-M.; Zhang, C.; Lin, L.-P.; Zhang, X.-W.; Ding, J. Pseudolaric acid B inhibits angiogenesis and reduces hypoxia-inducible factor 1alpha by promoting proteasome-mediated degradation. *Clin Cancer Res* **2004**, *10*, 8266-74.
31. Tan, W.-F.; Zhang, X.-W.; Li, M.-H.; Yue, J.-M.; Chen, Y.; Lin, L.-P.; Ding, J. Pseudolarix acid B inhibits angiogenesis by antagonizing the vascular endothelial growth factor-mediated anti-apoptotic effect. *Eur J Pharmacol* **2004**, *499*, 219-28.
32. Tong, Y.-G.; Zhang, X.-W.; Geng, M.-Y.; Yue, J.-M.; Xin, X.-L.; Tian, F.; Shen, X.; Tong, L.-J.; Li, M.-H.; Zhang, C.; Li, W.-H.; Lin, L.-P.; Ding, J. Pseudolarix acid B, a new tubulin-binding agent, inhibits angiogenesis by interacting with a novel binding site on tubulin. *Mol Pharmacol* **2006**, *69*, 1226-33.
33. Bacher, G.; Beckers, T.; Emig, P.; Klenner, T.; Kutscher, B.; and; Nickel, B. New small-molecule tubulin inhibitors. *Pure Appl.Chem.* **2001**, *73*, 149-1464.
34. Downing, K. H.; Nogales, E. Tubulin structure: insights into microtubule properties and functions. *Curr Opin Struct Biol* **1998**, *8*, 785-91.
35. Downing, K. H.; Nogales, E. Tubulin and microtubule structure. *Curr Opin Cell Biol* **1998**, *10*, 16-22.
36. Wong, K. W. The molecular mechanism of mitotic arrest induced by a novel diterpenoid pseudolaric acid B and a novel gene encoding RNA-binding protein 22. 2006.
37. Wong Vincent, K. W.; Chiu, P.; Chung Stephen, S. M.; Chow Larry, M. C.; Zhao, Y.-Z.; Yang Burton, B.; Ko Ben, C. B. Pseudolaric acid B, a novel microtubule-destabilizing agent that circumvents multidrug resistance phenotype and exhibits antitumor activity in vivo. *Clin Cancer Res* **2005**, *11*, 6002-11.

38. Liu, B.; Chen, H.; Lei, Z. Y.; Yu, P. F.; Xiong, B. Studies on anti-tumour activities of pseudolaric acid-B (PLAB) and its mechanism of action. *J Asian Nat Prod Res* **2006**, 8, 241-52.
39. Yang, S.-P.; Dong, L.; Wang, Y.; Wu, Y.; Yue, J.-M. Antifungal diterpenoids of *Pseudolarix kaempferi*, and their structure-activity relationship study. *Bioorg. Med. Chem.* **2003**, 11, 4577-4584.
40. Dong, X.; Ge, X.; Chen, H.; Li, L. Study on the antifungal activity of the derivatives of pseudolaric acid B. *Wujing Yixueyuan Xuebao* **2008**, 17, 365-367.
41. Yang, S.-P.; Cai, Y.-J.; Zhang, B.-L.; Tong, L.-J.; Xie, H.; Wu, Y.; Lin, L.-P.; Ding, J.; Yue, J.-M. Structural Modification of an Angiogenesis Inhibitor Discovered from Traditional Chinese Medicine and a Structure-Activity Relationship Study. *J. Med. Chem.* **2008**, 51, 77-85.
42. Pan, B.; Chang, H.; G, C.; Guo, Y. Synthetic studies on pseudolaric acid A. *Pure Appl.Chem.* **1989**, 61, 389-392.
43. Chiu, P.; Chen, B.; Cheng, K. F. A conjugate reduction-intramolecular aldol strategy toward the synthesis of pseudolaric acid A. *Tetrahedron Lett.* **1998**, 39, 9239-232.
44. Hu, Y.; Ou, L.; Bai, D. The synthesis of a 5,7-membered fused-ring compound by a tandem Pummerer rearrangement and intramolecular [4+3] cycloaddition. *Tetrahedron Lett.* **1999**, 40, 545-548.
45. Ou, L.; Hu, Y.; Song, G.; Bai, D. Diastereoselective intramolecular [4+3] cycloaddition: Synthesis of a versatile precursor for preparation of 5,7-fused ring compounds. *Tetrahedron* **1999**, 55, 13999-14004.
46. Chiu, P.; Chen, B.; Cheng, K. F. A Rhodium Carbene Cyclization-Cycloaddition Cascade Strategy toward the Pseudolaric Acids. *Org. Lett.* **2001**, 3, 1721-1724.

47. Chiu, P.; Chen, B.; Cheng, K. F. A rhodium carbene cyclization-cycloaddition cascade strategy toward the pseudolaric acids. *Org Lett* **2001**, 3, 1721-4.
48. Trost, B. M.; Waser, J.; Meyer, A. Total Synthesis of (-)-Pseudolaric Acid B. *J. Am. Chem. Soc.* **2008**, 130, 16424-16434.
49. Wu, B.; Karle, J. M.; Watkins, E. B.; Avery, M. A. Toward the total synthesis of pseudolaric acid B. Preparation of a key intermediate by degradation and its use in the reassembly of the natural product. *Tetrahedron Lett.* **2002**, 43, 4095-4098.
50. Bonk, J. D.; Avery, M. A. Synthetic studies on pseudolaric Acid B, the antifungal constituent of *Pseudolarix kaempferi*. *Book of Abstracts, 214th ACS National Meeting, Las Vegas, NV, September 7-11 1997*, MEDI-105.
51. Mullins, R. J.; Grote, A. L., . Wagner-Meerwein rearrangement. In *Name Reactions for Homologation, Part 2 (Comprehensive Name Reactions)*, Li, J. J., Ed. Wiley: 2009; pp 373-394.
52. Hubbard, R. D.; Miller, B. L. Lewis Acid Catalyzed Diels-Alder Reactions of Highly Hindered Dienophiles. *J. Org. Chem.* **1998**, 63, 4143-4146.
53. Martin, J. G.; Hill, R. K. Stereochemistry of the Diels-Alder reaction. *Chem. Rev. (Washington, DC, U. S.)* **1961**, 61, 537-62.
54. Sadeghi-Khomami, A.; Blake Alexander, J.; Wilson, C.; Thomas Neil, R. Synthesis of a carbasugar analogue of a putative intermediate in the UDP-galp-mutase catalyzed isomerization. *Org Lett* **2005**, 7, 4891-4.
55. Wijdeven Marloes, A.; Botman Peter, N. M.; Wijtmans, R.; Schoemaker Hans, E.; Rutjes Floris, P. J. T.; Blaauw Richard, H. Total synthesis of (+)-epiquinamide. *Org Lett* **2005**, 7, 4005-7.

56. Snape, T. J. Recent advances in the semi-pinacol rearrangement of alpha-hydroxy epoxides and related compounds. *Chem Soc Rev* **2007**, 36, 1823-42.
57. Wang, S.; Miura, M.; Jung, Y. K.; Zhu, H.; Li, E.; Yuan, J. Murine caspase-11, an ICE-interacting protease, is essential for the activation of ICE. *Cell* **1998**, 92, 501-9.
58. Grigg, R.; Sakee, U.; Sridharan, V.; Sukirthalingam, S.; Thangavelauthum, R. Palladium catalyzed bis- and tris-cyclizations furnishing fused cyclopropyl carbo/heterocycles. *Tetrahedron* **2006**, 62, 9523-9532.
59. Matovic, R.; Ivkovic, A.; Manojlovic, M.; Tokic-Vujosevic, Z.; Saicic, R. N. Ring Closing Metathesis/Fragmentation Route to (Z)-Configured Medium Ring Cycloalkenes. Total Synthesis of (+)-Periplanone C. *J. Org. Chem.* **2006**, 71, 9411-9419.
60. Fuerstner, A.; Thiel, O. R.; Ackermann, L.; Schanz, H.-J.; Nolan, S. P. Ruthenium Carbene Complexes with N,N'-Bis(mesityl)imidazol-2-ylidene Ligands: RCM Catalysts of Extended Scope. *J. Org. Chem.* **2000**, 65, 2204-2207.
61. Nicolaou, K. C.; Zhang, H.; Ortiz, A.; Dagneau, P. Total synthesis of the originally assigned structure of vannusal B. *Angew. Chem., Int. Ed.* **2008**, 47, 8605-8610.
62. Cabeza, M.; Heuze, I.; Bratoeff, E.; Ramirez, E.; Martinez, R. Evaluation of new pregnane derivatives as 5alpha -reductase inhibitor. *Chem. Pharm. Bull.* **2001**, 49, 525-530.
63. Cho, B. T.; Shin, S. H. Enantioselective ring opening of meso- and racemic epoxides with phenyl lithium catalyzed by chiral gamma -amino alcohols derived from alpha -D-xylose. *Bull. Korean Chem. Soc.* **2006**, 27, 1283-1284.
64. Clement, R.; Grise, C. M.; Barriault, L. Stereocontrolled synthesis of carbocycles via four successive pericyclic reactions. *Chem. Commun. (Cambridge, U. K.)* **2008**, 3004-3006.

65. Hattori, H.; Abbas, A. A.; Kobayashi, Y. Palladium-catalyzed reaction of 4-cyclopentene-1,3-diol monoacetate with Grignard reagents producing hitherto unreachable cis-1,2-isomers. *Chem. Commun. (Cambridge, U. K.)* **2004**, 884-885.
66. Vrancken, E.; Alexakis, A.; Mangeney, P. Organolithium/chiral Lewis base/BF₃: A versatile combination for the enantioselective desymmetrization of meso-epoxides. *Eur. J. Org. Chem.* **2005**, 1354-1366.
67. Jones, J. B.; Grayshan, R. New approach to the introduction of corticoid-like C-17 functions via 2-lithio-1,3-dithian-epoxide reactions. *J. Chem. Soc. D* **1970**, 741-2.
68. Kirsch, S. F.; Bach, T. Diastereoselective reactions of enantiomerically pure, sterically congested cyclohexanes as an entry to wailupemycins A and B: Total synthesis of (+)-wailupemycin B. *Chem.--Eur. J.* **2005**, 11, 7007-7023.
69. Semmelhack, M. F.; Hooley, R. J.; Kraml, C. M. Synthesis of Plakortone B and Analogs. *Org. Lett.* **2006**, 8, 5203-5206.
70. Yuan, J.; Shaham, S.; Ledoux, S.; Ellis, H. M.; Horvitz, H. R. The *C. elegans* cell death gene *ced-3* encodes a protein similar to mammalian interleukin-1 beta-converting enzyme. *Cell* **1993**, 75, 641-52.
71. Thornberry, N. A.; Lazebnik, Y. Caspases: enemies within. *Science* **1998**, 281, 1312-6.
72. Talanian, R. V.; Allen, H. J. Roles of caspases in inflammation and apoptosis: prospects as drug discovery targets. *Annu. Rep. Med. Chem. FIELD Full Journal Title:Annual Reports in Medicinal Chemistry* **1998**, 33, 273-282.
73. Talanian, R. V.; Brady, K. D.; Cryns, V. L. Caspases as targets for anti-inflammatory and anti-apoptotic drug discovery. *J Med Chem* **2000**, 43, 3351-71.

74. Earnshaw, W. C.; Martins, L. M.; Kaufmann, S. H. Mammalian caspases: structure, activation, substrates, and functions during apoptosis. *Annu Rev Biochem* **1999**, *68*, 383-424.
75. Slee, E. A.; Adrain, C.; Martin, S. J. Serial killers: ordering caspase activation events in apoptosis. *Cell Death Differ* **1999**, *6*, 1067-74.
76. Nicholson, D. W. Caspase structure, proteolytic substrates, and function during apoptotic cell death. *Cell Death Differ* **1999**, *6*, 1028-42.
77. Muzio, M.; Stockwell, B. R.; Stennicke, H. R.; Salvesen, G. S.; Dixit, V. M. An induced proximity model for caspase-8 activation. *J Biol Chem* **1998**, *273*, 2926-30.
78. Chai, J.; Shiozaki, E.; Srinivasula, S. M.; Wu, Q.; Datta, P.; Alnemri, E. S.; Shi, Y. Structural basis of caspase-7 inhibition by XIAP. *Cell* **2001**, *104*, 769-80.
79. Mittl, P. R.; Di Marco, S.; Krebs, J. F.; Bai, X.; Karanewsky, D. S.; Priestle, J. P.; Tomaselli, K. J.; Grutter, M. G. Structure of recombinant human CPP32 in complex with the tetrapeptide acetyl-Asp-Val-Ala-Asp fluoromethyl ketone. *J Biol Chem* **1997**, *272*, 6539-47.
80. Kang, B. H.; Ko, E.; Kwon, O. K.; Choi, K. Y. The structure of procaspase 6 is similar to that of active mature caspase 6. *Biochem J* **2002**, *364*, 629-34.
81. Salvesen, G. S.; Dixit, V. M. Caspase activation: the induced-proximity model. *Proc Natl Acad Sci U S A* **1999**, *96*, 10964-7.
82. Boatright, K. M.; Renatus, M.; Scott, F. L.; Sperandio, S.; Shin, H.; Pedersen, I. M.; Ricci, J. E.; Edris, W. A.; Sutherlin, D. P.; Green, D. R.; Salvesen, G. S. A unified model for apical caspase activation. *Mol Cell* **2003**, *11*, 529-41.
83. Thornberry, N. A.; Bull, H. G.; Calaycay, J. R.; Chapman, K. T.; Howard, A. D.; Kostura, M. J.; Miller, D. K.; Molineaux, S. M.; Weidner, J. R.; Aunins, J.; et al. A novel

heterodimeric cysteine protease is required for interleukin-1 beta processing in monocytes. *Nature* **1992**, 356, 768-74.

84. Thornberry, N. A. Caspases: key mediators of apoptosis. *Chem Biol* **1998**, 5, R97-103.

85. Gurcel, L.; Abrami, L.; Girardin, S.; Tschopp, J.; van der Goot, F. G. Caspase-1 activation of lipid metabolic pathways in response to bacterial pore-forming toxins promotes cell survival. *Cell* **2006**, 126, 1135-45.

86. Nadiri, A.; Wolinski, M. K.; Saleh, M. The inflammatory caspases: key players in the host response to pathogenic invasion and sepsis. *J Immunol* **2006**, 177, 4239-45.

87. Faucheu, C.; Blanchet, A. M.; Collard-Dutilleul, V.; Lalanne, J. L.; Diu-Hercend, A. Identification of a cysteine protease closely related to interleukin-1 beta-converting enzyme. *Eur J Biochem* **1996**, 236, 207-13.

88. Faucheu, C.; Diu, A.; Chan, A. W.; Blanchet, A. M.; Miossec, C.; Herve, F.; Collard-Dutilleul, V.; Gu, Y.; Aldape, R. A.; Lippke, J. A.; et al. A novel human protease similar to the interleukin-1 beta converting enzyme induces apoptosis in transfected cells. *EMBO J* **1995**, 14, 1914-22.

89. Lin, X. Y.; Choi, M. S.; Porter, A. G. Expression analysis of the human caspase-1 subfamily reveals specific regulation of the CASP5 gene by lipopolysaccharide and interferon-gamma. *J Biol Chem* **2000**, 275, 39920-6.

90. Creagh, E. M.; Conroy, H.; Martin, S. J. Caspase-activation pathways in apoptosis and immunity. *Immunol Rev* **2003**, 193, 10-21.

91. Thome, M.; Hofmann, K.; Burns, K.; Martinon, F.; Bodmer, J. L.; Mattmann, C.; Tschopp, J. Identification of CARDIAK, a RIP-like kinase that associates with caspase-1. *Curr Biol* **1998**, 8, 885-8.

92. Kobayashi, K.; Inohara, N.; Hernandez, L. D.; Galan, J. E.; Nunez, G.; Janeway, C. A.; Medzhitov, R.; Flavell, R. A. RICK/Rip2/CARDIAK mediates signalling for receptors of the innate and adaptive immune systems. *Nature* **2002**, 416, 194-9.
93. Chin, A. I.; Dempsey, P. W.; Bruhn, K.; Miller, J. F.; Xu, Y.; Cheng, G. Involvement of receptor-interacting protein 2 in innate and adaptive immune responses. *Nature* **2002**, 416, 190-4.
94. Poyet, J. L.; Srinivasula, S. M.; Tnani, M.; Razmara, M.; Fernandes-Alnemri, T.; Alnemri, E. S. Identification of Ipaf, a human caspase-1-activating protein related to Apaf-1. *J Biol Chem* **2001**, 276, 28309-13.
95. Wang, L.; Manji, G. A.; Grenier, J. M.; Al-Garawi, A.; Merriam, S.; Lora, J. M.; Geddes, B. J.; Briskin, M.; DiStefano, P. S.; Bertin, J. PYPAF7, a novel PYRIN-containing Apaf1-like protein that regulates activation of NF-kappa B and caspase-1-dependent cytokine processing. *J Biol Chem* **2002**, 277, 29874-80.
96. Grenier, J. M.; Wang, L.; Manji, G. A.; Huang, W. J.; Al-Garawi, A.; Kelly, R.; Carlson, A.; Merriam, S.; Lora, J. M.; Briskin, M.; DiStefano, P. S.; Bertin, J. Functional screening of five PYPAF family members identifies PYPAF5 as a novel regulator of NF-kappaB and caspase-1. *FEBS Lett* **2002**, 530, 73-8.
97. Mariathasan, S.; Newton, K.; Monack, D. M.; Vucic, D.; French, D. M.; Lee, W. P.; Roose-Girma, M.; Erickson, S.; Dixit, V. M. Differential activation of the inflammasome by caspase-1 adaptors ASC and Ipaf. *Nature* **2004**, 430, 213-8.
98. Yu, H. B.; Finlay, B. B. The caspase-1 inflammasome: a pilot of innate immune responses. *Cell Host Microbe* **2008**, 4, 198-208.

99. Mariathasan, S.; Monack, D. M. Inflammasome adaptors and sensors: intracellular regulators of infection and inflammation. *Nat Rev Immunol* **2007**, *7*, 31-40.
100. Thornberry, N. A. Interleukin-1 beta converting enzyme. *Methods Enzymol* **1994**, *244*, 615-31.
101. Thornberry, N. A.; Molineaux, S. M. Interleukin-1 beta converting enzyme: a novel cysteine protease required for IL-1 beta production and implicated in programmed cell death. *Protein Sci* **1995**, *4*, 3-12.
102. Walker, N. P.; Talanian, R. V.; Brady, K. D.; Dang, L. C.; Bump, N. J.; Ferenz, C. R.; Franklin, S.; Ghayur, T.; Hackett, M. C.; Hammill, L. D.; et al. Crystal structure of the cysteine protease interleukin-1 beta-converting enzyme: a (p20/p10)₂ homodimer. *Cell* **1994**, *78*, 343-52.
103. Wilson, K. P.; Black, J. A.; Thomson, J. A.; Kim, E. E.; Griffith, J. P.; Navia, M. A.; Murcko, M. A.; Chambers, S. P.; Aldape, R. A.; Raybuck, S. A.; et al. Structure and mechanism of interleukin-1 beta converting enzyme. *Nature* **1994**, *370*, 270-5.
104. Romanowski, M. J.; Scheer, J. M.; O'Brien, T.; McDowell, R. S. Crystal structures of a ligand-free and malonate-bound human caspase-1: implications for the mechanism of substrate binding. *Structure* **2004**, *12*, 1361-71.
105. Hardy, J. A.; Wells, J. A. Dissecting an allosteric switch in caspase-7 using chemical and mutational probes. *J Biol Chem* **2009**, *284*, 26063-9.
106. Scheer, J. M.; Romanowski, M. J.; Wells, J. A. A common allosteric site and mechanism in caspases. *Proc Natl Acad Sci U S A* **2006**, *103*, 7595-600.
107. Datta, D.; Scheer, J. M.; Romanowski, M. J.; Wells, J. A. An allosteric circuit in caspase-1. *J Mol Biol* **2008**, *381*, 1157-67.

108. Vezzani, A.; Balosso, S.; Maroso, M.; Zardoni, D.; Noe, F.; Ravizza, T. ICE/caspase 1 inhibitors and IL-1beta receptor antagonists as potential therapeutics in epilepsy. *Curr Opin Investig Drugs* 11, 43-50.
109. Ravizza, T.; Gagliardi, B.; Noe, F.; Boer, K.; Aronica, E.; Vezzani, A. Innate and adaptive immunity during epileptogenesis and spontaneous seizures: evidence from experimental models and human temporal lobe epilepsy. *Neurobiol Dis* **2008**, 29, 142-60.
110. Vezzani, A. Innate immunity and inflammation in temporal lobe epilepsy: new emphasis on the role of complement activation. *Epilepsy Curr* **2008**, 8, 75-7.
111. Viviani, B.; Bartesaghi, S.; Gardoni, F.; Vezzani, A.; Behrens, M. M.; Bartfai, T.; Binaglia, M.; Corsini, E.; Di Luca, M.; Galli, C. L.; Marinovich, M. Interleukin-1beta enhances NMDA receptor-mediated intracellular calcium increase through activation of the Src family of kinases. *J Neurosci* **2003**, 23, 8692-700.
112. Balosso, S.; Maroso, M.; Sanchez-Alavez, M.; Ravizza, T.; Frasca, A.; Bartfai, T.; Vezzani, A. A novel non-transcriptional pathway mediates the proconvulsive effects of interleukin-1beta. *Brain* **2008**, 131, 3256-65.
113. Maroso, M.; Balosso, S.; Ravizza, T.; Iori, V.; Wright, C. I.; French, J.; Vezzani, A. Interleukin-1beta Biosynthesis Inhibition Reduces Acute Seizures and Drug Resistant Chronic Epileptic Activity in Mice. *Neurotherapeutics*.
114. Vezzani, A.; Baram, T. Z. New roles for interleukin-1 Beta in the mechanisms of epilepsy. *Epilepsy Curr* **2007**, 7, 45-50.
115. Cornelis, S.; Kersse, K.; Festjens, N.; Lamkanfi, M.; Vandenabeele, P. Inflammatory caspases: targets for novel therapies. *Curr Pharm Des* **2007**, 13, 367-85.

116. VERTEX PHARMACEUTICALS; VEZZANI, A.; RANDLE, J. R. TREATING SEIZURES USING ICE INHIBITORS. WO/2005/115362, 2005.
117. Furlan, R.; Filippi, M.; Bergami, A.; Rocca, M. A.; Martinelli, V.; Poliani, P. L.; Grimaldi, L. M.; Desina, G.; Comi, G.; Martino, G. Peripheral levels of caspase-1 mRNA correlate with disease activity in patients with multiple sclerosis; a preliminary study. *J Neurol Neurosurg Psychiatry* **1999**, 67, 785-8.
118. Dowling, P. C.; Cook, S. D. Disease markers in acute multiple sclerosis. *Arch Neurol* **1976**, 33, 668-7.
119. Linton, S. D. Caspase inhibitors: a pharmaceutical industry perspective. *Curr Top Med Chem* **2005**, 5, 1697-717.
120. Rudolphi, K.; Gerwin, N.; Verzijl, N.; van der Kraan, P.; van den Berg, W. Pralnacasan, an inhibitor of interleukin-1beta converting enzyme, reduces joint damage in two murine models of osteoarthritis. *Osteoarthritis Cartilage* **2003**, 11, 738-46.
121. Ku, G.; Faust, T.; Lauffer, L. L.; Livingston, D. J.; Harding, M. W. Interleukin-1 beta converting enzyme inhibition blocks progression of type II collagen-induced arthritis in mice. *Cytokine* **1996**, 8, 377-86.
122. Feldmann, M.; Brennan, F. M.; Maini, R. N. Rheumatoid arthritis. *Cell* **1996**, 85, 307-10.
123. Feldmann, M.; Brennan, F. M.; Maini, R. N. Role of cytokines in rheumatoid arthritis. *Annu Rev Immunol* **1996**, 14, 397-440.
124. Howley, B.; Fearnhead, H. O. Caspases as therapeutic targets. *J Cell Mol Med* **2008**, 12, 1502-16.
125. O'Brien, T.; Lee, D. Prospects for caspase inhibitors. *Mini Rev Med Chem* **2004**, 4, 153-65.

126. Talanian, R. V.; Quinlan, C.; Trautz, S.; Hackett, M. C.; Mankovich, J. A.; Banach, D.; Ghayur, T.; Brady, K. D.; Wong, W. W. Substrate specificities of caspase family proteases. *J Biol Chem* **1997**, *272*, 9677-82.
127. Brady, K. D.; Giegel, D. A.; Grinnell, C.; Lunney, E.; Talanian, R. V.; Wong, W.; Walker, N. A catalytic mechanism for caspase-1 and for bimodal inhibition of caspase-1 by activated aspartic ketones. *Bioorg Med Chem* **1999**, *7*, 621-31.
128. Randle, J. C.; Harding, M. W.; Ku, G.; Schonharting, M.; Kurrle, R. ICE/Caspase-1 inhibitors as novel anti-inflammatory drugs. *Expert Opin Investig Drugs* **2001**, *10*, 1207-9.
129. Okamoto, Y.; Anan, H.; Nakai, E.; Morihira, K.; Yonetoku, Y.; Kurihara, H.; Sakashita, H.; Terai, Y.; Takeuchi, M.; Shibamura, T.; Isomura, Y. Peptide based interleukin-1 beta converting enzyme (ICE) inhibitors: synthesis, structure activity relationships and crystallographic study of the ICE-inhibitor complex. *Chem Pharm Bull (Tokyo)* **1999**, *47*, 11-21.
130. Dolle, R. E.; Hoyer, D.; Prasad, C. V.; Schmidt, S. J.; Helaszek, C. T.; Miller, R. E.; Ator, M. A. P1 aspartate-based peptide alpha-((2,6-dichlorobenzoyl)oxy)methyl ketones as potent time-dependent inhibitors of interleukin-1 beta-converting enzyme. *J Med Chem* **1994**, *37*, 563-4.
131. Dolle, R. E.; Prasad, C. V.; Prouty, C. P.; Salvino, J. M.; Awad, M. M.; Schmidt, S. J.; Hoyer, D.; Ross, T. M.; Graybill, T. L.; Speier, G. J.; Uhl, J.; Miller, B. E.; Helaszek, C. T.; Ator, M. A. Pyridazinodiazepines as a high-affinity, P2-P3 peptidomimetic class of interleukin-1 beta-converting enzyme inhibitor. *J Med Chem* **1997**, *40*, 1941-6.
132. Dolle, R. E.; Singh, J.; Rinker, J.; Hoyer, D.; Prasad, C. V.; Graybill, T. L.; Salvino, J. M.; Helaszek, C. T.; Miller, R. E.; Ator, M. A. Aspartyl alpha-((1-phenyl-3-(trifluoromethyl)pyrazol-5-yl)oxy)methyl ketones as interleukin-1 beta converting enzyme inhibitors.

Significance of the P1 and P3 amido nitrogens for enzyme-peptide inhibitor binding. *J Med Chem* **1994**, 37, 3863-6.

133. Karanewsky, D. S.; Bai, X.; Linton, S. D.; Krebs, J. F.; Wu, J.; Pham, B.; Tomaselli, K. J. Conformationally constrained inhibitors of caspase-1 (interleukin-1 beta converting enzyme) and of the human CED-3 homologue caspase-3 (CPP32, apopain). *Bioorg Med Chem Lett* **1998**, 8, 2757-62.

134. Wilson, K. P.; Black, J.-A. F.; Thomson, J. A.; Kim, E. E.; Griffith, J. P.; Navia, M. A.; Murcko, M. A.; Chambers, S. P.; Aldape, R. A.; et al. Structure and mechanism of interleukin-1beta converting enzyme. *Nature (London)* **1994**, 370, 270-5.

135. Kulkarni, S. S.; Kulkarni, V. M. Three-Dimensional Quantitative Structure-Activity Relationship of Interleukin 1-beta Converting Enzyme Inhibitors: A Comparative Molecular Field Analysis Study. *J. Med. Chem.* **1999**, 42, 373-380.

136. O'Brien, T.; Linton, S. D. *Design of caspase inhibitors as potential clinical agents*. 1 ed.; CRC press: 2009; p 1-289.

137. O'Brien, T.; Fahr, B. T.; Sopko, M. M.; Lam, J. W.; Waal, N. D.; Raimundo, B. C.; Purkey, H. E.; Pham, P.; Romanowski, M. J. Structural analysis of caspase-1 inhibitors derived from Tethering. *Acta Crystallogr Sect F Struct Biol Cryst Commun* **2005**, 61, 451-8.

138. Asgian, J. L.; James, K. E.; Li, Z. Z.; Carter, W.; Barrett, A. J.; Mikolajczyk, J.; Salvesen, G. S.; Powers, J. C. Aza-peptide epoxides: a new class of inhibitors selective for clan CD cysteine proteases. *J Med Chem* **2002**, 45, 4958-60.

139. Ekici, O. D.; Gotz, M. G.; James, K. E.; Li, Z. Z.; Rukamp, B. J.; Asgian, J. L.; Caffrey, C. R.; Hansell, E.; Dvorak, J.; McKerrow, J. H.; Potempa, J.; Travis, J.; Mikolajczyk, J.;

Salvesen, G. S.; Powers, J. C. Aza-peptide Michael acceptors: a new class of inhibitors specific for caspases and other clan CD cysteine proteases. *J Med Chem* **2004**, *47*, 1889-92.

140. Lauffer, D. J.; Mullican, M. D. A practical synthesis of (S) 3-tert-butoxycarbonylamino-2-oxo-2,3,4,5-tetrahydro-1,5-benzodiazepine-1-a cetic acid methyl ester as a conformationally restricted dipeptido-mimetic for caspase-1 (ICE) inhibitors. *Bioorg Med Chem Lett* **2002**, *12*, 1225-7.

141. Shahripour, A. B.; Plummer, M. S.; Lunney, E. A.; Sawyer, T. K.; Stankovic, C. J.; Connolly, M. K.; Rubin, J. R.; Walker, N. P.; Brady, K. D.; Allen, H. J.; Talanian, R. V.; Wong, W. W.; Humblet, C. Structure-based design of caspase-1 inhibitor containing a diphenyl ether sulfonamide. *Bioorg Med Chem Lett* **2001**, *11*, 2779-82.

142. IDdb3 drug alert: VX-740, july 12 2006. In.

143. Harter, W. G.; Albrect, H.; Brady, K.; Caprathe, B.; Dunbar, J.; Gilmore, J.; Hays, S.; Kostlan, C. R.; Lunney, B.; Walker, N. The design and synthesis of sulfonamides as caspase-1 inhibitors. *Bioorg Med Chem Lett* **2004**, *14*, 809-12.

144. Fahr, B. T.; O'Brien, T.; Pham, P.; Waal, N. D.; Baskaran, S.; Raimundo, B. C.; Lam, J. W.; Sopko, M. M.; Purkey, H. E.; Romanowski, M. J. Tethering identifies fragment that yields potent inhibitors of human caspase-1. *Bioorg Med Chem Lett* **2006**, *16*, 559-62.

145. Oppong, K. A.; Ellis, C. D.; Laufersweiler, M. C.; O'Neil, S. V.; Wang, Y.; Soper, D. L.; Baize, M. W.; Wos, J. A.; De, B.; Bosch, G. K.; Fancher, A. N.; Lu, W.; Suchanek, M. K.; Wang, R. L.; Demuth, T. P., Jr. Discovery of novel conformationally restricted diazocan peptidomimetics as inhibitors of interleukin-1beta synthesis. *Bioorg Med Chem Lett* **2005**, *15*, 4291-4.

146. Soper, D. L.; Sheville, J. X.; O'Neil, S. V.; Wang, Y.; Laufersweiler, M. C.; Oppong, K. A.; Wos, J. A.; Ellis, C. D.; Baize, M. W.; Chen, J. J.; Fancher, A. N.; Lu, W.; Suchanek, M. K.; Wang, R. L.; Schwecke, W. P.; Cruze, C. A.; Buchalova, M.; Belkin, M.; Wireko, F.; Ritter, A.; De, B.; Wang, D.; Demuth, T. P., Jr. Synthesis and evaluation of novel 8,5-fused bicyclic peptidomimetic compounds as interleukin-1beta converting enzyme (ICE) inhibitors. *Bioorg Med Chem* **2006**, *14*, 7880-92.
147. O'Neil, S. V.; Wang, Y.; Laufersweiler, M. C.; Oppong, K. A.; Soper, D. L.; Wos, J. A.; Ellis, C. D.; Baize, M. W.; Bosch, G. K.; Fancher, A. N.; Lu, W.; Suchanek, M. K.; Wang, R. L.; De, B.; Demuth, T. P., Jr. Synthesis and evaluation of novel 8,6-fused bicyclic peptidomimetic compounds as interleukin-1beta converting enzyme inhibitors. *Bioorg Med Chem Lett* **2005**, *15*, 5434-8.
148. Ellis, C. D.; Oppong, K. A.; Laufersweiler, M. C.; O'Neil, S. V.; Soper, D. L.; Wang, Y.; Wos, J. A.; Fancher, A. N.; Lu, W.; Suchanek, M. K.; Wang, R. L.; De, B.; Demuth, T. P., Jr. Synthesis and evaluation of thiazepines as interleukin-1beta converting enzyme (ICE) inhibitors. *Bioorg Med Chem Lett* **2006**, *16*, 4728-32.
149. Laufersweiler, M. C.; Wang, Y.; Soper, D. L.; Suchanek, M. K.; Fancher, A. N.; Lu, W.; Wang, R. L.; Oppong, K. A.; Ellis, C. D.; Baize, M. W.; O'Neil, S. V.; Wos, J. A.; Demuth, T. P., Jr. Synthesis and evaluation of tricyclic pyrrolopyrimidinones as dipeptide mimetics: inhibition of interleukin-1beta-converting enzyme. *Bioorg Med Chem Lett* **2005**, *15*, 4322-6.
150. Soper, D. L.; Sheville, J.; O'Neil, S. V.; Wang, Y.; Laufersweiler, M. C.; Oppong, K. A.; Wos, J. A.; Ellis, C. D.; Fancher, A. N.; Lu, W.; Suchanek, M. K.; Wang, R. L.; De, B.; Demuth, T. P., Jr. Synthesis and evaluation of novel 1-(2-acylhydrazinocarbonyl)-cycloalkyl

carboxamides as interleukin-1beta converting enzyme (ICE) inhibitors. *Bioorg Med Chem Lett* **2006**, 16, 4233-6.

151. Loser, R.; Abbenante, G.; Madala, P. K.; Halili, M.; Le, G. T.; Fairlie, D. P. Noncovalent tripeptidyl benzyl- and cyclohexyl-amine inhibitors of the cysteine protease caspase-1. *J Med Chem* **53**, 2651-5.

152. Howley, B.; Fearnhead, H. O. Caspases as therapeutic targets. *J. Cell. Mol. Med.* **2008**, 12, 1502-1516.

153. Randle, J. C. R.; Harding, M. W.; Ku, G.; Schonharting, M.; Kurrle, R. ICE/caspase-1 inhibitors as novel anti-inflammatory drugs. *Expert Opin. Invest. Drugs FIELD Full Journal Title:Expert Opinion on Investigational Drugs* **2001**, 10, 1207-1209.

154. Stierle, A. A.; Stierle, D. B.; Patacini, B. The berkeleyamides, amides from the acid lake fungus *Penicillium rubrum*. *J. Nat. Prod.* **2008**, 71, 856-860.

155. Sperry, J.; Harris, E. B. J.; Brimble, M. A. Total Synthesis and Absolute Configuration of (-)-Berkeleyamide A. *Org. Lett.*, ACS ASAP.

156. Palomo, C.; Oiarbide, M.; Garcia Jesus, M. Current progress in the asymmetric aldol addition reaction. *Chem Soc Rev* **2004**, 33, 65-75.

157. Evans, D. A.; Bartroli, J.; Shih, T. L. Enantioselective aldol condensations. 2. Erythro-selective chiral aldol condensations via boron enolates. *Journal of the American Chemical Society* **1981**, 103, 2127-2129.

158. Evans, D. A.; Downey, C. W.; Shaw, J. T.; Tedrow, J. S. Magnesium Halide-Catalyzed Anti-Aldol Reactions of Chiral N-Acylthiazolidinethiones. *Org. Lett.* **2002**, 4, 1127-1130.

159. Oppolzer, W.; Lienard, P. Efficient asymmetric synthesis of anti-aldols from bornane sultam derived boryl enolates. *Tetrahedron Lett.* **1993**, 34, 4321-4.

160. Oikawa, Y.; Sugano, K.; Yonemitsu, O. Meldrum's acid in organic synthesis. 2. A general and versatile synthesis of beta -keto esters. *J. Org. Chem.* **1978**, 43, 2087-8.
161. Hwu, J. R.; Leu, L. C.; Robl, J. A.; Anderson, D. A.; Wetzel, J. M. General scope of 1,3-dioxolanation of alpha ,beta -unsaturated aldehydes with 1,2-bis(trimethylsilyloxy)ethane and trimethylsilyl trifluoromethanesulfonate. *J. Org. Chem.* **1987**, 52, 188-91.
162. Goel, O. P.; Krolls, U.; Stier, M.; Kesten, S. N-tert-Butoxycarbonyl- L -leucinal. *Org. Synth.* **1989**, 67, No pp given.
163. Bang, J. K.; Naka, H.; Teruya, K.; Aimoto, S.; Konno, H.; Nosaka, K.; Tatsumi, T.; Akaji, K. Solid-Phase Syntheses of Olefin-Containing Inhibitors for HTLV-1 Protease Using the Horner-Emmons Reaction. *J. Org. Chem.* **2005**, 70, 10596-10599.
164. Martin, M. E.; Rice, K. G. A Novel Class of Intrinsic Proteasome Inhibitory Gene Transfer Peptides. *Bioconjugate Chem.* **2008**, 19, 370-376.
165. Gessier, F.; Schaeffer, L.; Kimmerlin, T.; Flogel, O.; Seebach, D. Preparation of beta 2-amino acid derivatives (beta 2hThr, beta 2hTrp, beta 2hMet, beta 2hPro, beta 2hLys, pyrrolidine-3-carboxylic acid) by using DIOZ as chiral auxiliary. *Helv. Chim. Acta* **2005**, 88, 2235-2249.
166. Goddard-Borger, E. D.; Stick, R. V. An Efficient, Inexpensive, and Shelf-Stable Diazotransfer Reagent: Imidazole-1-sulfonyl Azide Hydrochloride. *Org. Lett.* **2007**, 9, 3797-3800.
167. Crimmins, M. T.; King, B. W.; Tabet, E. A.; Chaudhary, K. Asymmetric aldol additions: use of titanium tetrachloride and (-)-sparteine for the soft enolization of N-acyl oxazolidinones, oxazolidinethiones, and thiazolidinethiones. *J Org Chem* **2001**, 66, 894-902.
168. Seco, J. M.; Quiñero, E.; Riguera, R. The Assignment of Absolute Configuration by NMR. *Chemical Reviews* **2004**, 104, 17-118.

169. Lipshutz, B. H.; Pollart, D.; Monforte, J.; Kotsuki, H. Palladium(II)-catalyzed acetal/ketal hydrolysis/exchange reactions. *Tetrahedron Lett.* **1985**, 26, 705-8.
170. Ghosh, A. K.; Onishi, M. Synthesis of Enantiomerically Pure Anti-Aldols: A Highly Stereoselective Ester-Derived Titanium Enolate Aldol Reaction. *J. Am. Chem. Soc.* **1996**, 118, 2527-8.
171. Datta, D.; Scheer, J. M.; Romanowski, M. J.; Wells, J. A. An Allosteric Circuit in Caspase-1. *J. Mol. Biol.* **2008**, 381, 1157-1167.

VITA

Born in 1978, Swapnil Jayant Kulkarni received a Bachelor's degree in Pharmacy (B.Pharm. Sci) from SVB College of Pharmacy, Dombivli, State of Maharashtra, India in 2000. Immediately after completing his graduation, he joined the Graduate school at Bombay College of Pharmacy, Mumbai India for a Master's Degree in Pharmaceutical Sciences. Swapnil worked as a Graduate research Assistant (08/2001-08/2002) under the guidance of Dr. Evans Coutinho, also his Major Professor at Bombay College of Pharmacy while implementing his research project for a Master's degree. He completed Master's in Pharmaceutical Sciences with emphasis on studies in enzymatic resolution of drugs in August 2002.

After completion of Masters, he worked at two well-known pharmaceutical research companies in India, RPG Life Sciences (formerly Searle India Ltd) and USV Ltd in the capacity of Research Scientist from 2002-2004. At USV Ltd, his work on novel process development of synthesis of Carvedilol led to the world wide WIPO patent.

In 2005, Mr .Swapnil J Kulkarni commenced the graduate studies for the Doctoral degree at The University of Mississippi. He joined Dr. Mitchell A. Avery's group in 2005. Since then, he has worked in the capacity of a graduate research assistant in Dr.Avery's group. The main focus of Swapnil's research in his graduate studies was total synthesis of biologically active anti-cancer and anti-Alzheimer's natural products, Pseudolaric acid B and Berkeleyamide A. He has accomplished the total synthesis of Berkeleyamide A with 18% yield and in nine steps. He was also successful in completing the total synthesis of model system for Pseudolaric acid B

Mr. Swapnil Kulkarni has been selected as 'Class Marshal' to lead the class of 2011 in the graduation ceremony to be held in May 2011. Swapnil was recognized by honor societies of Phi Kappa Phi and Rho Chi for his academic and scholastic achievements. In addition to academic achievements, he has also received dissertation fellowship in recognition of outstanding PhD research.

Swapnil has received numerous awards for his outstanding research presented in the form of posters and oral talk in Malto regional conference (2010) as well as AAPS National Conference (2009, 2010). He also received "Graduate Symposium Award" for oral presentation at AAPS national meeting in 2010 and "Drug discovery and design" section Travelship award sponsored by AAPS for travel to AAPS Annual Meeting and Exposition at Los Angeles CA in 2009.

Mr. Swapnil has also offered his services to the University and his professional community, American Association of Pharmaceutical Scientists (AAPS) in the capacity of the student representative of Drug discovery and design (DDD) section of AAPS.

Additionally, Mr. Swapnil received a NIH Predoctoral Fellowship sponsored by Center of Biomedical Research and Excellence, The University of Mississippi for consecutively two years (2008-2009 & 2009-2010) for pursuing research in the field of neuroscience.

He has published research as well as patents as listed below and presented her research in various national and international conferences.

List of Patents and Publications

Patents

1. T.V. Radhakrishnan, D.G. Sathe, **S.J. Kulkarni**; “A novel process for the preparation of 1-(9H-carbazol-4-yloxy)-3-[2-(-methoxyphenoxy)-ethyl] amino]-propan-2-ol (carvedilol)” *PCT Int. Appl. (2005), WO 2005115981 A2 20051208*

Publications

1. R. Ahmed, Z. Ali, Y. Wu, **S.J. Kulkarni**, M.A. Avery, M.I. Choudhary, A. Rahman, I.A. Khan; Steroids and other Secondary Metabolites from *Commiphora wightii* (*Commiphora mukul*), *Accepted Planta Medica*.
2. **S.J. Kulkarni**, Y. Pedduri, A.G. Chittiboyina, M.A. Avery; Asymmetric Total Synthesis of the Caspase-1 Inhibitor (-)-Berkeleyamide A, *Journal of Organic Chemistry*, **2010**, 75, 3113.
3. S.B. Upadhye, **S.J. Kulkarni**, S. Majumdar, M.A. Avery, W. Gul, M. ElSohly, M.A. Repka; Preparation and characterization of Δ^9 -Tetrahydrocannabinol hemisuccinate-cyclodextrin complexes, *AAPS PharmSciTech*, **2010**, 11(2), 509-517.
4. S.Q. Zhang, A.G. Chittiboyina, **S.J. Kulkarni**, M.A. Avery, B.A. Avery; LC Determination of a Novel Synthetic Thiazolidinedione (BP-1107) in Rat Plasma and Its Application to a Pharmacokinetic Study, *Chromatographia*, **2008**, (7/8), 68.
5. **S.J. Kulkarni**, B. Watkins, B. Wu, M.A. Avery; Studies towards total synthesis of Pseudolaric acid, (*In preparation*).
6. M.A. Avery, **S.J. Kulkarni**, T. Simmons, A.G. Chittiboyina; Synthesis and biological testing of novel Triazolyl derivatives of Artemisinin, (*In preparation*).
7. **S.J. Kulkarni**, Y. Pedduri, M.A. Avery; Synthesis and biological evaluation of Berkeleyamide A analogs, (*In preparation*).
8. **Presentations**
9. **S.J. Kulkarni**, Y. Pedduri, A.G. Chittiboyina, M.A. Avery; Total synthesis of Caspase-1 inhibitor Berkeleyamide-A, *American Association of Pharmaceutical Scientists*, November 2010, New Orleans, LA (*Outstanding Graduate Research Award*)

10. **S.J. Kulkarni**, E.B. Watkins, A.G. Chittiboyina, M.A. Avery; Studies towards total synthesis of Pseudolaric acid B, MALTO, May 2010, Oxford, MS (*Outstanding Poster*).
11. **S.J. Kulkarni**, Y. Pedduri, A.G. Chittiboyina, M.A. Avery; Total synthesis of Berkeleyamide-A: A potent caspase-1 inhibitor, *239th American Chemical Society National Meeting*, March 2010, San Francisco, CA.
12. **S.J. Kulkarni**, A.G. Chittiboyina, M.A. Avery; Studies towards Total Synthesis of Berkeleyamide A, *American Association of Pharmaceutical Scientists*, November 2009, Los Angeles, CA.
13. S.B. Upadhye, **S.J. Kulkarni**, S. Majumdar, M.A. Avery, W. Gul, M.A. ElSohly, M.A. Repka; Preparation and characterization of an inclusion complex of a hemisuccinate ester prodrug of delta-9-tetrahydrocannabinol with modified beta-cyclodextrins, *AAPS Annual meeting 2008*, Atlanta, GA.
14. S.P. Boddu, D. Pabbisetty, S.Q. Zhang, A.G. Chittiboyina, **S.J. Kulkarni**, M.A. Avery, B.A. Avery; Method development and intravenous pharmacokinetic study of a novel synthetic thiazolidinedione (bp-1107) in rats, *AAPS Annual meeting 2008*, Atlanta, GA.